FATIGUE BEHAVIOR OF PRETENSIONED CONCRETE GIRDERS

T. R. Overman, J. E. Breen,
and K. H. Frank

RESEARCH REPORT 300-2F

PROJECT 3-5-80-300

CENTER FOR TRANSPORTATION RESEARCH
BUREAU OF ENGINEERING RESEARCH
THE UNIVERSITY OF TEXAS AT AUSTIN
NOVEMBER 1984

PARTIAL LIST OF REPORTS PUBLISHED BY THE CENTER FOR TRANSPORTATION RESEARCH

This list includes some of the reports published by the Center for Transportation Research and the organizations which were merged to form it: the Center for Highway Research and the Council for Advanced Transportation Studies. Questions about the Center and the availability and costs of specific reports should be addressed to: Director; Center for Transportation Research; ECJ 2.5; The University of Texas at Austin; Austin, Texas 78712.

7-1 "Strength and Stiffness of Reinforced Concrete Rectangular Columns Under Biaxially Eccentric Thrust," by J. A. Desai and R. W. Furlong, January 1976.

7-2F "Strength and Stiffness of Reinforced Concrete Columns Under Biaxial Bending," by V. Mavichak and R. W. Furlong, November 1976.

16-1F "Oil, Grease, and Other Pollutants in Highway Runoff," by Bruce Wiland and Joseph F. Malina, Jr., September 1976.

23-1 "Prediction of Temperature and Stresses in Highway Bridges by a Numerical Procedure Using Daily Weather Reports," by Thaksin Thepchatri, C. Philip Johnson, and Hudson Matlock, February 1977.

23-2 "Analytical and Experimental Investigation of the Thermal Response of Highway Bridges," by Kenneth M. Will, C. Philip Johnson, and Hudson Matlock, February 1977.

23-3F "Temperature Induced Stresses in Highway Bridges by Finite Element Analysis and Field Tests," by Atalay Yargicoglu and C. Philip Johnson, July 1978.

29-2F "Strength and Behavior of Anchor Bolts Embedded Near Edges of Concrete Piers," by G. B. Hasselwander, J. O. Jirsa, J. E. Breen, and K. Lo, May 1977.

114-4 "Durability, Strength, and Method of Application of Polymer-Impregnated Concrete for Slabs," by Piti Yimprasert, David W. Fowler, and Donald R. Paul, January 1976.

114-5 "Partial Polymer Impregnation of Center Point Road Bridge," by Ronald Webster, David W. Fowler, and Donald R. Paul, January 1976.

114-6 "Behavior of Post-Tensioned Polymer-Impregnated Concrete Beams," by Ekasit Limsuwan, David W. Fowler, Ned H. Burns, and Donald R. Paul, June 1978.

114-7 "An Investigation of the Use of Polymer-Concrete Overlays for Bridge Decks," by Huey-Tsann Hsu, David W. Fowler, Mickey Miller, and Donald R. Paul, March 1979.

114-8 "Polymer Concrete Repair of Bridge Decks," by David W. Fowler and Donald R. Paul, March 1979.

114-9F "Concrete-Polymer Materials for Highway Applications," by David W. Fowler and Donald R. Paul, March 1979.

118-9F "Observation of an Expansive Clay Under Controlled Conditions," by John B. Stevens, Paul N. Brotcke, Dewaine Bogard, and Hudson Matlock, November 1976.

123-30F "Overview of Pavement Management Systems Developments in the State Department of Highways and Public Transportation," by W. Ronald Hudson, B. Frank McCullough, Jim Brown, Gerald Peck, and Robert L. Lytton, January 1976 (published jointly with the Texas State Department of Highways and Public Transportation and the Texas Transportation Institute, Texas A&M University).

172-1 "Axial Tension Fatigue Strength of Anchor Bolts," by Franklin L. Fischer and Karl H. Frank, March 1977.

172-2F "Fatigue of Anchor Bolts," by Karl H. Frank, July 1978.

176-4 "Behavior of Axially Loaded Drilled Shafts in Clay-Shales," by Ravi P. Aurora and Lymon C. Reese, March 1976.

176-5F "Design Procedures for Axially Loaded Drilled Shafts," by Gerardo W. Quiros and Lymon C. Reese, December 1977.

177-1 "Drying Shrinkage and Temperature Drop Stresses in Jointed Reinforced Concrete Pavement," by Felipe Rivero-Vallejo and B. Frank McCullough, May 1976.

177-3 "A Study of the Performance of the Mays Ride Meter," by Yi Chin Hu, Hugh J. Williamson, and B. Frank McCullough, January 1977.

177-4 "Laboratory Study of the Effect of Nonuniform Foundation Support on Continuously Reinforced Concrete Pavements," by Enrique Jimenez, B. Frank McCullough, and W. Ronald Hudson, August 1977.

177-6 "Sixteenth Year Progress Report on Experimental Continuously Reinforced Concrete Pavement in Walker County," by B. Frank McCullough and Thomas P. Chesney, April 1976.

177-7 "Continuously Reinforced Concrete Pavement: Structural Performance and Design/Construction Variables," by Pieter J. Strauss, B. Frank McCullough, and W. Ronald Hudson, May 1977.

177-9 "CRCP-2, An Improved Computer Program for the Analysis of Continuously Reinforced Concrete Pavements," by James Ma and B. Frank McCullough, August 1977.

177-10 "Development of Photographic Techniques for Performing Condition Surveys," by Pieter Strauss, James Long, and B. Frank McCullough, May 1977.

177-11 "A Sensitivity Analysis of Rigid Pavement Overlay Design Procedure," by B. C. Nayak, W. Ronald Hudson, and B. Frank McCullough, June 1977.

177-12 "A Study of CRCP Performance: New Construction Vs. Overlay," by James I. Daniel, W. Ronald Hudson, and B. Frank McCullough, April 1978.

177-13 "A Rigid Pavement Overlay Design Procedure for Texas SDHPT," by Otto Schnitter, W. R. Hudson, and B. F. McCullough, May 1978.

177-15 "Precast Repair of Continuously Reinforced Concrete Pavement," by Gary Eugene Elkins, B. Frank McCullough, and W. Ronald Hudson, May 1979.

177-16 "Nomographs for the Design of CRCP Steel Reinforcement," by C. S. Noble, B. F. McCullough, and J. C. M. Ma, August 1979.

177-17 "Limiting Criteria for the Design of CRCP," by B. Frank McCullough, J. C. M. Ma, and C. S. Noble, August 1979.

177-18 "Detection of Voids Underneath Continuously Reinforced Concrete Pavements," by John W. Birkhoff and B. Frank McCullough, August 1979.

183-7 "Permanent Deformation Characteristics of Asphalt Mixtures by Repeated-Load Indirect Tensile Test," by Joaquin Vallejo, Thomas W. Kennedy, and Ralph Haas, June 1976.

(Continued inside back cover)

TECHNICAL REPORT STANDARD TITLE PAGE

1. Report No.	2. Government Accession No.	3. Recipient's Catalog No.
FHWA/TX-85/39+300-2F		

4. Title and Subtitle	5. Report Date
FATIGUE BEHAVIOR OF PRETENSIONED CONCRETE GIRDERS	November 1984
	6. Performing Organization Code
7. Author(s)	8. Performing Organization Report No.
T. R. Overman, J. E. Breen, and K. H. Frank	Research Report 300-2F
9. Performing Organization Name and Address	10. Work Unit No.
Center for Transportation Research The University of Texas at Austin Austin, Texas 78712-1075	11. Contract or Grant No. Research Study 3-5-80-300
	13. Type of Report and Period Covered
12. Sponsoring Agency Name and Address Texas State Department of Highways and Public Transportation; Transportation Planning Division P. O. Box 5051 Austin, Texas 78763	Final
	14. Sponsoring Agency Code

15. Supplementary Notes
Study conducted in cooperation with the U. S. Department of Transportation, Federal Highway Administration
Research Study Title: "Fatigue Strength of Prestressed Concrete Girders"

16. Abstract

This report summarizes the fatigue testing of full scale precast pretensioned girders with unshored cast-in-place slabs. It includes an extensive literature review of prestressed concrete fatigue and of development of design specifications relating to fatigue of prestressed concrete. Detailed summaries are given of the fatigue and ultimate behavior of a series of full scale test specimens including static and dynamic loads, deflections, stresses, and crack measurements. The main variables included maximum nominal concrete tensile stress level; girder strand stress ranges; cross sections (both Texas Type C and AASHTO Type II girders); strand patterns (both straight and draped); passive reinforcement; degree of precracking; presence of occasional overloading; and prestressing losses. A nonlinear program was used in the analysis of experimental results to determine the effective prestressing extent of prestress losses, and the effective strand stress ranges. Comparisons were made to other reported test results and to recommended and existing fatigue design procedures. The report synthesizes this information and presents design recommendations suitable for inclusion within the general AASHTO fatigue design framework.

17. Key Words	18. Distribution Statement
girders, concrete, pretensioned, fatigue behavior, testing, full scale, design recommendations	No restrictions. This document is available to the public through the National Technical Information Service, Springfield, Virginia 22161.

19. Security Classif. (of this report)	20. Security Classif. (of this page)	21. No. of Pages	22. Price
Unclassified	Unclassified	382	

Form DOT F 1700.7 (8-69)

FATIGUE BEHAVIOR OF PRETENSIONED CONCRETE GIRDERS

by

T. R. Overman
J. E. Breen
and
K. H. Frank

Research Report No. 300-2F

Research Project 3-5-80-300

"Fatigue Strength of Prestressed Concrete Girders"

Conducted for

Texas
State Department of Highways and Public Transportation

In cooperation with the
U. S. Department of Transportation
Federal Highway Administration

by

Center for Transportation Research
Bureau of Engineering Research
The University of Texas at Austin

November 1984

The contents of this report reflect the views of the authors who are responsible for the facts and accuracy of the data presented herein. The contents do not necessarily reflect the official views or policies of the Federal Highway Administration. This report does not constitute a standard, specification, or regulation.

There was no invention or discovery conceived or first actually reduced to practice in the course of or under this contract, including any art, method, process, machine, manufacture, design or composition of matter, or any new and useful improvement thereof, or any variety of plant which is or may be patentable under the patent laws of the United States of America or any foreign country.

PREFACE

This is the final report on Project 3-5-80-300, "Fatigue of Prestressed Concrete Girders," sponsored by the State Department of Highways and Public Transportation of the State of Texas, and the Federal Highway Administration. It was administered by the Center for Transportation Research. The research was conducted at the Phil M. Ferguson Structural Engineering Laboratory, Balcones Research Center, The University of Texas at Austin, Austin, Texas. Close liaison with the Texas State Department of Highways and Public Transportation was maintained through their contact representative, Mr. A. B. Matejowsky. Mr. D. E. Harley and Mr. R. Stanford aided as contact representatives for the Federal Highway Administration. Mr. Louis Garrido of the Louisiana Highway Department and Professor Robert Bruce of Tulane University provided valuable assistance in arranging for construction of the Louisiana AASHTO Type girders. Mr. Kent Preston, representing Florida Wire and Cable, was of great assistance in securing the pretensioning strand used in the Texas girders. The assistance of all of these gentlemen in obtaining test specimens and in providing valuable suggestions throughout the testing is greatly appreciated.

The authors are particularly indebted to the technical staff who worked on this project at the Ferguson Laboratory and particularly to Research Engineers Conrad Paulson, Gregg Reese, Patrick Bachman, and Nobuyuki Matsumoto, who provided careful documentation of all tests in this series and who each contributed significantly to the development of the data bank and the analysis of specimens.

This report contains both a summary of the main fatigue testing program of full scale pretensioned girders and the design recommendations which can be drawn from those tests. An earlier report in this program summarized the fatigue tests of pretensioning strand in air and suggested a fatigue design model based on an extensive data bank. That model is further developed herein into a general design philosophy for flexural fatigue of pretensioned concrete girders.

SUMMARY

This report summarizes the fatigue testing of full scale precast pretensioned girders with unshored cast-in-place slabs. It includes an extensive literature review of prestressed concrete fatigue and of development of design specifications relating to fatigue of prestressed concrete. Detailed summaries are given of the fatigue and ultimate behavior of a series of full scale test specimens including static and dynamic loads, deflections, stresses, and crack measurements. The main variables included maximum nominal concrete tensile stress level; girder stand stress ranges; cross sections (both Texas Type C and AASHTO Type II girders); strand patterns (both straight and draped); passive reinforcement; degree of precracking; presence of occasional overloading; and prestressing losses. A nonlinear program was used in the analysis of experimental results to determine the effective prestressing extent of prestress losses, and the effective strand stress ranges. Comparisons were made to other reported test results and to recommended and existing fatigue design procedures. The report synthesizes this information and presents design recommendations suitable for inclusion within the general AASHTO fatigue design framework.

IMPLEMENTATION

The results of this study indicate that present AASHTO indirect design criteria for flexural fatigue strength of pretensioned concrete girders through limitation of the nominal tensile stress in the precompressed tensile zone will not ensure adequate fatigue life. Pretensioned concrete bridge girders without well-distributed, confined passive reinforcement which are actually subjected to loads producing nominal tensile stresses of $6\sqrt{f'_c}$ can fail as a result of fatigue of prestressing strands at less than 3 million cycles. Based on an extensive comparison of experimental results and computer studies, it appears adequate to relate the design of such girders to stress ranges similar to AASHTO structural steel Category B values for redundant load path structures.

The test results indicate the extremely detrimental effects of occasional modest overload cycles and the marked influence of strand stress ranges due to excessive prestress losses.

The report presents a general fatigue design methodology for pretensioned concrete girders which should result in substantially improved design of such girders. This can lead to development of the full design life and ensure satisfactory performance of this widely used bridge type over full design life. In addition, it will provide important information for the evaluation of occasional overloads and assist in the rating of bridges for both normal and permit loads.

C O N T E N T S

T A B L E S

F I G U R E S

CHAPTER 1

INTRODUCTION

1.1 General

The utilization of new materials or new applications of existing materials is a slow and usually conservative process. Building codes and design specifications do not address these new applications immediately. Only after widespread acceptance, which often means extensive testing, will a consensus specification writing organization provide guidelines. As engineers and the public gain confidence in the new development, codes and design specifications are relaxed to allow more efficient use of materials. However, both design and construction engineers' responsibilities increase as the factors of safety are decreased. They must understand how materials behave under various loading conditions and ensure that strict quality standards are observed. In some cases, more unconservative limits are required for a given application as a result of new findings. This is understandable because bridge and building standards are framed in a general way so that they can be used for many different structural applications. Prestressed concrete has followed this evolutionary path in the United States over the past three decades.

This chapter is divided into four main sections. The first section provides historical information on the beginnings of linear prestressing in the United States. The AASHTO Specifications for prestressed concrete and fatigue design recommendations are briefly reviewed in the second section. Previous tests by Rabbat et al. [76] are briefly discussed along with the purpose of this test program and the test variables in the following section. The last section provides an outline of the overall report which is based on the thesis of the senior author [95].

1.2 The Beginnings of Linear Prestressing in the United States

Professor Gustave Magnel of Belgium brought linear prestressing (as contrasted to circular prestressing used in tanks) to the United States in the 1940's [93,94]. He visited this country in 1946 as a "Belgium-American Educational Foundation Scientist" and lectured on structural engineering, reinforced concrete, and prestressed concrete. In 1948, Magnel was commissioned to design a prestressed concrete alternative to a variable depth box girder bridge for the Walnut Lane crossing in Philadelphia. Magnel's design involved prestressed concrete I-sections. The Walnut Lane Bridge was the first prestressed concrete bridge and the first application of linear prestressing in the United States.

The early days of prestressed concrete were characterized by a great deal of full-scale testing and the invention of new devices. A full-scale test to destruction of a typical girder was required by local authorities before construction began on the Walnut Lane Bridge. Additional extensive testing was carried out at Lehigh University in the early 1950's by Ekberg and Eney [34,51] to verify the feasibility of prestressed concrete and develop design criteria suited for U.S. applications. Stress-relieved wire, stressing beds, efficient chucks, and bundled wire (strand) were all developed in the 1950's as a result of the widespread interest in prestressed concrete. Most applications in the United States favored pretensioned concrete while European engineers generally worked with post-tensioned concrete.

1.3 Specifications and Recommendations for Prestressed Concrete Design

1.3.1 AASHTO Specifications

Specification writers must consider many factors, a large portion of which can vary greatly, before an acceptable specification is published. The applicability of the AASHTO Specification [7,8] maximum allowable nominal concrete tensile stress of $6\sqrt{f'_c}$ typifies the evolution of a design specification. Actual loads, including impact and the probability of overloads, had to be considered. Lateral and longitudinal (if applicable) distribution of loads is a factor. Once the effective section and loads are determined, the state of stress of the cross section is calculated. The calculation would include the initial prestress force and concrete properties (which vary depending on quality control at a given prestress plant) as well as prestress losses. Losses are a function of curing and storage conditions, material properties, atmospheric conditions, and loading history. The interdependence of losses add to their variability and uncertainty. After the state of stress is estimated given uncertain maximum loads, a designer compares the actual stresses with the allowable values assuming linear elastic behavior (no cracking). The allowable nominal concrete tensile stress limit is not valid if the concrete tensile cracking stress, which is also variable, is exceeded. Recognizing in some way these variable factors, the AASHO Specifications [3] first addressed prestressed concrete design in 1961.

The initial AASHO Specifications [3] (1961) pertaining to prestressed concrete design restricted the tensile stress to zero in the extreme fibers of the precompressed tension zone. In 1965 [4] the maximum allowable tensile stress was increased to $3\sqrt{f'_c}$. The present value of $6\sqrt{f'_c}$ was first allowed in the 1971 Interim Specifications [1]. As the maximum allowable tensile stress increases, variability in loads, losses and material properties become more of a factor, and the designer's responsibilities increase. If cracking occurs as a result of

an adverse change in one or more of the variables, fatigue as well as corrosion become potential problems. Figure 1.1 shows the drastic increase in local strand stress that accompanies the opening of flexural cracks (which can result in fatigue problems). The AASHTO Specifications [8] do not specifically address fatigue of prestressed concrete, but several ACI committee reports [19,24,44] do.

1.3.2 ACI Recommendations for Fatigue Design

The ACI Committee 215 and Committee 443 reports provide guidelines for fatigue design. Committee 215, Fatigue of Concrete, [44] suggests maximum strand stress ranges of 0.10 f_{pu} for uncracked sections and 0.04 f_{pu} for cracked sections for fatigue design. Committee 443, Concrete Bridge Design [24], suggests maximum nominal concrete tensile stresses of $6\sqrt{f'_c}$ for members with bonded auxiliary reinforcement, $3\sqrt{f'_c}$ for members with bonded auxiliary reinforcement in corrosive environments, and zero tension for members without bonded auxiliary reinforcement. The Committee 443 recommendations appear to be based on both corrosion and fatigue considerations.

1.4 Purpose of Test Program

As a result of potentially unfavorable results found in previous pretensioned girder tests by Rabbat et al. [76], this test program was initiated to determine the fatigue strength of full scale pretensioned concrete bridge girders.

1.4.1 Previous Tests by Rabbat et al.

Rabbat et al. [76] tested six full-scale AASHTO-PCI Type II girders with composite decks. The main purpose of the experimental program was "to determine the effect of repetitive loading on the behavior and strength of girders with draped and blanketed strands" [76]. Three specimens were cycled at a maximum load that produced zero tension in the extreme fibers of the precompressed tension zone. These girders withstood 5.0 million fatigue cycles with no indication of fatigue distress. The subsequent ultimate tests to failure (at loads slightly above the calculated ultimate capacities) confirmed that fatigue testing did not reduce the girders' strength. Three other girders were cycled in a cracked state at loads that produced a maximum, nominal, uncracked tensile stress of $6\sqrt{f'_c}$. These three girders experienced fatigue distress between 3.2 and 3.8 million cycles. Subsequent ultimate tests on two of the specimens and post mortem investigations on all three specimens revealed extensive wire fatigue failures.

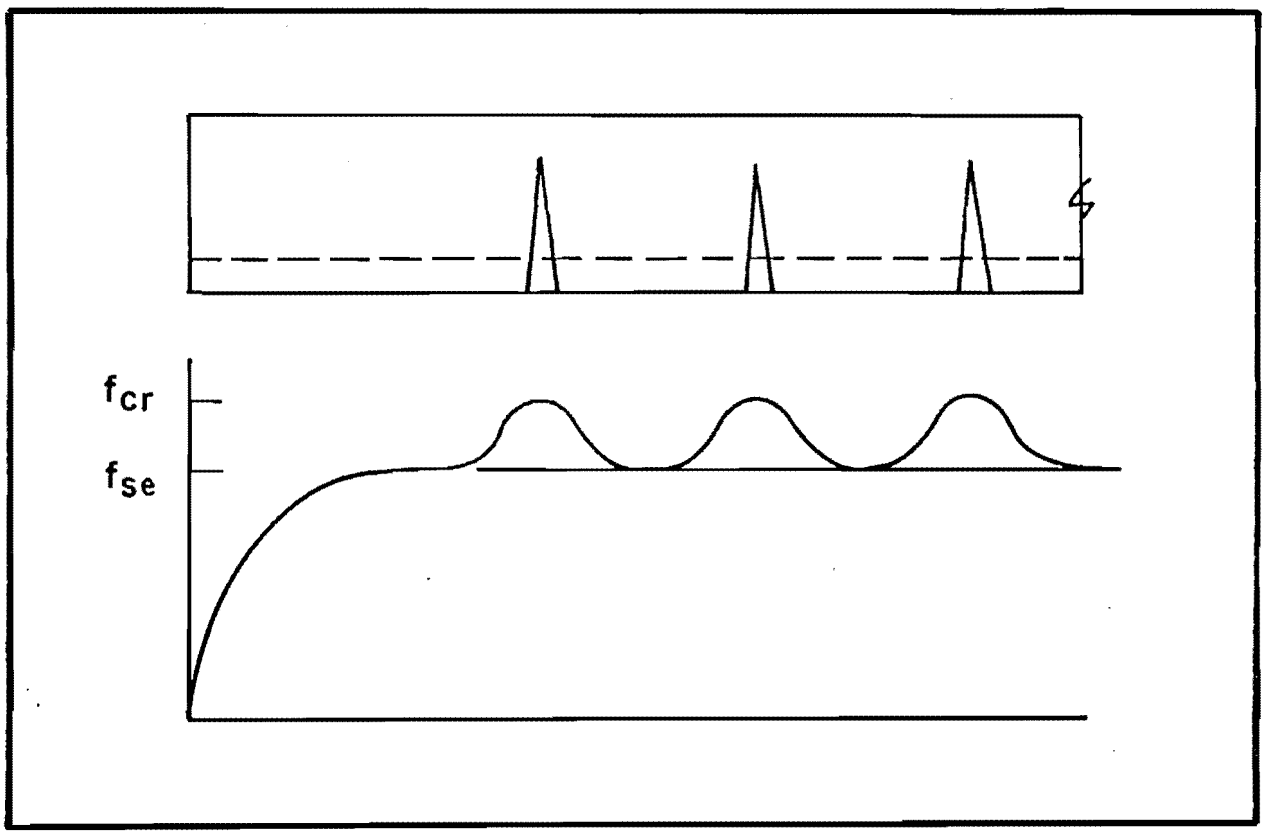

Fig. 1.1 Strand stress increase at flexural cracks

The application of the results of the tests by Rabbat et al. were questioned by the prestressed concrete industry as a result of fabrication and material unknowns and experimental techniques. The strand fatigue properties and initial conditions (rusted or unrusted surfaces) were questioned. In the study, prestress losses were assumed at 20 percent based on an initial prestress of 70 percent f_{pu}. The initial prestress, losses, and effective prestress values were questioned. The use of crack formers (which eliminated random cracking) was questioned. Some critics suggested possible dynamic amplification due to the loading rate of 265 cycles per minute, and they subsequently cast doubt on the results. This project was initiated to clarify some of these effects and to further explore variables affecting the fatigue strength of pretensioned girders.

1.4.2 Description of Test Program

The current test program was divided into three phases. The initial portion of the test program was reported on by Paulson et al. [73] and involved the development of a strand in air fatigue model based on both previously reported tests and new data (including tests on the strand used in the present study's Texas Type C and AASHTO-PCI Type II specimens). Eleven full-scale pretensioned girder specimens were tested in the current flexural fatigue portion of the research project. Several of these girder tests were previously reported by Reese [77]. The last portion of the study involves shear fatigue tests of full-scale girders and will be reported by Bachman [26].

1.4.2.1 Failure Modes of Prestressed Concrete Beams

T.Y. Lin [53] observed that "the fatigue strength of prestressed concrete can be studied from three approaches: that of concrete itself, that of high strength steel, and that of the combination." While some mention will be made of both concrete and steel fatigue, the third case, fatigue of prestressed members will be the major focus of this report. Emphasis will be given to predicting girder fatigue life from strand fatigue data.

The possible modes of fatigue failure of prestressed concrete beams are:

1. Cyclic compression failure of the concrete.

2. Tension failure of concrete due to overloads or repetitive loads followed by brittle fracture of steel at cracks due to high steel stress ranges.

3. Progressive bond failure between concrete and pretensioned steel originating at cracks due to high bond stresses. This

results in excessive slip of the prestressing steel which essentially causes a loss of effective prestress and may result in brittle fracture of steel at cracks due to high steel stress ranges.

4. Cyclic diagonal tension or shear failure resulting in stirrup fatigue fractures.

By far the most prevalent mode of failure encountered in girder fatigue tests is due to fatigue fractures of the prestressing strand at crack locations [41,47,62,64,65,76,77,91]. Shear fatigue failures have not been widely investigated although such failures have occurred and are being studied in a parallel test series [26]. This report will focus on the failure modes which involve brittle fracture of flexural steel, both prestressing and passive reinforcement.

1.4.2.2 Flexural Fatigue Tests

The flexural fatigue girder phase was designed solely as a fatigue test of full-scale pretensioned concrete girders. The strand fatigue properties for both the Texas Type C and AASHTO-PCI Type II specimens were known. The strand used in the Texas Type C specimens was considered to have average fatigue characteristics when compared to test data on all strand. The spool from which all strand for the Texas Type C girders was taken was stored inside the laboratory to prevent rusting. Initial prestress levels were known accurately as a result of ram pressure, strand-elongation, and strand strain gage and strand load cell instrumentation. Losses were calculated using PBEAM [85], a time-dependent computer program. Actual losses and the effective prestress level were determined from cracked section behavior with the aid of deflection and strain measurements. All but one specimen were precracked to determine the effective prestress level, but no crack formers were used. The cyclic loading rate was between 2.5 and 3.0 cycles per second, somewhat above the actual field loading rate which might approximate 1.7 cycles per second based on truck passages. However, the rate was below the ACI Committee 215 [19] suggested loading rate of 3.3 to 10 cycles per second for prestressing strand. All but one girder specimen was taken to fatigue failure to determine the fatigue life of various strand stress ranges.

1.4.2.3 Flexural Fatigue Test Variables

The main experimental variables included: maximum load level as indicated by the nominal concrete tensile stresses based on uncracked transformed section calculations; girder strand stress ranges; cross sections (which included AASHTO-PCI Type II girders and Texas Type C girders); strand pattern including both draped and straight strands;

provision of passive reinforcing steel in the precompressed tension zone; distribution and confinement of passive reinforcement; degree of precracking of sections; and the presence or absence of occasional modest overloads during static tests.

1.5 Description of the Following Chapters

This report summarizes the flexural fatigue tests of eleven full scale precast pretensioned concrete girders with unshored cast-in-place slabs [95]. The following chapter (second of six) includes an extensive literature review of fatigue of the constituent materials (concrete, reinforcing steel, and prestressing steel), of fatigue of prestressed members, of the evolution of prestressed concrete in the AASHTO Specifications, and of the development of specifications and code provisions relating to fatigue of prestressed concrete. The third chapter includes a detailed description of the fabrication procedure, material properties, initial static loading procedure, the technique used to determine the actual prestress force, and the fatigue and ultimate testing procedures. Chapter 4 provides detailed summaries of the static, fatigue and ultimate behavior of the eleven specimens including: static and dynamic loads, deflections, stresses and crack measurements. It reports results of a post mortem investigation which was performed on all specimens to determine the locations and types of wire and reinforcing steel fractures. Chapter 5 describes the nonlinear program used in the analysis of experimental results to determine prestress losses and strand stress ranges. It presents comparisons: among the eleven specimens, to other reported test results, and to various fatigue design procedures. The recommended design procedure developed in this study is outlined in detail in Chapter 5. The last chapter (Summary, Conclusions and Recommendations) synthesizes the reported information and presents design recommendations suitable for inclusion within the general AASHTO fatigue design framework.

The results of this limited number of tests must be put into perspective. The applied loads (static and dynamic), prestress losses, and material properties were known accurately for all specimens, unlike the situation with in-service girders. In actual service applications, these conditions could be better or worse. With single girder specimens, there is no possibility of lateral distribution of loads to adjacent girders. Lateral distribution occurs in actual bridges. Empirical procedures are used in design to estimate such distribution effects. These effects could reduce the possibility of fatigue if conservative distributions are assumed. Conversely, actual loads could be higher than design loads and material variations and construction variability could reduce girder strength and resistance to cracking. This could have a very damaging effect on the fatigue strength of actual applications. Finally, all girders tested in this program experienced a relatively large number of full live load cycles prior to failure. A highway girder would probably have to be in service a substantial number

of years before it accumulates cycles of this magnitude. Present favorable experience with pretensioned girders may not be a predictor of future experiences when longer lives result in substantial numbers of load applications.

CHAPTER 2

BACKGROUND

2.1 Introduction

In order to understand the behavior of prestressed concrete members subjected to fatigue loading, one must be aware of the limitations of the component materials, the interactions between the materials, and the behavior of the member as a whole. The first part of this chapter reviews previous studies regarding the fatigue of concrete and the fatigue of prestressing and reinforcing steel as well as their interaction. The next section reviews the available information on fatigue of prestressed concrete beams. The fatigue program with prestressed concrete bridges at the AASHO road test is reviewed in the third section. The application of partial prestressing with auxiliary nonprestressed mild reinforcement and its impact on fatigue is reviewed in the next section. Finally, the development of prestressed concrete fatigue related provisions in American regulatory standards is summarized.

2.2 Fatigue of Component Materials

2.2.1 Concrete

The mechanism of fatigue failure of concrete includes internal microcracking between the paste and the aggregate and within the paste itself. This network of cracks which develops under repeated loading is more extensive than that in specimens subjected to only static loading [79]. The ultimate result of this cracking is rupture of the concrete.

2.2.1.1 Concrete in Compression

The compression strain of concrete subjected to repetitive loading has two main components. A Rilem Report [79] states that one of these components is a function of the elastic strain and the endurance of the specimen, ϵ_e. The other component is a time-dependent function similar to creep, $_t$. Figure 2.1 shows the two components of cyclical compression strain. In this example the high initial strain corresponds to a level of upper stress equivalent to 0.75 f'_c.

Nordby [61], reporting on work by Mehmel and Probst, calls the two components of cyclical compression strain "elastic" and "remaining". The remaining part is the strain remaining after the load is removed. A portion of this is recoverable. Nordby states:

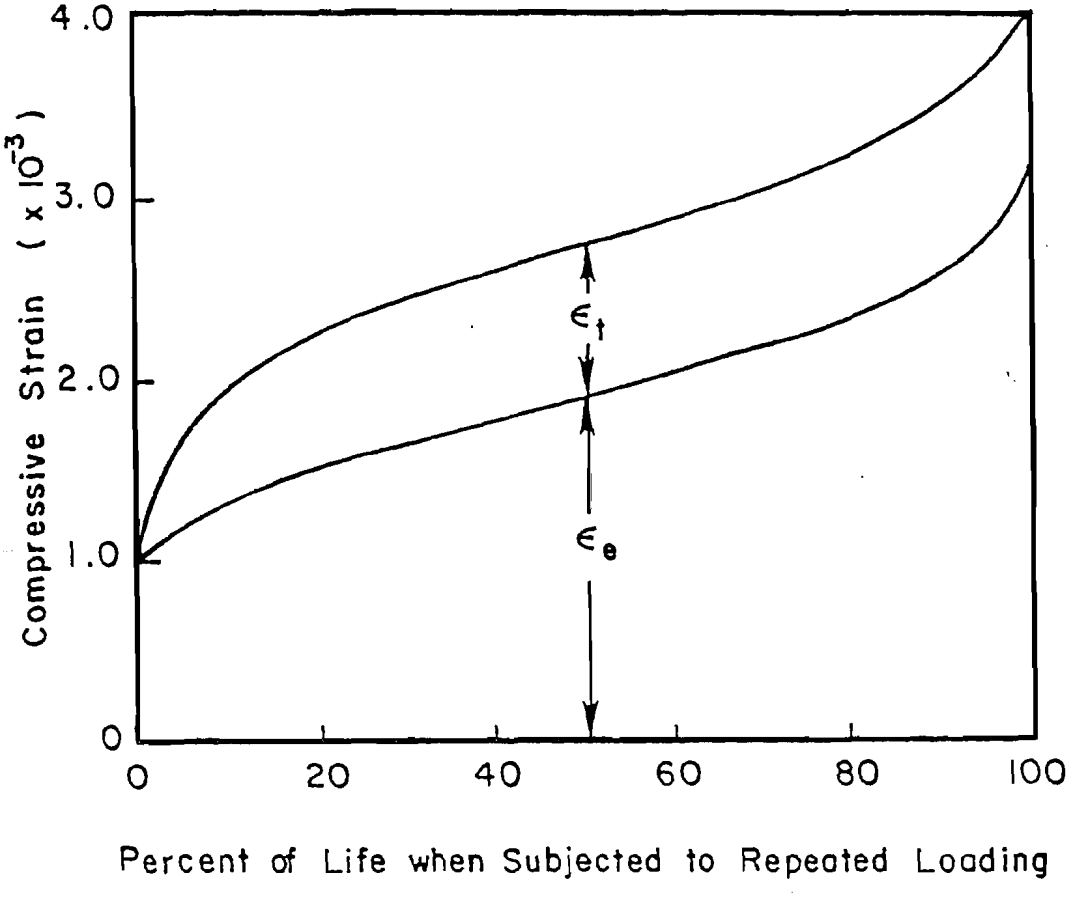

Fig. 2.1 The two components of cyclic strain

> It was found that elastic strains and remaining strains increase with the number of repetitions as long as a certain critical stress (endurance limit) is not exceeded and that the ratio (remaining strain/elastic strain) grows larger with the number of cycles. This critical stress was between 47 and 60 percent f'_c.

Figure 2.2 shows Mehmel's and Probst's results from which the conclusions are drawn. The tests were performed on compression cylinders.

Both studies indicate permanent strains result from compressive fatigue loading. The studies confirm Nordby's critical stress theory. For the high initial strains in the Rilem Report, in which the initial stress was 0.75 f'_c, the elastic portion dominates. The time component changed little after 20 percent of the life was reached. The Mehmel and Probst study, performed at stresses below the critical value, indicates a proportionally larger increase in time effects than the elastic effects.

ACI Committee 215 [19], reporting on work by Raju, states:

> Similar to the behavior of concrete under sustained loads, the strain of concrete during repeated loading increases substantially beyond the value observed after the first load application. The strain at fatigue failure is likely to be higher if the maximum stress is lower.

This would indicate larger strains develop in low stress, high cycle tests than develop in high stress, low cycle tests. For flexural members, this time or cyclical load effect would cause permanent deformations. Deflections should increase as cycling continues. In addition, with prestressed members the effective prestress force should decrease.

2.2.1.2 Concrete in Tension

Recent tests by Saito and Imai [81] indicate:

> ... that the S-N curve of concrete subjected to repeated tensile loads exhibits no fatigue limit less than 2 million cycles. The relationship between stress level S [percentage of ultimate stress] and average fatigue life N for P = 0.5 [50 percent probability] is

$$S = -4.12 \log N + 98.73$$

A plot of this curve is shown in Fig. 2.3. The Saito test specimen is shown in Fig. 2.4. The minimum stress level for all tests was 8.0

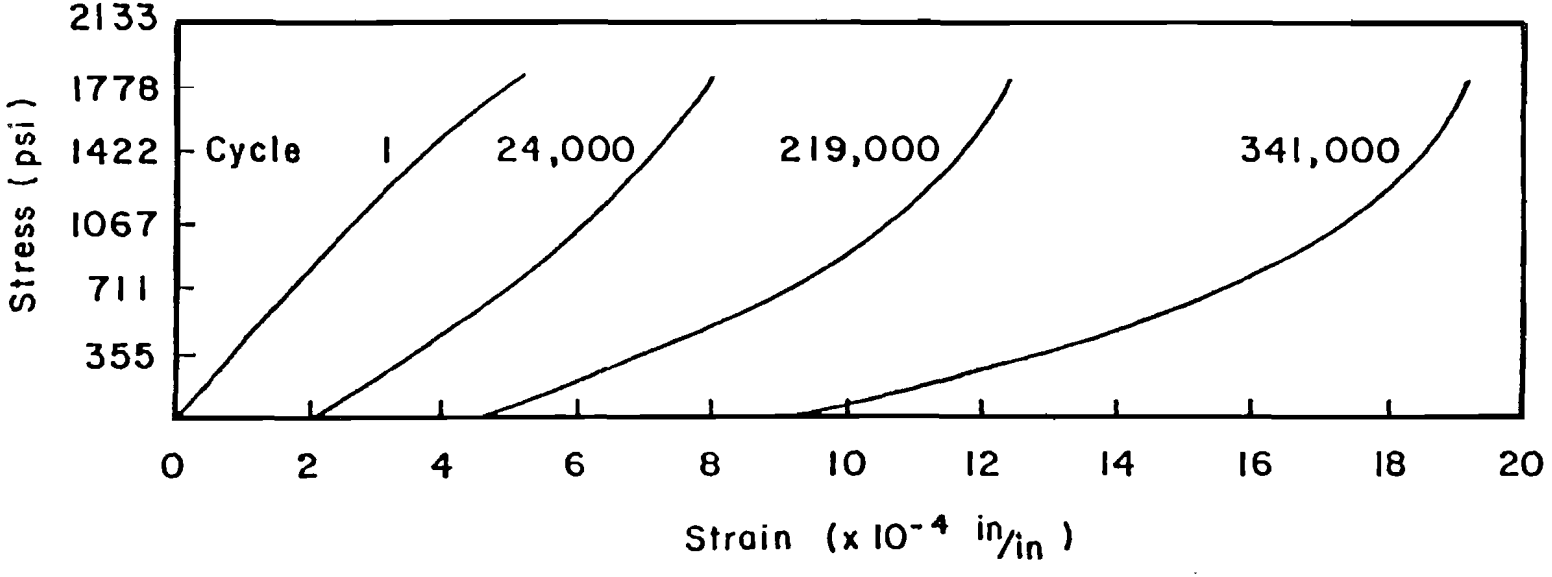

Fig. 2.2 Cyclic strain in compression specimens

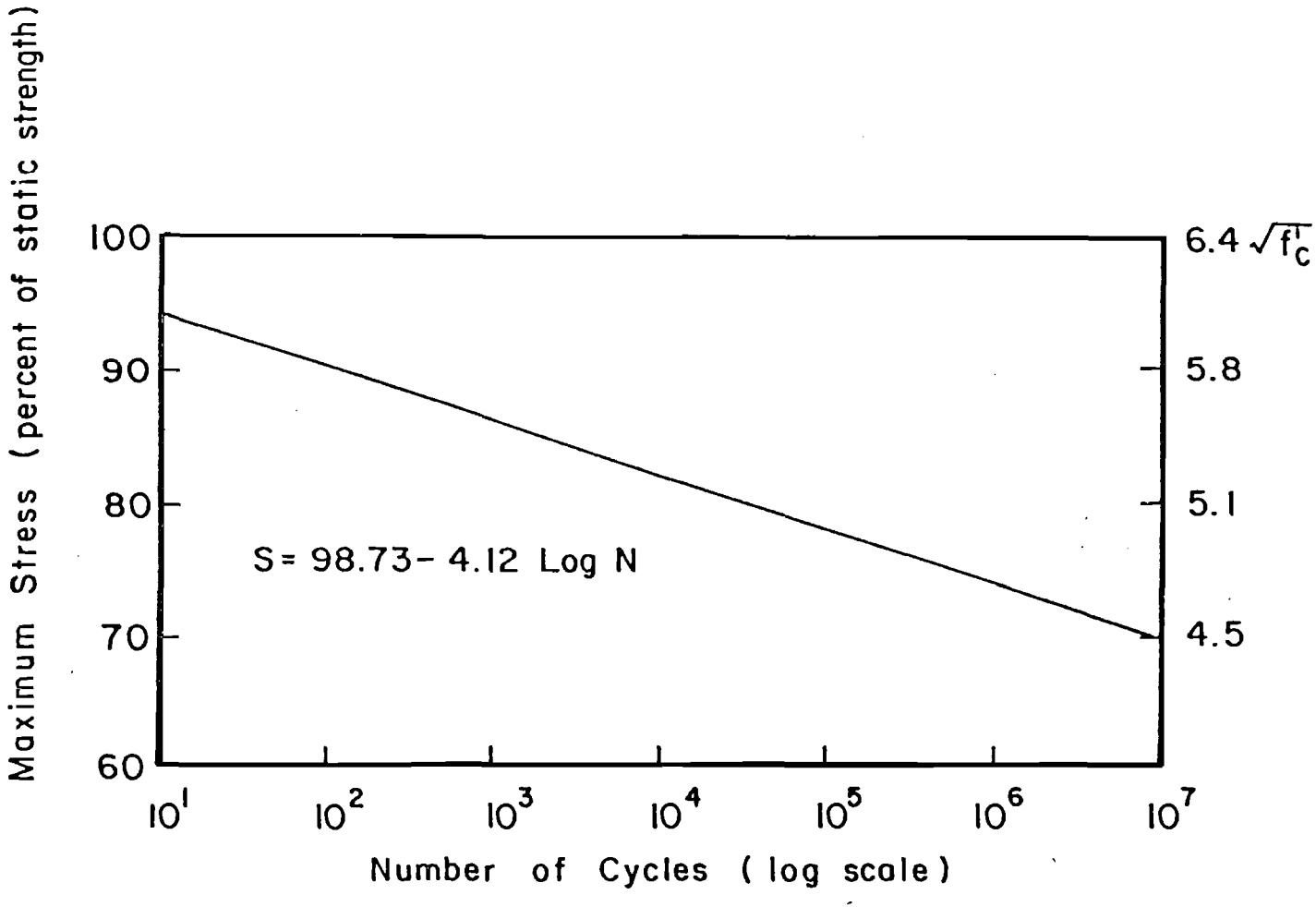

Fig. 2.3 Saito's S/N relationship for concrete in tension

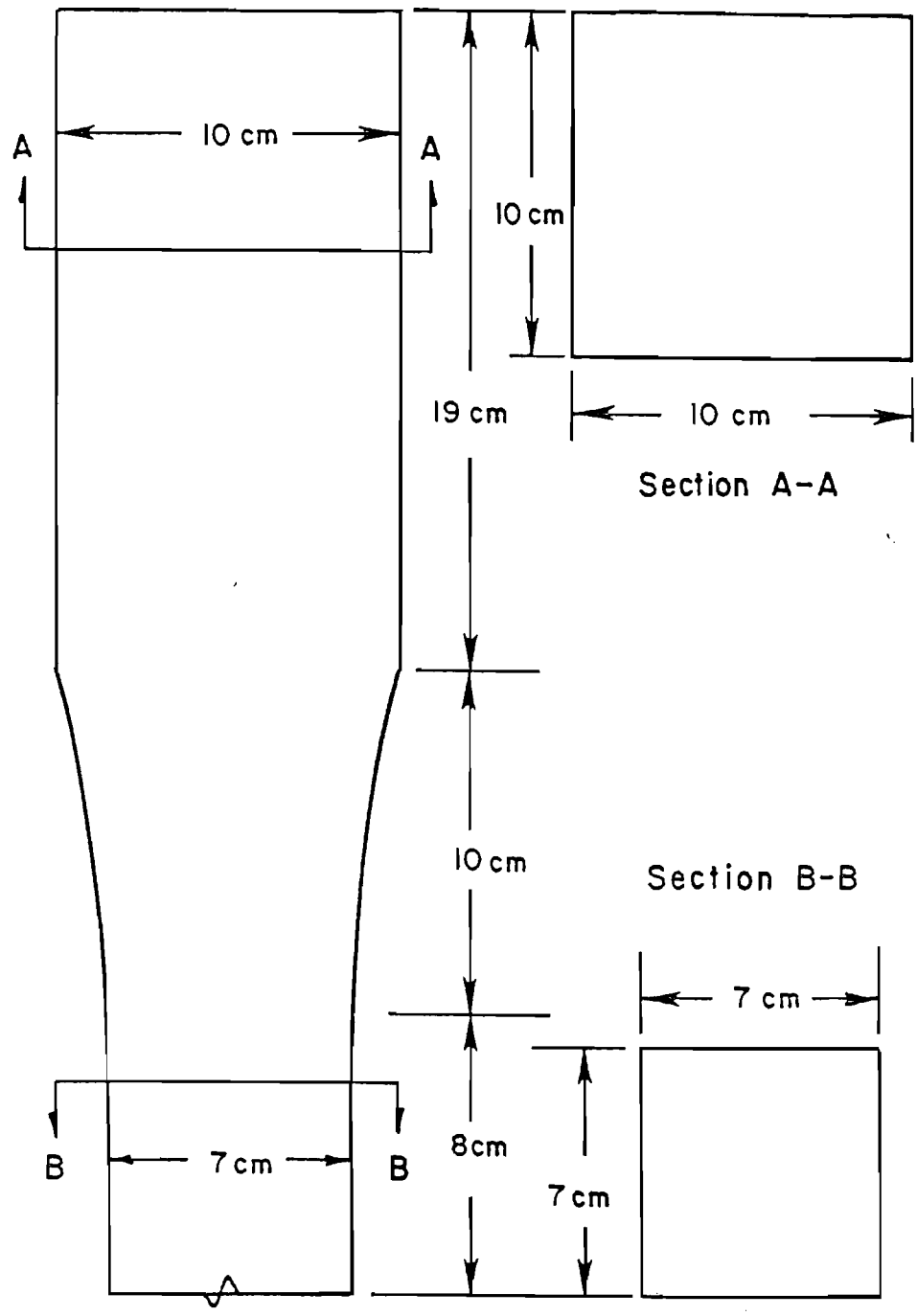

Fig. 2.4 Top half of Saito and Imai specimen

percent of the static tensile strength (f_t), which was approximately 480 psi. The compression strength was approximately 5600 psi. All compressive strength and tension test specimens were tested between eight and nine weeks after casting. A residual strain equal to the elastic strain was reported for a stress of 0.75 f_t.

ACI Committee 215 [19] reports that the fatigue strength of concrete for a life of 10 million cycles is roughly 55 percent of the static strength. The probability of failure is 5 percent. The ratio S_{min} (minimum stress)/S_{max} (maximum stress) was 0.15 for the test. For a probability of failure of 50 percent, the strength is approximately 60 percent of the static strength. If the Saito data can be extrapolated to N = 10 million cycles, the maximum stress would be 70 percent f_t. With a minimum stress of 8 percent f_t, S_{min}/S_{max} = 0.11. The probability of failure is 50 percent. The differences are probably due to the extrapolation of data, loading rate, and the difference in specimen geometry. The ACI Committee 215 limit of 55 percent is also applicable to concrete in compression or flexure. Both sources indicate that there is no fatigue limit for concrete in tension. However, the 10 million cycle limit should be a reasonable bound for almost all bridge applications.

Murdock and Kesler [58], reporting on their research as well as research by Clemmer, Hatt, and Creps, use the modified Goodman diagram shown in Fig. 2.5. For a flexural specimen tested with a minimum stress of zero, it would be expected to last 10 million cycles at a tensile stress of approximately 60 percent of the modulus of rupture. For a flexural specimen tested with complete stress reversals (the applied loads produce alternate tension and compression stresses that are equal), it can be expected to have a fatigue strength of 56 percent of the static flexural strength at 10 million cycles. This is the limit used in the ACI Committee 215 [19] report for tension, compression, and flexural specimens. As the minimum tensile stress increases above zero, the fatigue strength at 10 million cycles increases, but the stress range decreases due to the difference in slopes of the two lines.

2.2.1.3 Concrete in Flexure

The fatigue strength of concrete specimens with a strain gradient has been stated to be either slightly better or approximately the same as pure tension or compression fatigue specimens, depending on the type of loading. Ople and Hulsbos [63] reported an increase in fatigue life for column specimens tested with a strain gradient over pure compression specimens. The fatigue strength of specimens with a lin. load eccentricity (the maximum extreme fiber stress was from 0.85 f'_c to 0.95 f'_c; the minimum extreme fiber stress when the specimen was loaded was 0.0 f'_c; the unloaded extreme fiber stresses were 0.1 f'_c and 0.0 f'_c) was 15 to 18 percent above the fatigue strength of axially

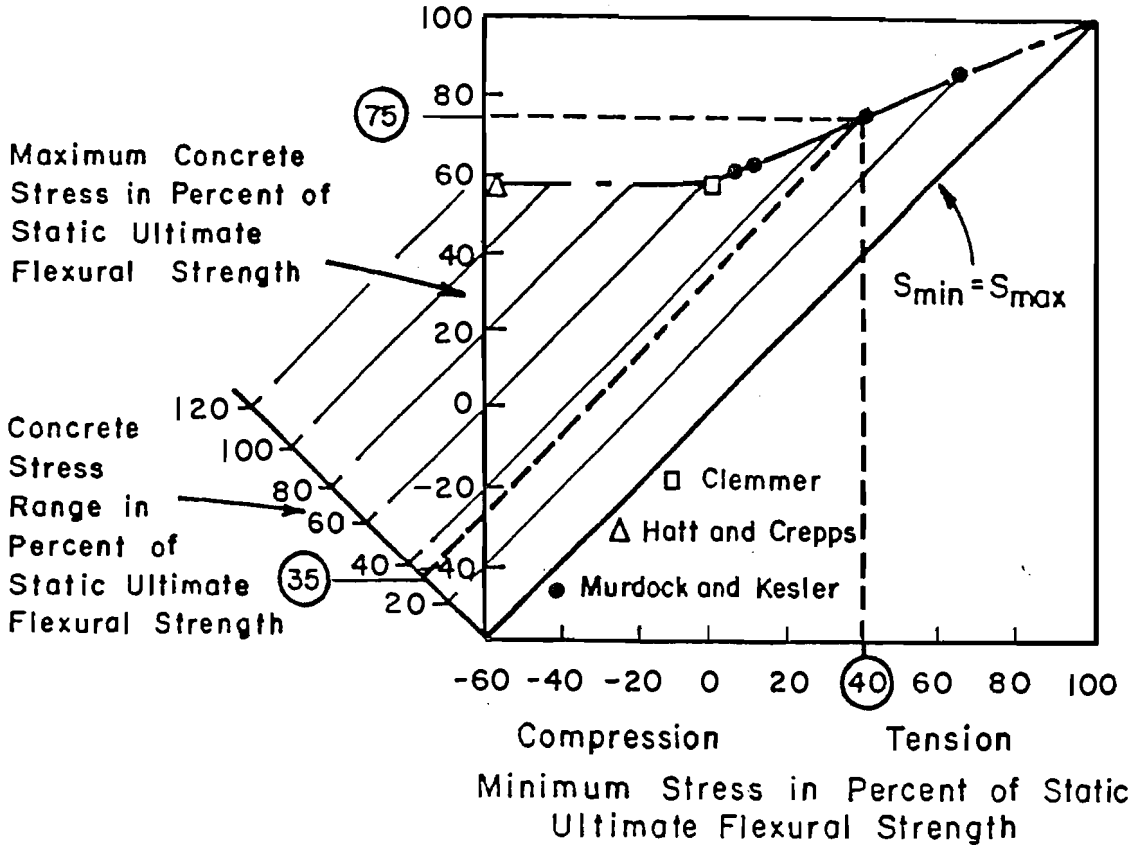

Use of the Modified Goodman Diagram

1. Determine the minimum stress and locate this value on the horizontal axis. Example: A minimum stress of 40 percent of the static ultimate flexural strength.

2. To find the maximum allowable tensile stress for a fatigue life of 10 million cycles, proceed vertically to the dashed line; read horizontally from this point to the vertical axis. Example: A maximum stress of 75 percent of the static ultimate flexural strength.

3. To find the corresponding concrete stress range move diagonally from the maximum stress point to the stress range axis. Example: A concrete stress range of 35 percent of the static ultimate flexural strength.

Fig. 2.5 Flexural fatigue strength at 10 million cycles

loaded (no stress gradient) specimens for a range of fatigue life of 40,000 to 1,000,000 cycles.

2.2.1.4 Bond Between Concrete and Steel

The bond characteristics of seven-wire strand and reinforcing bar greatly influence the fatigue life of prestressed and reinforced members. Abeles [15] states:

> It may be expected that with excellent bond the conditions in prestressed concrete beams are better than with the steel tested in the air, whereas with very bad bond the conditions are considerably worse because of mechanical influences, including friction between concrete and steel which occur in wide cracks when in addition to direct tension, additional stresses occur due to the steel curvature, i.e., bending occurs as [a] consequence of the great deformation in the beams in the state of high loading.
>
> ... The early occurrence of the bond break may reduce the fatigue life of a prestressed concrete beam to only 40% of that which it would have if bond break did not occur.

Bond deterioration occurs where steel strain exceeds concrete strain. This difference in strain exists at the ends of a member and at cracks. High steel strains at cracks destroy bond between concrete and steel at locations adjacent to these cracks. This distance of debonding is called the debond length. If the debond length at the ends of a member, due to shear or flexural cracks, overlap the transfer region, gross slippage will occur. At isolated cracks the slippage is less drastic. Lin [53] states that at flexural cracks, "the bond stress in the vicinity of the crack rises, and slip occurs over a small portion of the strand adjacent to the crack". Under fatigue loads which are at a level which produce significant tensile stresses in the concrete, flexural cracks are opened repeatedly. This causes a gradual increase in debond length and slip. Rabbat et al. [76] reported that twice the bond development length was required to prevent bond failure when cycling into the tensile range. Abeles [15] reported that varying ranges of loads intensify bond deterioration.

Debonding is characterized by forked cracks [15,24,47]. Figure 2.6 shows several typical forked flexural cracks. Extensive cracking occurs in specimens with unbonded tendons because there is no force normal to cracks to control crack propagation. With bonded construction, the reinforcing or prestressing steel arrests cracks; as debonding occurs, cracks fork similar to unbonded specimens.

Debonding can increase steel strains at a crack to values greater than those predicted by a cracked section analysis. Frantz and Breen [38], in a study to determine the effects of reinforcing

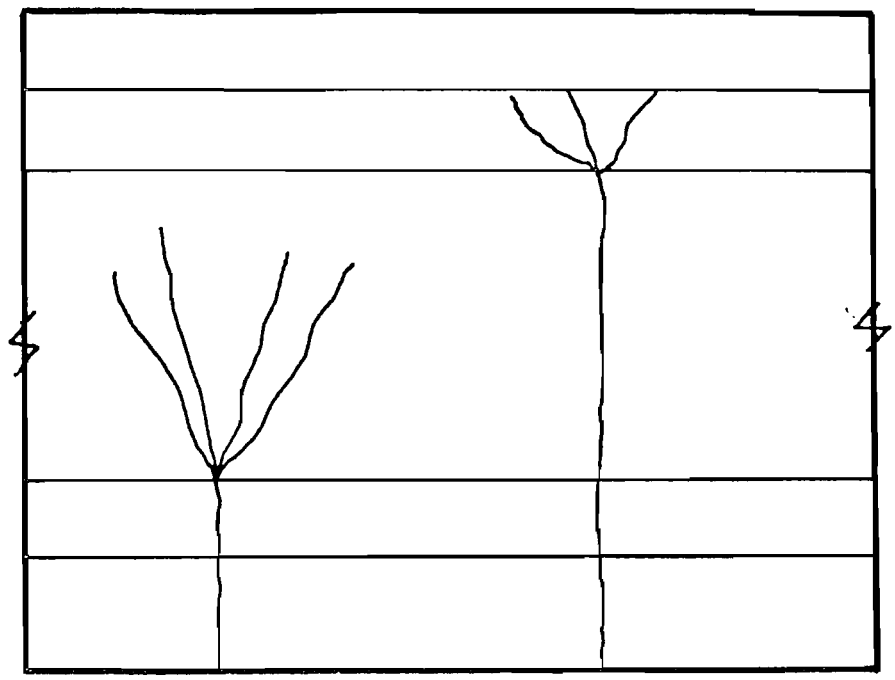

Fig. 2.6 Forking of flexural cracks due to debonding

distribution on cracking, reported local measured stresses at cracks 39 to 54 percent higher than those predicted by a cracked section analysis. Frantz points out that this is probably a low estimate of actual stresses since "... none of the gages lie directly across a crack. The stresses in the bars at a crack are probably higher....". Transfer of strain energy at a crack from concrete to steel could be the cause of this increase in steel stress. The degree of increase in stress is a function of the degree of debonding. The shorter the debond length, the higher the steel stress.

Debonding reportedly increases auxiliary passive reinforcement stresses for partially prestressed members. Gerwick and Venuti [39] report:

> When concrete is cracked and then cycled repeatedly into the "crack-reopening" tensile range, the steel is subjected to significantly increased stress ranges. Bond progressively is lost along the steel, particularly along smooth bars, strand, and wire.... Due to slippage of the prestressing steel, the conventional unstressed steel usually is subjected to a slightly higher stress range. As stiffness decreases and creep increases, the steel is subjected to ever greater stress ranges. These increase significantly after cracking and as failure approaches.

Bond characteristics appear random within a single specimen. A difference in bond at a flexural crack can cause one strand or reinforcing bar to be stressed more than an adjacent one. The element with the shortest bond length would have the highest stress. The varying load ranges, which increase steel stress as the specimen deteriorates due to different unbonded length, complicate the analysis.

2.2.2 Steel

The mechanism of fatigue failure of steels includes microcracks, or existing flaws, that propagate. There is generally little plastic deformation on the macroscopic scale before brittle failure. High strength steels, such as prestressing strand, have a low crack resistance (fracture toughness) compared to normal strength steels [30]. Higher strength materials permit the use of smaller sections and allow higher stresses. A small flaw in high strength materials, that produces large stress increases, due to stress concentrations at the crack tip and a slight decrease in section, can result in brittle fracture.

2.2.2.1 Prestressing Strand

Paulson [73] reported on over 700 prestressing wire and strand fatigue specimens in his literature review. In addition, he generated

over 60 new data points in the first phase of this project. His multivariate regression analysis for all valid data points produced the following equation:

$$\text{Log } N = 11.0 - 3.5 \text{ Log } S_r \qquad \text{(A-1L)}$$

where: N is the fatigue life in number of cycles

S_r is the stress range; maximum stress-minimum stress

He states that:

> For the purposes of design, lower limit regression model A-1L would be the most appropriate to use. Although it was previously stated that minimum stress was significant, it is desirable that design equations be kept straightforward. Also, design guides should be properly conservative. Modified regression model A-1L best fits these requirements.

The equation is for a conservative, one-sided tolerance limit where there is a 95 percent probability that at least 97.5 percent of the distribution will be above the limit. An endurance limit of 20 ksi is suggested, but not verified by Paulson's data.

A regression analysis based on fatigue tests of strand from the same spool as that used in all Texas Type C specimens in this study (excluding all failures in the prestressing chuck grips) indicated:

$$\text{Log } N = 13.51 - 4.16 \text{ Log } S_r - 0.446 \text{ Log } S_{min}$$

Excluding the minimum stress term, S_{min}, the suggested relationship is:

$$\text{Log } N = 12.67 - 4.23 \text{ Log } S_r$$

Paulson stated several limitations to these equations. One involved the test specimen length. All data was for lengths from 35 to 54 in. Statistically, the fatigue life should decrease as the specimen length increases; that is, a longer specimen has more possibility of flaws along its length than a shorter specimen. Canteli et al. [31] confirmed this length effect. They found a 7.1 percent reduction in the endurance limit with a 250 percent increase in specimen length. Considering that the girder specimens tested in the flexural series had constant moment regions of 16 and 24 ft, with 14 to 22 strands, this length effect could be very significant. A second limitation was that the minimum stress range included in Paulson's analysis was 22 ksi. There were only six recorded strand fatigue failures at stress ranges less than 30 ksi. Since most beam tests produced strand stress ranges less than 30 ksi, the "in-air"data had to be extrapolated. The endurance limit of 20 ksi was extrapolated from the very limited data

and is quite questionable. The third limitation involves the use of the equation with cracked girder sections. Paulson [73] states that:

> ... the designer must be cautioned that these recommendations do not apply to cracked sections. Any investigation of fatigue in a prestressed component has to include determining whether or not the section cracks. Only if the section remains uncracked can the above recommendations be applied.

This disclaimer was included because very few full-scale beam tests had been performed. As a result, the "in-air" data could not be compared to beam results with confidence. One of the purposes of the full-scale beam fatigue tests reported herein was to compare beam results with Paulson's model.

2.2.2.2 Reinforcing Steel

Tests by Hanson, Somes, and Helagson [42] indicate that reinforcing steel has an endurance limit of approximately 20 ksi. The study included 236 reinforcing bar specimens embedded in concrete. The report states that "test specimens simulated conditions found in bridge deck slabs and girders, and in other structures subjected to high amplitude repeated loading." Five bar sizes were tested, Nos. 5, 6, 8, 10, and 11. Minimum levels of 6 ksi compression, 6 ksi tension, and 18 ksi tension were investigated. Grade 40, 60, and 75 bars were tested. The primary emphasis was on Grade 60 reinforcement. Figure 2.7 shows the tolerance limits obtained from the test data.

ACI Committee 215 [19] included twenty-two studies, including the one by Hanson et al., in its report on fatigue. Numerous stress range, fatigue life, and S_r-N curves resulted from these studies. Figure 2.8 shows this data graphically. Important variables, in addition to stress range, were minimum stress, bar size and type of specimen, geometry of deformations, yield and tensile strength, bending, and welding. Analysis of the available literature resulted in the following recommendation:

> The stress range in straight deformed reinforcement that may be imposed on minimum stress levels up to 40 percent of the yield strength shall not exceed 20,000 psi (1406 kgf/cm^2) or one-half of that amount in bent bars or bars to which auxiliary reinforcement has been tack welded.

2.3 Fatigue of Prestressed Concrete Members

The fatigue life of cracked prestressed concrete members is primarily a function of strand cyclic stress range. Once a flexural specimen cracks, prestressing strand and reinforcing bars, if present,

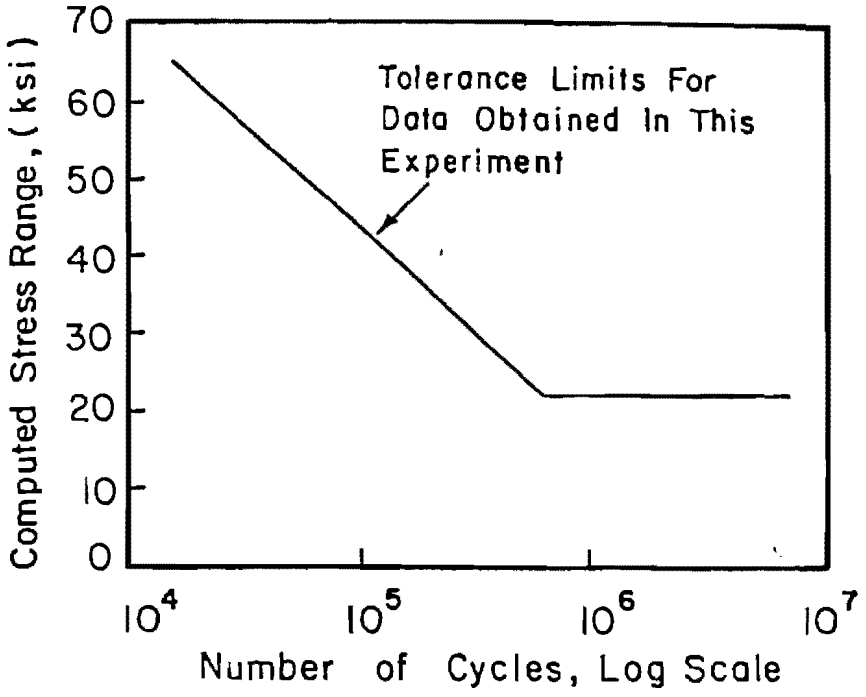

Fig. 2.7 Reinforcing bar tolerance limit obtained by Hanson et al.

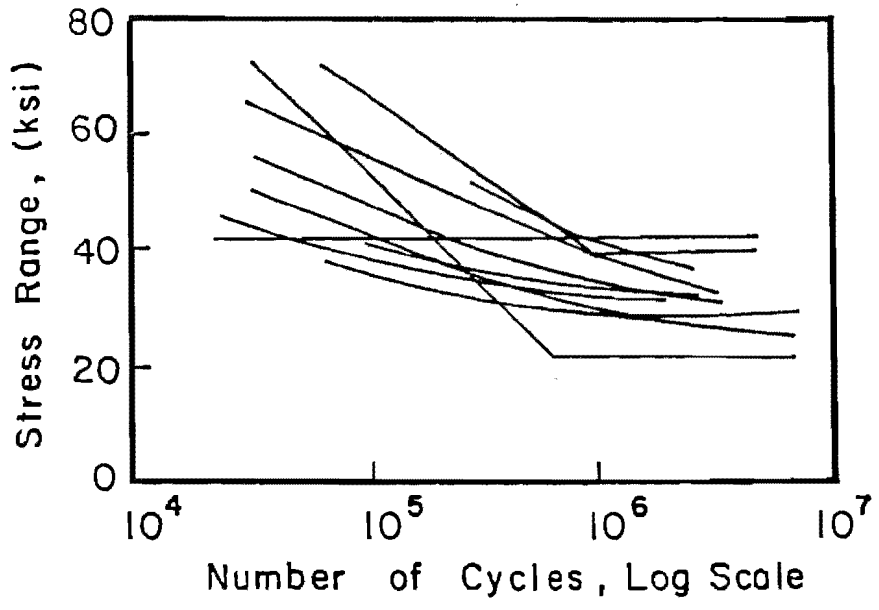

Fig. 2.8 Reinforcing bar S/N results reported in ACI Committee 215 report

provide the internal tension force. Failure is by progressive fatigue fracture of individual wires within a prestressing strand. Naaman [60] points out that there are signs of fatigue deterioration:

> In a cracked concrete member, whether reinforced, prestressed or partially prestressed, crack widths and deflections keep increasing from their first cycle static values with the number of loading cycles. The increase is mostly attributed to the cyclic creep of concrete and bond deterioration accompanied by slip between the reinforcement and concrete on either side of existing cracks.

Seventeen flexural fatigue test programs are described in this section. Strand stress ranges or adequate information to calculate stress ranges was reported in only six test reports. This information is summarized in Table 2.1.

2.3.1 1954: Abeles

The Abeles study [12] involved static and fatigue testing of partially prestressed railway slabs and beams. Fatigue stress ranges were not included for the prestressed or unstressed wires used in the assemblies. Abeles reported permanent deflections or set, stating: "It is seen that set gradually increased with an increase in the number of repetitions, but considerable recovery took place during the weekend when the specimen was allowed to rest."

2.3.2 1956: Ozell and Ardaman

Ozell and Ardaman reported [65] on eight static and fatigue tests. Results for the five fatigue tests in which failure resulted are shown in Table 2.1. Failure was defined as a 30 percent loss in the flexural spring constant (the design load divided by the corresponding center deflection). Fatigue testing was continued after this 30 percent loss for zero to 40,000 cycles (zero to 9 percent of the failure cycles). The specimens tested are shown in Fig. 2.9(a).

Information on permanent set was reported. Figure 2.10 shows the permanent set at various stages of loading for the seven fatigue specimens. Ozell and Ardaman [65] stated that:

> Beam specimens stressed beyond the cracking load showed slight change in their load-deflection characteristics and underwent a small amount of permanent set (0.10 to 0.18 in., depending on the test load) during the first 30,000 cycles. However, the continued repetitions of loading caused considerable change at greater number of cycles.

TABLE 2.1 Constant Stress Range Beam Test Results

Researchers (Year of Report)	Specimen	Stress Range (ksi)	Fatigue Life
Ozell and Ardaman (1956)	L-2	41.0	460,000
	M-1	60.0	280,000
	M-2	47.0	325,000
	M-3	18.0	940,000
	M-4	80.0	126,000
Nordby and Venuti (1957)	6A	23.9	136,000
	6B	23.9	186,000
	S6	29.4	842,000
Ozell and Diniz (1958)	S-2	49.0	780,000
	S-3	76.0	186,000[a]
	S-4	68.0	514,000
	S-5	43.5	870,000
	S-6	32.5	2,273,000
Warner and Hulsbos (1962)	F1	44.5	139,000
	F2	43.5	164,000
	F4	43.3	225,000
Ozell (1962)	I2	15.3[b]	2,500,000
	I3	28.3[b]	1,500,000
	I4	24.4[b]	760,000
	I5	25.0[b]	640,000
	I6	30.5[b]	210,000
Abeles, Brown and Hu (1974)	A3	58.3	114,800
	A5	89.9	24,200
	A6	94.2	21,300
	A7	114.5	11,500
	B1	13.0	2,517,500
	B3	79.7	57,700
	B4	54.3	168,300
	B5	84.0	48,300
	B6	58.1	144,000
	C1[c]	62.2	161,800
	C3[c]	60.8	165,300
	C4[c]	46.4	387,400

TABLE 2.1 Constant Stress Range Beam Test Results (continued)

Researchers (Year of Report)	Specimen	Stress Range (ksi)	Fatigue Life
Abeles, Brown and Hu (1974)	D4	53.7	207,500
	D5	86.7	53,800
	D6	89.1	41,400
	D7	51.3	223,800
	E1[c]	46.2	307,600
	E2[c]	27.5	2,048,000
	E3[c]	27.3	756,000
	E4[c]	42.4	285,700
	E5[c]	28.9	956,000
	F2	132.3	16,100
	F4	132.8	17,700
Rabbat et al. (1978)	G10	19.5[d]	3,630,000
	G11	18.2[d]	3,780,000
	G13	20.1[d]	3,200,000

[a] Bond failure
[b] Calculated using PBEAM
[c] Partially prestressed with nontensioned strands
[d] Static cycle stress range at 2.5 million cycles

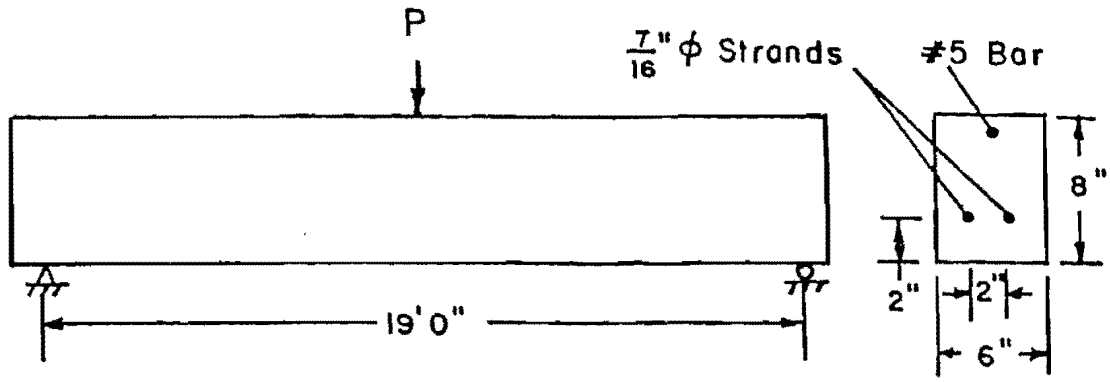

a) Ozell and Ardaman (1956)

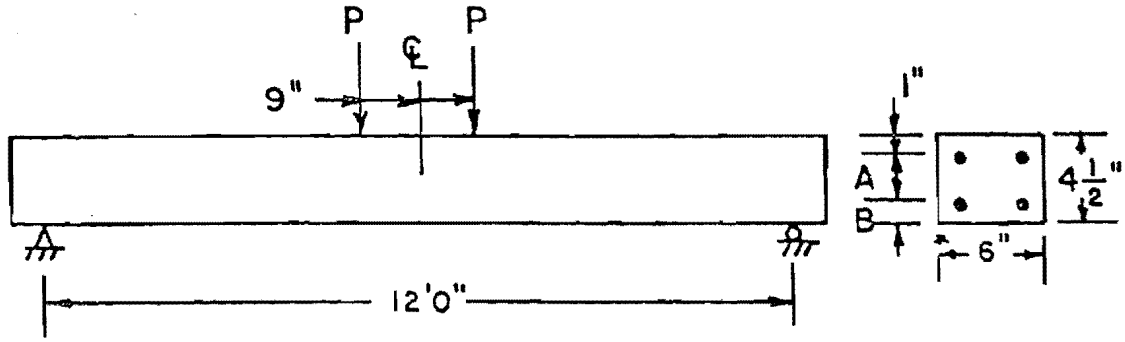

	Specimens 6A & 6B	Specimen S6
A	$2\frac{1}{4}$"	$2\frac{1}{2}$"
B	$1\frac{1}{4}$"	1"

b) Nordby and Venuti (1957)

Fig. 2.9 Beam fatigue test specimens

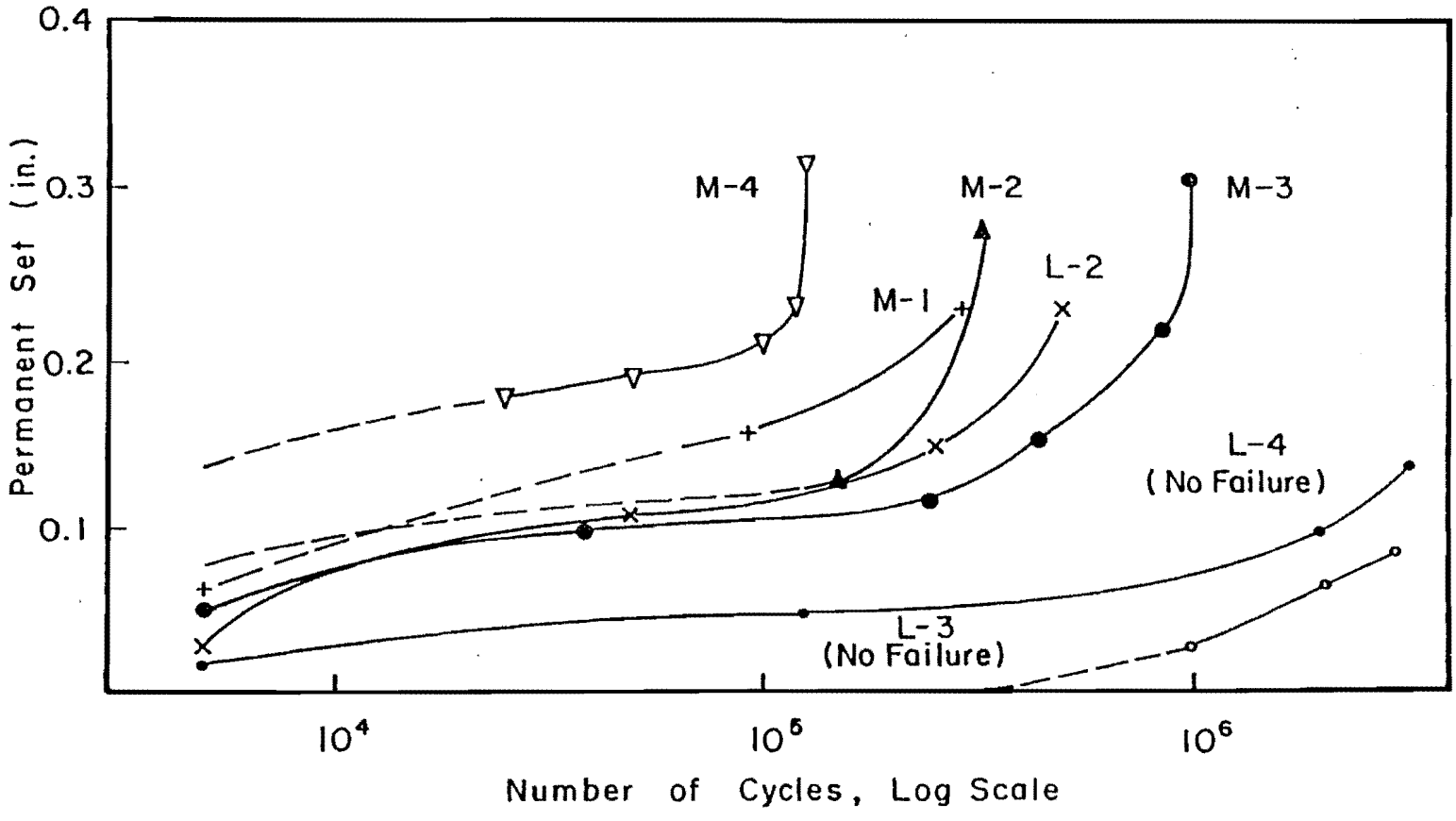

Fig. 2.10 Permanent set for Ozell and Ardaman test specimens

Ozell and Ardaman found fatigue breaks only at crack locations and evidence of bond failure in one specimen. The authors state that:

> The fracture of the wires at points bordering the tension cracks in the beam substantiates the belief that these cracks form stress concentrations in the strands, especially as a result of overloads, rendering them vulnerable to fatigue and ultimately causing the breaking of the wires.

Bond failure, indicated by smooth wires 1.5 in. from the point of fracture, was reported in specimen M-1.

2.3.3 1957: Nordby and Venuti

Nordby and Venuti [62] performed 24 static and fatigue tests on beams of expanded shale and conventional concrete. Two conventional concrete specimens and one expanded shale concrete specimen had prestressing steel fatigue fractures. The results of these tests are shown in Table 2.1. Notice that specimens 6A and 6B (constructed of conventional concrete) withstood fewer cycles at a lower stress range than specimen S6 which was constructed of expanded shale concrete. The cross section and loading configuration for these three beams is shown in Fig. 2.9(b).

Nordby and Venuti reported fatigue breaks at flexural crack as well as bond failures. Bond failures generally occurred (six out of nine specimens) in specimens with 36 in. shear spans. Analysis of fatigued specimens revealed that:

> The three fatigue failures occurred when the beams were severely cracked during the repetitive loading; this failure was a result of stress concentrations and abrasion between the strands and the concrete.

Nordby's and Venuti's conclusions state that:

> Cracks should not be allowed in beams in which repeated overloads occur, since those fatigue failures that did occur appeared to be directly related to cracking. Slip also seemed to be dependent upon cracking to a great extent....

The authors reported that there was no significant loss of prestress in any of the fatigue specimens.

2.3.4 1958: Ozell and Diniz

Ozell and Diniz [66,67] reported on two fatigue test programs in 1958. The first involved four composite beams while the second involved testing of six specimens of the type shown in Fig. 2.11(a).

One beam failed due to fatigue of the prestressing strands in the first test series. This specimen was loaded to a maximum nominal (uncracked section) concrete stress of 367 psi ($7.1\sqrt{f'_{ct}}$) for 580,000 fatigue cycles. The remaining three beams were loaded to maximum uncracked section nominal concrete tensile stresses of 247 psi, 572 psi, and 667 psi, which is 3.1, 7.2, and 8.4 times the square root of 6350 psi (the average concrete compressive strength at the time of testing). Fatigue lives were 452,000, 860,000, and 865,000 cycles, respectively. Permanent sets at various stages of loading for two specimens are shown in Fig. 2.12. No strand stress range information was provided.

Five specimens failed due to fatigue in the second test series. The strand stress ranges and number of cycles to failure are shown in Table 2.1. Strand fractures were found in four of the specimens while the fifth, S-3, experienced bond failure between the two extreme flexural cracks. All specimens were cracked during the initial static tests.

Permanent set measurements were similar to those reported in previous tests. The "set" increases gradually during a large portion of fatigue cycling. Towards the end of testing, the increase is more pronounced. Permanent sets from 0.140 to 0.308 in. were reported.

Ozell and Diniz attributed early strand fatigue failure to cracking. They state that "the cracks in the concrete act as stress raisers and the consequent stress concentrations in the strands contributed to the fatigue failure of the wires at those points."

2.3.5 1962: Warner and Hulsbos

Warner and Hulsbos [91] tested six prestressed concrete beams, like the one shown in Fig. 2.11(b), to compare actual fatigue lives to the one predicted by a model. The model was based on fatigue tests of prestressing strand tested in-air, not encased with concrete. Three of the specimens had a constant load range while the remaining three had varying load ranges. The specimens tested under varying loads will not be described here because of the problem of determining the cumulative damage from different load ranges. Stress ranges and fatigue lives are shown in Table 2.1.

Warner and Hulsbos [91] described the statistical problems with determining the fatigue life and did not describe the behavior of the

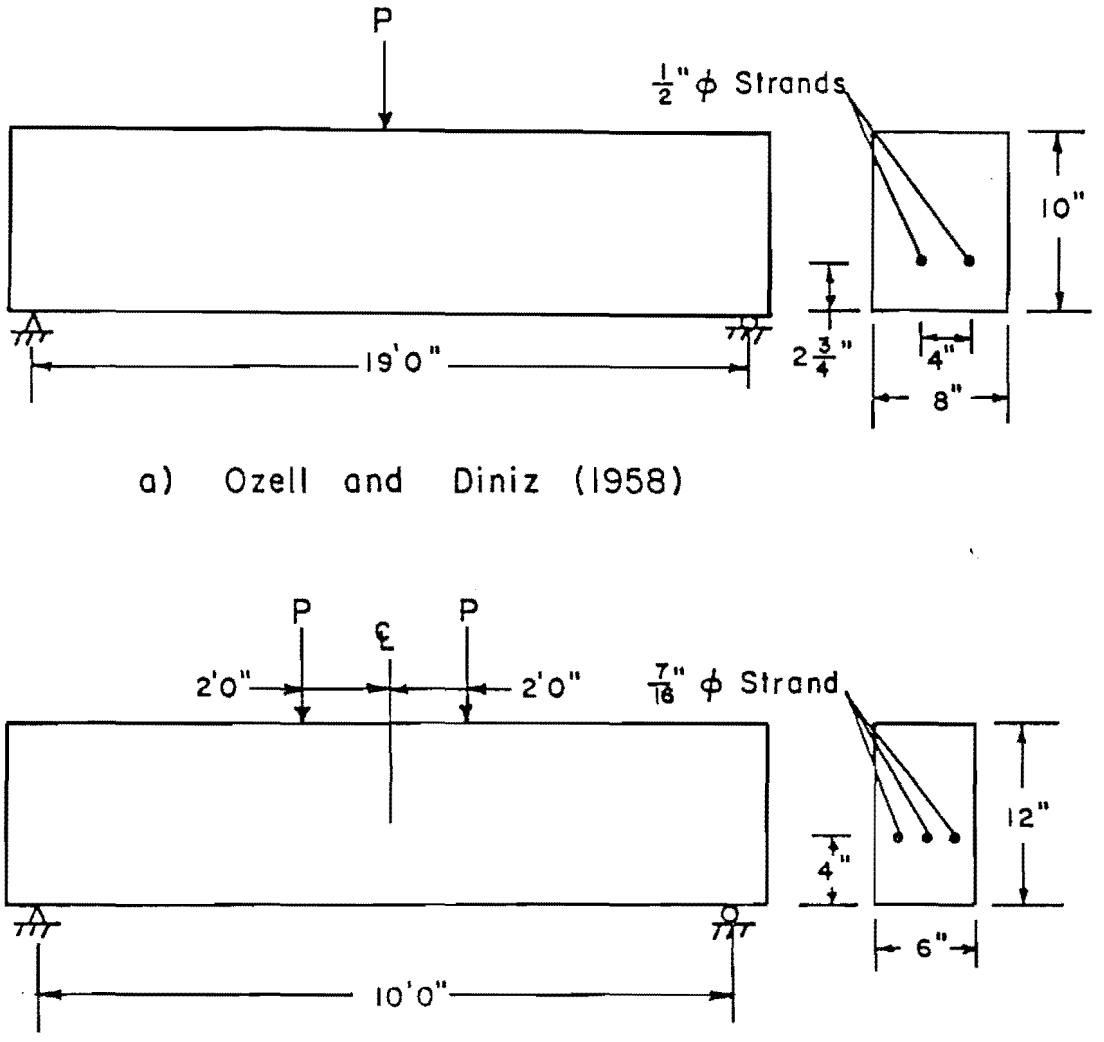

Fig. 2.11 Beam fatigue test specimens

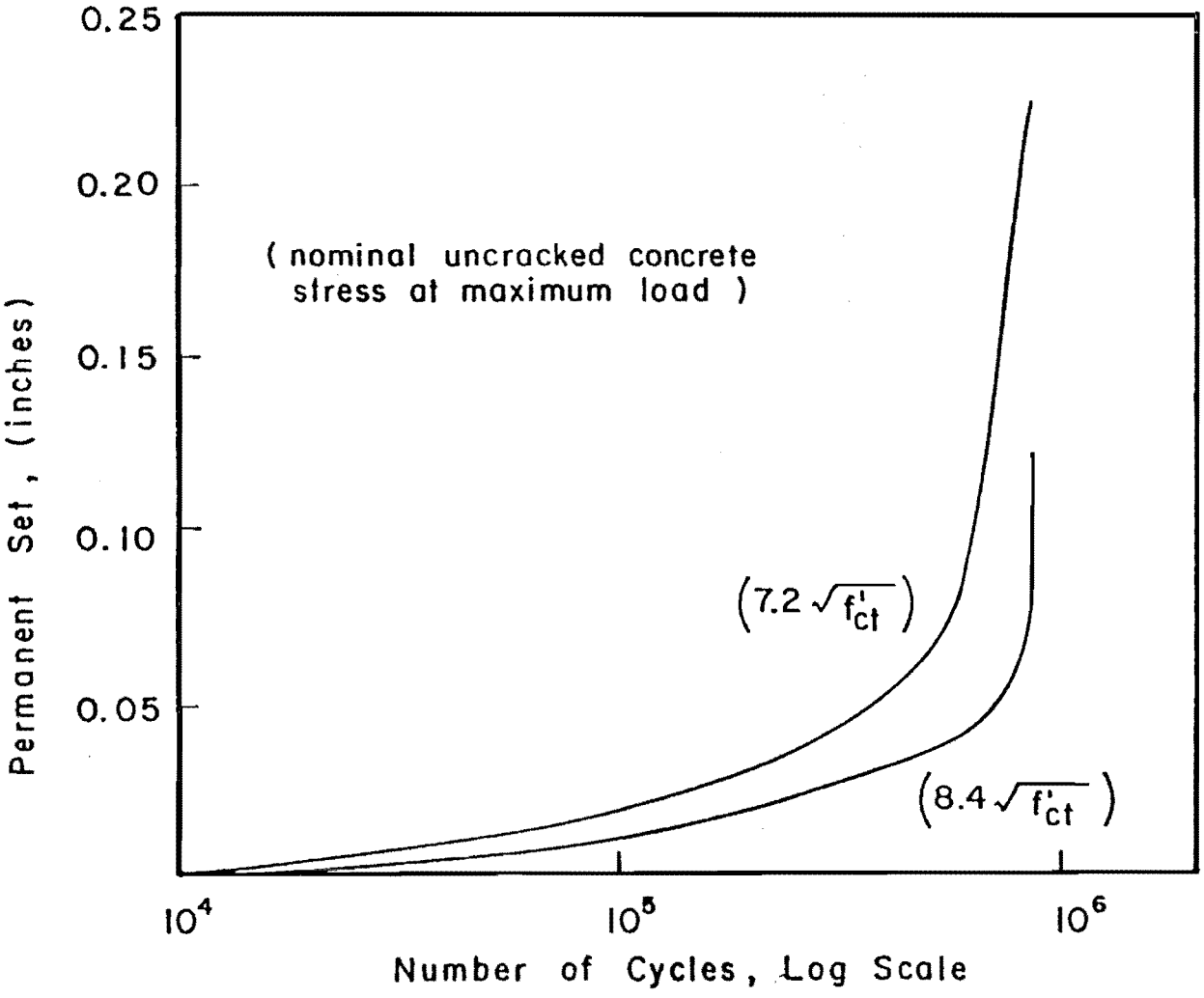

Fig. 2.12 Permanent set for Ozell and Diniz test specimens

specimens. Problems with determination of the maximum stress range are addressed in the following statement:

> ... an examination of the deformations measured in the test beams indicates that steel stress varies greatly along the length of the beam, even in regions of constant moment, and in fact will attain a maximum value only at the widest crack.

The strand stress range does not only vary along the member, it also varies as a beam deteriorates during cyclic loading. The authors [91] discuss this problem in their conclusions, stating that:

> The response of a prestressed concrete beam may be expected to vary considerably as a result of the application of fatigue loading. This variation is probably due to creep effects, changes in the concrete stress-strain relation, and progressive bond failure between the tension steel and surrounding concrete in the vicinity of the tension cracks.

Strand stress ranges vary along a beam as well as during cyclic testing. Warner and Hulsbos [91] made the following note concerning the scatter encountered in beam fatigue results: "... variability in predicted beam fatigue life is likely to be much greater even than indicated by the variability in the strand fatigue data."

2.3.6 1962: Ozell

Ozell [64] tested six prestressed concrete I-beams without slabs. Five of the specimens failed due to fatigue loading. Fatigue lives and calculated strand stress ranges are shown in Table 2.1. The main purpose of the test program was to determine if the bend in draped strands decreased a beam's fatigue life. This was the first test of large prestressed concrete I-beams. The test specimen is shown in Fig. 2.13.

The applied load caused maximum nominal bottom flange tensile stresses of between 740 and 1100 psi (8.7 to 13.0$\sqrt{7200}$; 7200 psi was the concrete compressive strength at the time of testing) for the five specimens that failed due to fatigue loading. The concrete stress was termed "nominal" because all specimens cracked during the initial loading, so the concrete tensile stress was actually zero. The beams were never loaded above the maximum cyclic load value [64].

Permanent set data were recorded. Figure 2.14 shows the permanent set at various phases of loading. The problem with determining actual permanent set is addressed in the following statement:

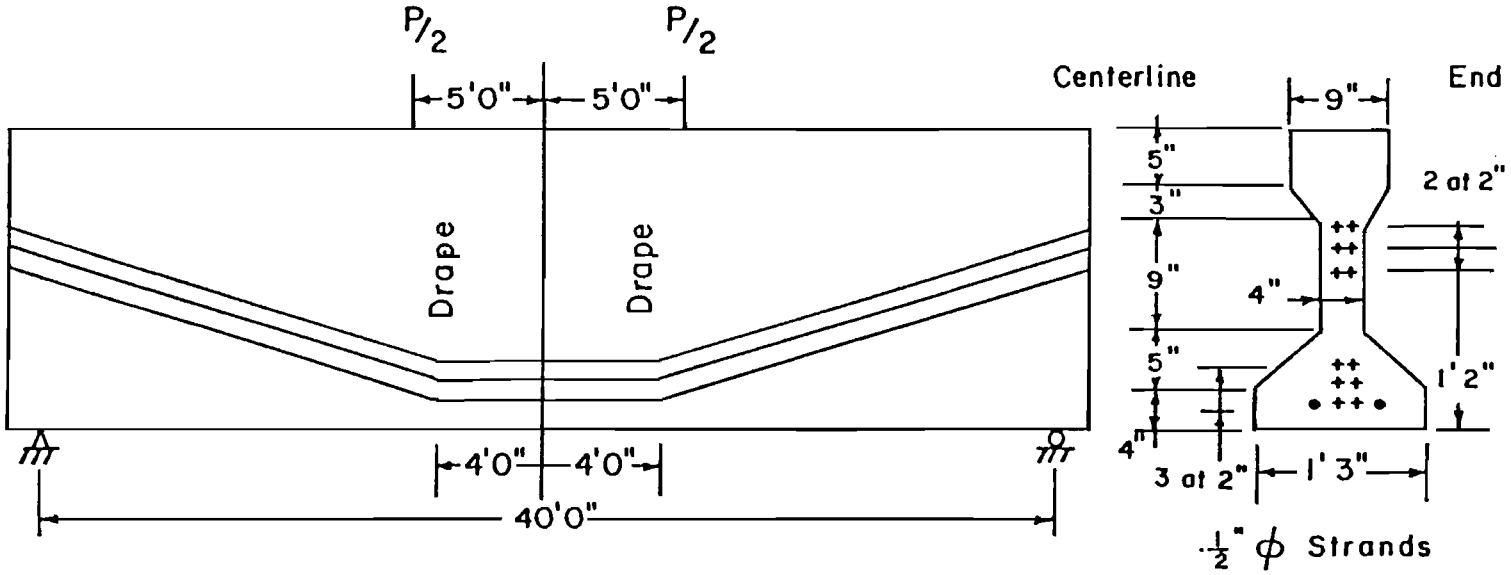

a) Ozell (1962)

Fig. 2.13 Beam fatigue specimen, Ozell (1962)

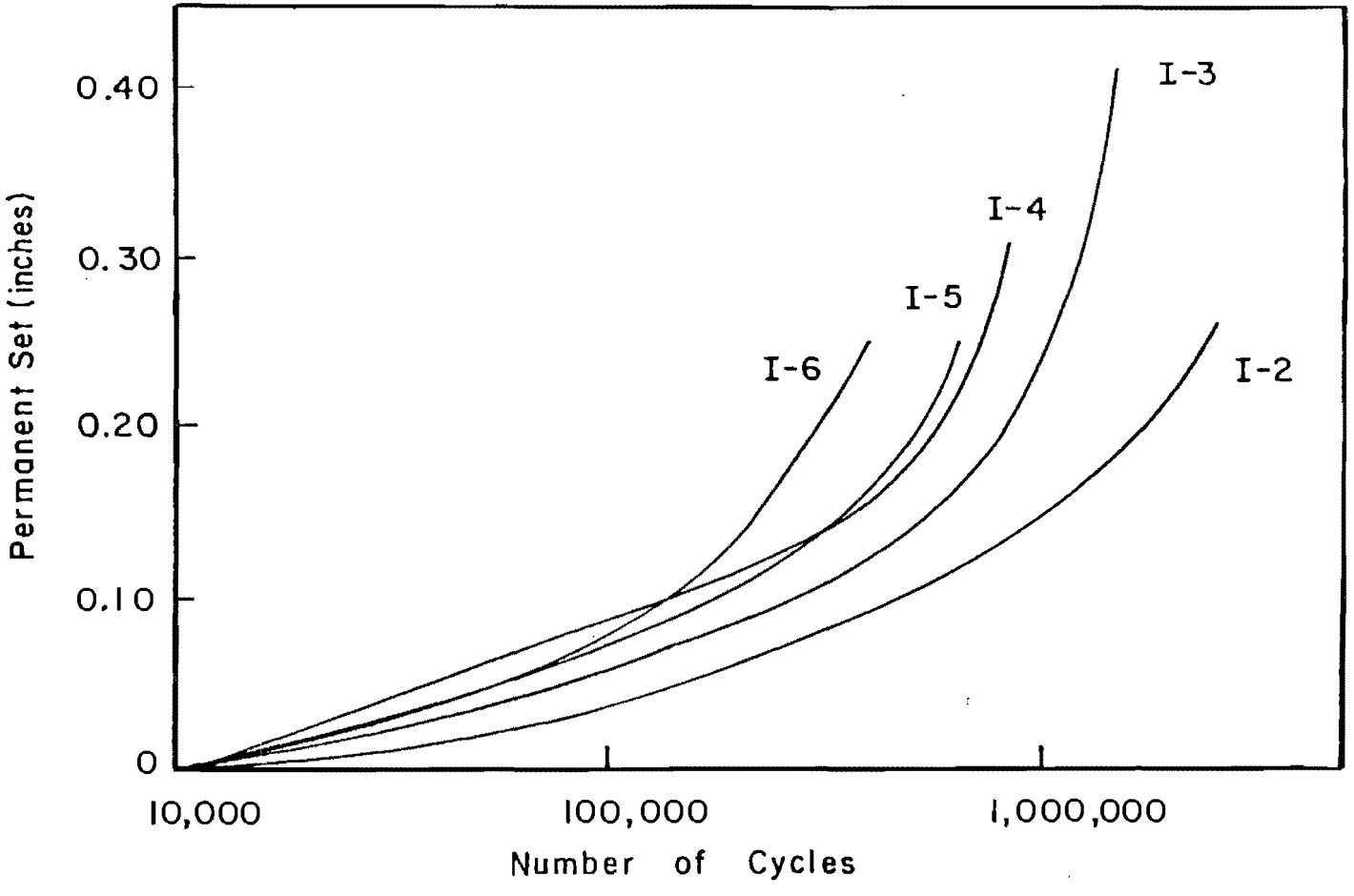

Fig. 2.14 Permanent set for Ozell test specimens

> A further complication was met in establishing the permanent set. Beams start to camber (hysteresis) immediately following the stopping of the cyclic load application. This behavior, which occurs in a few minutes, makes it difficult to obtain consistent results since the rate and amount of recovery are affected by the magnitude of load and extent of damage to the beam.

Ozell concluded that strand failures occur at flexural cracks and that draping did not reduce the fatigue life of a specimen [64].

2.3.7 1962: Bate

Bate [28] performed four beam fatigue tests on specimens with 0.3 in. diameter seven-wire strands. The purpose of this test series was to compare the results with those obtained from a previous test on specimens with 0.2 in. diameter prestressing wire. Of the four specimens tested only one failed due to fatigue of prestressing strands. The remaining three were tested to determine ultimate capacity after 3.0 million fatigue cycles. No strand fatigue fractures were found in these three specimens. The fatigued specimen withstood 2.71 million cycles at a maximum stress range of 23 ksi. Few details concerning fatigue behavior are presented in Bate's [28] paper, but he does indicate that there were no signs of strand fretting.

2.3.8 1965: Hanson and Hulsbos

Hanson and Hulsbos [40] fatigue tested two 1'6" deep model prestressed I-beams without slabs to determine the effect inclined cracks have on fatigue life. One specimen withstood 2.0 million cycles, at which time fatigue fracture occurred in one stirrup. The load range was constant. The other specimen failed due to fatigue fracture of one wire after 4.5 million cycles. The load range in this case was not constant. The variable load range in the second specimen, and the shear failure in the first, make these specimens incompatible with the constant load, flexural fatigue data in Table 2.1.

2.3.9 1965: Karr and Magura

Karr and Magura [50] performed three fatigue tests and two static tests to determine the effects of strand blanketing. Half-scale AASHO-PCI Type III specimens were tested. The actual cast-in-place deck dimensions were 3 x 39 in.

The three fatigue specimens were tested under constant loads for 5.0 million cycles. The beams had non-blanketed, partially blanketed, and fully blanketed strands. The ultimate strength-calculated ultimate capacity ratios were 0.98, 0.96, and 0.84,

respectively. All blanketed strands sustained some bond failure, while no bond failure occurred in unblanketed strands [50]. The premature failure of the specimen with fully blanketed strands occurred in a region where two strands were not effective due to blanketing.

2.3.10 1966: Magura and Hognestad

The purposes of the tests by Magura and Hognestad [54] were to correlate field and laboratory performance of bridge girders subjected to fatigue loads and to add to the AASHO Road Test findings. (The AASHO Road Test is discussed in Section 2.4 of this report.) Girders 5A and 5B were post-tensioned with parallel-wire cables, then grouted. Girders 6A and 6B were pretensioned with 3/8 in. seven-wire strands.

Girders 5A and 6A were cycled to a constant maximum load which produced a nominal concrete tensile stress of approximately 660 psi. The compression cylinder strengths at the time of testing for 5A and 6A were 8830 and 10,070 psi, respectively. The 660 psi tensile stress was $7\sqrt{f'_c}$ for 5A and $6.6\sqrt{f'_c}$ for 6A. Beam 5A cracked during the first application of live load. The cracking stress was 86 percent of the modulus of rupture. All major cracks were established by 200,000 cycles. The only change after this point was that the existing cracks extended and increased in width. After approximately 2.7 million cycles, the strand stress range and centerline deflection under static load increased drastically. The strand stress range increased from 9 ksi to 22 ksi. The deflection increased from 0.3 in. to 0.45 in. Fatigue testing was stopped at 5.0 million cycles. Loss of bond was reported during ultimate test of beam 5A. The ratio of the measured moment capacity to the calculated moment capacity ratio was 0.90. The ultimate midspan deflection was approximately 10 in. No strand fatigue fractures were reported.

Girder 6A (a pretensioned specimen) did not crack during the initial loading. Flexural cracks were first noticed after 5000 cycles. The tensile stress was 86 percent of the modulus of rupture. The maximum crack width at this time was 0.003 in. At 300,000 cycles the maximum width was 0.005 in. After this, the maximum crack width did not increase, but new cracks did form. The specimen withstood approximately 3.5 million fatigue cycles before the ultimate test. The ultimate strength to calculated capacity ratio was 1.04. The ultimate deflection was approximately 22 in.

Girders 5B and 6B were tested at varying load ranges. Beam 5B withstood 4.59 million fatigue cycles before flexural cracking was observed. The cracking stress was 92 percent of the modulus of rupture. After 5.028 million cycles, the specimen was tested to determine ultimate strength. The ultimate strength was 104 percent of the calculated ultimate capacity. The centerline deflection was approximately 30 in.

Girder 6B withstood 4.7 million cycles before flexural cracking was noticed. The tensile stress was 94 percent of the modulus of rupture. The specimen was tested to destruction after 5.2 million cycles. The ultimate strength was 106 percent of the calculated ultimate capacity. No strand fatigue fractures were reported in any of the test specimens.

Magura and Hognestad [54] made the following conclusions:

1. The behavior under repeated loads of the full-scale girders tested in the laboratory compared satisfactorily with the behavior of the bridges in the AASHO Road Test.

2. For both pretensioned and post-tensioned bridge girders stressed under live load to a maximum concrete tension of approximately 300 psi, which was approximately $3\sqrt{f'_c}$, no cracks or only microcracks were formed, and no deterioration in performance resulted from continued applications of load.

3. The pretensioned bridge girders with a concrete tension of about 700 psi, which was approximately $7\sqrt{f'_c}$, showed no significant detrimental effects from flexural cracks under repeated loading, whereas similarly stressed and cracked post-tensioned bridge girders showed serviceability distress and reduced capacity from load repetitions.

2.3.11 1969: Abeles, Barton, and Brown

Abeles et al. [13] tested four 4 x 9 in. partially prestressed specimens under varying load ranges to study the fatigue resistance of prestressed concrete bridge elements subjected to fatigue loadings. The maximum applied load varied from 33 to 78 percent of the ultimate capacity. No information was included on strand stress ranges.

2.3.12 1970: Hanson, Hulsbos, and Van Horn.

Hanson et al. [41] tested six prestressed concrete I-beams to determine the fatigue life of beams with flexural and inclined cracking. No slabs were cast on the 1'6" deep models. All specimens were initially loaded to approximately 80 percent of their calculated ultimate flexural capacity. Flexural and inclined cracks resulted from this initial loading. The specimens were then subjected to 2.0 million fatigue cycles at "design" loads. The nominal concrete tensile stress was approximately $5.5\sqrt{f'_c}$. After this, the six specimens were tested at "above-design" loads producing nominal concrete tensile stresses between 8 and $10\sqrt{f'_c}$.

Four specimens failed due to fatigue of prestressing wires in the strands. A fifth failed due to fatigue of stirrups. The sixth specimen experienced shear and flexural fatigue fractures. Table 2.2 shows the average strand stress ranges at design and above design load. The number of cycles to failure and the type of failures are also shown.

Stress concentrations at cracks were addressed. Hanson et al. state that:

> ... the stress range in the strand of the location of the crack was probably significantly greater than the measured strain range [Table 2.2], which was an average range over a length that included several cracks. Finally, when the bond was destroyed between the strand and the concrete, abrasion occurred which may have reduced the fatigue life.

The conclusion of this paper [41] also recommends additional tests to determine the effect that conditions at a crack have on the fatigue strength of a strand in a beam.

2.3.13 1974: Abeles, Brown and Hu

Abeles, Brown and Hu [14,15] reported on the static and fatigue testing of 52 beams. The 21 constant load tests results are presented in Table 2.1. The objective was to study the influence of strand stress, steel ratio, group strand action, bond, and non-pretensioned strand on fatigue life. Specimens from series A through E are shown in in Fig. 2.15. A series F specimen is shown in Fig. 2.16. Typical centerline deflections, permanent sets, and crack widths of various stages of loading are shown in Figs. 2.17 through 2.19 [14].

Abeles et al. [15] made the following conclusion regarding fatigue behavior of prestressed concrete beams:

- Extent of deflection and of cracking depends on the bond resistance.... The bond is gradually broken by the fatigue loading; this is intensified by varying ranges of loading.

- The addition of non-tensioned strands acts favorably at fatigue loading for they improve the resistance to cracking and bond.

- The magnitude of the effective prestress gradually decreases particularly over large ranges during load cycling so that even with constant load ranges varying strand stress ranges in the steel occur.

- The loss of prestress equivalent to a reduction in steel stress as mentioned [previously] was ascertained to be gradual, corresponding to the number of cycles, until a state is reached

TABLE 2.2 Stress Ranges and Fatigue Lives of Specimens Tested by Hanson et al. [41]

Specimen	Average Strand Stress Range at "Design" Loads[a] ($2x10^6$ cycles) (ksi)	Average Strand Stress Range at "Above-Design" Loads[a] (ksi)	Number of Cycles at Above-Design Loading			
			First Indication of Damage		End of Test	Failure Type
			Flexural	Shear		
H-40	16.0	29.1	304,000	None	458,000	Flexure
H-50	14.9	18.9	455,000	None	570,000	Flexure
H-60	13.5	17.0	714,000	None	906,000	Flexure
H-70	13.7	26.2	576,000	267,000	691,000	Flexure/ Shear
H-80	13.0	21.2	None	274,000	401,000	Shear
H-90	14.9	22.5	1,082,000	None	1,201,000	Flexure

[a] E is assumed as 29,000 ksi

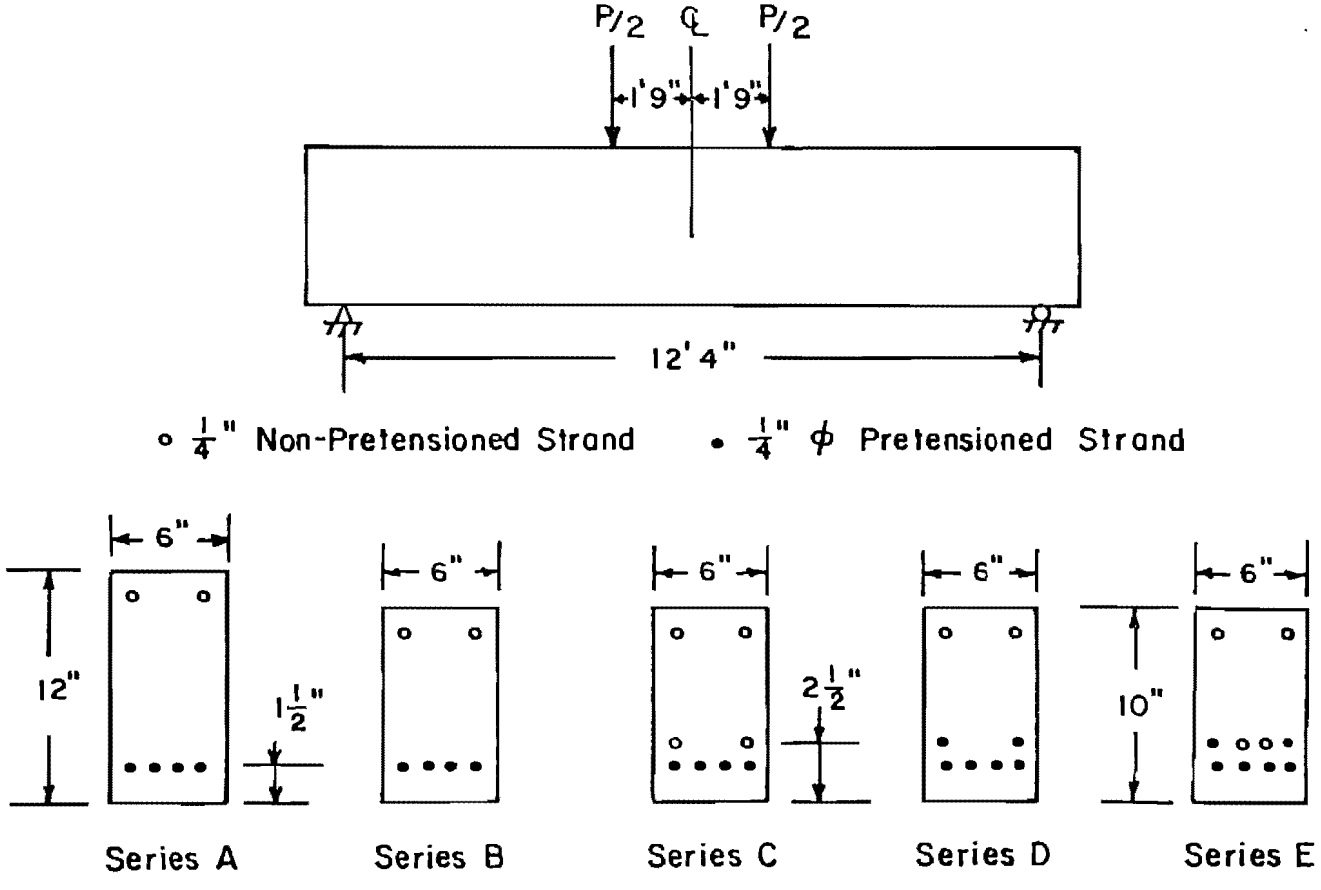

Fig. 2.15 Beam fatigue specimens; Abeles, Brown, and Hu (1972)

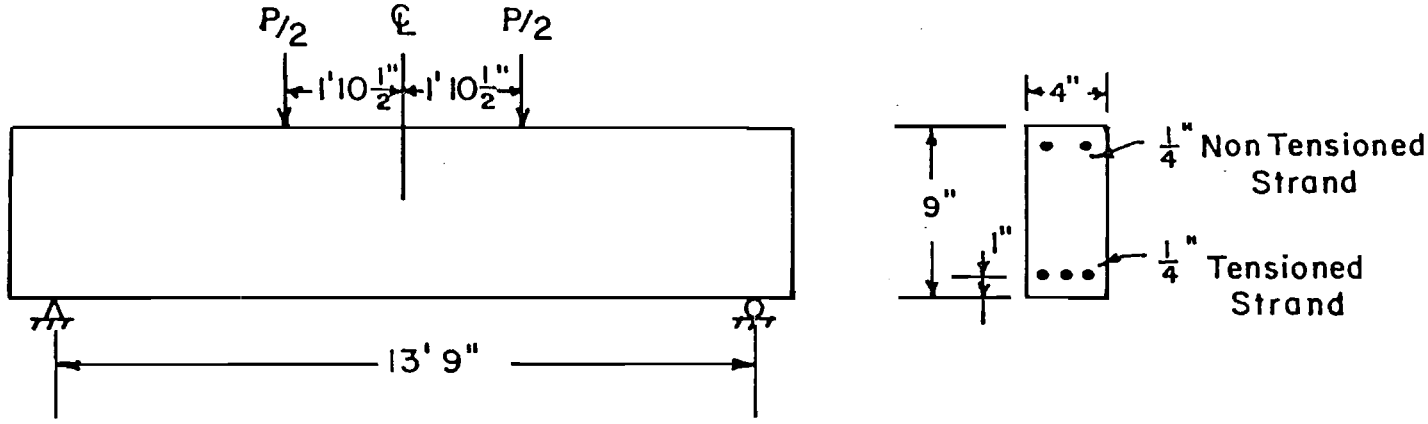

Abeles, Brown and Hu (Series F) (1974)

Fig. 2.16 Beam fatigue specimen; Abeles, Brown, and Hu (1974)

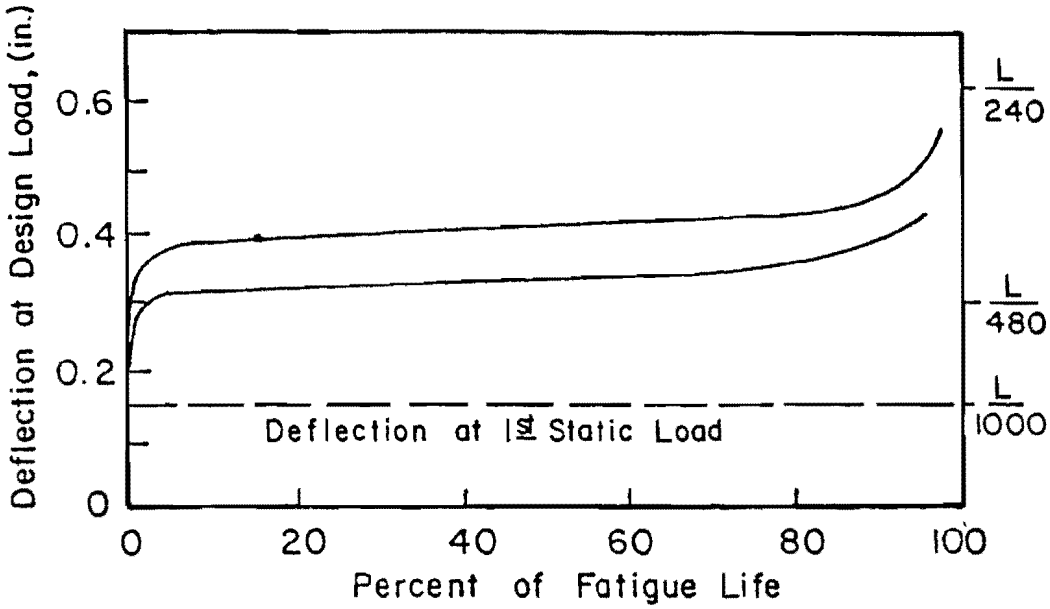

Fig. 2.17 Deflection of typical beams tested by Abeles et al. at design load

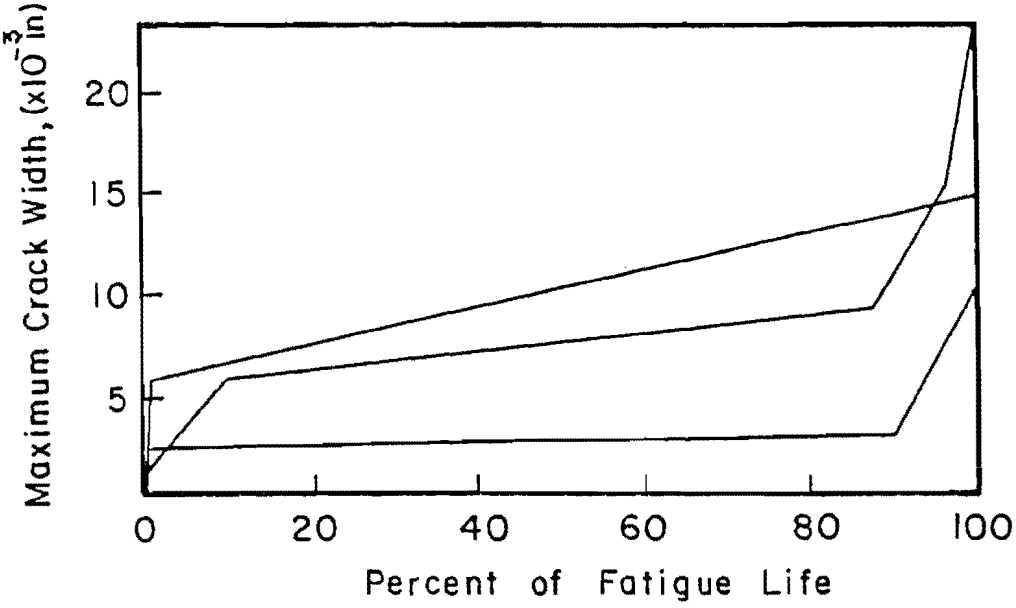

Fig. 2.18 Maximum crack width at level of strand at design load in beams tested by Abeles et al.

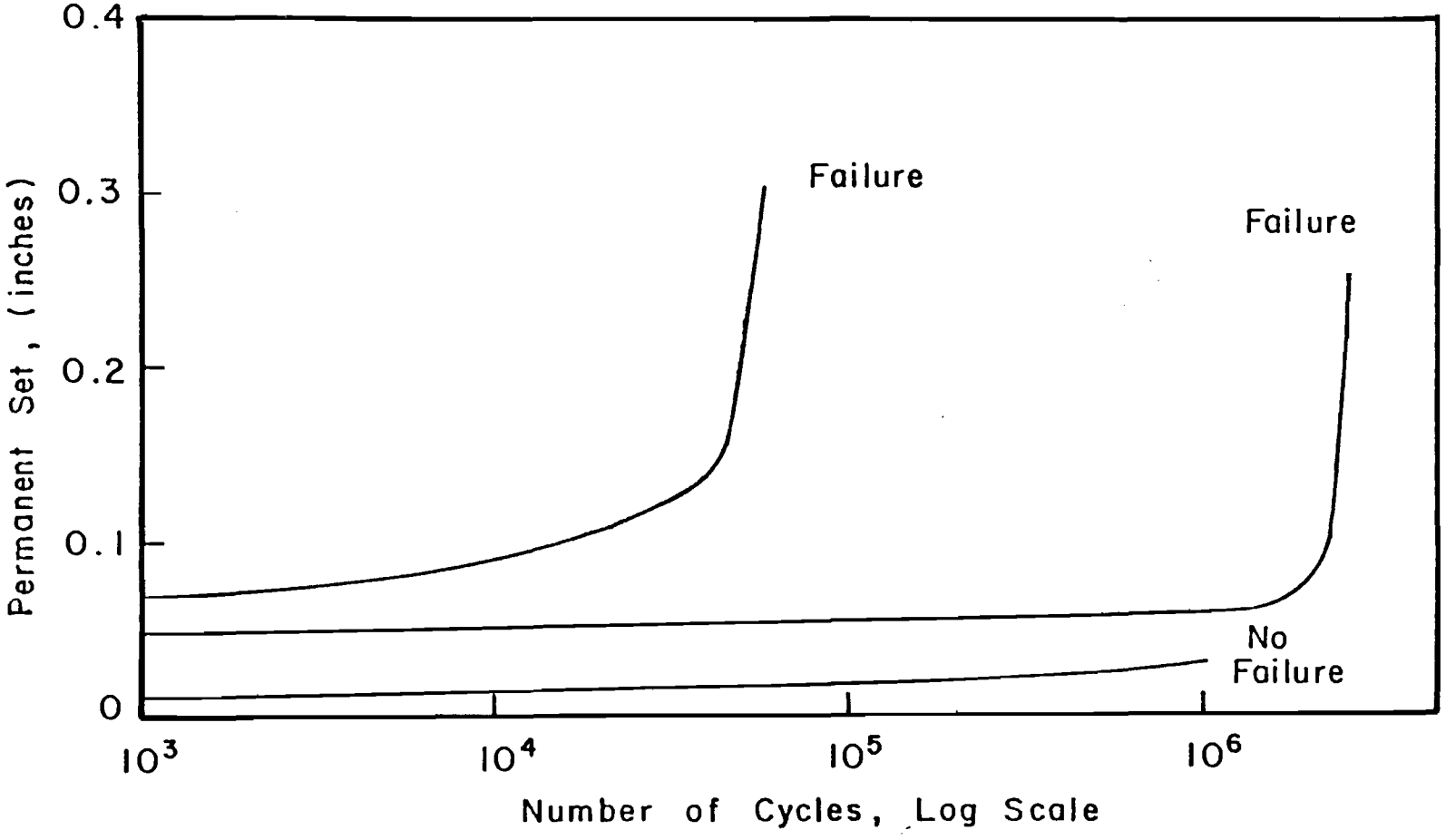

Fig. 2.19 Permanent set for several specimens tested by Abeles et al.

> when the bond is broken to a greater extent and suddenly a much greater loss of prestress occurs and thus reduction in the steel stress takes place with consequent substantial increase in deflection and crack width.

2.3.14 1977: Irwin

Irwin [47] tested three 21 in. deep pretensioned concrete I-beams with cast-in-place slabs to study the static and fatigue behavior of fully prestressed beams and to gather information on the behavior of prestressed concrete and prestressing strand when a cross section is cracked. Fatigue tests were performed on two of the specimens while the third specimen was tested statically. Table 2.3 presents information about cracking and cyclic concrete and strand stresses. Notice the increase in strand stress range for beam one. Irwin states that:

> ... the stress in some strands may have been higher than nominal because of the method of calculation, [or] redistribution associated with differing unbonded lengths of strand....

Post mortem investigation of beam one revealed white powdery deposits on the prestressing strands 6 in. each side of the failure crack. A 2 in. deposit was found in an area where two wires fractured. Beam two had large areas with the white deposit, which generally extended 2.4 in. both sides of flexural cracks. Light rusting was found within these powdery regions; the following conclusions presented by Irwin [47] indicate that bond deterioration is a problem.

- Fatigue failures in the prestressing strands in beam 1 led to collapse after 3.2×10^6 repetitions of load.... The breakdown of bond between the prestressing strands and the concrete appeared to be an important feature.

- ... The extensive breakdown of bond is important because of the implications that the strands cannot be relied upon to assist in controlling crack widths under certain conditions and that fatigue problems may require consideration.

2.3.15 1977: Howells and Raithby

Howells and Raithby [46] tested four lightweight prestressed concrete I-girders to determine their ultimate strength under static and repeated loading. Two beams were tested under varying fatigue loads; a third was statically tested to failure. The fourth beam was cycled at 60 percent of its ultimate capacity. The strand stress range at the beginning of testing of the fourth beam was approximately 27.2 ksi. Fatigue testing was stopped after 289,000 cycles. Little information was provided concerning the static and variable load fatigue tests.

TABLE 2.3 Static and Cyclic Stresses for Beams Tested by Irwin [47]

	Beam #1	Beam #2	
Cracking Stress (psi)	540	430[a]	
Modulus of Rupture (psi)	700	680	
Cyclic Nominal Concrete Stresses	380/1.5	430	4.2
Stress (psi)/Cycles (million)	400/1.5	460 to 980 by 140 psi	10,000 cycles at each step
	430/0.2		
		1220	10,000
Strand Stress Range (ksi) Initial/Final	7.3/30	3.0/41	

[a] Cracked during repetitive testing after 300 cycles.

2.3.16 1978: Rabbat, Karr, Russell, and Bruce

Rabbat et al. [76] tested six AASHTO-PCI Type III I-girders to determine how repetitive loading effects the behavior and strength of girders with blanketed strands. The specimens tested were similar to the one shown in Fig. 2.20. The only difference was that several specimens had blanketed instead of draped strands. The development length, ℓ_d, used in determining blanketing layout was defined as

$$\ell_d = (f^*_{su} - 2/3\ f_{se})\ D$$

where: f^*_{su} = average stress in prestressing steel at ultimate load;

f_{se} = effective steel prestress after losses; and

D = nominal diameter of prestressing steel.

Three girders were cycled at a nominal concrete tensile stress of $6\sqrt{f'_c}$ while the remaining three were cycled at zero tension for 5.0 million cycles. In addition to development length and concrete tensile stress level, the presence or absence of confining ties was a variable. Table 2.4 summarizes the test program.

All girders had artificial cracks formed by cast-in crack formers and were cracked before fatigue testing. The maximum nominal concrete tensile stress during static tests on all specimens was $6\sqrt{f'_c}$. The three girders which were cycled to $6\sqrt{f'_c}$ and failed prior to 5.0 million cycles will be discussed. No fatigue failures were encountered in the other specimens.

Specimen G10 withstood 3.63 million fatigue cycles. At that time, a large crack at a drape point was observed. A crack former was also located at this point. The crack pattern, which forked at the lower flange-web intersection, indicated strand slippage--none was reported. Fifty-nine wires fractured in fatigue at the critical location. Rabbat et al. [76] indicate that "the hold-down device did not seem to be the cause of fatigue of strands."

Specimen G11 had blanketed strands with a development length of ℓ_d. It withstood 3.78 million fatigue cycles. At this time a large crack was observed at a crack former 8 ft from the centerline. During the subsequent static test to destruction all but two strands fractured. The two were blanketed at the ends of the girder and slipped inside the blanketing. Crack patterns indicated strand slip prior to the ultimate test.

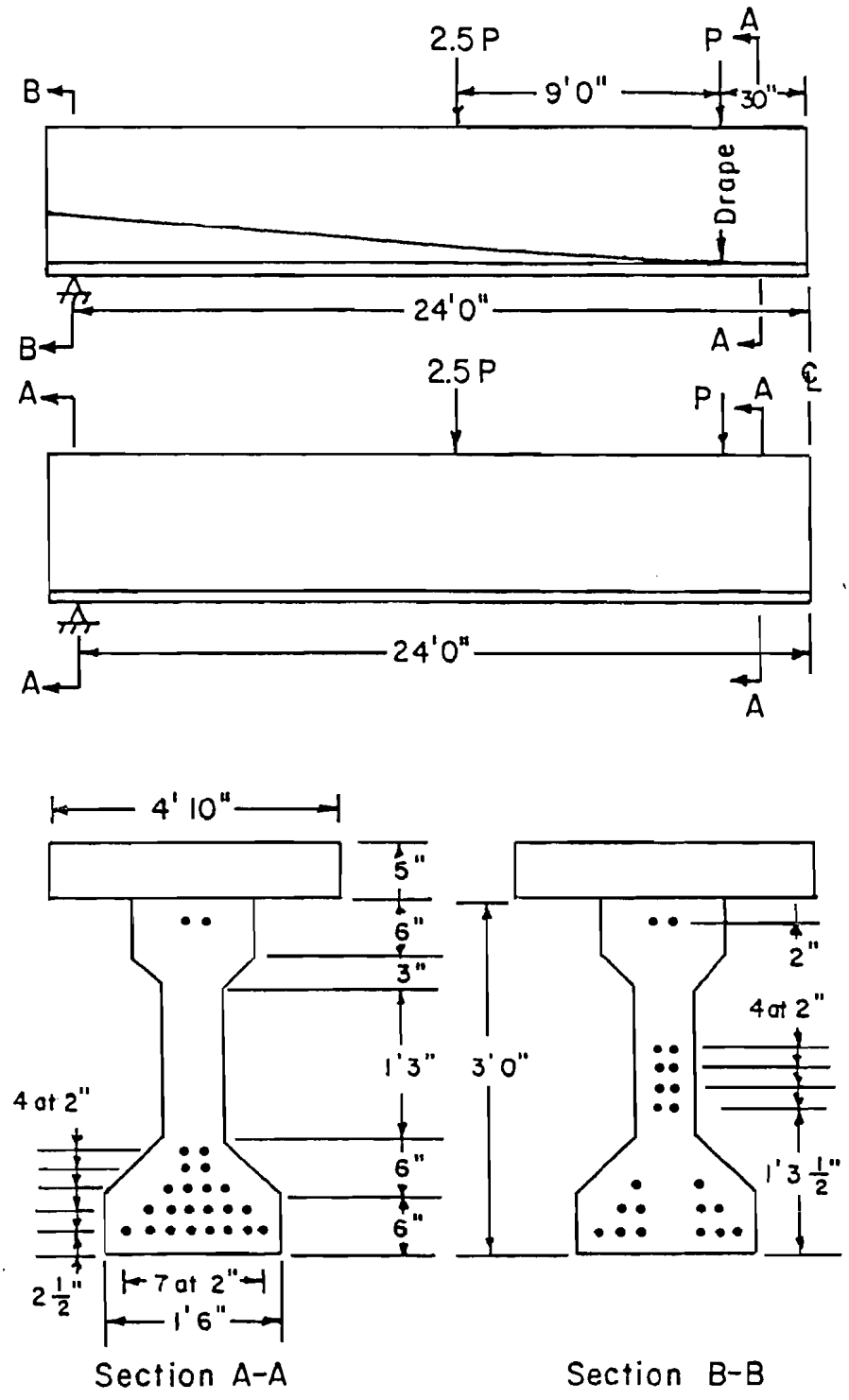

Fig. 2.20 Beam fatigue specimen, Rabbat et al. (1978)

TABLE 2.4 Test Variables and Results of Fatigue Tests by Rabbat et al. [76]

Specimen	Nominal Concrete Tensile Stress[a]	Development Length	Confinement Reinforcement	Static Strand Stress at First Static Cycle (ksi)	Static Strand Stress Range at 1.0 Million Cycles (ksi)	Static Strand Stress Range at 2.5 Million Cycles (ksi)	Fatigue Life ($\times 10^6$)[d]
G10	$6\sqrt{f'_c}$	Draped strands	No	8.5	19.5	19.0	3.63 -F
G10A	0	Draped strands	No	NA[c]	NA	NA	5.0 -NF
G11	$6\sqrt{f'_c}$	ℓ_d [b]	No	10.6	14.2	18.2	3.78 -F
G12	0	ℓ_d	No	12.7	14.2	15.5	5.0 -NF
G13	$6\sqrt{f'_c}$	$2\ell_d$	No	12.3	13.8	20.1	3.2 -F
G14	0	ℓ_d	Yes	11.8	12.9	12.8	5.0 -NF

[a] All specimens were cracked before cycling began.
[b] $\ell_d = (f_{su} - 2/3\ f_{se})D$
where: f_{su} = average stress in prestressing steel at ultimate load
f_{se} = effective stress in prestressing steel after losses
D = nominal diameter of prestressing steel
[c] The strands in girder G10A were not instrumented.
[d] F indictes failure; NF indicates no failure.

Specimen G13 was cycled at a maximum nominal concrete tensile stress of $6\sqrt{f'_c}$. The development length for this girder was 2 ℓ_d. After 3.2 million cycles, a crack at a crack former had propagated into the upper portion of the web. A subsequent static test indicated a loss in stiffness. When the specimen was cut open, 61 wire fatigue fractures were found at the critical crack.

2.3.17 1982: Bieschke and Klingner

Bieschke and Klingner [29] fatigue tested a 50-ft, three-girder bridge to study the behavior of precast deck panels with and without transverse strand extensions. The girders were pretensioned TDHPT Type B I-beams. Fatigue testing began after an initial static test. The first 1.5 million cycles of fatigue loading simulated AASHTO HS-20 vehicle loads. The fatigue loads were then increased, producing a concrete tensile stress of less than $3\sqrt{f'_c}$. No flexural cracking resulted from the 5.0 million cycles at this load level. At this time, the bridge was statically loaded to produce flexural cracks in all three girders. The bridge was then fatigue tested in a cracked state for 5.0 million cycles at a maximum nominal concrete tensile stress of less than $3\sqrt{f'_c}$. There was no visible indication of fatigue distress at this time. Flexural cracks closed after removal of load and load-deflection behavior did not significantly change from that recorded prior to the last 5.0 million cycles.

2.3.18 Analysis of Beam Fatigue Test Data

A linear regression analysis of the previously reported constant load range, beam fatigue data using the least squares method was performed. The population consisted of the 47 data points reported in Table 2.1. It has been established [73] that strand fatigue lives are log normally distributed and that the relationship between the log of the fatigue life (Log N) and the log of the strand stress range (Log S_R) is linear. Using the data from Table 2.1, the mean regression line was found to be:

$$\text{Log } N = 9.45 - 2.41 \text{ Log } S_R$$

The correlation coefficient was 0.909, and the standard error of estimate was 0.239. Figure 2.21 shows the mean regression line along with Paulson's [73] Model A-1L. For stress ranges below 26 ksi beam fatigue lives are shorter than strand "in-air" lives. The beam fatigue results do not indicate an endurance limit (a stress range below which no fatigue failures occur).

Size of test specimen and length of constant moment region are significant variables. The solid symbols in Fig. 2.21 indicates specimens with single point loadings. These beams tested by Ozell,

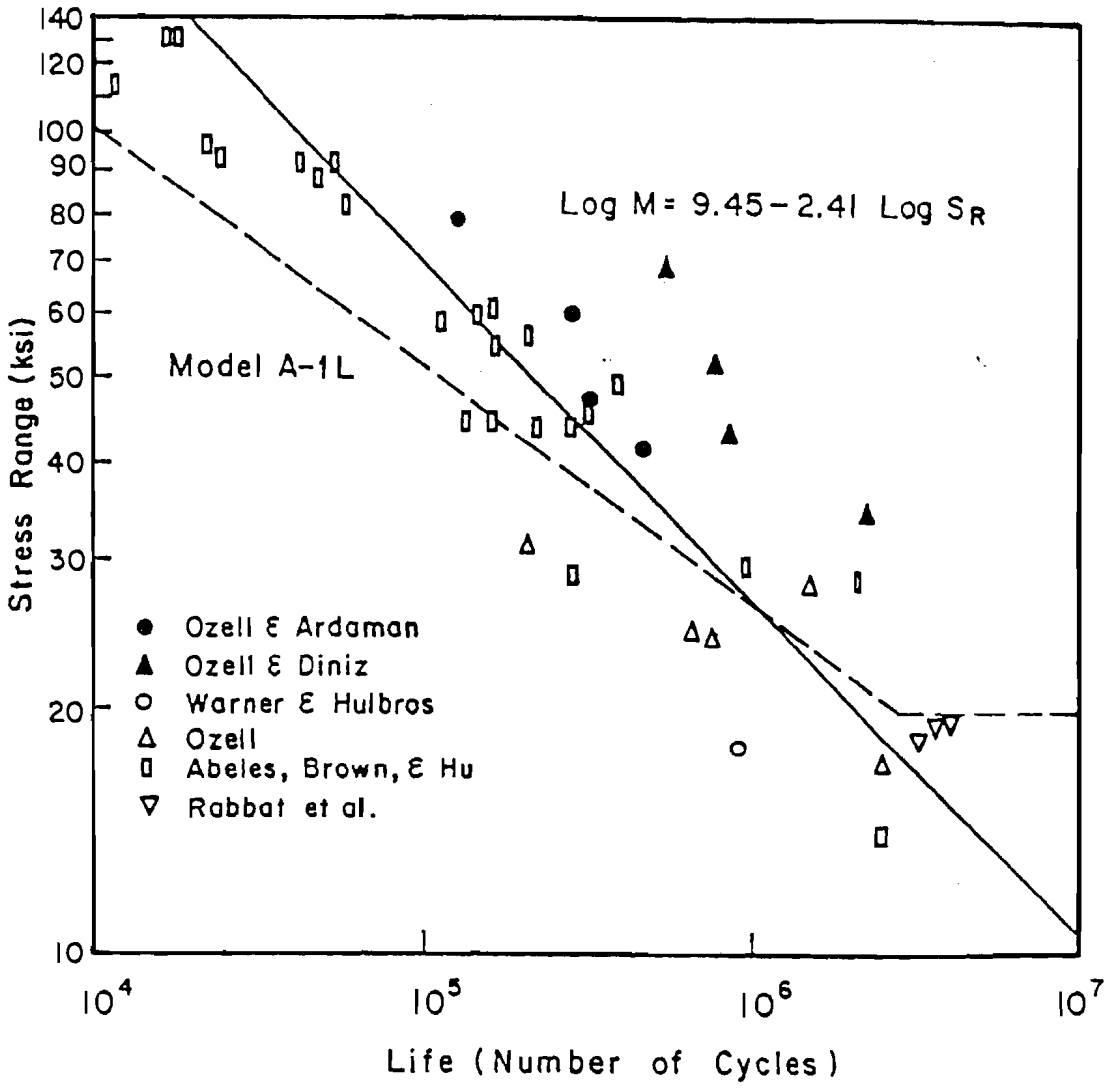

Fig. 2.21 Constant stress range beam fatigue results and mean regression line

Ardaman, and Diniz [65,66,67] had longer fatigue lives in general compared to tests with constant moment regions. Figure 2.22 shows the large scale results reported by Ozell and Rabbat et al. The mean regression line is approximately parallel to Paulson's [73] Model A-1L line, which is also shown in the figure. This type behavior would be expected as a result of the longer lengths of stressed strand as reported by Canteli [31] or a constant stress increase caused by flexural cracking.

2.4 AASHO Road Test of Prestressed Concrete Bridges

The American Association of State Highway Officials (AASHO) conducted full scale road tests [37] on eighteen slab and beam bridges between 1958 and 1960 on an "outside" test track. Two of the bridges were post-tensioned while two others were pretensioned. The AASHO test, reported by Fisher and Viest, included approximately 556,000 vehicle trips on each of the four prestressed concrete bridges and approximately 1.0 million additional accelerated fatigue test cycles on three of the bridges. The prestressed concrete bridges were designed for a maximum nominal tensile stress in the center beams under passage of the test vehicle of 300 and 800 psi in the bottom concrete fibers. Fisher and Viest [37] state that:

> The choice of these stress levels evolved from the objective of the research. In prestressed concrete bridges the primary concern was the fatigue cracking of concrete subjected to tensile stresses and the fatigue strength of the prestressing steel in cracked beams.

Table 2.5, taken from the report [37] indicates that the actual concrete stresses due to dead and live loads were often significantly different from the design stresses. The large live load prestressing steel stresses in post-tensioned bridge 5A can be attributed to flexural cracking. Figure 2.23 shows the typical three girder bridge tested in the AASHO road test. Bond, shear keys, and extensions of stirrups into the slab ensured composite action between the cast-in-place concrete slab and the precast concrete girders.

2.4.1 Post-Tensioned Bridges

Post-tensioned beams for bridges 5A and 5B were stressed with cables made of 10 parallel wires enclosed in a flexible metal conduit. The high carbon steel, stress relieved wires were then encased with grout.

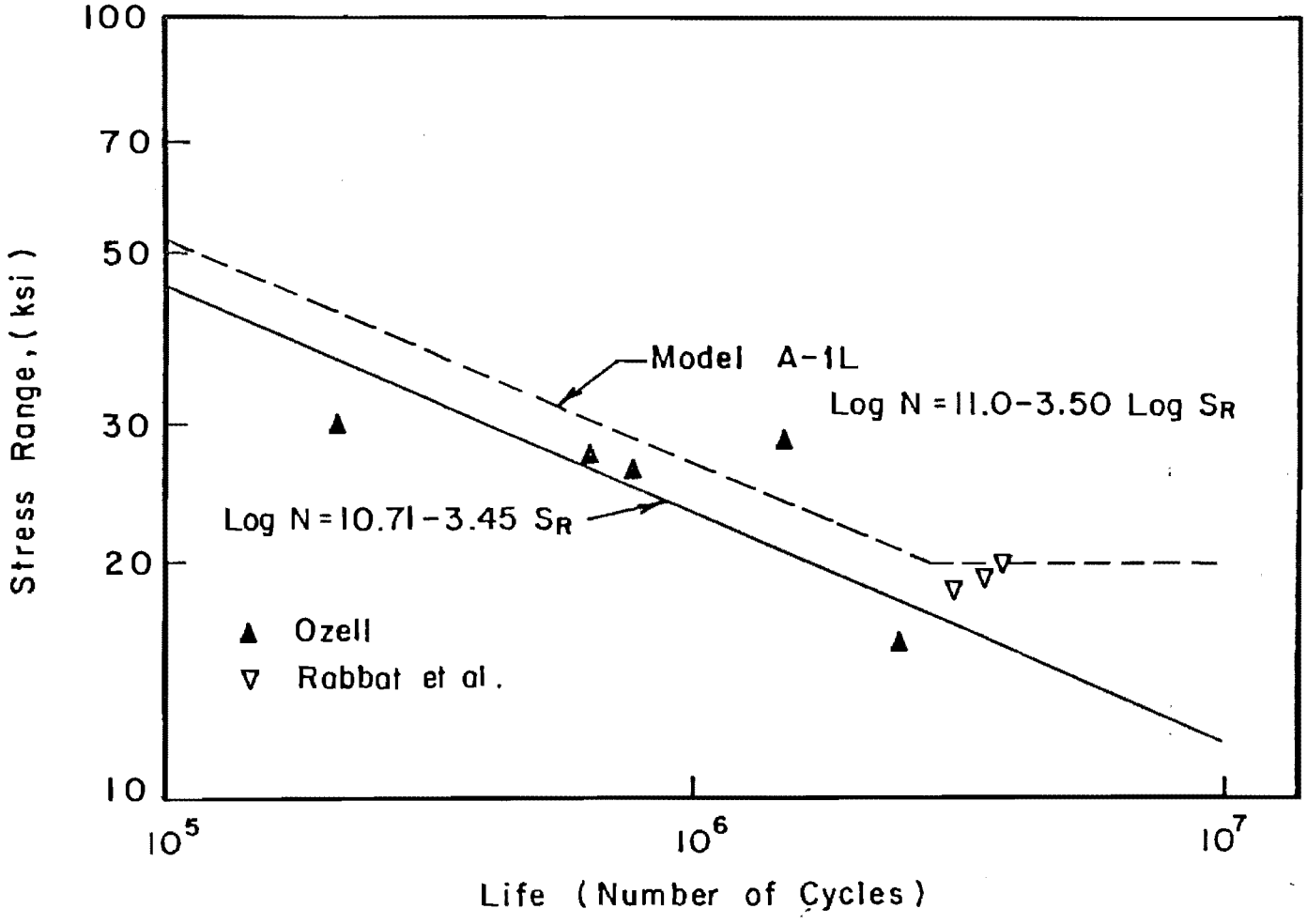

Fig. 2.22 Large scale constant stress range beam fatigue results and mean regression line

TABLE 2.5 Initial Stresses at Midspan of AASHO Road Test Prestressed Concrete Beams [37]

Bridge	Beam	Concrete Stress on Bottom Surface (psi)				Modulus of Rupture (psi)	Stress in Bottom Layer Prestressing Steel (psi)			
		DL	LL[1]	Total	Design		DL	LL	Total	Design
5A	Interior	- 84	(1019)[2]	(935)		742	144.9	23.4	168.3	
Post-	Center	22	(1020)	(1042)	820	742	145.0	18.4	163.4	150.6
Tensioned	Exterior	398	(968)	(1366)		742	150.5	26.1	176.6	
5B	Interior	-859	1019	160		742	152.8	4.5	157.3	
Post-	Center	-643	1020	377	346	742	149.1	4.3	153.6	152.2
Tensioned	Exterior	-321	968	647		742	152.9	4.3	157.2	
6A	Interior	5	530	535		742	164.6	2.6	167.2	
Pre-	Center	129	570	699	828	742	163.5	2.8	166.3	148.1
tensioned	Exterior	473	(549)	(1022)		742	167.8	4.6	172.4	
6B	Interior	-470	468	-1		742	170.1	2.3	172.4	
Pre-	Center	-374	489	115	310	742	171.1	2.4	173.5	150.0
tensioned	Exterior	9	549	358		742	172.3	2.7	175.0	

[1] Stress caused by regular test vehicle moving at 30 mph.
[2] Values in parentheses are fictitious estimates based on live load stresses of tandem uncracked bridges.

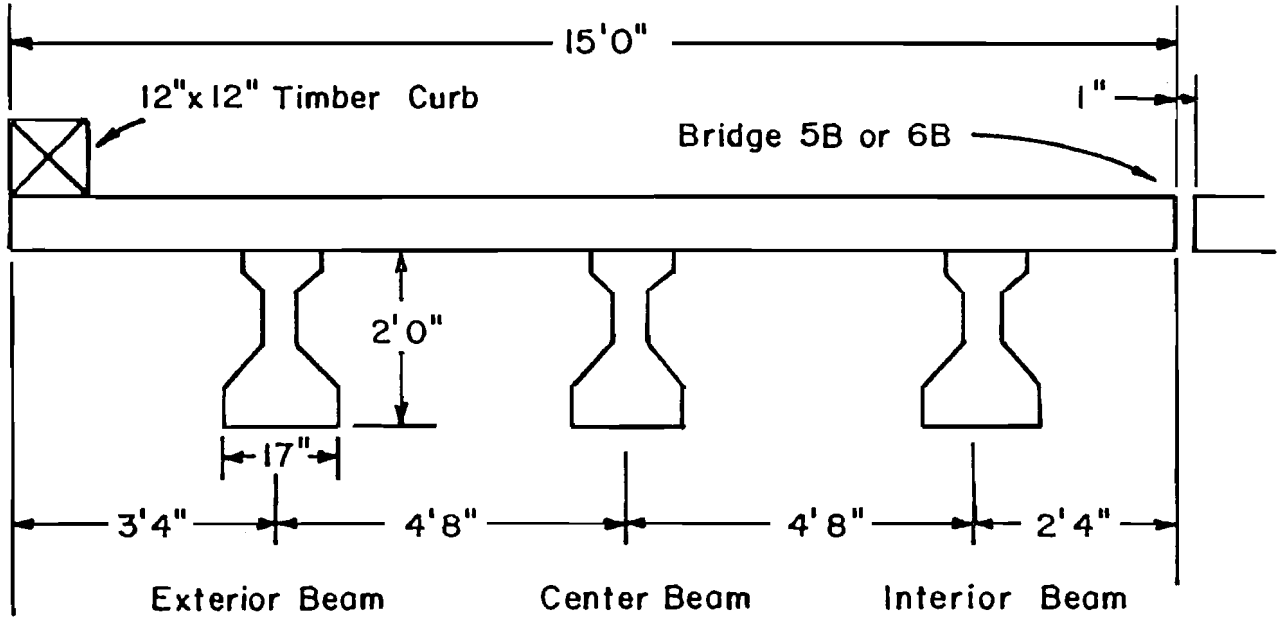

Fig. 2.23 Typical AASHO Road Test prestressed bridge section

2.4.1.1 Bridge 5A

All three girders in bridge 5A cracked during the first passages of regular test vehicles. The actual concrete stress exceeded the modulus of rupture (742 psi) and the design stress of 820 psi. Additional cracks formed, and the existing ones propagated, during the first 100,000 vehicle trips. After the initial 100,000 trips, few new cracks formed, but the existing ones widened. At the end of traffic testing, the maximum dead load crack width was 0.01 in. The average crack spacing was 22 in. Figure 2.24(a) indicates that the dead load strain increased significantly during vehicular testing. This would indicate large creep strains due to cyclic loading and an accompanying loss of prestress force. Contrary to this, Fisher and Viest [37] state that "No correlation was found between the losses and the repeated applications of load." The measured live load strains remained essentially constant throughout the vehicular test. The live load strand stress range was between 18.4 ksi for the center girder and 26.1 ksi for the exterior girder.

2.4.1.2 Bridge 5B

The behavior of bridge 5B remained virtually unchanged throughout vehicular testing. Figure 2.24(b) indicates a relatively constant dead load concrete strain. The small fluctuations are due to seasonal changes. Steel strains also remained constant during testing. No cracking was reported at the end of vehicular testing.

Bridge 5B withstood an additional 949,000 accelerated fatigue cycles with no substantial changes in bridge appearance or behavior. Cracks did form during this last phase of testing, but they were generally only visible with the aid of a 40-power microscope. Fisher and Viest [37] report that:

> These hairline or micro-cracks were apparently the result of the repeated loading. They did not influence appreciably the bridge stiffness nor cause noticeable increases in the live load stress in steel.

2.4.2 Pretensioned Bridges

Pretensioned beams for bridges 6A and 6B were stressed with seven-wire, high carbon steel, stress relieved strands. The pretensioned as well as the post-tensioned beams had end blocks.

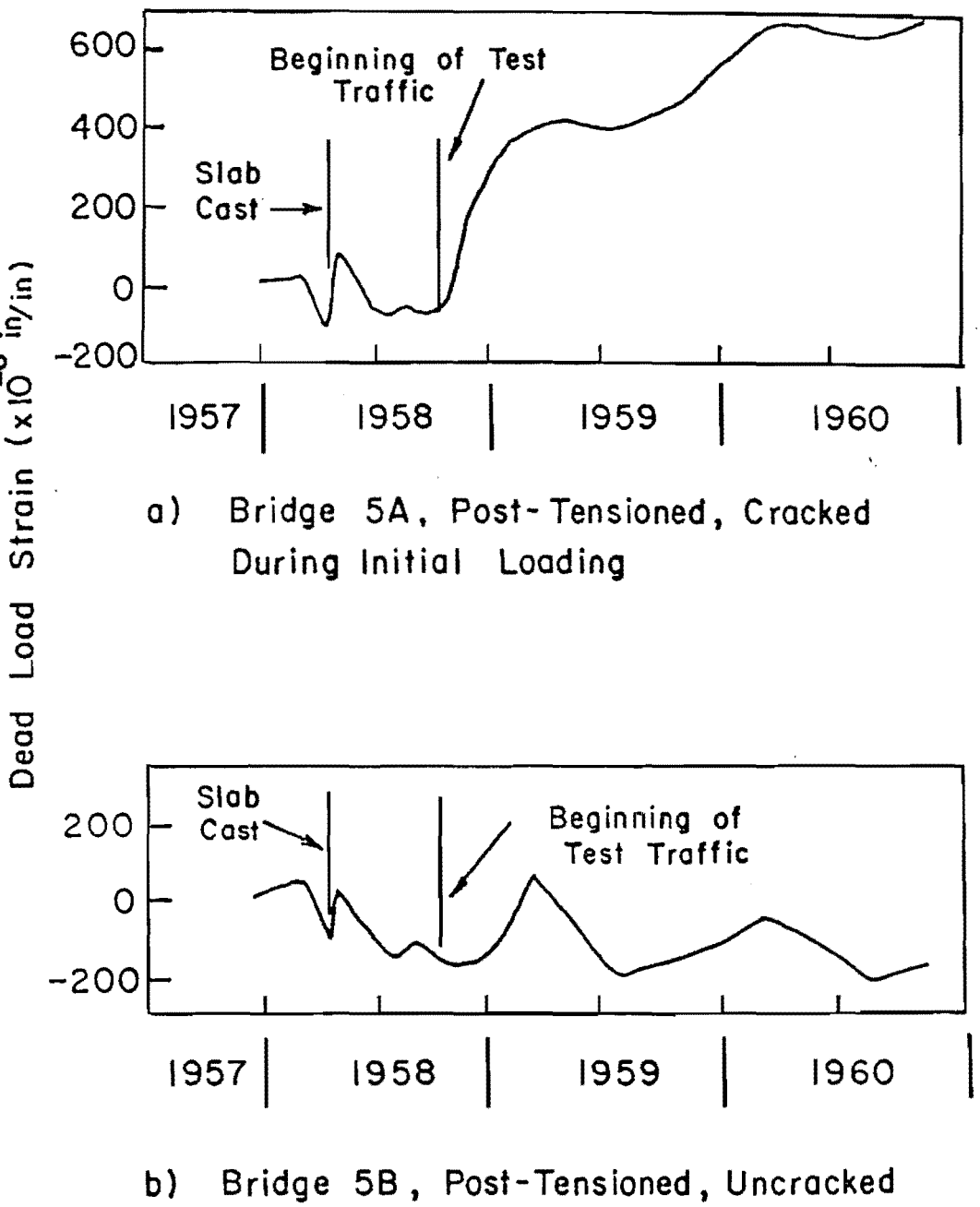

Fig. 2.24 Strain histories for AASHO Road Test posttensioned bridges

2.4.2.1 Bridge 6A

The exterior beam of bridge 6A was cracked during the first passages of regular test vehicles. Similar to the three cracked beams in bridge 5A, new cracks formed and existing cracks widened in the exterior beam of bridge 6A during the first 100,000 cycles. The bond characteristics of strand proved superior to the bond characteristics of wire. The maximum crack width in the exterior beam of bridge 6A after the vehicular testing was 0.005 in., half the value reported in the post-tensioned beams. The average crack spacing for the exterior beam was 10 in. Fisher and Viest [37] report that:

> Apparently the prestressing strand was more effective in retaining the bond between the concrete and prestressing steel for beams subjected to high tensile stress. This would account for the better crack distribution in the prestressed beams.

The result of the better bond characteristics can be seen in Fig. 2.25. Both crack patterns were recorded at the end of vehicular testing. Notice the forked cracks, several researchers [15,25,47] have reported that this forking is indicative of bond failure, in Fig. 2.25(a) for the post-tensioned specimen.

An additional 943,400 accelerated fatigue cycles did not substantially change the behavior of bridge 6A. Micro-cracks formed during this phase of testing, but the bridge stiffness changed little.

2.4.2.2 Bridge 6B

Bridge 6B withstood 556,000 vehicular cycles without cracking. The design extreme fiber concrete tensile stress in the center girder was 310 psi. The actual stress was 115 psi. An additional 942,100 accelerated fatigue cycles produced only microcracks with no substantial change in bridge stiffness.

2.4.3 Results of Prestress Concrete Bridge Tests

None of the prestressed concrete bridges failed during vehicular or accelerated fatigue testing. Flexural cracking did not appreciably decrease the stiffness of pretensioned bride 6A. Cracking did significantly change the behavior, increased strand stresses and increased dead load concrete strains of post-tensioned bridge 6A during vehicular testing.

The AASHO road test significantly affected the AASHO specifications. The test indicated that small tensile stresses were not detrimental to the behavior of prestressed highway girders for approximately 1.5 million cycles. This is a relatively low number of

a) Exterior Post-Tensioned Beam From Bridge 5A

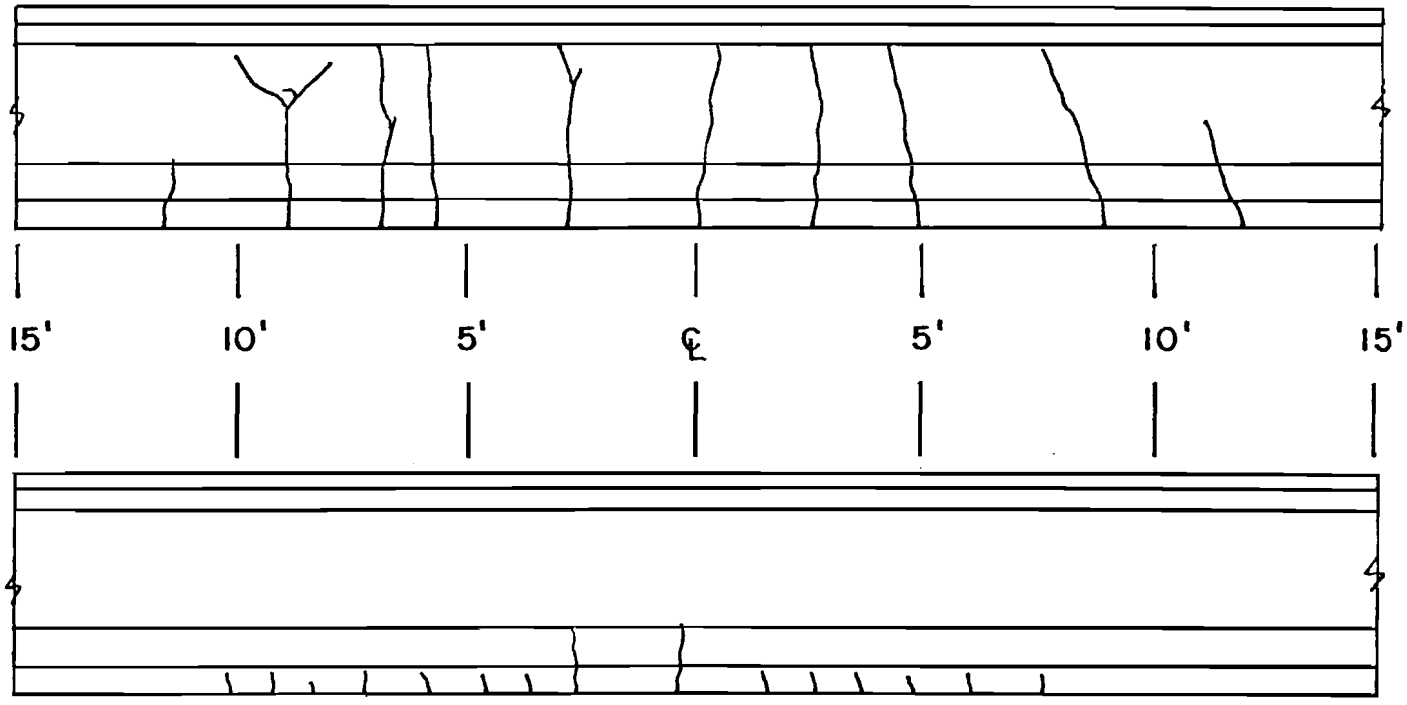

b) Exterior Pre-Tensioned Beam From Bridge 6A

Fig. 2.25 Crack patterns of prestressed concrete beams in AASHO Road test

cycles on which to base specifications involving fatigue. Previous tests indicated that fatigue is only a problem with cracked sections. Considering the cracking and the cyclical deterioration of concrete, the following questions were asked. How would the bridges behave after 5.0 million cycles? What would the fatigue life be if the girders were cracked due to overloads, high prestress losses, or fabrication errors? Why was post-tensioned bridge 5A not tested after the vehicular loading? Why was testing stopped after approximately 1.5 million cycles?

2.5 Partial Prestressing Philosophy

2.5.1 Definition

Full and partial prestressing has been defined in several ways [27,52,60]. The following definitions will be used in this report. Full prestressing: the entire prestressed section remains in compression at service load levels. Partial prestressing: like reinforced concrete, the concrete portion of the cross section cannot resist tensile stresses. For loads that produce stresses above the decompression stresses (zero stress in the extreme fibers of the precompressed tension zone), auxiliary reinforcement in the form of reinforcing bars or bonded prestressing steel must be proportioned to transmit tensile forces, control cracking and control deflections. Bachman [27] cites the following disadvantages of full prestressing:

- considerable upward creep deflections [camber] caused by prestressing calculated to offset even the tensile stresses arising from the maximum live load, though this might seldom or indeed never occur.

- a large consumption of prestressing steel even in zones of the structure where high prestressing is not required.

Reinforcing steel is often used in partially prestressed elements to reduce the amount of prestressing steel. Cracking of partially prestressed beams at service load levels can cause fatigue problems as Naaman [60] points out:

> In partially prestressed concrete beams the section is generally uncracked under the sole effect of the dead load and will crack due to the first application of the live load. Subsequent applications of live loads will lead to cracks opening at the decompression stress which is lesser than the cracking stress. First cracking or subsequent crack opening will shift upward the location of the neutral axis of bending of the section leading to a higher rate of increase in the steel and correspondingly in the concrete extreme fiber compressive strain (to maintain equilibrium of forces and moments in the section). These repetitive changes in stresses create fatigue, damage in the corresponding materials, reduce bond

properties at the interface between steel and concrete and lead to steady deflections with the number of cycles of loading.

The initial specimens tested in this study had only prestressing strand in the lower flange. Widely spaced cracks initiated during static and fatigue testing and often propagated to and forked in the web. The forking was similar to that reported in specimens with unbonded or poorly bonded prestressing steel [15,25,47]. As a result of the wide spacing, the flexural cracks were relatively broad. The flexural curvature was concentrated at these locations. Auxiliary passive reinforcing steel was added to the precompressed tension region to control crack distribution and width but not to resist service load moments; it was "auxiliary" to the active, stressed, prestressing steel.

Several guidelines [8,22,24,55] for partial prestressing and post-tensioned unbonded construction were used to determine the amount and distribution of the auxiliary reinforcement. This steel reduced the strand stress range due to the larger area of steel and reduced losses.

2.5.2 Auxiliary Passive Reinforcement Design Procedure

Existing specifications and recommendations were used as guidelines to determine the amount and distribution of auxiliary passive reinforcement. Menn [55] states that "to insure crack control the designer must provide a minimum percentage of mild steel of about 0.6 percent of the concrete area and it must be well distributed throughout the zone of tension." AASHTO Standard Specifications for Highway Bridges [8] addresses minimum reinforcing steel requirements in Section 1.6.24(D), Minimum Bar Reinforcement for Cast-in-Place Post-Tensioned Box Girders. Part (2) states: "The minimum bottom flange reinforcement shall be the same as for reinforced concrete box girders except the minimum reinforcement shall be 0.3 percent of the flange section." No minimum requirements for other types of structures are specified in the AASHTO Specifications. For construction with unbonded tendons, the ACI Building Code [22] requires:

$$A_s = 0.004A \qquad \text{(Eq.18-6)}$$

where: A_s = area of nonprestressed tension reinforcement, sq. in.

A = area of that part of cross section between flexural tension tension face and center of gravity of gross section, sq. in.

This provision is for flexural members with unbonded prestressing tendons. The Code states in Section 18.9.2.1 that "bonded reinforcement required by Eq. (18-6) shall be uniformly distributed over precompressed tensile zone as close as practicable to extreme tension fiber."

The actual design approach used in this study involved proportioning auxiliary reinforcement to resist the entire nominal concrete tensile force carried by an uncracked section with the extreme tensile fibers at 6 $\sqrt{f'_c}$. The reinforcing steel design tensile stress was limited to 25 ksi for fatigue considerations. For the Texas C-16 section tested, with a 77 in. wide, 7-3/4 in. deep slab, 5000 psi girder and slab 28-day concrete strength, and assuming 18 percent losses, the calculated uncracked section neutral axis, at 6 $\sqrt{f'_c}$ extreme fiber concrete tensile stress, was 11.8 in. above the bottom of the section. The calculated area of auxiliary steel required was 2.15 sq. in. Approximately 2.0 sq. in. of steel was used in the three specimens. Menn's [55] recommendation of 0.6 percent of the concrete area (girder only) would result in a required steel area of 2.97 sq. in. ACI 318-83 [22] called for 1.54 sq. in. for unbonded construction. The lower flange and the angled transition between the lower flange and the web were used in the AASHTO [8] calculation; 0.79 sq. in. of auxiliary steel was required for this area.

2.6 Design Provisions for Prestressed Concrete

The American Association of State Highway and Transportation Officials (AASHTO) Specifications and ACI Committee reports by Committee 215, Considerations for Design of Concrete Structures Subjected to Fatigue Loading, and Committee 443, Analysis and Design of Reinforced Concrete Bridge Structures, along with other pertinent specifications and codes will be reviewed in this section.

2.6.1 Historical Review of Prestressed Concrete Provisions in the AASHTO Specifications

The AASHTO Specifications first addressed prestressed concrete in the introduction to the 1957 Specifications [2] with the following statement:

> The committee has given much study to prestressed concrete design and construction, a field in which general agreement on specifications is impossible at this time because of the rapid development taking place both in research and in utilization.

The introduction went on to say that a report of the Joint ASCE-ACI Committee on Prestressed Concrete would be available in early 1958.

The Joint Committee Report [17] was published in January 1958. The authors of this report were concerned with repetitive loads and fatigue as can be seen in the following provisions which were part of Section 206, Repetitive Loads:

206.1 General

Ultimate strength of concrete or steel subjected to repetitive loading may be less than static strength because of the phenomenon of fatigue. Full importance of fatigue in prestressed concrete members has not yet been determined. Fatigue failure may occur in concrete, steel, anchorages, splices or bond.

206.3 Prestressing Steel

... Range of stress under service loads will usually be small unless concrete is cracked. Cracking may occur if tension is permitted in concrete. Fatigue failure of steel should be considered in such cases, especially when a high percentage of ultimate strength is used for prestress.

206.5 Bond

Failure of bond under repetitive loading is unlikely unless the member is cracked under design loads or a significant number of repetitions of overload. High bond stresses adjacent to racks may be a source of progressive failure under repeated loads.

206.7 Design Recommendations

Fatigue should not result in a reduction of strength if the following recommendations are observed. When the recommendations cannot be followed, fatigue strength of all elements comprising the prestressed member should be considered.

...

b. Tension should not be permitted in concrete at the critical cross section under either design load or overloads that may be repeated a large number of times.

Section 207.3.2, Stresses at Design Loads, called for zero flexural tension in the precompressed tensile zone of single element bridge members.

The Prestressed Concrete Institute (PCI) published tentative provisions, "PCI Standard Building Code for Prestressed Concrete," in November 1959 [69]. The tentative code stated in Section 304, Allowable Stresses:

...

2. At design loads the fiber stresses should generally not exceed the following:

...

Tension, without bonded reinforcement (either prestressed or nonprestressed) on the tension side ... $3\sqrt{f'_c}$

Tension, with bonded reinforcement (either prestressed or nonprestressed) on the tension side ... $6\sqrt{f'_c}$

Although tensile stresses are permitted to exist in concrete, they should not be considered as effective in resisting the bending moment, except for convenience in computation where the errors involved are known to be within limits.

This indicates that a cracked section analysis is required if there is a possibility of concrete tensile stresses.

Fatigue was addressed in Section 305, Repetitive Load and Stress Reversals. The introduction stated that repetitive loads would decrease the ultimate strength but that the possibility (in buildings) "... is usually so rare that a lower factor of safety is considered sufficient when considered fatigue loadings." The PCI provisions [69] used the same wording as the ASCE-ACI Joint Committee Report [17] in terms of bond fatigue. Steel fatigue was considered a problem only when cracks in concrete were expected to extend beyond the level of the tendons.

The actual "PCI Standard Building Code for Prestressed Concrete" [70] published in 1961 deemphasized fatigue problems. A reduced capacity due to fatigue was not mentioned. The wording of Section 203, Allowable Stresses in Concrete, was changed to:

...

(b) Stresses at design loads after allowance for all prestress losses shall not exceed the following:

...

2. Tension in the precompressed tensile zone:
Members, not exposed to a corrosive environment, which contain bonded prestressed or unprestressed reinforcement located so as to control cracking ... $6\sqrt{f'_c}$

All other members ... 0

Section 211, Repeated Loads, only addressed fatigue of anchorages, inclined diagonal tension cracks, and stated that:

> (a) The possibility of bond failure due to repeated loads shall be investigated in regions of high bond stress and where flexural cracking is expected at design loads.

The AASHO allowable tensile stress of service load levels has slowly increased from zero to $6\sqrt{f'_c}$. The 1961 Specifications [3] provided a section for prestressed concrete. At that time the allowable tensile stress after losses was zero.

The 1965 AASHO Specifications [4] were published after the AASHO Road Test report [37]. The Road Test indicated that small tensile stresses did not adversely effect behavior of pretensioned beams up to 1.5 million cycles. Post-tensioned beams showed more distress in the tests. The 1965 AASHO Specifications [4] reflected the confidence gained from the Road Test. The allowable stress at service load levels after losses in the precompressed tensile zone was $3\sqrt{f'_c}$, but not more than 250 psi, for pretensioned members and zero for post-tensioned members.

Wording of Section 1.6.7(B), Allowable Stresses in Concrete, in the 1969 AASHO Specifications [5] was changed from that used in the 1965 Specifications [4]. Section 1.6.7(B)(2) stated that:

> Stresses at design load after losses have occurred:
>
> ...
>
> Tension
>
> In zones initially precompressed with prestressed reinforcement or, in zones with nonprestressed reinforcement that is sufficient to resist the total tension force in the concrete computed on the assumption of an uncracked section ... $3\sqrt{f'_c}$ (but not to exceed 250 psi).
>
> In zones without reinforcement ... zero.

The 1971 Interim Specifications [1] increased the allowable tensile stresses to control camber and as a result of confidence gained from the building industry. The commentary states that:

> The allowable tensile stress in the precompressed tensile zone has been increased to $6\sqrt{f'_c}$. This is below the modulus of rupture and is well below the stress level where a member displays a marked difference between cracked and uncracked behavior. The building industry has used this level of stress for many years without adverse effects and although this is a significant percentage

increase the actual behavior should not be significantly altered. The increased stress should improve long-time riding characteristics in structures where camber growth occurs under present stress levels.

Section 1.6.6(B), Allowable Stresses for Concrete, states that:

...

(2) Stress at service load after losses have occurred:

...

Tension in the precompressed tensile zone

(a) For members with bonded reinforcement ... $6\sqrt{f'_c}$

For severe corrosive exposure conditions, such as coastal areas ... $3\sqrt{f'_c}$

(b) For members without bonded reinforcement ... 0

It is interesting to note that the AASHO Specifications [1] were changed as a result of success in the building industry. The actual loads on building structures are usually small compared to the dead load and do not occur a large number of times. The consequences of flexural cracking, visible cracks and larger deflections when full live load is applied, is mainly a serviceability problem in building structures. The small number of cycles does not affect the ultimate capacity. For bridge structures, full live load and often overloads must be resisted a large number of cycles. The consequence of flexural cracking is serviceability problems initially and strength problems ultimately as the number of cycles increase and fatigue fracture of prestressing steel occurs.

The 1971 Interim Specification [1] would have been more effective if two sets of allowable stresses were presented. The steel fatigue specifications in the 1969 Specifications [5] divided roads into two cases. Case I was for freeways, expressways, and major highways and streets which experience a larger number of cycles. Case II was for other highways and streets not included in Case I. This case was for roads that did not experience a large number of cycles. The allowable tensile stresses in Case I were lower than for Case II as a result of fatigue of the materials caused by the increased number of cycles. The $6\sqrt{f'_c}$ tensile stress limit could have been applied to the Case II type structures, with low traffic volume, where creep deflections would be most severe. The $3\sqrt{f'_c}$ limit could have been applied to Case I type structures, where fatigue may be an eventual problem.

The 1971 Interim Specifications [1] also addressed partial prestressing to control service load behavior. Section 1.6.1, General, states that:

> The specifications of this section are intended for design of prestressed concrete bridge members. Members designed as reinforced concrete, except for a percentage of tensile steel stressed to improve service behavior, shall conform to the applicable specifications of Section 5.

Commentary Section 1.6.1 explained this wording by stating that:

> ... The intent of this reason is to provide a specification for prestressed concrete bridge structures that would be self-contained. However, because partial prestressing provides the Engineer the opportunity to use a limited amount of prestress to control service load behavior characteristics, some references are required to Section 5.

Section 5 included specifications for reinforced concrete.

The 1973 AASHO Specifications [6] included these changes. There was no change in the allowable tensile stress in the precompressed tensile zone in the 1977 Specifications [8].

2.6.2 ACI and Other Recommendations for Prestressed Concrete

The ACI Building Code [22] is for buildings and therefore does not address all problems encountered in bridge structures. ACI does address bridge structures and fatigue in committee reports.

2.6.2.1 ACI Committee 215 Report: Considerations for Design of Concrete Structures Subjected to Fatigue Loading

ACI Committee 215 published its first state-of-the-art report on fatigue [19] in 1974. In Chapter 3, Fatigue of Beams and Pavements, the following statement regarding prestressing strand stress range was made:

> The stress range in prestressed reinforcement that may be imposed on minimum stress levels up to 60 percent of the tensile strength shall not exceed the following:
>
> | | |
> |---|---|
> | Strand and bars | $0.10\ f_{pu}$ |
> | Wires | $0.12\ f_{pu}$ |

... results of recent research [reference was made to the tests by Hanson et al. (41)] indicate that if the nominal tensile stress in the precompressed tensile zone does not exceed $6\sqrt{f'_c}$, it may be assumed that fatigue of the prestressing reinforcement is not critical.

2.6.2.2 ACI Committee 443: Analysis and Design of Reinforced Concrete Bridge Structures

A draft of the Committee Report [23] was first published in 1974. The official report [24] was published in 1977. Section 8.3, Fatigue of Materials, stated the same allowable stress ranges as Committee 215 for prestressing steel. Section 8.7, Permissible Stresses for Prestressed Flexural Members at Service Conditions, addresses flexural stresses, after losses, in Part 2:

> Flexural stresses in concrete of service loads, after allowance for all prestress losses, should not exceed the following:
>
> ...
>
> (b) Tension in precompressed tension zone: Members with bonded auxiliary reinforcement to control cracking ... $6\sqrt{f'_c}$
>
> Members with bonded auxiliary reinforcement to control cracking, but exposed to corrosive environments or severe exposure conditions ... $3\sqrt{f'_c}$
>
> Members without bonded auxiliary reinforcement ... 0

Section 9.12, Repetitive Loads, states that "the possibility of rupture of steel due to repeated loads should be investigated in regions where flexural cracking is expected at design loads."

2.6.2.3 American Concrete Institute Considerations of Fatigue

Hawkins and Shah addressed ACI fatigue recommendations in a paper [44] published in 1982. The summary states that:

> Consideration relevant to the high cycle fatigue design of concrete structures have been developed by American Concrete Institute's Committee 215 on Fatigue, 357 on Offshore Structures, and 443 on Concrete Bridge Design. The bases for these recommendations are described and findings from recent investigations that are likely to influence future recommendations are summarized.

Appendix A, Provisions for Fatigue of Concrete, suggested by ACI Committee 215, states that:

> Fatigue shall be considered by rational evaluation when the stress range in concrete members under a large number of repeated loads exceed the following:
>
> ...
>
> 4.1 Where the nominal tensile stress in the precompressed tensile zone does not exceed $6\sqrt{f'_c}$ and the member is uncracked:
>
> $$f_{tr} = 0.10\ f_{pu} \qquad \text{(A3)}$$
>
> 4.2 Where the nominal tensile stress in the precompressed tensile zone exceeds $6\sqrt{f'_c}$ or the member is cracked:
>
> $$f_{tr} = 0.04\ f_{pu} \qquad \text{(A4)}$$
>
> where: f_{tr} = stress range in prestressing tendons under repeated service loadings; i.e., difference between maximum and minimum stress in psi;
>
> f_{pu} = specified ultimate capacity of prestressing tendons in psi.

The text limits the applicability of equation A3 by stating that:

> Prestressing steels do not seem to have an endurance limit and the values predicted by Eq. (A3) correspond to the likely fatigue life for 2×10^6 cycles. Eq. (A3) is intended primarily for pretensioned construction. In post-tensioned construction bending of the anchorage and anchorage details can cause stress concentrations that reduce the fatigue strength below that given by Eq. (A3). Unless there are data to the contrary the fatigue strength of anchorages should not be taken as greater than half the fatigue strength of the steel.

There is a large variation in allowable tensile stresses in prestressed concrete [8,19,24,44]. Several specifications [8,24] are based on concrete stresses and several [19,24,44] are based on steel stresses. With increasing vehicle weights, overloads, and the reduced tensile capacity of concrete due to cyclic loading, there appears to be a high probability that prestressed concrete highway members will crack when the design stress if $6\sqrt{f'_c}$. This, coupled with the fact that partially prestressed members are assumed to be cracked at service load levels, makes concrete tensile stresses meaningless. The provisions [19,24,44] based on strand stress range are the most rational ones.

CHAPTER 3

EXPERIMENTAL PROGRAM

3.1 Introduction

The main purpose of the experimental program was to study the effects of repeated cyclic loads on the fatigue life and behavior of pretensioned girders. Both Texas Type "C" and AASHTO-PCI Type II I-beams were tested so as to involve slightly different cross sections. Additional variables included range of applied load, and hence strand stress range, straight and draped strand profiles, presence of passive reinforcement, distribution of passive reinforcement, precracked and uncracked members, and overloads during static testing.

The basic approach was to use a number of tests of standard girders to develop a stress range vs. number of cycles (S/N) curve. In order to determine if fatigue of pretensioned girders was actually a problem and to define the shape of the short fatigue life portion of the S/N curve, the first specimens were tested with an upper nominal concrete tensile stress, in the precompressed tension zone, greater than $6\sqrt{f'_c}$. The remaining girders were cycled at or below $6\sqrt{f'_c}$.

Eight Texas Type "C" girders were fabricated at the Ferguson Structural Engineering Laboratory. Three additional AASHTO-PCI Type II girders were cast in a commercial prestressing plant and shipped to Austin. All testing was performed at the Ferguson Laboratory after unshored slabs were cast to form composite members. The testing setup is shown in Fig. 3.1.

An alphanumeric label will be used for each specimen. From left to right the designation indicates six items. The first indicates the section type. "C" is the Texas Type C while "A" is AASHTO-PCI Type II. The next indicator gives the number of strands. The C-16 specimens had straight strands while the C-14 and A-22 specimens had draped strands. The third figure indicates the presence or absence of passive (unstressed) reinforcing steel in the precompressed tension zone. "NP" represents no passive reinforcement. "UP" represents unconfined passive reinforcement. "CP" represents confined passive reinforcement. The next indicator gives the maximum nominal tensile fiber concrete stress in multiples of $\sqrt{f'_{ct}}$, where $\sqrt{f'_{ct}}$ is the concrete cylinder strength at the time testing began. The next figure indicates the presence or absence of overloads. "OL" indicates occasional modest overloads (greater than 4 percent of the load) during static tests. "NO" represents no overloads. The last indicator gives the number of fatigue cycles when testing was discontinued, in millions.

C-16-CP-5.5-OL-9.43

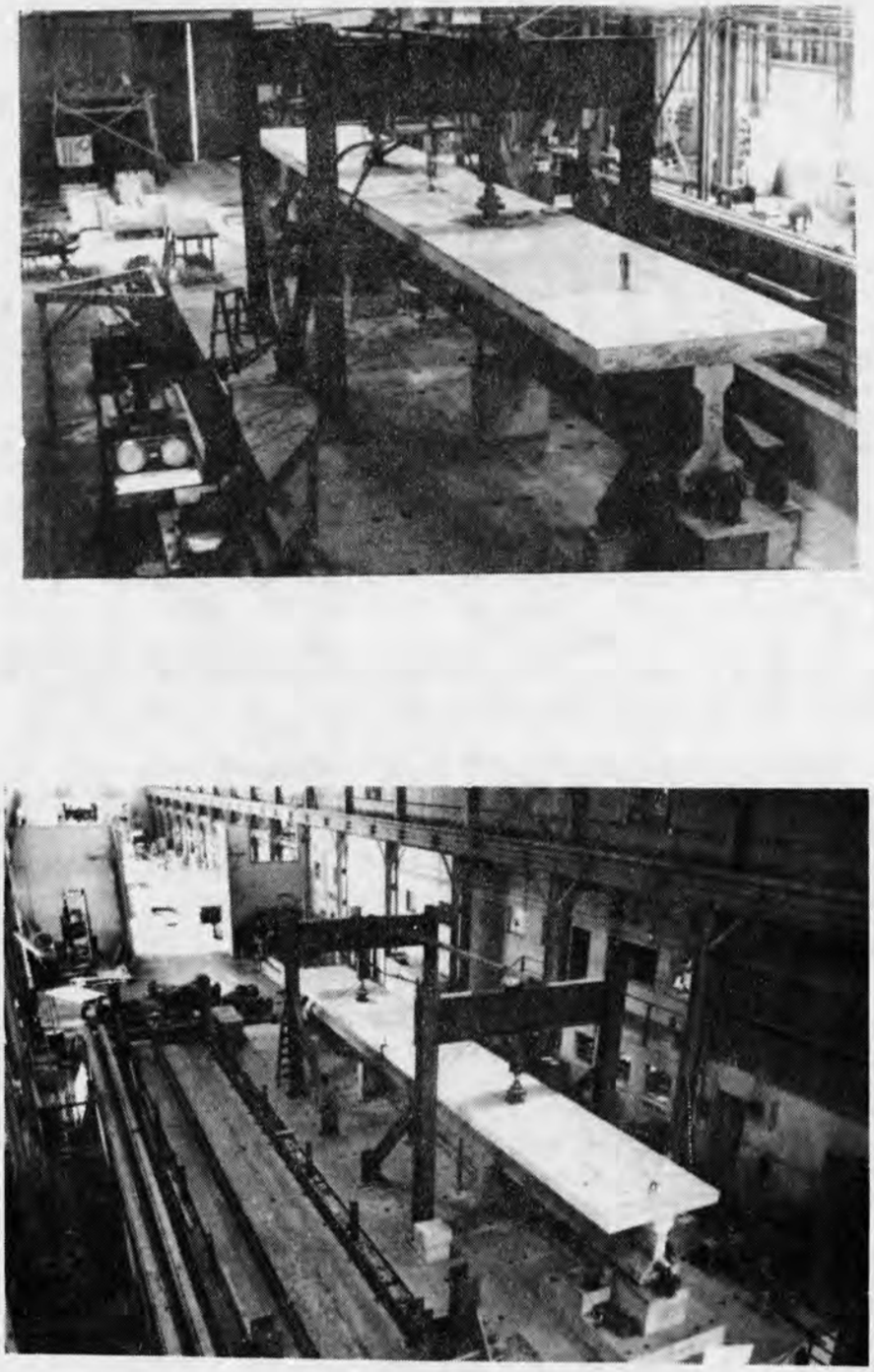

Fig. 3.1 Test setup

C = Texas Type C

16 = 16 straight strands

CP = Confined passive reinforcing steel

5.5 = Maximum nominal concrete stress was $5.5\sqrt{f'_{ct}}$

OL = Occasional overloads

9.43 = Fatigue testing was stopped at 9.43 million cycles

3.2 Fabrication of Texas Type C Girders

The Texas Type C pretensioned girders are shown in Fig. 3.2. The C-16 members, shown in Fig. 3.3, had 16 straight strands. The C-14 member shown in Figs. 3.4 through 3.6 had 10 straight strands and four draped strands. All strands were seven wire, 1/2-in. diameter, Grade 270 stress relieved.

3.2.1 Strand Stressing Procedure and Instrumentation

The initial prestress was carefully measured in the fabrication of the Texas Type C girders. Two to four strands were instrumented with Micro-Measurements EA-06-062AP-120 electrical resistance strain gages. The gages were located on individual wires of the strands and were used to determine the prestress force. Strain measurements were accurate to $\pm$ 10 $\mu\varepsilon$, which is less than 0.2 percent of the total strain. Ram pressure, determined by a pressure transducer and pressure gage, strand elongation, and two load cells (on uninstrumented strands) were used to check the prestress force.

Steps were taken to ensure that all strands were stressed equally. All strands were cut from the same reel with a grinder. Strain gages were installed prior to stressing. To eliminate any difference in initial stress, all strands were dead loaded with 1000 lb weight. The draped strands were pulled down before dead loading. The drape hardware is shown in Fig. 3.7. Both ends of the strands were gripped and restrained with standard chucks. All strands were then tensioned simultaneously (with a 1000 kip ram) in 10 percent increments to approximately 70 percent of their specified ultimate capacity. Specimen C-16-NP-10.5-NO-0.91 was intentionally prestressed to approximately 60 percent F_{pu} to simulate an older girder with increased losses. Table 3.1 shows the initial prestress values for all specimens. The stressing bed is shown in Fig. 3.8. Figures 3.9 and 3.10 show the stressing end of the prestressing bed. Notice the spool of prestressing strand in the lower right corner of Fig. 3.10. The strand was stored

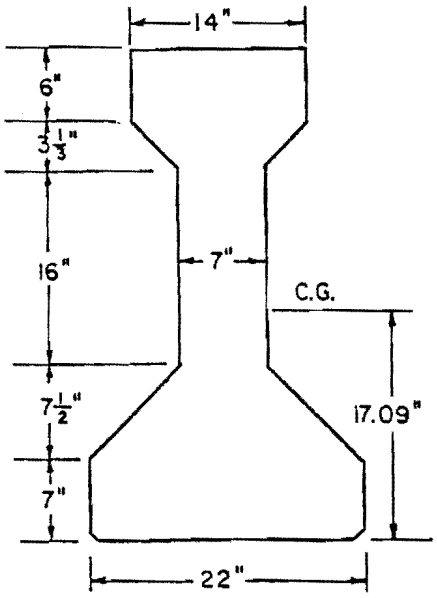

A = 494.9 in^2

Cb = 17.09 in

Ct = 22.91 in

I = 82,602 in^4

Sb = 4833 in^3

St = 3605 in^3

Fig. 3.2 Texas Type C girder properties

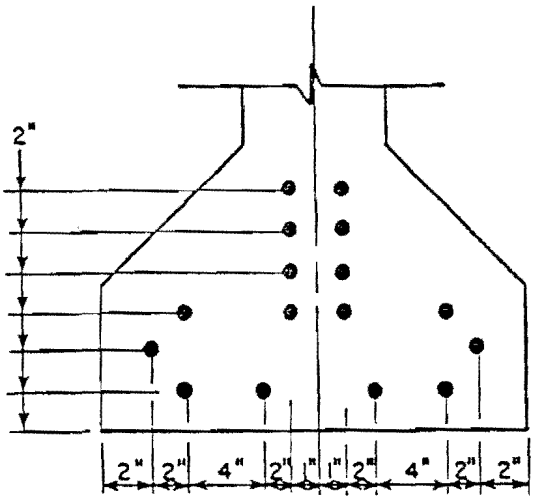

Fig. 3.3 C-16 strand pattern

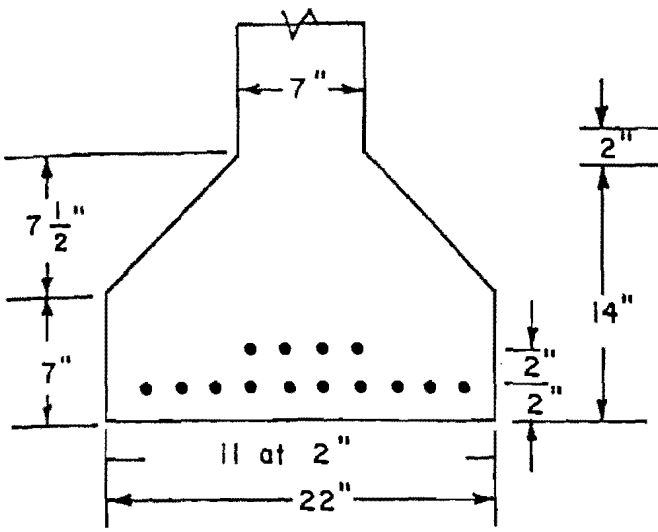

Fig. 3.4

C-14 centerline strand pattern

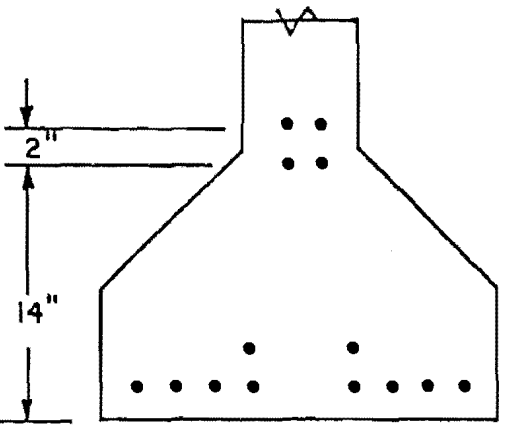

Fig. 3.5

C-14 end strand pattern

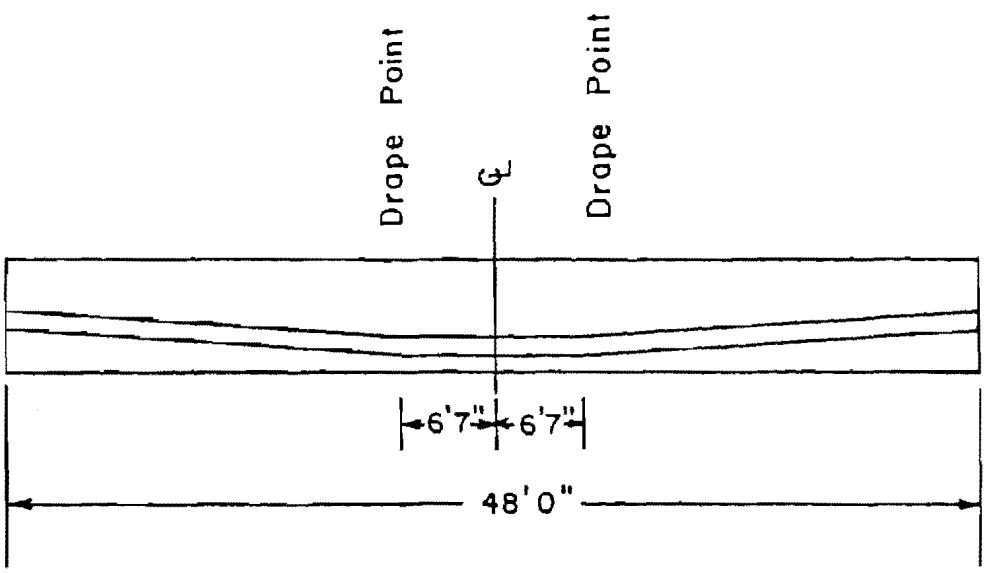

Fig. 3.6 C-14 strand layout

Fig. 3.7 C-14 drape hardware

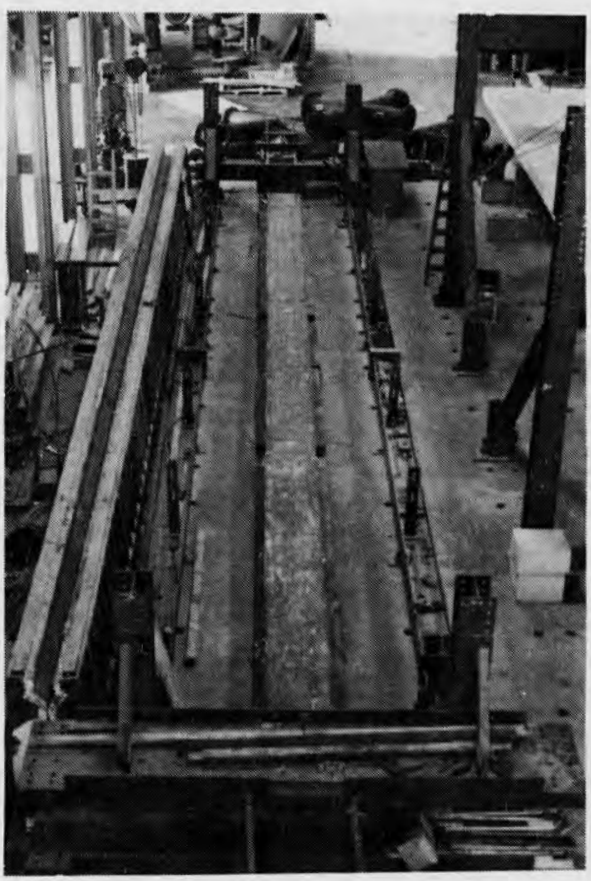

Fig. 3.8 Stressing bed

TABLE 3.1 Initial Prestress for Test Specimens

Specimen	Initial Stress f_{si} (ksi)	Percent f_{pu}	Prestressing Steel Area A_{ps} ($in.^2$)	Initial Force P_2 (kips)
C-16-NP-10.5-NO-0.58	185	68.5	2.45	453
C-16-NP-7.2-OL-1.48	183	67.8	2.45	448
C-16-NP-10.1-NO-0.91	159	58.9	2.45	390
C-16-NP-6.0-NO-1.91	187	69.3	2.45	458
C-14-NP-5.5-OL-2.29	198	73.3	2.14	424
A-22-NP-6.2-OL-2.84	157	62.8	2.40	337
A-22-NP-6.2-NO-5.00	157	62.8	2.40	337
A-22-NP-3.5-OL-5.95(NF)	157	62.8	2.40	337
C-16-UP-8.0-NO-1.73	205	75.9	2.45	502
C-16-CP-7.2-NO-2.54	200	74.0	2.45	490
C-16-CP-5.5-OL-9.43	192	71.1	2.45	470

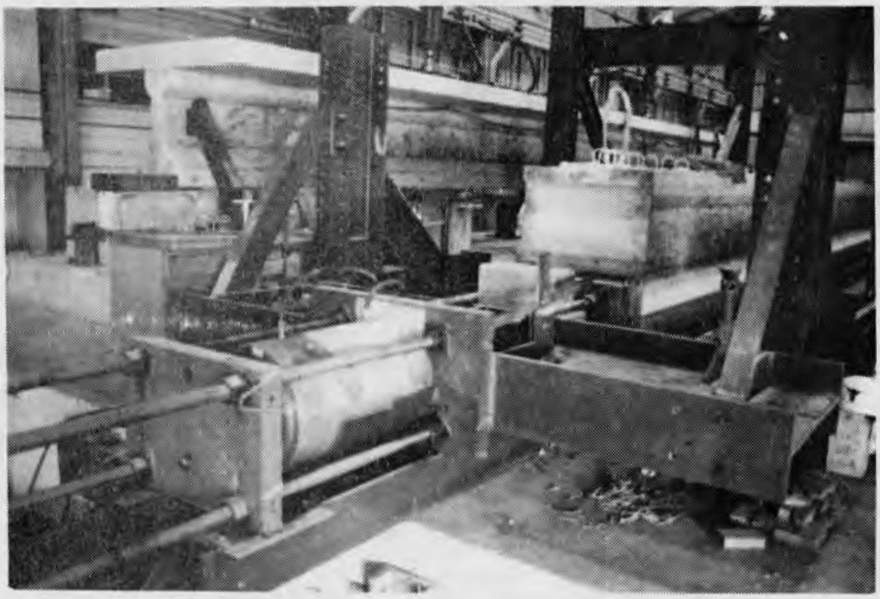

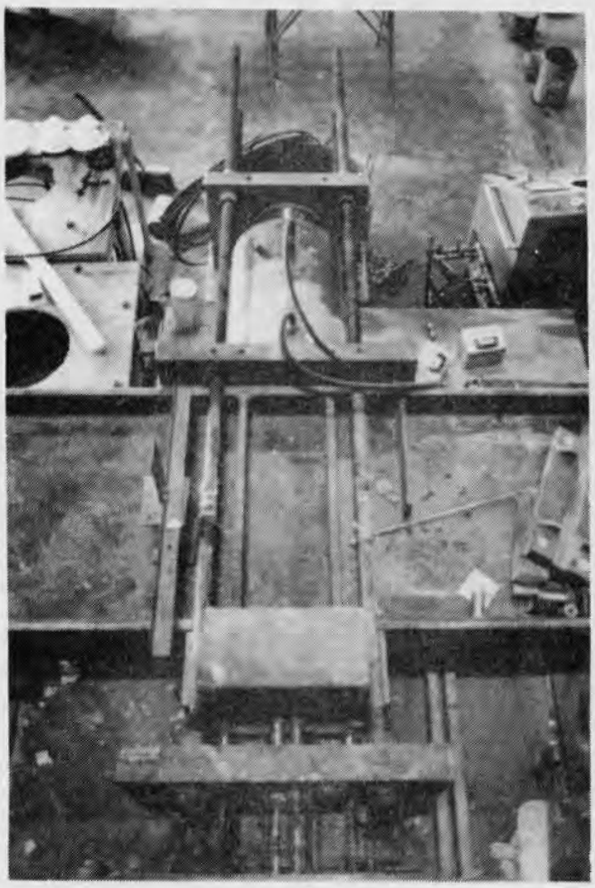

Fig. 3.9

Pretensioning mechanism

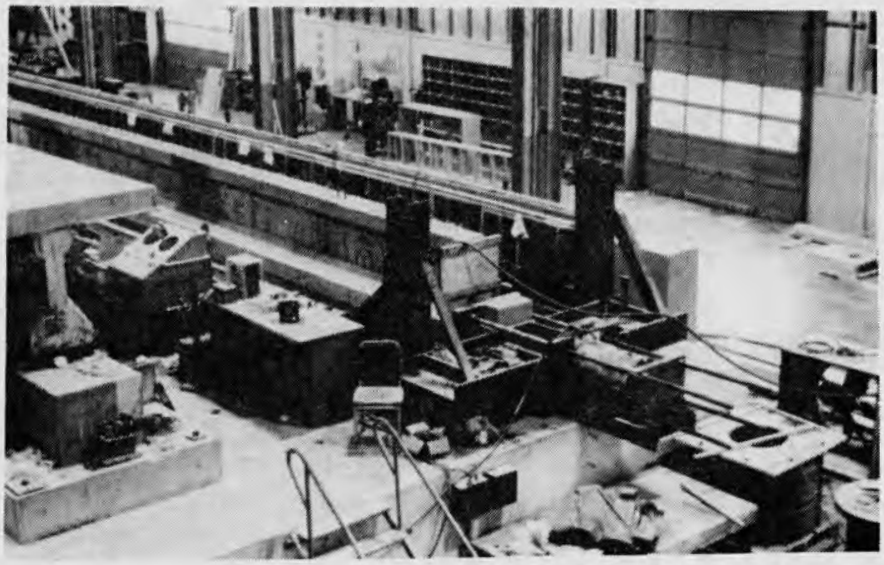

Fig. 3.10 Stressing end of the prestressing bed

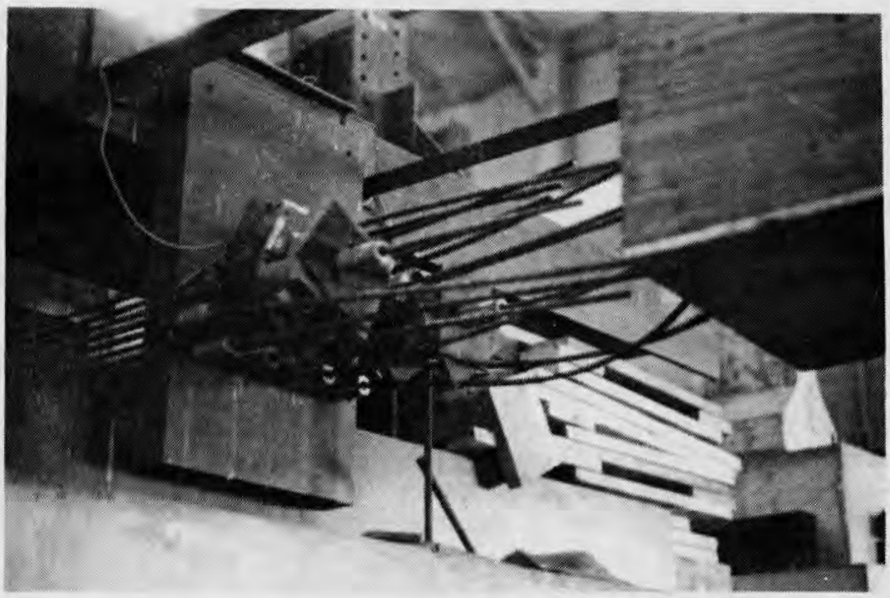

Fig. 3.11 "Dead-end" of the prestressing bed

inside the laboratory to prevent corrosion. Figures 3.11 and 3.12 show the "dead end" of the stressing bed with load cells to monitor load and a dial gage to determine bulk head movement.

Strain gage, pressure, elongation, and load readings were recorded at each 10 percent increment. The entire strand stressing procedure, beginning with application of load by the hydraulic ram, took approximately 50 minutes. After tensioning, the strands were "locked-off" at the stressing end so ram pressure could be relieved. The reinforcing steel cage was then tied.

3.2.2 Shear and Confining Reinforcement

All shear and confining reinforcement conformed to Texas Highway Department drawing Gp-A. The basic shear reinforcement, shown in Fig. 3.13, consisted of number 3 hairpin stirrups spaced at 1'0" on center. Additional shear and confining steel was placed at the ends of the members. Two number 5 longitudinal bars were hung from the transverse number 3 bars (which were attached to the hairpin stirrups) in the upper flange to reduce tensile stresses at release. Instrumentation wires were then attached to the stirrups and longitudinal bars with nylon ties. Beam pickup loops were also installed at this time.

3.2.3 Passive Reinforcement

The conventional reinforcing bars shown in Figs. 3.14 and 3.15 were added to the lower flange of three specimens (indicated by "CP", confined passive reinforcement and "UP", unconfined passive reinforcement) to control crack width, reduce crack spacing, and reduce strand stress range. This steel, which is normally considered as tension steel since it is in the lower flange, actually worked as compression steel in the precompressed region to reduce creep losses. The passive reinforcement was tied along with the shear and confining reinforcement after the strands were stressed. Confining links shown in Fig. 3.15 were added to the specimens designated with "CP" (confined passive reinforcement) to prevent the "compression" steel from buckling. These closed number three links, positioned adjacent to the stirrups at 1'0" spacing, were placed before the strands were stressed. Figure 3.16 shows shear reinforcement and confining links prior to installation of forms. Figure 3.17 shows one girder side form installed.

3.2.4 Placement of Girder Concrete

Ready mix concrete from local suppliers was used for the girders. Before placing the concrete, the strands were retensioned to the desired stress. This was done to reduce relaxation losses which

Fig. 3.12 "Dead-end" of the prestressing bed with load cells and dial gage

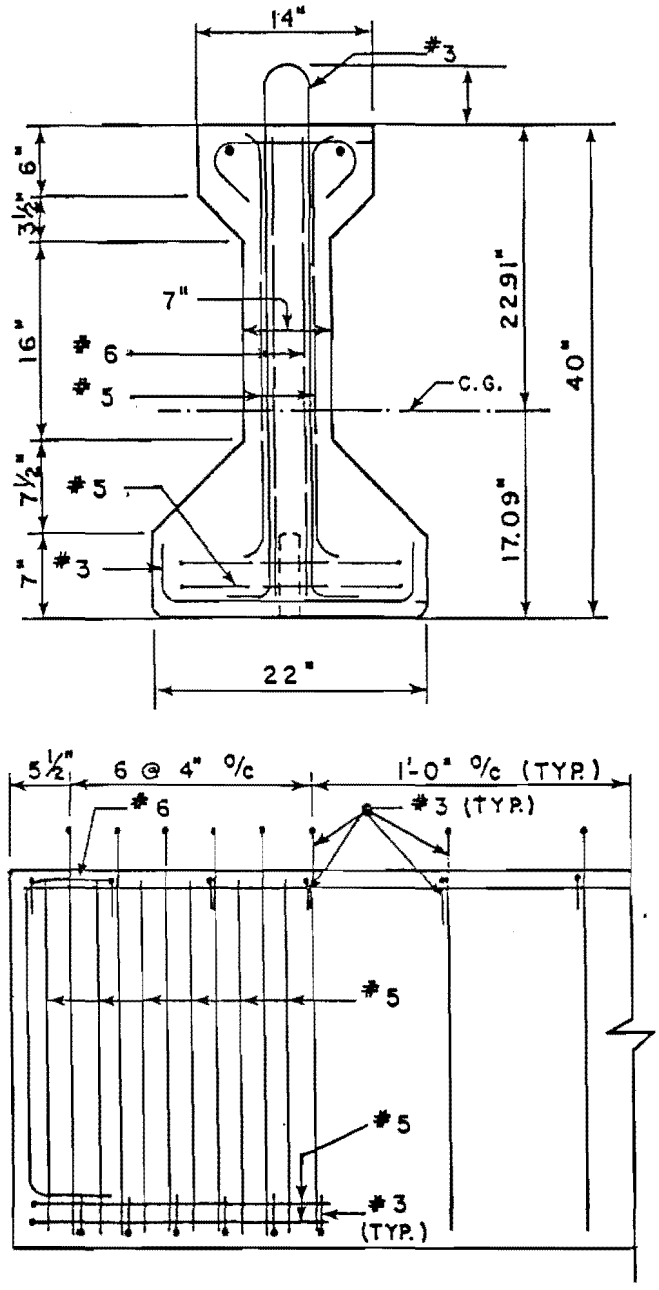

Fig. 3.13 Texas Type C shear and confining reinforcement

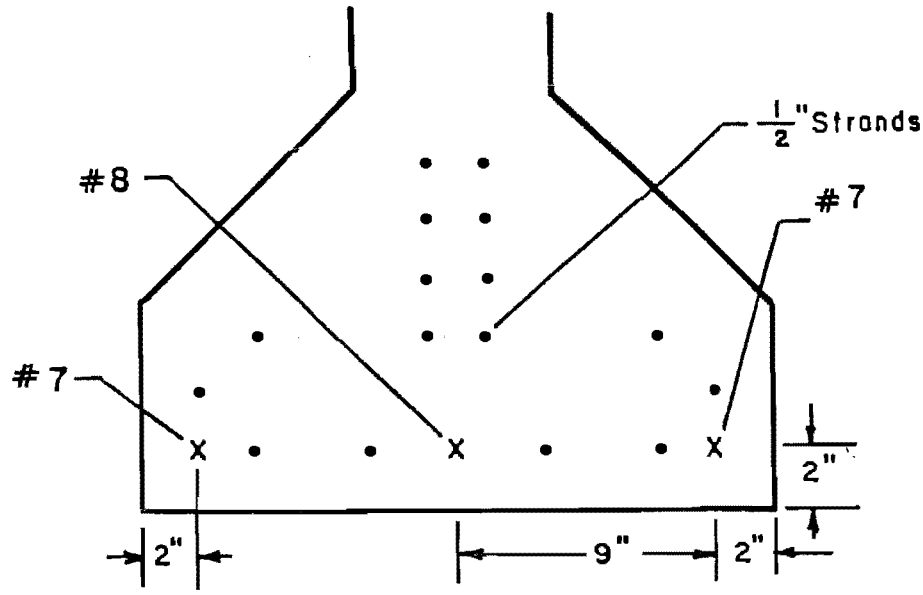

Fig. 3.14 Specimen C-16-UP-8.0-NO-1.73 passive reinforcement layout

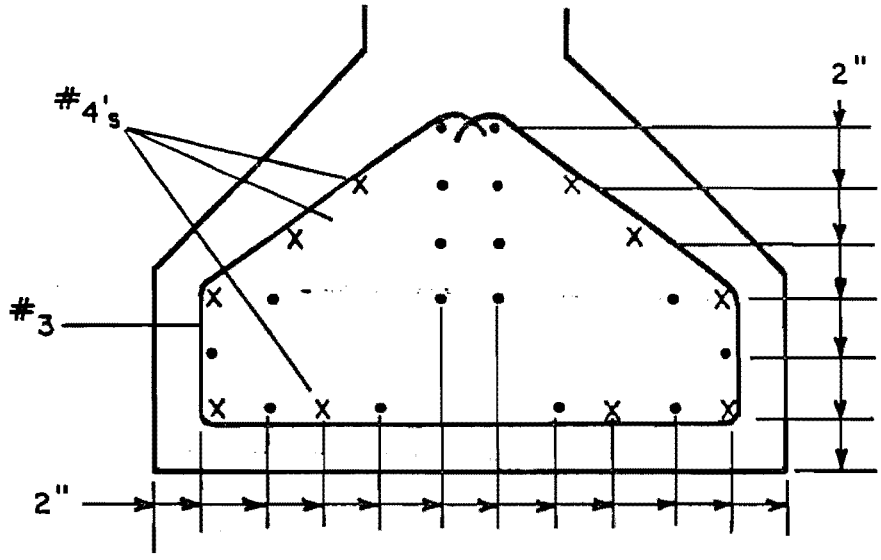

Fig. 3.15 Specimens C-16-CP-7.2-NO-2.54 and C-16-CP-5.5-OL-9.43 passive and confining reinforcement layout

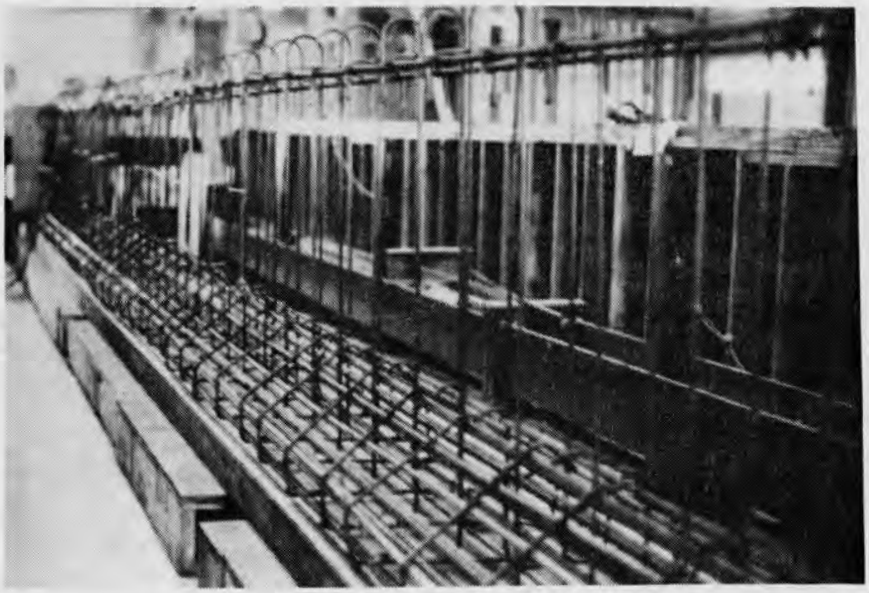

Fig. 3.16 Shear reinforcement and confining links

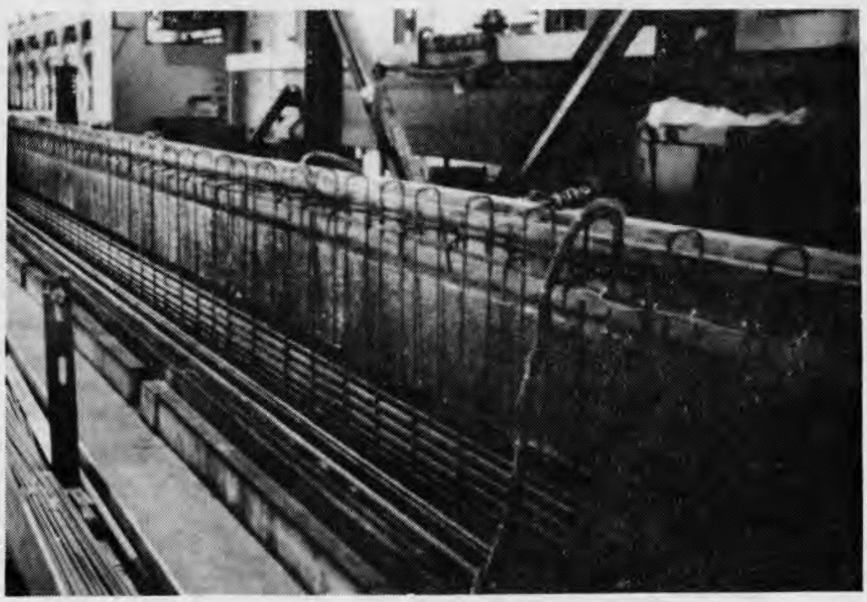

Fig. 3.17 Shear reinforcement and one girder form installed

occurred in the week the steel was tied and the forms were set. Once the ready mix truck was onsite, the slump was checked according to ASTM procedures. A slump of approximately 5 in. was desirable. Water was added as needed and the slump was rechecked. The concrete was placed in three lifts with a 1/2 cu. yd. bucket. Flexible shaft vibrators were used to consolidate each lift. The top surface was roughened to the 1/4 in. ACI Building Code requirement [22], Section 17.5.2.3, for shear transfer. AASHTO Specifications Section 1.6.14(B) through (C) [8] only call for a clean, intentionally roughened surface. Figure 3.18 shows the roughened surface.

Twelve to fifteen 6x12 cylinders were cast according to ASTM procedures. The cylinders, like the girder, were covered with polyethylene sheets for curing. The cylinder molds were removed the same day as the girder forms. The compression specimens were capped with a sulphur compound. A cylinder strength of 4000 psi was required before release of prestress force.

3.2.5 Release of Prestress Force

The prestress force was released gradually. After the desired cylinder strength was attained, the prestress force was applied to the member by slowly releasing the ram pressure. This controlled release is recommended by ACI Committee 443 [24], Concrete Bridge Structures. The strands were then cut with a grinder.

3.3 Fabrication of AASHTO-PCI Type II Girders

The three AASHTO-PCI Type II girders are shown in Fig. 3.19. These members, designated by the prefix A-22, had 22-7/16 in. diameter, Grade 250, seven wire stress relieved strands. Ten of these strands were draped as shown in Figs. 3.20 and 3.21. The girders were cast simultaneously in a commercial long line stressing bed.

3.3.1 Strand Stressing Procedure and Instrumentation

Three methods were used to monitor the initial prestress force. Electrical resistance strain gages were applied to individual wires on two strands after the strands were tensioned to approximately 1000 lbs. The strands were then tensioned to 70 percent of their specified ultimate capacity. Strand elongation and ram hydraulic pressure were used to determine the prestress force. Because of the accuracy of the strain gages and the lack of well documented elongation and pressure readings, strain gage readings were used to determine the actual initial prestress for testing purposes.

Fig. 3.18 Roughened girder surface for shear transfer

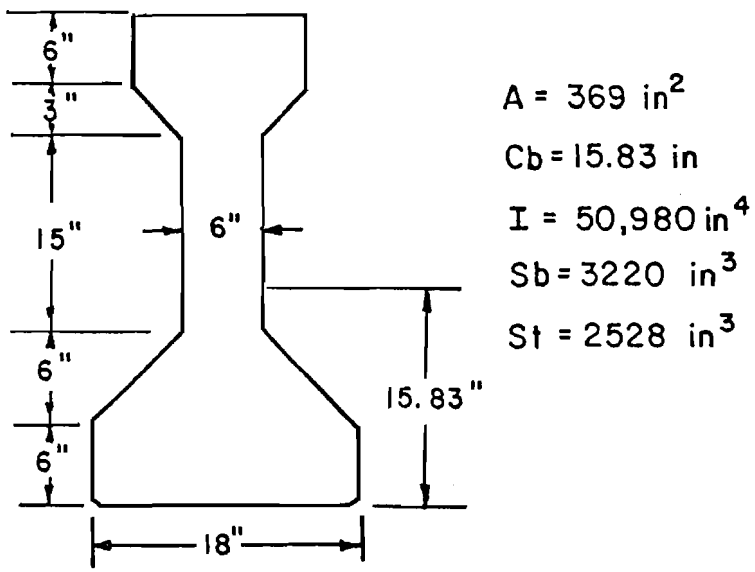

Fig. 3.19 AASHTO-PCI Type II girder properties

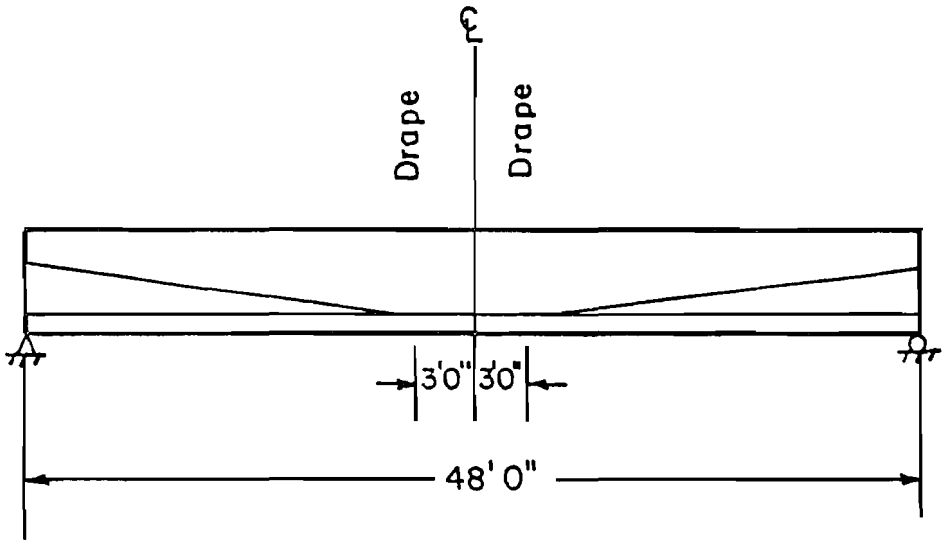

Fig. 3.20 A-22 strand layout

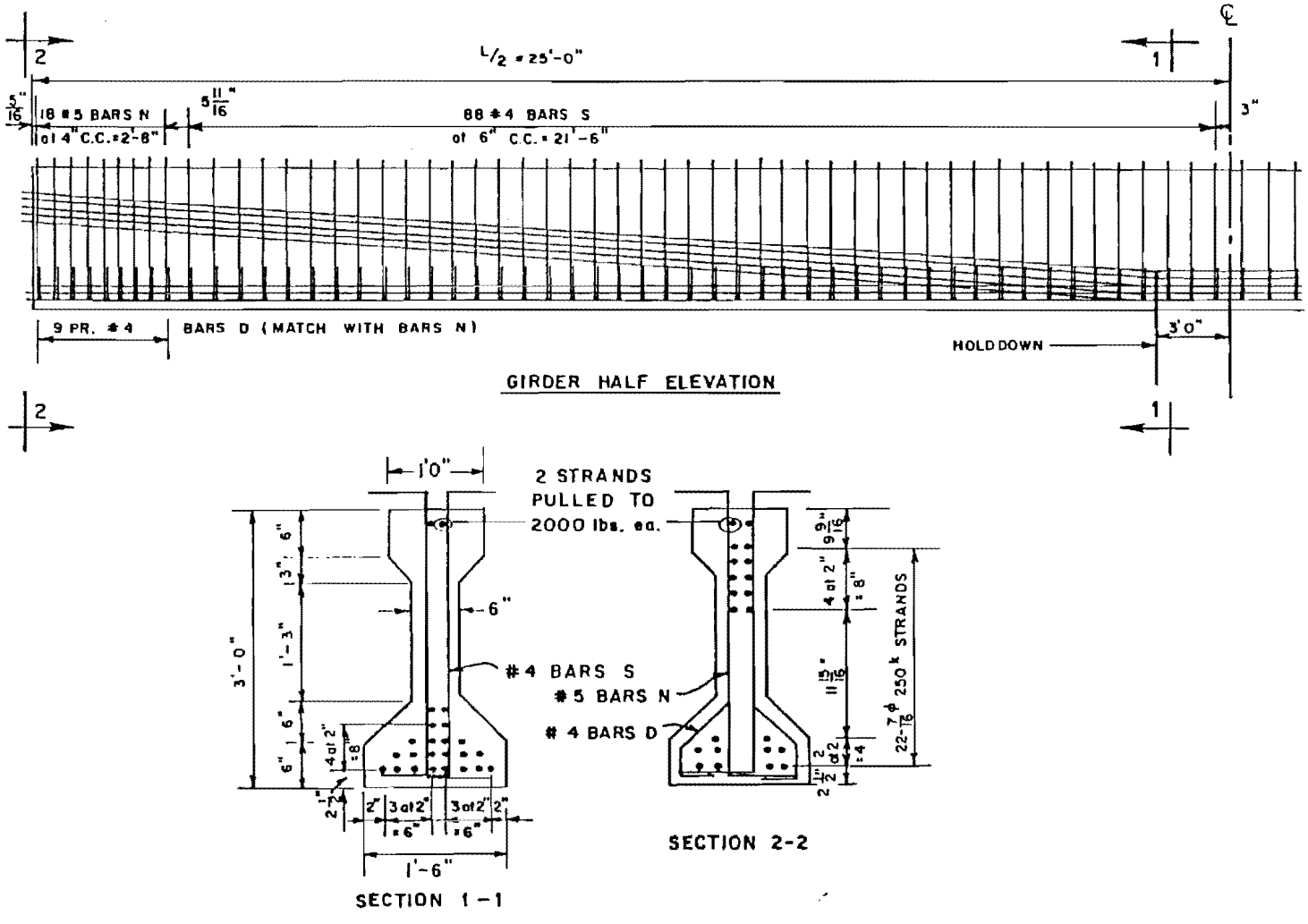

Fig. 3.21 A-22 centerline and end sections

3.3.2 Shear and Confining Reinforcement

All shear and confining reinforcement was Grade 40 and conformed to PCPC, Inc., drawing 201-S-2. Figure 3.21 shows this reinforcement. The basic shear reinforcement consisted of number 4 stirrups spaced at 6 in. on center. Two 7/16 in. diameter, Grade 250 strands stressed to 2000 lbs each were used in the top flange to reduce tensile stresses at release.

3.3.3 Release of Prestress Force

The prestress force was released suddenly after the concrete cured overnight. Steel forms were removed prior to release. Compression cylinder strength was checked by plant personnel. The actual strength was above the required 4000 psi strength for release. The prestress force was then applied to the members as the strands were heated with a cutting torch.

3.4 Slab Construction

Unshored cast-in-place slabs were added to all girders to form the composite sections shown in Figs. 3.22 and 3.23. The I-beam was moved to the loading frame where plywood forms were installed, as shown in Fig. 3.24. Slab steel was placed, as shown in Fig. 3.25, and the concrete was cast. Flexible shaft vibrators were used to consolidate the concrete which was placed in a single lift. Nine to twelve cylinders were cast according to ASTM procedures. The cylinders, like the slab, were covered with polyethylene for curing. The cylinder molds were removed the same day as the slab forms.

After the slab was cast on specimen A-22-NP-3.5-OL-5.95 (NF), a narrow section at midspan was trowelled to facilitate application of concrete strain gages. Five SR-4 A-9-5 electrical resistance strain gages were installed, as shown in Fig. 3.26, prior to testing to determine the effective slab width.

3.5 Plywood Girder and Slab Forms

Reusable plywood forms were used for Texas Type-C girders and all deck slabs. They were constructed of 3/4 in. plywood with 2x4, 2x6, and 2x12 in. ribs. Several coats of varnish were applied to the forms for protection.

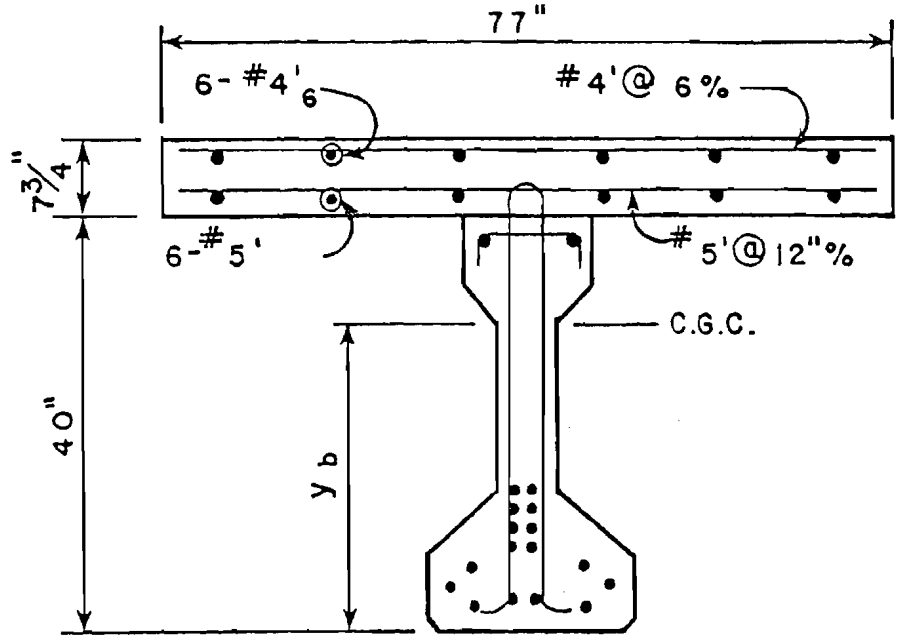

Fig. 3.22 Texas Type C slab reinforcement

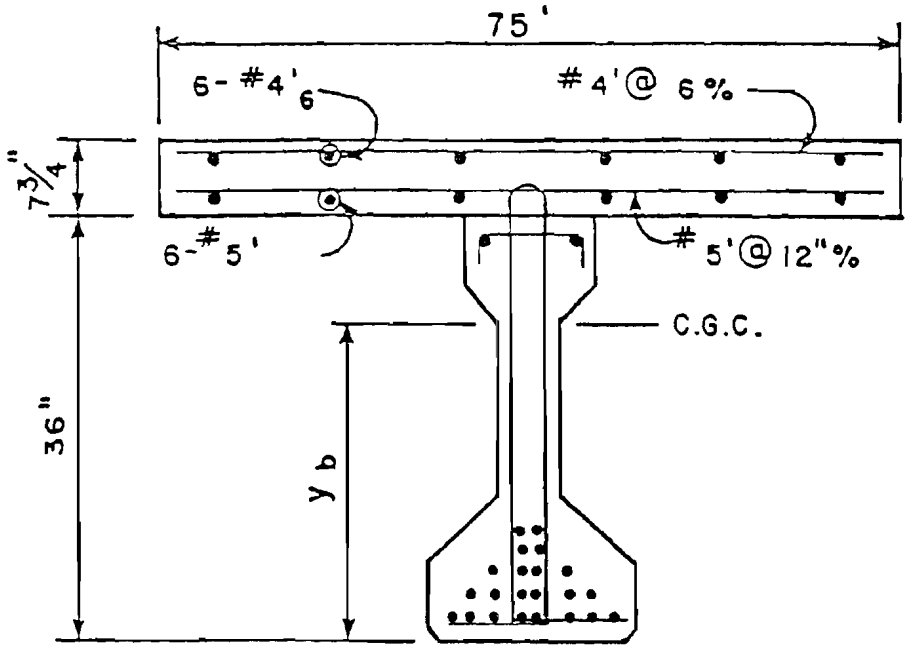

Fig. 3.23 AASHTO-PCI Type II slab reinforcement

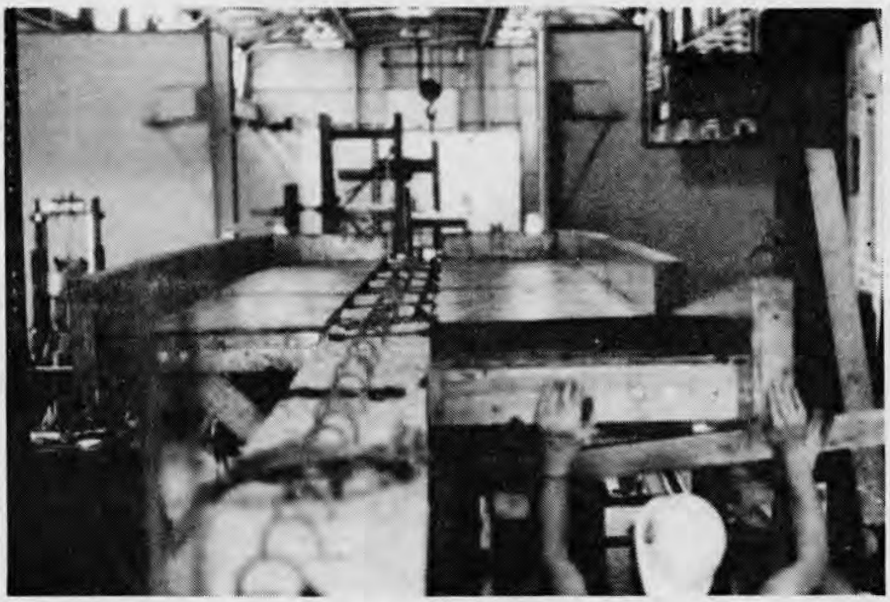

Fig. 3.24 Slab forms

Fig. 3.25 Slab reinforcement

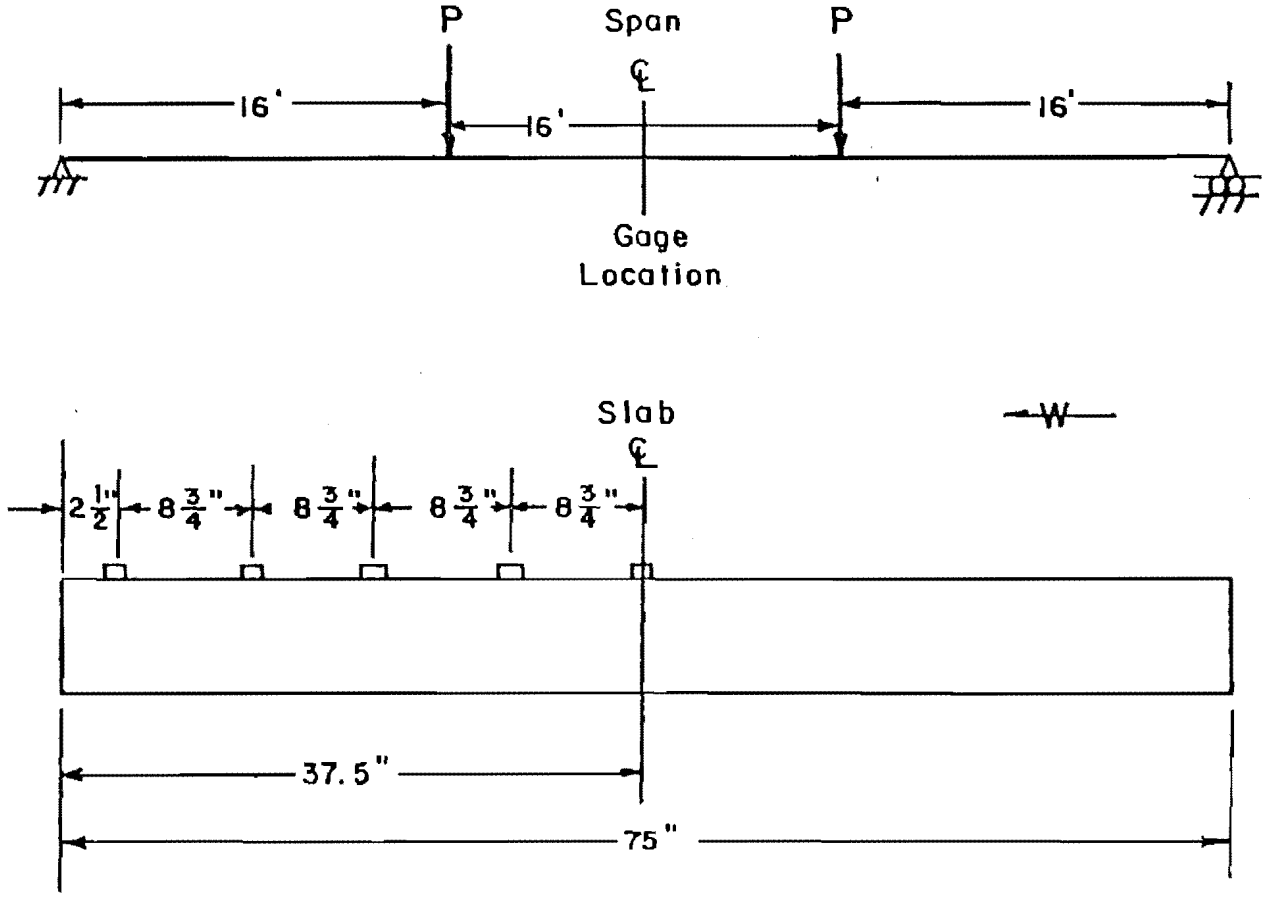

Fig. 3.26 Slab strain gage locations for Specimen A-22-NP-3.5-OL-5.95 (NF)

3.6 Materials

3.6.1 Concrete

The concrete mixes were designed using TDHPT Standard Specifications. Concrete used for the beams was Class H. Slab concrete was Class C. Both mixes had a minimum cement factor of six sacks per cubic yard. The concrete consisted of Type I portland cement, Colorado River sand and crushed limestone coarse aggregate. The maximum size aggregate was one inch. Table 3.2 gives the mix proportions and concrete strengths for all girders. The initial strength in Table 3.2 is the concrete compressive strength at the time the prestress force was applied to the girders or the time slab forms were removed. The origin of the materials used in the Louisiana Specimens was unknown.

3.6.2 Prestressing Steel

One-half inch diameter, Grade 270, seven wire strand was used in the Texas Type C specimens. This strand was stress relieved and was manufactured under ASTM Specification A-416-74. All specimens were fabricated from a single 12,000 ft spool. The spool was stored inside the laboratory to prevent corrosion.

Seven-sixteenths inch Grade 250 seven wire strand was used in the AASHTO Type II specimens. This strand was also stress relieved and was manufactured under ASTM Specification A-416-80.

Stress versus strain curves were provided by the manufacturer for both strand types. Laboratory tests confirmed these values. The strand modulus of elasticity for the 1/2 in. strand was 29,000 ksi; for the 7/16 in. strand it was 28,600 ksi.

To determine the wire modulus, which was needed to interpret strain readings, strain gages were applied to specimens which were loaded in a testing machine. The 1/2 in. diameter wire modulus was 30,500 ksi. It is compared to the strand modulus in Fig. 3.27. The 7/16 in. diameter wire modulus was 29,100 ksi. The wire and strand modulus for this strand is shown in Fig. 3.28.

3.6.3 Reinforcing Steel

The reinforcement used for the Texas Type C beams and all slabs was as specified in THPT drawing Gp-A. All bars were ASTM A615 Grade 60 and were purchased from a local supplier. The reinforcement used in the three AASHTO specimens was as specified on PCPC drawing 201-S-2. This reinforcing steel was ASTM A615, Grade 40.

TABLE 3.2 Concrete Properties for Test Specimens

Specimen (g)=girder (d)=deck	Weights per Cubic Yard (lbs) Coarse Agg.	Fine Agg.	Cement	Water (gal)	Slump (in.)	W/C Ratio	Cement Factor (sacks)	Specimen Strength (psi) Initial (days)	28 Day	Test (days)	Flexural
C-16-NP-10.5											
-NO-0.58 (g)	1810	1160	677	256 (31)	8.0	0.396	7.2	4300 (14)	5300	5350 (91)	NA
(d)	2050	1050	564	240 (29)	4.0	0.443	6.0	NA	5500	5780 (36)	NA
C-16-NP-7.2											
-OL-1.48 (g)	1905	1205	580	216 (26)	6.0	0.388	6.2	4800 (7)	5970	6350 (167)	NA
(d)	2100	1100	564	240 (29)	3.0	0.443	6.0	NA	4430	4200 (16)	NA
C-16-NP-10.1											
-NO-0.91 (g)	1900	1140	640	228 (27)	6.0	0.371	6.8	4700 (14)	5780	6610* (84)	NA
(d)	1950	1200	564	240 (29)	6.0	0.443	6.0	NA	3750	2800* (8)	NA
C-16-NP-6.0											
-NO-1.19 (g)	2028	1217	679	236 (28)	3.5	0.348	7.2	4950 (6)	6690	6870 (35)	NA
(d)	1984	1330	560	247 (30)	4.0	0.441	6.0	4430 (5)	5910	4950 (7)	NA

TABLE 3.2 Concrete Properties for Test Specimens (continued)

Specimen (g)=girder (d)=deck	Weights per Cubic Yard (lbs) Coarse Agg.	Fine Agg.	Cement	Water (gal)	Slump (in.)	W/C Ratio	Cement Factor (sacks)	Specimen Strength (psi) Initial (days)	28 Day	Test (days)	Flexural
C-14-NP-5.5											
-OL-2.29 (g)	1990	1200	667	261 (31)	6.0	0.391	7.1	4500 (6)	5600	5791* (55)	460
(d)	2390	856	600	264 (32)	8.0	0.440	6.4	4370 (8)	5600	5500* (23)	NA
A-22-NP-6.2											
-OL-2.84 (g)	2108	1118	705	197 (24)	4.5	0.279	7.5	4032 (1)	6880*	7050 (455)	NA
(d)	2180	990	652	273 (33)	5.5	0.419	6.9	4950 (6)	5300	5050* (8)	NA
A-22-NP-6.2											
-NO-5.00 (g)	2018	1118	705	197 (24)	4.5	0.279	7.5	4032 (1)	6880*	7050 (490)	NA
(d)	2200	1000	658	262 (31)	6.0	0.398	7.0	4820 (7)	5750	5170 (14)	NA
A-22-NP-3.5											
-OL-5.95(NF)											
(g)	2018	1118	705	197 (24)	4.5	0.279	7.5	4032 (1)	6880*	7050 (672)	NA
(d)	2023	1355	570	219 (26)	8.0	0.384	6.1	4400 (5)	6400	5540 (11)	NA

TABLE 3.2 Concrete Properties for Test Specimens (continued)

Specimen (g)=girder (d)=deck	Weights per Cubic Yard (lbs) Coarse Agg.	Fine Agg.	Cement	Water (gal)	Slump (in.)	W/C Ratio	Cement Factor (sacks)	Specimen Strength (psi) Initial (days)	28 Day	Test (days)	Flexural
C-16-UP-8.0											
-NO-1.73 (g)	2040	1220	683	228 (27)	7.0	0.334	7.3	5730 (13)	5800	5800 (30)	653
(d)	2050	1080	644	291 (35)	8.0	0.452	6.9	2750 (5)	3630	3000* (8)	NA
C-16-CP-7.2											
-NO-2.54 (g)	2040	1220	682	228 (33)	6.5	0.334	7.3	6330 (3)	7100	7200 (15)	592
(d)	1968	1181	659	278 (33)	8.0	0.422	7.0	4097 (3)	5435	4900* (15)	NA
C-16-CP-5.5											
-OL-9.43 (g)	2006	1204	672	251 (30)	5.0	0.374	7.2	5210 (11)	5840	5600 (24)	NA
(d)	2021	1354	570	220 (26)	6.5	0.386	6.1	1310 (1)	4400	3550 (8)	NA

* Calculated value

NA - Not Available

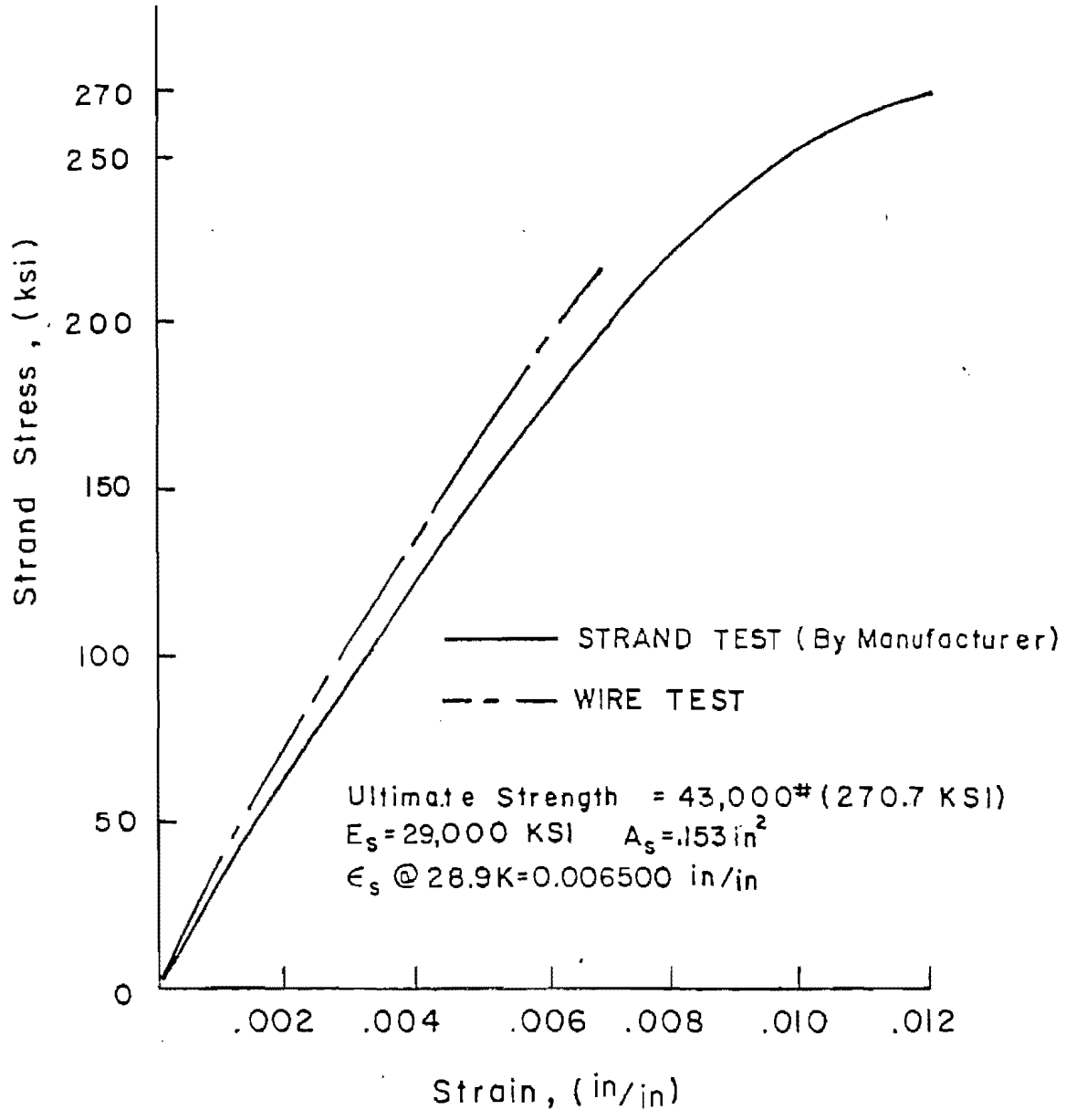

Fig. 3.27 Stress versus strain curves for the prestressing steel used in the Type C specimens

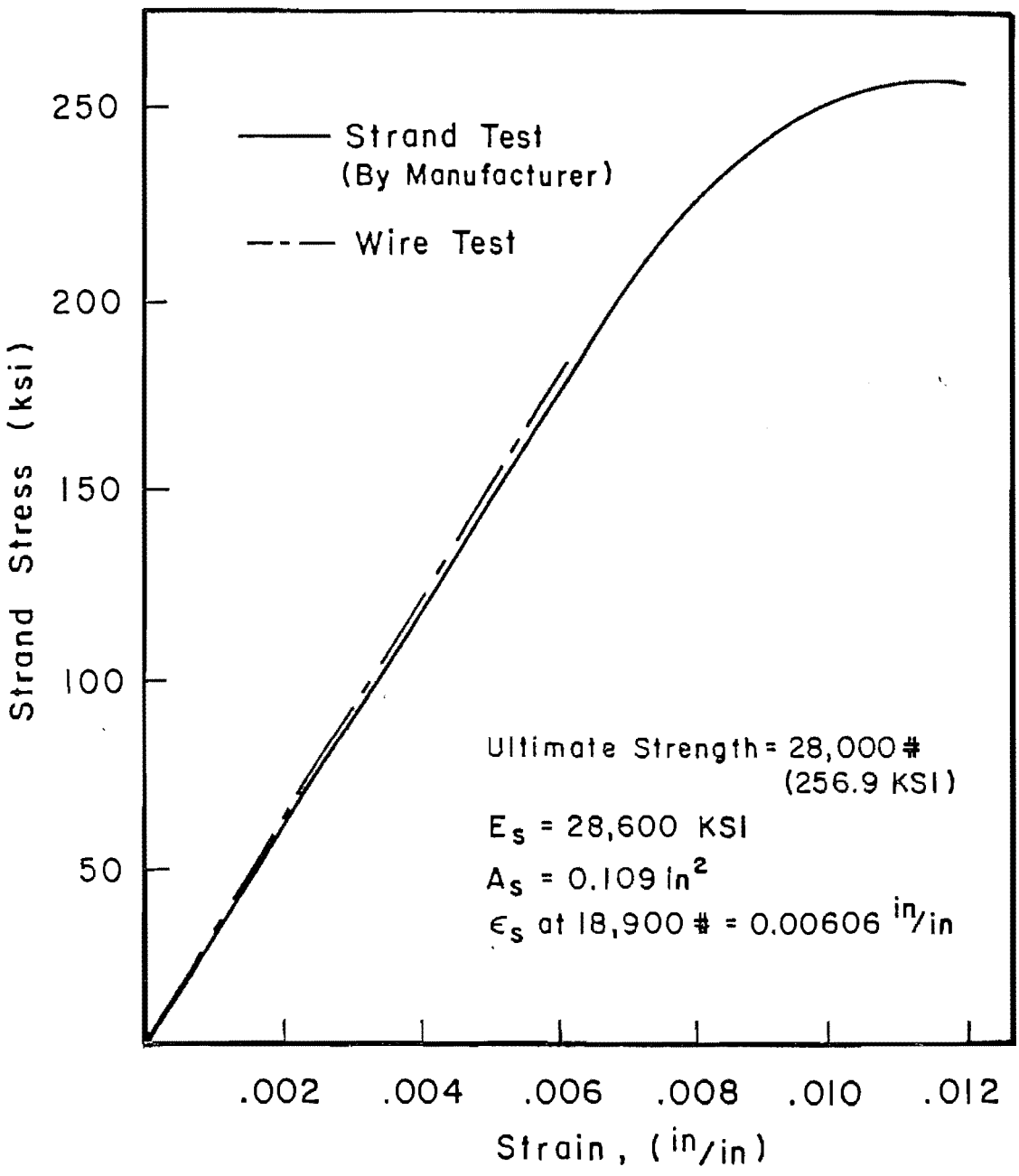

Fig. 3.28 Stress versus strain curves for the prestressing steel used in the AASHTO-PCI Type II specimens

3.7 Instrumentation for Static and Fatigue Testing

3.7.1 Concrete Instrumentation

Demec mechanical strain gages were used to measure concrete strain and crack opening width. Demec points were installed on the lower flange and nine locations prior to release of the prestressing force. The distances between the points were read, using a 6 in. Demec gage, before and after release to determine the effective prestress force. Demec points were also placed on both sides of selected flexural cracks after they developed. The points were read with a 2-in. gage to measure crack opening displacement. The strain indicated by the Demec gage was multiplied by the 2 in. gage length to determine crack widths. It was assumed that the concrete strain adjacent to the crack was negligible compared to the crack width. A 2-in. potentiometer was also installed across selected cracks to monitor static and dynamic crack openings. Figure 3.29 shows 2 and 6 in. Demec points.

Concrete strain indicators, as shown in Fig. 2.30 and 2.31, consisted of a 1/2 in. diameter aluminum bar instrumented with a strain gage. A washer and nut were placed on the ends of each bar. The bars were embedded in the center of the lower flange, at the level of the bottom layer of prestressing steel. The washer and nut assemblies ensured that the bar's strain was compatible with the adjacent concrete.

3.7.2 Deflection Measurements

Deflection was measured using three separate devices. Mechanical dial gages were located at the centerline, load points, and three feet from the ends of the specimen. Transit points were located at the centerline and at quarter points of the span. A fixed benchmark was used so all transit reading could be compared. A potentiometer was permanently attached at the centerline of several specimens to determine permanent set (deflection with zero load) at various stages of fatigue loading. Figure 3.32 shows a dial gage, a permanently fixed potentiometer, a 2-in. potentiometer for static tests and a limit switch to stop fatigue testing when the centerline deflection increases.

3.7.3 Data Acquisition

A strain indicator and switch and balance boxes were used to read strain gages on the first three specimens. An Acurex Autodata Ten/10 electronic scanner was used on all other tests. A Nova Three was used to reduce the data from the Acurex.

A Vishay 2310 four channel power supply/amplifier was used for load cells, potentiometers, and selected strain gages during static and fatigue testing. The voltages were read using an MTS Model 464 peak

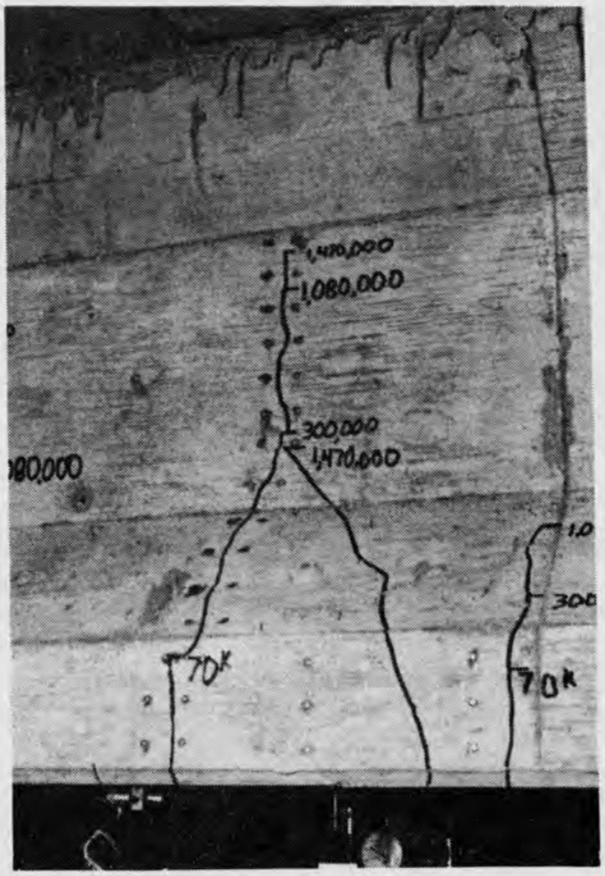

Fig. 3.29 Two and six in. Demec points and an instrumented flexural crack

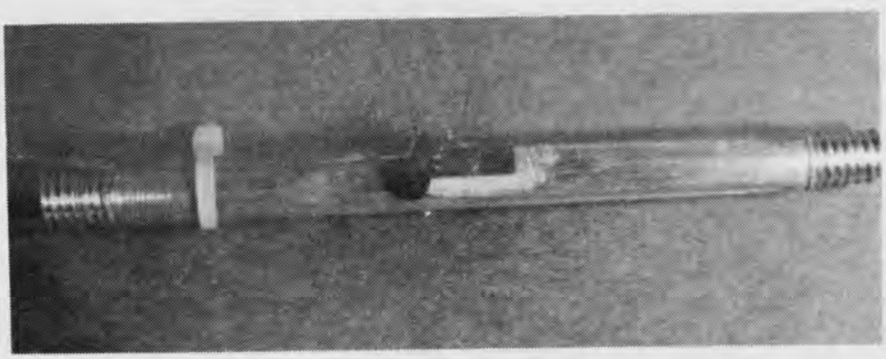

Fig. 3.30 Instrumented aluminum bar used to determine concrete strain

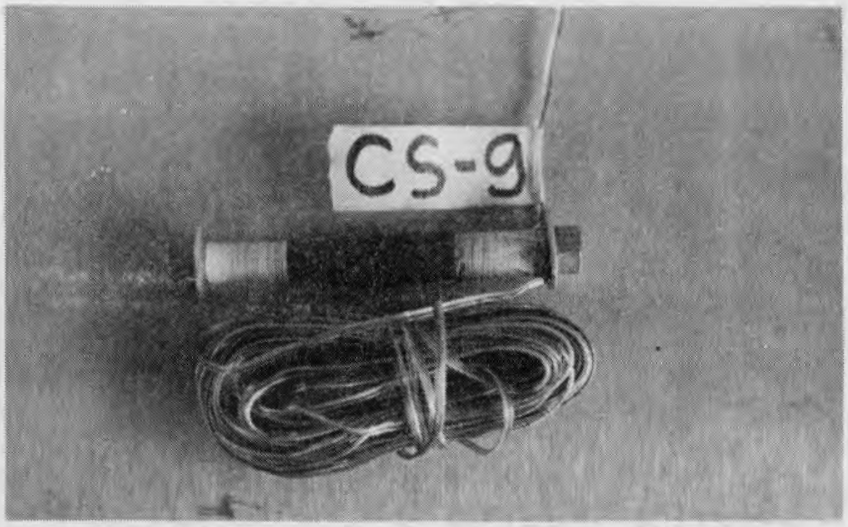

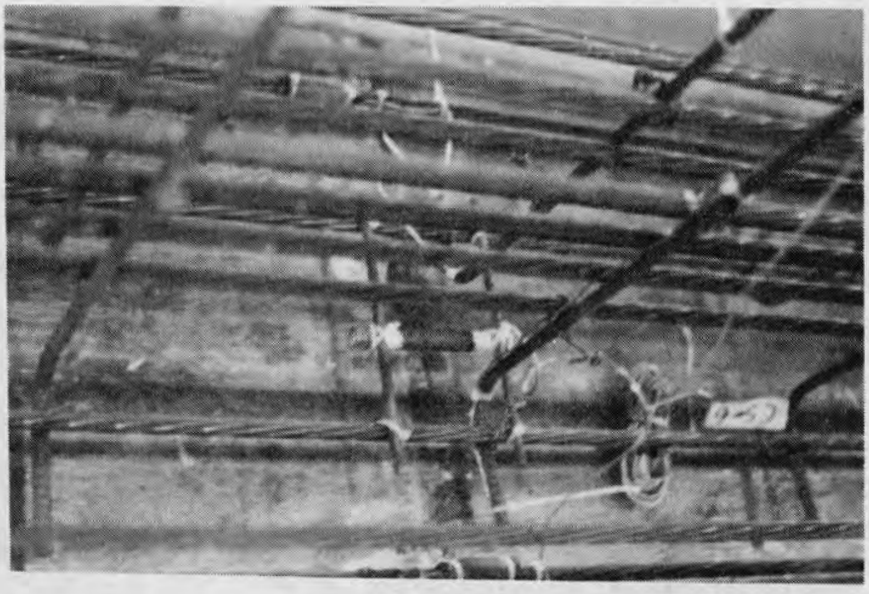

Fig. 3.31 Concrete strain indicators

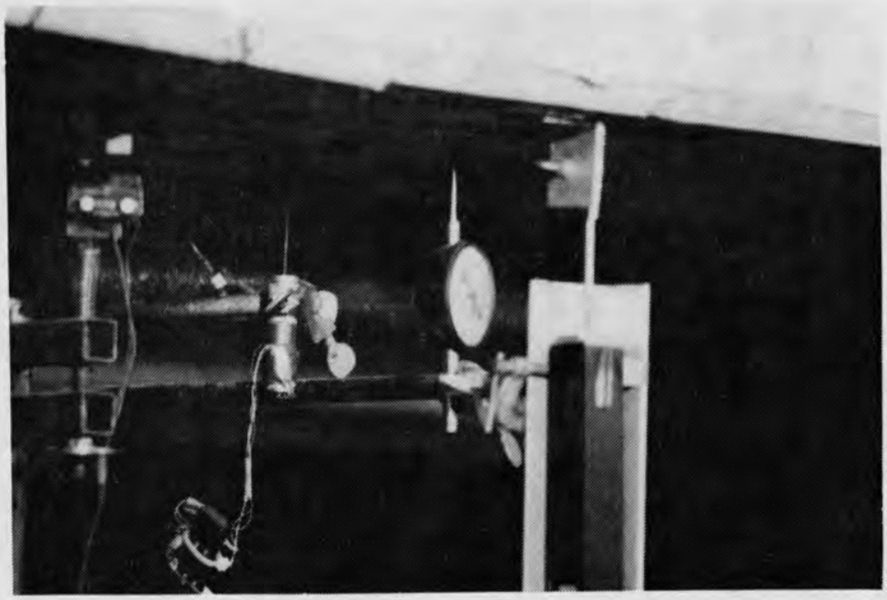

Fig. 3.32 Dial gage and linear potentiometers

Fig. 3.33 Test setup; pulsator pump and pressure gages, plotters, power supply, peak detector, and computer terminal

detector. Several Houston Instruments Model 2000 plotters were also used. The electronic system made it possible to measure load, strain, deflection, and crack opening width during static and fatigue testing. Figure 3.33 shows the test setup.

3.8 Testing Bed and Hydraulic System

3.8.1 Testing Bed

The testing frame, shown in Fig. 3.1, consisted of four steel columns and two beams to form two bents. Diagonal braces, to the laboratory floor, stabilized the columns. The specimens were supported off the test floor by reinforced concrete pedestals. The specimens rested on 20x9x1 in., 70 Duro hardness, neoprene pads. Lateral restraint for the specimens was provided by four knee braces at the ends of the member. Hand tightened springs prevented longitudinal movement. A 1-in. neoprene pad for fatigue tests and a 5-in. pad for ultimate tests are shown in Fig. 3.34.

3.8.2 Hydraulic System

A Riehle Los pulsator pump was used for static and fatigue testing. Two 150 kip single acting Miller rams were used. The oil level was maintained on the unpressurized side to prevent damage to the rams during loading.

The fatigue load range was obtained by adjusting the piston stroke on the pulsator pump. The loads were monitored using load cells mounted under each loading ram. Figure 3.35 shows the ram and load cell assembly. The top connection was pinned, and the bottom assembly included a spherical head to allow only vertical loading. The load cell is between the spherical head and the ram piston. Loads were read dynamically with a peak detector. As the specimen softened, a larger deflection was required to achieve the desired load. The dynamic stroke had to be increased to maintain the load range. Basic load control was used throughout the fatigue tests to maintain a constant load range by frequent adjustment of the pulsator pump's stroke as the girder softened.

3.9 Test Procedure

3.9.1 Determination of Prestress Losses

The effective prestress force at the time of testing must be known to determine the effective concrete tensile stress range. The initial force was determined using strand strain gages and was checked using ram pressure, elongation, and strand load determined by load

Fig. 3.34 One and five in. neoprene pads

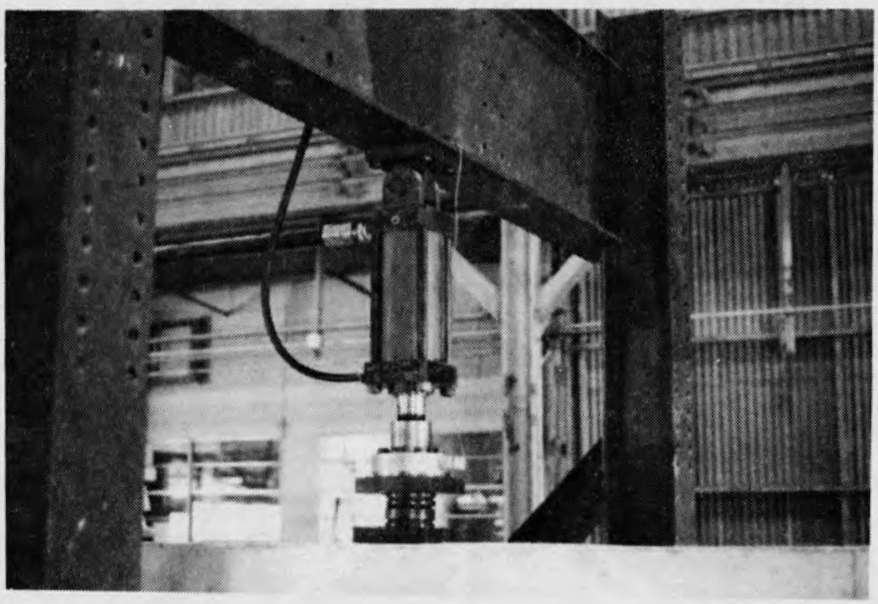

Fig. 3.35 Loading ram with upper pinned connection and lower spherical head and load cell assembly

cells. At release and after, Demec gages were used on several specimens to monitor the concrete strains as an indication of the state of stress in the precompressed zones.

In all cases the effective prestress force was not known precisely. All specimens except A-22-NP-6.2-NO-5.0 were cracked prior to fatigue loading. This allowed a reasonable determination of the effective prestress. Once the section is cracked, the load versus deflection, the strand strain at a crack, the concrete strain at a crack, and the crack opening versus load plots deviate from linear behavior when the extreme fibers experience tension. The deviation is not sudden, but gradual. It usually occurs over a 2 to 5 kip load increment. Because of this transition, determination of the zero tension point (P_o, the load at which the extreme precompressed tension fibers experienced tension) required judgment. Figures 3.36 through 3.38 show the zero tension load as determined from load versus deflection, load versus wire strain, and load versus concrete strain plots. A time dependent analysis program for prestressed concrete developed by Suttikan [85] was used to assist in the determination of the theoretical force. The input included, among other things, concrete properties to determine creep and shrinkage effects, strand properties to determine relaxation, and days to release and loading to determine loading effects.

3.9.2 Static Tests.

Before fatigue testing and at various intervals during fatigue testing, static tests were performed. Deflections, crack widths, and concrete and steel strains were monitored during these static tests.

3.9.2.1 Initial Static Tests

All but one of the sections were initially subjected to monotonically increasing load until cracking occurred to simulate the effect of moderate overloads and to produce realistic loading conditions which might induce fatigue failure. The effective prestress was estimated from Demec and strain readings (concrete and prestressing steel) as well as from the analytical model. This provided a target cracking load. The specimen was loaded incrementally until it cracked. After cracking, several more static cycles were applied. Cracks were marked during the initial and subsequent static tests.

3.9.2.2 Periodic Static Tests

At various stages of fatigue testing, the testing was halted and static tests were performed. The first periodic static test was generally after 10,000 to 30,000 cycles. The subsequent static tests

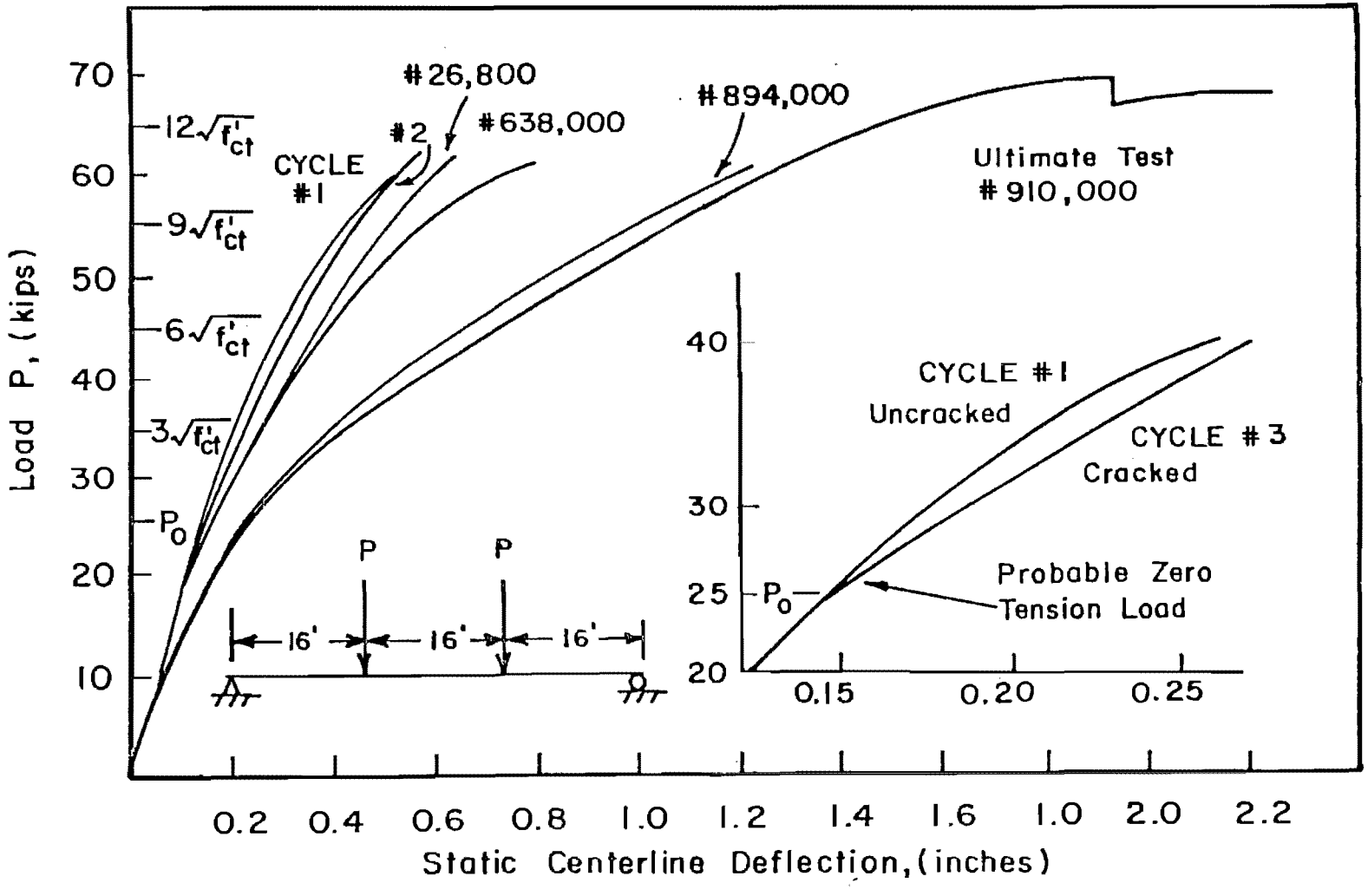

Fig. 3.36 Zero tension load from a load versus deflection curve

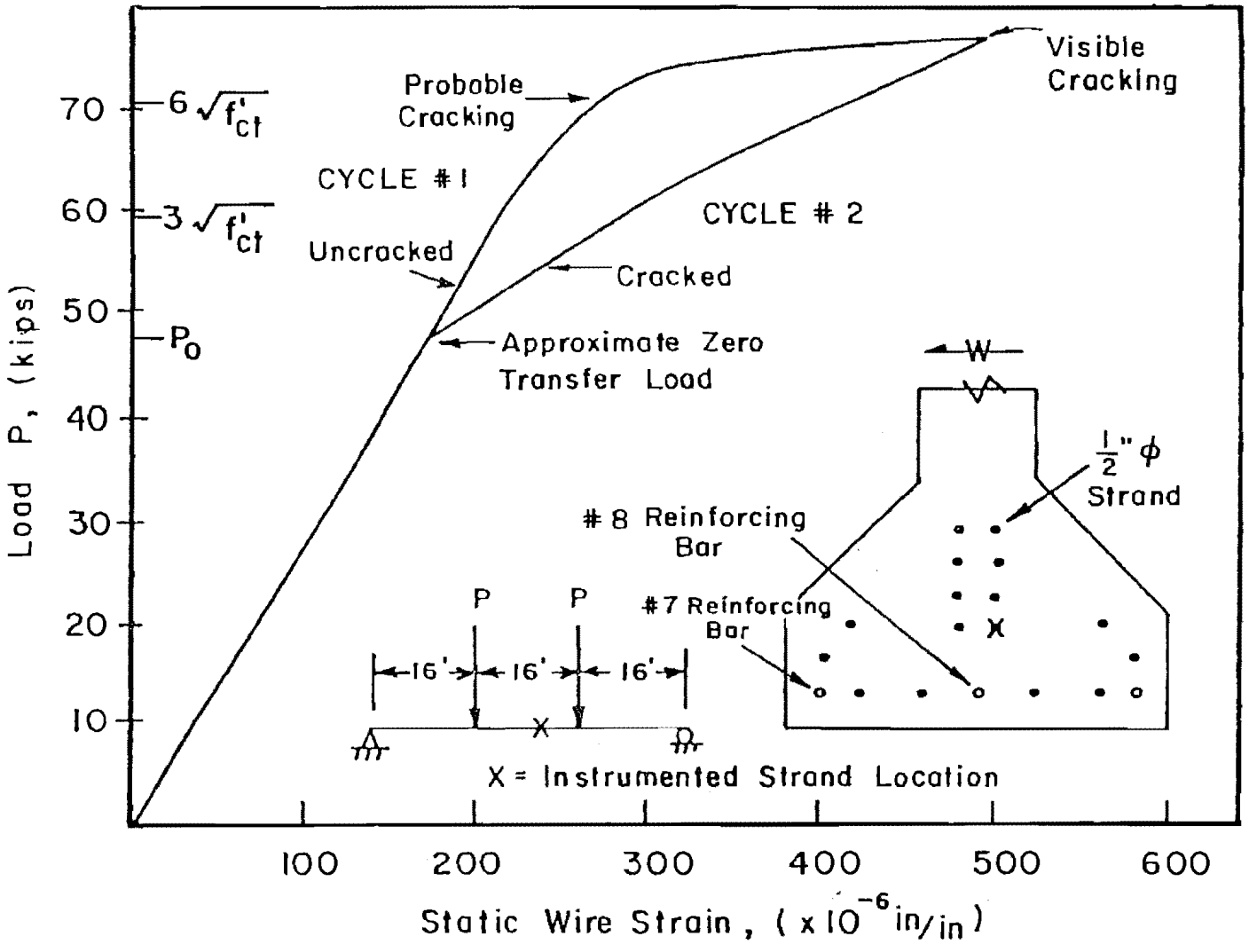

Fig. 3.37 Zero tension load from a load versus wire strain curve

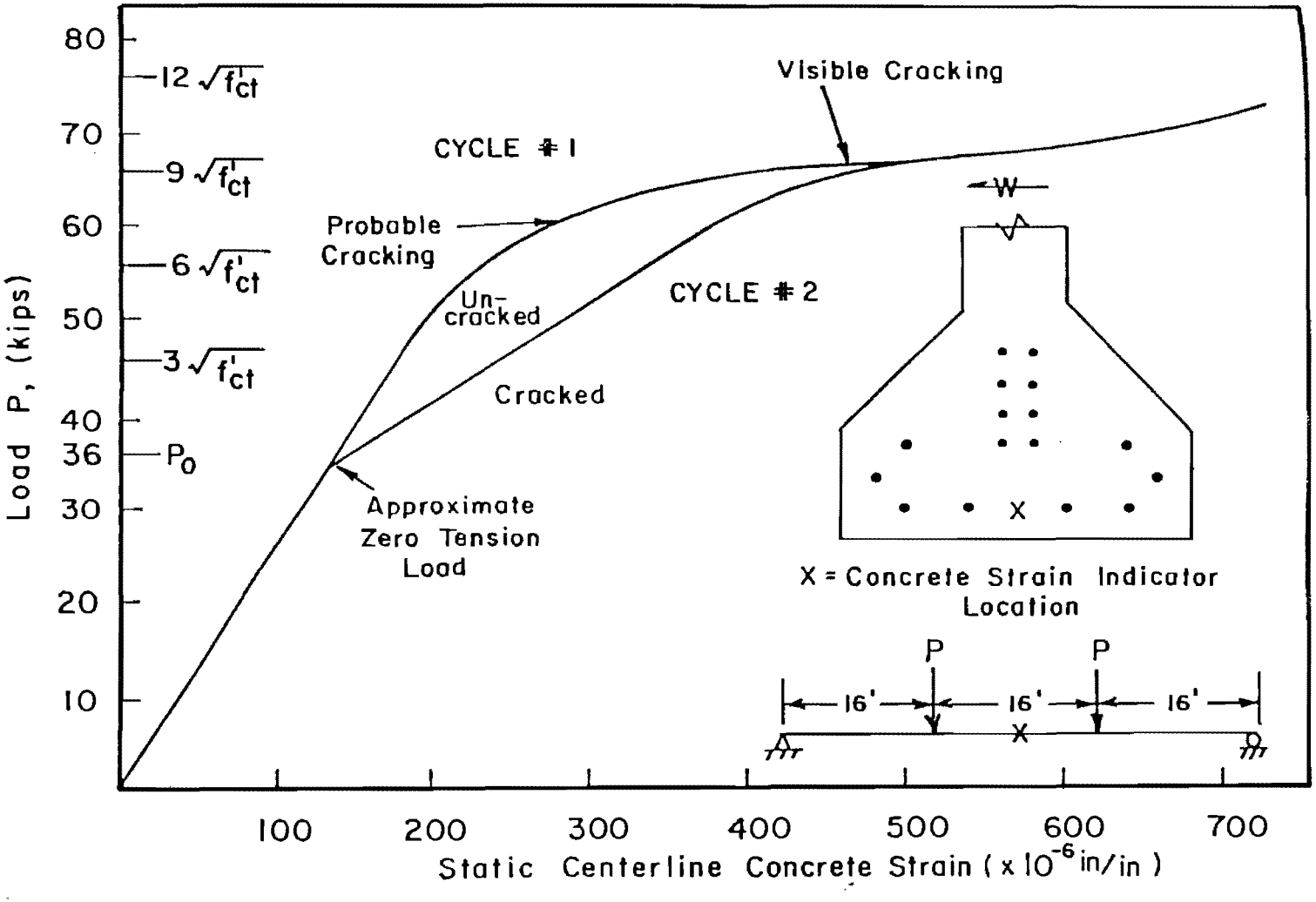

Fig. 3.38 Zero tension load from a load versus concrete strain curve

were performed every 700,000 to 1.0 million cycles or whenever a limit switch stopped the pulsator pump, indicating an increase in centerline deflection.

Periodic static tests were repeats of the initial static test. Crack opening, concrete and steel strain, and deflection data were gathered; cracks were located and marked, and pictures were taken if required. While moderate overloads were required to crack the sections, overloads were generally not applied to specimens during subsequent static tests.

3.9.3 Fatigue Tests

To define the S/N curve for beams, high nominal, or uncracked, maximum concrete tensile stresses were applied to early specimens. The last specimens tested were cycled at or below a maximum concrete tensile stress of $6\sqrt{f'_c}$. The effective prestress force was determined from the data obtained during the initial static tests. The fatigue load was determined using the effective prestress and the concrete cylinder strength at the time of testing, f'_{ct}. The fatigue loads were calculated by setting the extreme fiber tensile stress equal to a multiple of $\sqrt{f'_{ct}}$.

Loads, centerline deflection, crack opening, and strand wire strains were monitored during fatigue loading. The fatigue load fluctuated at most by 3 kips (approximately 5 percent) and generally less than 1 kip (approximately 2 percent).

3.9.4 Ultimate Tests

Fatigue loading was discontinued and the specimens were prepared for ultimate testing after numerous wire fatigue fractures had occurred. Generally, fatigue testing was stopped after approximately 30 percent of the wires had fractured due to fatigue. Specimen A-22-NP-3.5-OL-5.95 (NF) had no fatigue fractures, hence the "NF". Fatigue fractures were indicated by a marked increase in centerline deflection at the upper static load, an increase in permanent deflection under no load, concrete spalling, visible wire breaks, increased strand stress ranges, and flexural cracks that failed to close after removal of load.

The loading bed was modified slightly for the ultimate test. Five inch neoprene pads were used to support the specimen instead of the one inch pads to permit large end rotations. A 12 in. linear potentiometer was installed above the specimen at the centerline so large deflections could be monitored.

Ultimate testing was stopped after the specimen collapsed or ceased to carry additional load due to yielding of the tension steel. The ultimate test on the specimen with no fatigue fractures (A-22-NP-

3.5-0L-5.95 (NF)) was stopped for safety reasons after the centerline deflection reached 23 in. The theoretical ultimate capacity was determined using the principles of equilibrium and the concrete stress distribution defined in AASHTO Specifications [8] Section 1.5.31 (ACI 318-77 [21] Section 10.2.7.

3.9.5 Post Mortem Investigation

A post mortem investigation was performed on each girder after the ultimate test to determine the location and types of wire fractures. Pictures were taken and a crack map was drawn before dissection of the specimen. Lower flange concrete was removed by jackhammering, as shown in Fig. 3.39. The strands were cut with a torch or grinder, cleaned and sprayed with a clear sealer to prevent corrosion. The locations and types of steel fractures were then carefully examined and catalogued. Static breaks, as shown in the strand in the center of Fig. 3.40, were characterized by necking and a cup and cone type fracture. Fatigue breaks, as shown in Fig. 3.41, had jagged surfaces with little or no sign of necking. Figure 4.42 shows two strands; the upper one sustained fatigue failure in a beam specimen; the lower strand was an "in-air" specimen tested by Paulson. Notice the same jagged surface in both strand breaks. Figure 4.43 shows a ductile reinforcing bar static break. Figure 4.44 shows the oval surface at a fatigue initiation crack. The reinforcing bar had not failed at this point.

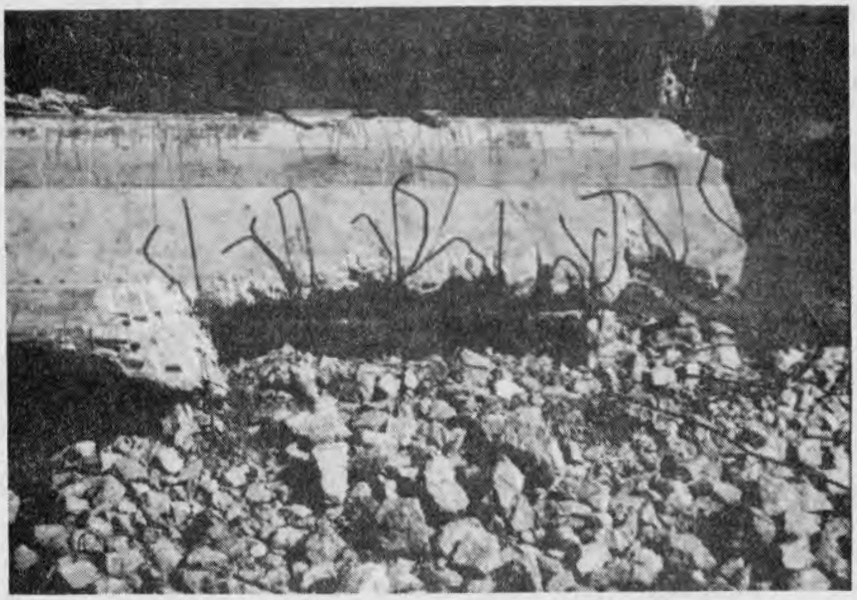

Fig. 3.39 Lower flange concrete removed for post mortem investigation

Fig. 3.40 Static wire break with necking

Fig. 3.41 Beam specimen wire fatigue fractures

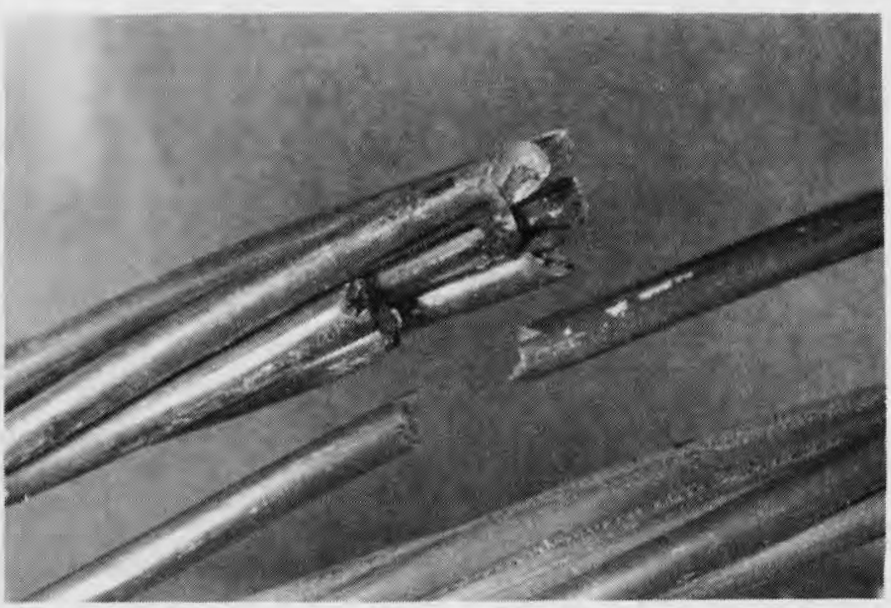

Fig. 3.42 Wire fatigue fractures from beam specimen (upper) and "in-air" specimen (lower)

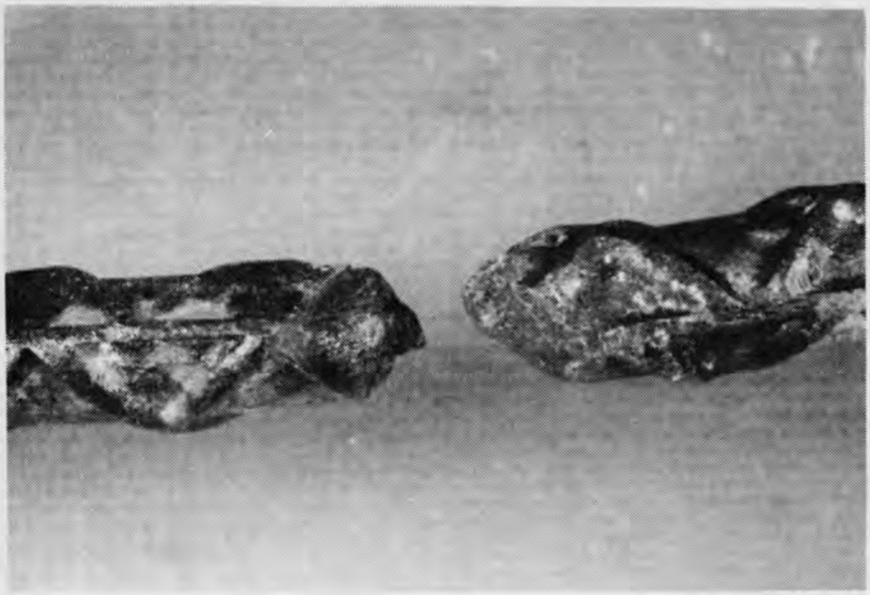

Fig. 3.43 Ductile reinforcing bar static fracture

Fig. 3.44 Oval surface at a fatigue initiation crack

CHAPTER 4

EXPERIMENTAL RESULTS

4.1 Introduction

Eleven pretensioned concrete girder specimens were tested in the flexural fatigue series. All tests will be described using the following order: four straight strand girders, four draped strand girders and then three girders with supplementary conventional reinforcing steel in the lower flange to control cracking. Table 4.1 presents material and composite properties.

All loads referred to in this chapter are loads per ram. The maximum and minimum fatigue loads, P_{max} and P_{min}, represent the average load readings taken during fatigue testing. A peak detector permitted constant monitoring of maximum and minimum fatigue loads as well as centerline deflection, strand stress range, and crack opening displacements. Small variations in the loads ($\pm$ 5 percent) occurred due to changes in the girders' dynamic response, as a result of cracking, and drift in the pulsater pump. The loads were readjusted periodically to minimize the effects of such variations.

Throughout the discussion of the tests, references are made to nominal concrete tensile stresses, which refer to the computed concrete stress in the extreme fibers of the precompressed tension zone. These stresses were computed based on uncracked, transformed cross sections. They are given only for reference to existing design provisions. In actuality, once a section is cracked, this parameter is meaningless. Prestressing strand stress range is more meaningful for cracked sections and will be used in addition to nominal tensile stresses throughout.

4.2 Specimen C-16-NP-10.5-NO-0.58

This specimen was a Texas Type C with sixteen straight strands. There was no passive (unstressed) reinforcing steel in the lower flange. The specimen was cycled at an upper fatigue load, P_{max}, that produced $10.5\sqrt{f'_{ct}}$ nominal tensile stress in the extreme tension fibers. There were no loads above P_{max} during the periodic static tests. The specimen withstood 0.58 million fatigue cycles before failure.

4.2.1 Initial Static Tests

Specimen C-16-NP-10.5-NO-0.58 was initially loaded incrementally to a maximum load of 72.8 kips. Flexural cracks became visible at 70 kips and extended into the web. Figure 4.1 shows measured

TABLE 4.1 Material and Section Properties on Day Testing Was Started

Specimen	Concrete Strength Initial Loading Day $f_{cgirder}$ f'_{ct} (psi)	f'_{cslab} (psi)	Effective Slab Width (in.)	C.G.-bottom (in.)	I_{total} ($in.^4$)	S_x ($in.^3$)
C-16-NP-10.5-NO-0.58	5350	5780	80.03	31.99	283,200	8850
C-16-NP-7.2-OL-1.48	6350	4200	62.62	30.35	260,880	8590
C-16-NP-10.1-NO-0.91	6610*	2800*	50.12	28.87	240,700	8340
C-16-NP-6.0-NO-1.91	6870	4950	65.36	30.64	264,700	8640
C-14-NP-5.5-OL-2.29	5790*	5500*	75.04	31.56	277,400	8790
A-22-NP-6.2-OL-2.84	7050	5050*	63.48	29.57	175,300	5930
A-22-NP-6.2-NO-5.00	7050	5170	64.23	29.64	176,000	5940
A-22-NP-3.5-OL-5.95(NF)	7050	5540	66.48	29.84	177.900	5960
C-16-UP-8.0-NO-1.73	5800	3000*	55.38	29.53	249,700	8460
C-16-CP-7.2-NO-2.54	7200	4900*	63.52	30.45	262,100	8610
C-16-CP-5.5-OL-9.43	5600	3550	61.31	30.21	258,900	8570

* Calculated from 28 day value

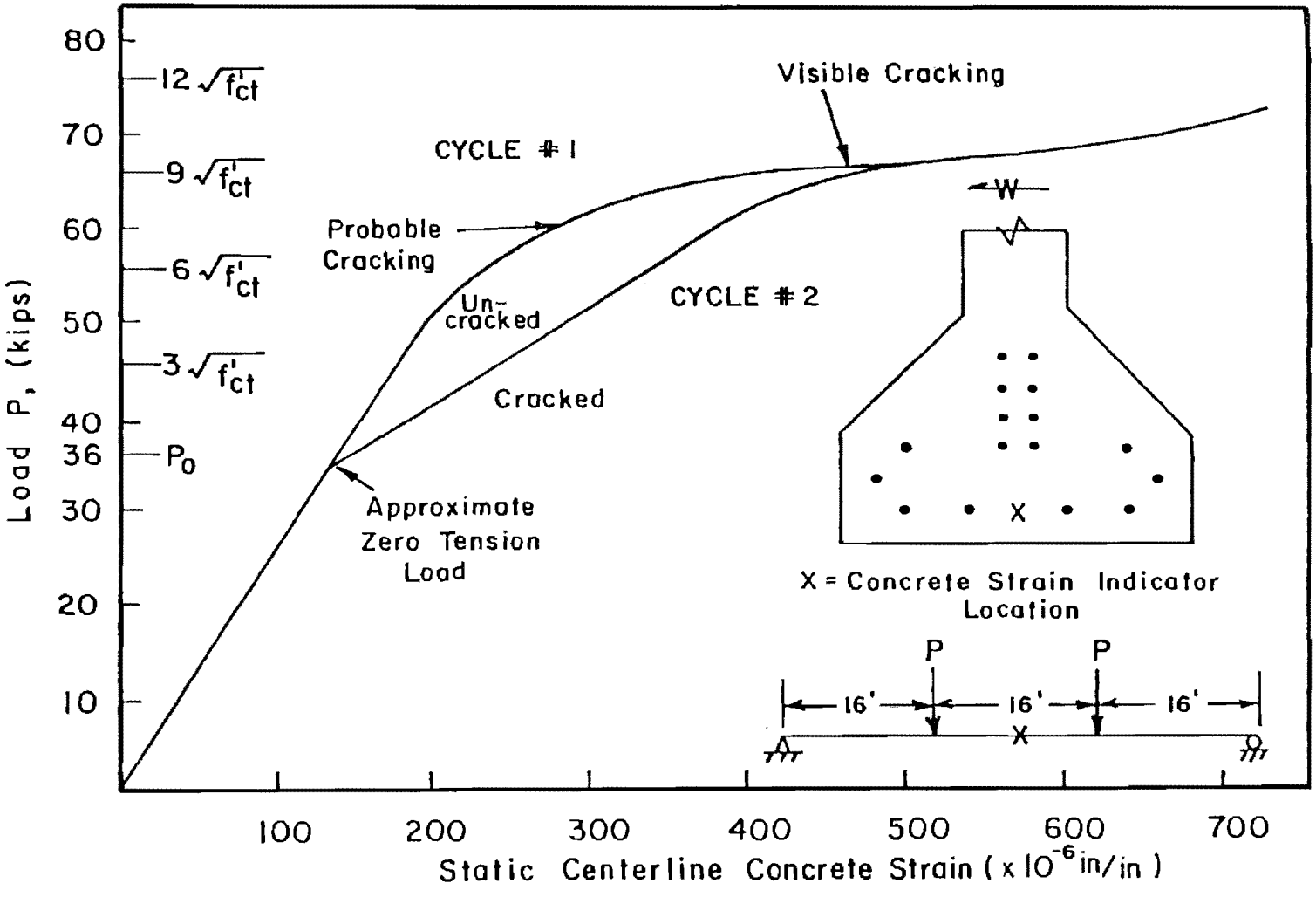

Fig. 4.1 Load versus concrete strain for Specimen C-16-NP-10.5-N0-0.58

concrete strain versus load and indicates that first cracking probably occurred at approximately 60 kips. Figure 4.2 shows measured wire strain on a pretensioned strand located near the centerline versus load. It also indicates probable cracking in the vicinity of 60 kips. Three static tests were run to the same maximum load level of 72.8 kips before cycling began. The reduction in stiffness between the first and second cycles, due to flexural cracking, can be clearly seen in Figs. 4.1 and 4.2. Seven flexural cracks formed during these initial cycles.

4.2.2 Zero Tension Load, P_o

Figures 4.1 and 4.2 of load versus concrete and strain strain and Fig. 4.3 of load vs. deflection during static tests indicate a change in behavior at approximately 36 kips. This is the load at which the precompressed concrete tension zone first experienced tension. The change is a result of a decreased moment of inertia due to flexural cracking. The centerline deflection at 36 kips was 0.190 in.

4.2.3 Fatigue Loads

A severe maximum nominal concrete tensile stress of $10.5\sqrt{f'_{ct}}$ was purposely selected for the upper fatigue load for Specimen C-16-NP-10.5-NO-0.58 to define the low cycle portion of the S/N (stress range versus number of cycles) curve. Based on the uncracked section modulus given in Table 2.1 and a zero tension load of 36 kips, the maximum fatigue load was 71.5 kips. The minimum load was 47.5 kips. The load program can be seen in Fig. 4.4.

4.2.4 Fatigue Behavior

The specimen's deflection remained stable for the majority of the fatigue test. Figure 4.5 shows that the live load centerline deflection during the initial three cycles of 0.53 in. had stabilized at 0.87 in. by 11,000 cycles, when the next static test was performed. Dynamic strand wire strains of approximately 0.00100 in./in. were consistently read on the peak detector during the initial 26,000 fatigue cycles. During a static test at 25,000 cycles, the static strain range between 47.5 and 71.5 kips was 0.00083 in./in. The deflection remained virtually unchanged after 11,000 cycles until approximately 435,000 cycles. A static cycle at 315,000 cycles indicated that the centerline and third-point deflections were 0.87 and 0.74, respectively, at 72.8 kips.

Flexural cracks continued to form and propagate to the top of the web for the first 440,000 cycles. At that time there were 14 flexural cracks in the 16 ft constant moment region. After 440,000 cycles, the cracks began to fork and propagate horizontally. The

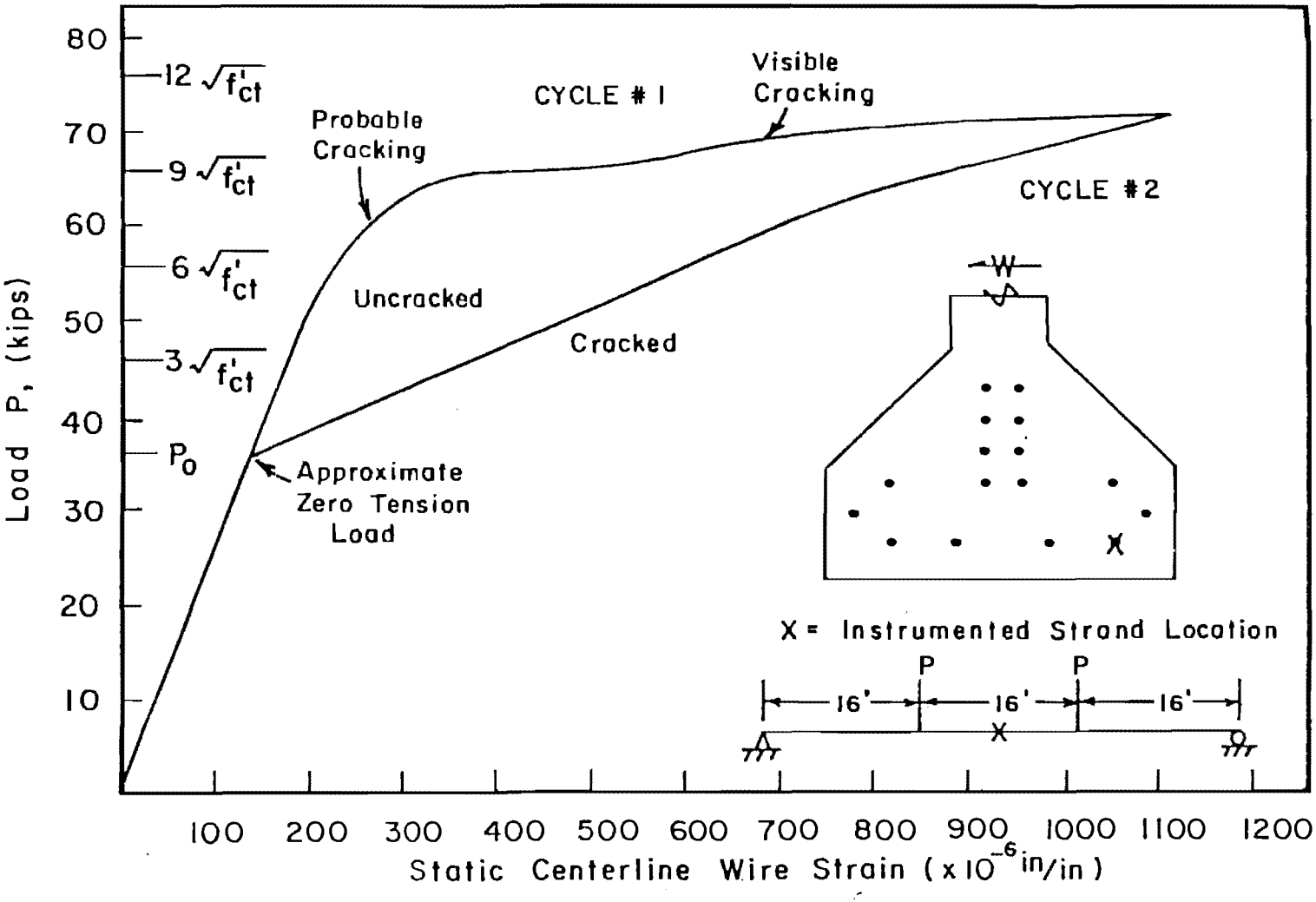

Fig. 4.2 Load versus wire strain for Specimen C-16-NP-10.5-NO-0.58

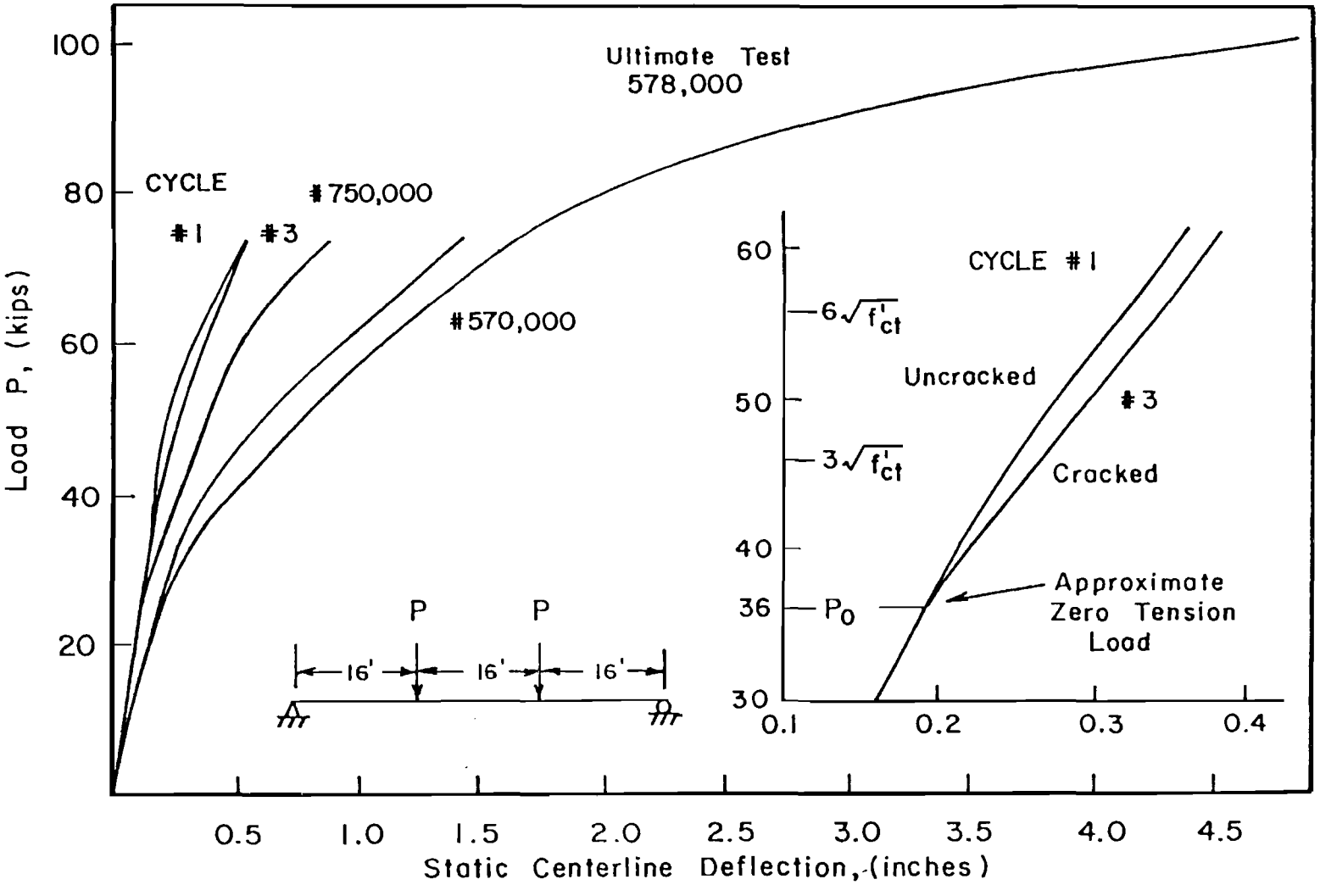

Fig. 4.3 Load versus deflection during static tests for Specimen C-16-NP-10.5-NO-0.58

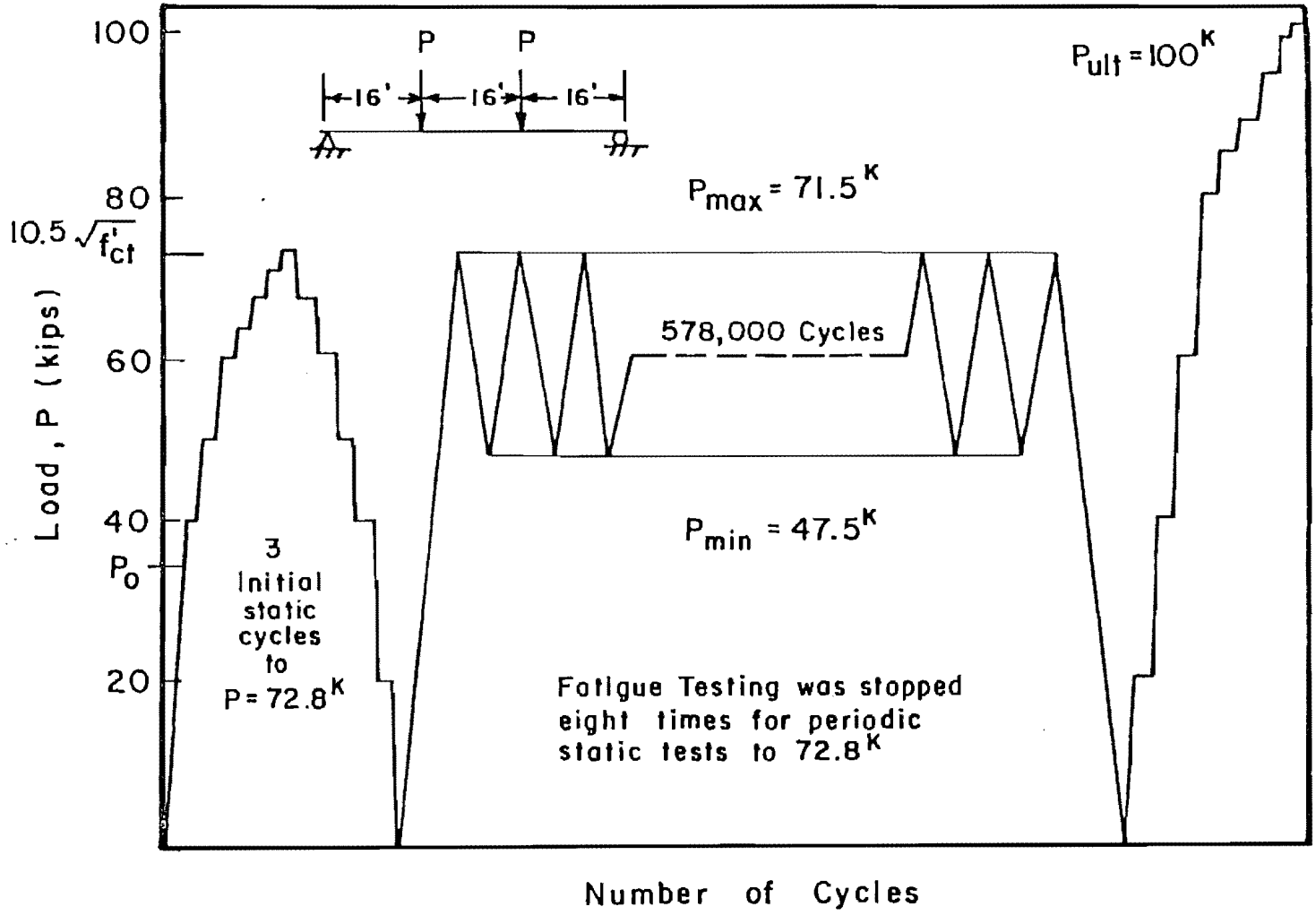

Fig. 4.4 Load program for Specimen C-16-NP-10.5-NO-0.58

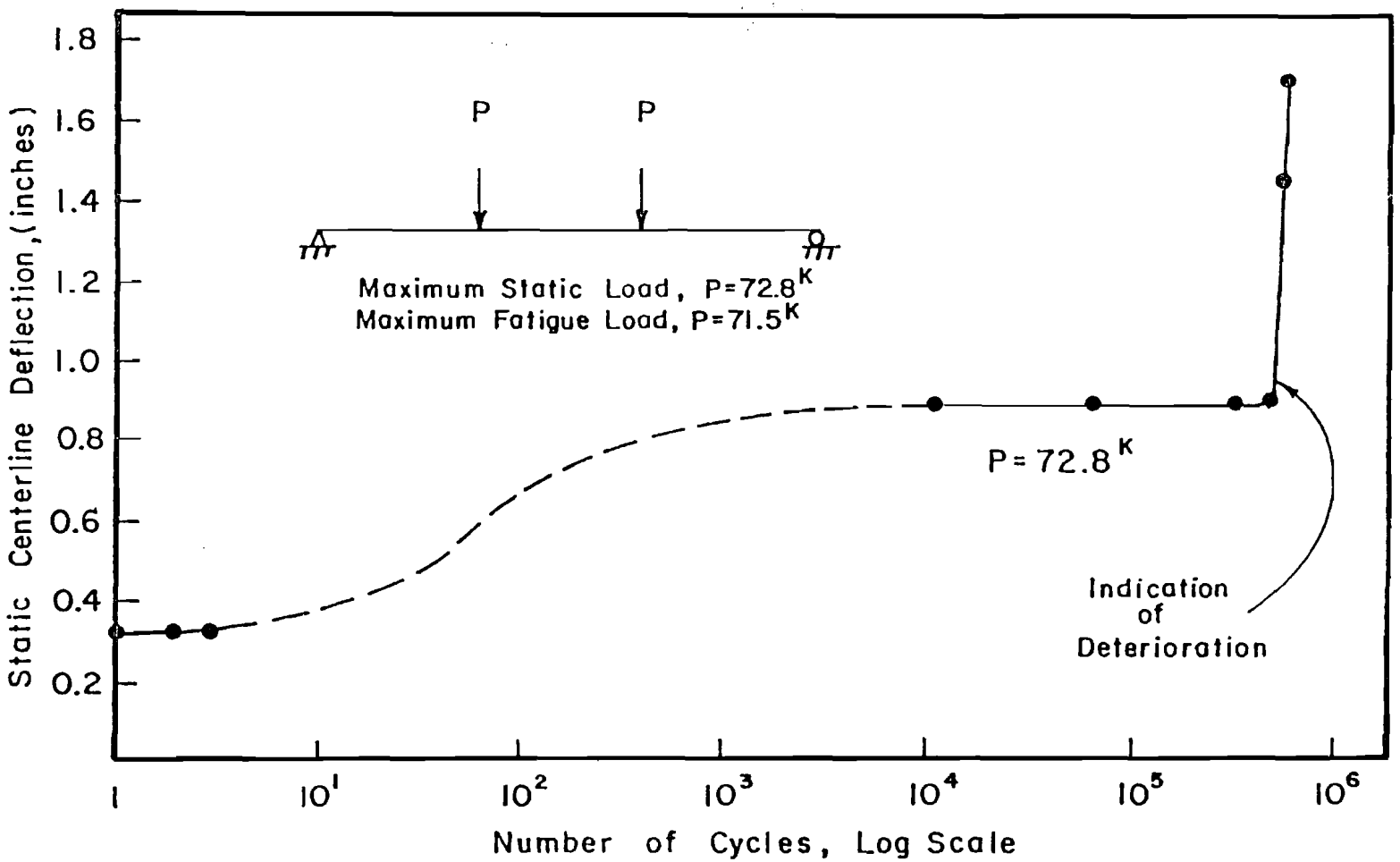

Fig. 4.5 Maximum centerline deflection during static tests for Specimen C-16-NP-10.5-NO-0.58

cracking pattern of 480,000 cycles is shown in Fig. 4.6. Note the several forked flexural cracks.

The specimen's stiffness deteriorated rapidly after 480,000 fatigue cycles. The maximum centerline deflection increased from 0.90 at 480,000 cycles to 1.70 in. at 578,000 cycles. This 58 percent increase in deflection can be seen in Fig. 4.5. As the concrete and steel properties degraded, flexural cracks extended into the top flange. Horizontal cracks in the lower flange were noticed at 570,000 cycles. Wire breaks were heard at 540,000 cycles and could be seen at 578,000 cycles when severe concrete spalling on the lower flange occurred. Figure 4.7 shows the extent of spalling prior to the ultimate test. When fatigue testing was discontinued at 578,000 cycles, there were 15 flexural cracks in the 16 ft constant moment region.

4.2.5 Static Ultimate Test

The specimen was loaded incrementally to failure, which occurred at 100 kips. This is 85 percent of the calculated ultimate capacity of 117 kips. Failure was by brittle failure of the prestressing strands. Figure 4.3 shows the ultimate load deflection curve which indicates that the specimen exhibited some ductility. The ultimate centerline deflection of 4.8 in. is approximately one-fifth of that expected for a monotonically loaded specimen and a 48 ft span.

4.2.6 Post Mortem Investigation

After the ultimate load test, the concrete cover was removed, and the strands were exposed. Thirty-three fatigue breaks were discovered on eleven strands at six locations. All wire fractures occurred at concrete crack locations. Figure 4.8 shows the fatigue fracture locations along the member. Figure 4.9 indicates the fracture locations relative to the cross section.

4.2.7 Dynamic Load Amplification

The static centerline deflection between 47.5 and 71.5 kips at 315,000 cycles, which was in the stable region of the fatigue testing, was 0.52 in. (0.36 in. to 0.88 in.). The dynamic deflection at 312,000 cycles was 0.60 in. (0.34 in. to 0.94 in.) which indicates slight dynamic amplification. The static loads corresponding to these dynamic deflections were approximately 46 and 74 kips.

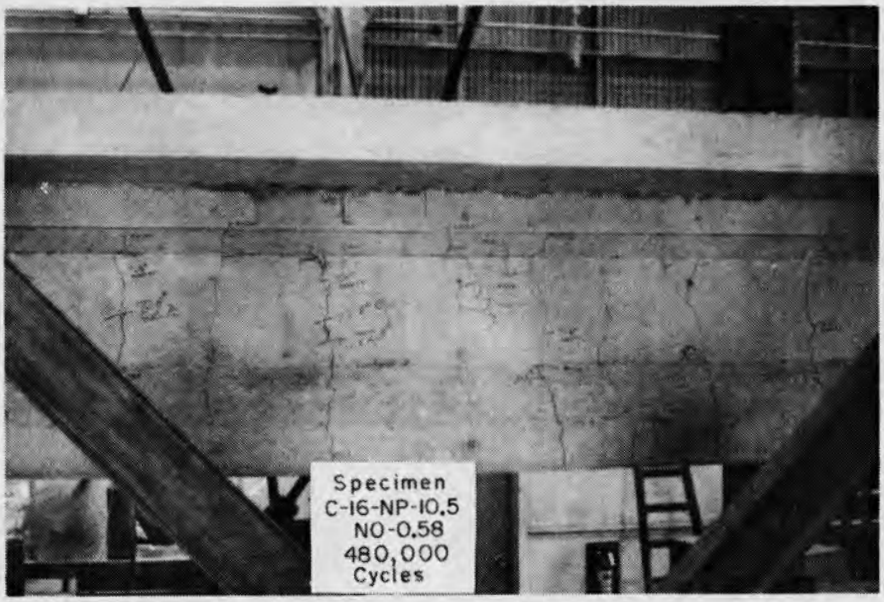

Fig. 4.6 Cracking pattern for Specimen C-16-NP-10.5-NO-0.58 after 480,000 cycles

Fig. 4.7 Concrete spalling prior to static ultimate test

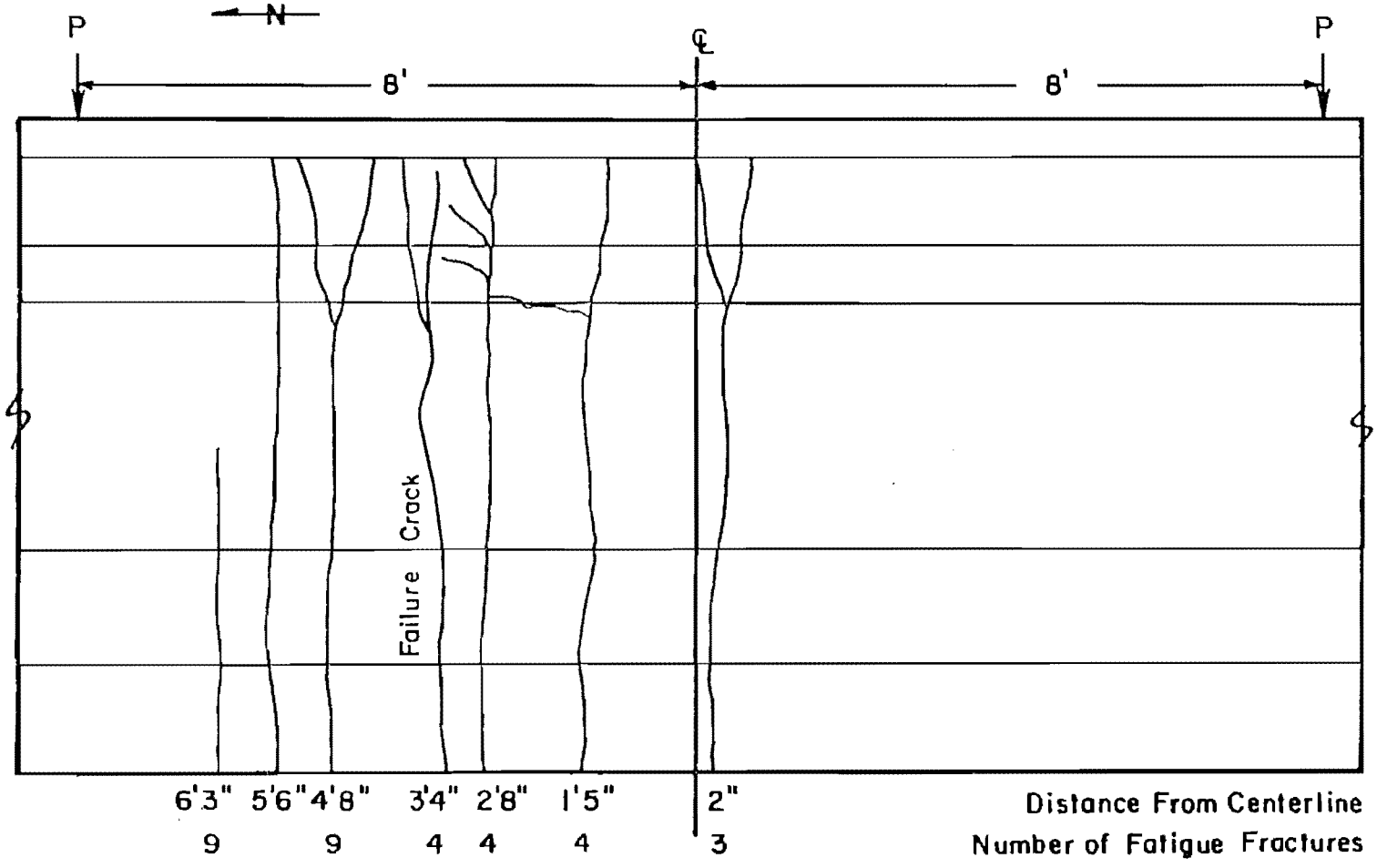

Fig. 4.8 Location and number of wire fatigue fractures and corresponding concrete cracks for Specimen C-16-NP-10.5-NO-0.58

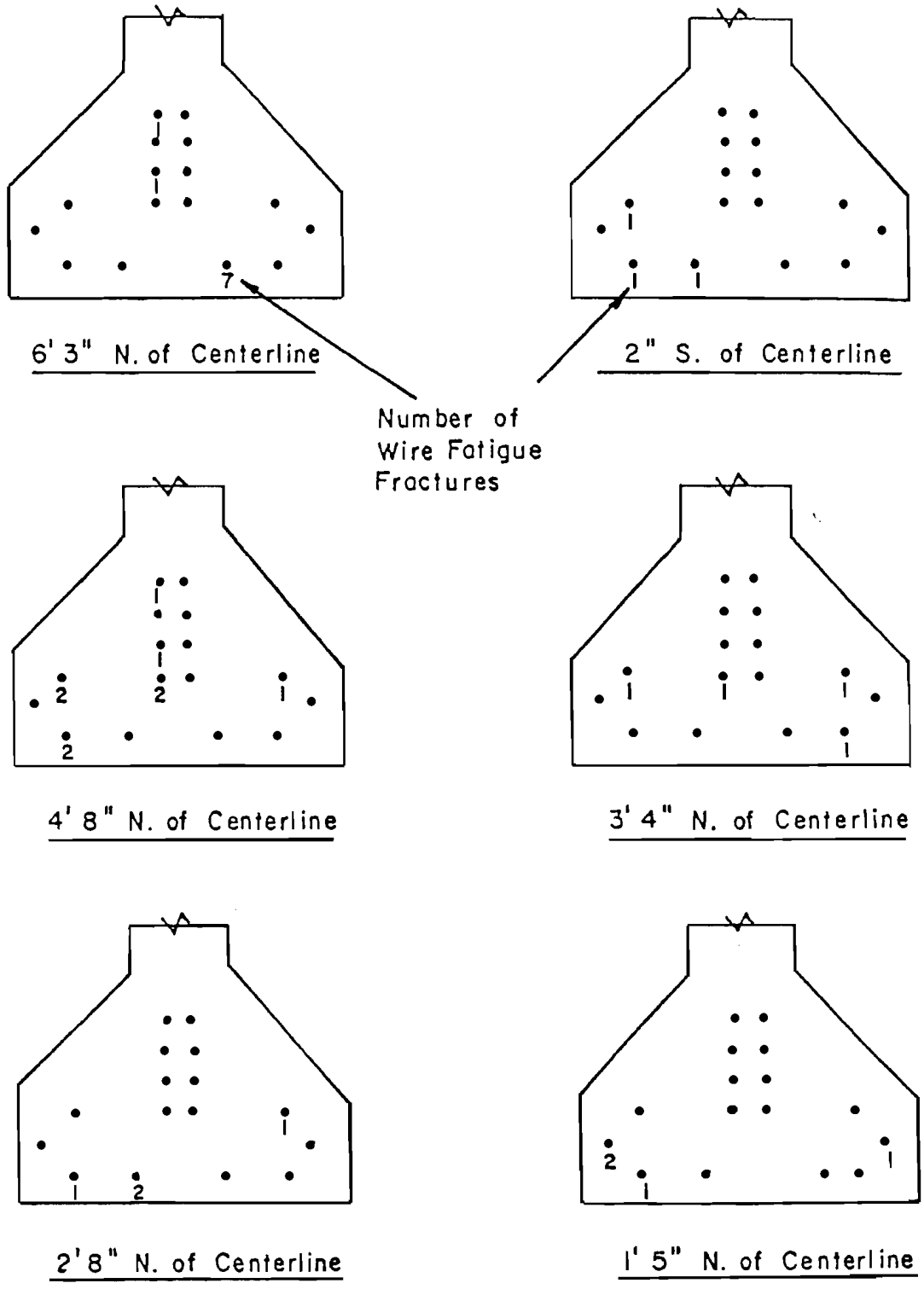

Fig. 4.9 Fatigue fracture locations for Specimen C-16-NP-10.5-NO-0.58

4.3 Specimen C-16-NP-7.2-OL-1.48

This specimen was a Texas Type C with 16 straight strands. There was no passive reinforcing steel in the lower flange. The specimen was cycled at an upper fatigue load, P_{max}, that produced a nominal concrete tensile stress of $7.2\sqrt{f'_c}$ in the extreme tension fibers. There were overloads above P_{max} during periodic static tests. The specimen withstood 1.48 million fatigue cycles before failure.

4.3.1 Initial Static Tests

Specimen C-16-NP-7.2-OL-1.48 was initially loaded monotonically to a maximum load of 73 kips. Flexural cracks became visible at 67.5 kips. Figure 4.10 of static centerline deflection versus load indicates an appreciable reduction in stiffness between 60 and 65 kips. Cracking probably first began in this region. Five flexural cracks formed and propagated to the middle portion of the web during the initial three static cycles.

4.3.2 Zero Tension Load, P_o

The insert of load versus centerline deflection between 30 and 50 kips in Fig. 4.10, indicates a change in stiffness at approximately 35 kips. The change is a result of a decreased moment of inertia and occurs when flexural cracks begin to open (the zero tension load). The centerline deflection at 35 kips was 0.190 in.

4.3.3 Fatigue Loads

The specimen was cycled at a maximum load (P_{max}) of 60.8 kips. Based on the zero tension load of 35 kips, this load produced a nominal concrete tensile stress of $7.2\sqrt{f'_{ct}}$. The concrete compressive strength at the time testing began (f'_{ct}) and composite properties are given in Table 2.1. The minimum load was 10 kips. The load program for Specimen C-16-NP-7.2-OL-1.48 can be seen in Fig. 4.11.

4.3.4 Fatigue Behavior

The maximum static centerline deflection remains essentially constant for the initial 990,000 cycles, as shown in Fig. 4.12. The maximum static load was 72 kips for the first four periodic static tests (at 2000, 145,000, 325,000, and 990,000 cycles). The maximum static load of 1.478 million cycles was limited to 61.5 kips as a result of the large number of wire fractures.

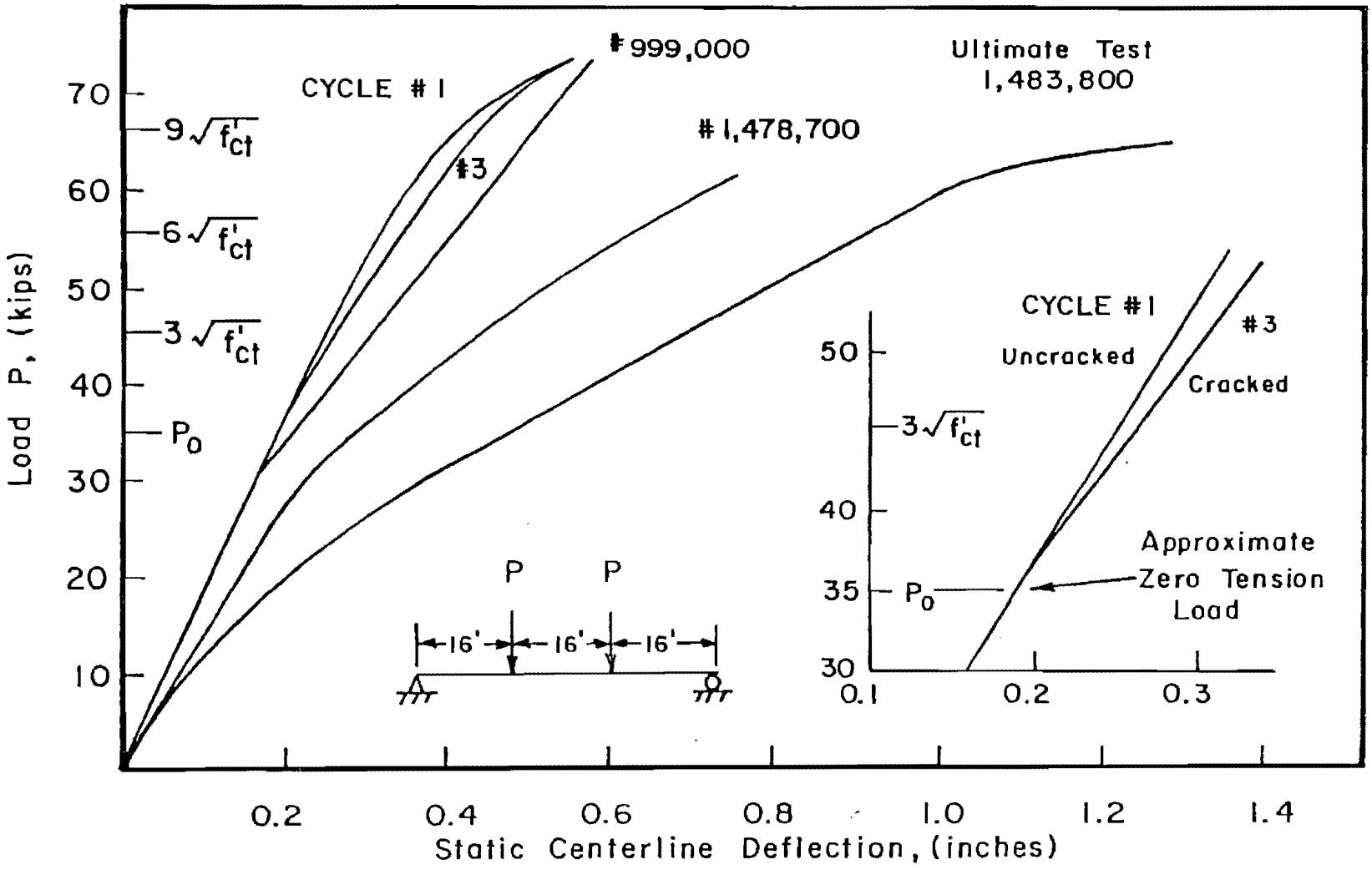

Fig. 4.10 Load versus deflection during static tests for Specimen C-16-NP- 7.2-OL-1.48

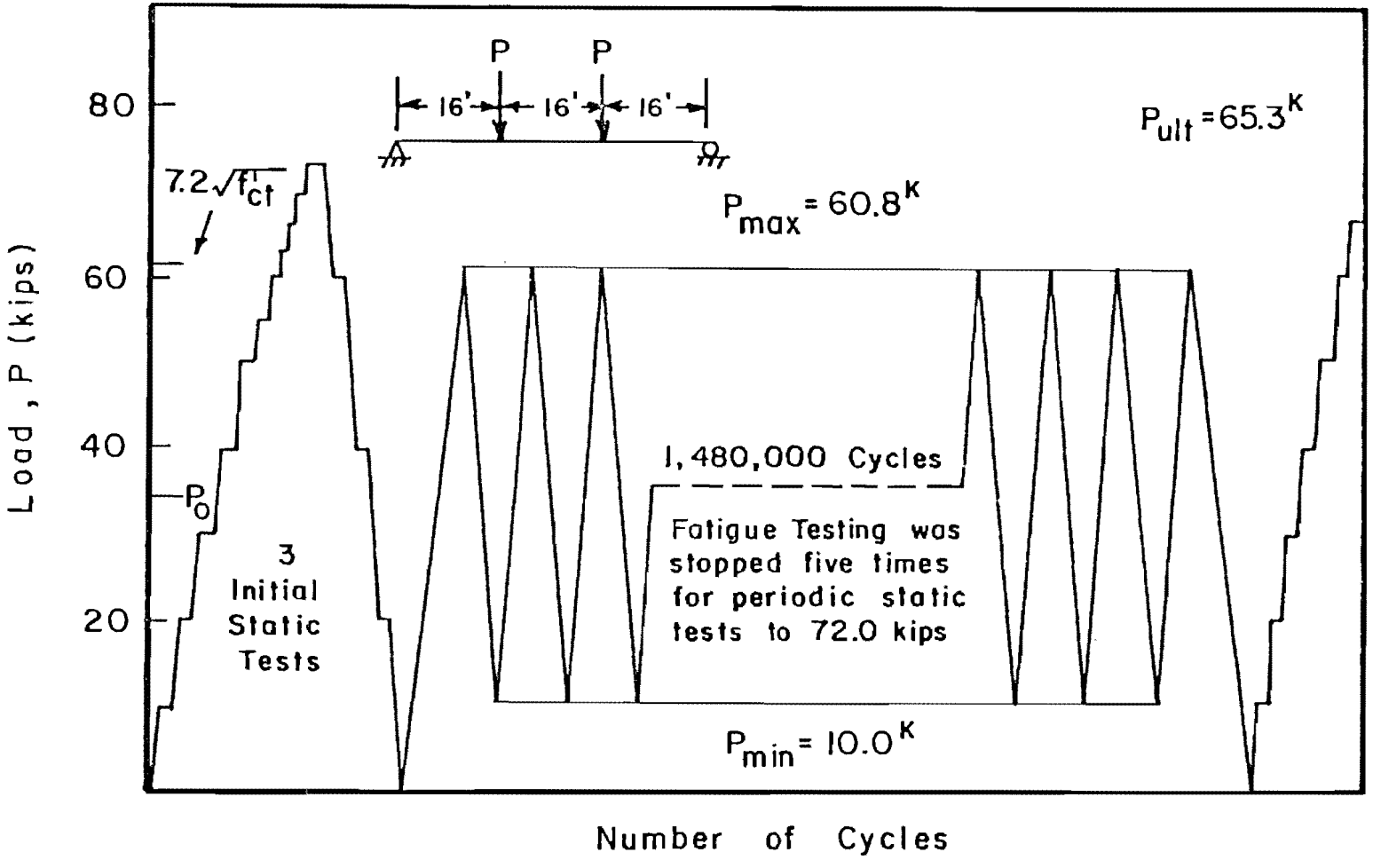

Fig. 4.11 Load program for Specimen C-16-NP-7.2-OL-1.48

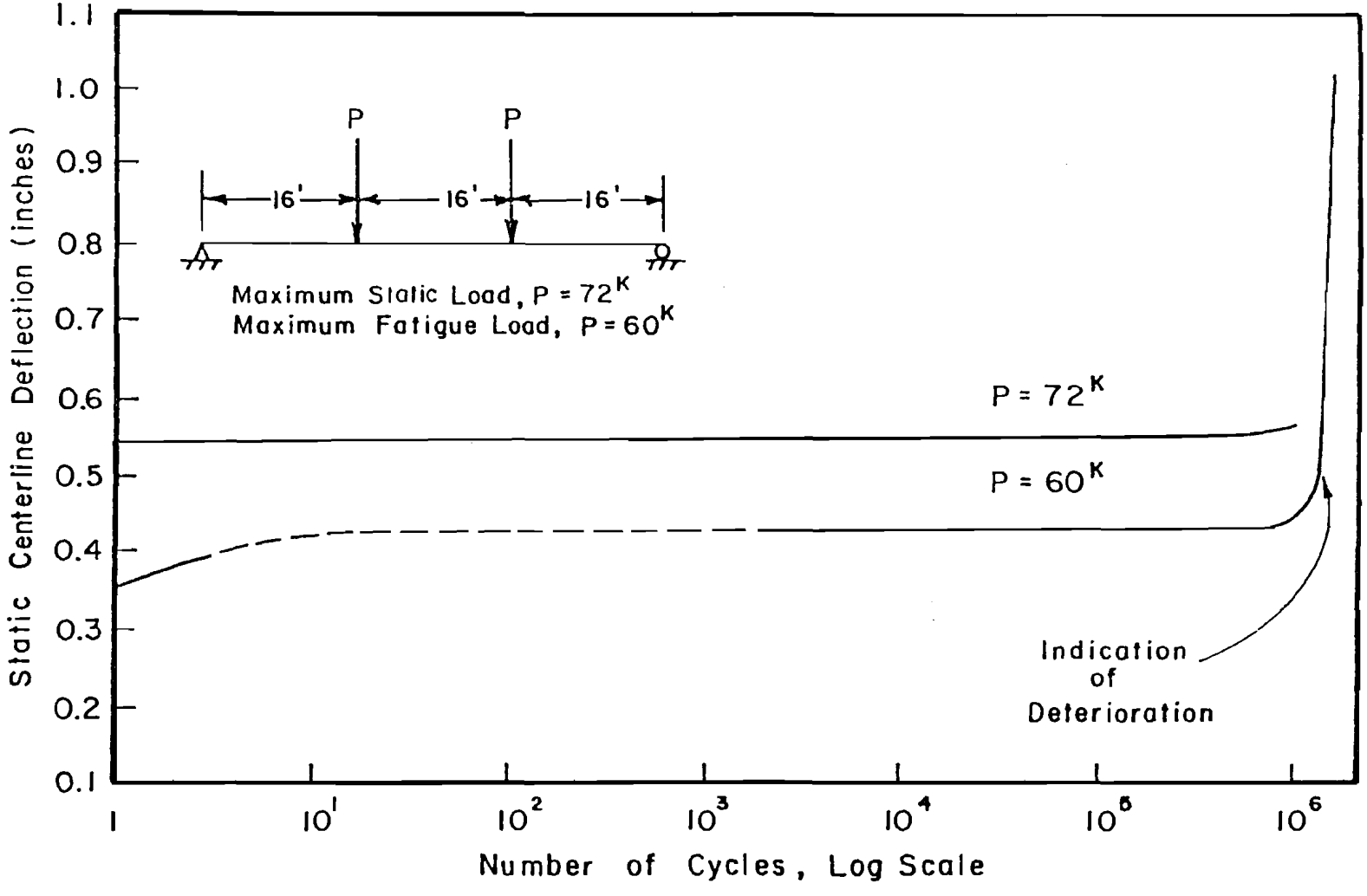

Fig. 4.12 Centerline deflection during static tests for Specimen C-16-NP-7.2-OL-1.48

The measured load strain behavior, as indicated by an instrumented strand wire at the centerline (shown in Fig. 4.13), changed little during the first 990,000 cycles. This gage was not at a flexural crack, so maximum strain could not be measured initially. However, as the member deteriorated, the strain increased drastically. The increased strain, as shown in Fig. 4.13, is probably a result of debonding because the nearest flexural crack was 1'9" from the strain gage. The dynamic strain range was approximately 0.00026 in./in. The static range between 10 and 61 kips determined from Fig. 4.13 was approximately 0.00125 in./in.

The static centerline deflection at 60 kips increased from 0.425 in. at 990,000 cycles to 0.608 in. at 1,478,000 cycles. The 43 percent increase in deflection is shown in Figs. 4.8 and 4.12. The third point deflection at 990,000 cycles, at 60 kips, was 0.365 in. Spalling occurred and wire fatigue breaks could be seen at 1.46 million cycles. The extent of spalling at 1.484 million cycles is shown in Fig. 4.14. Additional wire fractures could be heard during a static test at 1.478 million cycles. The maximum static load at 1.478 million cycles was limited to 61.5 kips as a result of the visible wire fractures and the increased centerline deflection. Figure 4.16 indicates a significant increase in crack opening width between 990,000 and 1,478,000 cycles. The crack opening increased from 0.024 in. at 990,000 cycles to 0.123 in. at 1,478,000 cycles, under a load of 60 kips. The flexural cracks did not close upon removal of load at 1.478 million cycles. There was only one additional crack formed during fatigue loading.

4.3.5 Static Ultimate Test

After completion of cyclic loading, the specimen was loaded incrementally to failure which occurred at 65.3 kips (56 percent of the calculated ultimate capacity). Figure 4.9 demonstrates that the member lacked ductility. The ultimate centerline deflection was only 1.3 in. Failure was by brittle fracture of the remaining prestressing strands. Cracking incurred during the ultimate test is shown in Fig. 4.15.

4.3.6 Post Mortem Investigation

The post mortem investigation revealed 56 wires in the 16 strands had undergone fatigue fractures, but they were all concentrated at one crack location. The failure crack, shown in Fig. 4.17, was located 1'9" north of the centerline. Distribution of the fatigue fractures relative to the cross section is shown in the insert on Fig. 4.17.

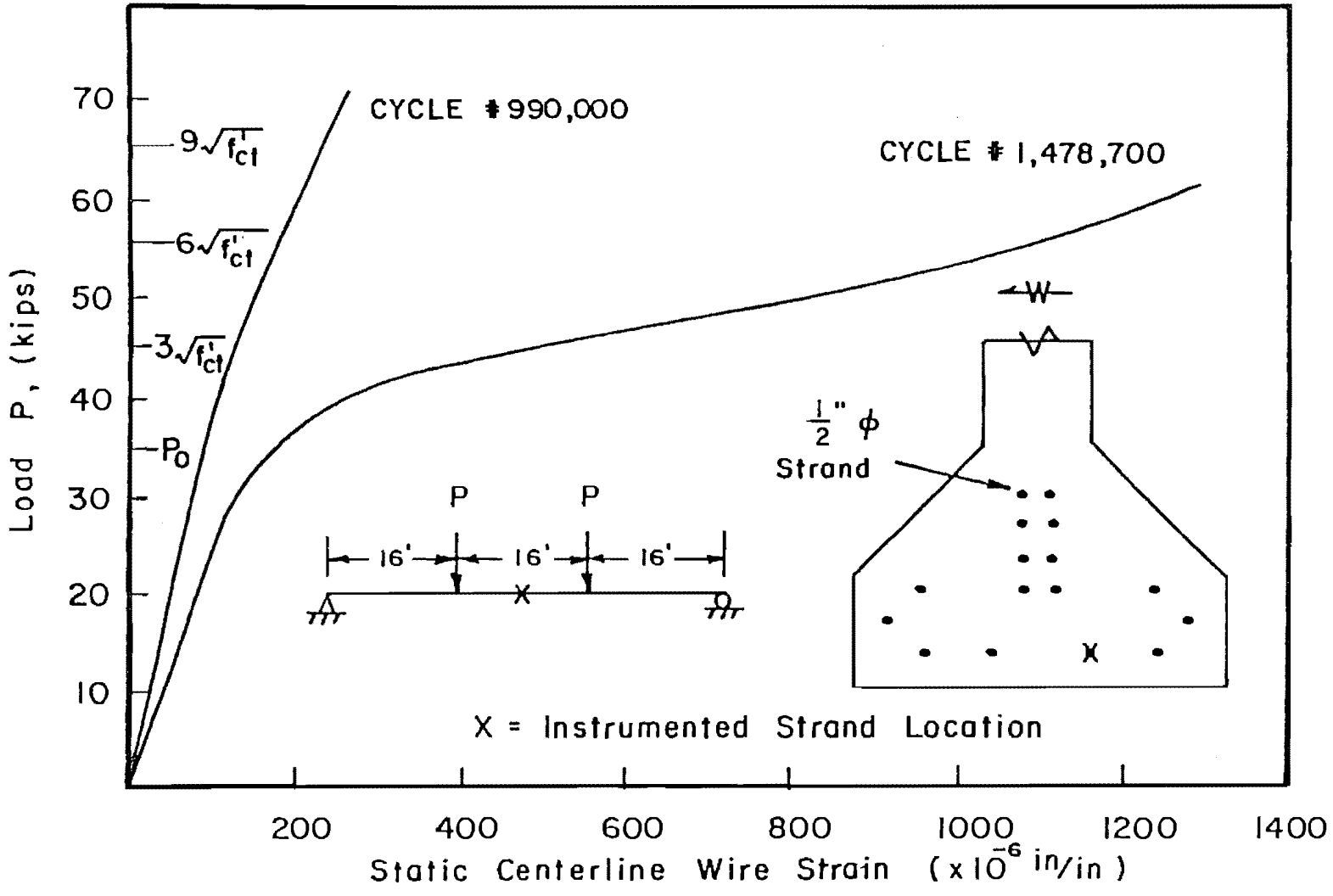

Fig. 4.13 Load versus wire strain for Specimen C-16-NP-7.2-OL-1.48

Fig. 4.14 Concrete spalling at 1.484 million cycles

Fig. 4.15 Cracking after static ultimate test

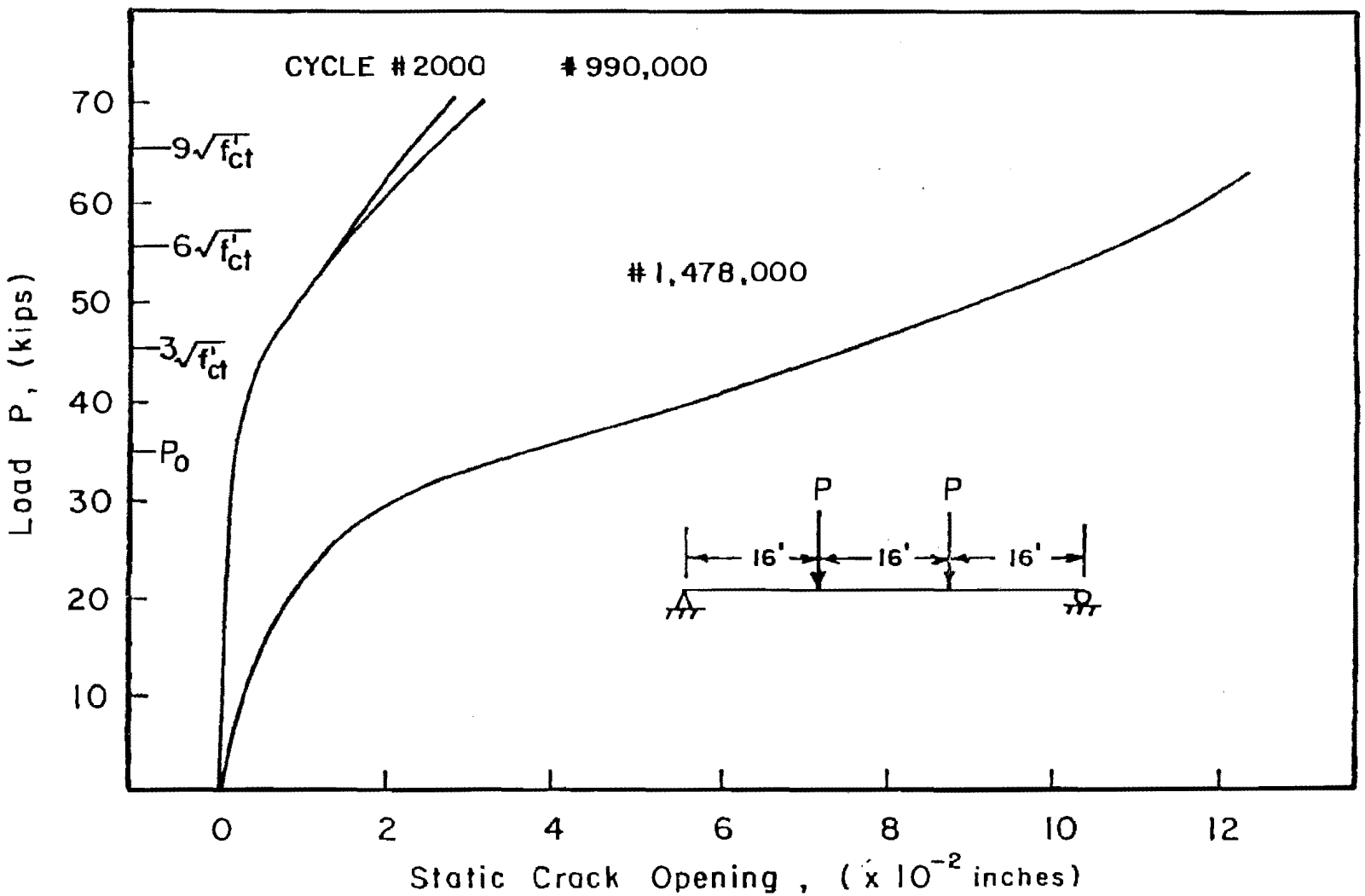

Fig. 4.16 Load versus crack opening 1 ft 9 in. north of centerline for Specimen C-16-NP-7.2-0L-1.48

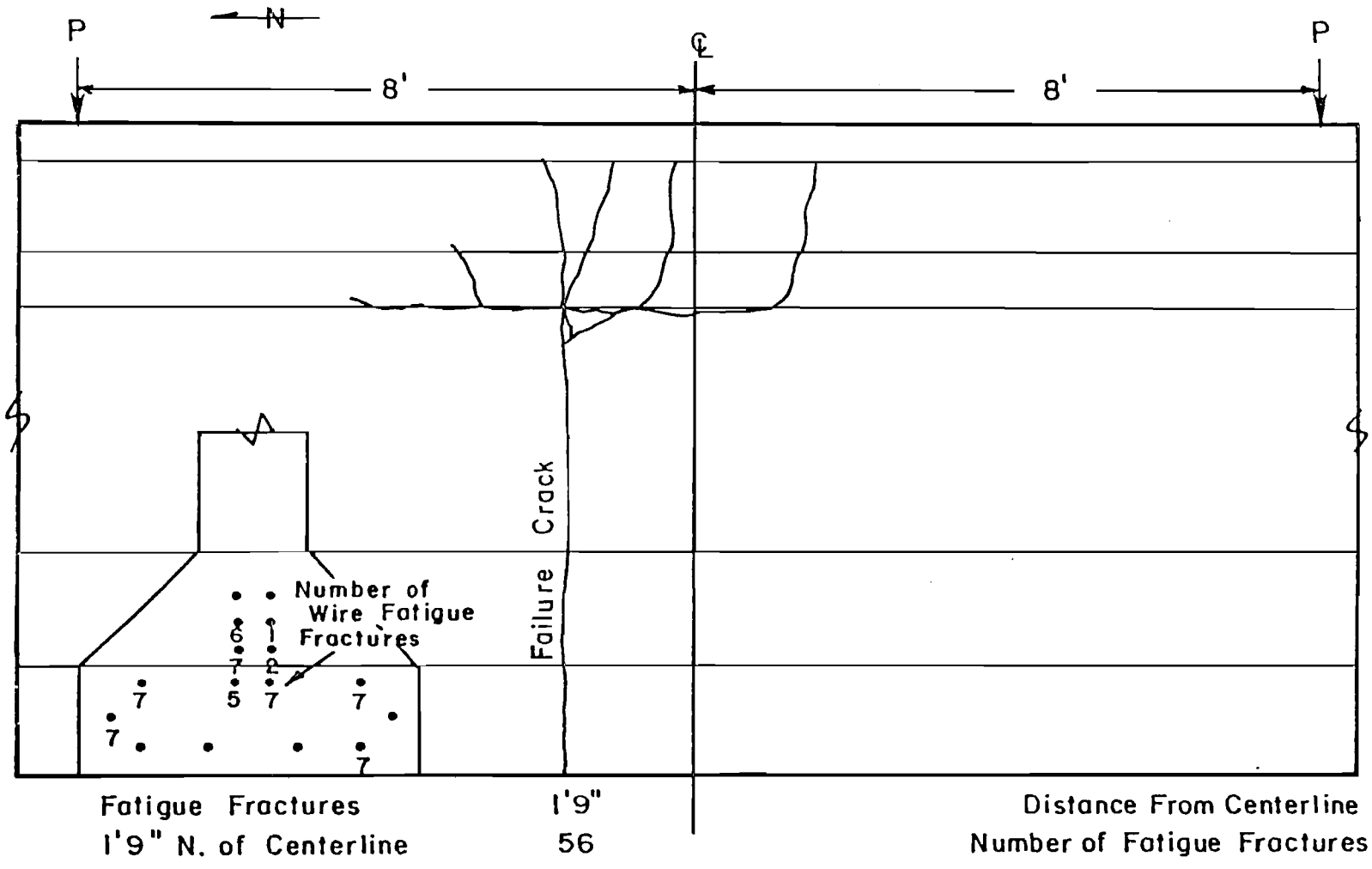

Fig. 4.17 Location and number of wire fatigue fractures and corresponding concrete crack for Specimen C-16-NP-7.2-OL-1.48

4.3.7 Dynamic Load Amplification

The static centerline deflection between 10 and 60.8 kips at 990,000 cycles, which was in the stable range of fatigue testing, as shown in Fig. 4.12, was 0.38 in. (0.05 in. to 0.43 in.). The dynamic deflection at 975,000 was also 0.38 in. (0.05 to 0.43 in.) indicating no measurable dynamic amplification.

4.4 Specimen C-16-NP-10.1-NO-0.91

This specimen was a Texas Type C with 16 straight strands. There was no passive reinforcing steel in the lower flange. The maximum fatigue load (P_{max}) produced a nominal concrete tensile stress of $10.1\sqrt{f'_{ct}}$. No loads above P_{max} were applied to the specimen during static testing. Fatigue loads were applied for 0.91 million cycles.

4.4.1 Initial Static Tests

Specimen C-16-NP-10.1-NO-0.91 was intentionally prestressed to approximately 0.6 f_{pu} to simulate the effects of long term losses or fabrication errors. It was initially loaded incrementally to 61.5 kips. Flexural cracks became visible at a load of 56 kips. Figure 4.18 of static centerline concrete strain versus load and Fig. 4.19 of static centerline wire, strain versus load, indicate that cracking probably occurred at approximately 50 kips. A substantial reduction in stiffness as a result of flexural cracking is shown in Figs. 4.18 and 4.19 between the first and second cycles. Seven flexural cracks were formed during the initial static cycles.

4.4.2 Zero Tension Load, P_o

The insert in Fig. 4.20 of static load versus deflection between 20 and 40 kips indicates a change in stiffness between the first and second cycles at approximately 25 kips. This is the zero tension load. The centerline deflection at this load, during the initial cycles, was 0.148 in.

4.4.3 Fatigue Loads

Specimen C-16-NP-10.1-NO-0.91 was designed as a companion to Specimen C-16-NP-7.2-OL-1.48. The major variable was the initial prestress level. Both specimens were cycled at 60.8 kips. Based on a zero tension load of 25 kips, this produced a nominal concrete tensile stress in Specimen C-16-NP-10.1-NO-0.91 of $10.1\sqrt{f'_{ct}}$. The minimum load was 27.1 kips. The initial static strain range between 27.1 and 60.8

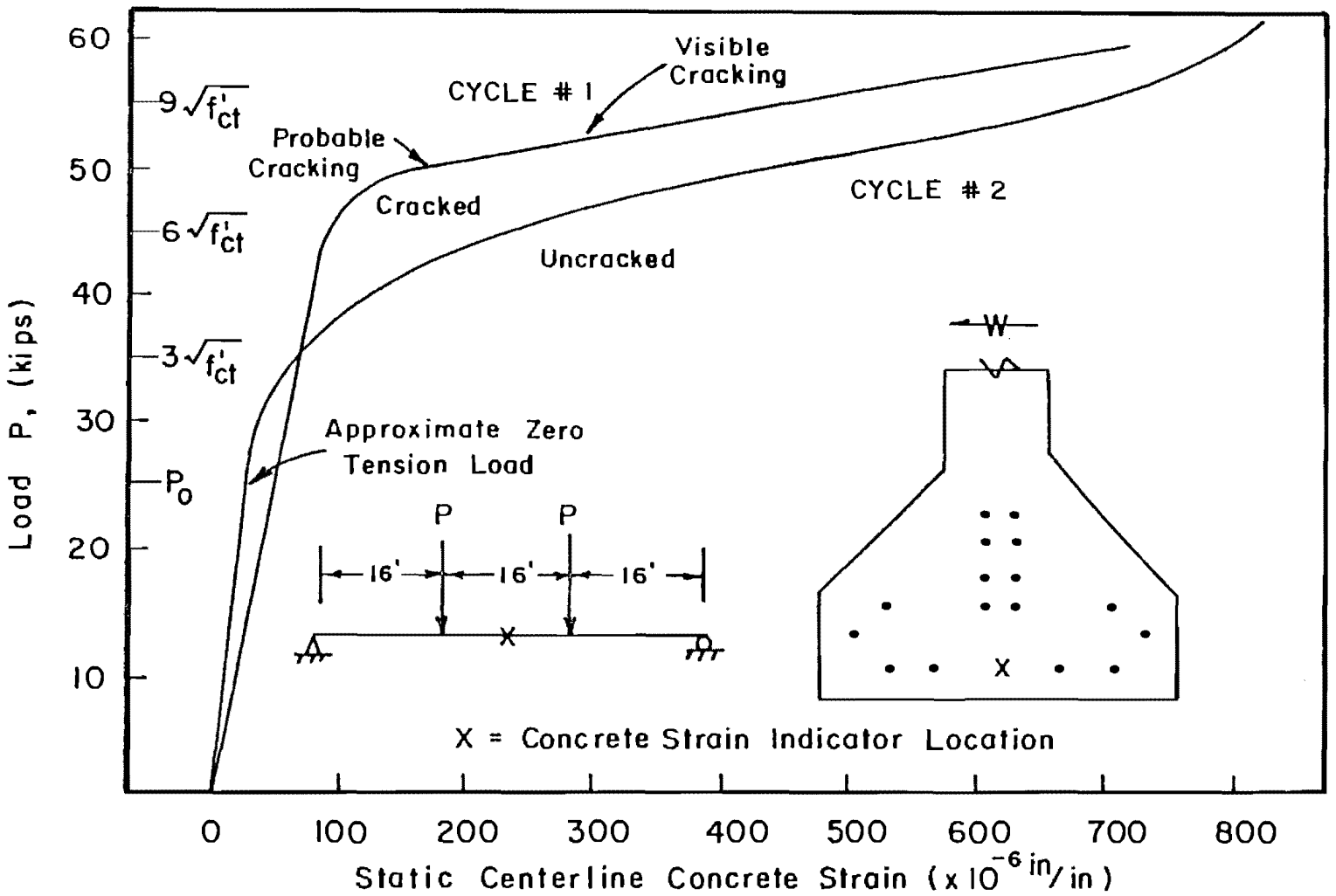

Fig. 4.18 Load versus concrete strain for Specimen C-16-NP-10.1-NO-0.91

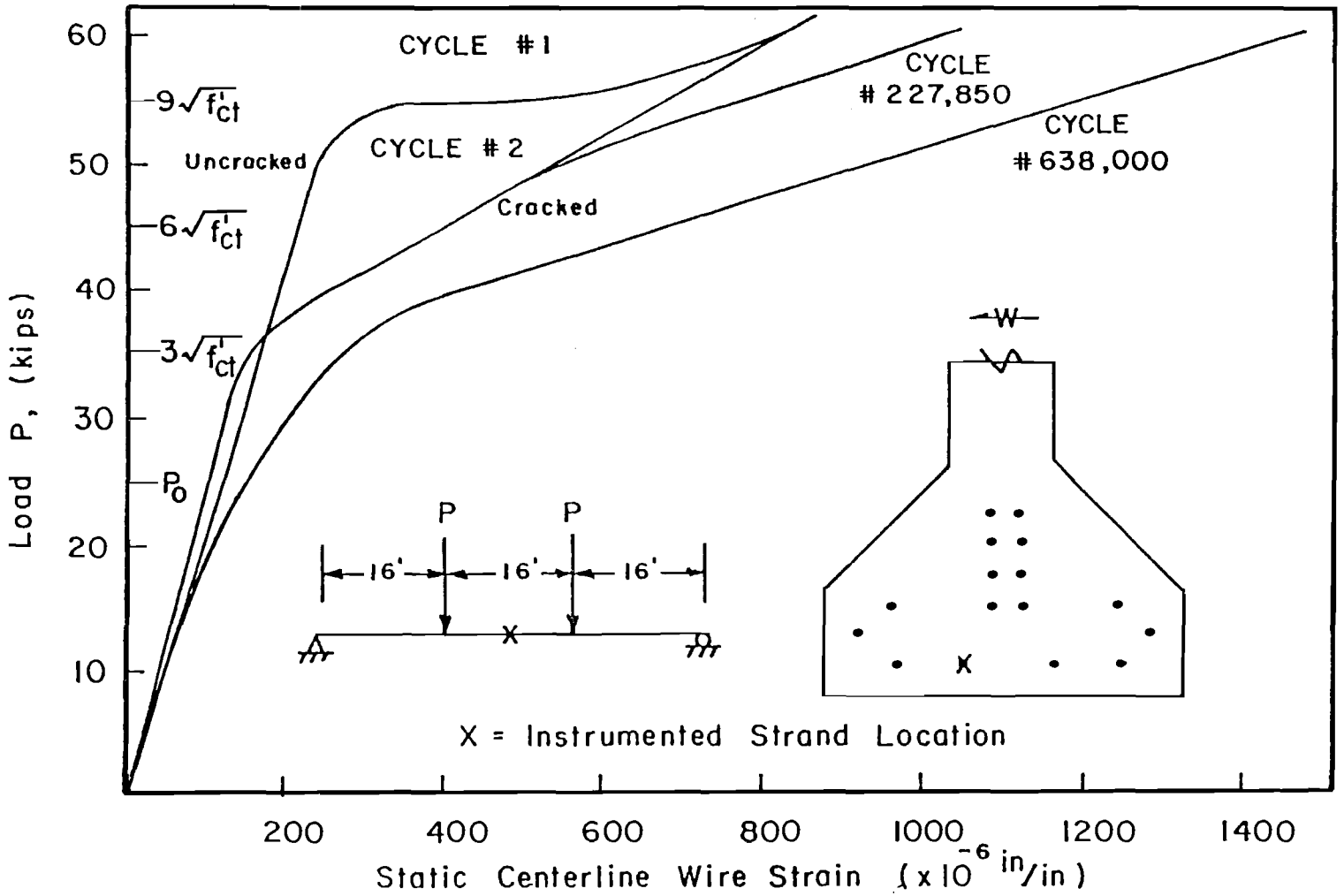

Fig. 4.19 Load versus wire strain for Specimen C-16-NP-10.1-NO-0.91

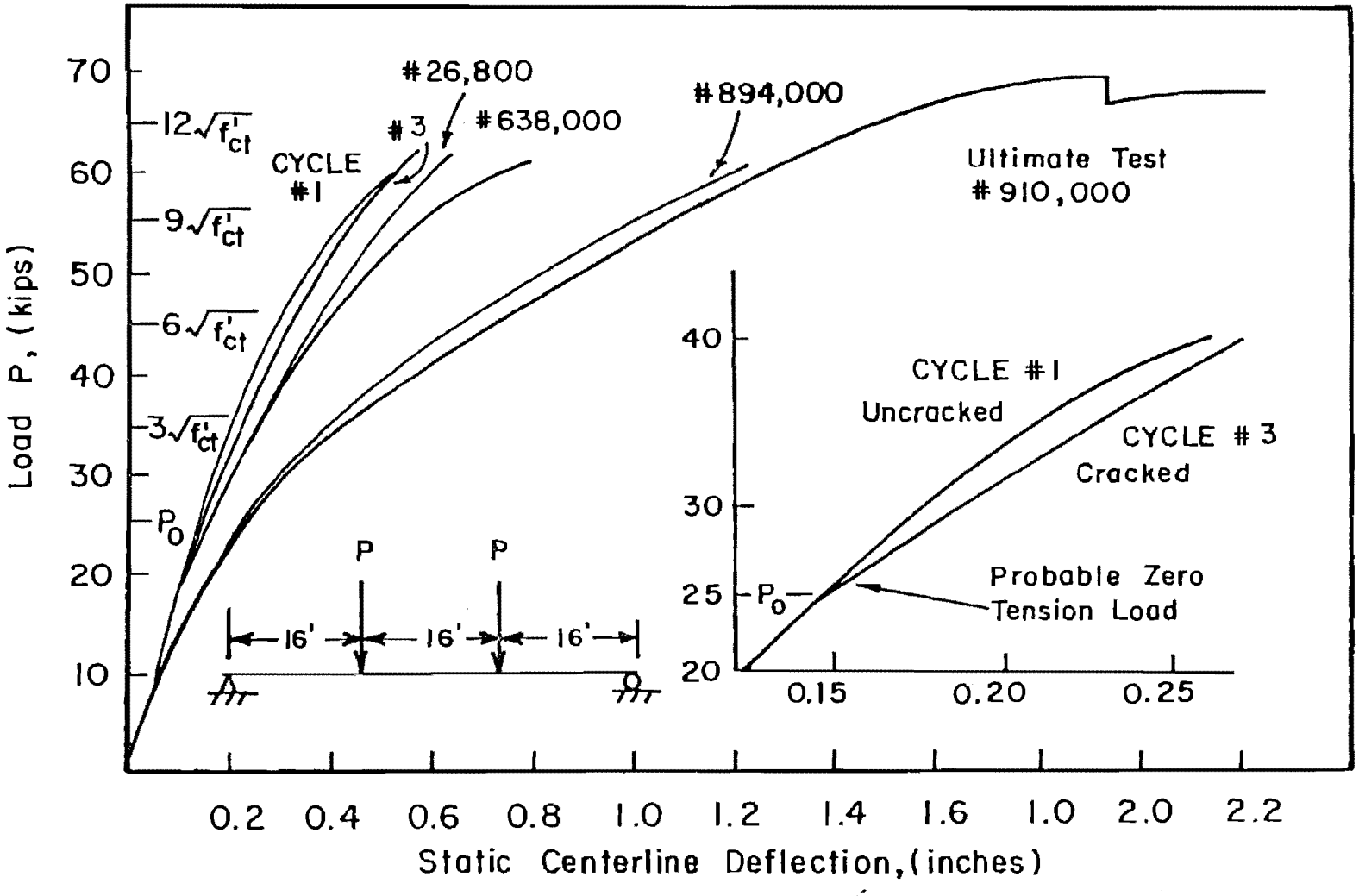

Fig. 4.20 Load versus deflection during static tests for Specimen C-16-NP-10.1-NO-0.91

kips was approximately 0.00070 in./in. The load program for this specimen can be seen in Fig. 4.21.

4.4.4 Fatigue Behavior

The specimen's behavior degraded slowly throughout most of the fatigue test. Figure 4.22 shows that the static centerline deflection never stabilized. Figure 4.20 shows the load deflection curves at various phases of fatigue testing. Notice the decrease in the initial linear portion of the curves as cycling progressed. This phenomenon can also be seen in Fig. 4.19.

Flexural cracks continued to form and propagate during fatigue testing. After 369,000 cycles two forked cracks were marked. These two cracks can be seen in Fig. 4.23, 1 in. and 2 ft 6 in. south of the centerline. This forked configuration often indicates bond degradation [15,25,47]. There were 13 flexural cracks at 369,000 cycles in the center 17 ft of the span. Dynamic strain readings during the initial 471,000 cycles indicated a strain range of 0.00079 in./in.

The specimen deteriorated rapidly after 638,000 cycles. The static centerline deflection at 61.5 kips increased from 0.79 in. at that time (the third point deflection was 0.67 in.) to 1.22 in., a 54 percent increase, at 894,000 cycles, to 1.31 in., a 66 percent increase, at 910,000 cycles. Wire breaks could be heard periodically from 837,000 cycles to the end of fatigue testing. Cracks did not close upon removal of load at 837,000 cycles. Horizontal cracking of the lower flange and substantial concrete spalling 2 ft north of the centerline occurred after 894,000 cycles. Cracking at 894,000 cycles is shown in Fig. 4.24. There were 15 flexural cracks prior to the ultimate test at 910,000 cycles in the center 19 ft of the specimen. Figure 4.25 shows a slight offset in the lower flange prior to the ultimate test probably as a result of unsymmetrical wire fractures.

4.4.5 Static Ultimate Test

The specimen was loaded incrementally to failure at 69.8 kips, which is 60 percent of the calculated ultimate capacity. Failure was by brittle fracture of the remaining prestressing strands. The ultimate deflection, as shown in Fig. 4.20, was 2.22 in. The deflection at 69.8 kips was 1.93 in.

4.4.6 Post Mortem Investigation

The concrete cover was removed from the prestressing strands after the ultimate test to reveal 88 fatigue fractures on 15 of the 16 strands at eight locations. Figure 4.23 shows the fatigue fracture

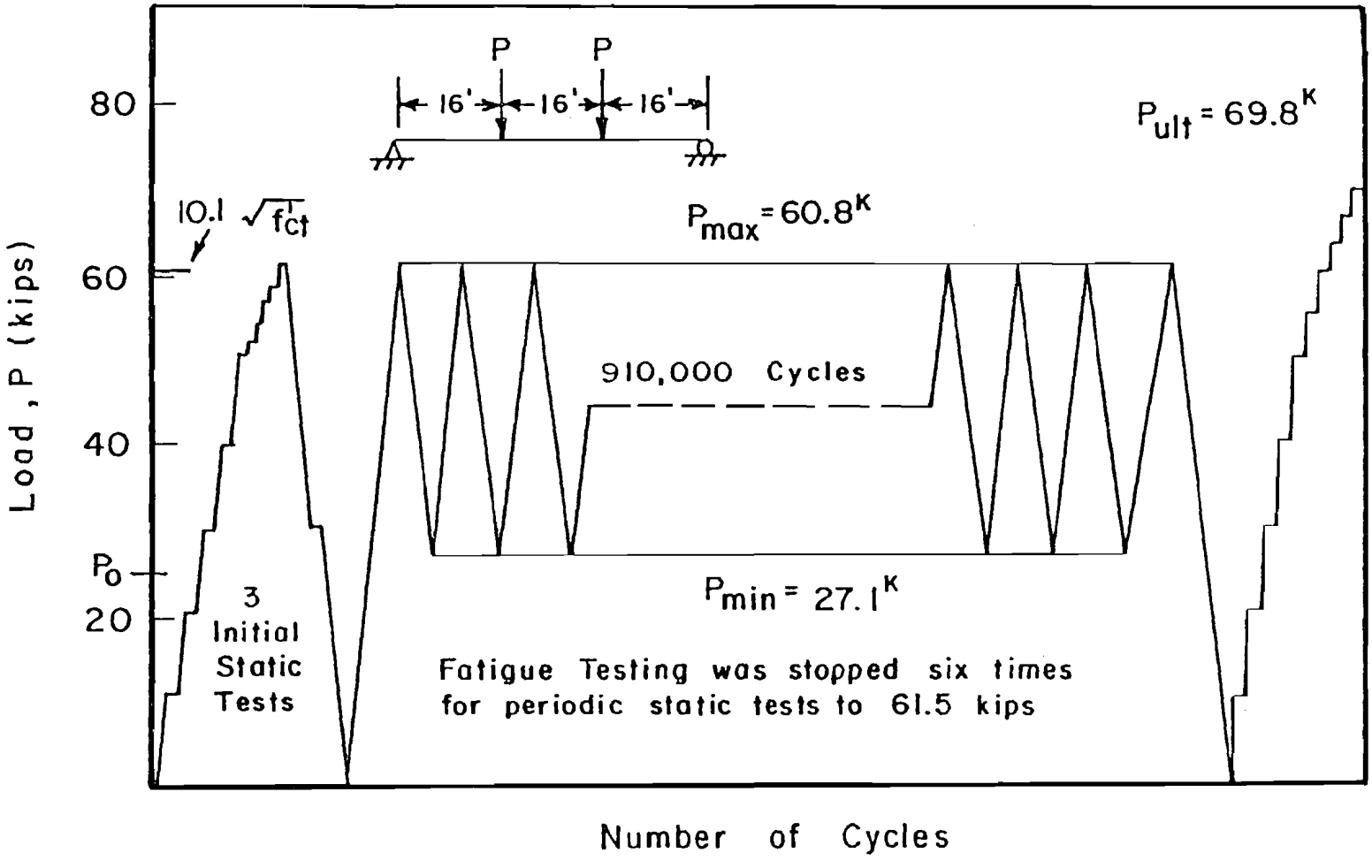

Fig. 4.21 Load program for Specimen C-16-NP-10.1-NO-0.91

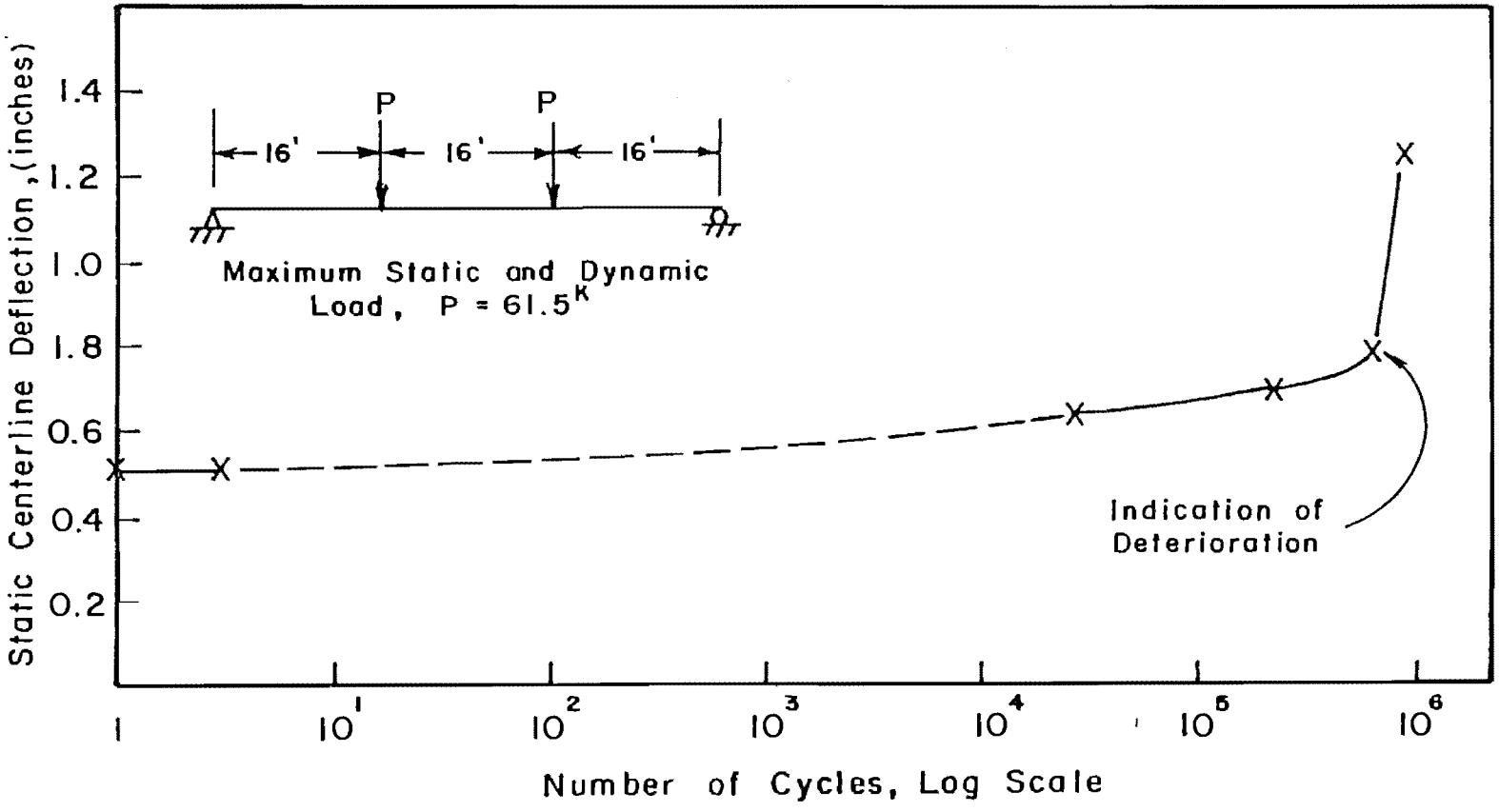

Fig. 4.22 Maximum centerline deflection during static tests for Specimen C-16-NP-10.1-NO-0.91

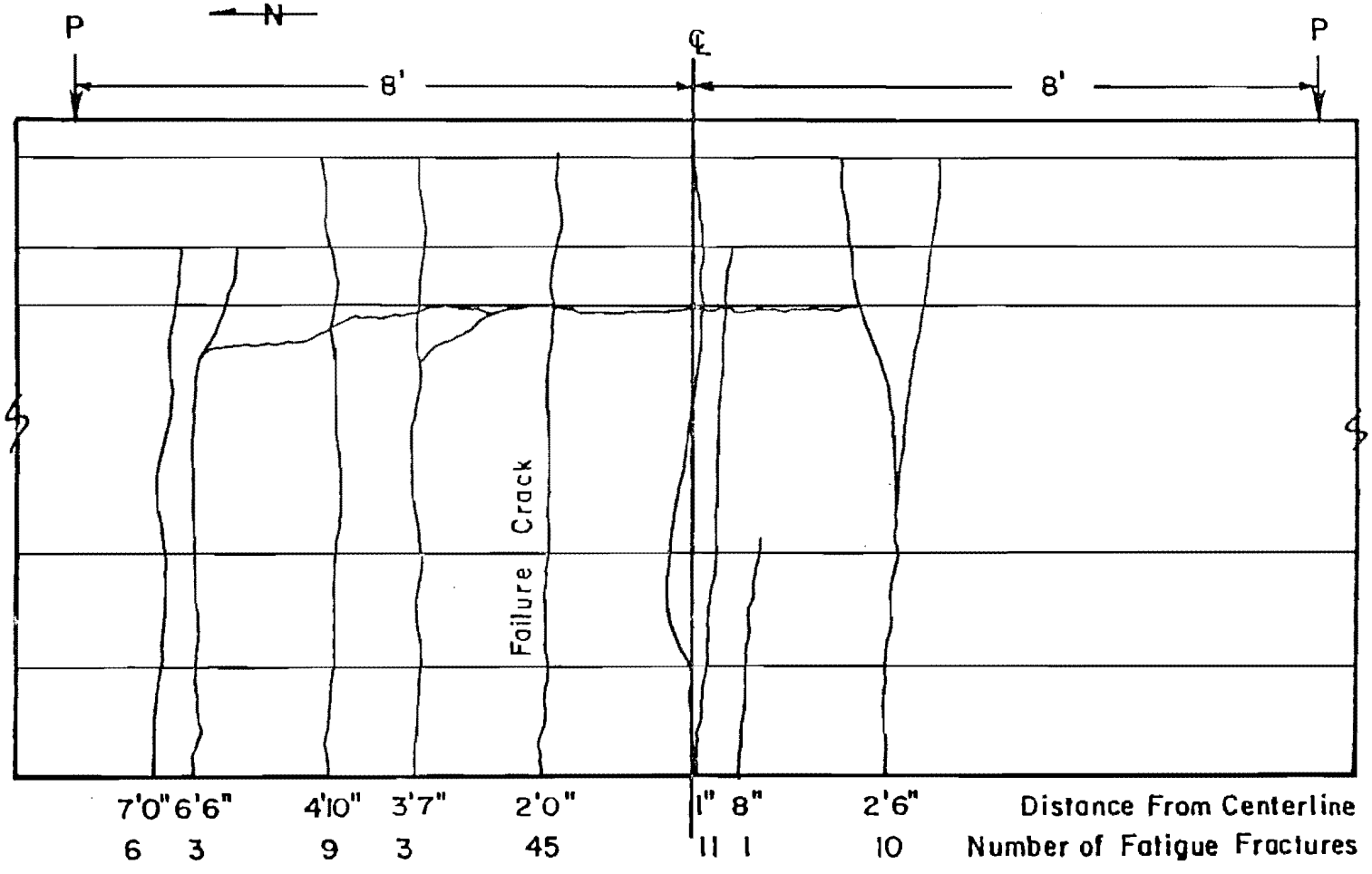

Fig. 4.23 Location and number of wire fatigue fractures and corresponding concrete cracks for Specimen C-16-NP-10.1-NO-0.91

locations along the member. Figure 4.26 shows the breaks with respect to the cross section.

4.4.7 Dynamic Load Amplification

The static centerline deflection between 27.1 and 60.8 kips at 638,000 cycles was 0.61 in. (0.18 in. to 0.79 in.). This is before the specimen began to deteriorate significantly. The dynamic centerline deflection between these two loads was 0.65 in. (0.23 in. to 0.88 in.) which indicates dynamic amplification. The static loads corresponding to these dynamic deflections were approximately 34 and 64 kips.

4.5 Specimen C-16-NP-6.0-NO-1.91

This was a Texas Type C specimen with 16 straight strands. There was no passive (NP) reinforcing steel in the lower flange. The maximum fatigue load (P_{max}) produced a nominal concrete tensile stress at $6.0\sqrt{f'_{ct}}$. There were no overloads (NO), loads above P_{max}, during periodic static tests. The specimen experienced 1.91 million fatigue cycles.

4.5.1 Initial Static Tests

Specimen C-16-NP-6.0-NO-1.91 was designed as a combined flexural/shear specimen. For this reason, the member was initially loaded with a constant moment region of 16 ft to produce flexural cracks. The load frame was then modified to produce a higher shear to moment ratio. The constant moment region for fatigue testing was 24 ft.

Flexural cracking was first visible at 70 kips. Eight cracks formed during the initial five static cycles. None of them extended into the web. Figure 4.27 of load versus wire strain indicates that flexural cracking probably first began at approximately 60 kips.

4.5.2 Zero Tension Load, P_o

Figure 4.27 of load versus strain and Fig. 4.28 of load versus crack opening width during unloading indicate a deviation from the initial linear behavior at approximately 37.5 kips. This is the load at which the extreme tension fibers experienced tension, and as a result of flexural cracking, the cracks opened reducing the effective moment of inertia. A change in behavior results. The centerline deflection at 37.5 kips was 0.223 in.

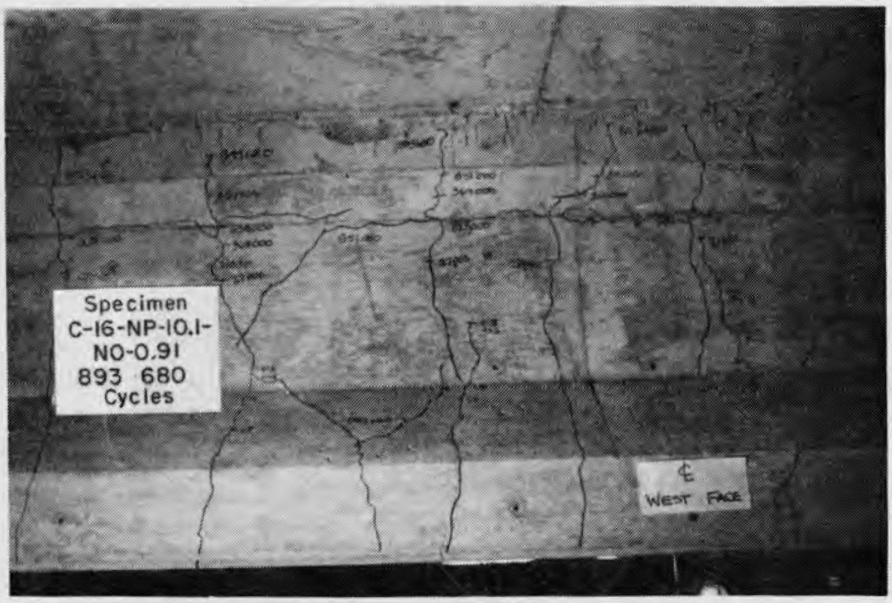

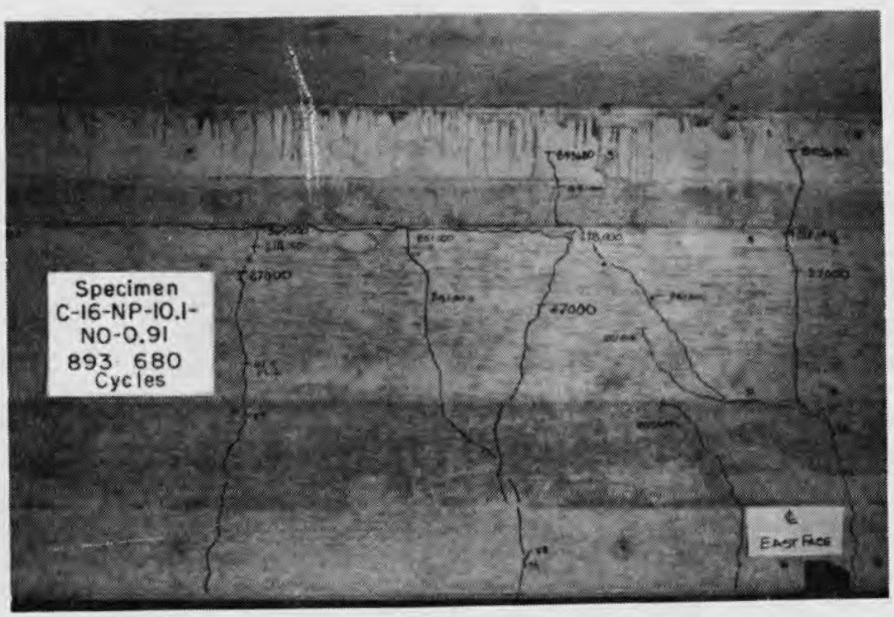

Fig. 4.24 Cracking at 893,680 cycles

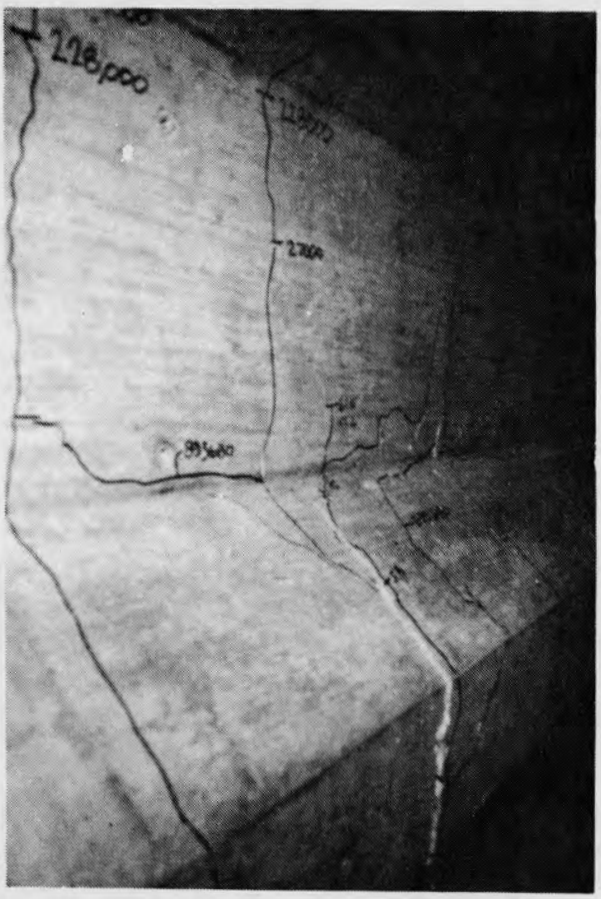

Fig. 4.25 Offset in the lower flange prior to the static ultimate test

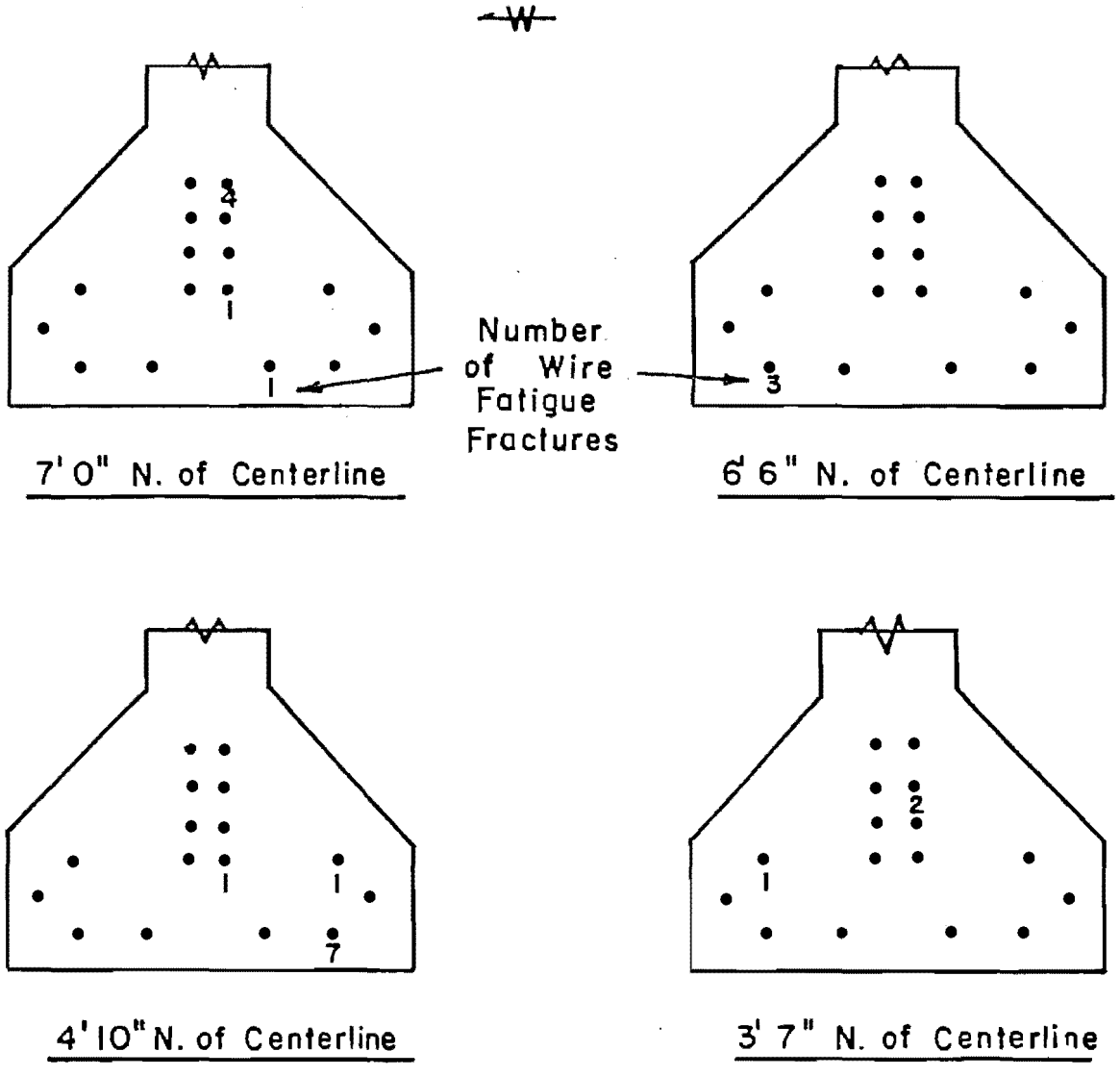

Fig. 4.26 Fatigue fracture locations for Specimen C-16-NP-10.1-NO-0.91

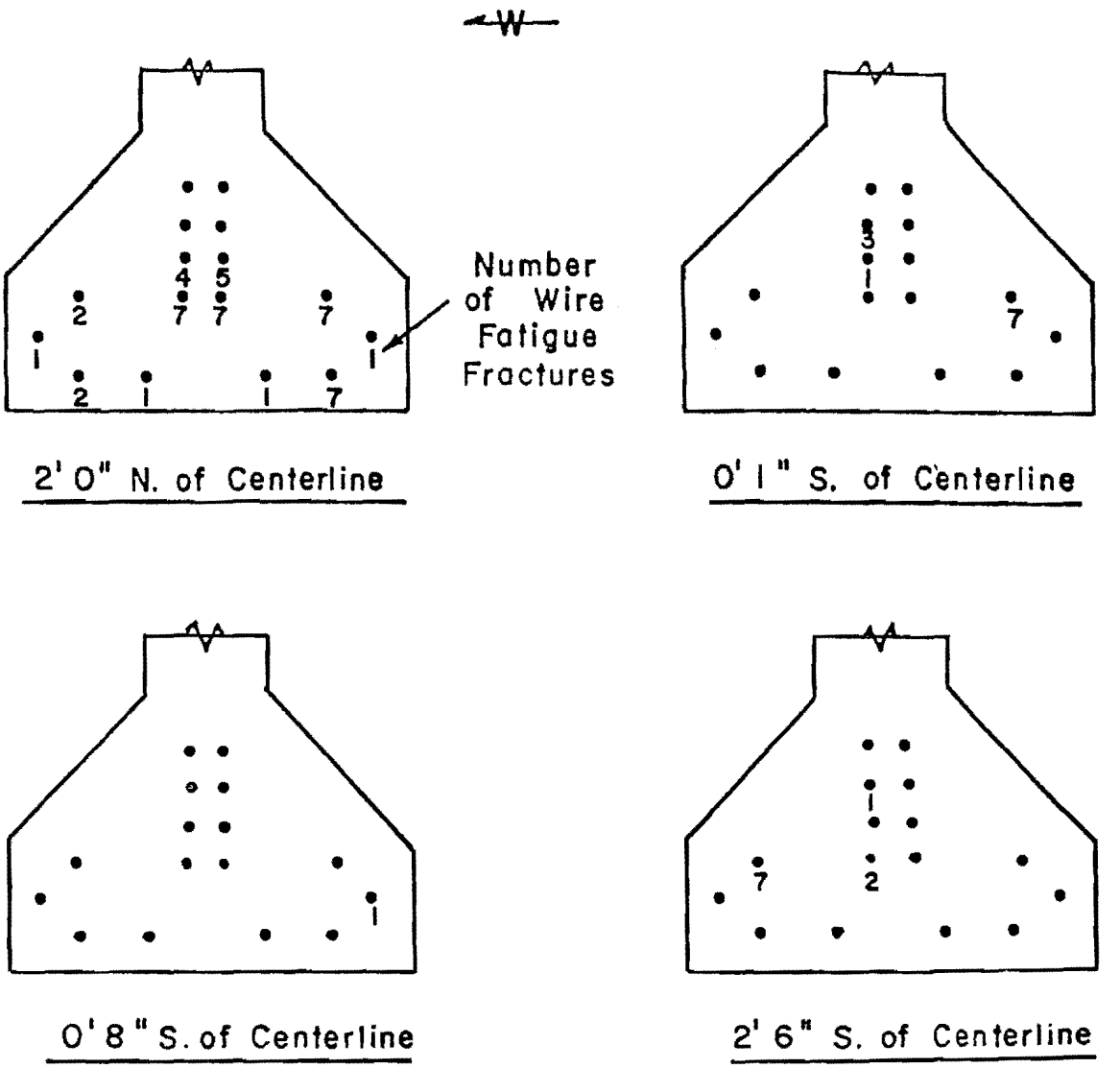

Fig. 4.26 Fatigue fracture locations for Specimen C-16-NP-10.1-NO-0.91 (continued)

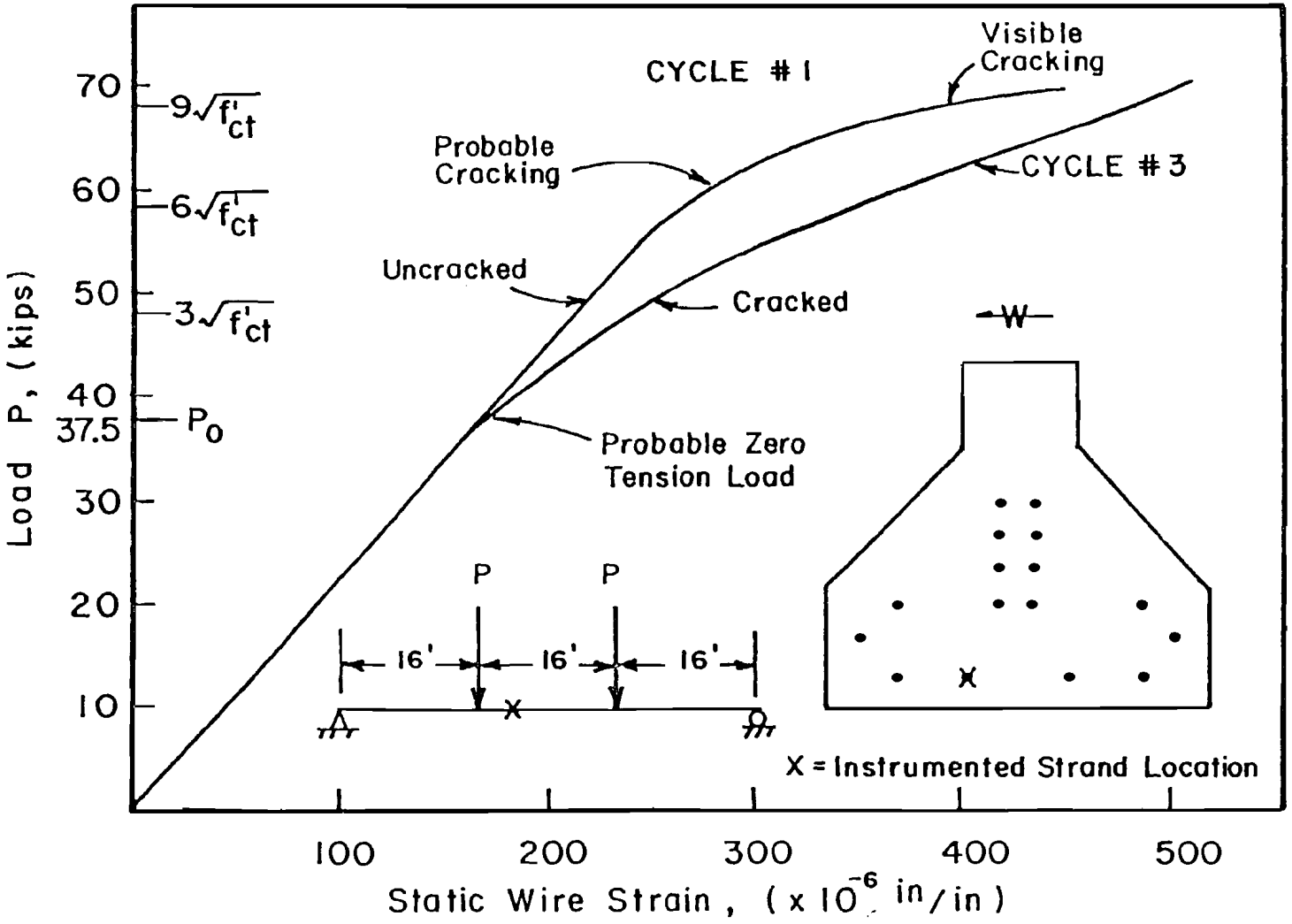

Fig. 4.27 Load versus static wire strain 4 ft 4 in. north of centerline during initial cycles for Specimen C-16-NP-6.0-NO-1.91

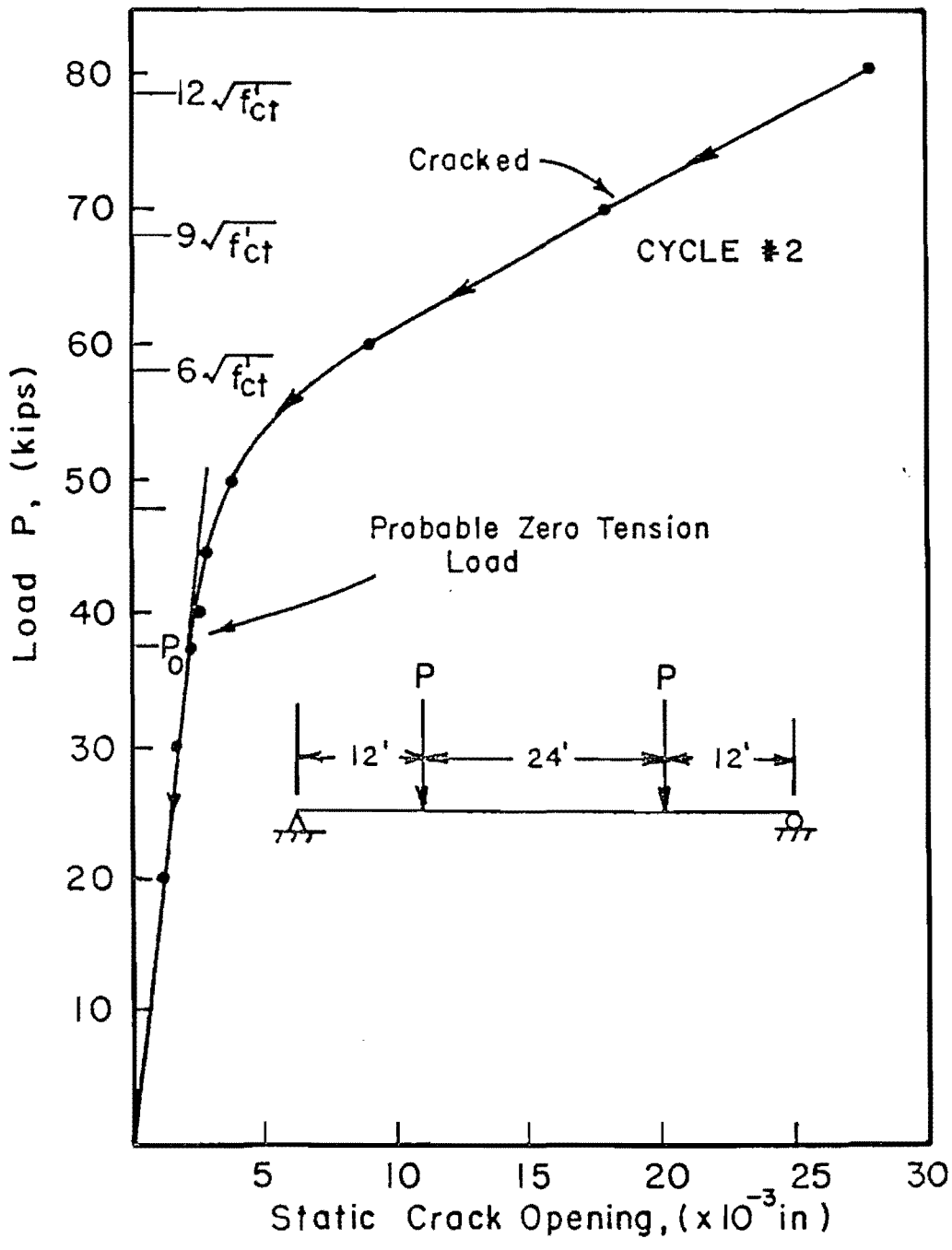

Fig. 4.28 Load versus static crack opening 7 in. north of centerline during unloading for Specimen C-16-NP-6.0-NO-1.91

4.5.3 Fatigue Loads

A nominal concrete tensile stress of $6.0\sqrt{f'_{ct}}$ was selected for Specimen C-16-NP-6.0-NO-1.91 to determine if increased shear coupled with flexural tension, at the AASHTO design level, would result in a failure at less than 5.0 million cycles. Based on uncracked section properties and a zero tension load of 50 kips (with a 12 ft shear span, 37.5 kips with a 16 ft shear span) the maximum fatigue load was 80 kips. The minimum load was 10 kips. The load program is shown in Fig. 4.24.

4.5.4 Fatigue Behavior

The specimen's behavior remained relatively stable for the first 1,080,000 cycles. Figure 4.30 indicates that the centerline deflection stabilized after the initial static tests at 0.41 in. The centerline deflection after 1,080,000 cycles for a load of 80 kips was 0.47 in., a 15 percent increase. The quarter point deflection at this point was 0.37 in. Permanent deflection, deflection with no load, was approximately 0.2 in., as shown in Fig. 4.31. This permanent deflection with no apparent loss of flexural stiffness is probably a result of shear cracking at the ends of the member and cyclic creep of concrete. There were 16 flexural cracks in the center 18.5 ft at 1.08 million cycles.

The member deteriorated rapidly after 1,080,000 cycles. Figures 4.30 and 4.31 show a marked increase in centerline deflection with and without load after 1.08 million cycles. Figure 4.32 indicates that an instrumented crack's opening increased drastically from 0.00498 in. to approximately 0.00988 in. between 1.08 and 1.47 million. The instrumented crack is shown in Fig. 4.37. The permanent crack opening from 300,000 cycles to 1.47 million cycles is shown in Fig. 4.32.

Strand slip at the north end of the specimen was visible at 1.080 million cycles, as shown in Fig. 4.33. Three of the top four strands had slipped at this time. Extensive shear cracking was also present at both ends of the member. Figures 4.34 through 4.36 indicate a marked increase in strain in the lower strands at approximately 40 kips. The top strands probably slipped at this load, and the bottom strands were required to resist more of the internal movement. The maximum record strain between 10 and 80 kips at this time was approximately 0.00060 in./in. The maximum strain during previous static tests was 0.000350 in./in. The dynamic strain range was approximately 0.00095 in./in. Spalling, as shown in Figs. 4.37, occurred at approximately 1.5 million cycles. Wire fractures could be seen at this time. Fatigue testing was stopped after 1.91 cycles as a result of a loss of stiffness due to flexural and shear cracking and wire fractures. There were 21 flexural cracks in the center 18.5 ft before the ultimate test. Three of the upper strands had slipped at this time.

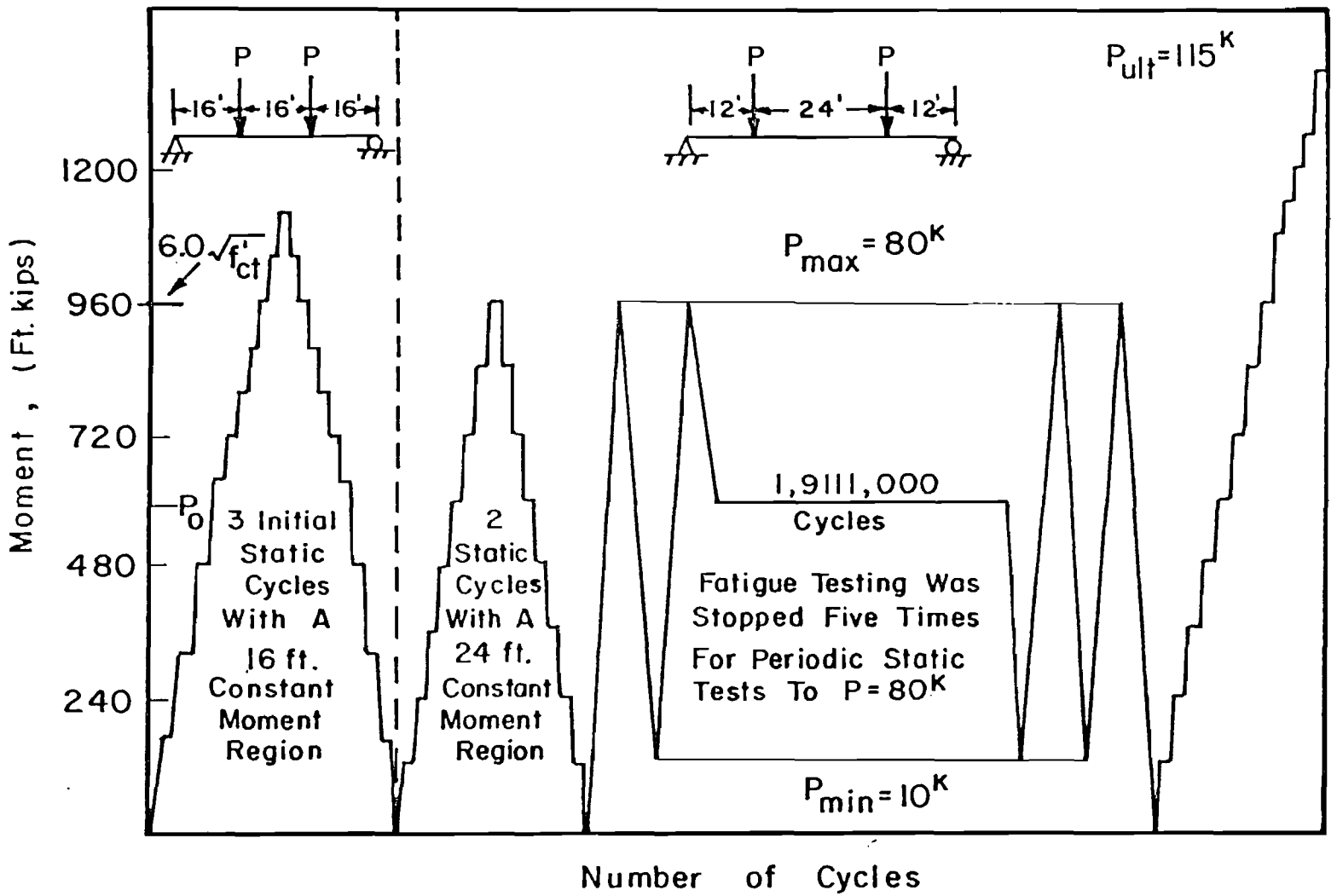

Fig. 4.29 Load program for Specimen C-16-NP-6.0-NO-1.91

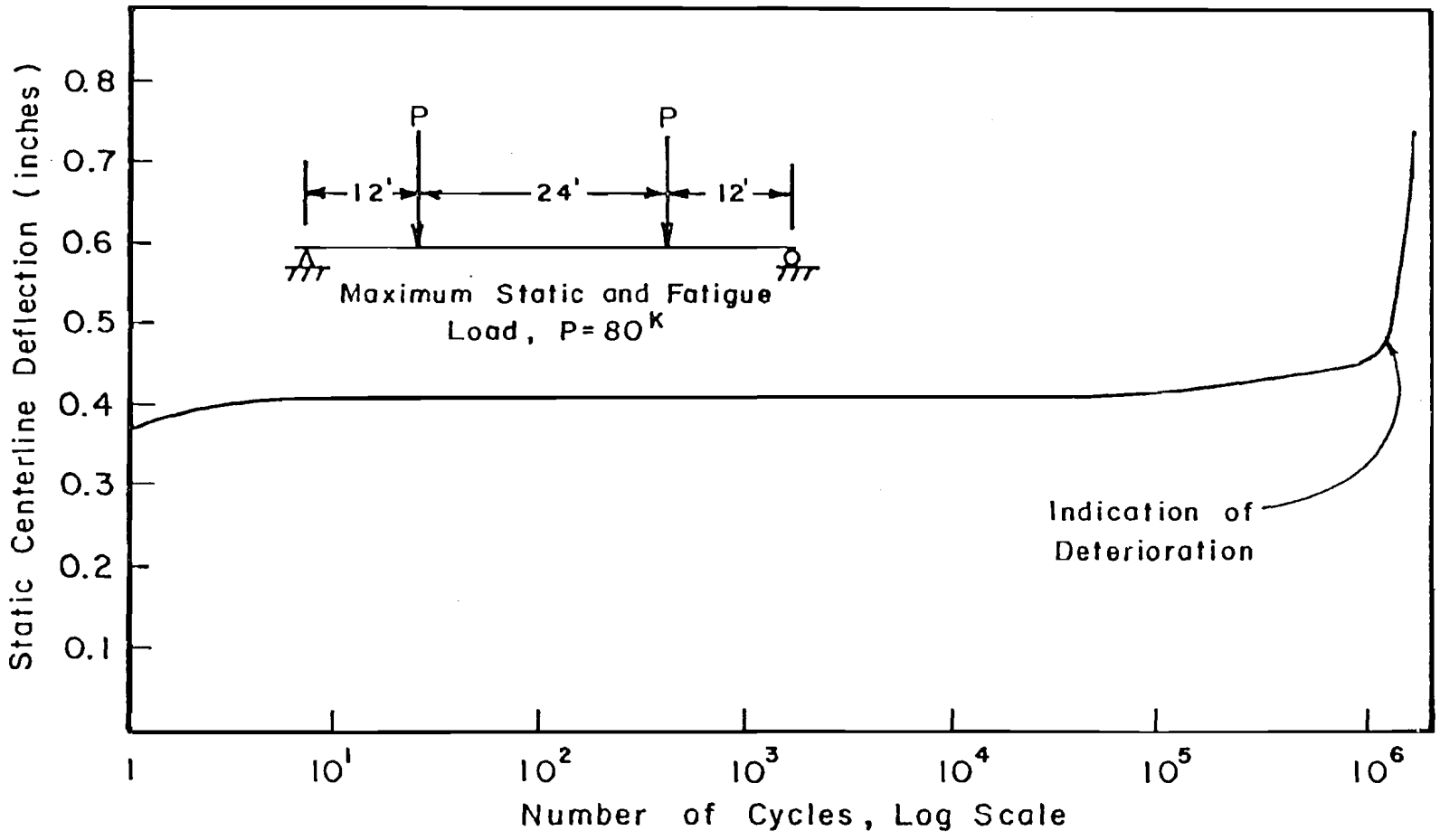

Fig. 4.30 Maximum centerline deflection during static tests for Specimen C-16-NP-6.0-NO-1.91

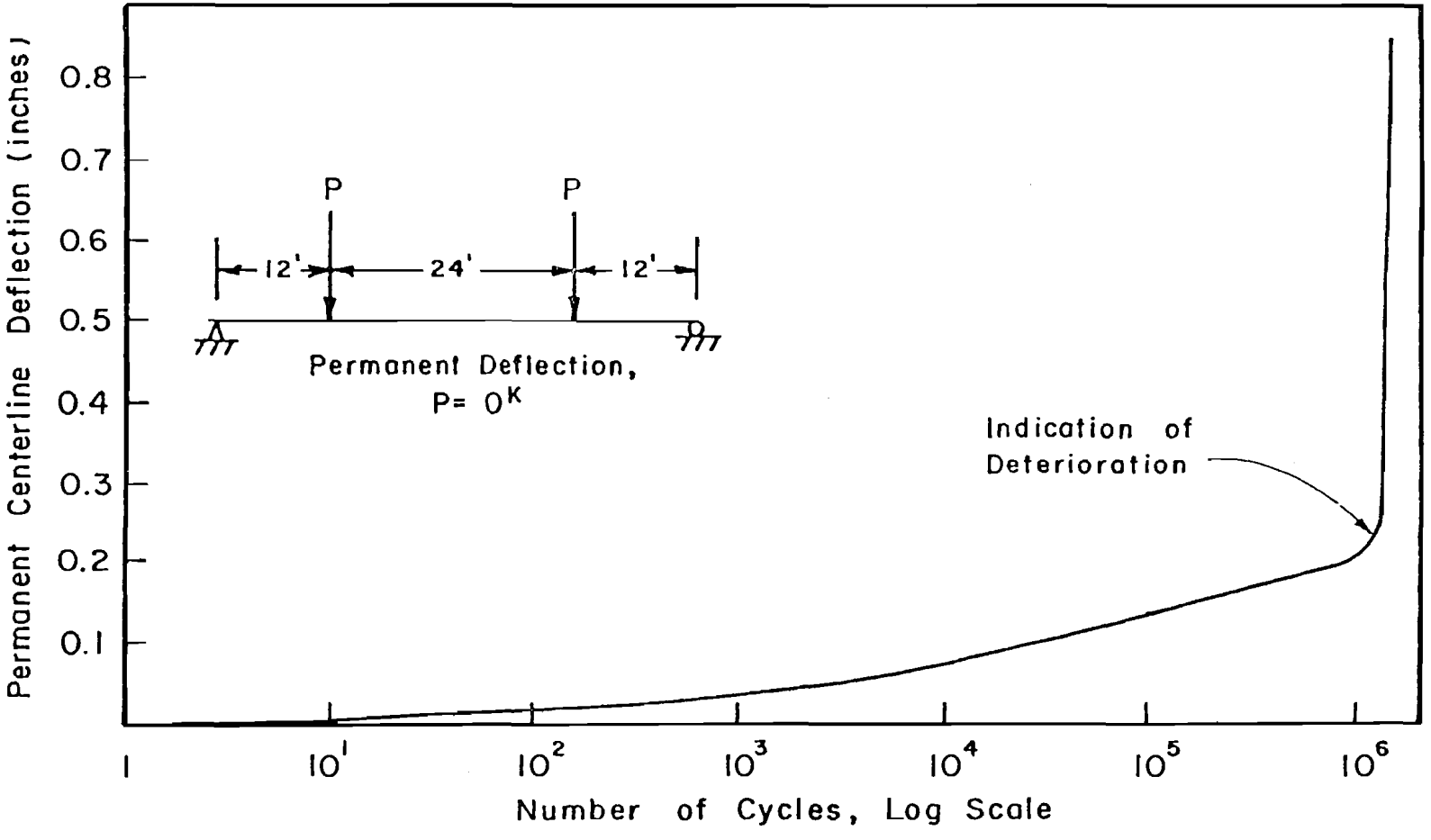

Fig. 4.31 Permanent centerline deflection during static tests for Specimen C-16-NP-6.0-NO-1.91

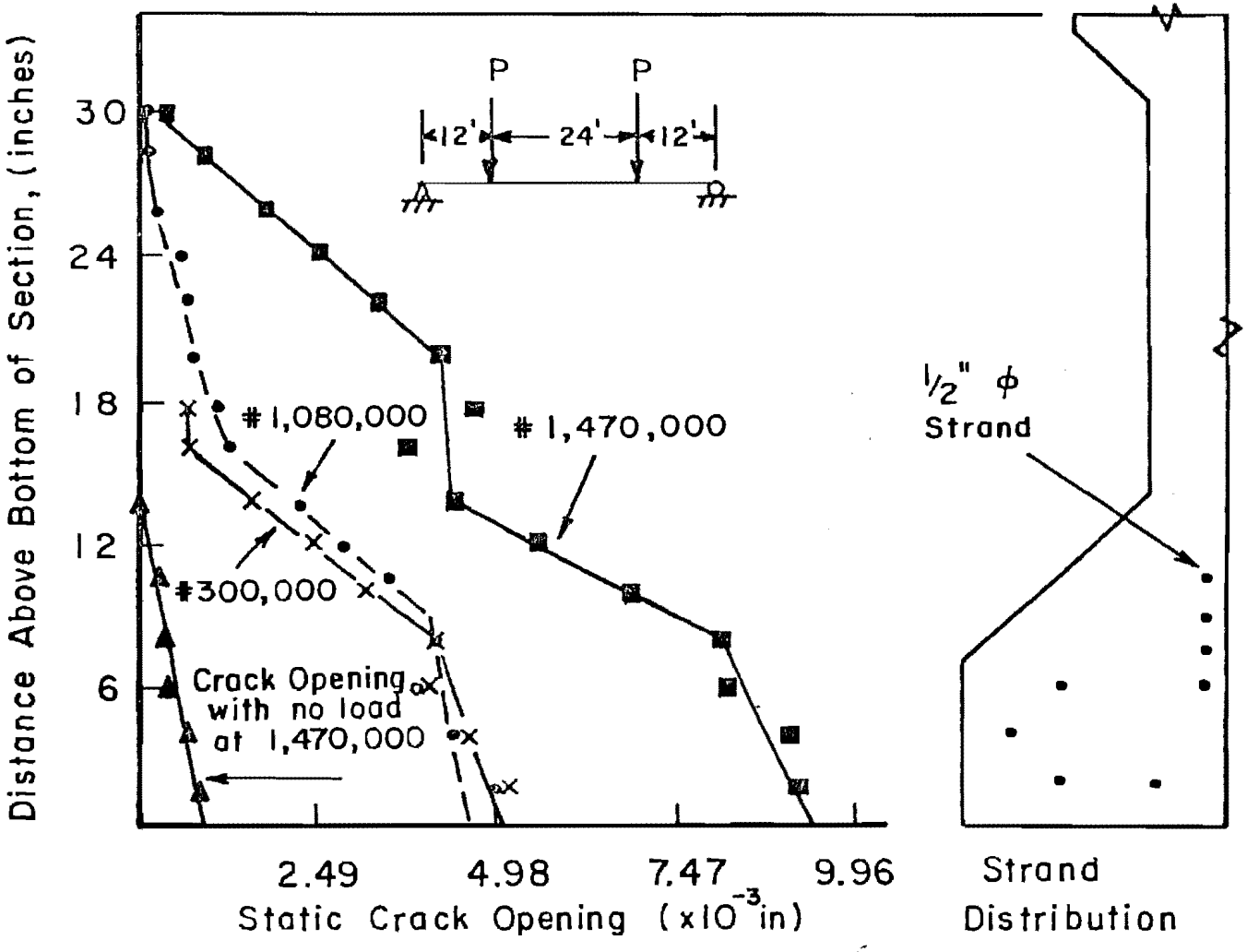

Fig. 4.32 Static crack profile 7 in. north of centerline at 80 kips during static tests

Fig. 4.33

Strand slip at

1.080 million cycles

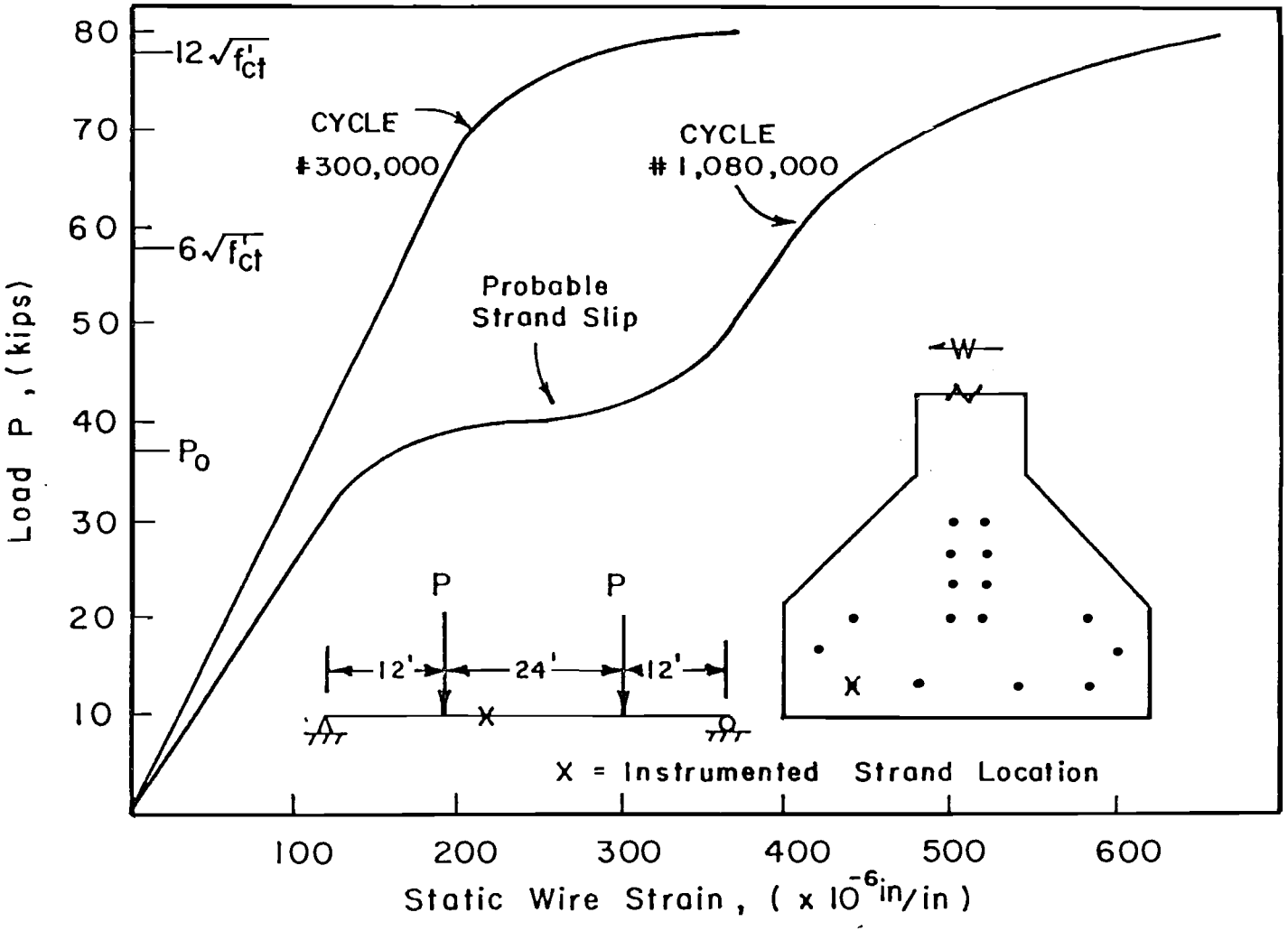

Fig. 4.34 Load versus wire strain 6 ft 8 in. north of centerline at 300,000 and 1.080 million cycles

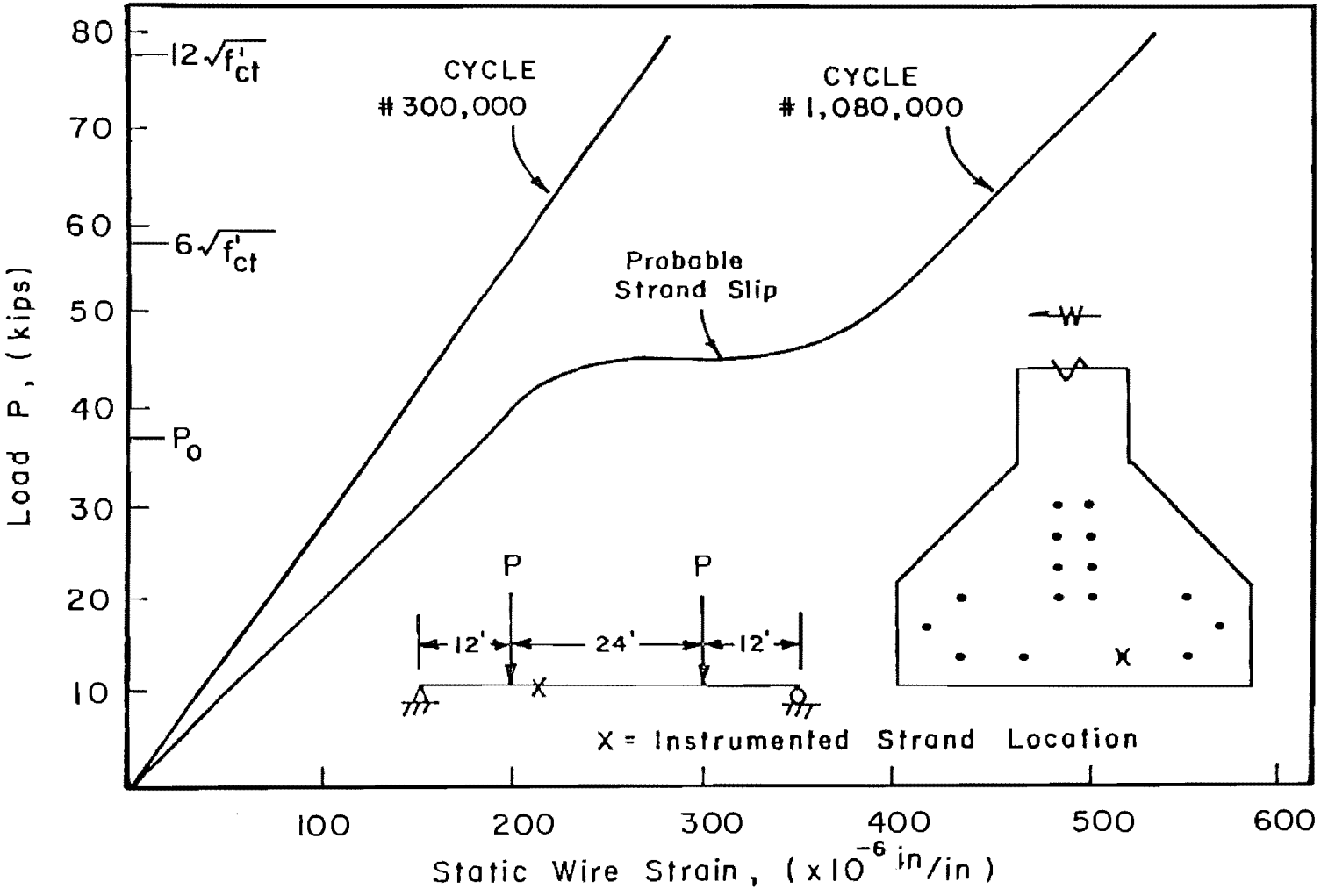

Fig. 4.35 Load versus wire strain 8 ft 6 in. north of centerline at 300,000 and 1.080 million cycles

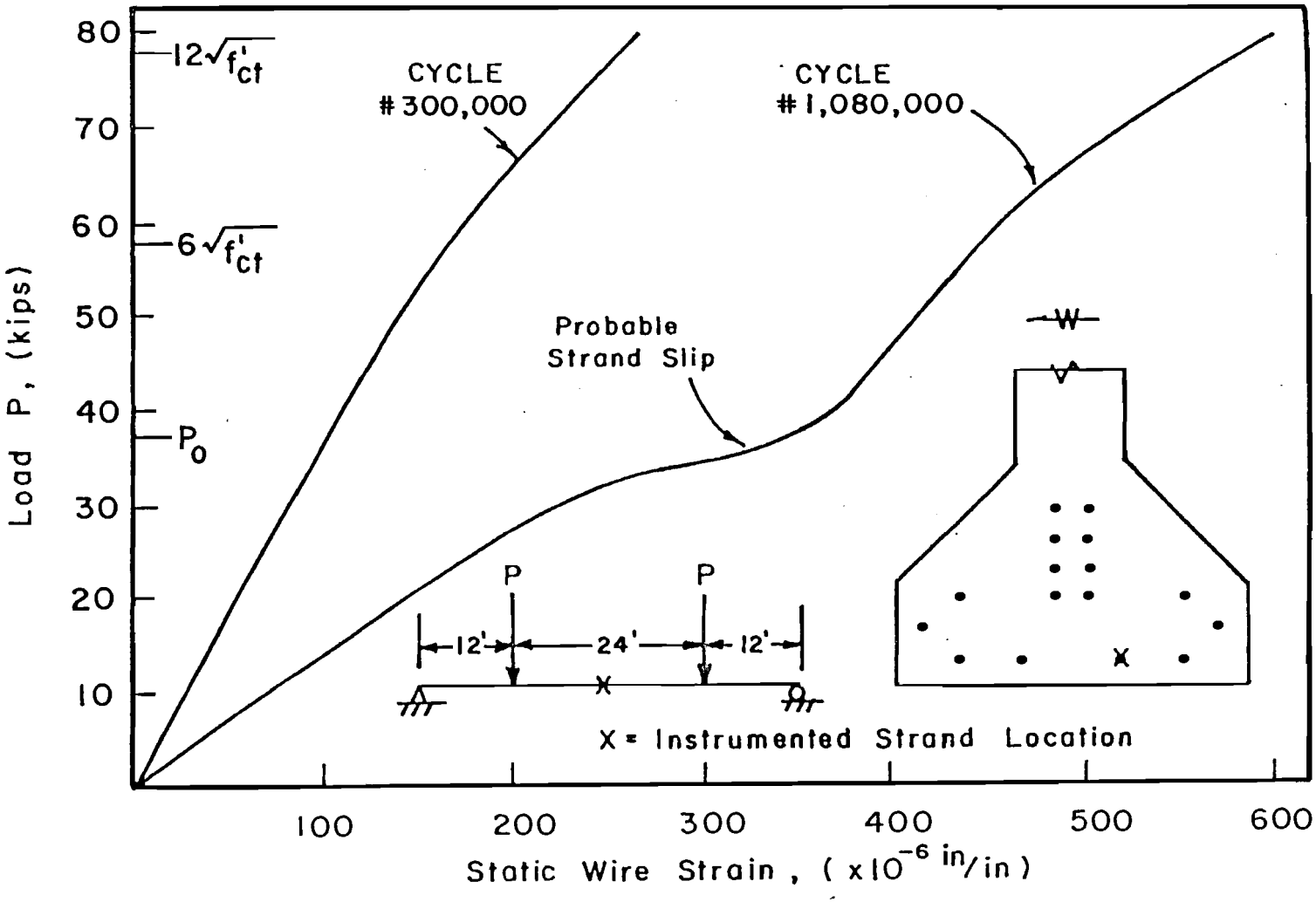

Fig. 4.36 Load versus wire strain 7 in. north of centerline at 300,000 and 1.080 million cycles

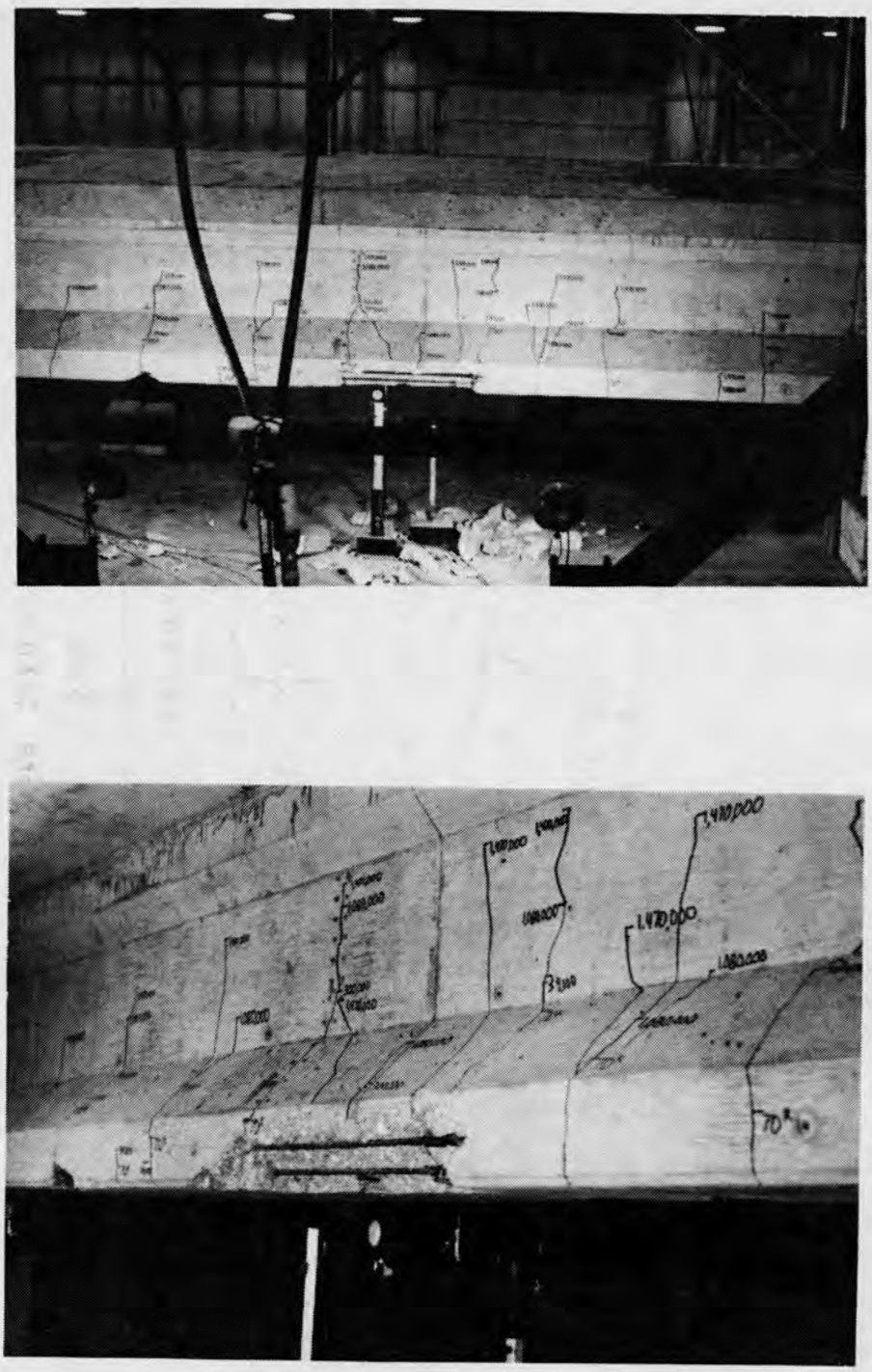

Fig. 4.37 Concrete spalling after approximately 1.5 million cycles

4.5.5 Static Ultimate Test

The specimen was loaded incrementally to 115 kips, which is 71 percent of the calculated ultimate capacity. Figure 4.38 indicates that the specimen possessed some ductility. The deflection at 115 kips was 5.25 in. The maximum deflection was approximately 6.0 in.

4.5.6 Post Mortem Investigation

The post mortem investigation revealed thirty-four fatigue fractures of the wires in the prestressing strand at five locations. Figure 4.39 shows the failure crack was 1 ft 11 in. north of the centerline. Figure 4.40 indicates the fatigue wire fractures relative to the cross section. Notice in Fig. 4.40 that none of the upper ten strands were fractured at any location. This would indicate that the lower strands experienced a higher stress.

4.5.7 Dynamic Load Amplification

The static centerline deflection at 300,000 cycles, which is in the stable portion of the centerline deflection number of cycles curve shown in Fig. 4.30, between 10 and 80 kips was 0.39 in. (0.05 in. to 0.44 in.). The dynamic deflection at 293,400 cycles was 0.42 in. (0.05 in. to 0.47 in.). At 345,000 cycles the dynamic deflection range was 0.41 in. (0.05 in. to 0.46 in.) which indicates slight dynamic amplification. The static loads corresponding to these dynamic deflections were approximately 10 and 83 kips.

4.6 Specimen C-14-NP-5.5-OL-2.29

This specimen was a Texas Type C with 14 strands. Four of these were draped. There was no passive reinforcing steel in the lower flange. The specimen was cycled at a maximum fatigue load (P_{max}) that produced a nominal tensile stress of $5.5\sqrt{f'_{ct}}$. There were overloads during static tests above P_{max}. Fatigue testing was stopped after 2.29 million cycles at $5.5\sqrt{f'_{ct}}$.

4.6.1 Initial Static Tests

Specimen C-14-NP-5.5-OL-2.29 was loaded monotonically to a maximum load of 80 kips. Flexural cracks were first visible at 77.5 kips. Figures 4.41 and 4.42 of load versus prestressing strand wire strain indicate that flexural cracking probably occurred at approximately 70 kips. Figures 4.43 and 4.44 of load versus measured

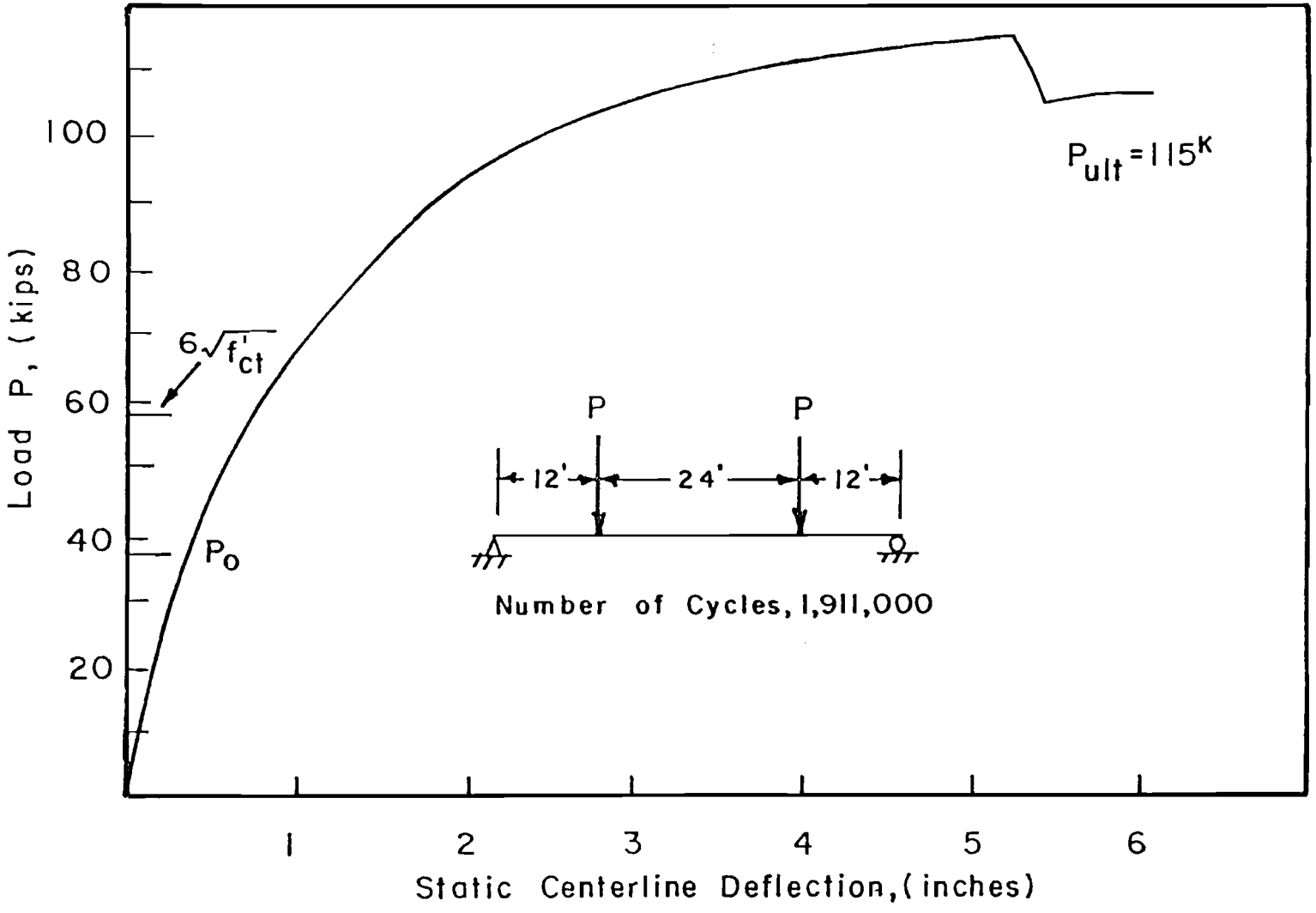

Fig. 4.38 Ultimate load versus deflection for Specimen C-16-NP-6.0-NO-1.91

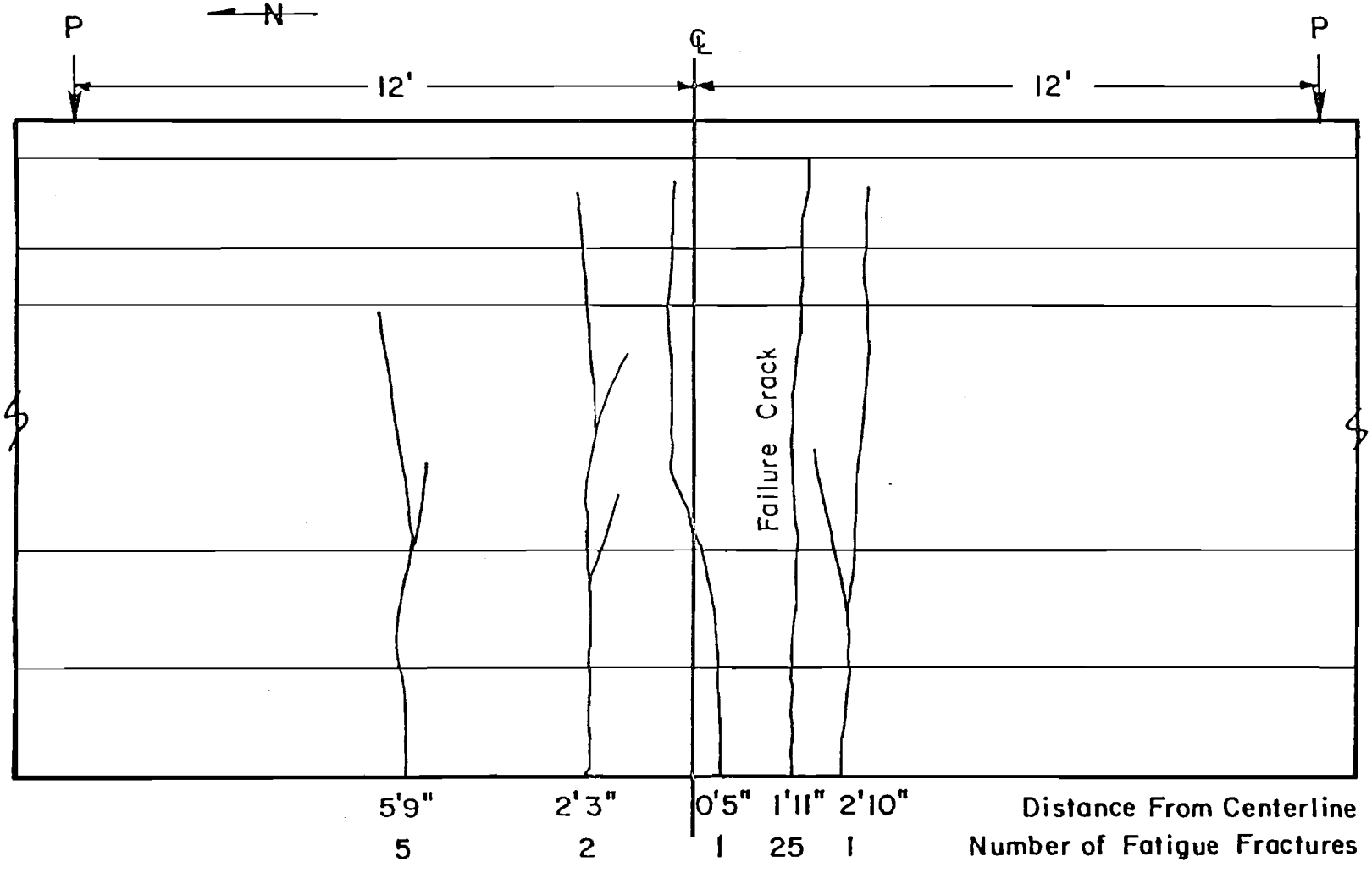

Fig. 4.39 Location and number of wire fatigue fractures and corresponding concrete cracks for Specimen C-16-NP-6.0-NO-1.91

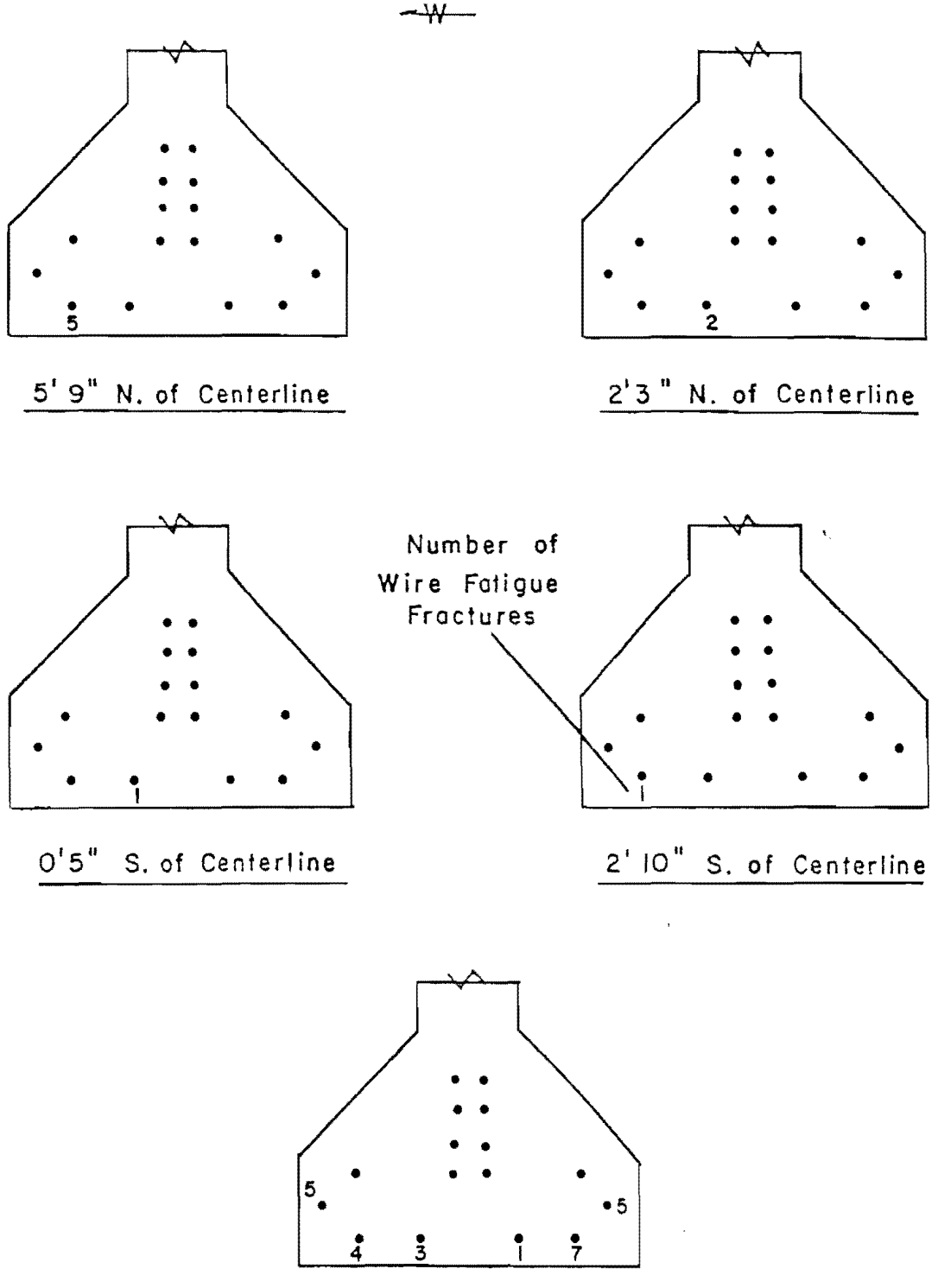

Fig. 4.40 Fatigue fracture locations for Specimen C-16-NP-6.0-NO-1.91

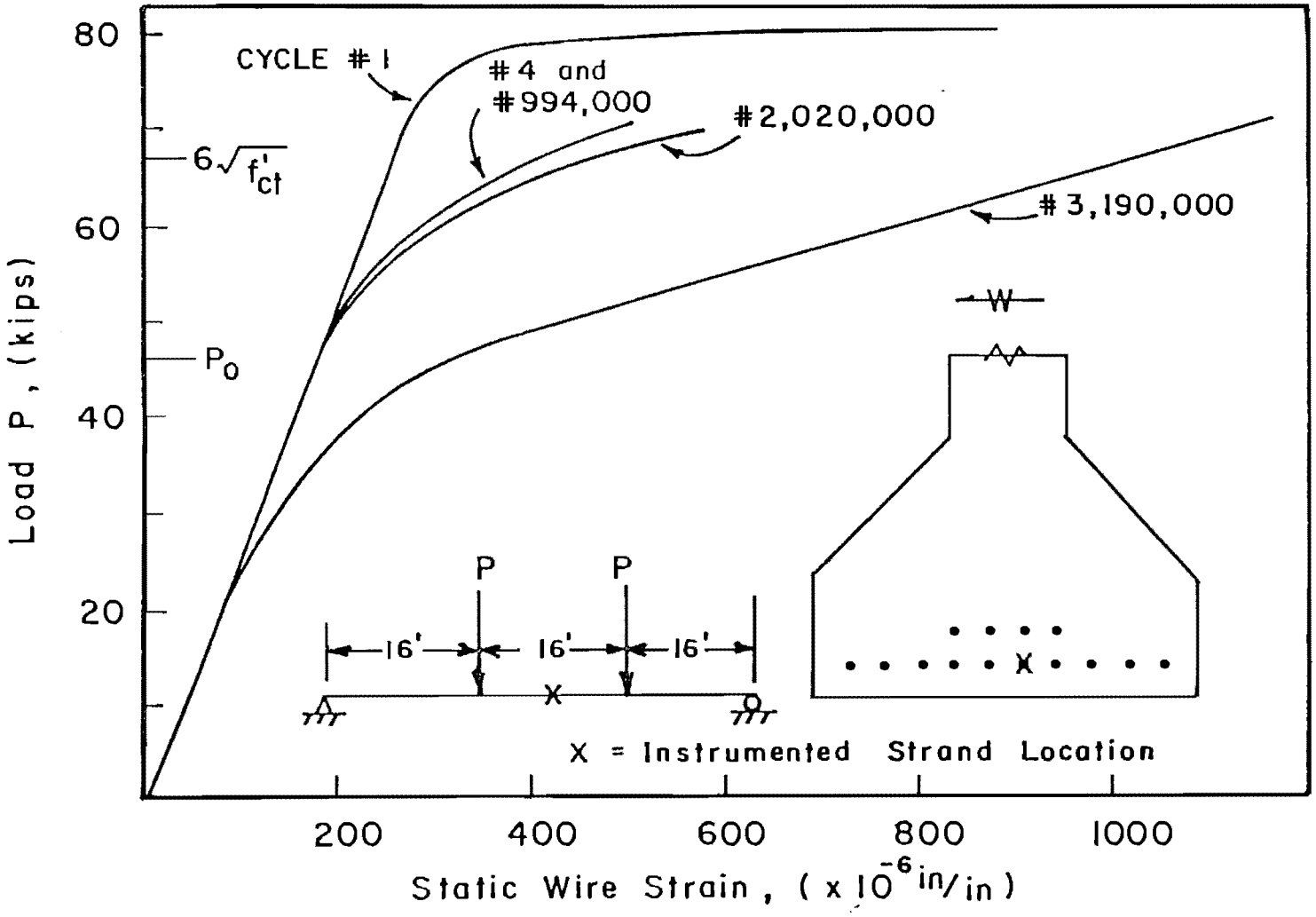

Fig. 4.41 Load versus wire strain 3 in. north of centerline for Specimen C-14-NP-5.5-OL-2.29

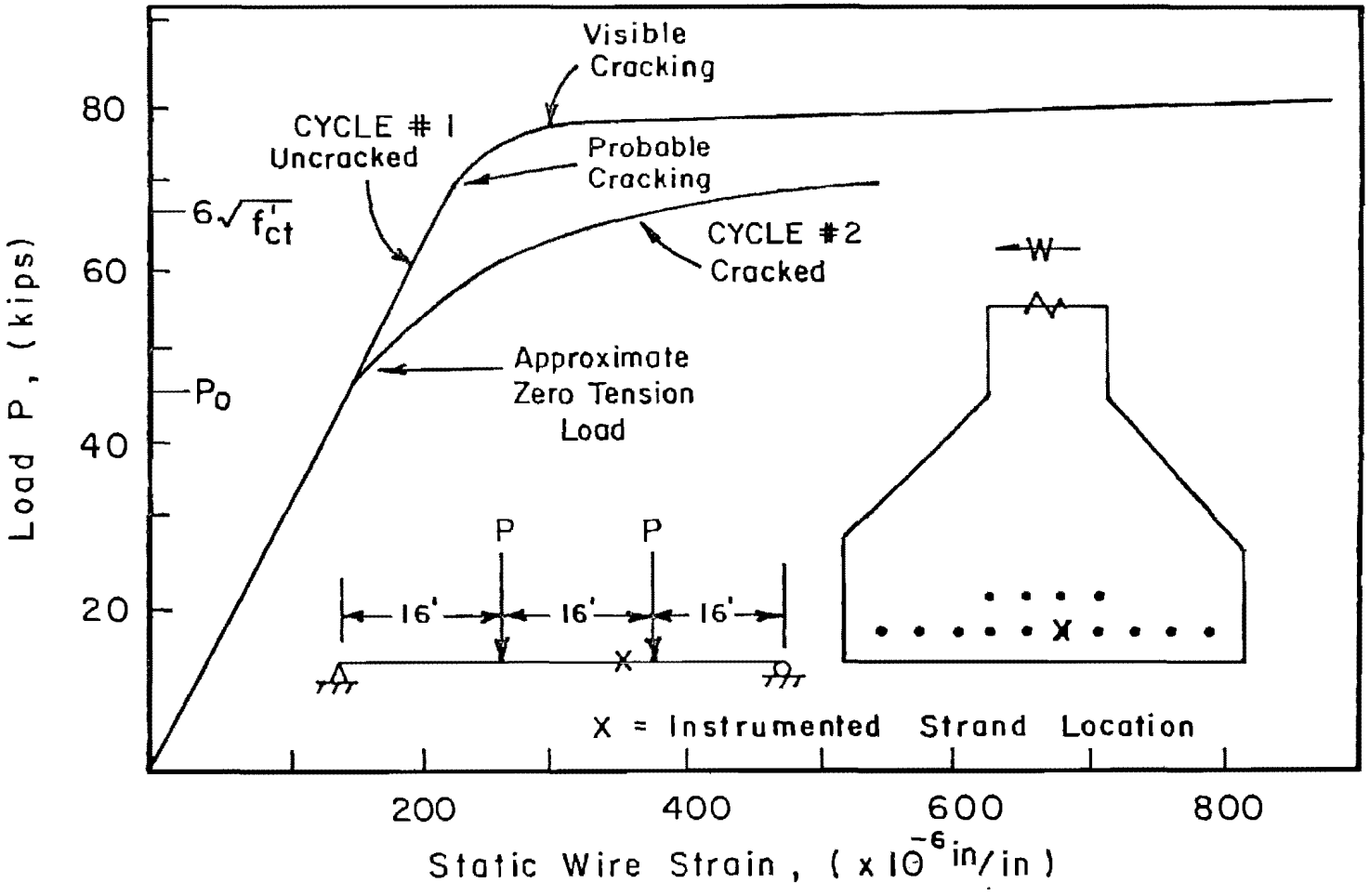

Fig. 4.42 Load versus wire strain 5 ft 10 in. south of centerline for Specimen C-14-NP-5.5-OL-2.29

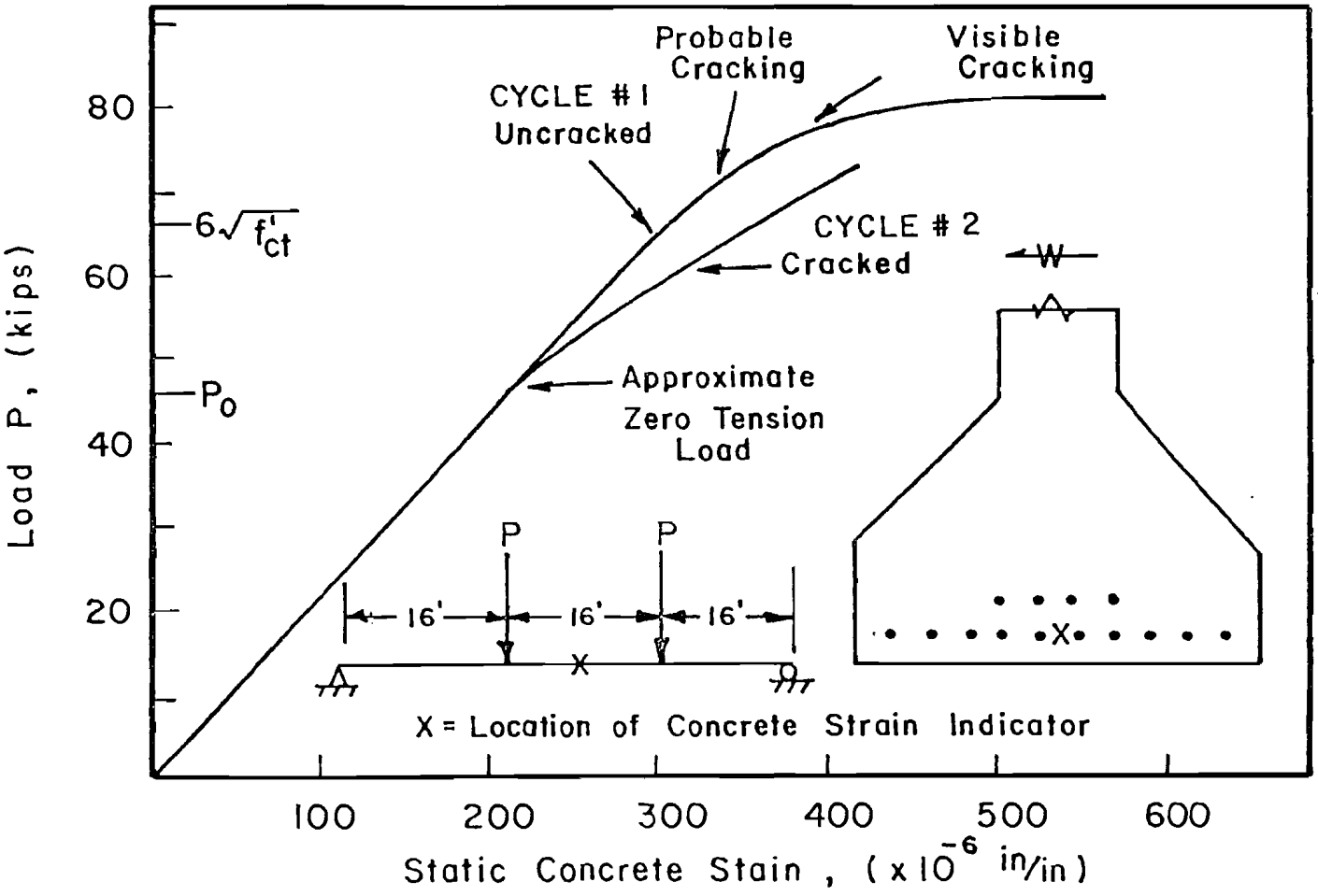

Fig. 4.43 Load versus measured concrete strain 1 ft 6 in. south of centerline for Specimen C-14-NP-5.5-OL-2.29

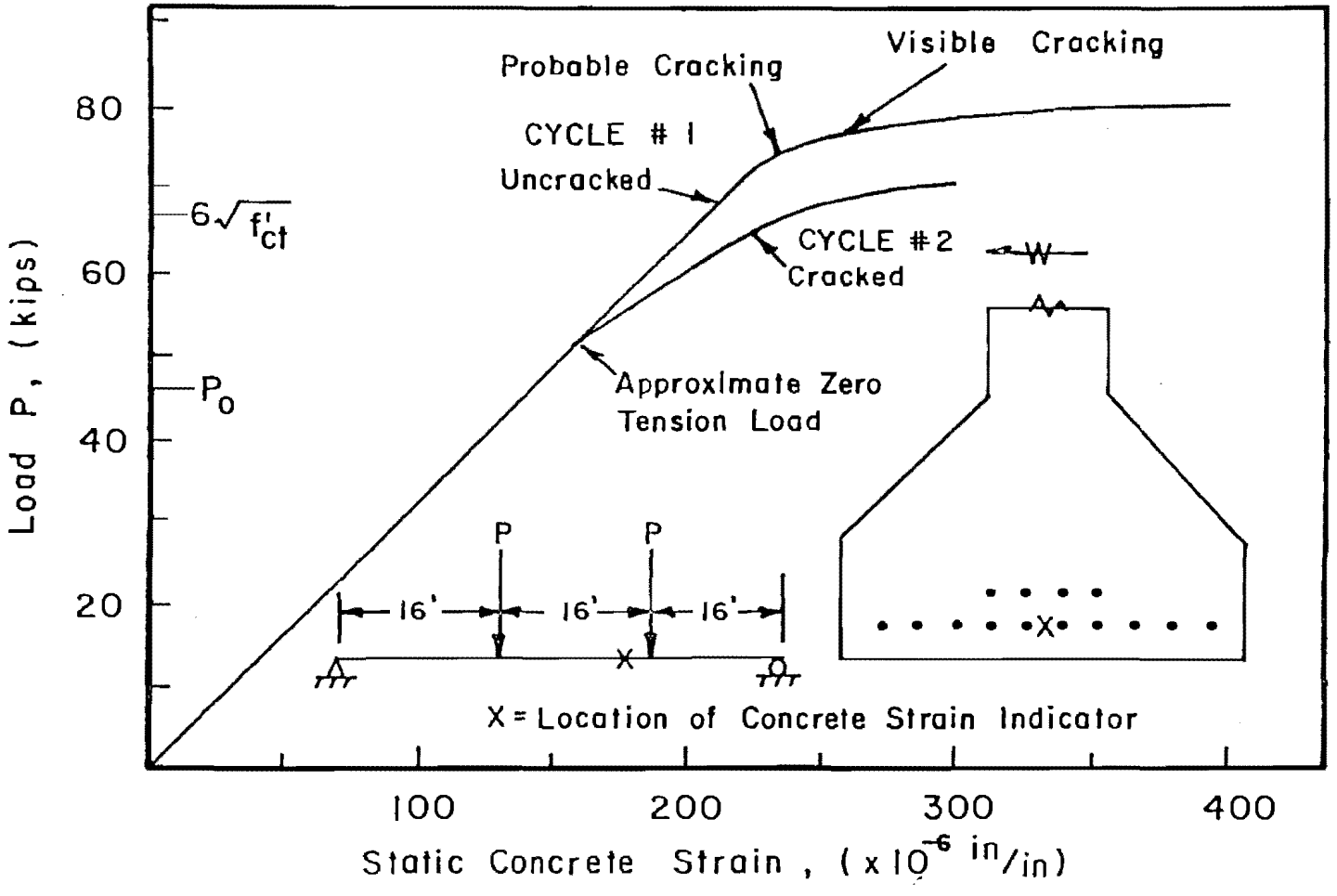

Fig. 4.44 Load versus measured concrete strain 5 ft 4 in. south of centerline for Specimen C-14-NP-5.5-OL-2.29

concrete strain also indicate that cracking probably occurred at approximately 70 kips. Figure 4.45 of load versus deflection indicates slight deviation from linear behavior at 70 kips and significant cracking at 80 kips. Six flexural cracks initiated and propagated to the top of the web during the initial four static cycles.

4.6.2 Zero Tension Load, P_o

Figures 4.41 through 4.45 during the initial static tests indicate a change in behavior of approximately 46 kips. The extreme tension fibers first experienced tension at this load (P_o). The change in behavior is a result of reduced stiffness due to flexural cracking. The cracks first opened at this load. The centerline deflection at 46 kips during the initial static tests was 0.235.

4.6.3 Fatigue Loads

Specimen C-14-NP-5.5-OL-2.29 was initially cycled at an upper fatigue load corresponding to a nominal concrete tensile stress of $4.0\sqrt{f'_{ct}}$. Based on the zero tension load of 46 kips, the maximum load was 60 kips. The minimum load was 5 kips. The dynamic strain range was approximately 0.00045 in./in. The static strain range was approximately 0.00034 in./in. After 994,000 cycles, three static tests wee performed to determine if there had been any deterioration in the member's behavior. Figures 4.41 and 4.45 of load versus wire strain and centerline deflection indicate only slight changes in behavior between the initial cycles after cracking and 994,000 cycles.

The maximum nominal concrete tensile stress was subsequently increased to $5.5\sqrt{f'_{ct}}$. The load corresponding to this concrete stress was 65 kips. The minimum load was increased to 10 kips to maintain the load range of 55 kips. However, the static strain range increased to 0.00040 in./in. The load program for this specimen is shown in Fig. 4.46.

4.6.4 Fatigue Behavior

Centerline wire strain and deflection increased gradually from 994,000 cycles to 2.02 million fatigue cycles. Figure 4.47 shows this change for centerline deflection. Figures 4.41 and 4.48 indicate the change for static wire strain. The dynamic wire strain was approximately 0.00060 in./in. at 2.0 million cycles.

The static wire strain increased drastically from 0.00055 in./in. at 2.02 million cycles to 0.00116 in./in. at 3.19 million cycles. Figures 4.41 and 4.48 show this increase. The increase in centerline deflection was less drastic. At 2.02 million cycles, the

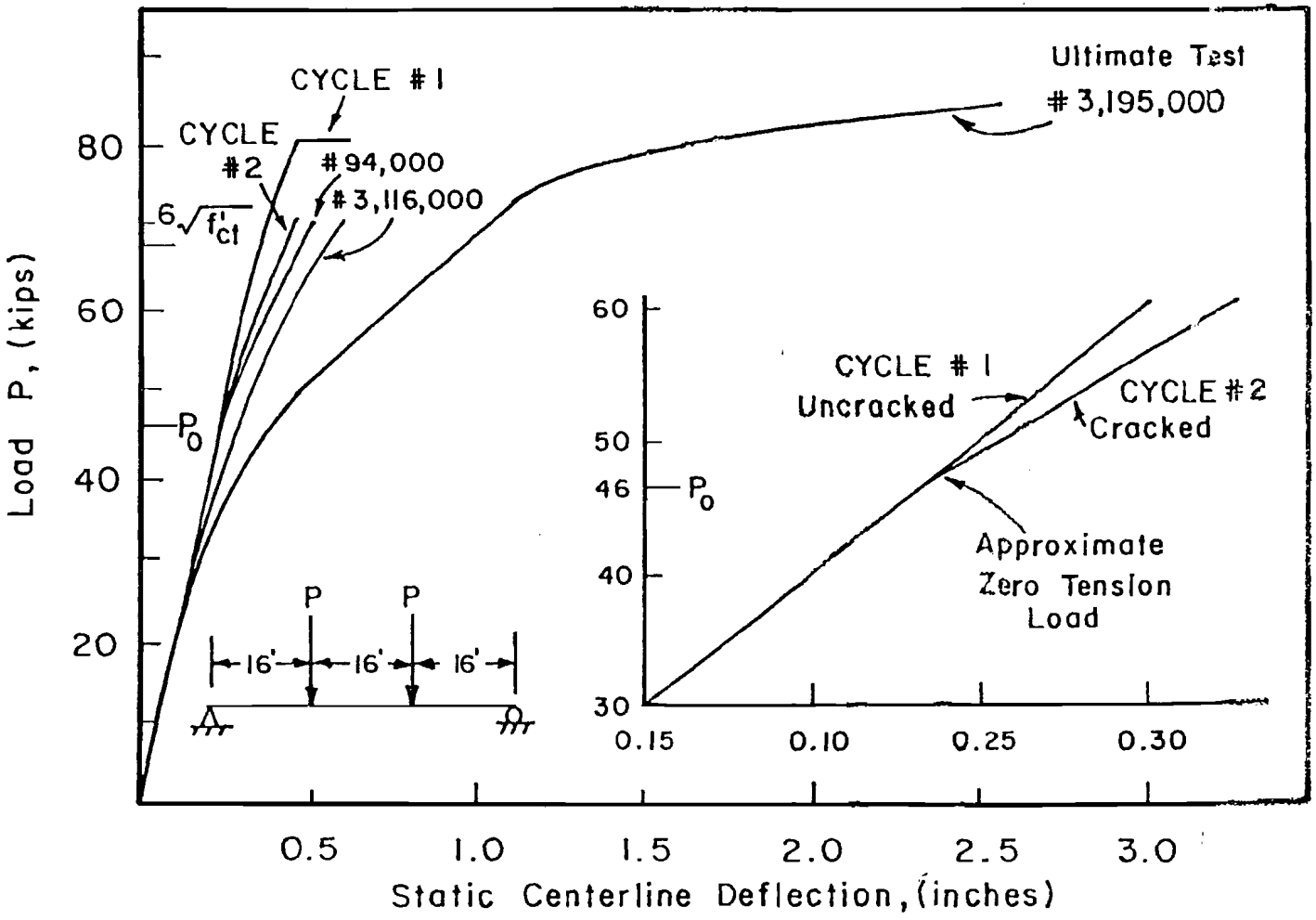

Fig. 4.45 Load versus centerline deflection during static tests for Specimen C-14-NP-5.5-OL-2.29

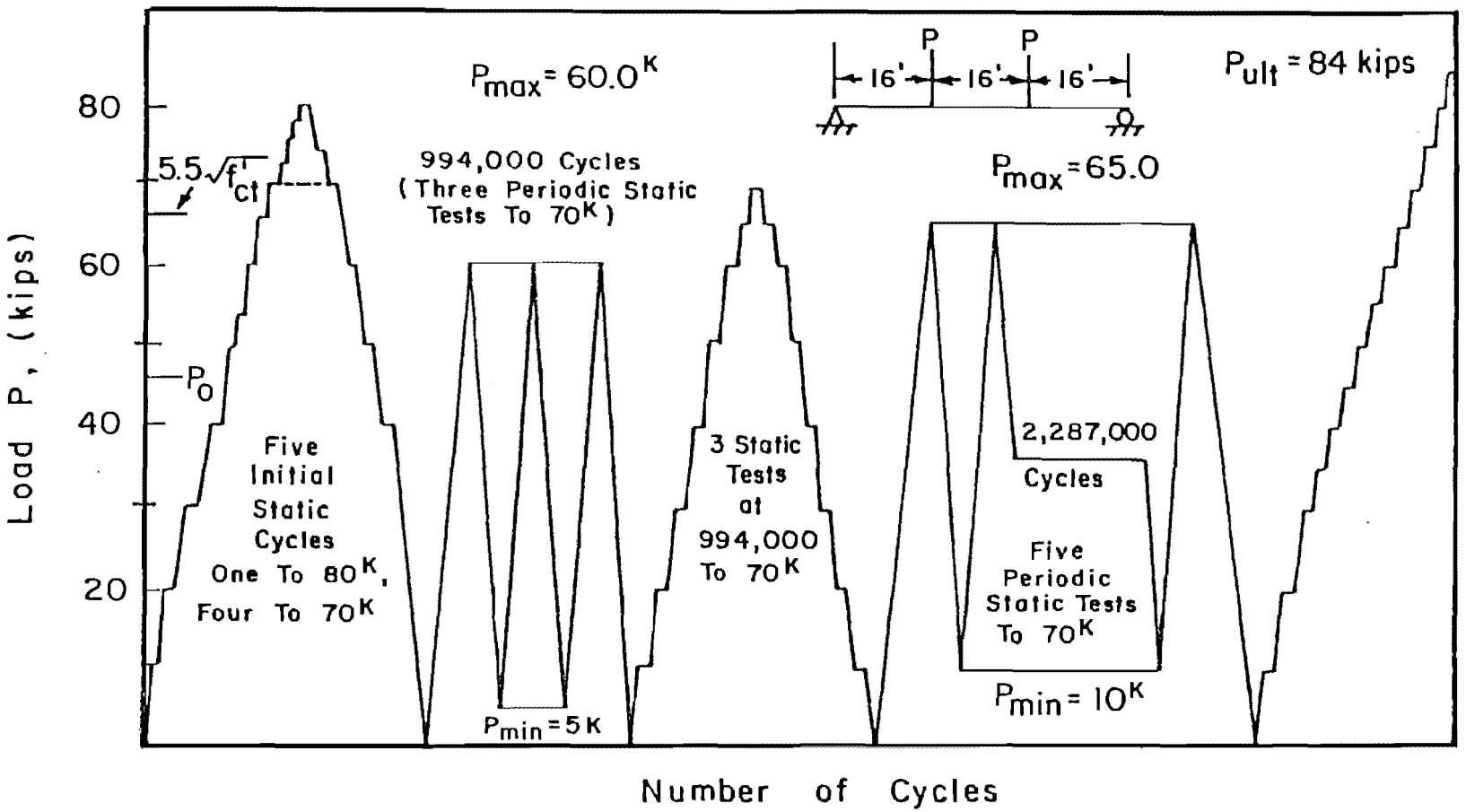

Fig. 4.46 Load program for Specimen C-14-NP-5.5-OL-2.29

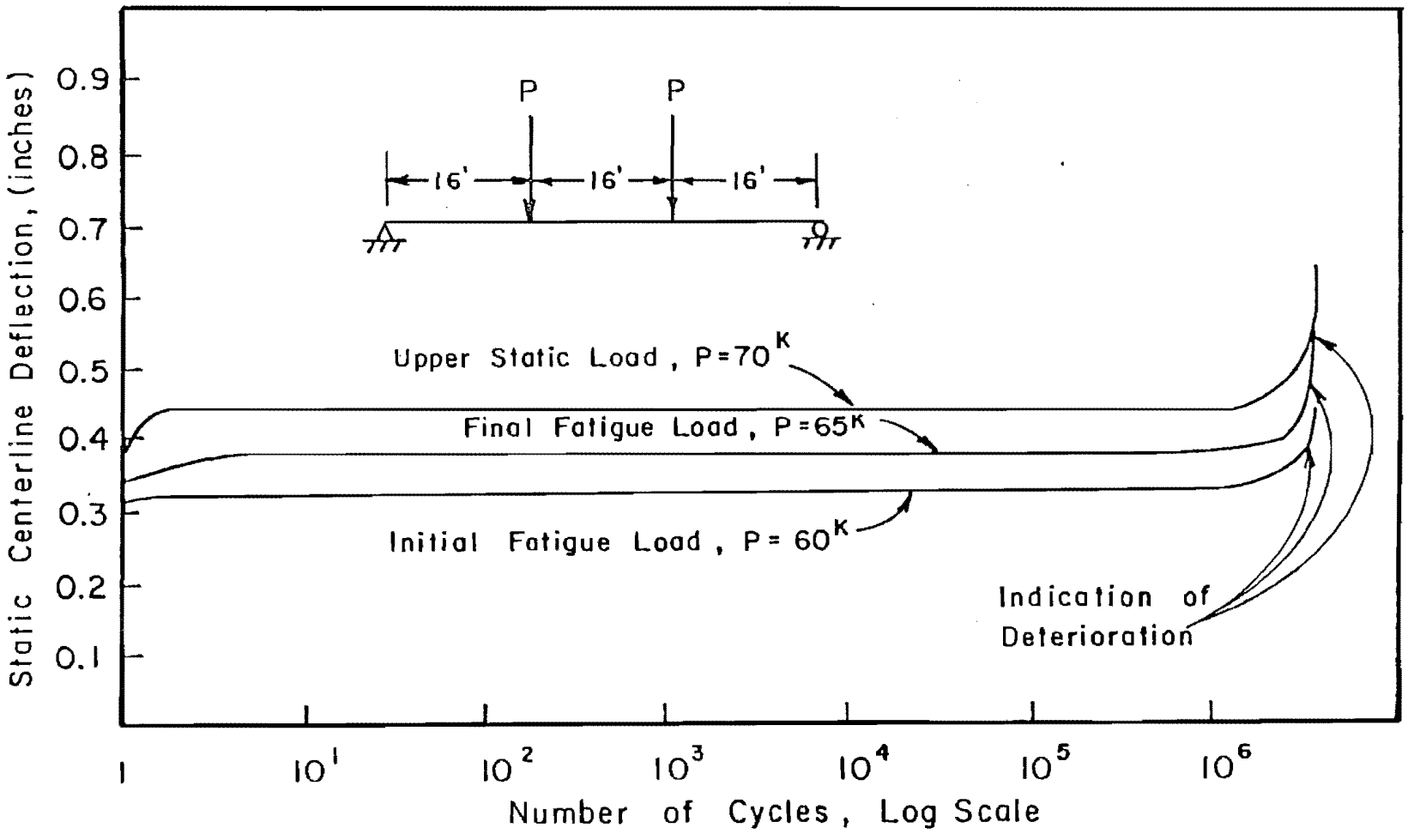

Fig. 4.47 Centerline deflection during static tests for Specimen C-14-NP-5.5-OL-2.29

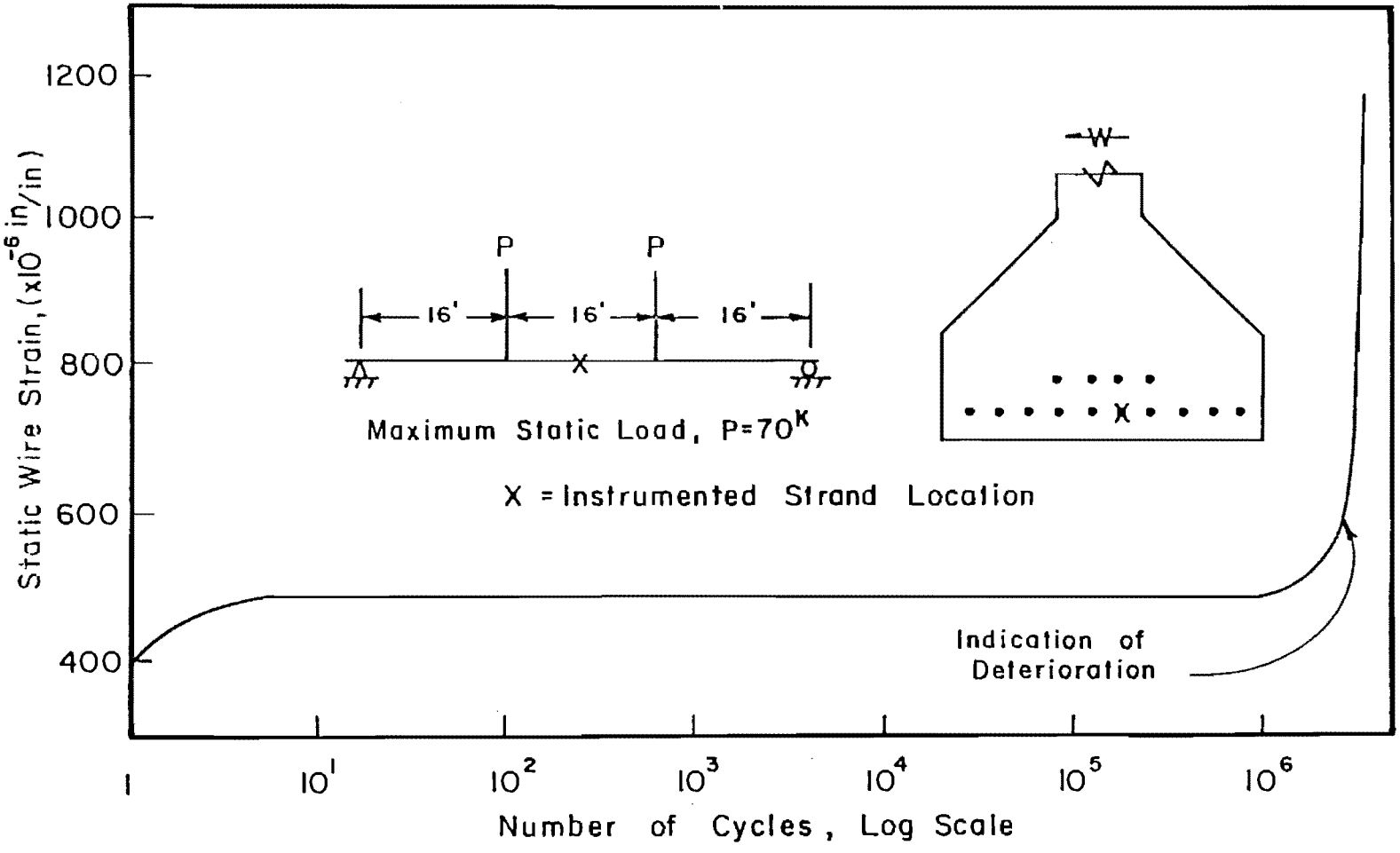

Fig. 4.48 Maximum wire strain during static tests for Specimen C-14-NP-5.5-0L-2.29

centerline deflection at 70 kips was 0.47 in. (the third point deflection was 0.40 in.). The deflections at 3.12 million cycles were 0.59 and 0.47 in. Notice again the more flexible behavior and decreased linear portions of the curves in Figs. 4.41 and 4.45. Figure 4.49 shows crack opening measurements from loads of zero to 70 kips. The flat portion at the top of the curves at 2.309 and 2.39 million cycles is probably due to slip of the strands.

By 3.05 million cycles wire fractures were audible during static testing. Breaks were also heard during fatigue testing at 3.07 million cycles. Flexural cracks ceased to close completely upon removal of load at 3.05 million cycles. Significant spalling as shown in Fig. 4.50 first occurred at 3.19 million cycles. Fatigue testing was discontinued after 3,281,000 cycles. Figures 4.51 show flexural cracks on the east side of the specimen prior to the ultimate test. There were eleven flexural cracks in the center 12 ft 8 in. of the span before the ultimate test.

4.6.5 Static Ultimate Test

The specimen was loaded incrementally to a failure load of 84 kips, which is 74 percent of the calculated capacity. Figure 4.45 shows that there was a deflection of 2.6 in. at the maximum load prior to failure. Strand fractures significantly reduced the ductility of the member. Static and fatigue wire fractures visible after the static ultimate tests are shown in Figs. 4.52 and 4.53.

4.6.6 Post Mortem Investigation

The concrete cover was removed and the strands were exposed after the ultimate test. Thirty-five wire fatigue fractures were discovered at the three locations shown in Fig. 4.54. No fractures occurred at the strand drape points which were approximately 6.5 ft from the centerline. These points were within the constant moment region. The wire fractures relative to the cross section are shown in Fig. 4.55.

4.6.7 Dynamic Load Application

The static centerline deflection between 10 and 65 kips at 2.02 million cycles was 0.34 in. (0.05 in. to 0.39 in.). The dynamic deflection range at 2.19 million cycles was 0.41 in. (0.03 in. to 0.44 in.) which indicates slight dynamic amplification. The static loads that correspond to these dynamic deflections were approximately 6 and 68 kips.

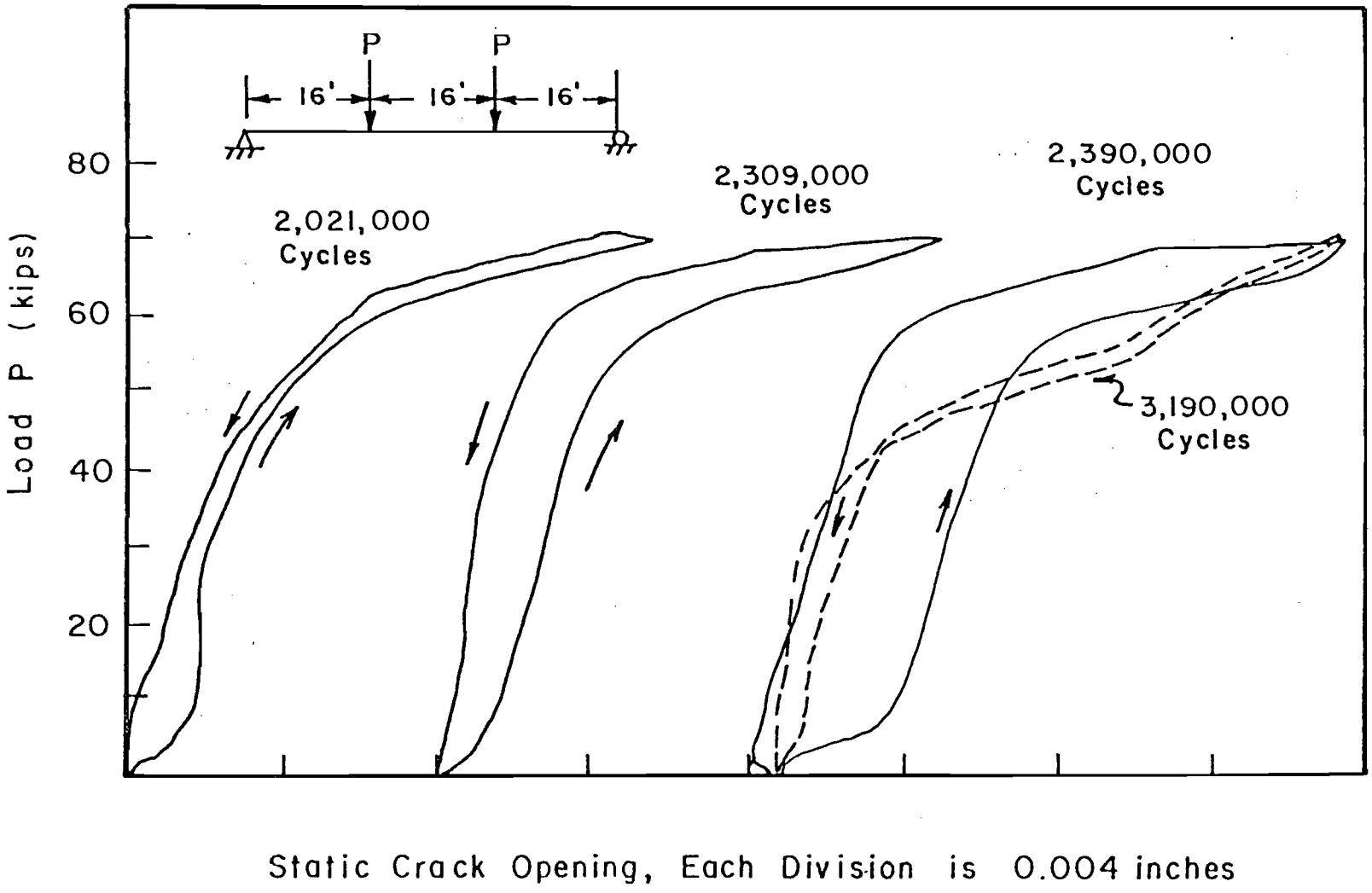

Fig. 4.49 Load versus crack opening during static tests for Specimen C-14-NP-5.5-0L-2.29

Fig. 4.50 Concrete spalling on the west side of the specimen which occurred at 3.19 million cycles

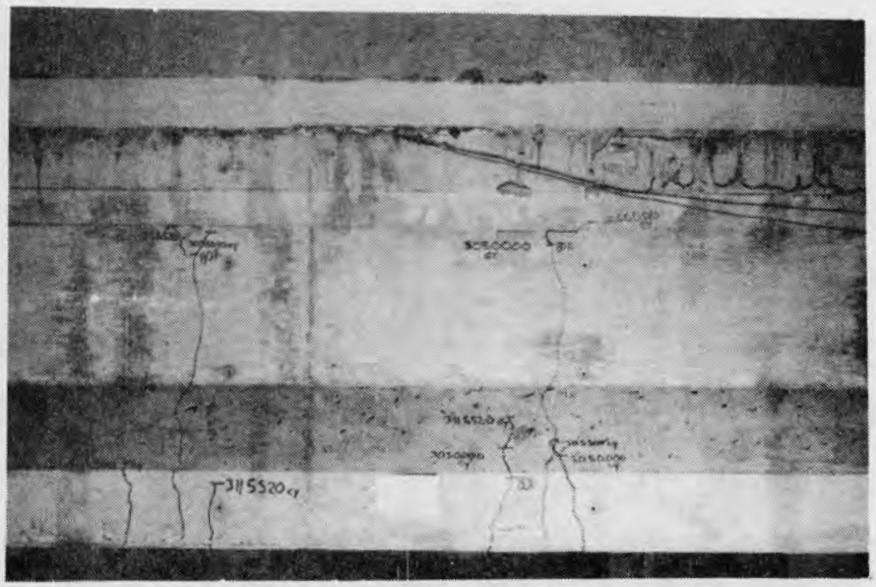

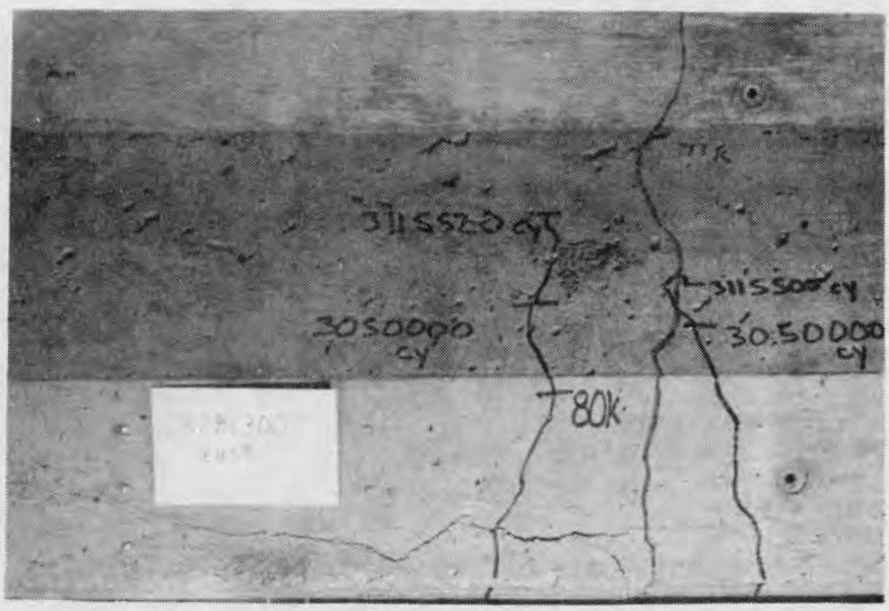

Fig. 4.51 Cracking on the east side of the specimen prior to the static ultimate test

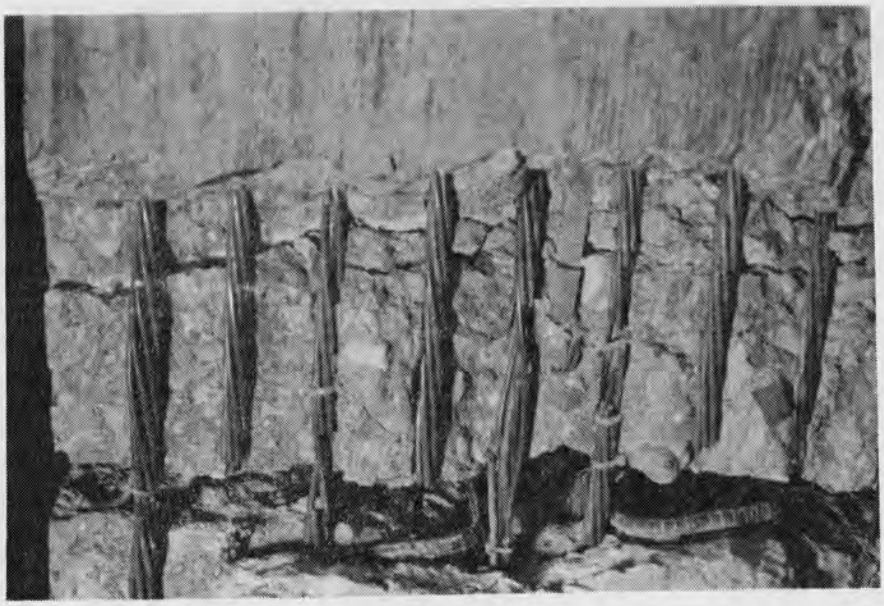

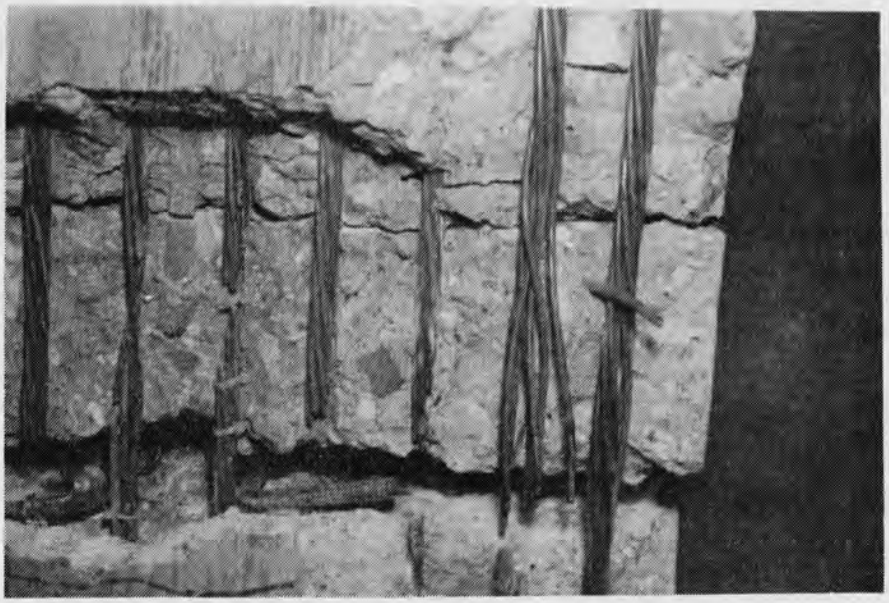

Fig. 4.52 Wire fractures for Specimen C-14-NP-5.5-OL-2.29

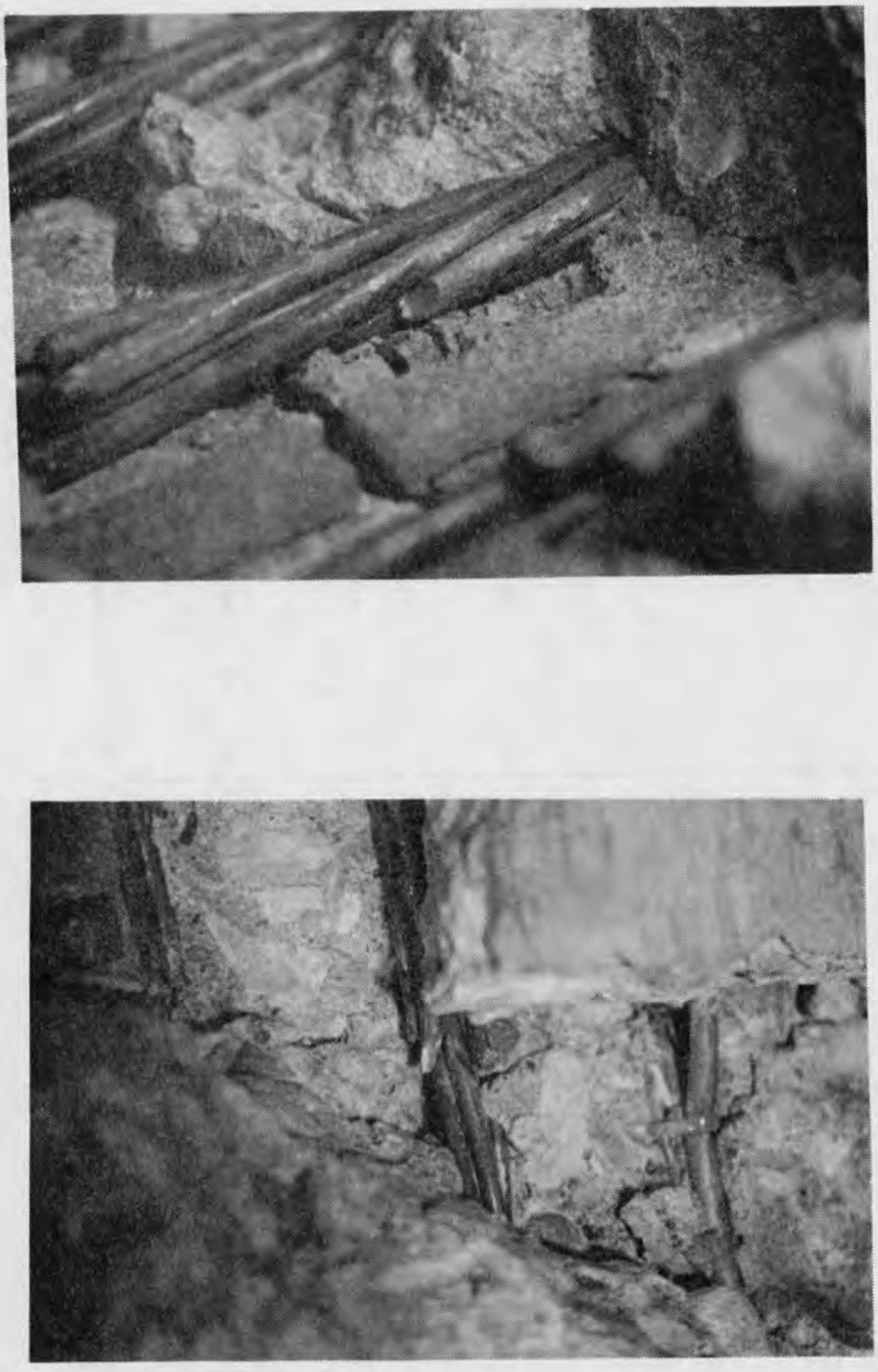

Fig. 4.53 Wire fatigue fractures for Specimen C-14-NP-5.5-OL-2.29

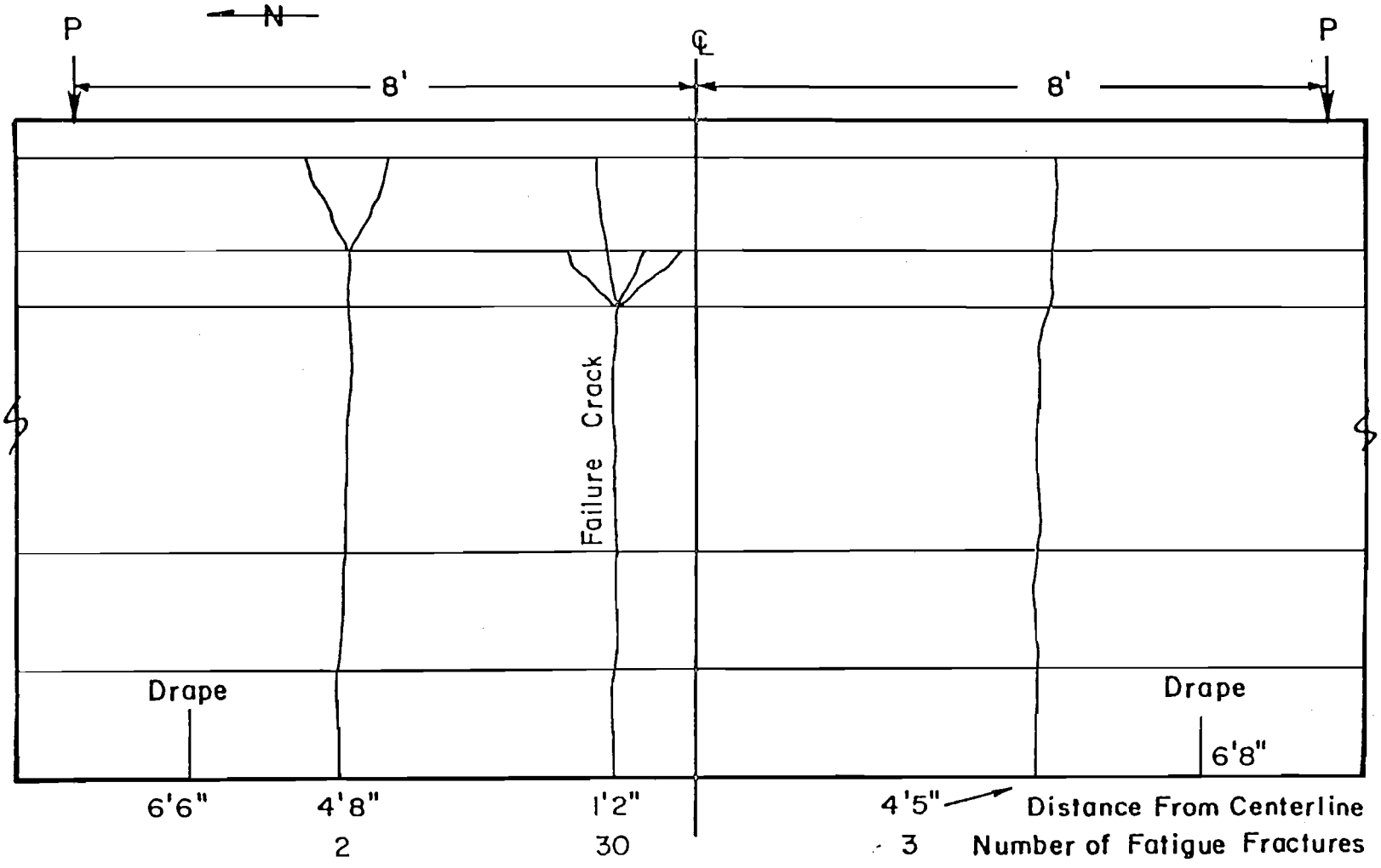

Fig. 4.54 Location and number of wire fatigue fractures and corresponding concrete cracks for Specimen C-14-NP-5.5-OL-2.29

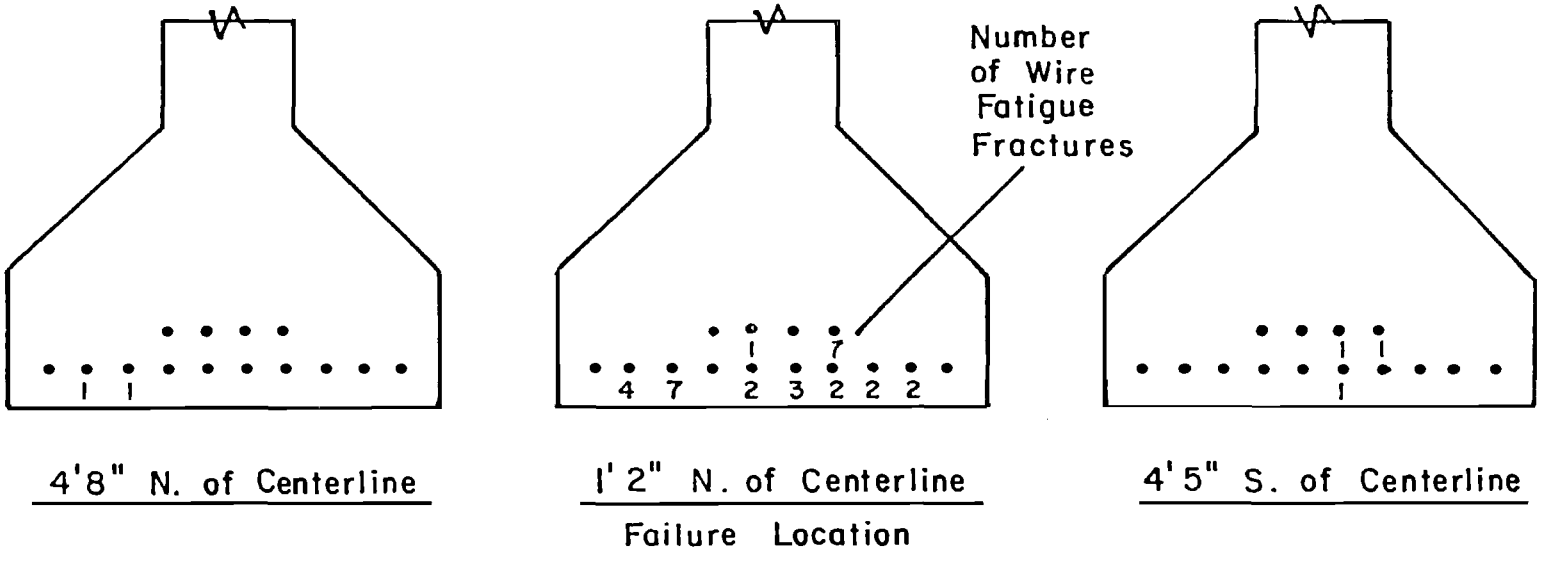

Fig. 4.55 Fatigue fracture locations for Specimen C-14-NP-5.5-OL-2.29

4.7 Specimen A-22-NP-6.2-OL-2.84

This specimen was an AASHTO-PCI Type II with 22 strands, ten of which were draped. There was no passive (unstressed) reinforcing steel in the lower flange. The specimen was cycled at an upper fatigue load (P_{max}) that produced 6.2 $\sqrt{f'_{ct}}$ nominal tensile stress in the extreme tension fibers (based on a transformed uncracked section). Loads above P_{max} (overloads) were applied to the member during static tests. The specimen experienced 2.84 million fatigue cycles before testing was discontinued.

4.7.1 Initial Static Tests

Specimen A-22-NP-6.2-OL-2.84 was loaded monotonically to a maximum load of 55 kips. Flexural cracks became visible at this load level. A slight increase in deflection with no increase in load at 45 kips, as shown in Fig. 4.56, indicates cracking probably began at this load. Seven flexural cracks formed and extended to the lower flange web boundary during the initial three static cycles.

4.7.2 Zero Tension Load, P_o

Fig. 4.57 of load versus static crack width during unloading indicates a significant increase in crack width beginning at approximately 30 kips. Figure 4.56 of load versus deflection indicates a deviation from linear behavior also at approximately 30 kips. The change in behavior at this load is the result of the extreme tensile fibers experiencing tension. This is the zero tension load (P_o). The centerline deflection at this load was 0.24 in.

4.7.3 Fatigue Loads

Specimen A-22-NP-6.2-OL-2.84 was cycled at a nominal concrete tensile stress of 6.2 $\sqrt{f'_{ct}}$, which is approximately the maximum allowable tensile stress specified by the AASHTO Specifications [8], to determine if failure could occur at the design stress. Based on the zero tension load of 30 kips, the maximum load was 46 kips. The minimum load was 10 kips. The load program for this specimen can be seen in Fig. 4.58.

4.7.4 Fatigue Behavior

The static centerline deflection at 55 kips, as shown in Fig. 4.59, remained stable during the initial 2.64 million fatigue cycles. There were ten flexural cracks in the 16 ft constant moment region at that time. The centerline and third point deflections at 55 kips were 0.56 in. and 0.49 in., respectively. Figures 4.60 and 4.61 of crack

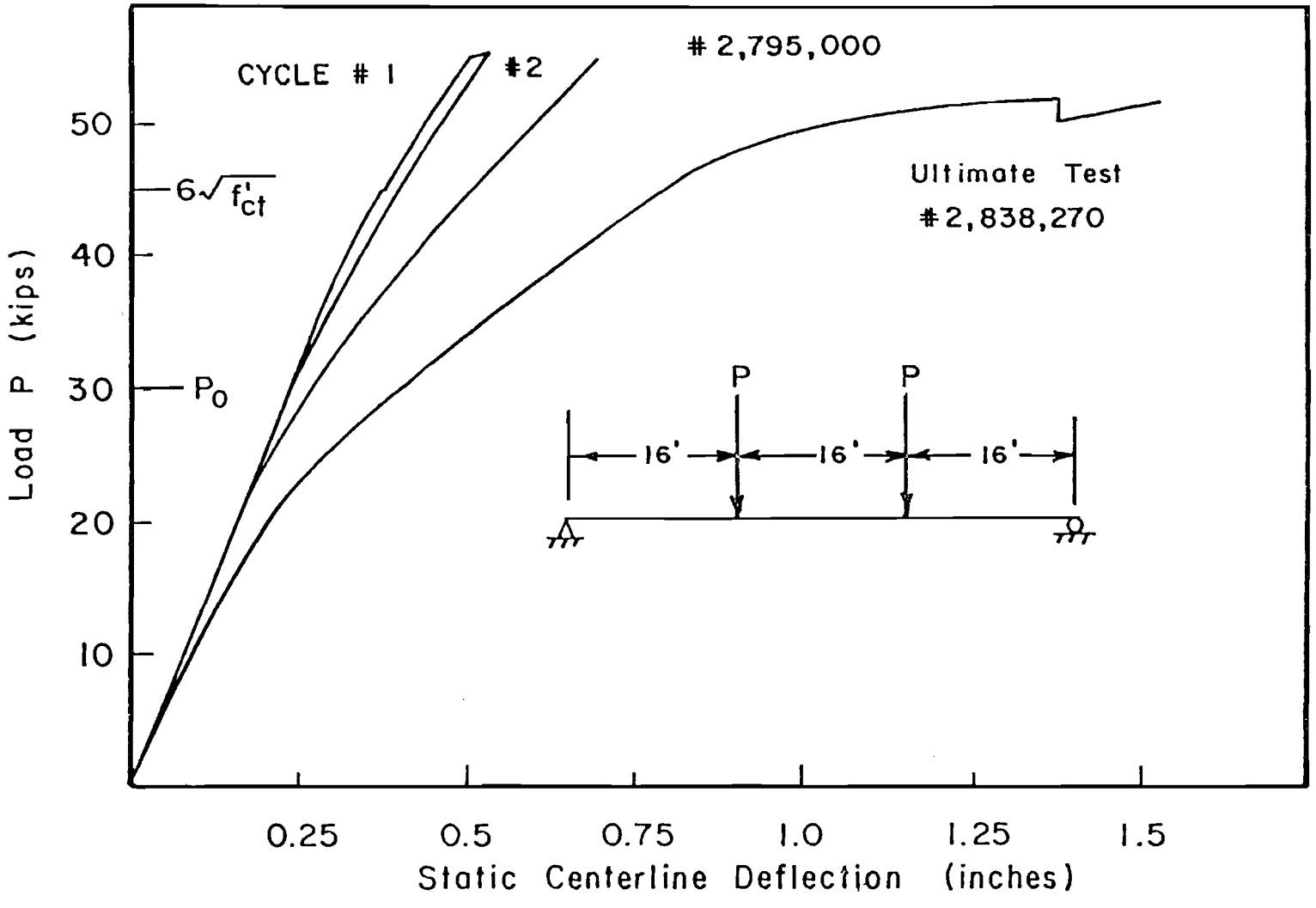

Fig. 4.56 Load versus centerline deflection during static tests for Specimen A-22-NP-6.2-OL-2.84

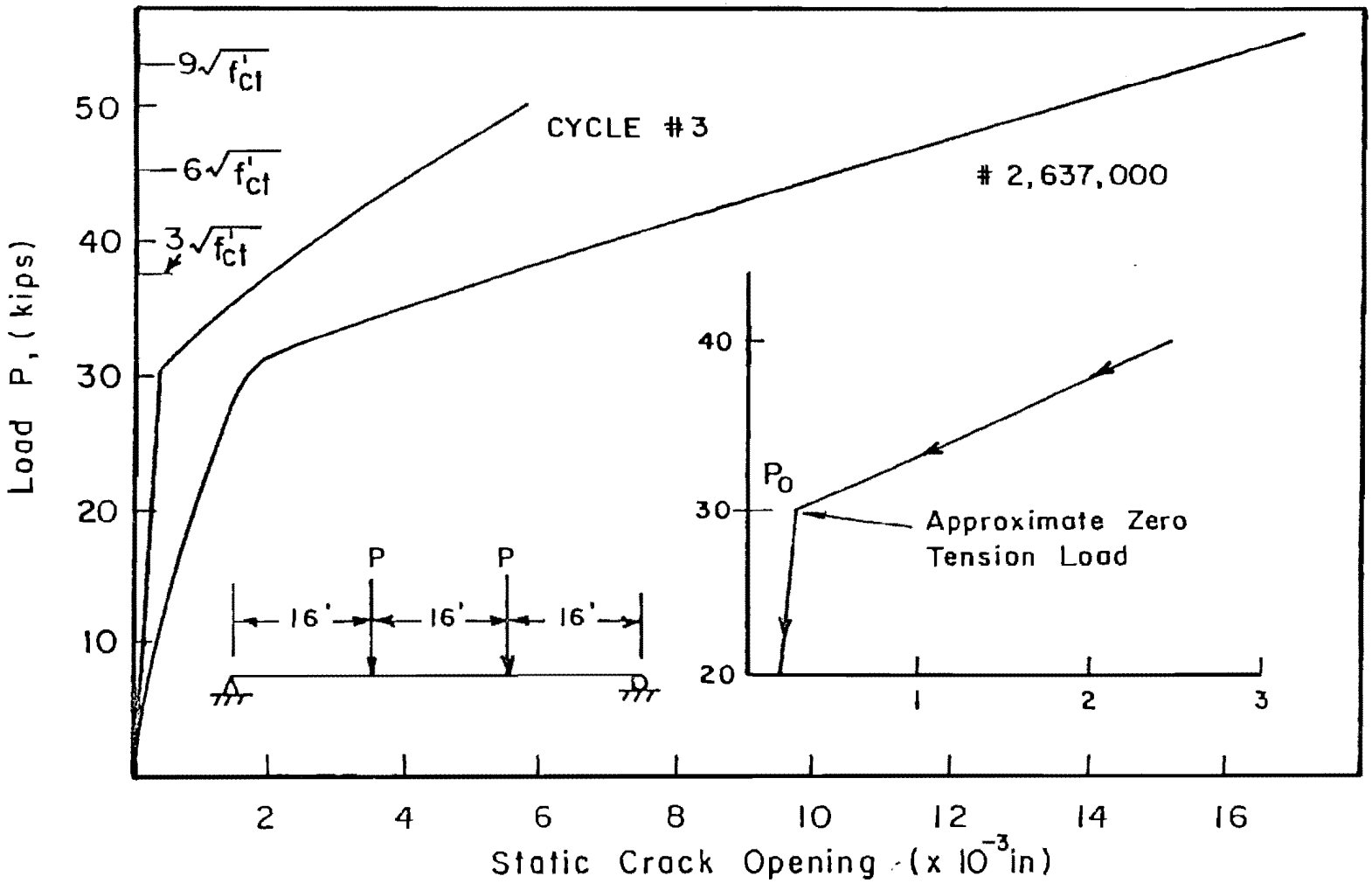

Fig. 4.57 Load versus crack opening during static tests for Specimen A-22-NP-6.2-OL-2.84

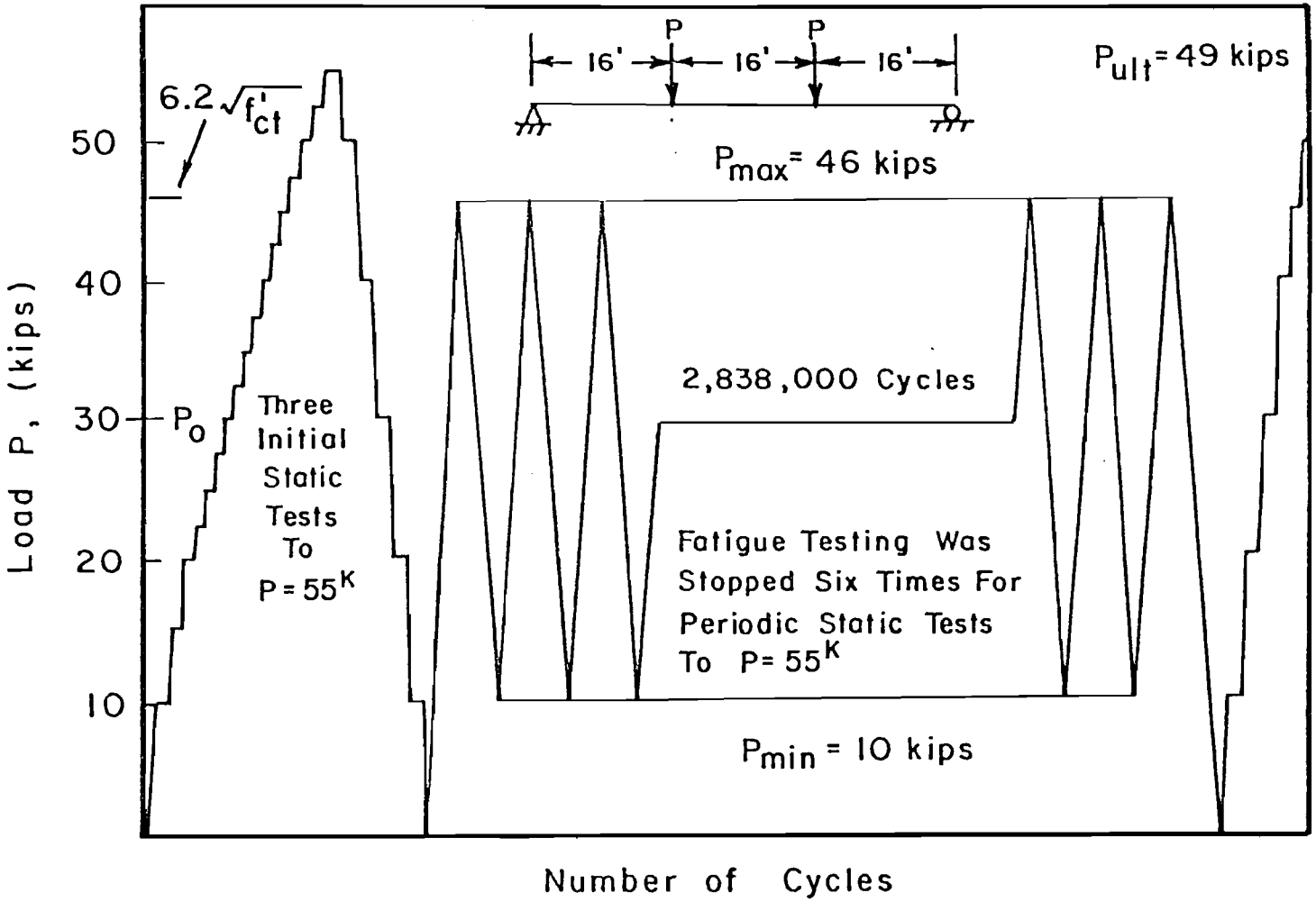

Fig. 4.58 Load program for Specimen A-22-NP-6.2-OL-2.84

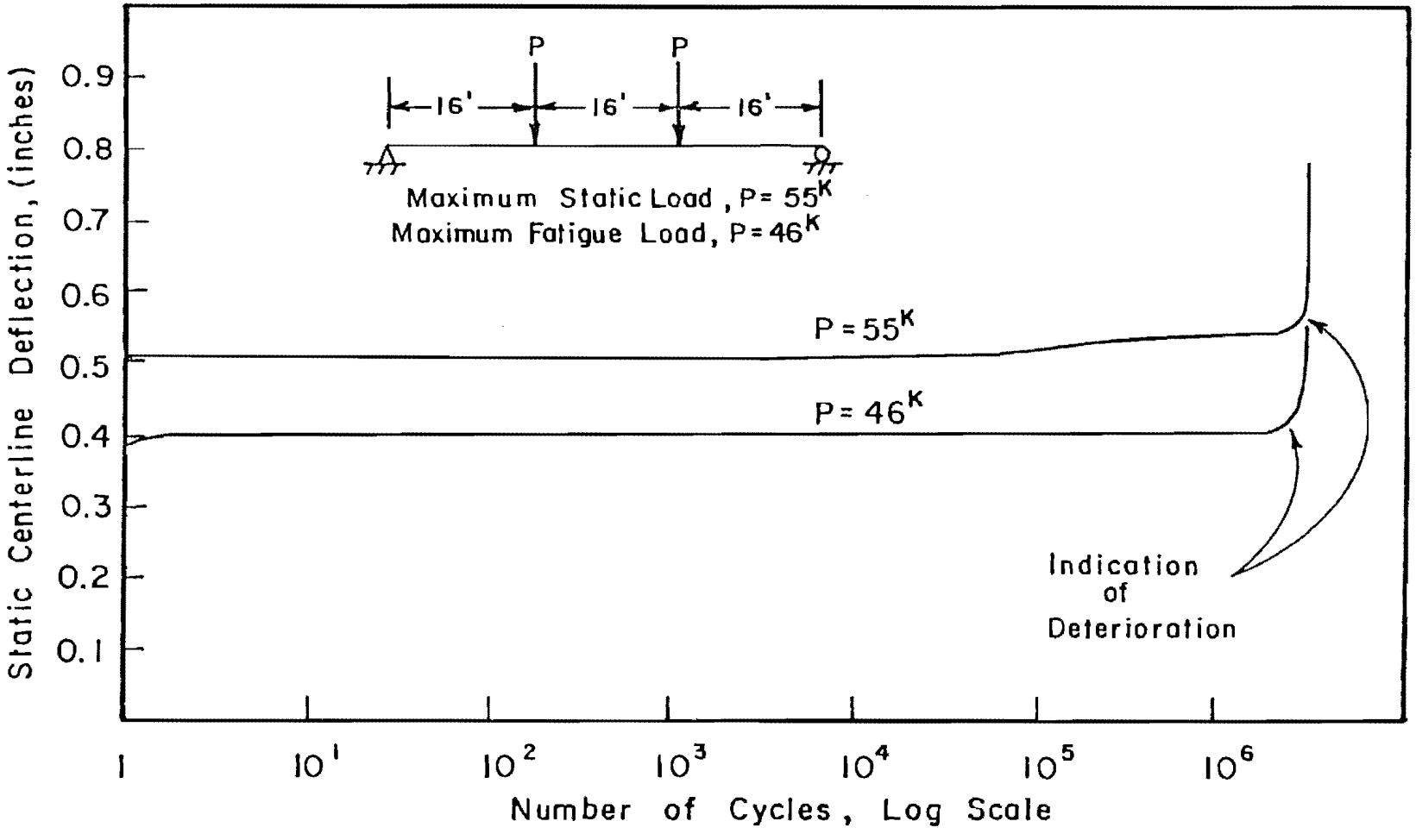

Fig. 4.59 Centerline deflection during static tests for Specimen A-22-NP-6.2-OL-2.84

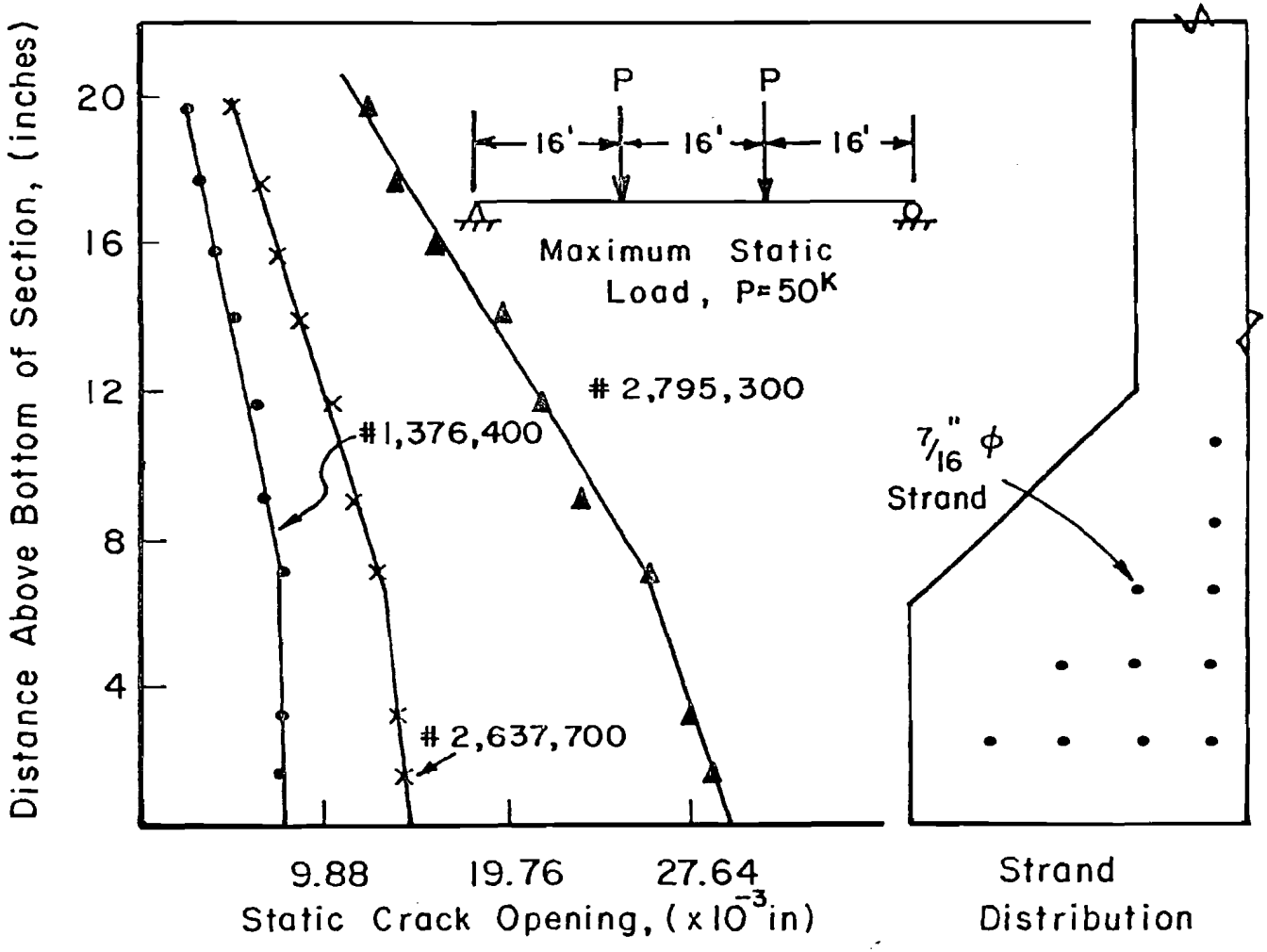

Fig. 4.60 Static crack profile 3 ft 6 in. south of centerline at 55 kips during static tests

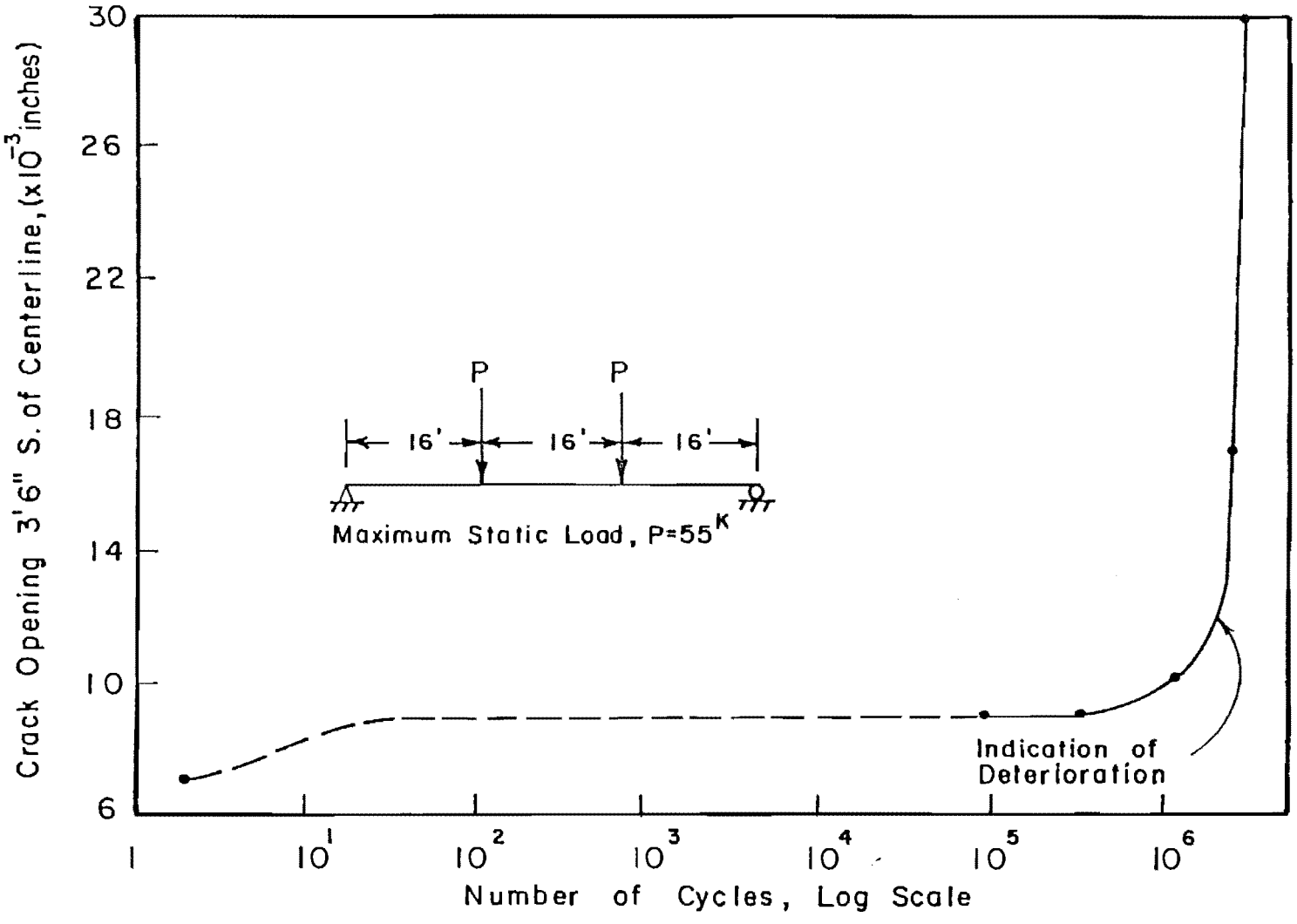

Fig. 4.61 Maximum crack opening during static test for Specimen A-22-NP-6.2-OL-2.84

opening at various phases of fatigue testing indicate that the specimen began to deteriorate as early as 1.38 million cycles. Figure 4.62 shows the drastic increase in crack opening between 40 and 50 kips at 2.63 million cycles. The decompression load was 30 kips. Figure 4.63 of permanent centerline deflection with no load shows a marked increase initially due to fatigue loading and another increase at 2.64 million cycles due to wire fractures, which were first heard during a static test at this time.

The stiffness decreased rapidly after 2.64 million cycles. Figure 4.59 shows an increase in centerline deflection from 0.56 in. at 2.64 million cycles to 0.68 in. at 2.80 million cycles at a load of 55 kips. The static crack opening at 50 kips, as shown in Fig. 4.60, increase approximately 90 percent between 1.38 and 2.64 million cycles. An increase of 120 percent occurred in the 158,000 cycles after 2.64 million cycles. Wire fatigue fractures could be heard during fatigue testing at 2.67 million cycles. No spalling occurred prior to the ultimate test at 2.84 million cycles, although there was an audible squeaking sound originating from the eventual failure crack at 2.81 million cycles. There were 12 flexural cracks in the constant moment region prior to the static ultimate test.

4.7.5 Static Ultimate Test

The specimen was loaded incrementally to a failure load of 49 kips, which was only three dips above the maximum fatigue load. The calculated ultimate capacity was 100 kips. Figure 4.56 indicates that there was little ductility at failure, which occurred at the south drape point. The maximum deflection was 1.53 in. Figure 4.64 shows flexural cracking and crack instrumentation after the ultimate test. The forking took place during the ultimate test.

4.7.6 Post Mortem Inspection

The concrete cover was removed and the strands were exposed after the ultimate test. The wire fatigue failures were concentrated at a flexural crack, at the drape point, 3.5 ft south of the centerline, as shown in Fig. 4.66. The 66 wire fatigue breaks at this location are shown in the insert on Fig. 4.66. No other fractures were found. Notice the high number of wire fractures on the center ten strands which were draped. Figure 4.66 shows the failure section and the drape hardware.

4.7.7 Dynamic Load Amplification

The static centerline deflection between 10 and 46 kips at 1.38 million cycles, which was in the stable portion of the deflection number

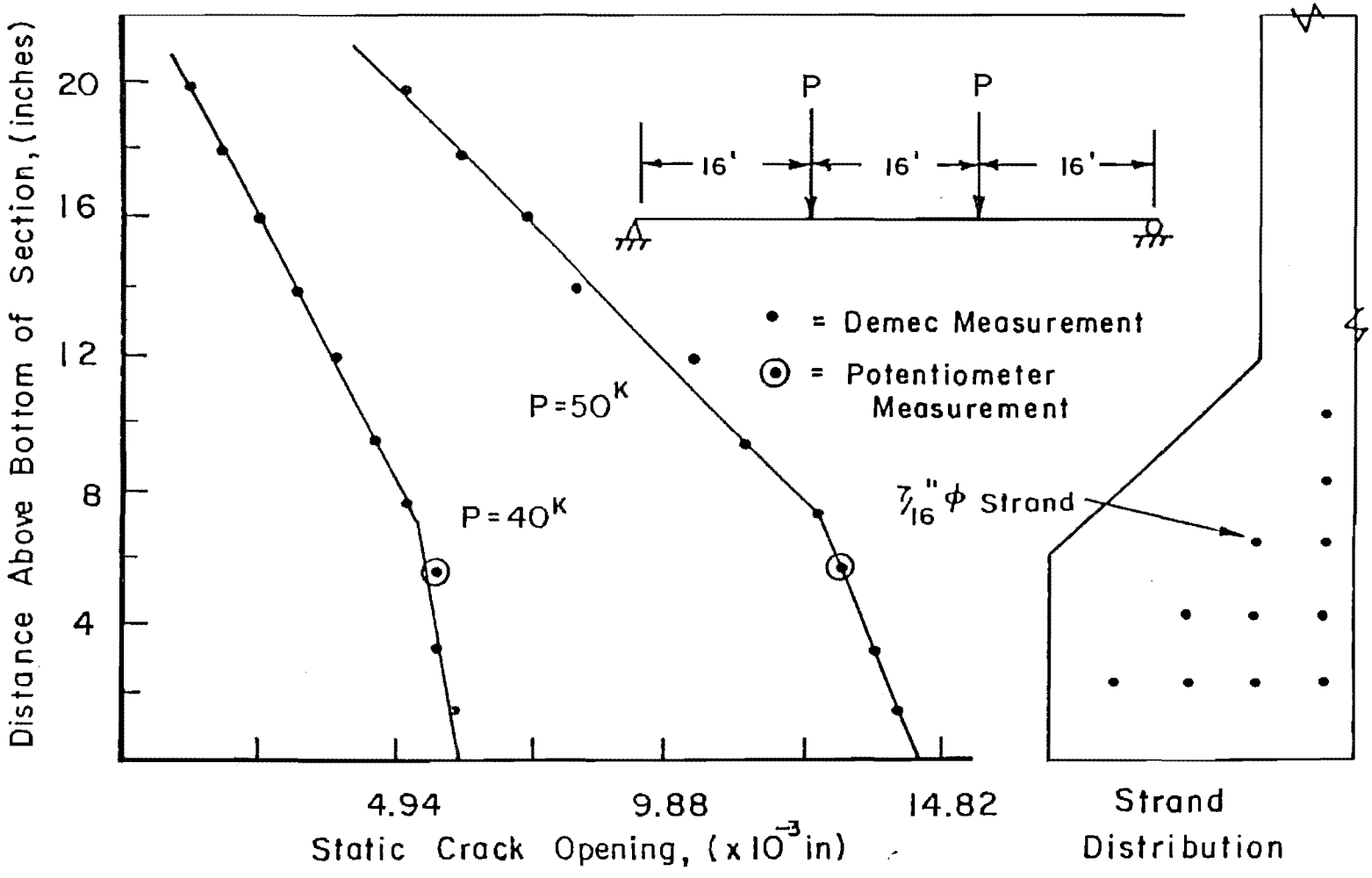

Fig. 4.62 Static crack profile 3 ft 6 in. south of centerline at 2.63 million cycles

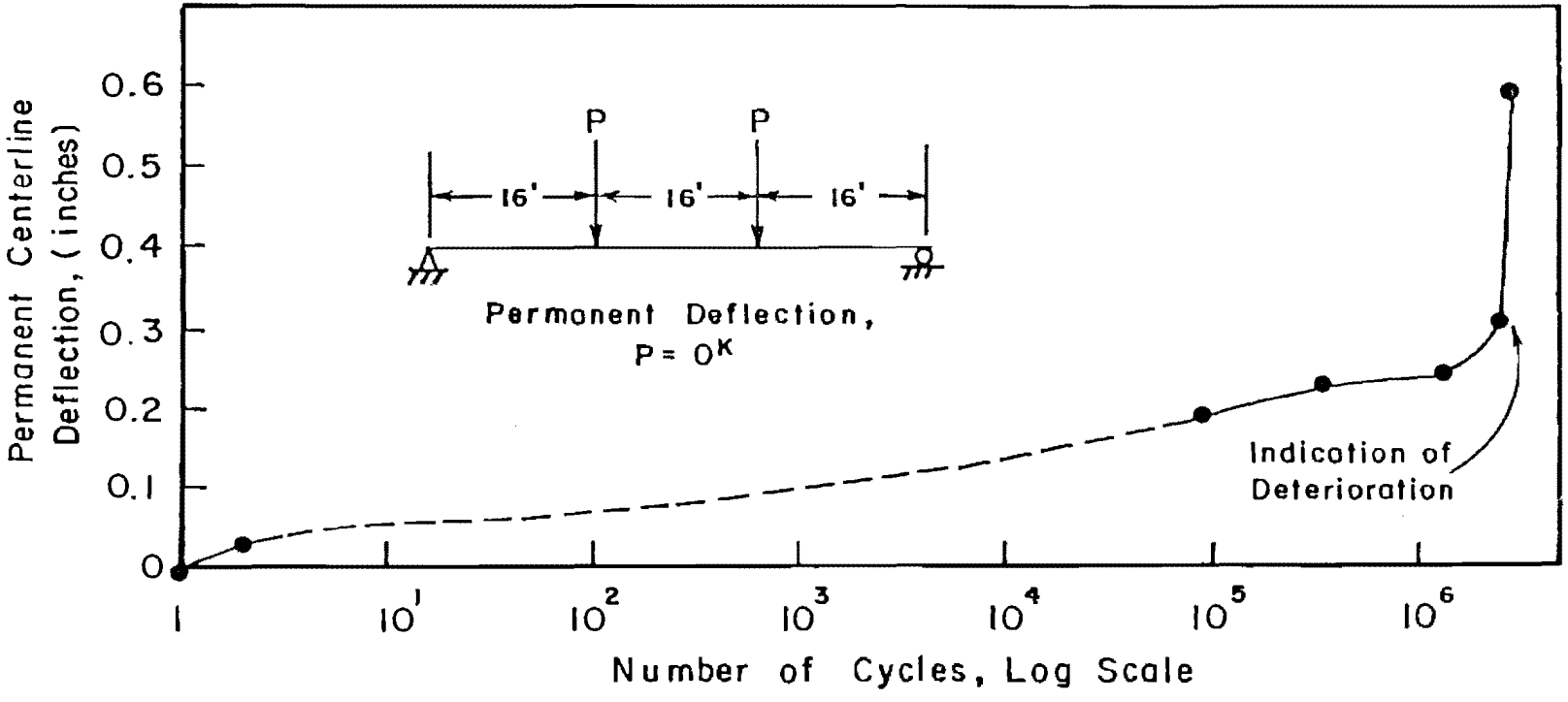

Fig. 4.63 Permanent centerline deflection during static tests for Specimen A-22-NP-6.2-OL-2.84

Fig. 4.64 Flexural cracking prior to the static ultimate test

Fig. 4.65 Drape hardware at the failure crack.

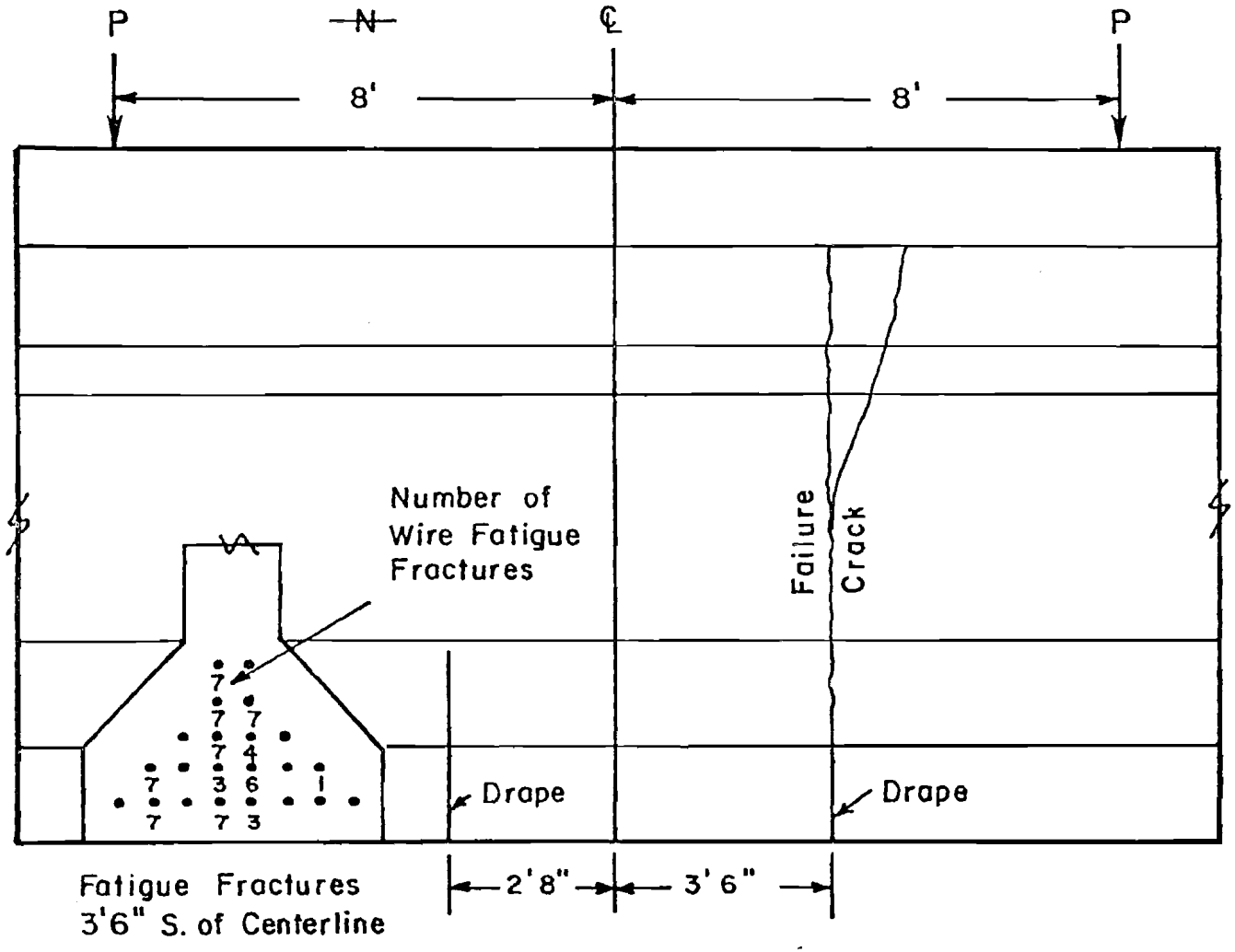

Fig. 4.66 Location of drape points and fatigue fractures for Specimen A-22-NP-6.2-OL-2.84

of cycles curve shown in Fig. 4.59, was 0.34 in. (0.07 in. to 0.41 in.). The dynamic deflection at 1.38 million cycles was 0.36 in. (0.08 in. to 0.44 in.) which indicates slight dynamic amplification. The static loads that correspond to these dynamic deflections were approximately 11 and 48 kips.

4.8 Specimen A-22-NP-6.2-NO-5.00

This specimen was an AASHTO-PCI Type II with 22 strands, ten of which were draped. There was no passive reinforcing steel in the lower flange. The specimen was cycled at an upper fatigue load (P_{max}) that produced $6.2\sqrt{f'_{ct}}$ nominal tensile stress in the extreme concrete tension fibers. No loads above P_{max} were applied to the member prior to the ultimate test. The specimen withstood 5.00 million fatigue cycles prior to the ultimate test.

4.8.1 Initial Static Test

Specimen A-22-NP-6.2-NO-5.00 was designed as a replicate to Specimen A-22-NP-6.2-OL-2.84. The main variable was the presence of overloads, as indicated in the alphanumeric title. The girders were cast simultaneously in a single prestressing bed. The section modulus at the time of testing was essentially identical (5930 $in.^3$ for the specimen with overloads, 5940 $in.^3$ for the specimen with no overloads). The loads applied to Specimen A-22-NP-6.2-NO-5.00 only produced nominal concrete tensile stresses greater than $6.2\sqrt{f'_{ct}}$, based on an uncracked section, during the ultimate test. Because the member was not overloaded, no flexural cracks formed during the initial static tests. Several cracks existed in the upper flange and the top portion of the web, as a result of mishandling and shipping, prior to loading.

4.8.2 Fatigue Loads

The maximum fatigue load was 46 kips. Based on the assumed zero tension load of 30 kips, determined from Specimen A-22-NP-6.2-OL-2.84, and uncracked section properties, this load produced a nominal concrete stress of $6.2\sqrt{f'_c}$. The minimum load was 10 kips. These are the same loads applied to Specimen A-22-NP-6.2-OL-2.84. The load program for Specimen A-22-NP-6.2-NO-5.00, which was not overloaded, is shown in Fig. 4.67. The centerline, at the assumed zero tension load of 30 kips prior to fatigue testing, was 0.23 in.

4.8.3 Fatigue Behavior

The specimen cracked during cyclic loading at 1180 cycles. The full load range, 10 to 46 kips, was reached at 850 cycles. (When

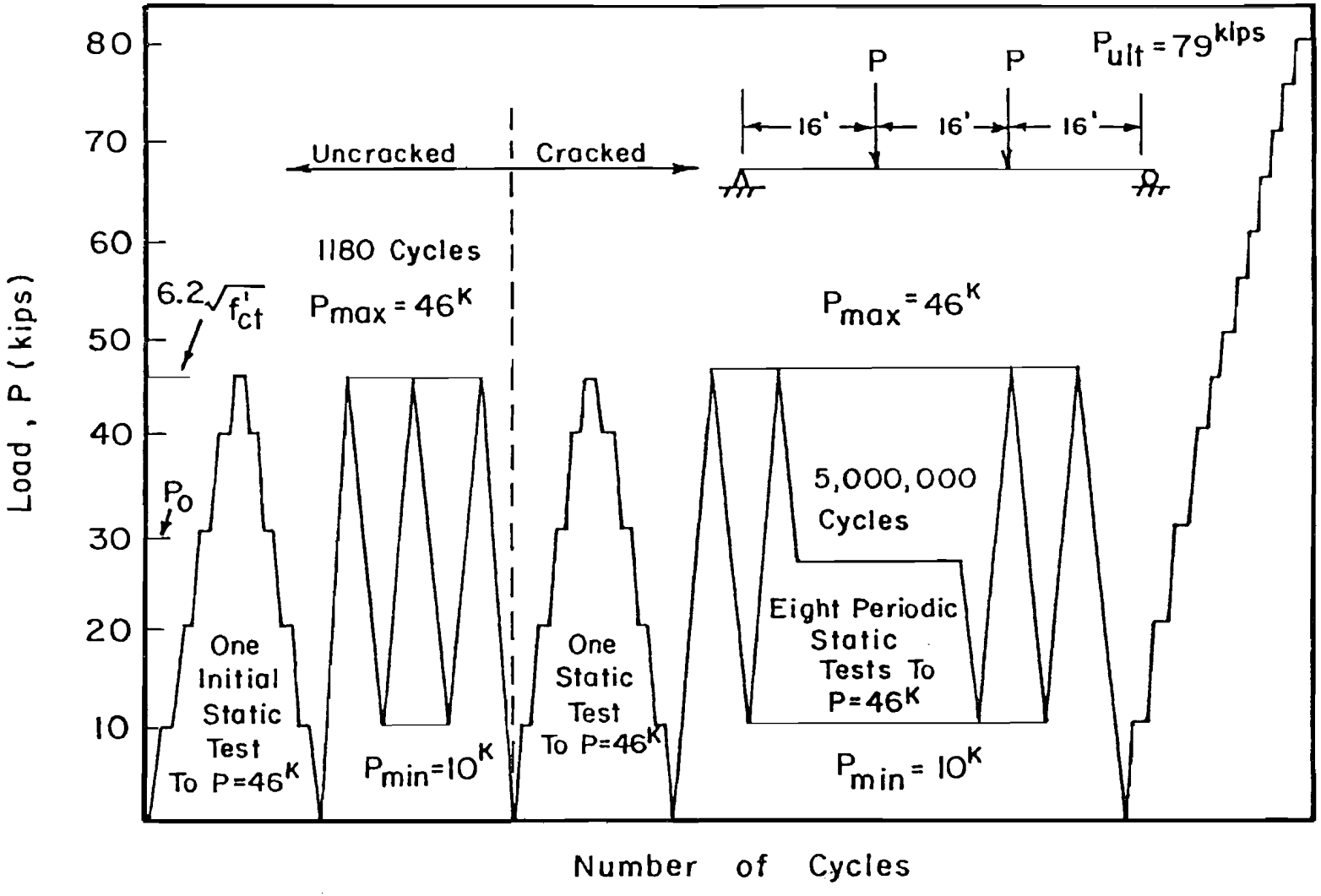

Fig. 4.67 Load program for Specimen A-22-NP-6.2-NO-5.00

fatigue loading is begun, the maximum and minimum are equal to P_{max} (the maximum fatigue load). As the stroke is increased on the pulsator pump, the minimum fatigue load decreases until the desired minimum fatigue load (P_{min}) is reached. For this reason, the minimum load prior to 850 cycles was greater than 10 kips, and the load range was less than 36 kips.) One crack 10 in. south of the centerline formed during the initial 1108 cycles. Figure 4.68 indicates that this crack was an extension of a handling crack. The handling cracks are indicated by dashed lines.

The centerline deflection at 46 kips increased from 0.355 in. during the initial static cycles to 0.369 in. at 1180 cycles. The permanent deflection (static centerline deflection with no load), shown in Fig. 4.69, was 0.025 in. after 1180 cycles. This is probably due to the cyclic creep of concrete during fatigue testing.

The centerline deflection at various phases of fatigue testing, as shown in Fig. 4.70, remained stable for the initial 4.5 million cycles. The static centerline deflection at 46 kips after 3.5 million cycles was 0.39 in. At 4.5 million cycles, when there were seven flexural cracks, the centerline deflection was 0.41 in. (only a 5 percent increase). By 5.0 million cycles there were 12 flexural cracks in the constant moment region and the centerline deflection was 0.51 in. (a 24 percent increase in 500,000 cycles).

Figure 4.71 shows a marked increase in crack width between 35 kips and 46 kips at 1.0 million cycles. Flexural cracks do not open until the extreme tension fibers experience tension, which first occurs at the zero tension load. The figure indicates that the zero tension load is slightly less than 35 kips. The 30 kip assumed value appears reasonable. Figures 4.72 and 4.73 show the gradual increase in crack opening during fatigue testing. A decreasing stiffness of the member, as indicated by increasing crack widths, is also apparent.

The specimen's behavior deteriorated rapidly after 4.50 million cycles when wire fatigue breaks were heard during a static test. Fatigue breaks could be heard during fatigue testing after this. Like the previous A-22 specimen, no concrete spalling occurred prior to the ultimate test. At 4.90 million cycles fine white powder was seen coming from the eventual failure crack. The concrete adjacent to this crack was noticeably warmer than other parts of the member indicating heat generated by friction.

4.8.4 Static Ultimate Test

The specimen was loaded monotonically to failure at 79 kips, 79 percent of the calculated ultimate capacity. Figure 4.74 shows the ultimate deflection before failure was 4.8 in. The deflection at maximum load of 2.93 in. was twice that of Specimen A-22-NP-6.2-OL-2.84,

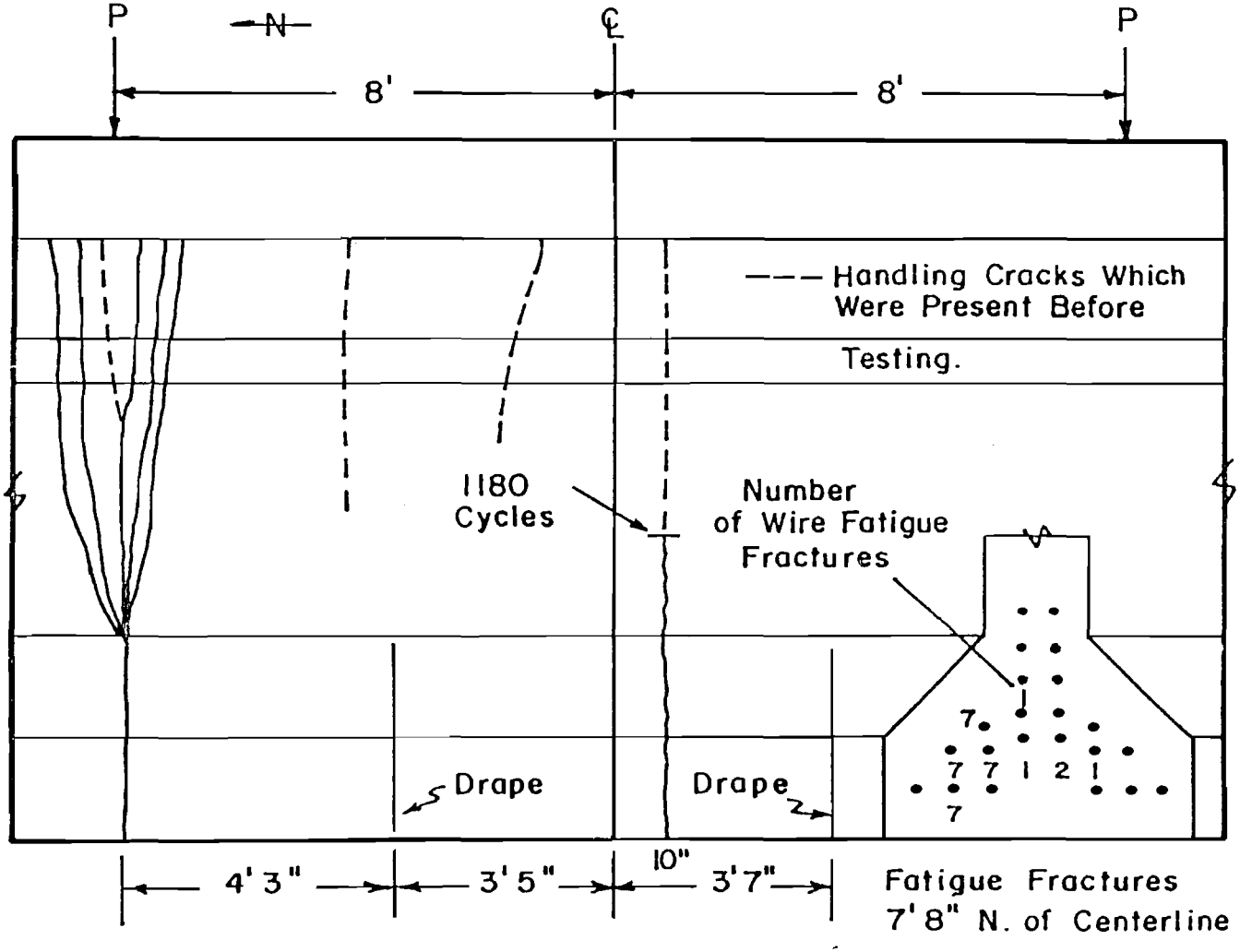

Fig. 4.68 Location of drape points and fatigue fractures for Specimen A-22-NP-6.2-NO-5.00

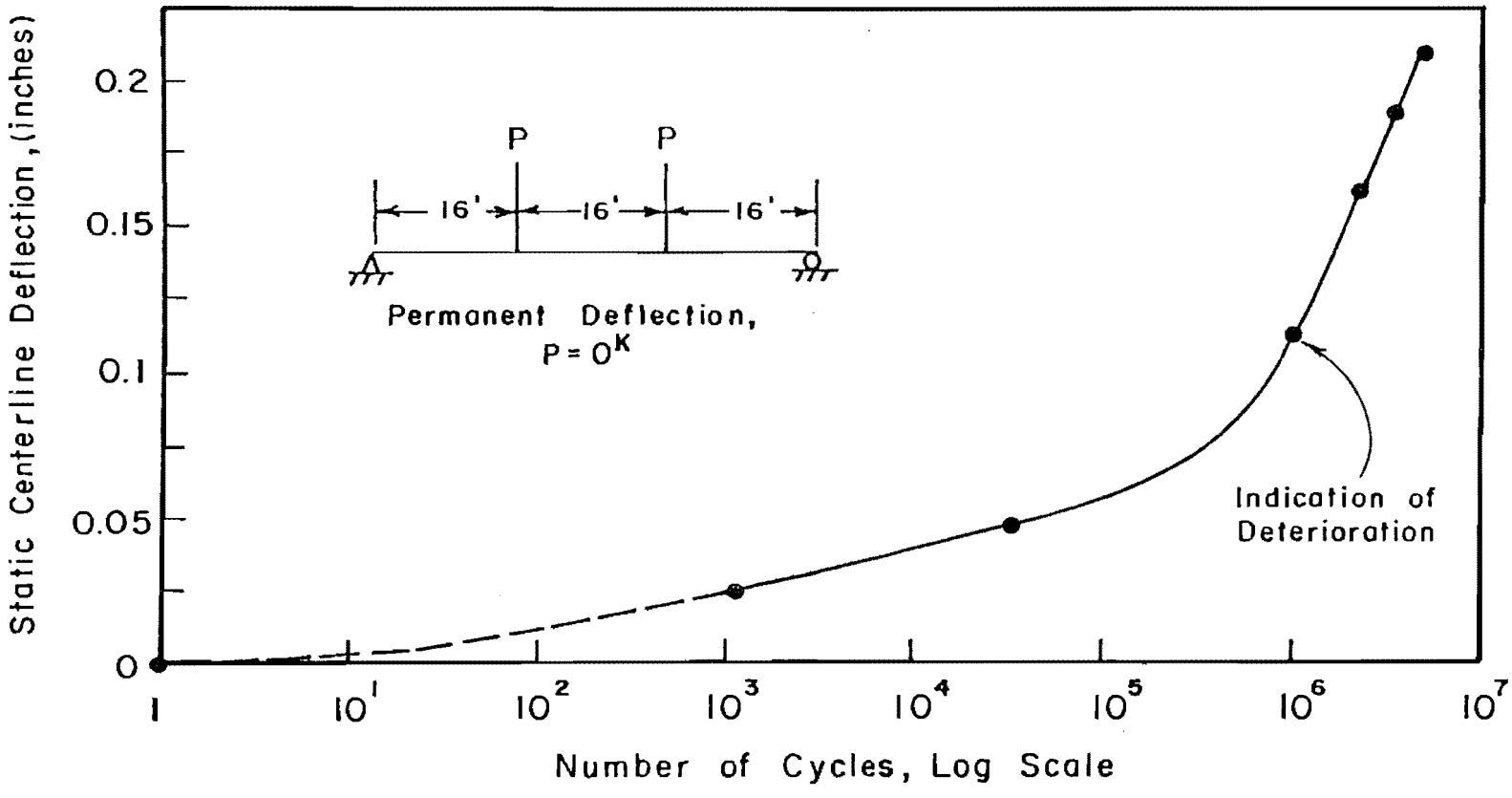

Fig. 4.69 Permanent deflection during static tests for Specimen A-22-NP-6.2-NO-5.00

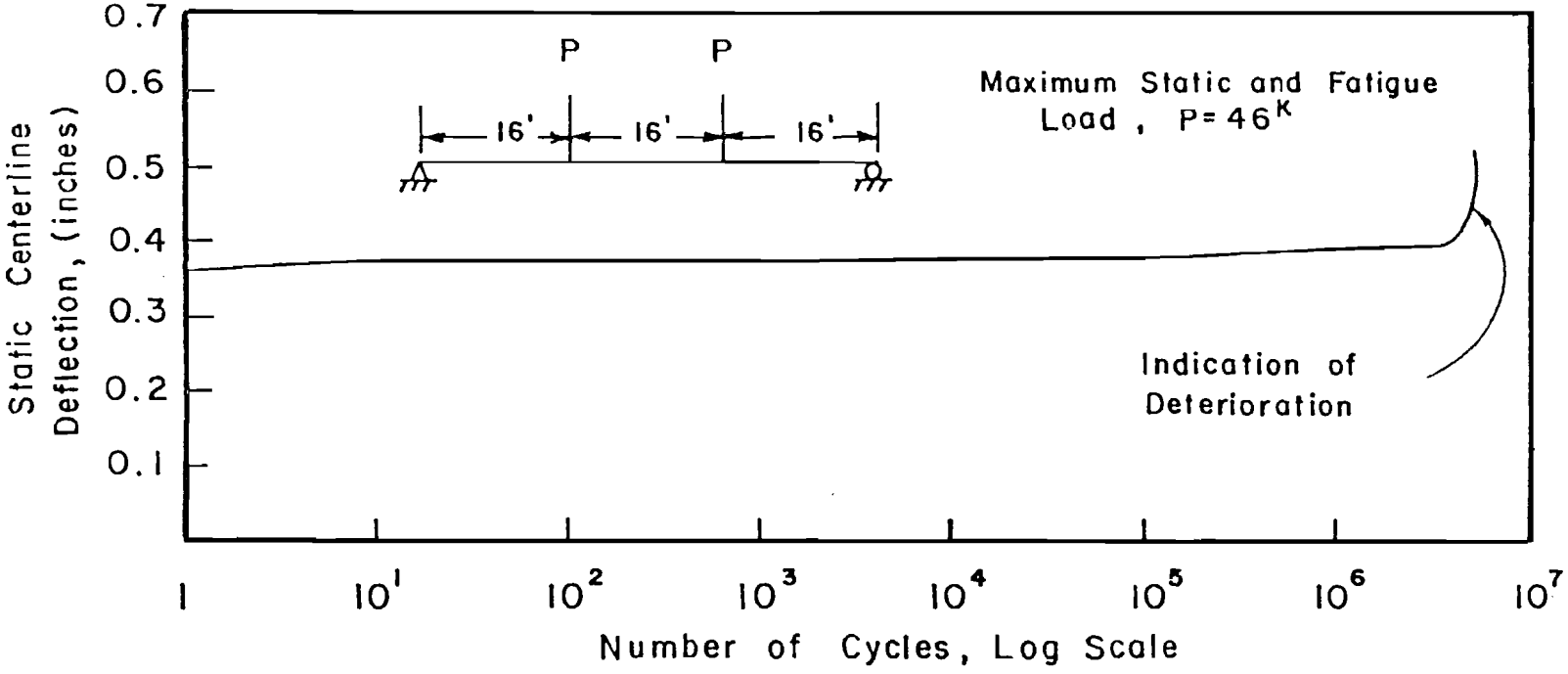

Fig. 4.70 Centerline deflection during static tests for Specimen A-22-NP-6.2-NO-5.00

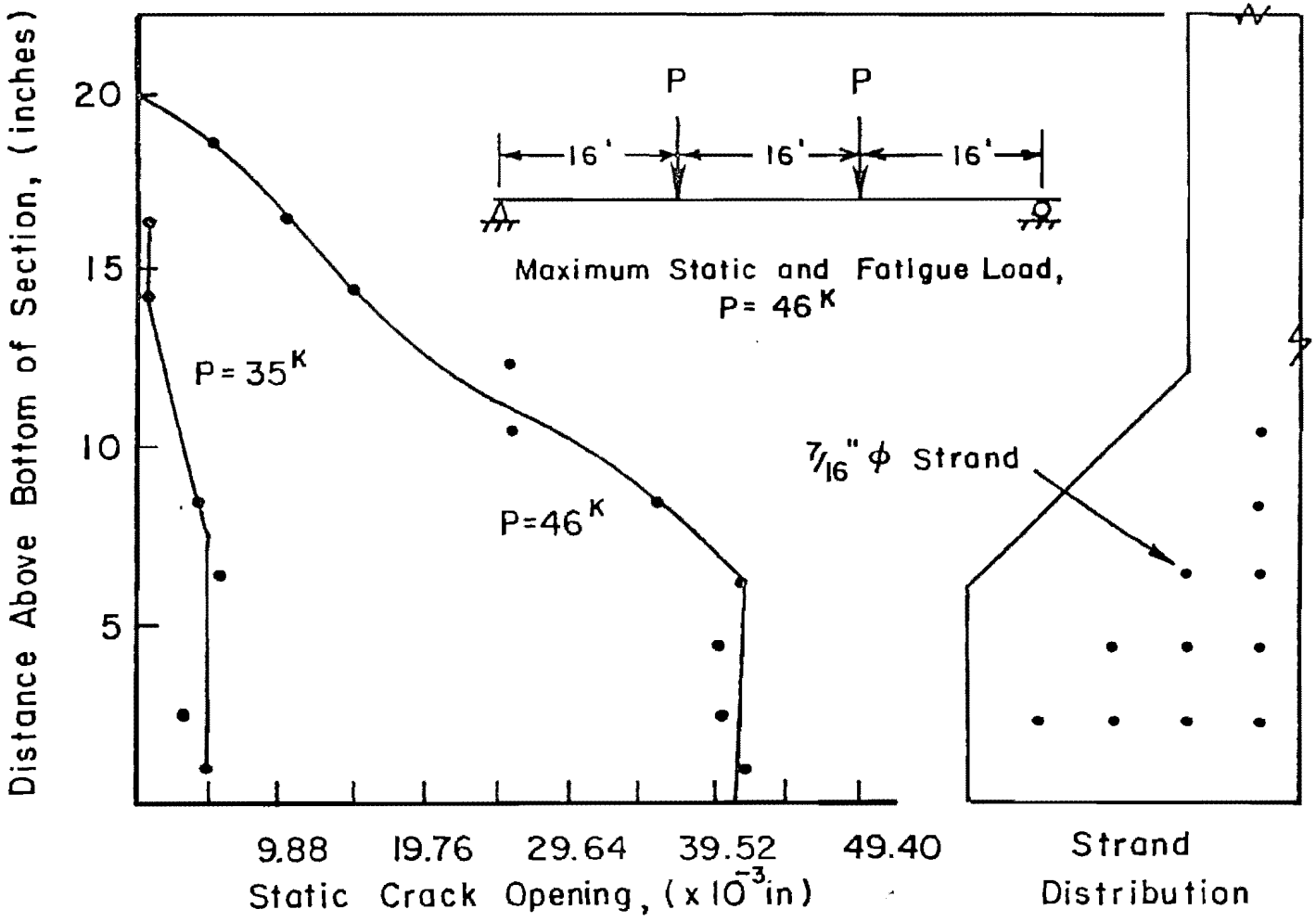

Fig. 4.71 Static crack profile 10 in. south of centerline at 1.0 million cycles

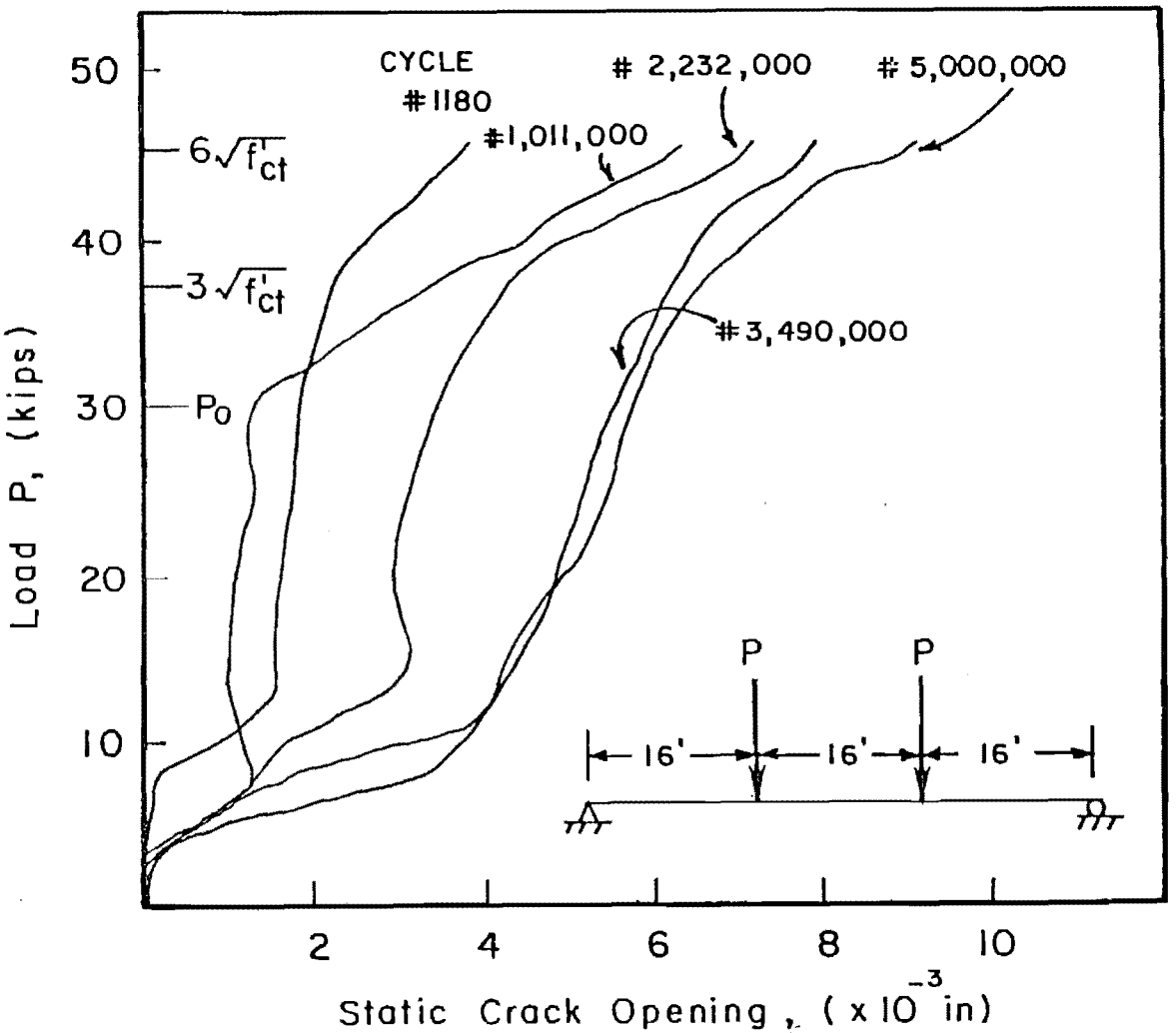

Fig. 4.72 Load versus crack opening 10 in. south of centerline during static tests

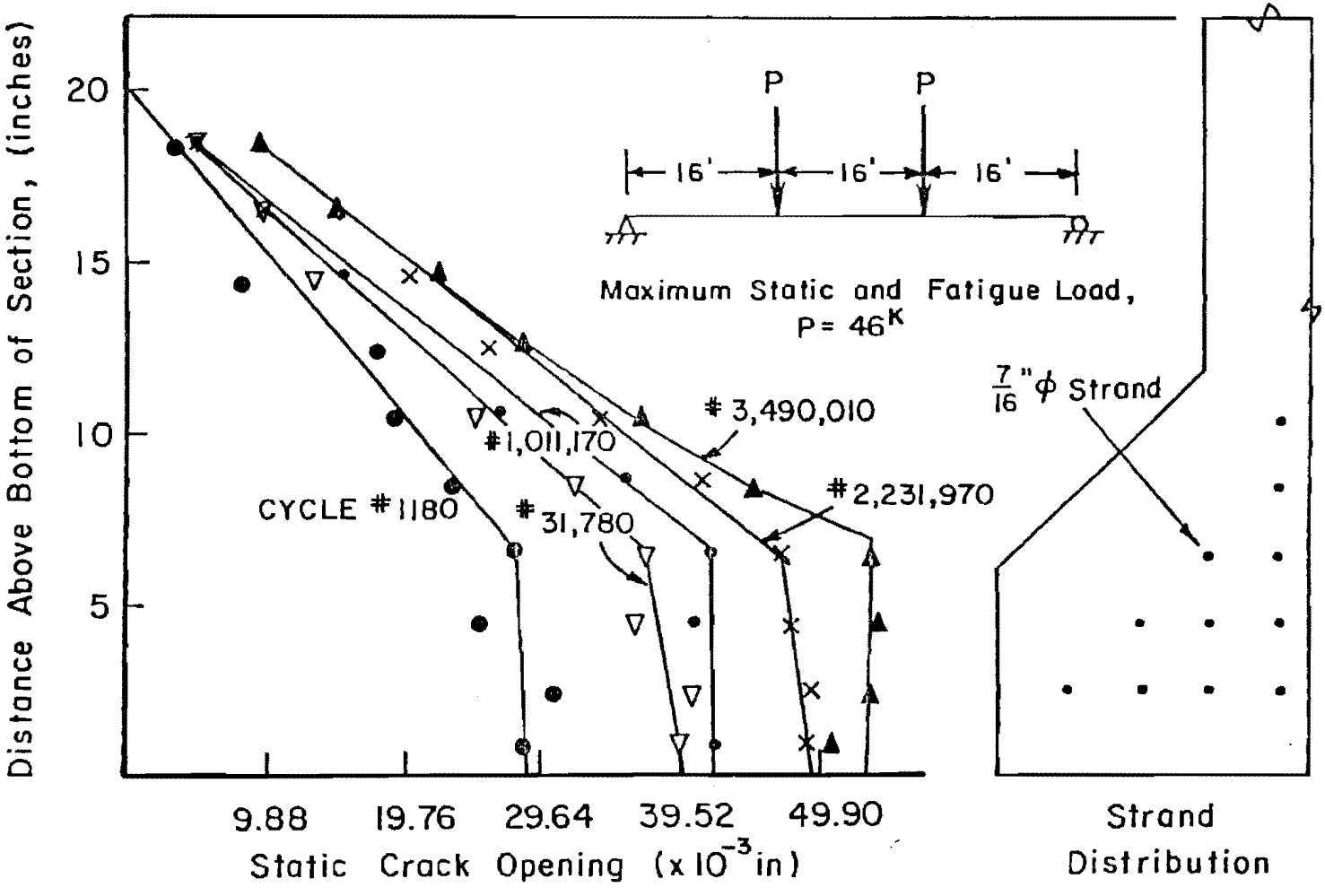

Fig. 4.73 Static crack profile 10 in. south of centerline during static tests

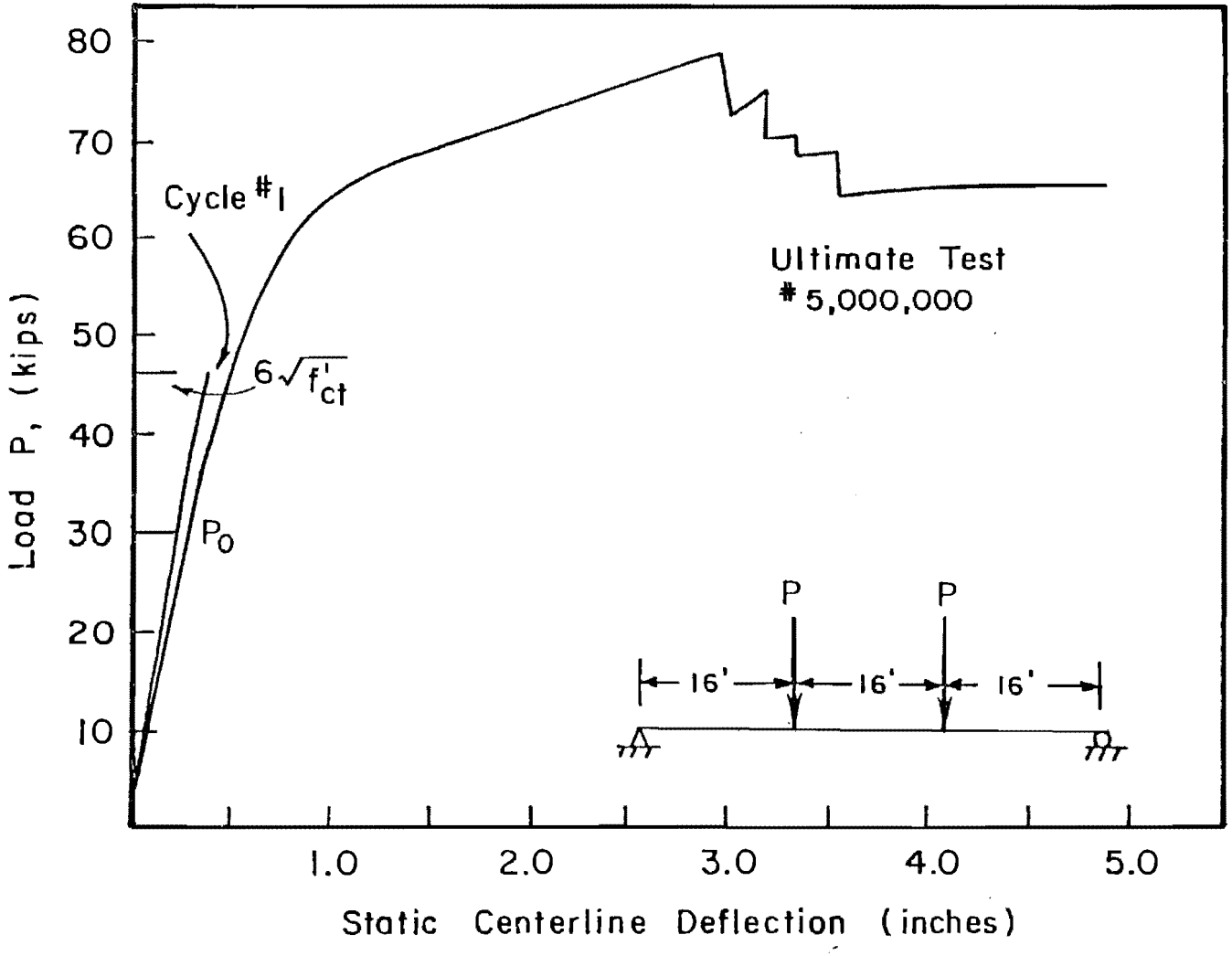

Fig. 4.74 Ultimate load versus deflection for Specimen A-22-NP-6.2-NO-5.00

but less than the expected deflection of 20 to 30 in. Figure 4.75 shows the failure crack after the ultimate test.

4.8.5 Post Mortem Inspection

The post mortem investigation revealed 33 fatigue fractures on eight strands. The failure crack, shown in Fig. 4.68, was 7 ft 8 in. north of the centerline, which is within the constant moment region but outside the drape point at 3 ft 5 in. from the centerline. The flexural crack at the south drape point extended 22 in. above the bottom of the section, which is approximately at the center of the web. The only fatigue breaks were those shown in the insert on Fig. 4.68, at the failure crack.

4.8.6 Dynamic Load Amplification

The static centerline deflection between 10 and 46 kips at 1.0 million cycles, which was in the stable region of fatigue testing, was 0.32 in. (0.07 in. to 0.39 in.). The dynamic deflection at 0.95 million cycles was 0.33 in. (0.09 in. to 0.42 in.), which indicates slight dynamic amplification. The static loads corresponding to these dynamic deflections were 13 and 48 kips.

4.9 Specimen A-22-NP-3.5-OL-5.95 (NF)

This specimen was an AASHTO-PCI Type II with 22 strands, ten of which were draped. There was no passive (unstressed) reinforcing steel in the lower flange. The specimen was cycled at an upper fatigue load (P_{max}) that produced $3.5\sqrt{f'_{ct}}$ nominal tensile stress in the extreme tension fibers, based on an uncracked section. There were loads above P_{max} (overloads) applied to the member during periodic static tests. Fatigue testing was stopped after 5.95 million cycles. No failure (NF) occurred at this load level, at this number of cycles.

4.9.1. Initial Static Tests

Specimen A-22-NP-3.5-OL-5.95 (NF) was loaded incrementally to a maximum load of 55 kips. Flexural cracks became visible at this load. The load versus strain curves shown in Fig. 4.76 for the initial static cycle indicates a change in slope at 30 kips. The transition is gradual like that that occurs at the zero tension load, unlike the sudden increase that occurs at cracking, as shown in Fig. 4.2. This would indicate that the section was possibly cracked before loading. There was no indication of cracking prior to the initial static test and the load deflection curve indicated uncracked section behavior until

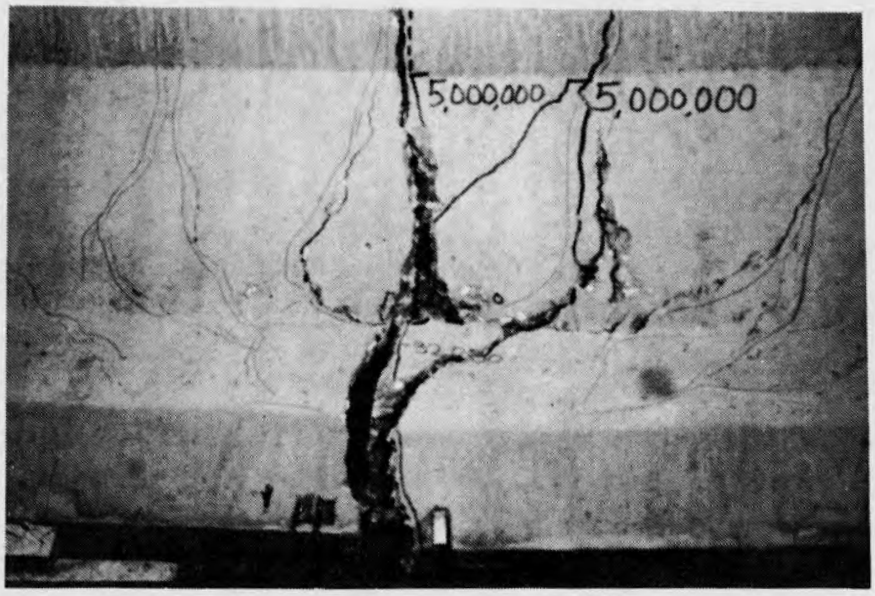

Fig. 4.75 Failure crack for Specimen A-22-NP-6.2-NO-5.00

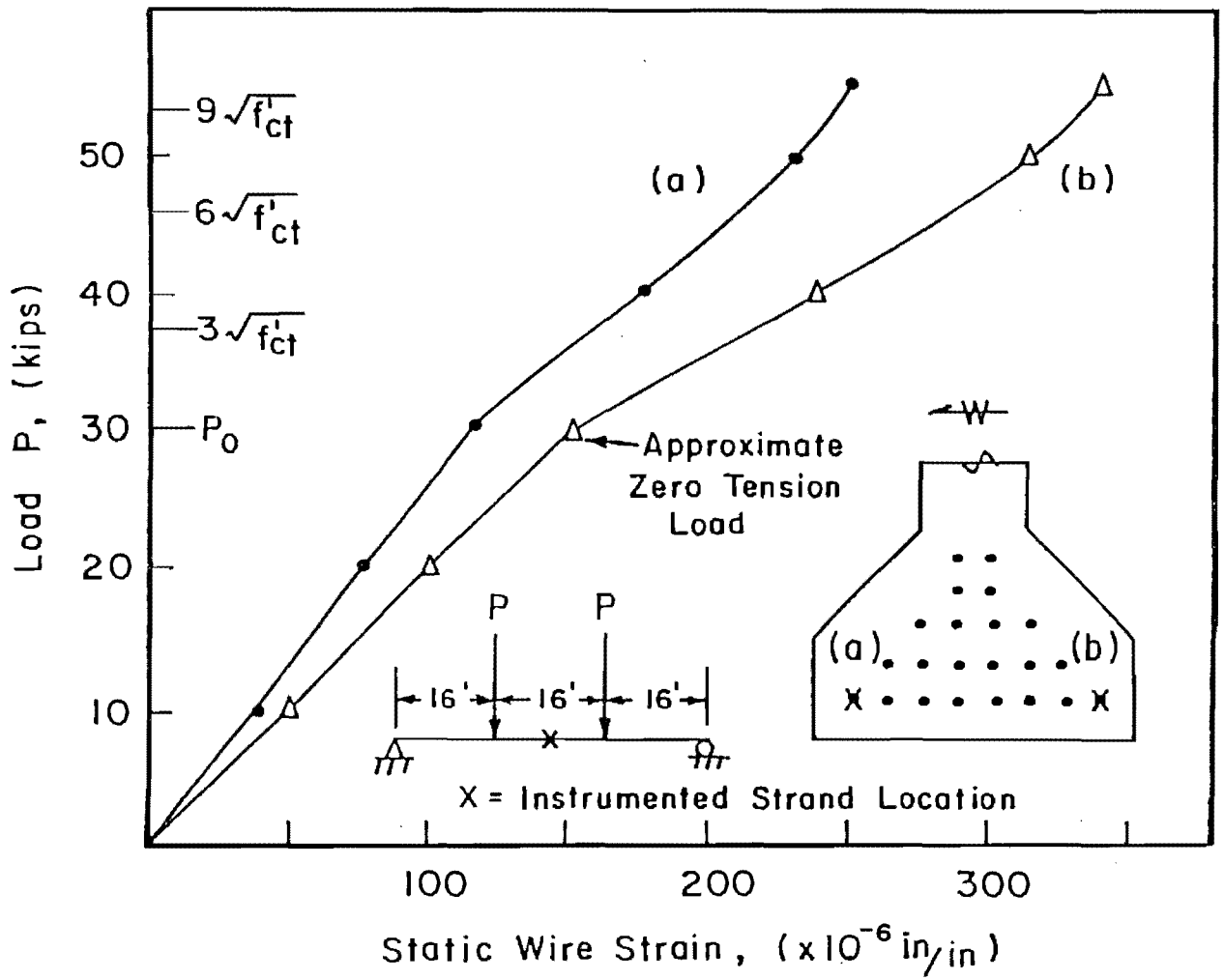

Fig. 4.76 Load versus centerline wire strain for Specimen A-22-NP-3.5-OL-5.95 (NF)

probable cracking occurred at 45 kips. An uncracked section was therefore assumed prior to loading.

Five static cycles were applied to the specimen before fatigue testing began. Four flexural cracks, as shown in Fig. 4.77, formed during these initial cycles. By the fifth cycle the inner two cracks had propagated to the bottom of the web. The crack 87 in. south of the centerline originated in the middle region of the bottom flange and propagated in two directions. The drape points are also shown in Fig. 4.77.

4.9.2 Zero Tension, P_o.

Figure 4.76 indicates a significant change in the load versus strain curve at 30 kips, typical of the change that occurs at the zero tension load. This is the same approximate load indicated as the zero tension load for Specimen A-22-NP-6.2-OL-2.84. This is reasonable since all A-22 specimens were cast simultaneously in a long-line casting bed. (The strands were continuous through all three girders.) The centerline deflection at 30 kips was 0.22 in.

4.9.3 Fatigue Loads

Specimen A-22-NP-3.5-OL-5.95 (NF) was cycled at a maximum nominal tensile stress of $3.5\sqrt{f'_{ct}}$ to assist in identifying an endurance limit. Based on a zero tension load of 30 kips and uncracked section properties, the maximum load required to produce a tensile stress of $3.5\sqrt{f'_{ct}}$ was 39 kips. The two previous A-22 specimens had failed at a cycle load that produced $6.2\sqrt{f'_{ct}}$ tensile stress. This specimen was cycled at approximately 60 percent of that value, based on an uncracked section, to determine if failure could occur at less than $6\sqrt{f'_{ct}}$ in hopes of defining the endurance limit. The load program for Specimen A-22-NP-3.5-OL-5.95 (NF) is shown in Fig. 4.78.

4.9.4 Fatigue Behavior

The specimen's behavior, as indicated by the centerline deflection during static tests shown in Fig. 4.79, remained constant throughout fatigue testing. The static centerline deflection at 55 kips increased from 0.46 in. during the initial static cycles to 0.53 in. at 5.95 cycles, only a 13 percent increase. The third point deflection at 5.95 cycles was 0.44 in.

Figure 4.80, of the static crack profile at 55 kips, indicates that the crack 4 ft 2 in. north of the centerline did not increase in width significantly between 63,000 and 5.95 million cycles. Figure 4.81 shows crack opening as a function of load. Here again, there is not a

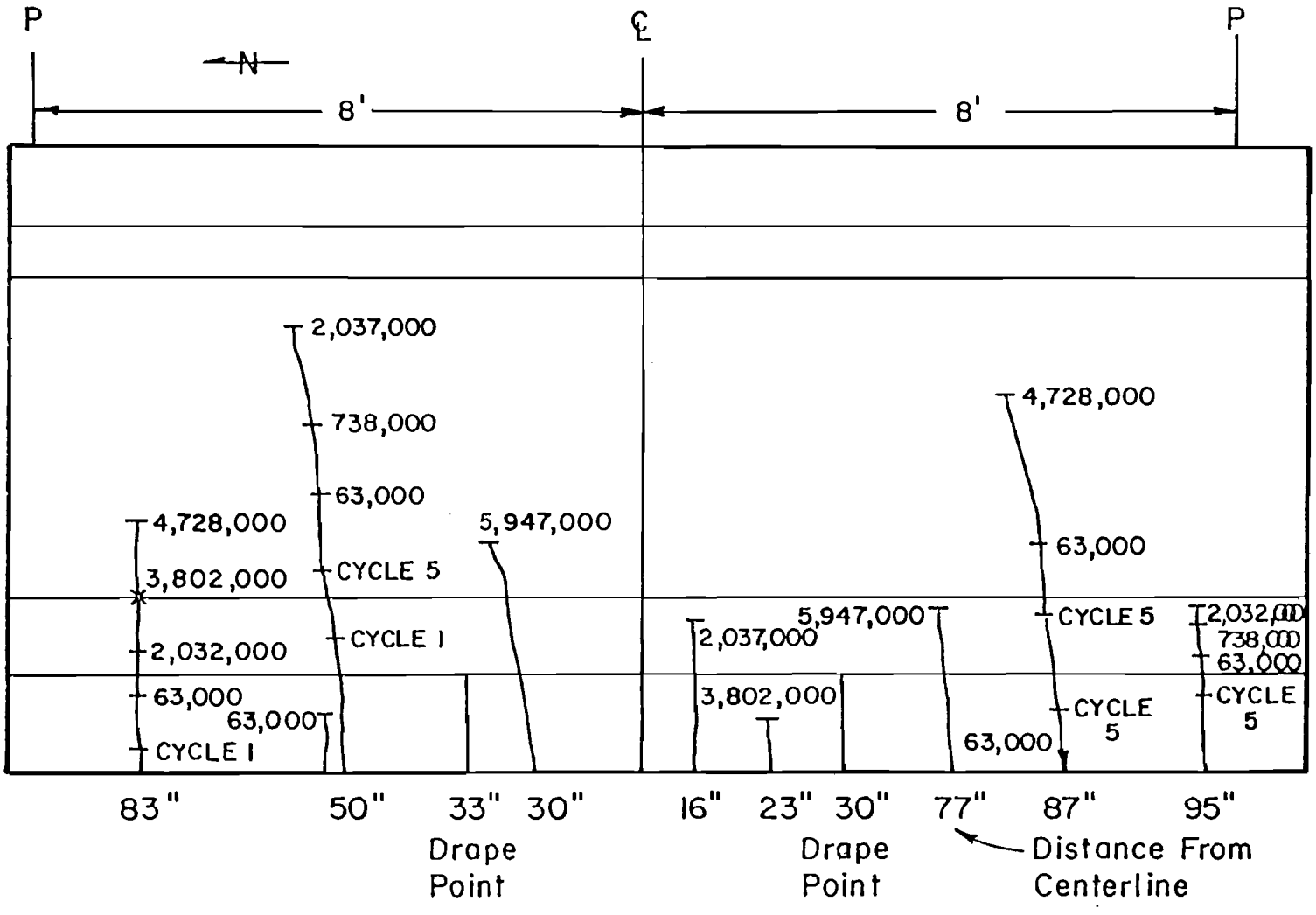

Fig. 4.77 Location of drape points and flexural cracks prior to ultimate testing

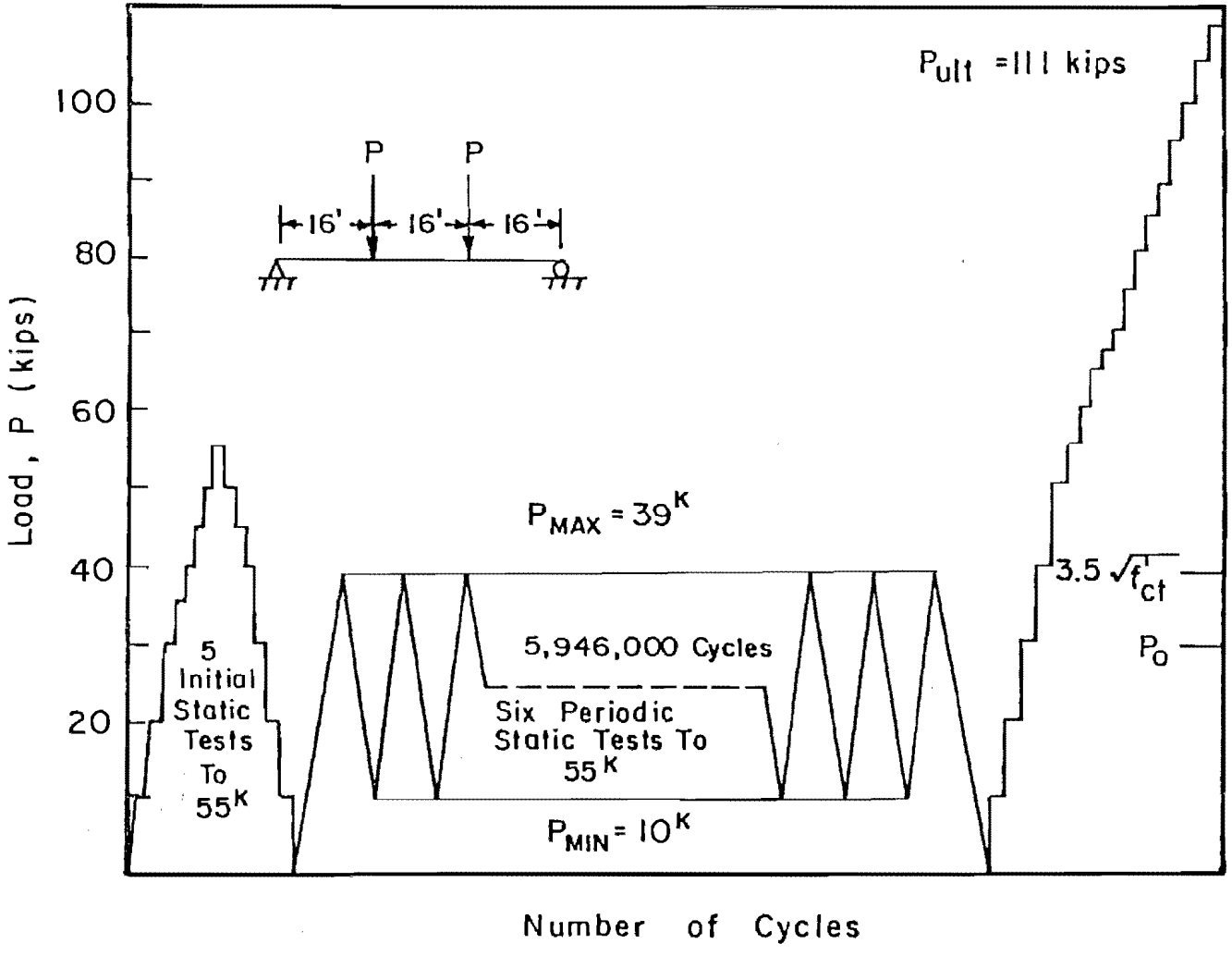

Fig. 4.78 Load program for Specimen A-22-NP-3.5-OL-5.95 (NF)

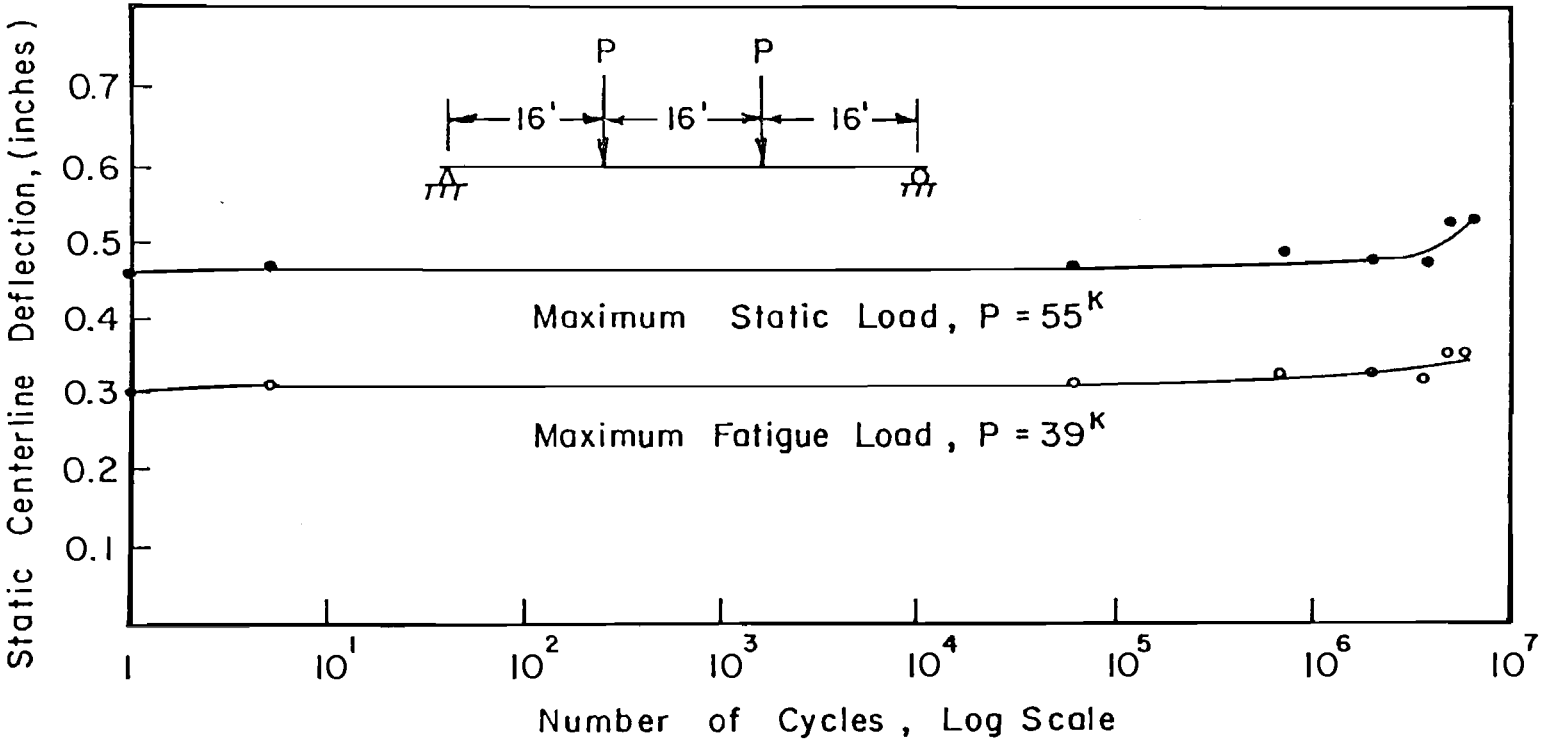

Fig. 4.79 Centerline deflection during static tests for Specimen A-22-NP-3.5-OL-5.95 (NF)

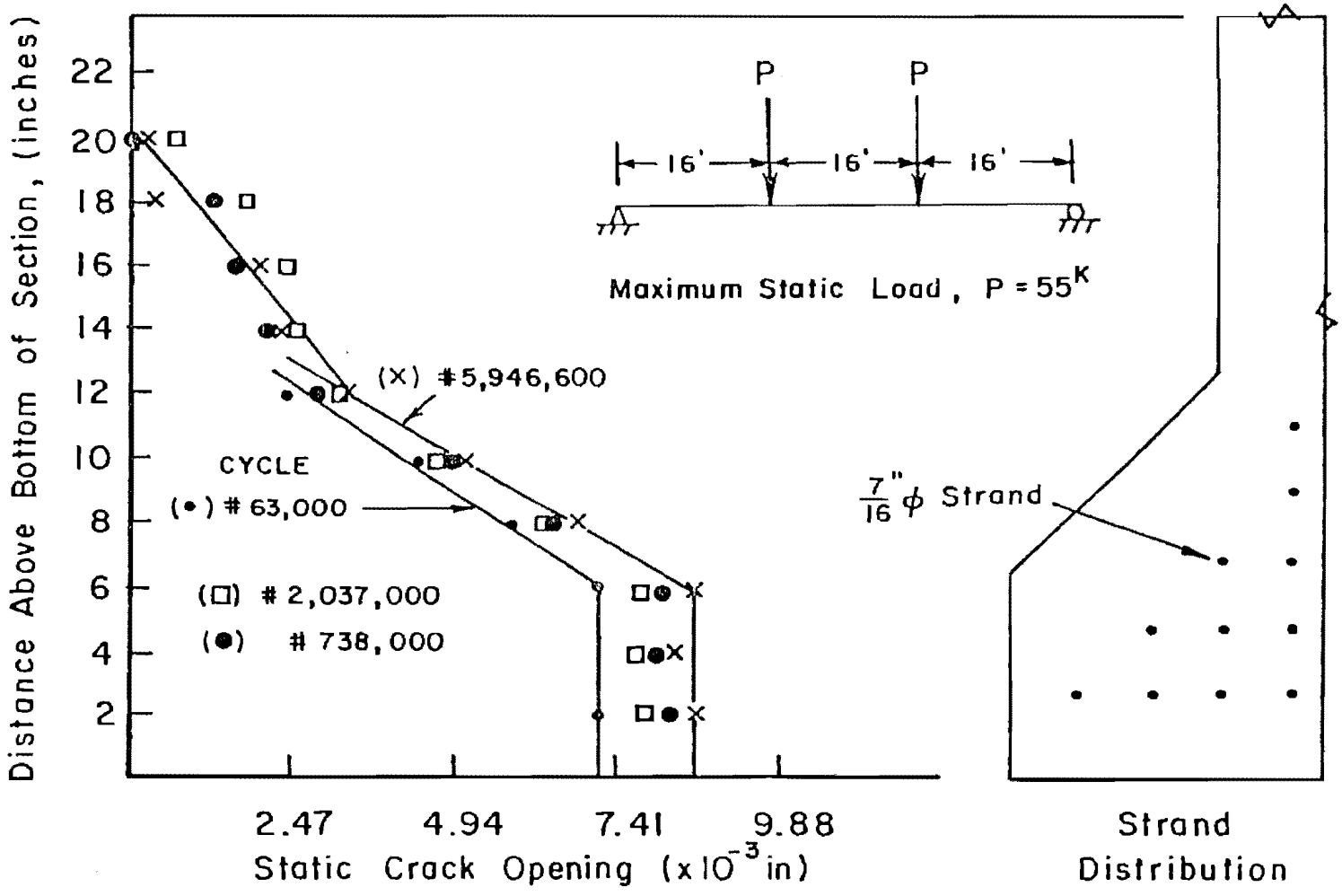

Fig. 4.80 Static crack profile 4 ft 2 in. north of centerline during static tests

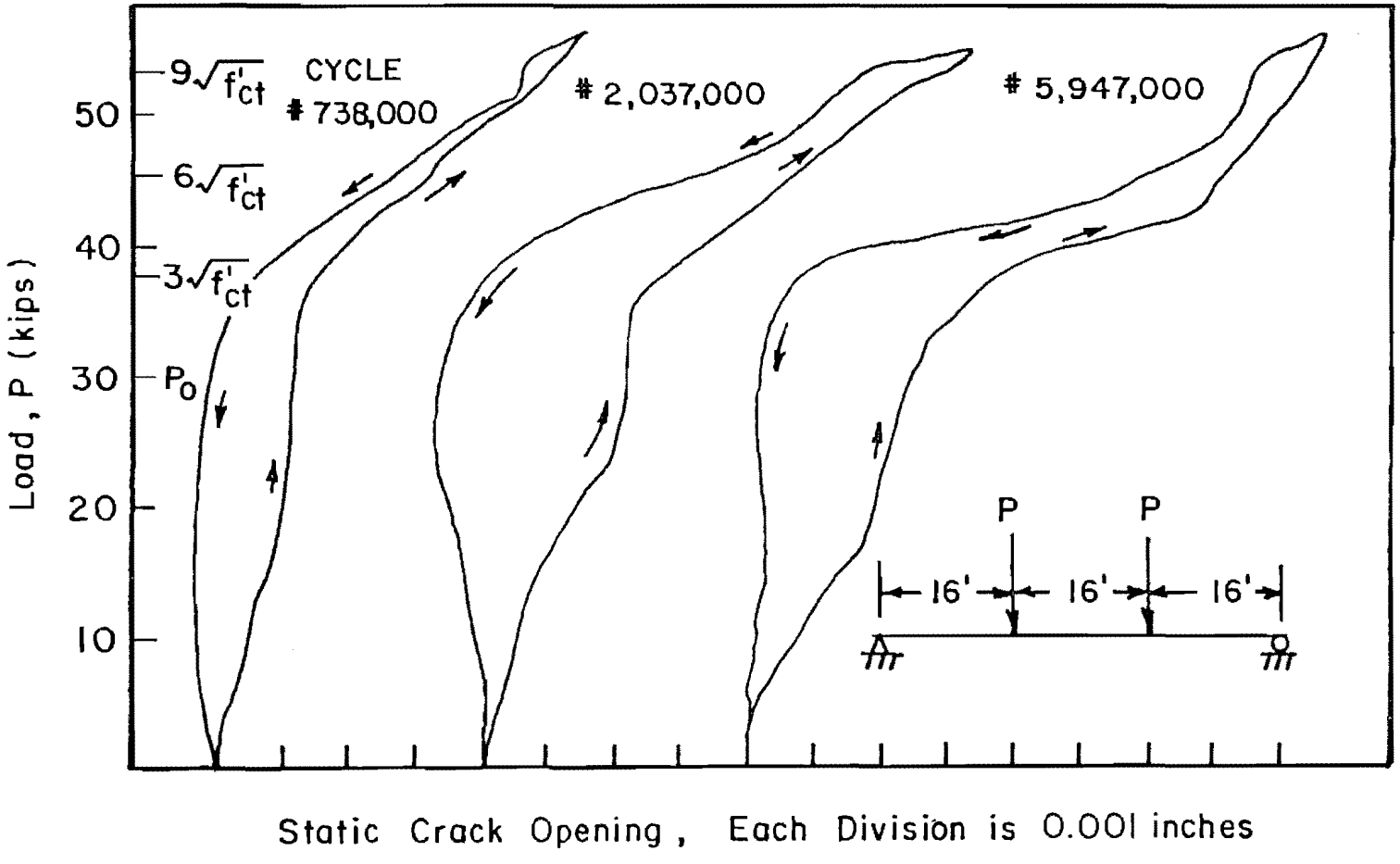

Fig. 4.81 Load versus crack opening 4 ft 2 in. north of centerline during static tests

significant change in behavior between 738,000 and 5.95 million cycles. There were nine flexural cracks, as shown in Fig. 4.77, in the center 14 ft 10 in. of the span before the static ultimate test.

Slab strain was monitored throughout testing of this specimen to determine the effective slab width. Figure 4.82 shows slab strains during the initial cycle and at 5.95 million cycles. The outside gage, which was the only active one for the ultimate test, indicates little change from the initial cycle. The change in slope at approximately 30 kips is a result of the reduced section modulus at the zero tension load. The slab concrete must strain more for an increment of load because of the reduced section, due to flexural cracking.

4.9.5 Static Ultimate Test

The specimen had to be loaded in four stages, as shown in Fig. 4.83, as a result of large deflections. The loading ram stroke was 12 in., so steel plates were inserted between the rams and the deck as the permanent deflection increased. The maximum load was 111 kips, which is 11 percent greater than the calculated ultimate capacity of 100 kips. The maximum deflection was 22.7 in. The specimen never lost its capacity to carry load. The test was stopped because of the safety hazards caused by excessive deflection and rotations. Figure 4.84 shows the specimen during the ultimate test. Figures 4.85 and 4.86 show the extensive cracking after the ultimate test was halted.

4.9.6 Post Mortem Investigation

The concrete cover for a distance of 11 ft was removed from the lower flange after the ultimate test. No static or fatigue fractures were located in this region.

4.9.7 Dynamic Load Amplification

The static centerline deflection range between 10 and 39 kips at 4.73 million cycles was 0.27 in. (0.07 in. to 0.34 in.), which was typical for all static tests. The dynamic deflection range between 10 and 39 kips, at 4.71 million cycles, was 0.27 in. (which indicates no dynamic amplification).

4.10 Specimen C-16-UP-8.0-NO-1.73

This specimen was a Texas Type C with 16 straight strands. There was 1.99 sq. in. (two number seven bars and one number eight bar) of passive steel in the lower flange at the level of the bottom strands to control cracking. This passive (unstressed) reinforcement was

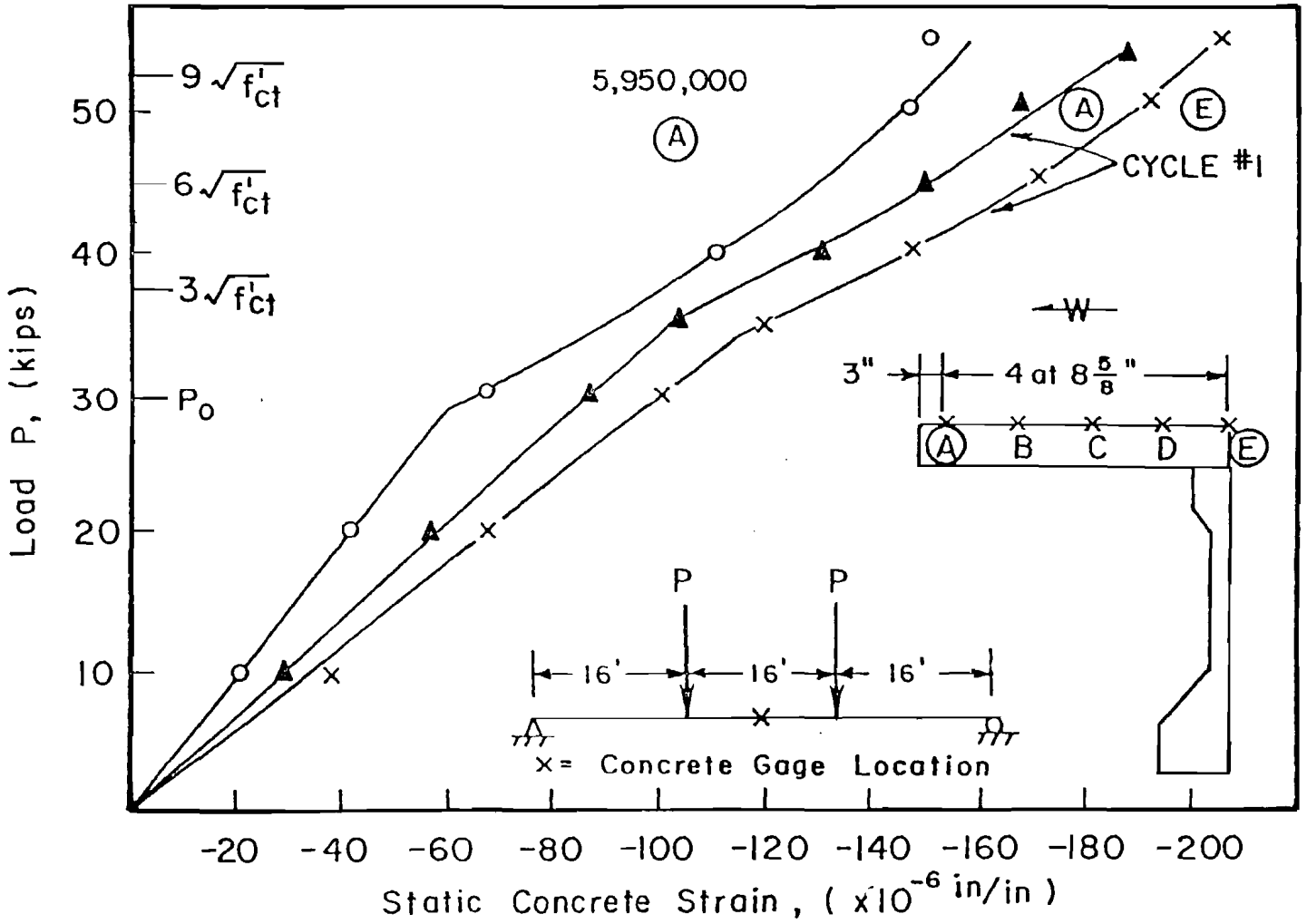

Fig. 4.82 Centerline slab strain during the initial cycle and at 5.95 million cycles

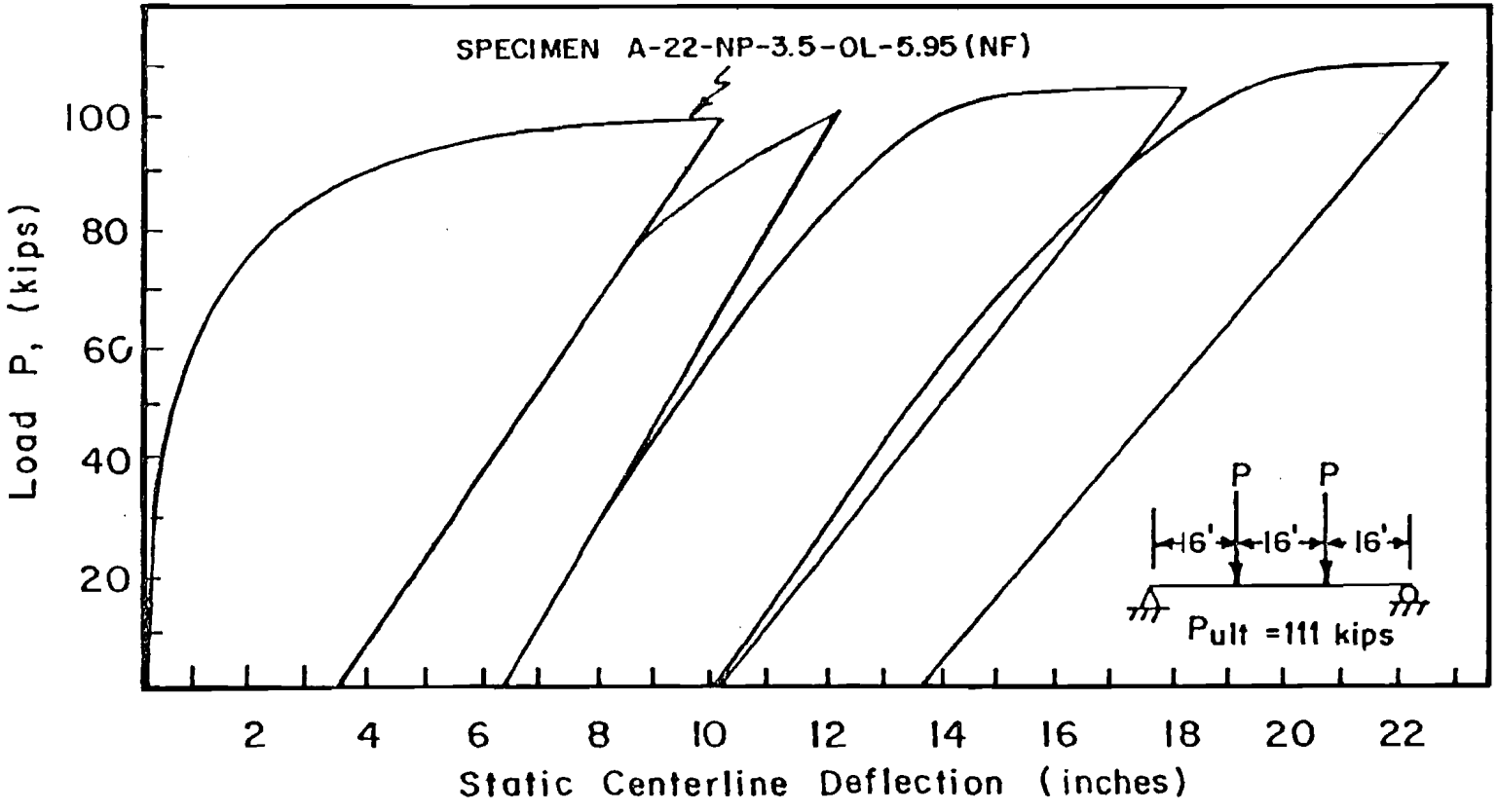

Fig. 4.83 Ultimate load versus deflection for Specimen A-22-NP-3.5-OL-5.95 (NF)

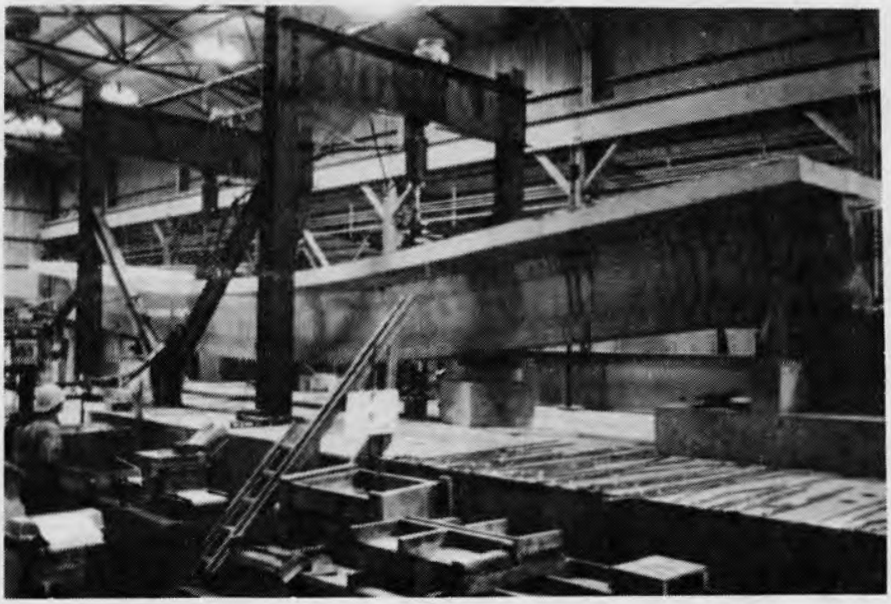

Fig. 4.84 Ultimate tests of Specimen A-22-NP-3.5-OL-5.95 (NF)

Fig. 4.85 Flexural cracking on the east side of Specimen A-22-NP-3.5-OL-5.95 (NF) after ultimate testing

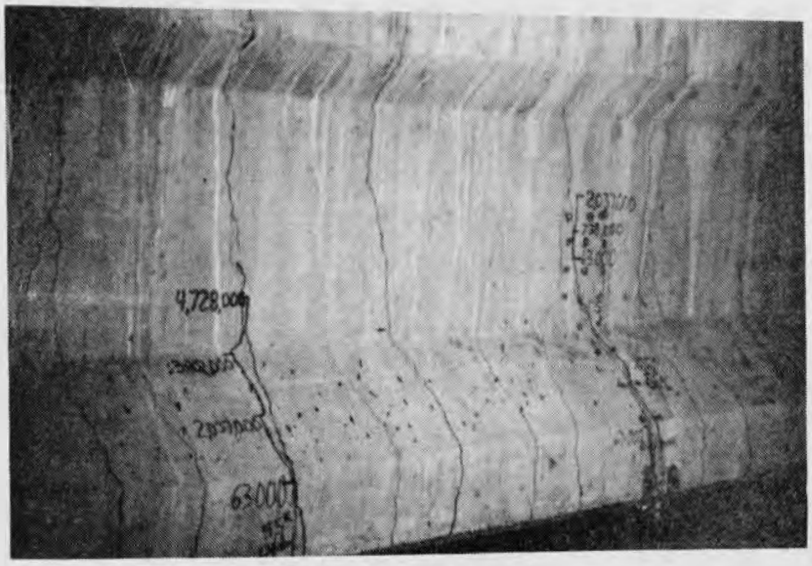

Fig. 4.86 Flexural cracking on the west side of Specimen A-22-NP-3.5-OL-5.95 (NF) after ultimate testing

unconfined. The insert on Fig. 4.87 shows the steel distribution in the lower flange. The specimen was cycled at an upper fatigue load (P_{max}) that produced $8.0\sqrt{f'_{ct}}$ nominal tensile stress, based on an uncracked section, in the extreme tension fibers. There were no loads (no overloads, NO) above P_{max} during the periodic static tests. The specimen experienced 1.73 million cycles prior to the ultimate test.

4.10.1 Initial Static Tests

The specimen was loaded incrementally to a maximum load of 75 kips. Flexural cracks were first visible at this load. Figures 4.87 and 4.88 of load versus strand wire strain indicate that cracking probably occurred at approximately 70 kips. Figure 4.89 of load versus deflection indicates a slight increase in deflection with no increase in load at 70 kips. This behavior typically occurs during flexural cracking. Another increase in deflection with no load increase was observed at 75 kips. Sixteen flexural cracks formed during the initial three cycles and were confined to the lower flange.

4.10.2 Zero Tension Load, P_o.

Figures 4.87 through 4.89 indicate a significant change in behavior at approximately 48 kips. This change marks the point at which the extreme tension fibers first experience tension, hence 48 kips is the zero tension load. The centerline deflection at this load was 0.31 in.

4.10.3 Fatigue Loads

Specimen C-16-UP-8.0-NO-1.73 was designed as a companion to Specimen C-16-NP-7.2-OL-1.48. The main variable was the addition of 1.99 sq. in. of nonprestressed reinforcing steel (two #7 reinforcing bars and one #8 bar) to the bottom flange of Specimen C-16-UP-8.0-NO-1.73. Based on the zero tension load of 48 kips, and uncracked section properties, a load of 75 kips was required to produce a nominal tensile stress at $8.0\sqrt{f'_{ct}}$. The minimum load of 24 kips was selected to maintain the same load range of 51 kips applied to Specimen C-16-NP-7.2-OL-1.48. The load program for Specimen C-16-UP-8.0-NO-1.73 is shown in Fig. 4.90.

4.10.4 Fatigue Behavior

The specimen's behavior remained stable for the initial 1.15 million fatigue cycles. Figure 4.92 indicates that the centerline deflection increased from 0.57 in. during the second cycles to 0.67 in.

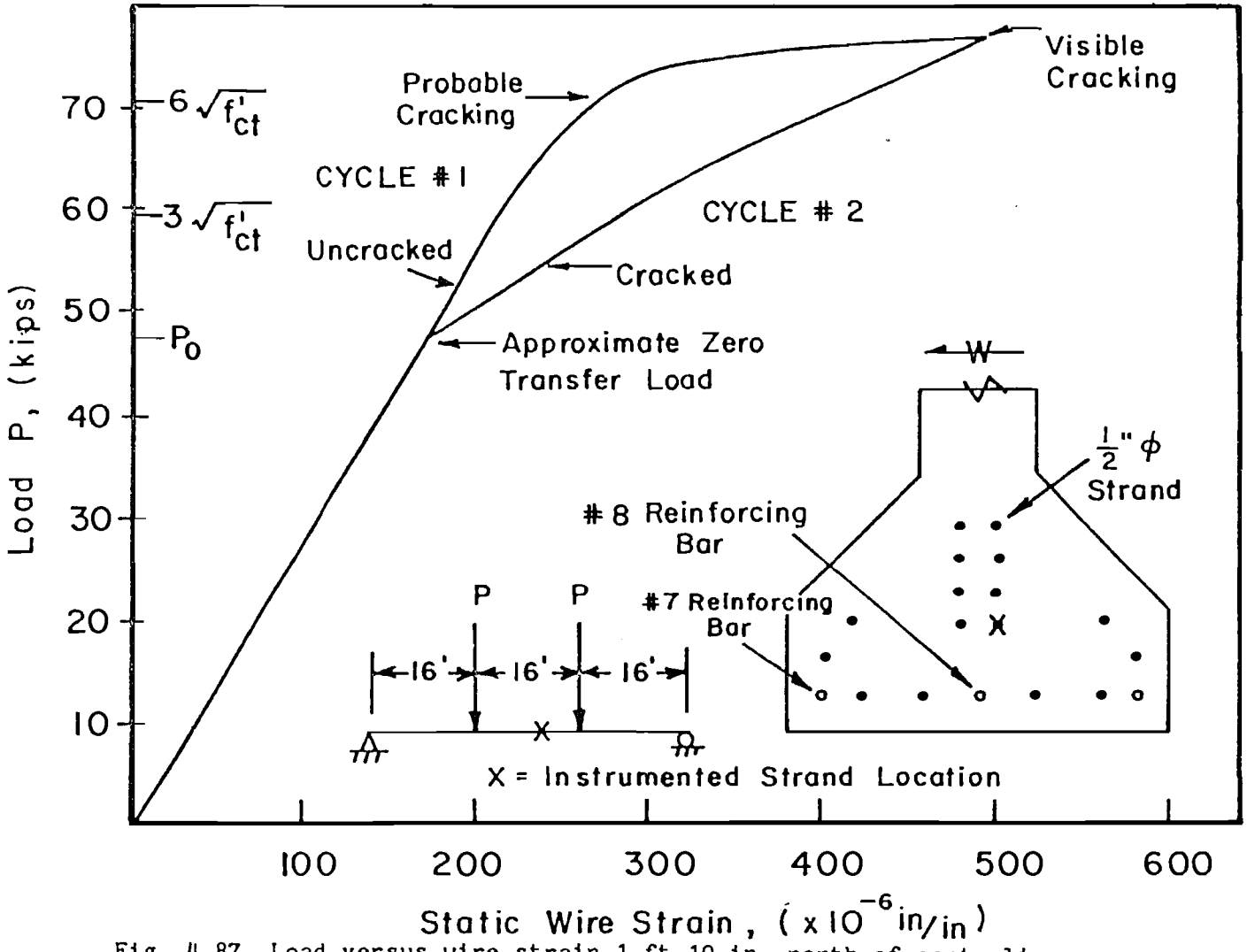

Fig. 4.87 Load versus wire strain 1 ft 10 in. north of centerline for Specimen C-16-UP-8.0-NO-1.73

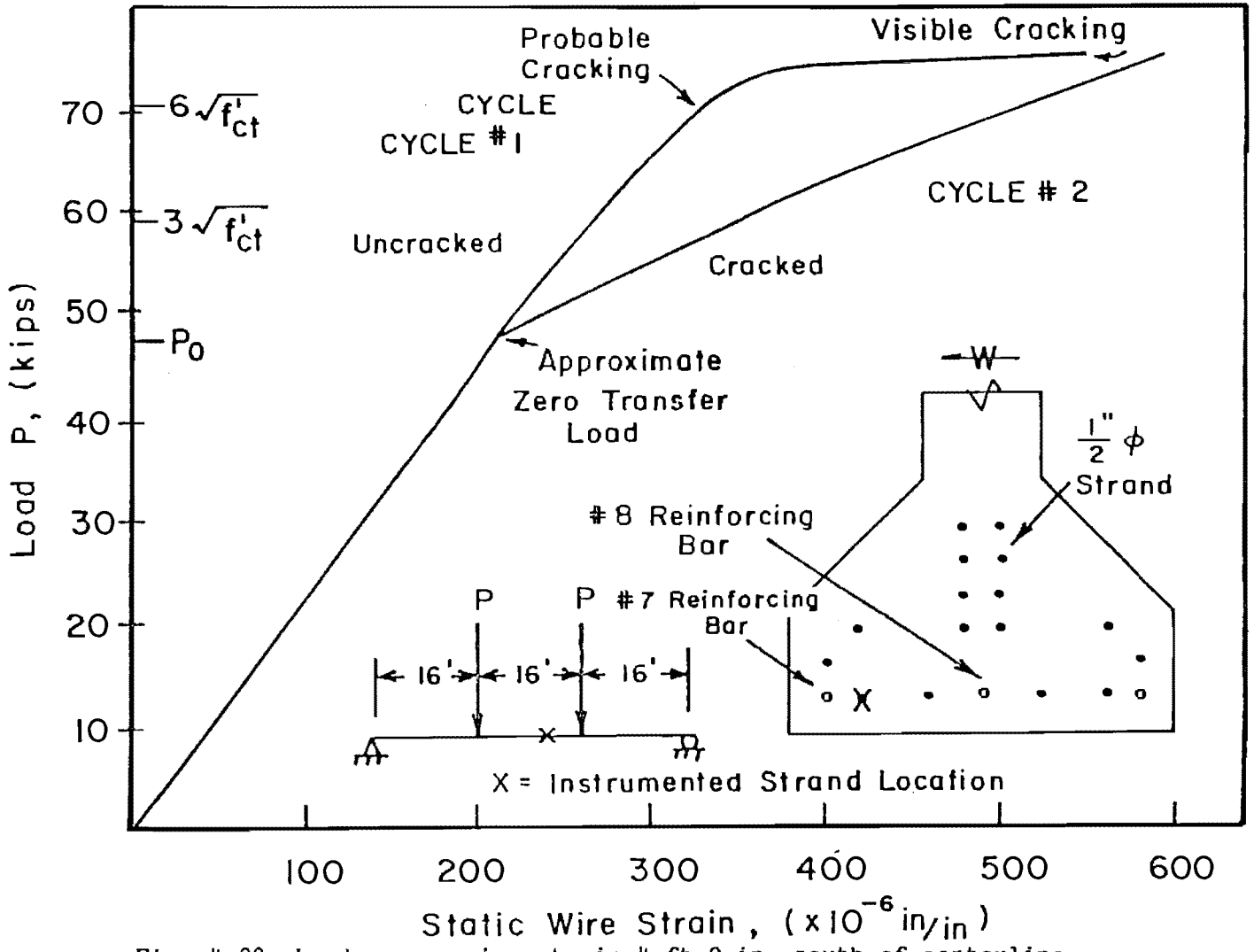

Fig. 4.88 Load versus wire strain 4 ft 0 in. south of centerline for Specimen C-16-UP-8.0-NO-1.73

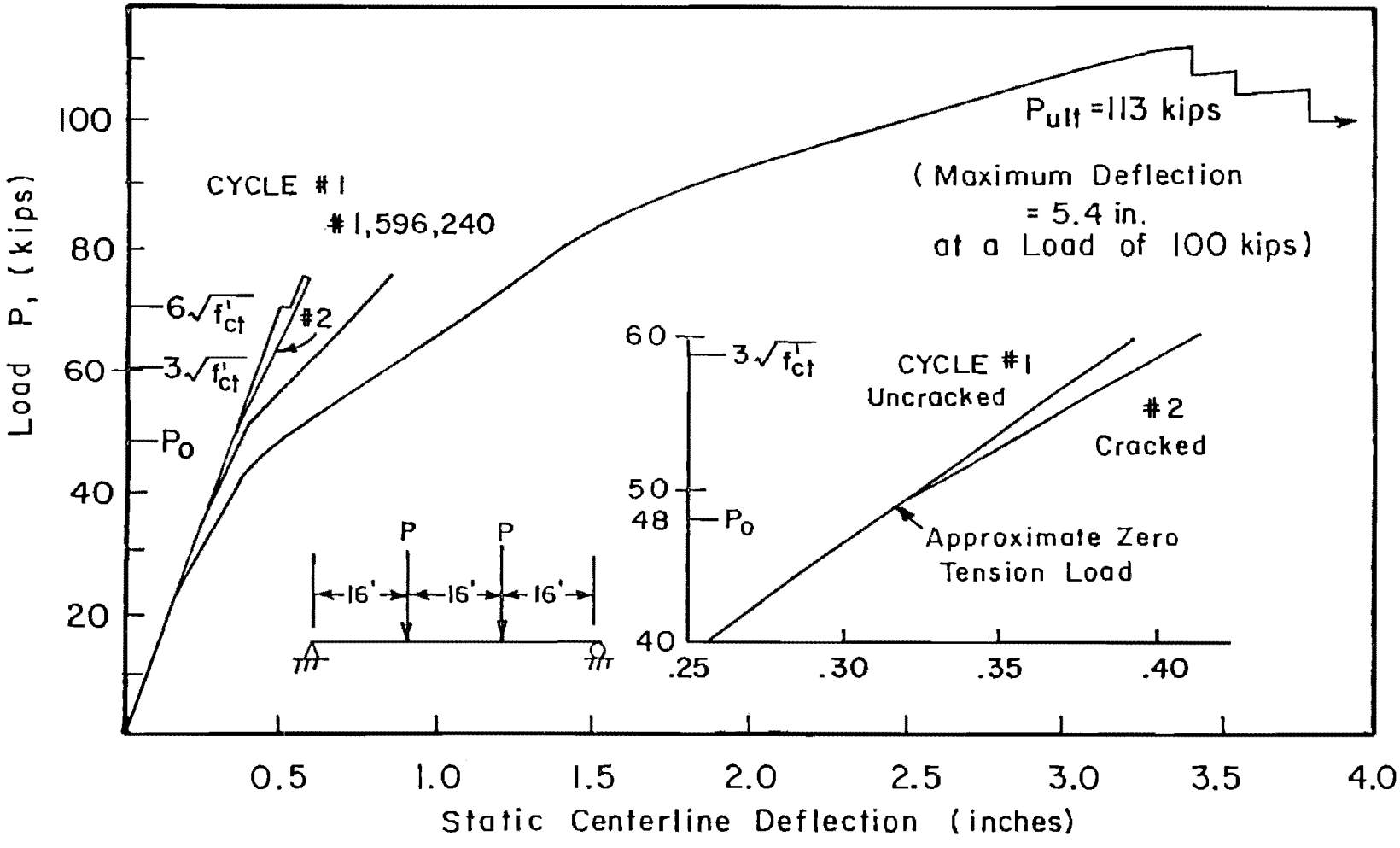

Fig. 4.89 Load versus deflection during static tests for Specimen C-16-UP-8.0-NO-1.73

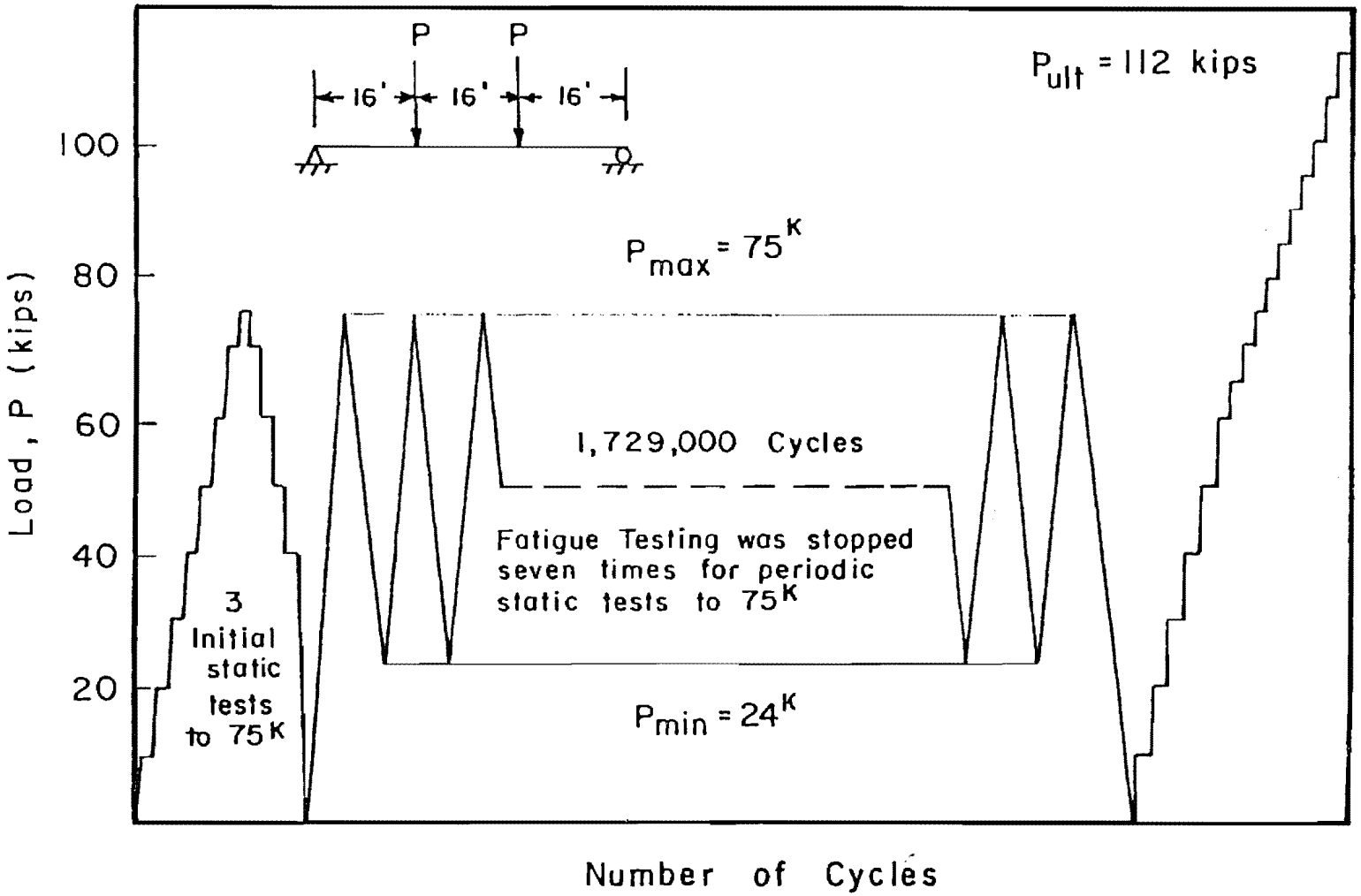

Fig. 4.90 Load program for Specimen C-16-UP-8.0-NO-1.73

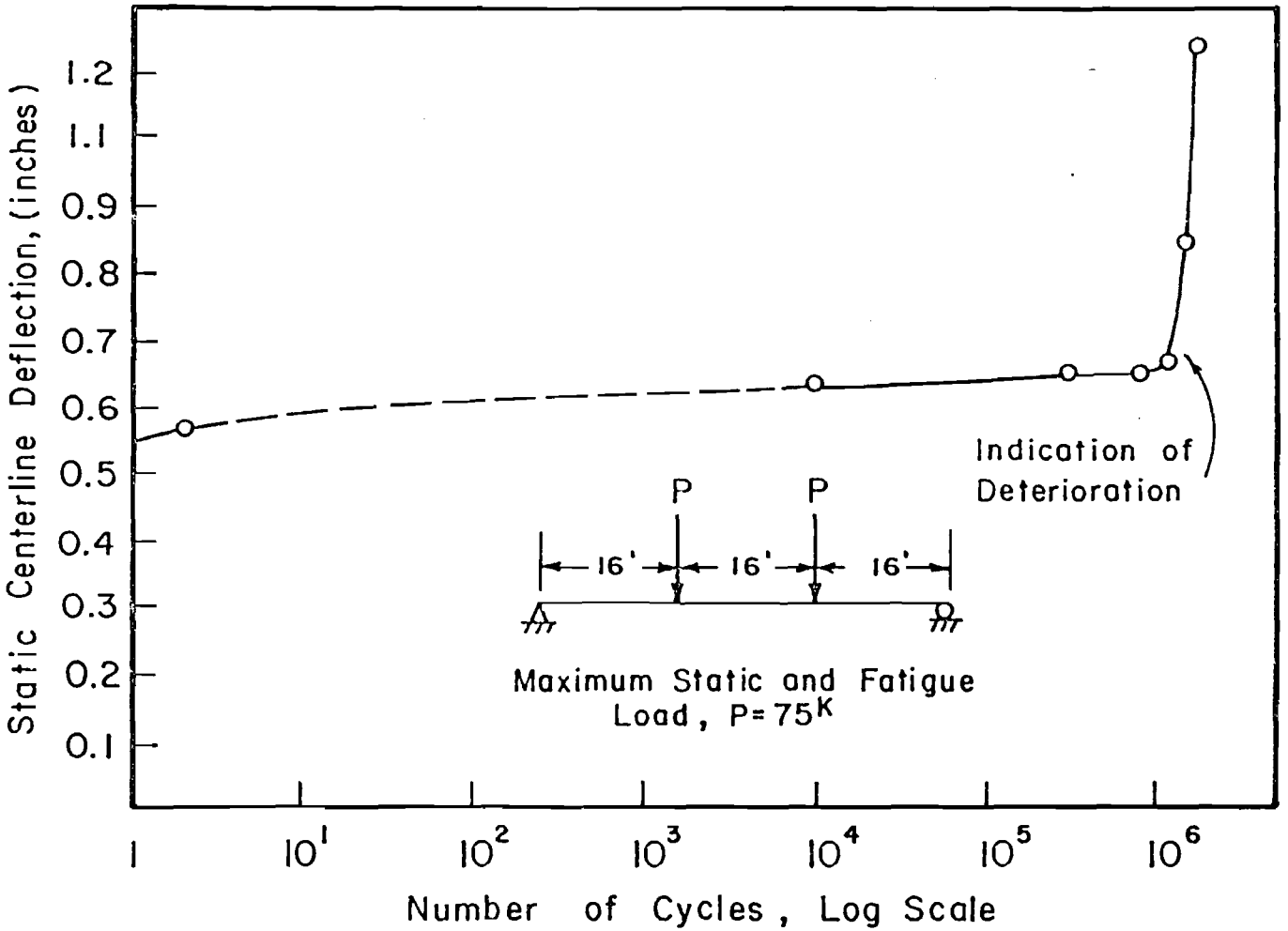

Fig. 4.91 Centerline deflection during static tests for Specimen C-16-UP-8.0-NO-1.73

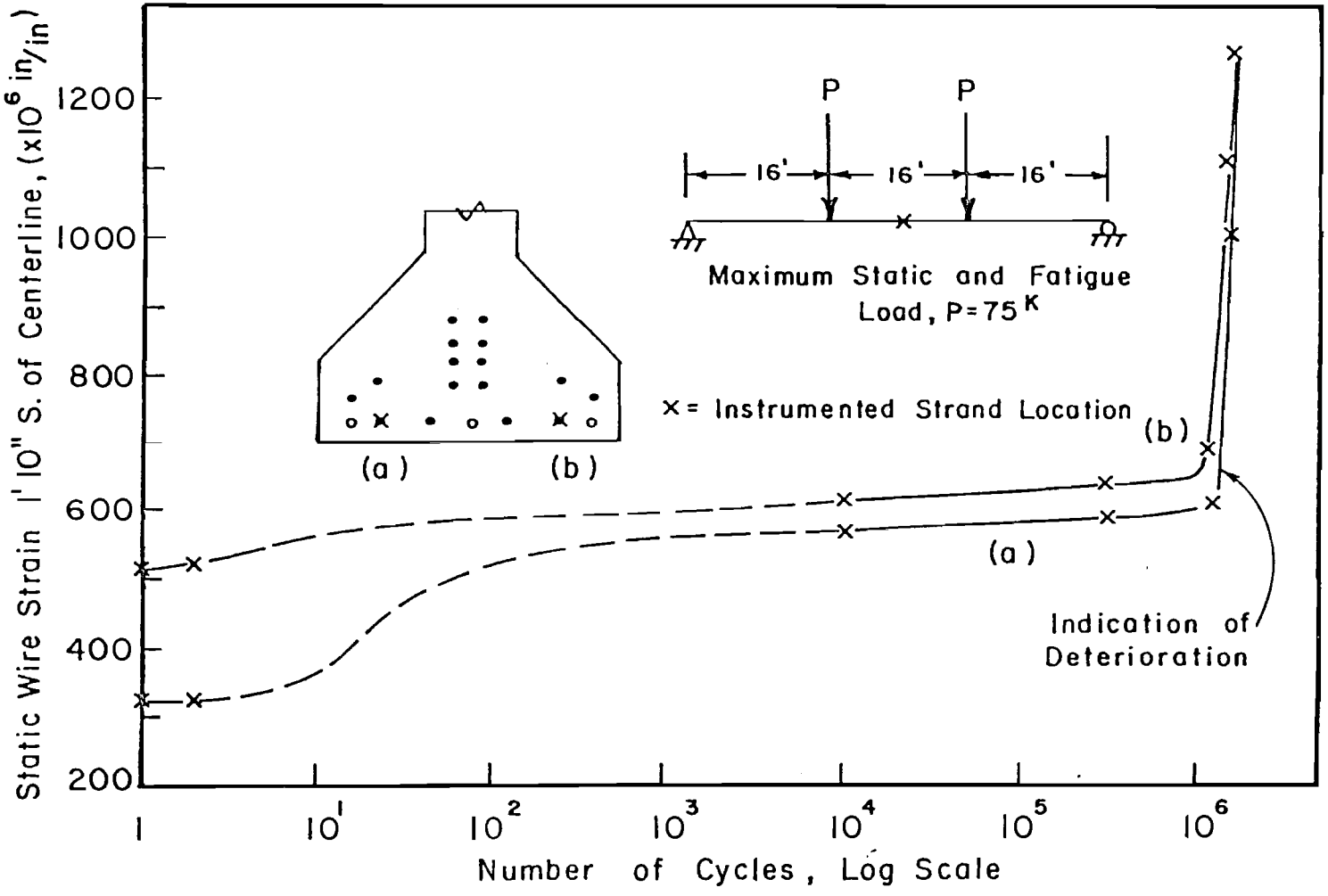

Fig. 4.92 Wire strain during static tests for

at 1.15 million cycles. The third point deflection at 75 kips after 1.15 million cycles was 0.58 in.

Strand wire strains at various phase stages of fatigue testing, as shown in Fig. 4.92, increased gradually during the initial 1.15 million cycles. The two strain gages were 24 in. from the centerline. The difference in strain can probably be attributed to different bond characteristics or unsymmetrical flexural cracking. The maximum static strain range between 24 and 75 kips at 1.15 million cycles was approximately 0.00061 in./in. measured at 22 in. north and 24 in. south of the centerline. The dynamic strain range over this interval was 0.00066 in./in. at this stage of fatigue testing.

Although the centerline deflection was stable for the initial 1.15 million cycles, the permanent centerline deflection with no load, as shown in Fig. 4.93, never stabilized. The rate of increase changed as the member began to deteriorate. There were 27 flexural cracks that generally extended to the middle portion of the web at 1.15 million cycles.

The member began to deteriorate rapidly after the initial stable period of 1.15 million cycles. Figures 4.91 through 4.93 indicate this behavior. Spalling occurred after 1.20 million cycles. This can be seen in Fig. 4.94. Wire breaks were visible at this location. By 1.60 million cycles the #7 bar on the west side of the specimen buckled due to the loss of confining concrete. Five wire fractures could be heard in succession at 1.61 million cycles. The bar buckled, as shown in Fig. 4.95, as a result of the compression force induced by the prestressing strands. The drastic increase in wire strains shown in Fig. 4.92 is the result of wire fractures. As adjacent wires fractured, the remaining wires experienced a higher stress for a given load.

The passive steel controlled crack width and spacing. Figure 4.96 shows a smaller crack width at the bottom of the member (at 1.61 million cycles) as a result of the presence of reinforcing steel. Figures 4.95 and 4.97 show the close crack spacing. There were 36 flexural cracks in the center 20 ft of the span before the ultimate test. There were several shear cracks in the shear span that formed from 1.63 million cycles to the end of fatigue testing.

4.10.5 Static Ultimate Test

The specimen was loaded incrementally to a maximum load of 112 kips, which was 77 percent of the calculated ultimate capacity. The centerline deflection, as shown in Fig. 4.83, was 3.4 in. The specimen lost strength at this point. Loading continued to a deflection of 3.8 in. was reached. The load was approximately 100 kips. At this point, the reinforcing steel appeared to yield, as shown in the load deflection graph, Figure 4.89. Testing was halted at a deflection of 5.4 in. The load was still approximately 100 kips.

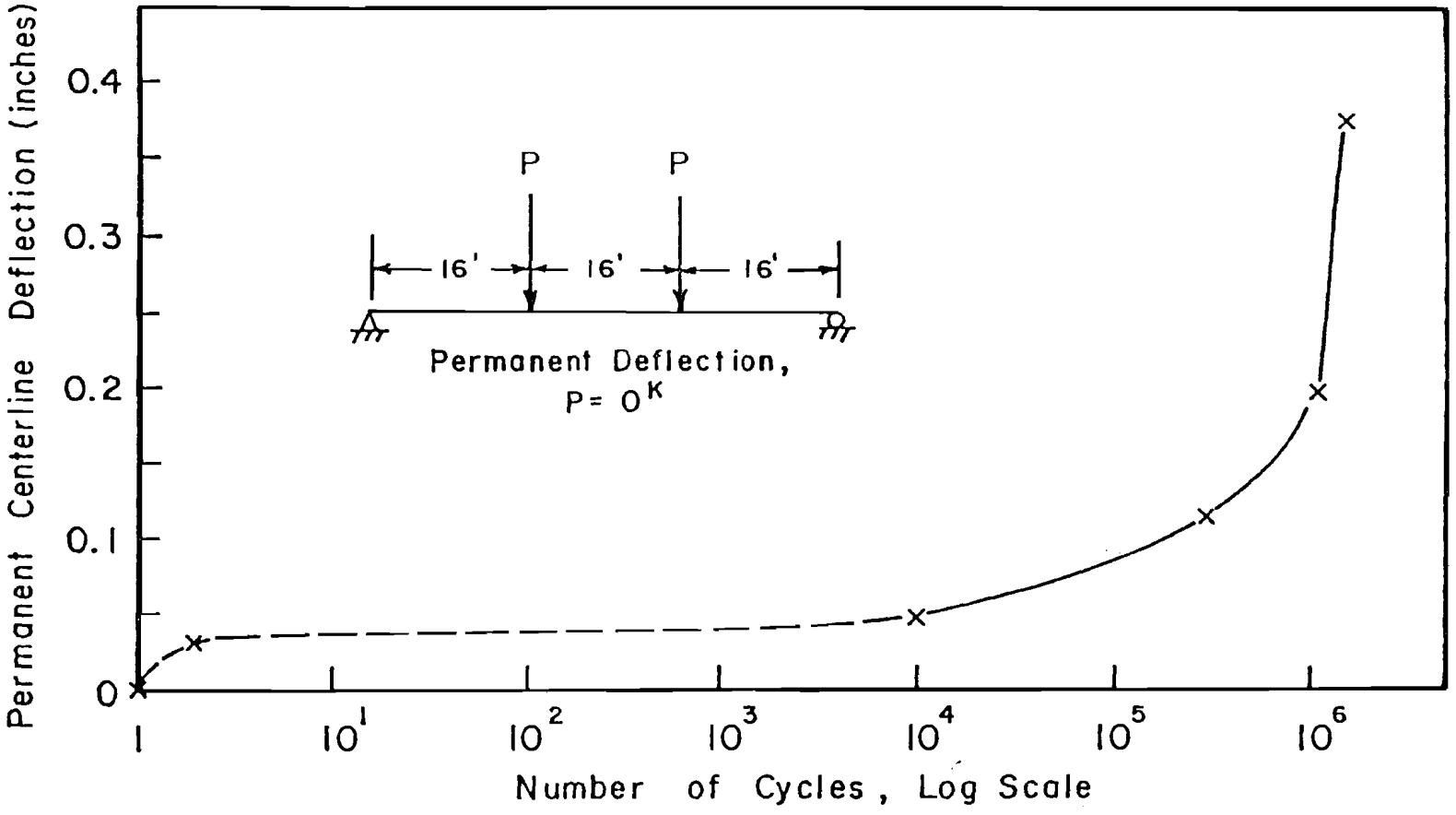

Fig. 4.93 Permanent centerline deflection during static tests for Specimen C-16-UP-8.0-NO-1.73

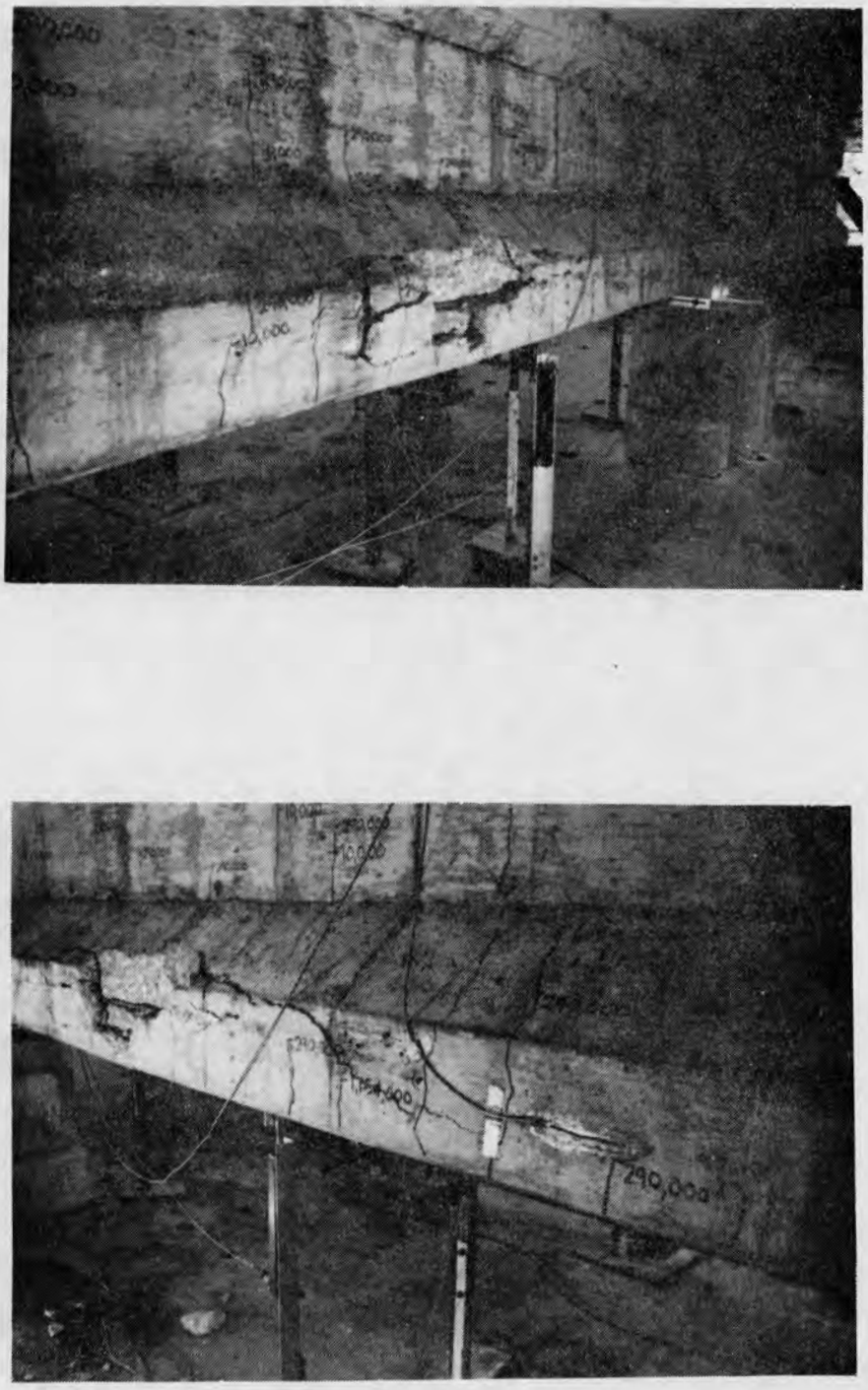

Fig. 4.94 Concrete spalling after 1.20 million cycles

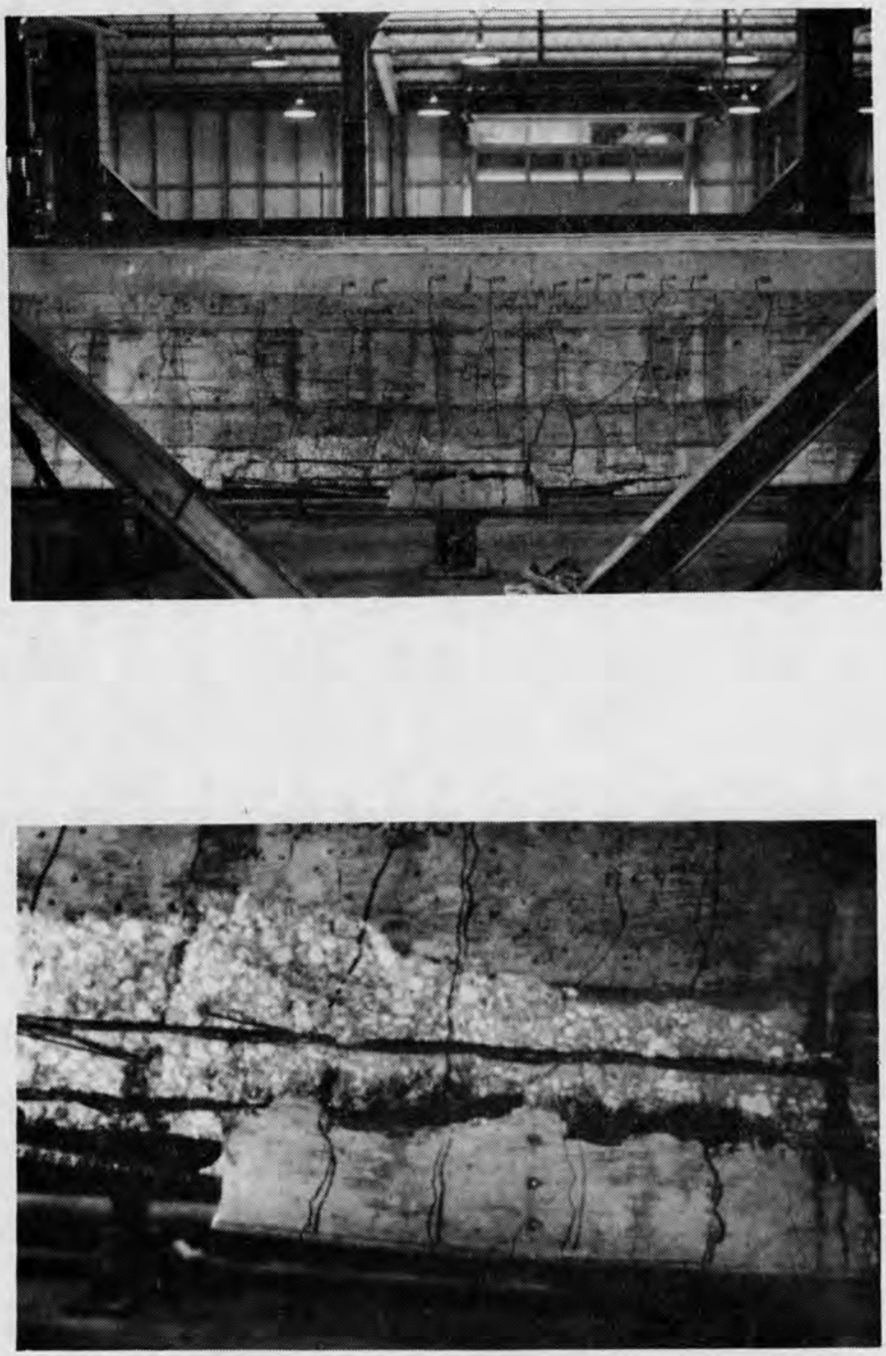

Fig. 4.95 Buckling of reinforcing steel due to a lack of confinement

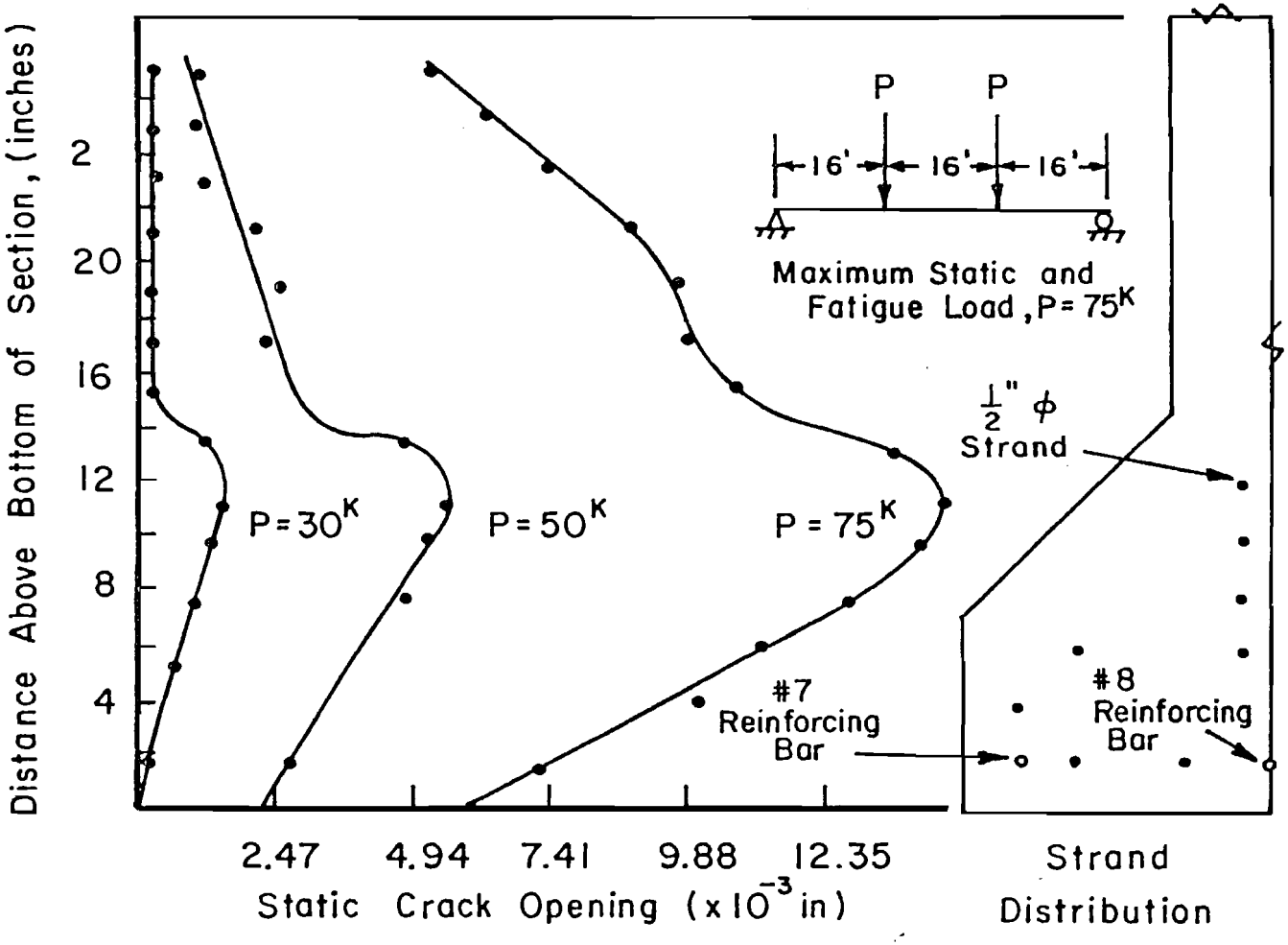

Fig. 4.96 Static crack profile 2 ft 0 in. north of centerline for Specimen C-16-UP-8.0-NO-1.73

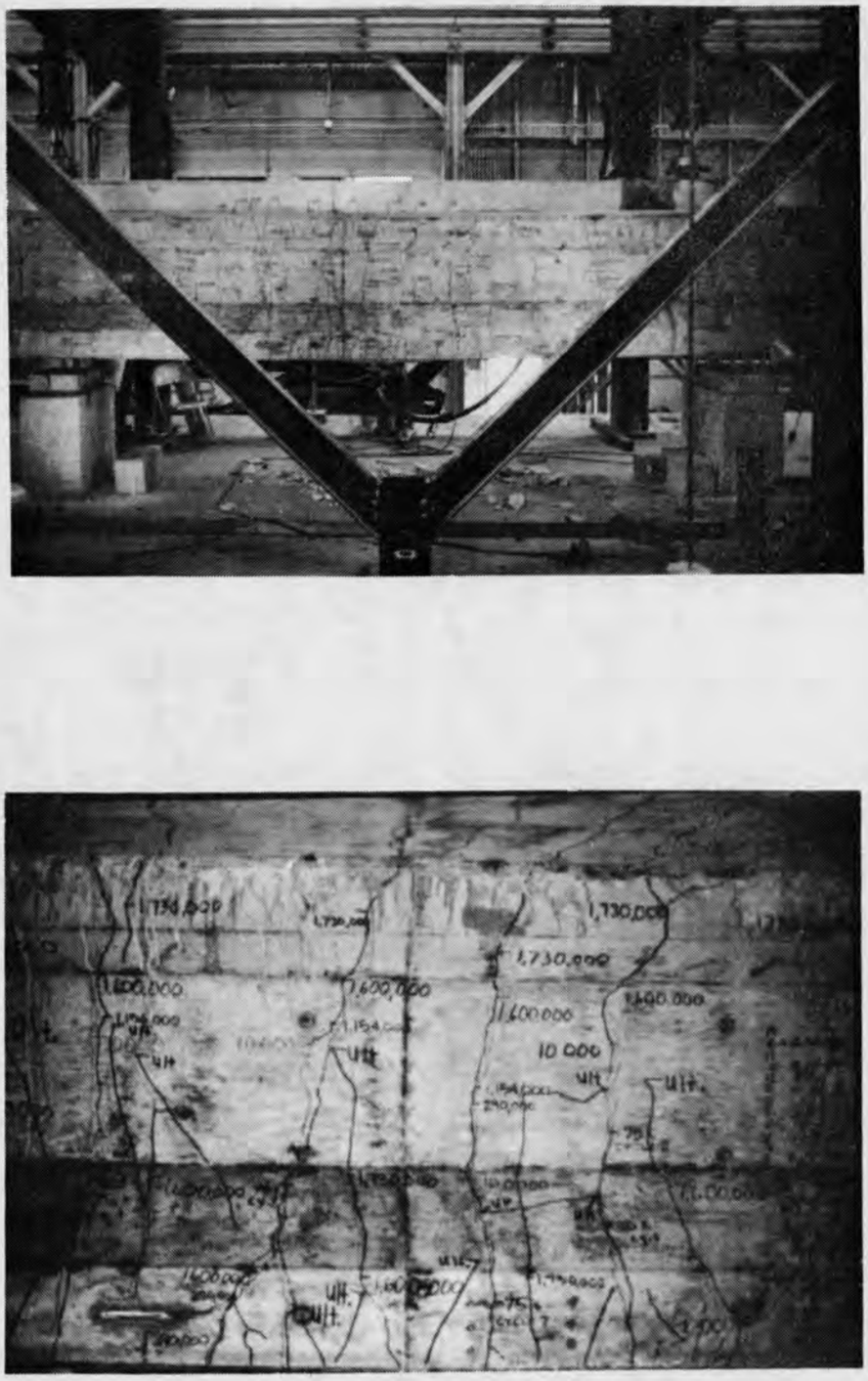

Fig. 4.97 Flexural cracking on the east side of Specimen C-16-UP-8.0-NO-1.73 after ultimate testing

4.10.6 Post Mortem Investigation

The post mortem investigation revealed 46 wire fractures at eight locations. A companion specimen C-16-NP-7.2-OL-1.48 had wire fatigue fractures at only one location. This indicates that the passive steel makes the strands more efficient by limiting the strand stress at a single isolated location. With passive steel, the strands were stressed more evenly in the constant moment region as can be seen in the excellent distribution of wire fractures in Fig. 4.98. Figure 4.99 shows the fractures relative to the cross section. Notice that only seven wires fractured at eight locations, at the level of the passive steel. No fatigue initiation cracks or fractures were found in the reinforcing steel.

4.10.7 Dynamic Load Amplification

The static centerline deflection range between 24 and 75 kips at 1.15 million cycles was 0.53 in. (0.14 in. to 0.67 in.). The dynamic deflection range between these two loads of 1.20 million cycles was 0.56 in. (0.14 to 0.70 in.) which indicates slight dynamic amplification. The static loads corresponding to these dynamic deflections were approximately 24 and 77 kips.

4.11 Specimen C-16-CP-7.2-NO-2.54

This specimen was a Texas Type C with 16 straight strands. There was 2.0 sq. in. (ten #4 reinforcing bars) of confined, passive (unstressed) reinforcing steel in the lower flange to control cracking. The confining steel consisted of #3 bars spaced adjacent to the stirrups at 1 ft intervals. The maximum fatigue load (P_{max}) produced a nominal concrete tensile stress of $7.2\sqrt{f'_{ct}}$ based on uncracked section properties. No loads above P_{max} were applied to the specimen during static tests. The specimen experienced 2.54 million fatigue cycles prior to the static ultimate test.

4.11.1 Initial Static Tests

Specimen C-16-CP-7.2-NO-2.54 was loaded incrementally to a maximum static load of 70 kips. Slight cracking was visible at this load level. Figure 4.100, which shows load versus strand wire strain during the initial two static cycles, indicates that cracking probably occurred at approximately 65 kips. During the second cycle a marked change in slope occurred at approximately 42.5 kips. This change is typical of the transition that takes place at the zero tension load (the load at which the extreme tension fibers first experience tension).

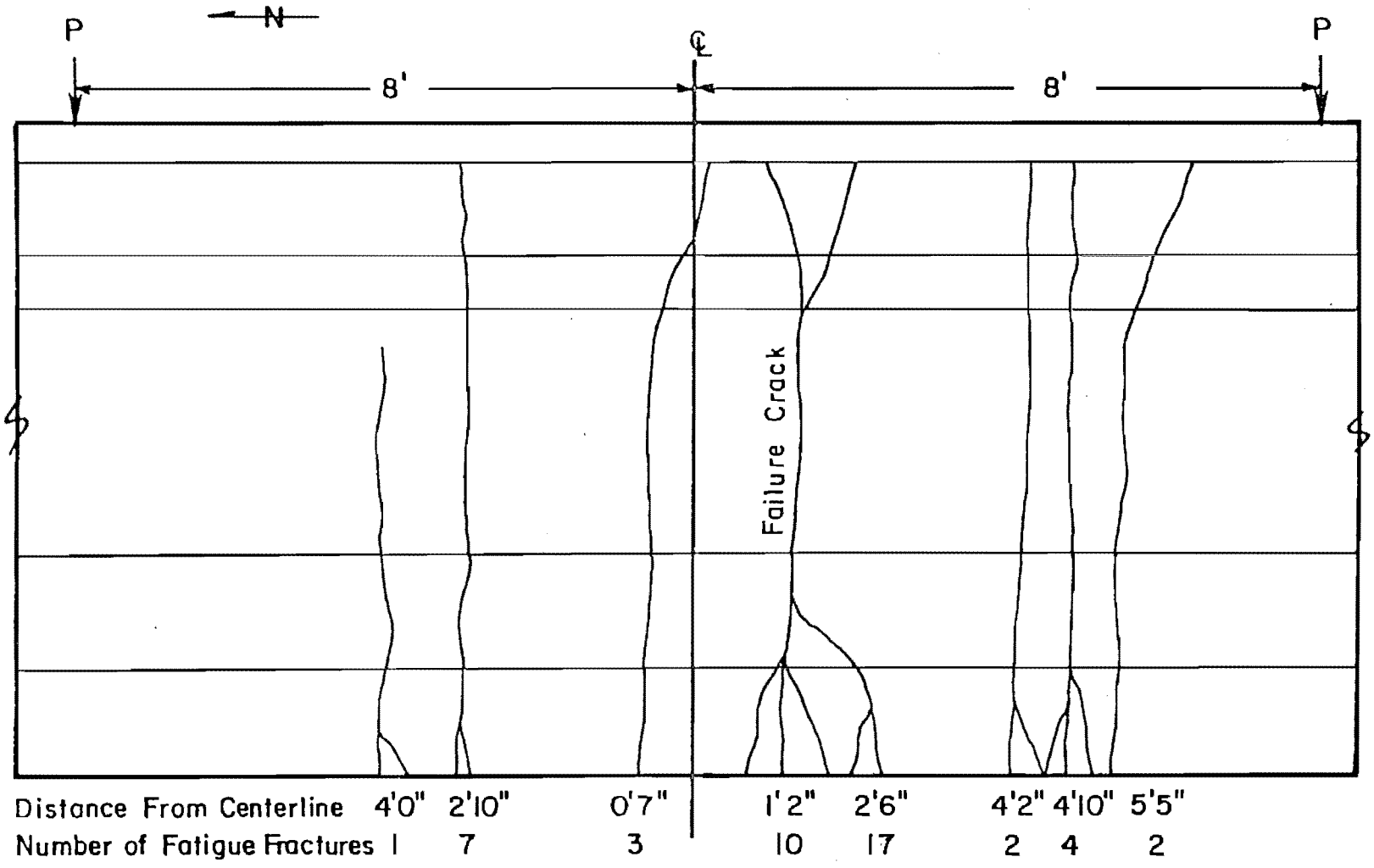

Fig. 4.98 Location and number of wire fatigue fractures and corresponding concrete cracks for Specimen C-16-UP-8.0-NO-1.73

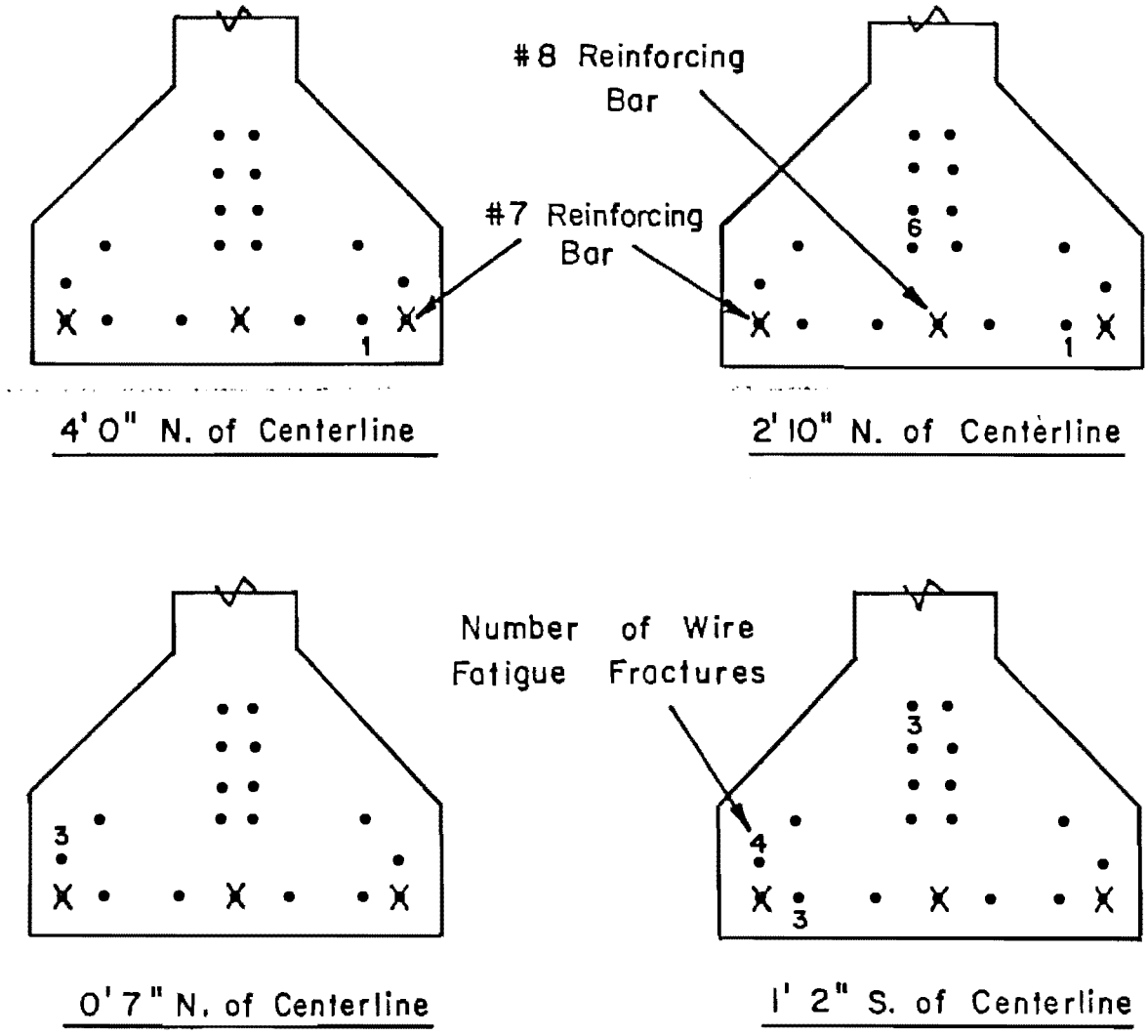

Fig. 4.99 Location of fatigue fractures for Specimen C-16-UP-8.0-NO-1.73

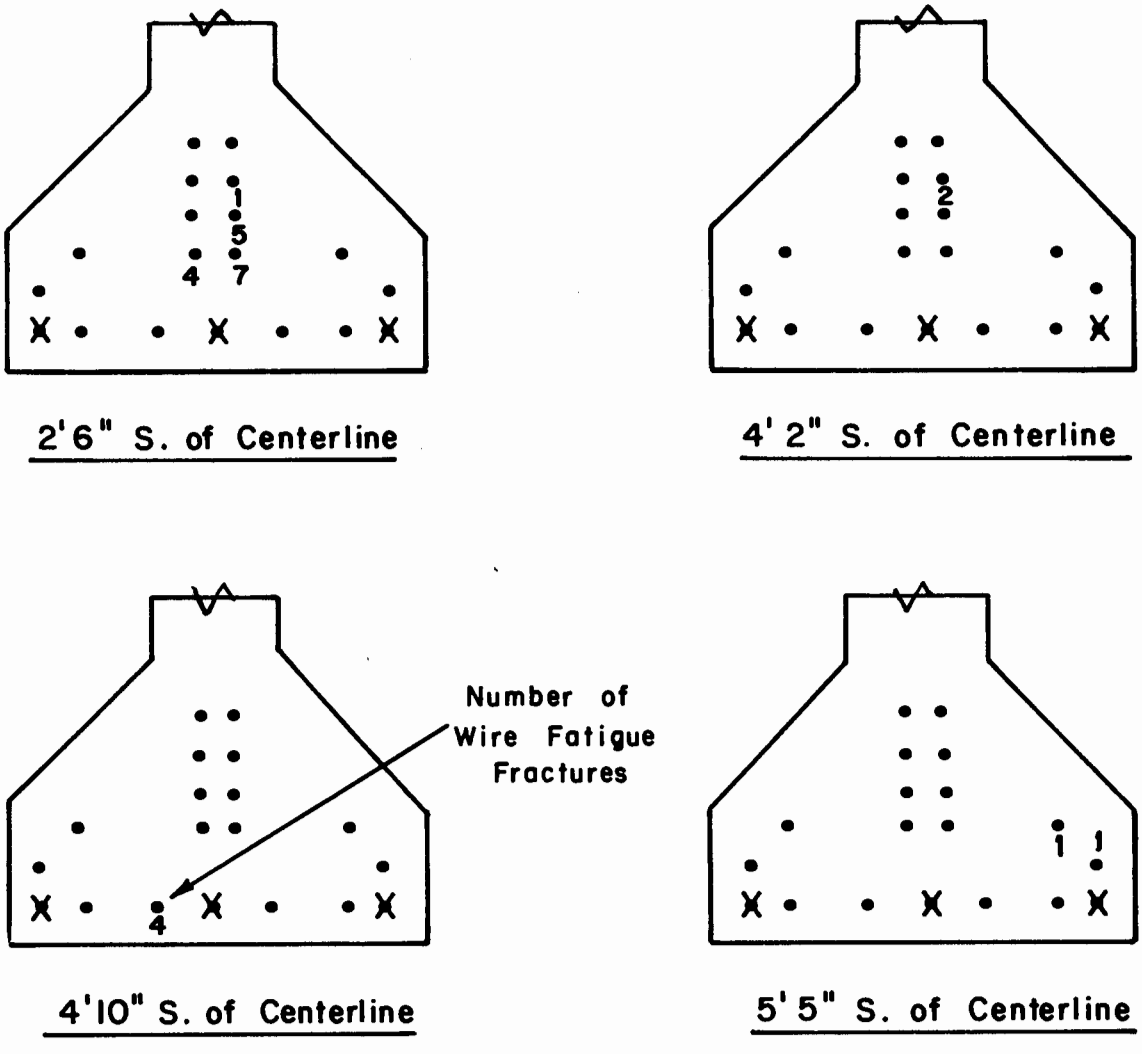

Fig. 4.99 Location of fatigue fractures for Specimen C-16-UP-8.0-NO-1.73 (continued)

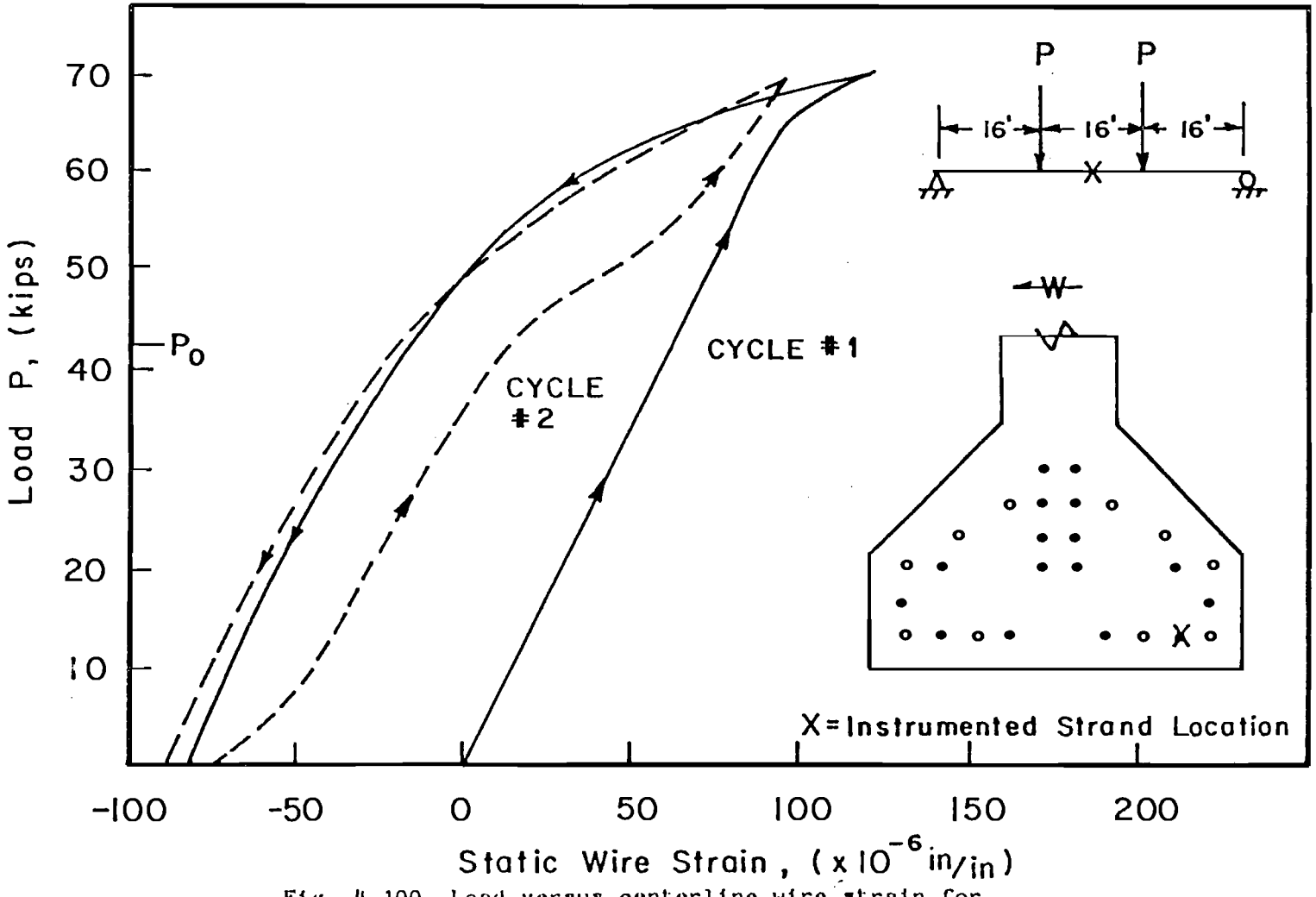

Fig. 4.100 Load versus centerline wire strain for Specimen C-16-CP-7.2-N0-2.54

Figure 4.101, of strand strain versus load 2 ft north of the centerline, demonstrates the same change at approximately 42.5 kips.

Figures 4.100 and 4.101 indicate a decrease in strain during unloading. This is probably the result of the superior bond characteristics of the reinforcing steel. Both figures indicate that as the specimen is loaded above the zero tension load, strand wire strain increases drastically, as would be expected, but the drastic increase does not continue. The slope actually increases before the maximum load is reached. This is the region of the loading curve that the reinforcing steel resist most of the applied load, due to its superior bond characteristics. During unloading, the reinforcing steel is stressed more at any given load than during loading. The prestressing steel is stressed less as indicated by Figs. 4.100 and 4.101. During loading, load is essentially transferred from the prestressing steel to the reinforcing steel.

Three cracks formed during the initial five static cycles. Two cracks were confined to the vertical portion of the web; both were approximately 5 in. above the bottom of the section. The remaining crack extended 1 in. into the angled portion of the lower flange.

4.11.2 Zero Tension Load, P_o

Figures 4.100 and 4.101 of load versus strand wire strain indicate a significant change in behavior at approximately 42.5 kips; that is typical of the change that occurs at the zero tension load. The passive reinforcing steel reduced crack width and extension so that a marked change in behavior did not occur in the load versus deflection curve. The centerline deflection at 42.5 kips was 0.26 in.

4.11.3 Fatigue Loads

Specimen C-16-CP-7.2-NO-2.54 was designed as a companion to Specimens C-16-NP-7.2-OL-1.48 and C-16-UP-8.0-NO-1.73. The main variable was the presence of passive reinforcement in the C-16-CP and C-16-UP specimens. The 2.0 sq. in. of reinforcing steel in Specimen C-16-CP-7.2-NO-2.54 was confined, as the alphanumeric label indicates. Specimen C-16-UP-8.0-NO-1.73 had 1.99 sq. in. of unconfined passive (UP) reinforcing steel. Based on a zero tension load of 42.5 kips and uncracked section properties, a load of 70 kips was required to produce a nominal concrete tensile stress of $7.2\sqrt{f'_{ct}}$, where f'_{ct} was the concrete strength at the time testing began. A minimum load of 19 kips was required to maintain the same load range of 51 kips applied to the other two companion specimens. Figure 4.102 shows the load program for Specimen C-16-CP-7.2-NO-2.54.

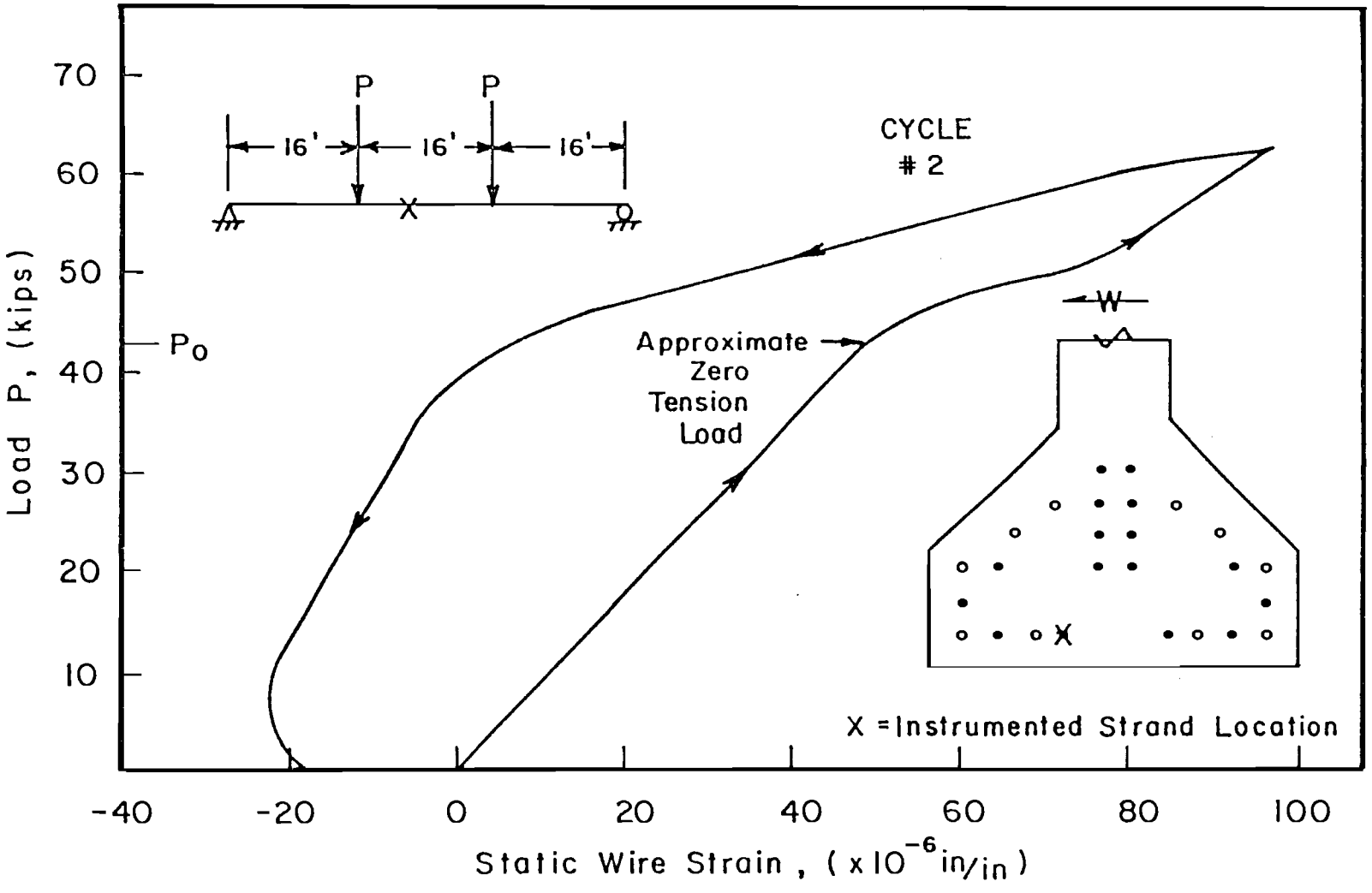

Fig. 4.101 Load versus wire strain 2 ft 0 in. north of centerline for Specimen C-16-CP-7.2-NO-2.54

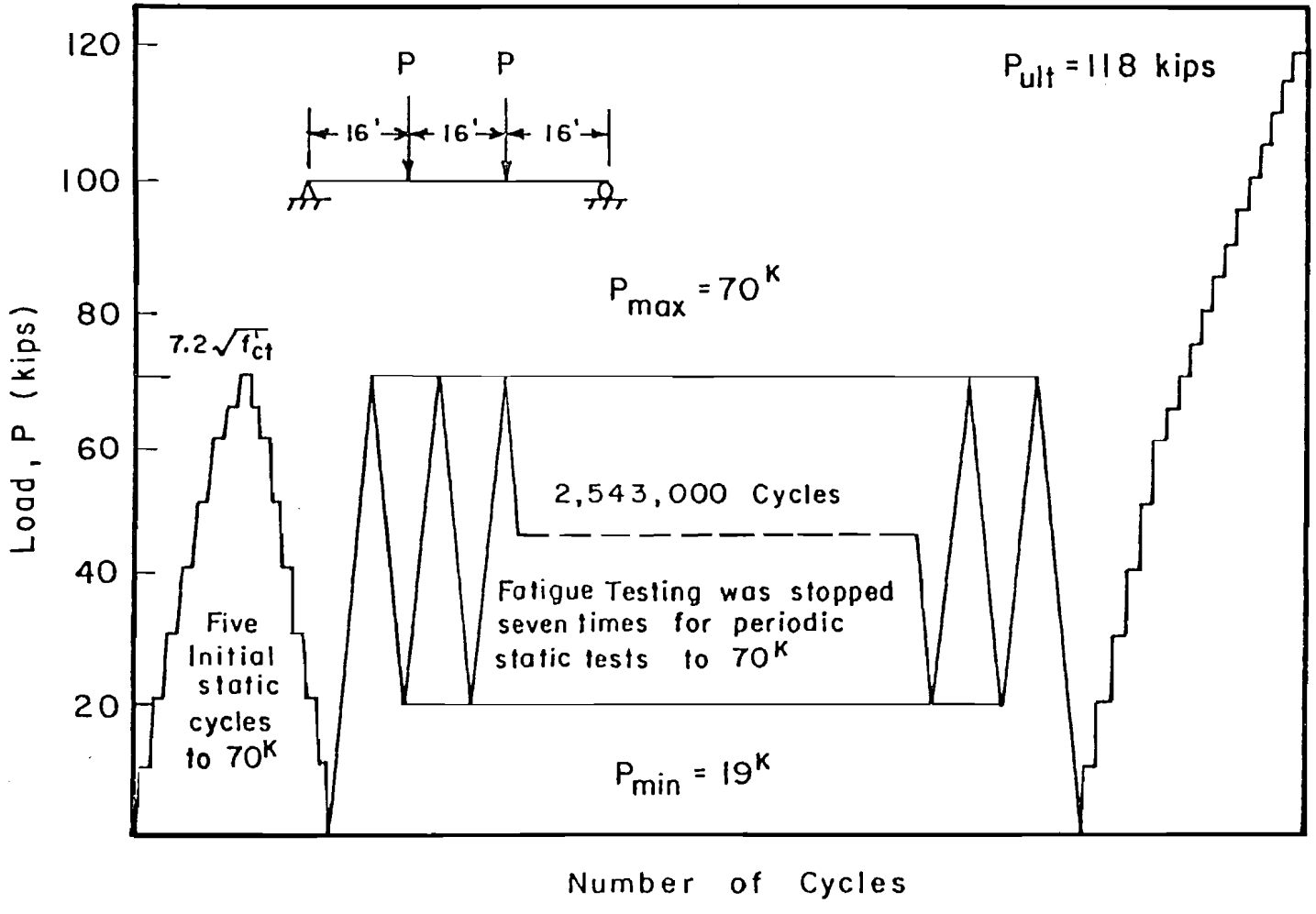

Fig. 4.102 Load program for Specimen C-16-CP-7.2-NO-2.54

4.11.4 Fatigue Behavior

Figure 4.103 shows static centerline deflection at various phases of fatigue testing and indicates that after a slight increase in deflection at approximately 400,000 cycles, the centerline deflection was stable until 2.30 million cycles. The permanent deflection plotted against number of cycles shown in Fig. 4.104 indicates this same type of behavior. Other specimen results had indicated a continuous increase in permanent deflection.

Figure 4.105 indicates that static wire strain was not consistent during multiple cycles. This is similar to the behavior shown in Fig. 4.100. Notice the continuously decreasing strain at zero load indicated in both figures.

Figure 4.106 of static crack opening versus load shows a sudden change in crack width when the specimen was loaded or unloaded. This drastic change does not appear to be a function of the load but of loading and unloading. It occurred during two loading cycles at approximately 10 and 25 kips and during unloading at 70 and 55 kips.

Figure 4.107 shows crack opening at a selected flexural crack, at various phases of fatigue loading, and indicates that the passive steel controlled crack width for the initial 2.30 million cycles. The crack profile at 70 kips changed from bilinear at 55,000 cycles to linear at 2.30 million cycles. The increased crack opening in the web is due to the extension of flexural cracks. The instrumented crack was visible 20 in. above the bottom of the section after 55,000 cycles. At 2.30 million cycles the crack was visible 28 in. above the bottom of the section.

The specimen deteriorated rapidly after 2.30 million cycles as indicated by Figs. 4.103 and 4.104. The static centerline deflection increased from 0.61 in. at 1.40 million cycles (the third point deflection was 0.53 in.) to 0.65 in. at 2.30 million cycles to 1.1 in. at 2.54 million cycles. Neither the static nor dynamic strain increased significantly as a result of fatigue testing. The maximum static strain between 20 and 70 kips was approximately 0.00055 in./in. during periodic static tests. The maximum dynamic strain between these loads was consistently 0.00025 in./in. The drastic difference is probably a result of the location of the strain gages. The static gage reading indicates that that gage was probably adjacent to a flexural crack. The strain gage wired to the peak detector and monitored during fatigue testing was not in the vicinity of a significant flexural crack.

Wire fatigue breaks could be heard during fatigue testing at 2.37 million cycles. At approximately 2.50 million cycles significant concrete spalling, as shown in Fig. 4.108, occurred. After the static test at 2.30 million cycles there were 36 flexural cracks. By 2.50 million cycles seven additional cracks had formed and several extended

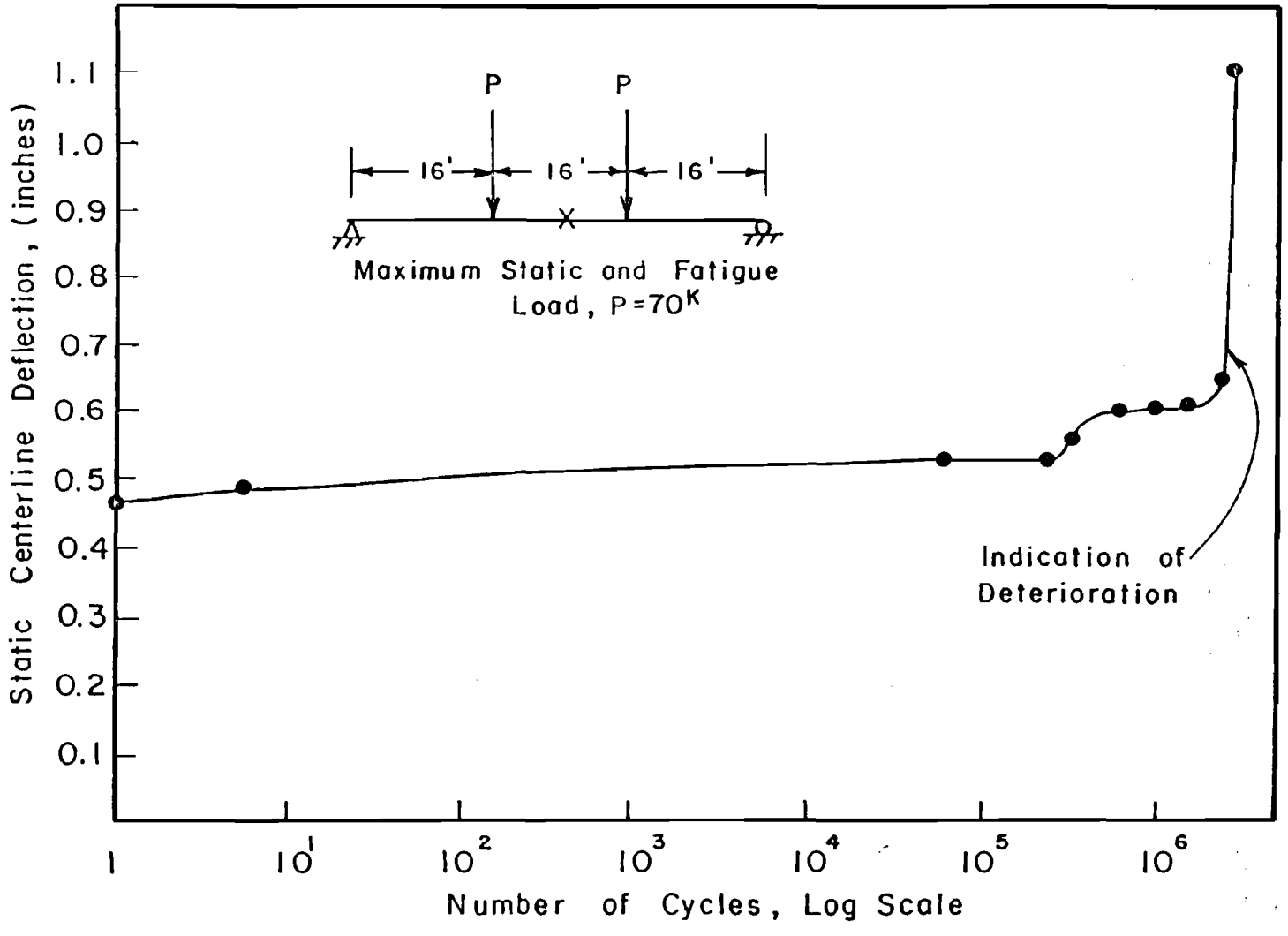

Fig. 4.103 Centerline deflection during static tests for Specimen C-16-CP-7.2-NO-2.54

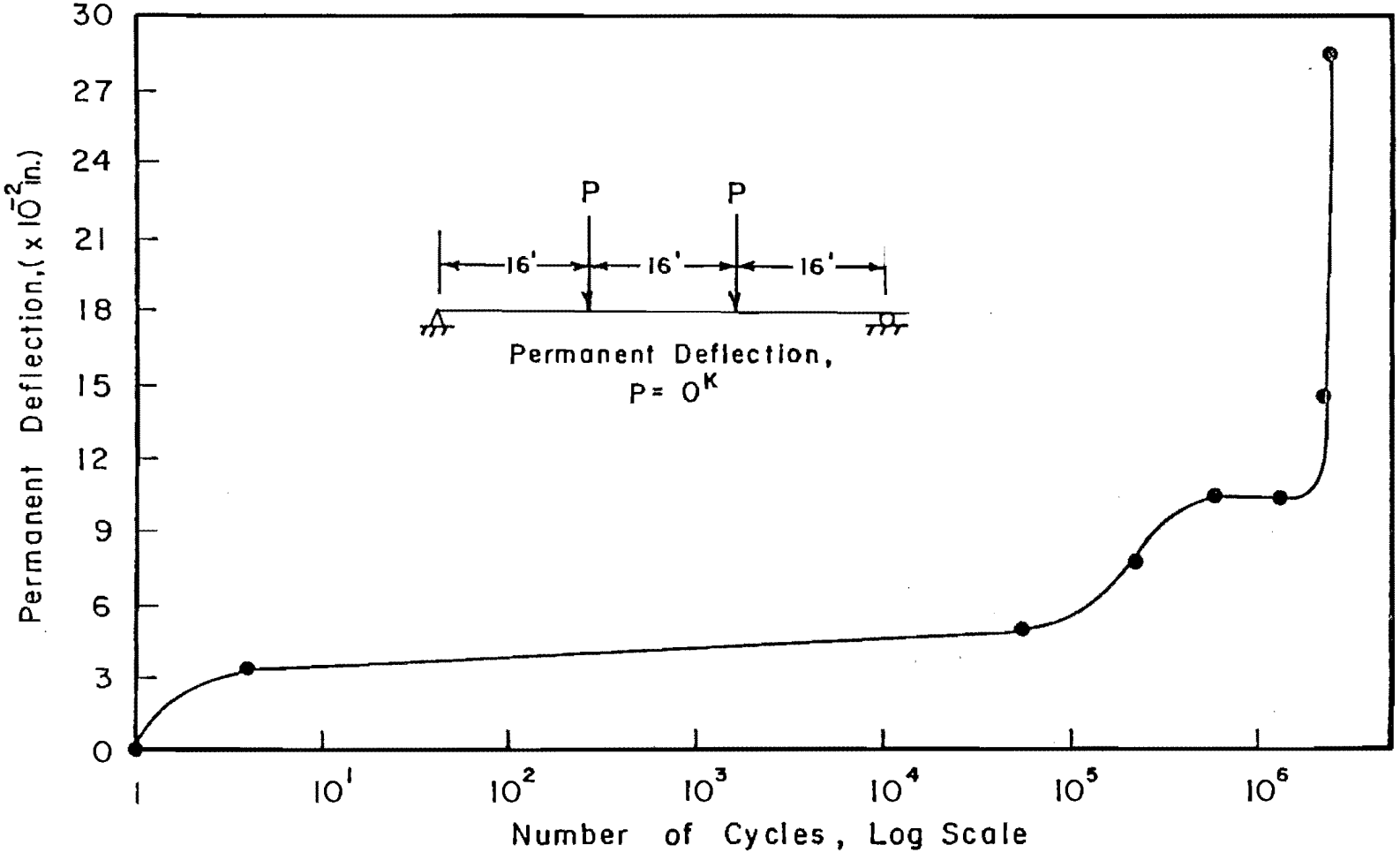

Fig. 4.104 Permanent deflection during static tests for Specimen C-16-CP-7.2-NO-2.54

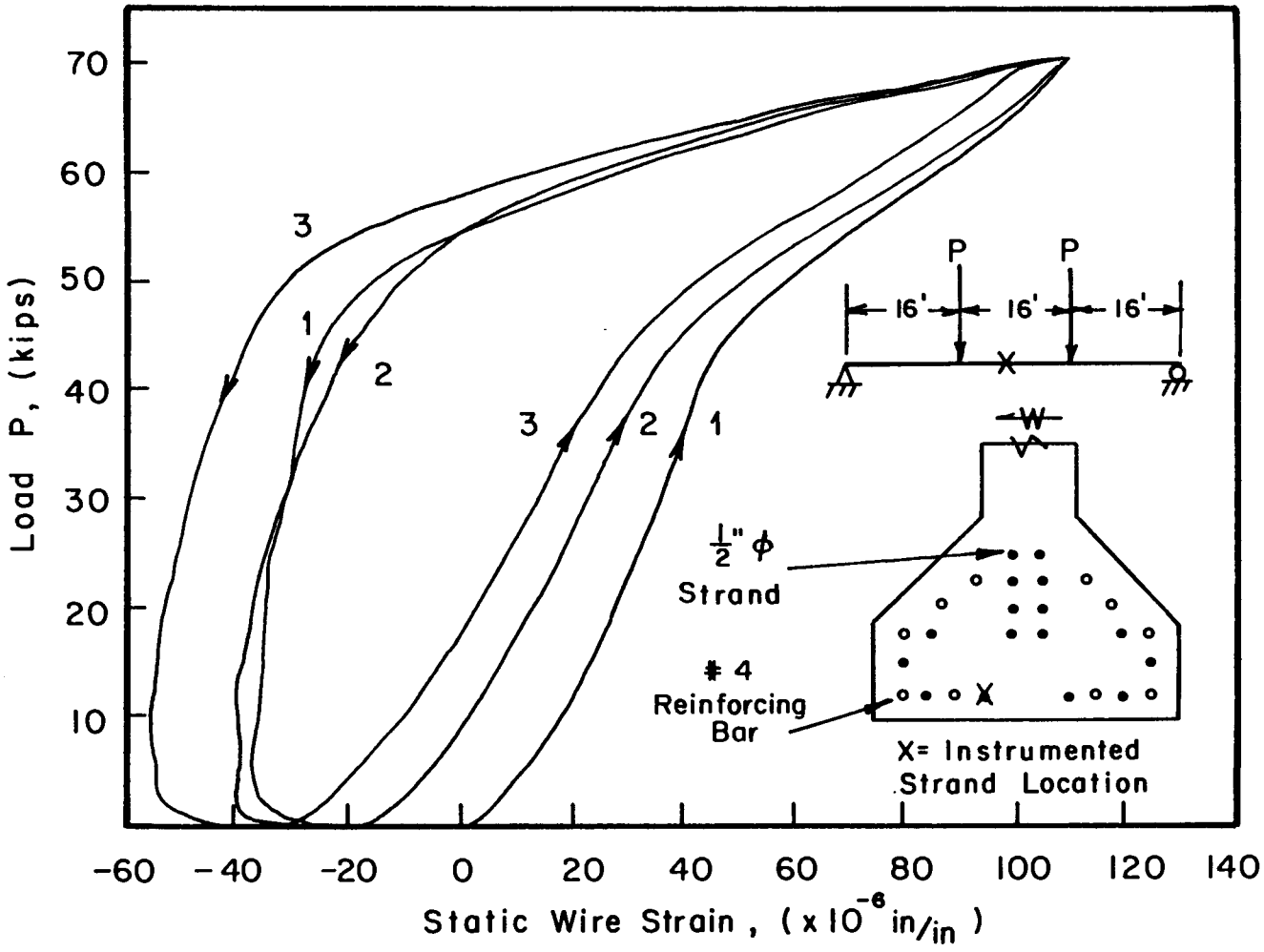

Fig. 4.105 Reduction of wire stress during three static cycles after 306,900 fatigue cycles

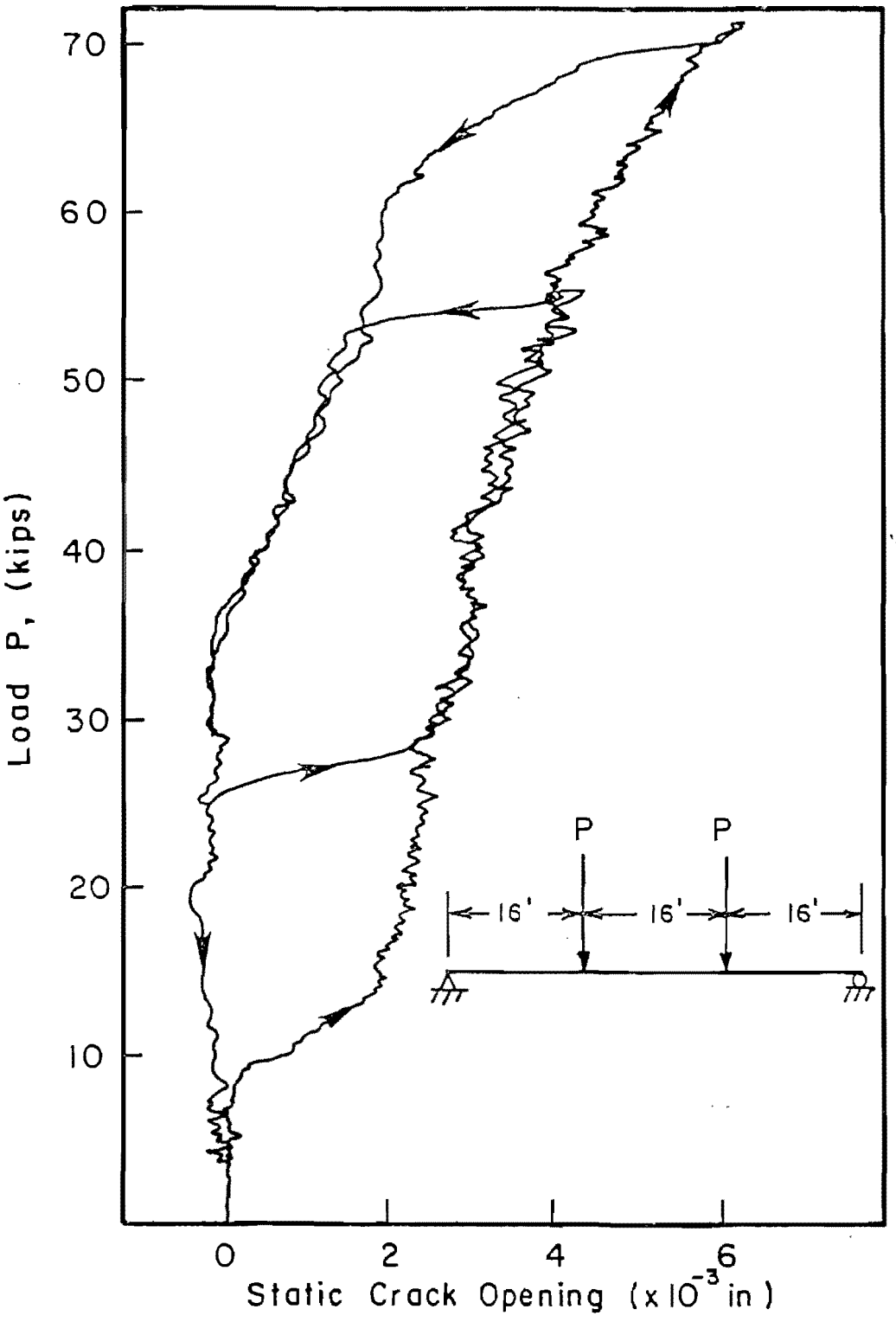

Fig. 4.106 Load versus crack opening at 2.3 million cycles

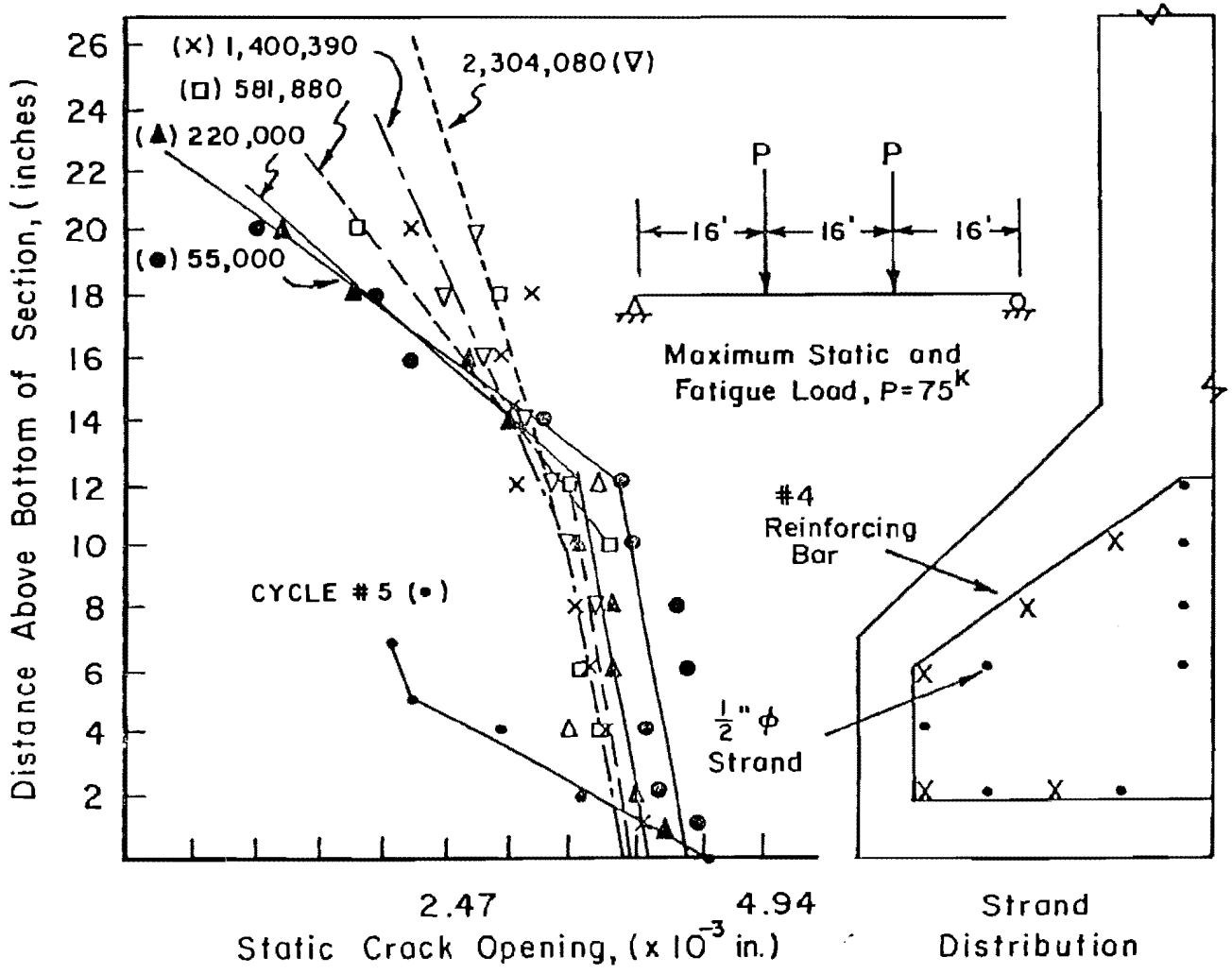

Fig. 4.107 Crack profile 6 ft 5 in. north of centerline during static testing for Specimen C-16-CP-7.2-NO-2.54

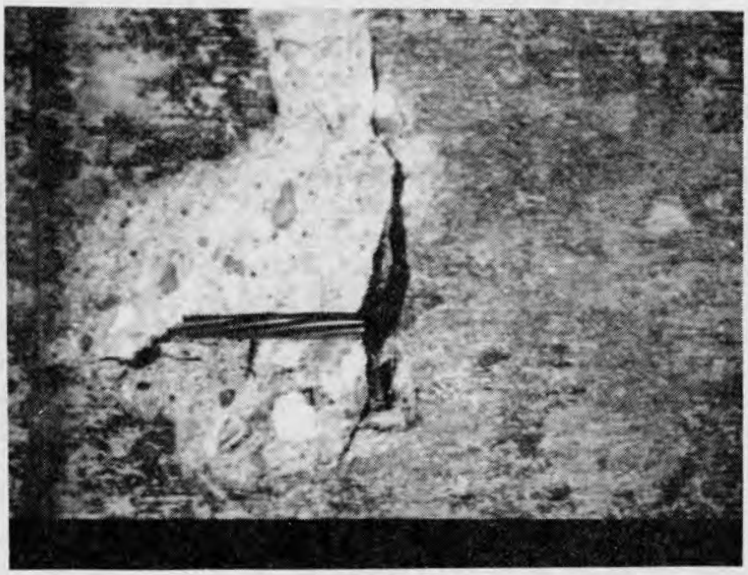

Fig. 4.108 Spalling after 2.50 million cycles for Specimen C-16-CP-7.2-NO-2.54

into the top flange. Fatigue testing was stopped after 2.54 million cycles.

4.11.5 Static Ultimate Test

The specimen was loaded incrementally to a failure load of 118 kips, which was 82 percent of the calculated ultimate capacity. Figure 4.102 shows the ultimate load versus deflection curve. The centerline deflection at 118 kips was 4.9 in. The member continued to support a reduced load until a deflection of 6.8 in. was reached. The load was approximately 90 kips at this time. Wire breaks were heard at 93 kips and again at 111, 115, and 118 kips. Additional breaks were heard at the loss of strength locations indicated on the load-deflection curve.

4.11.6 Post Mortem Investigation

The concrete cover was removed and the strands were exposed after the ultimate test. Figure 4.110 shows the location of the fatigue breaks and fatigue initiation cracks along the member. Figure 4.111 shows the fatigue breaks relative to the cross section. Notice the good distribution of fatigue breaks in the constant moment region as seen in the previous specimen with passive reinforcement. Figure 4.98 shows the fatigue fractures along the member for Specimen C-16-UP-8.0-NO-1.73.

4.11.7 Dynamic Load Amplification

The static centerline deflection range between 19 and 70 kips at 1.40 million cycles was 0.49 in. (0.11 in. to 0.60 in.). This is typical of the periodic static tests after 300,000 cycles and before 2.30 million cycles. The dynamic deflection range at 1.41 million cycles was 0.50 in. (0.14 in. to 0.64 in.), which indicates slight dynamic amplification. The static loads corresponding to these dynamic deflections were approximately 24 and 73 kips.

4.12 Specimen C-16-CP-5.5-OL-9.43

This specimen was a Texas Type C with 16 straight strands. There was 2.0 sq. in. (ten #4 reinforcing bars) of confined, passive (unstressed) reinforcing steel in the lower flange to control cracking. The confining steel consisted of #3 bars spaced adjacent to the stirrups at 1 ft intervals. The maximum fatigue load (P_{max}) produced a nominal concrete tensile stress of $5.5\sqrt{f'_{ct}}$ based on uncracked section properties. Loads above P_{max} (overloads) were applied to the member during static tests. The specimen experienced 9.43 million fatigue cycles prior to the static ultimate test.

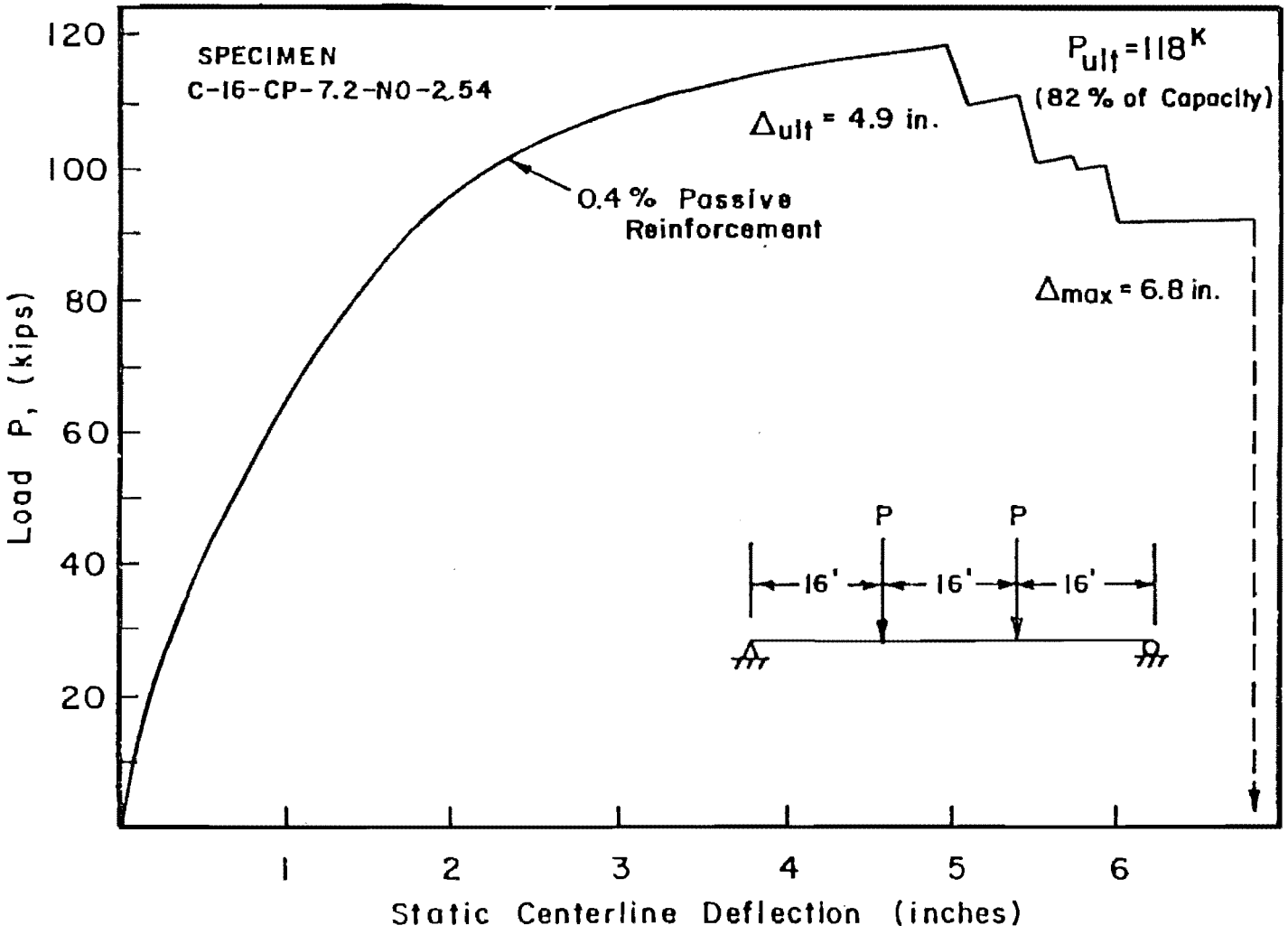

Fig. 4.109 Ultimate load versus deflection for Specimen C-16-CP-7.2-NO-2.54

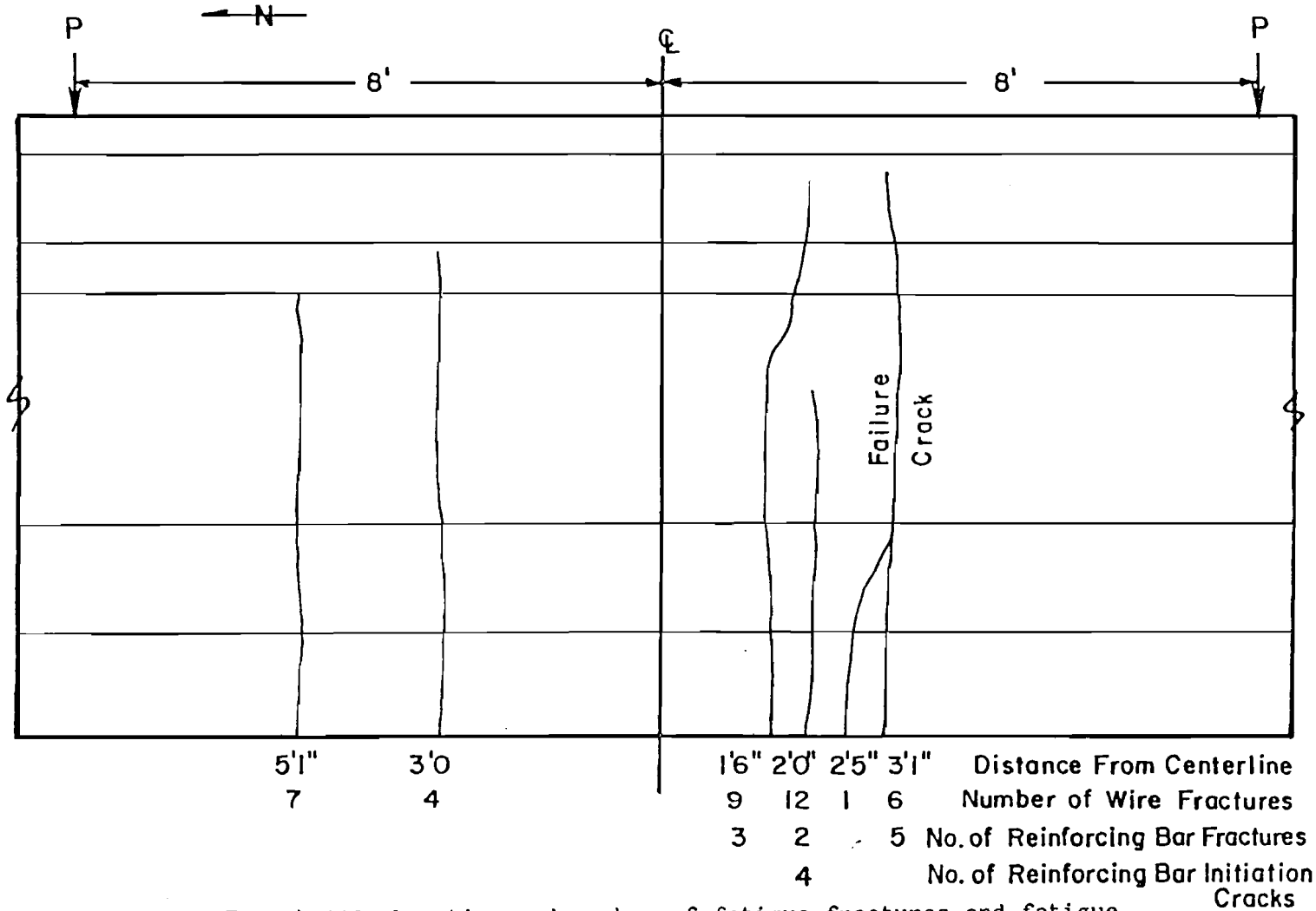

Fig. 4.110 Location and number of fatigue fractures and fatigue initiation cracks and corresponding concrete cracks for Specimen C-16-CP-7.2-NO-2.54

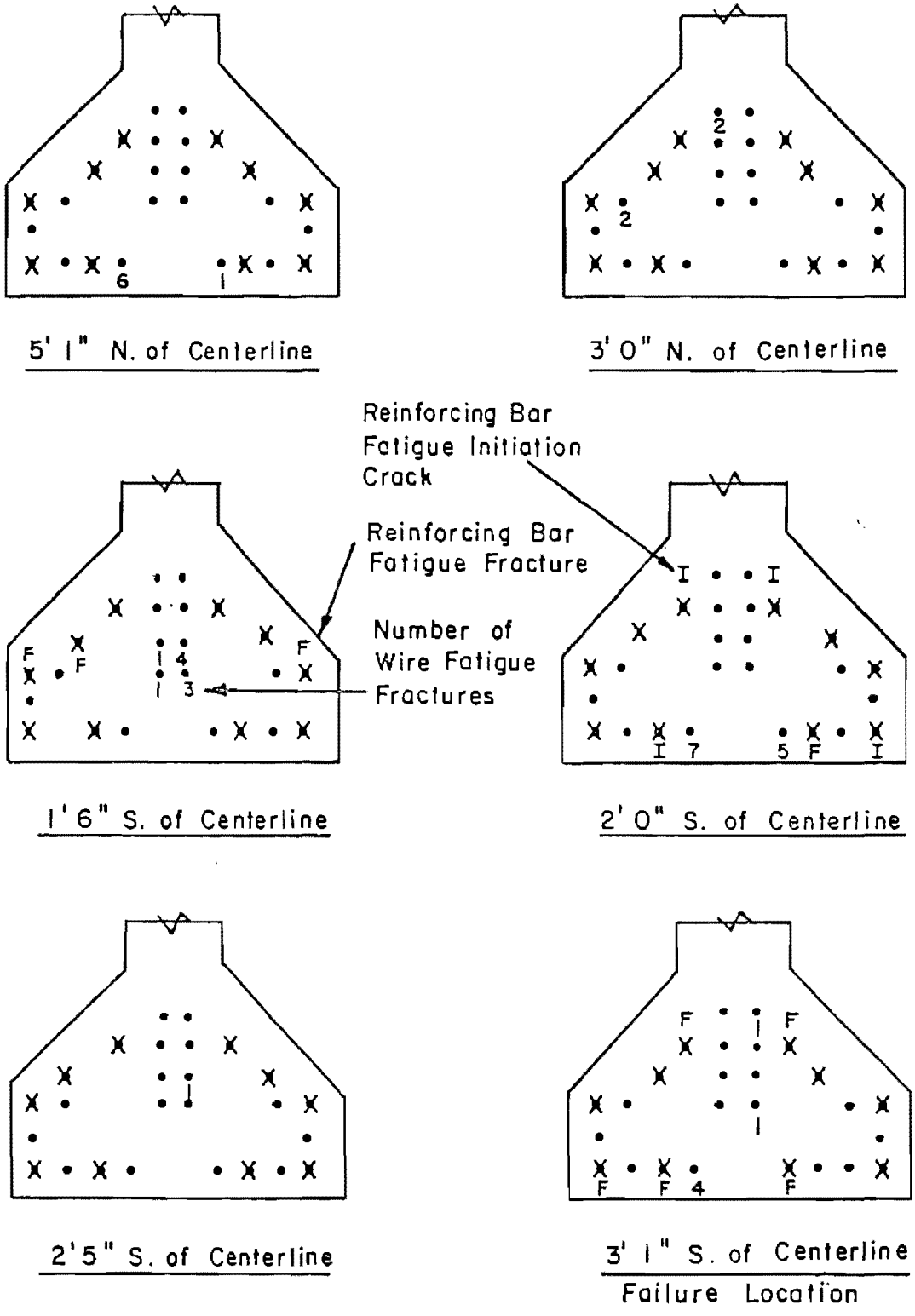

Fig. 4.111 Location of fatigue fractures and initiation cracks for Specimen C-16-CP-7.2-NO-2.54

4.12.1 Initial Static Tests

Specimen C-16-CP-5.5-OL-9.43 was loaded incrementally to a maximum load of 70 kips. Flexural cracking was first visible at 65 kips. Figures 4.112 and 4.113 also indicate a deviation from linear behavior at approximately 65 kips. Flexural cracking probably began at this load level. Both figures show a decrease in wire strain for an increment of load once the section cracked. While the section is decompressed, the strand, reinforcing steel, and concrete theoretically strain equally. Once the section is cracked and experiences tension, the well bonded reinforcing steel resists the applied moment, leaving the strand to strain with the adjacent concrete.

Two flexural cracks formed during the initial five static cycles. One crack extended 10 in. above the bottom of the section. The other crack extended 3 in. above the bottom of the section.

4.12.2 Zero Tension Load, P_o

Figure 4.114 shows a deviation from linear behavior at approximately 42.5 kips. Figures 4.112 and 4.113 show a return to linear behavior in the vicinity of this load. This change is a result of flexural cracks opening or closing and is defined as the zero tension load.

4.12.3 Fatigue Loads

A maximum concrete tensile stress of $5.5\sqrt{f'_{ct}}$ was selected for this specimen to determine the fatigue life of a member with passive reinforcement cycled at approximately the AASHTO design level. Based on a zero tension load of 42.5 kips and uncracked section properties, a load of 61 kips was required to produce a nominal concrete tensile stress of $5.5\sqrt{f'_{ct}}$. The minimum load was 20 kips. The centerline deflection at 42.5 kips was 0.24 in. The load program for this specimen can be seen in Fig. 4.115.

4.12.4 Fatigue Behavior

The specimen's behavior remained relatively stable for the initial 6.92 million cycles Figure 4.116 indicates that the centerline deflection at 65 kips increased from 0.45 in. at 6.06 million cycles (the third point deflection was 0.37 in.) to 0.48 in. at 6.92 million cycles, a 7 percent increase. The deflection continued to increase until 9.43 million cycles when testing was stopped. The centerline deflection at that time was 1.01 in. at 65 kips. Figure 4.117 shows that the permanent set with no load increased throughout fatigue testing. The increase was more drastic after 6.06 million cycles.

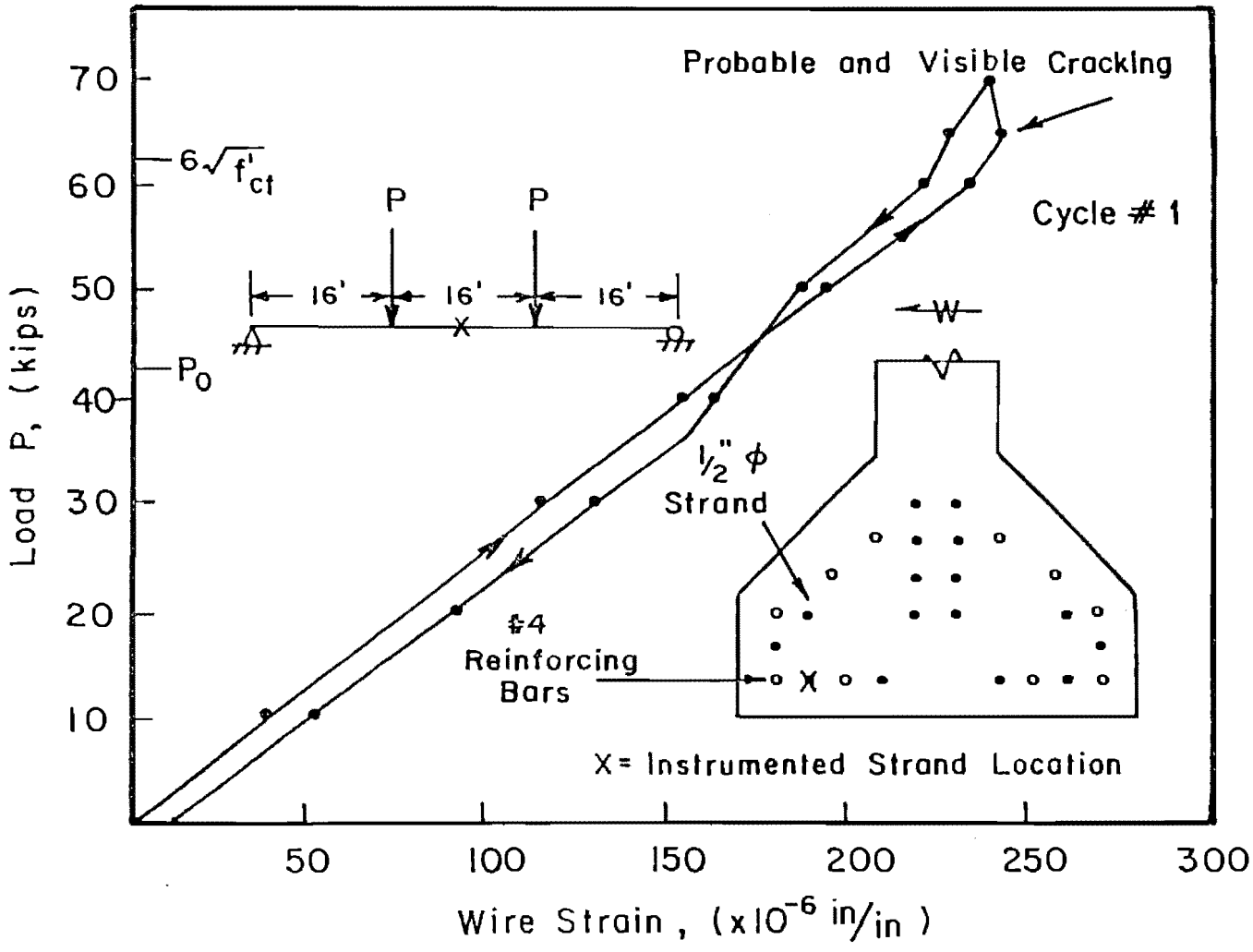

Fig. 4.112 Load versus wire strain 6 in. north of centerline for Specimen C-16-CP-5.5-OL-9.43

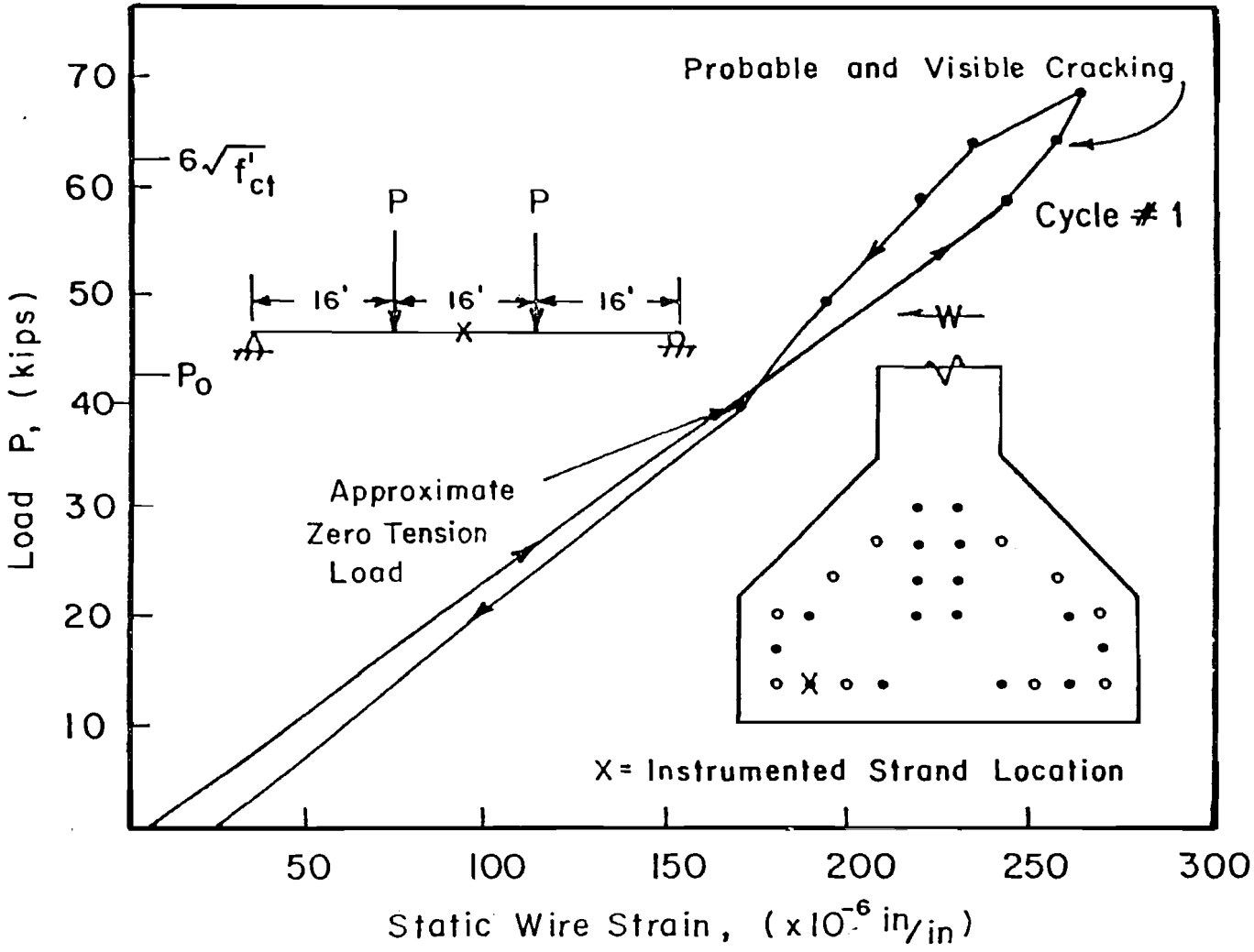

Fig. 4.113 Load versus wire strain 4 ft 6 in. north of centerline for Specimen C-16-CP-5.5-0L-9.43

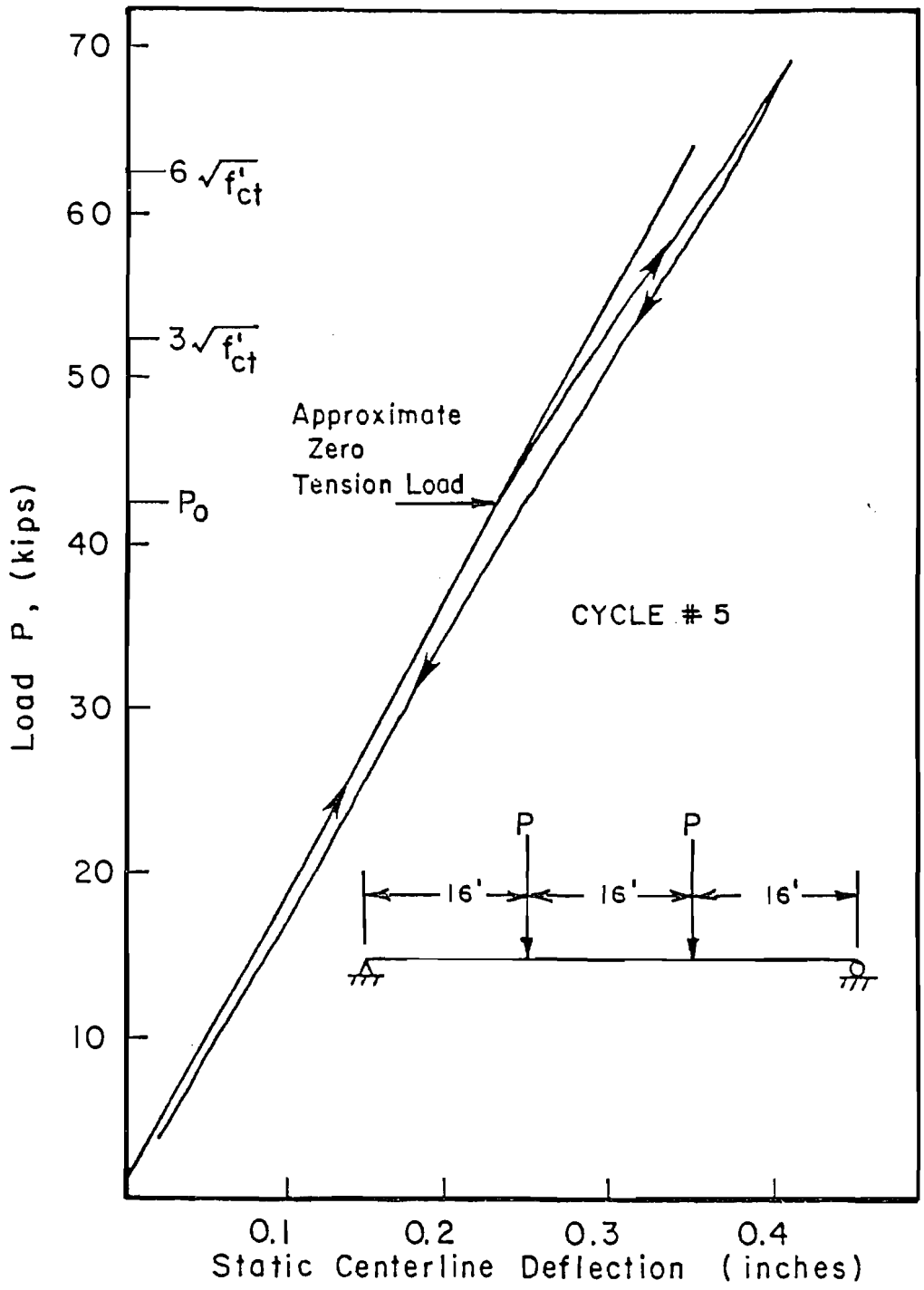

Fig. 4.114 Load versus deflection during cycle five for Specimen C-16-CP-5.5-0L-9.43

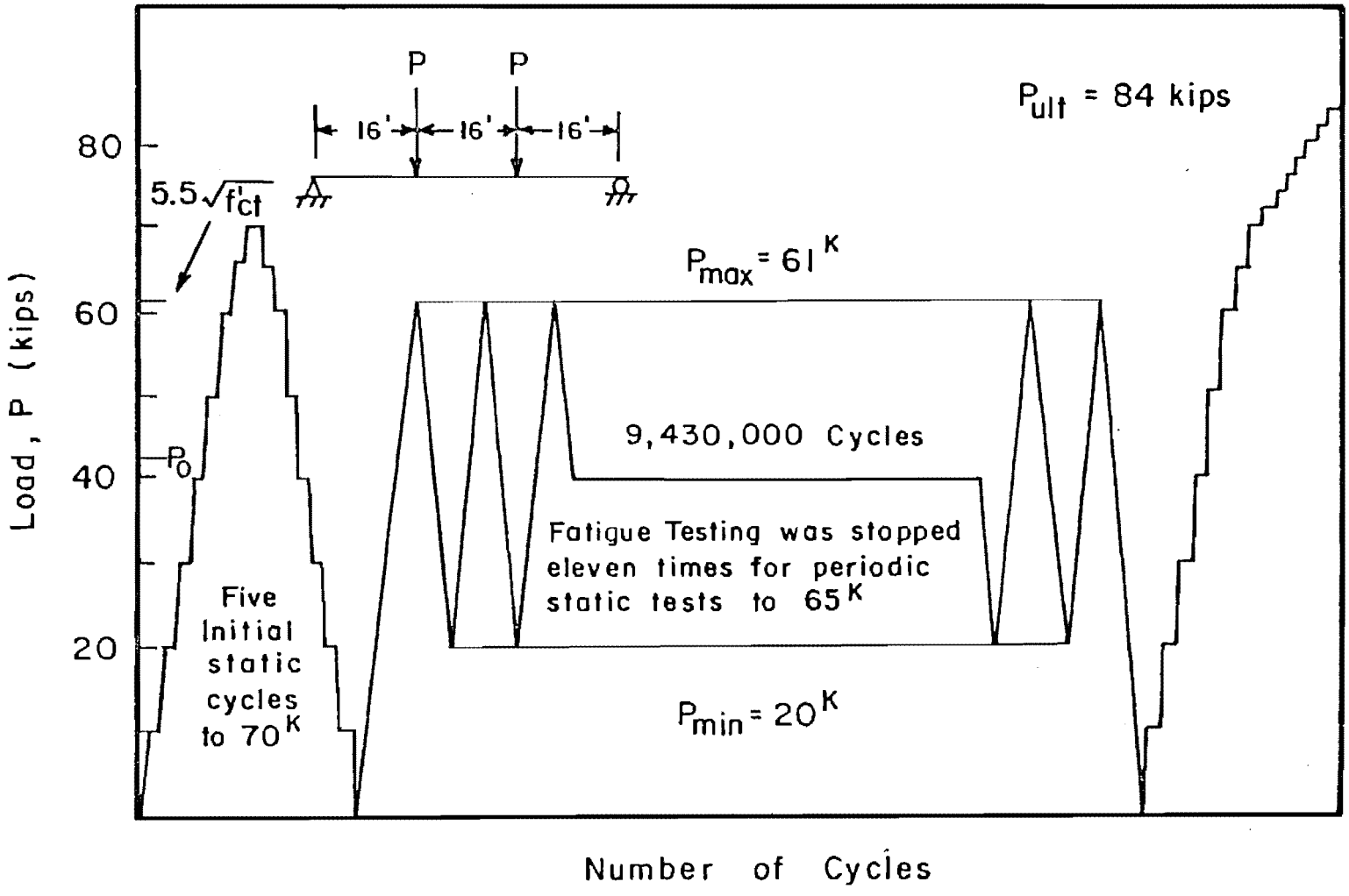

Fig. 4.115 Load program for Specimen C-16-CP-5.5-OL-9.43

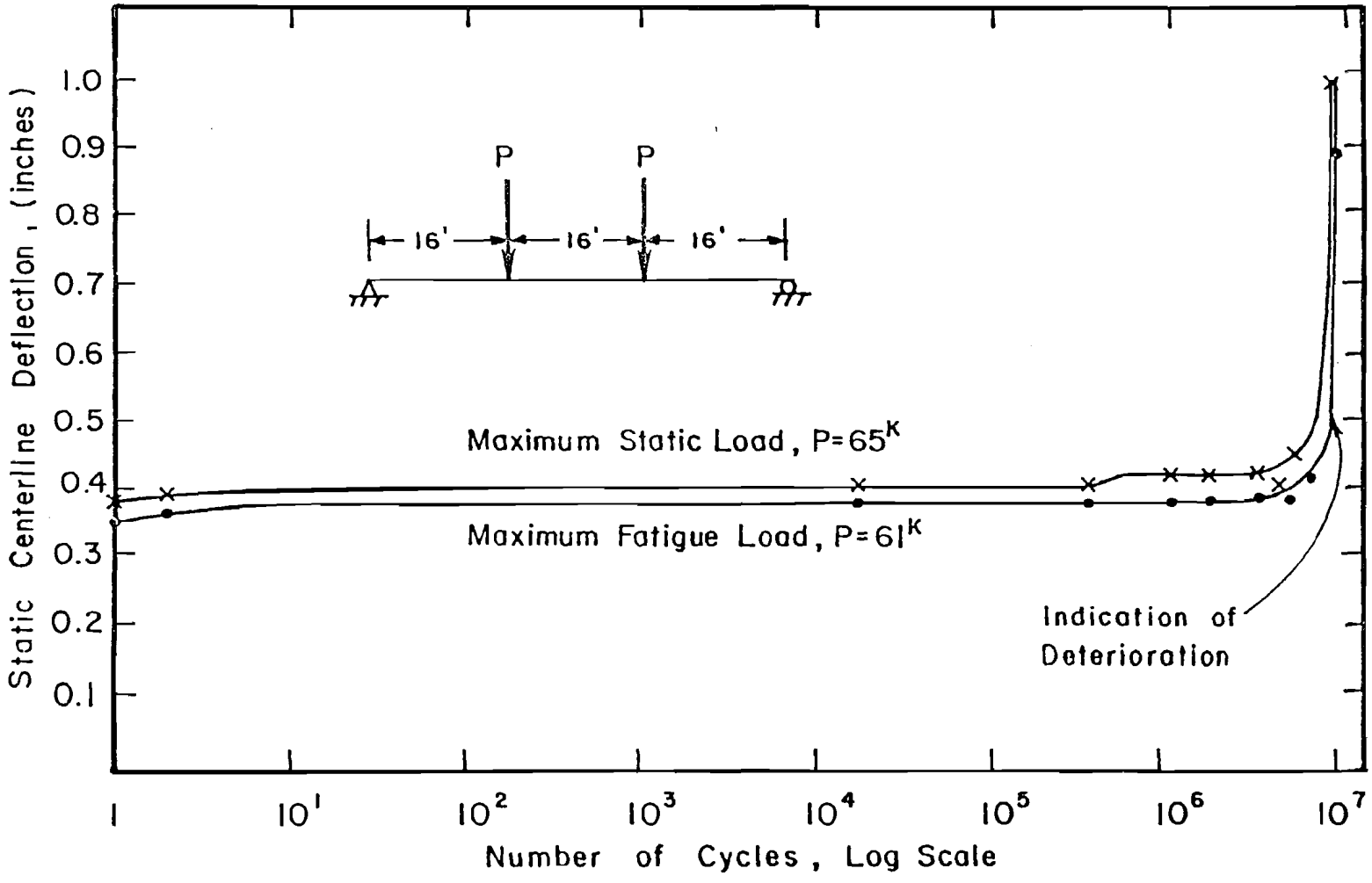

Fig. 4.116 Centerline deflection during static tests for Specimen C-16-CP-5.5-0L-9.43

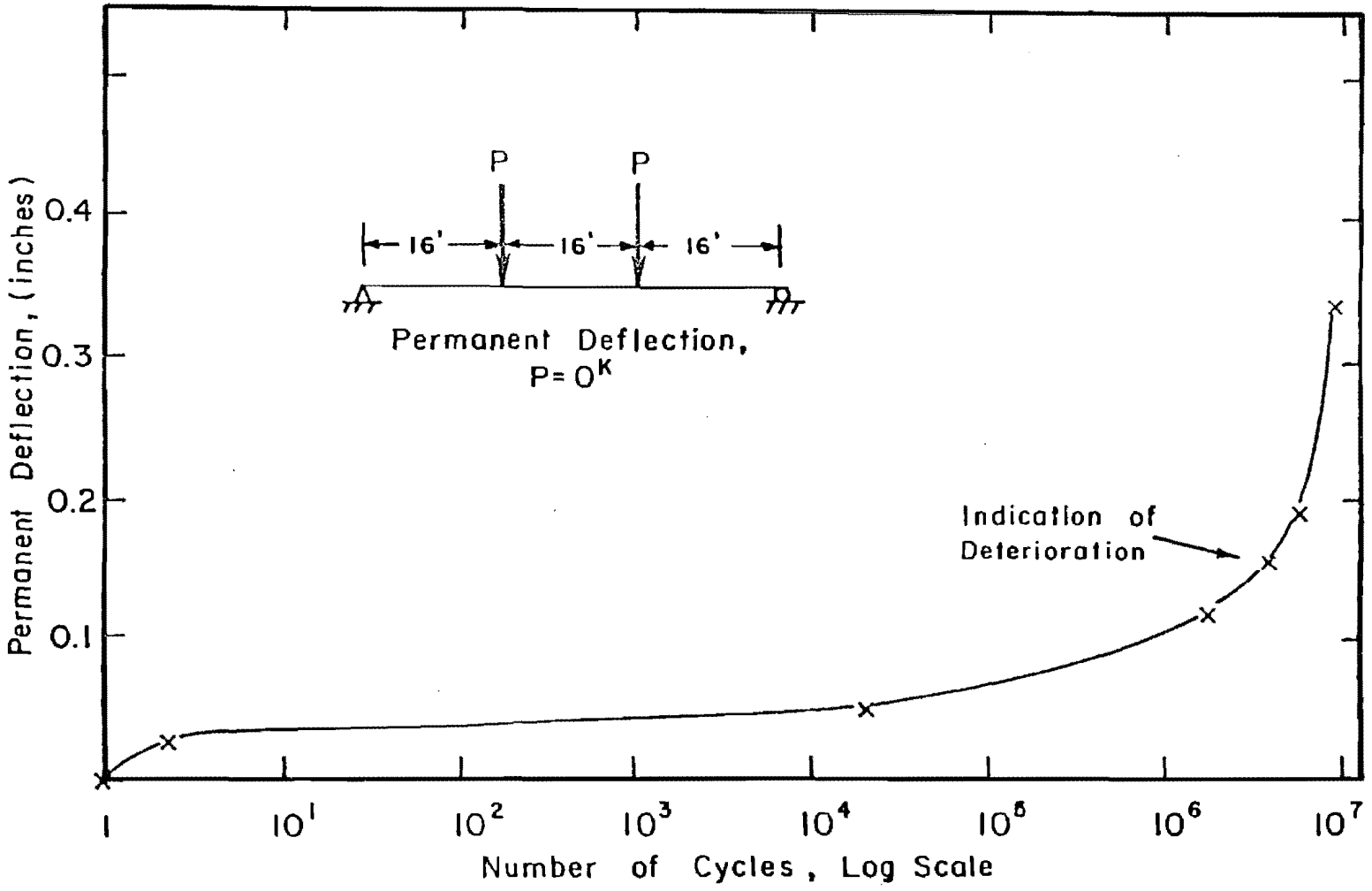

Fig. 4.117 Permanent centerline deflection during static tests for Specimen C-16-CP-5.5-OL-9.43

Figure 4.118 indicates that the wire strain remained relatively constant for the initial 5.0 million cycles. The two sets of strains plotted in this figure were from gages at the same location along the member. The only difference was their location relative to the cross section. The strains were significantly different throughout fatigue testing. This difference is probably a result of different bond characteristics or unsymmetrical flexural cracking. The maximum measured static strain between 20 and 61 kips, considering all gages, during the initial 5.0 million cycles, was approximately 0.00024 in./in. The dynamic strain range, between these loads, over this interval, remained fairly constant at 0.00030 in./in.

The specimen began to deteriorate after 6.92 million cycles. Although strain increased significantly after 5.0 million cycles, as shown in Fig. 4.118, centerline deflection (shown in Fig. 4.116) and crack opening (shown in Fig. 4.119), did not increase significantly until after 6.92 million cycles. Unlike previous tests, the degradation was gradual. Figure 4.119 shows crack profiles at various phases of fatigue loading and indicates a gradual increase after 6.92 million cycles. The passive reinforcing steel controlled cracking throughout fatigue testing. Figure 4.120 shows the instrumented flexural crack and flexural cracking on the west side of the specimen prior to the ultimate test.

A single wire fracture was heard during a static test at 6.01 million cycles. No other breaks were heard prior to the ultimate test. There were 35 flexural cracks in the center 17.5 ft of the span at 6.92 million cycles. At 9.43 million cycles, two additional cracks had formed. Ten of these flexural cracks extended into the top flange. No spalling occurred prior to the ultimate test.

4.12.5 Static Ultimate Test

After 9.43 million fatigue cycles, a static ultimate test to failure was performed. Figure 4.121 shows that the maximum load was 84 kips with a deflection of 2.75 in. This load was 58 percent of the calculated ultimate capacity. The maximum deflection was 3.55 in. at a load of 63 kips. Figure 4.122 shows the flexural crack distribution after the ultimate on the east face of the specimen. The unlabeled lines on the slab and girder indicate cracks that initiated during the ultimate test.

4.12.6 Post Mortem Investigation

After the ultimate test, the concrete cover was removed, and the strands were exposed. Forty-eight wire fatigue fractures, eight reinforcing bar fatigue fractures, and three reinforcing bar fatigue initiation cracks were discovered at the three locations labeled in Fig.

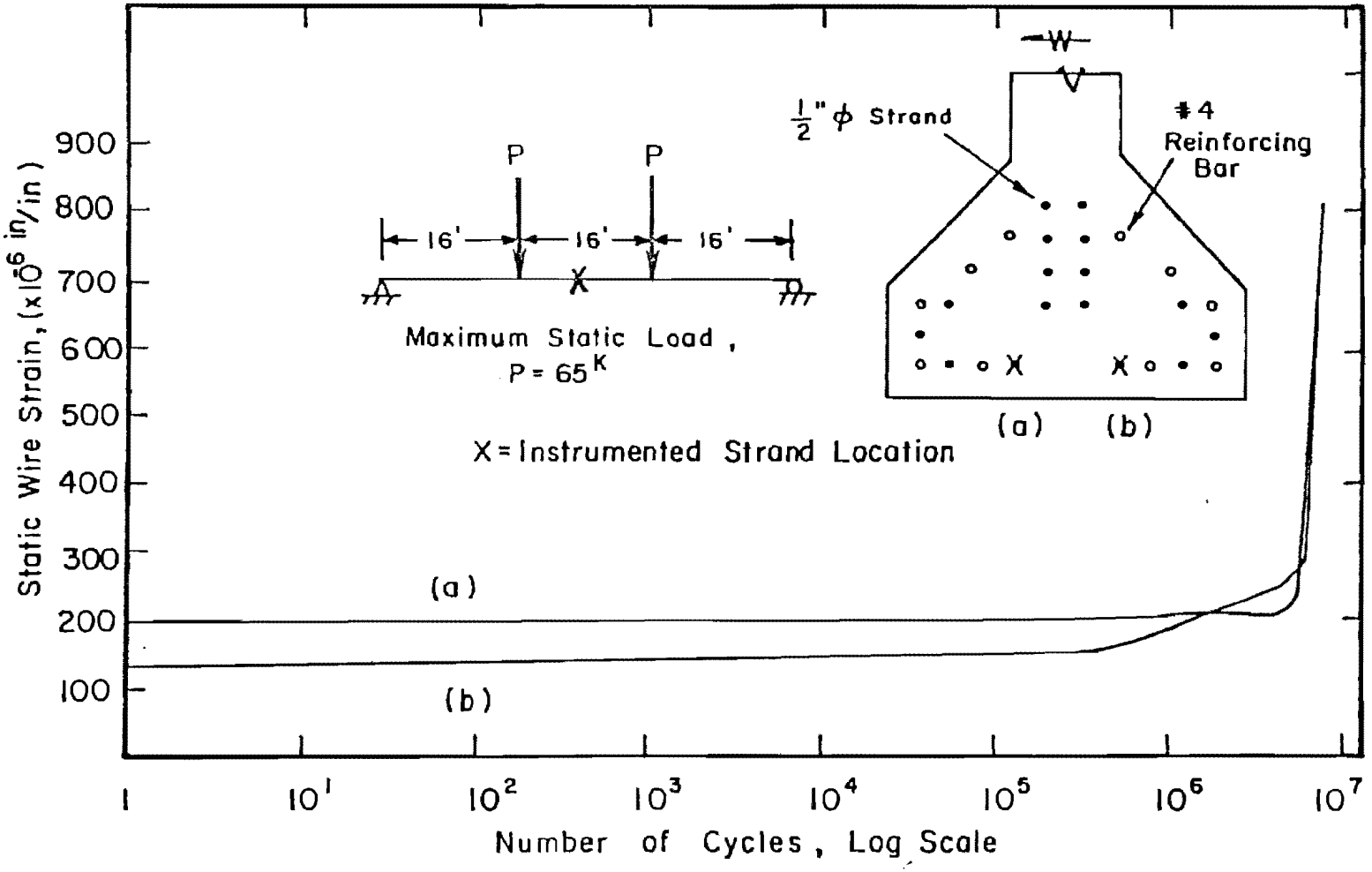

Fig. 4.118 Wire strains 1 ft 6 in. north of centerline during static tests for Specimen C-16-CP-5.5-OL-9.43

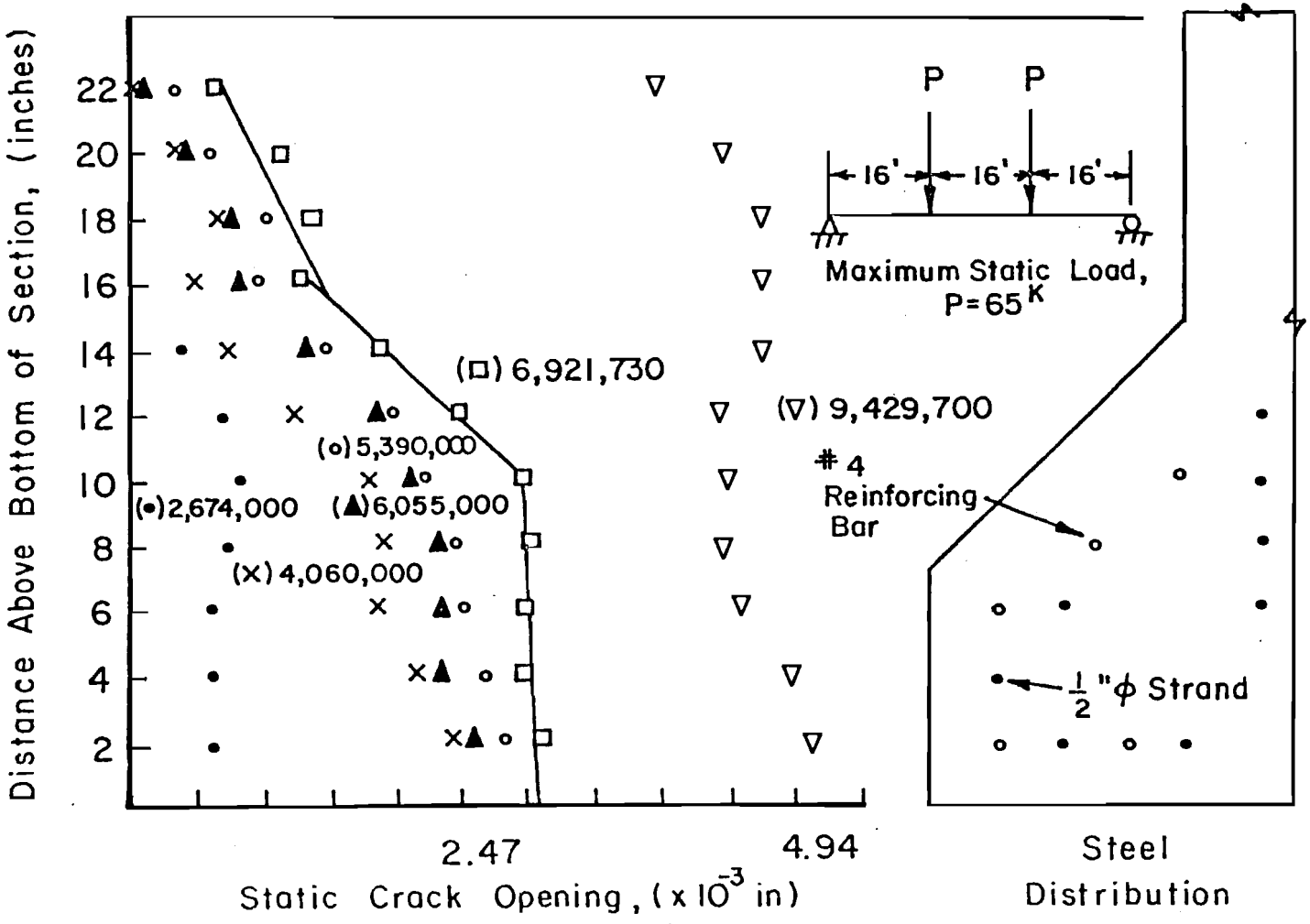

Fig. 4.119 Static crack profile 4 ft 1 in. north of centerline for Specimen C-16-CP-5.5-OL-9.43

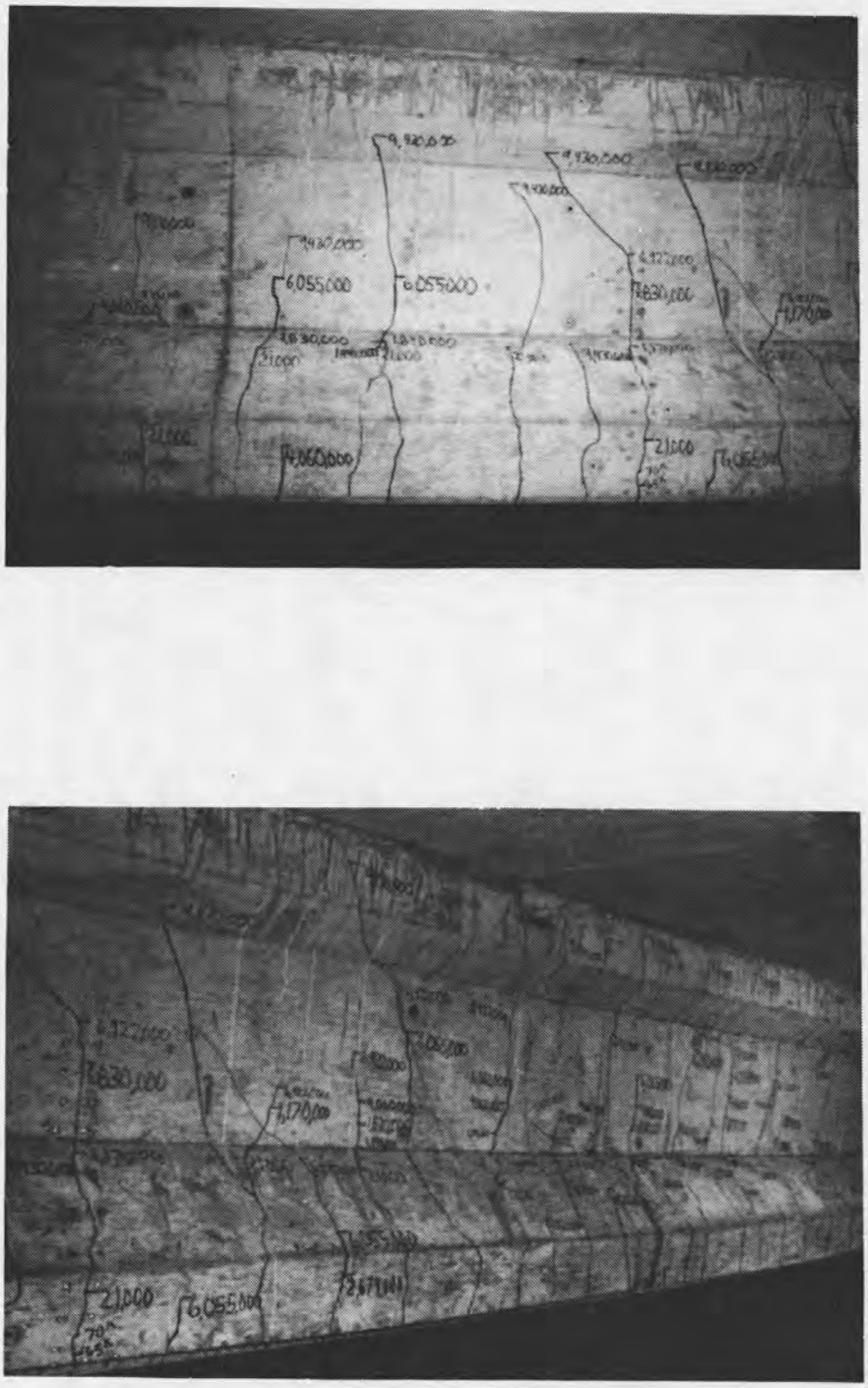

Fig. 4.120 Instrumented flexural crack and flexural cracking on the west face prior to the ultimate test

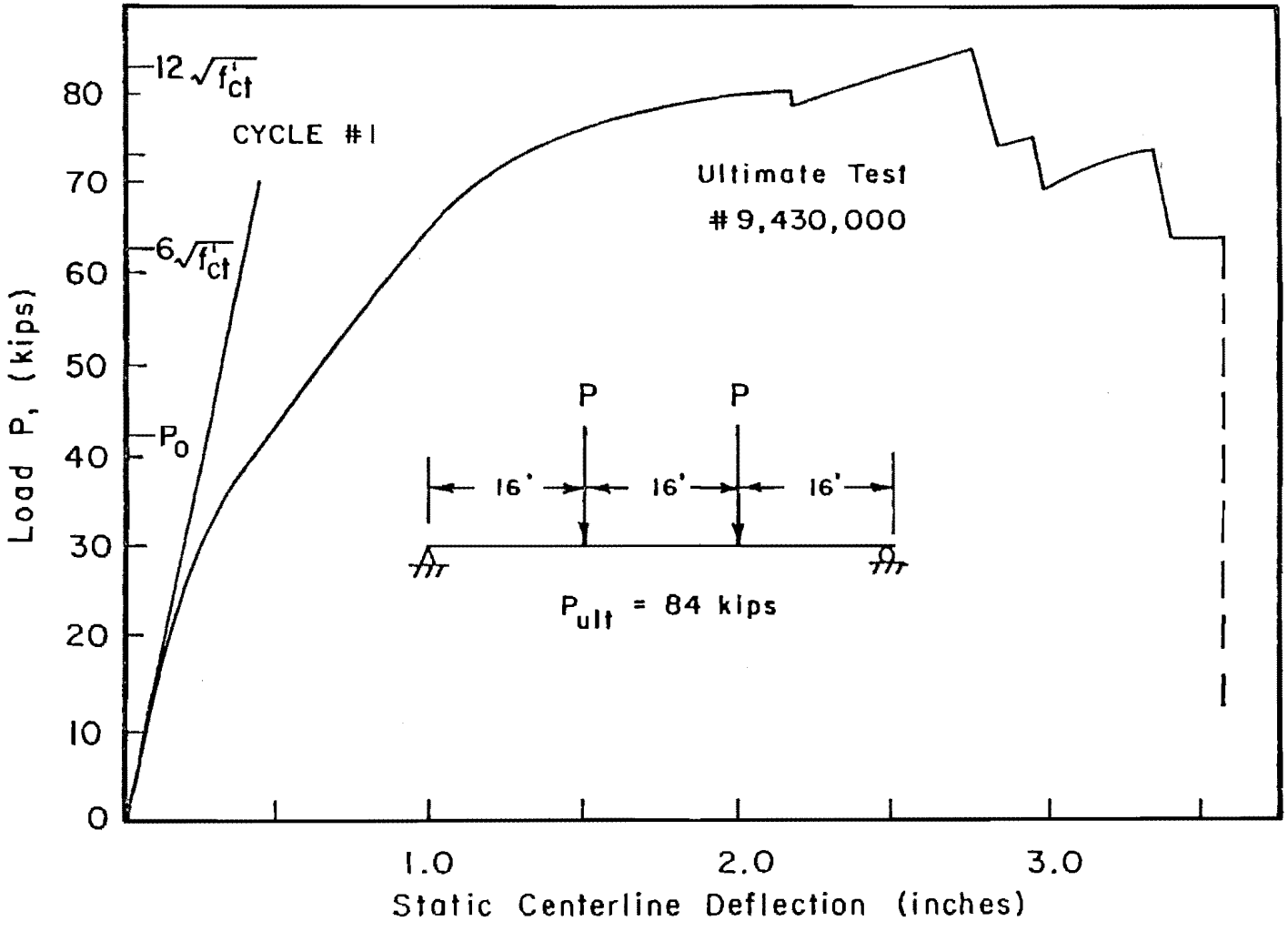

Fig. 4.121 Ultimate load versus deflection for Specimen C-16-CP-5.5-OL-9.43

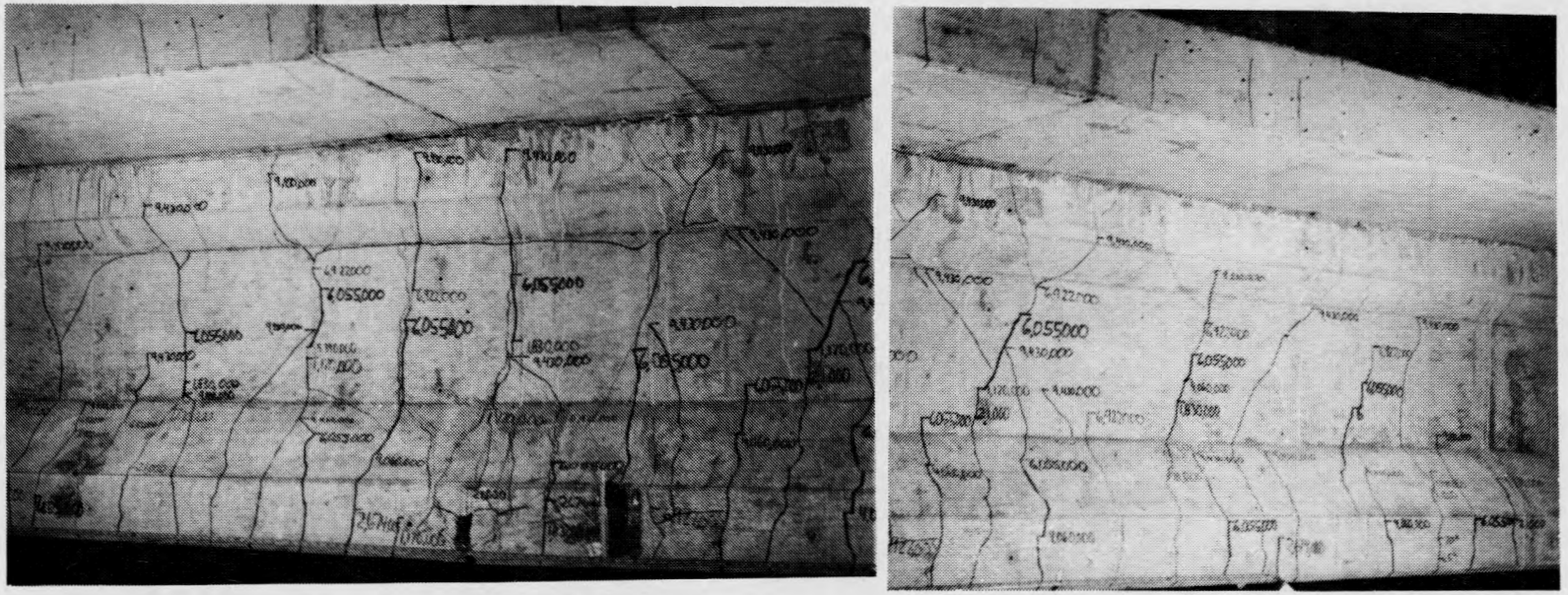

Fig. 4.122 Flexural cracking on the east face after the static ultimate test

4.123. The distribution of fatigue initiation cracks and breaks relative to the cross section is shown in Fig. 4.124.

4.12.7 Dynamic Load Amplification

The static centerline deflection between 20 and 61 kips at 5.39 million cycles was 0.28 in. (0.11 in. to 0.39 in.). The dynamic deflection between 20 and 61 kips at 5.39 million cycles (after the static test) was 0.28 in. (0.11 in. to 0.39 in.) indicating no dynamic amplification.

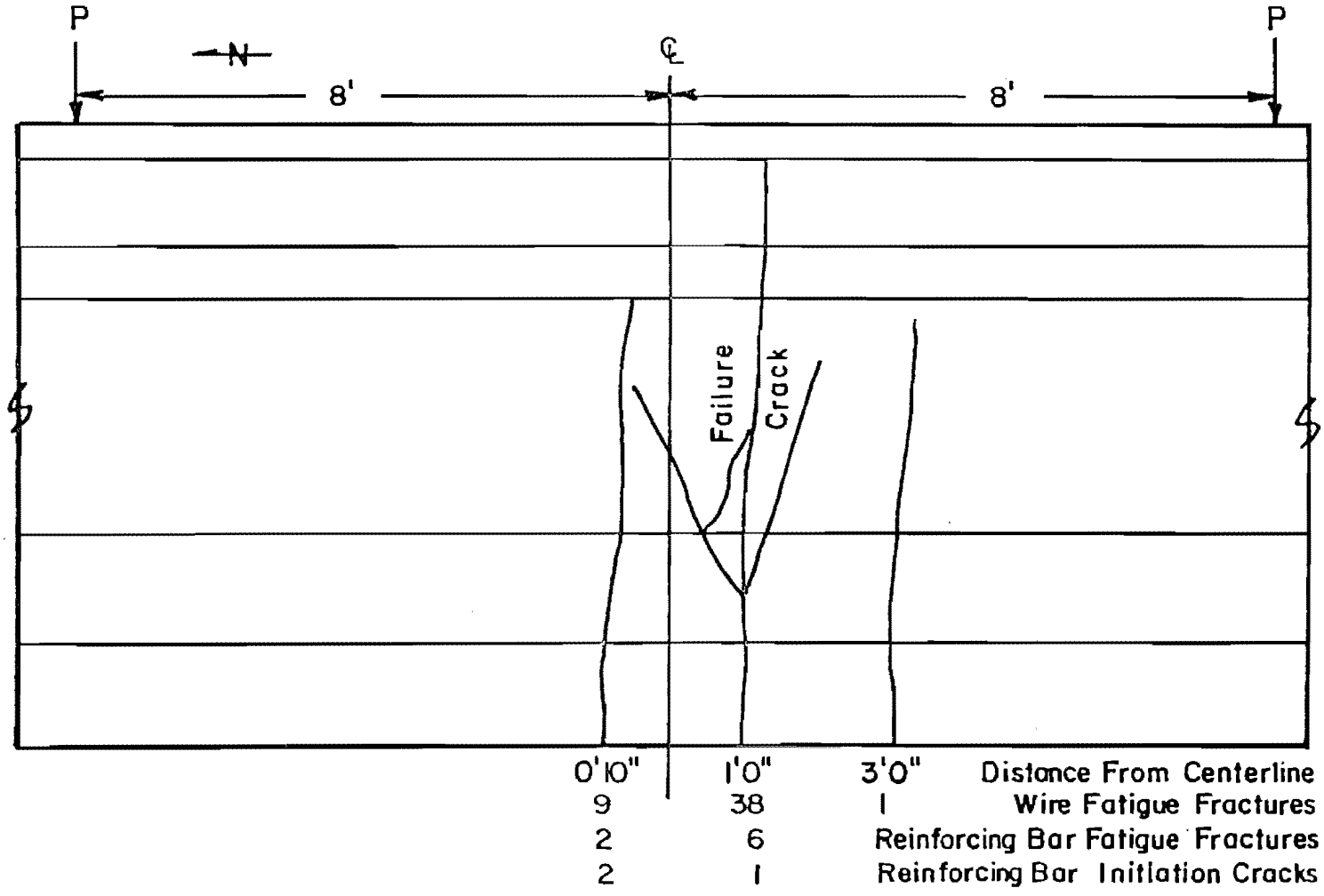

Fig. 4.123 Location and number of fatigue fractures and fatigue initiation cracks and corresponding concrete cracks for Specimen C-16-CP-5.5-0L-9.43

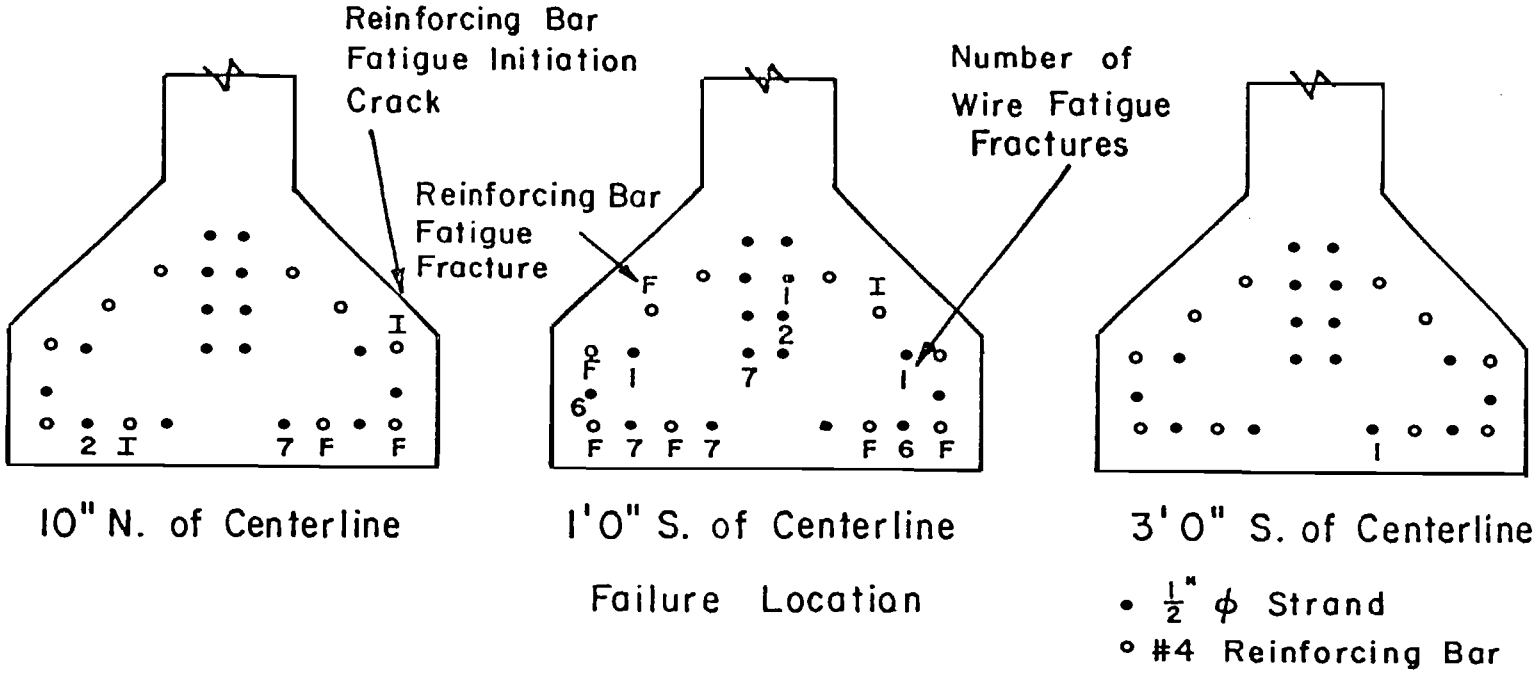

Fig. 4.124 Location of fatigue fractures and initiation cracks for Specimen C-16-CP-5.5-OL-9.43

CHAPTER 5

EVALUATION AND COMPARISON OF TEST RESULTS

5.1 Introduction

The experimental results from the eleven flexural specimens reported in Chapter 4 will be evaluated and compared in this chapter. The first portion of the chapter includes a typical girder design using the AASHTO Specifications [7,8]. The resulting girder design shows that bridge members can experience loads similar to the ones applied during static and fatigue tests in this study. The following section presents a brief discussion of PBEAM [85], an analytical program used for calculating prestress losses and for evaluating strand stress ranges using nonlinear material properties, including cracking. The next portion of this chapter provides an evaluation and comparison of all specimens at various stages of loading as well as evaluation of test results using current design parameters and models. The last section of this chapter presents the design process recommended for evaluation of the fatigue life of pretensioned concrete girders subjected to fatigue loading.

The evaluation and comparison among test specimens section includes a comparison of measured stiffness values determined from load-deflection behavior and of calculated stiffness values determined from material and cross section properties; a comparison of actual losses to those calculated using PBEAM; an evaluation of the effect that prestress losses have on strand stress range; a comparison of cracking stresses relating the level of first visible cracking to probable cracking as determined from load-deflection and load-strain curves; a comparison of applied fatigue loads to effective dynamic loads determined from dynamic deflections; and a comparison of dynamic, static, and analytical strand stress ranges. The last portion of this section includes a presentation of cracked section stiffness values for calculating deflections; an attempt to relate the number of cycles at failure (and the percentage of fatigue life) to both the first indication of deterioration (significant increases in deflections, strand stresses, and crack widths) and the first visible (spalling, cracking) and audible (wire fatigue fractures) indications of deterioration; presentation and comparison of average crack spacings; actual and calculated ultimate capacities and deflections; and relation of the number of fatigue breaks and break locations to the presence or absence of overloads.

The final section gives an evaluation of test results using design parameters (concrete and strand stress ranges) and existing fatigue models. Paulson's [73] failure model for strand tested in air is utilized along with the AASHTO Bridge Specifications model for

fatigue of redundant structural steel members (Category B) and the ACI Fatigue Committee's (Committee 215) strand fatigue recommendations.

5.1.1 Alphanumeric Labels

Throughout this chapter an alphanumeric label will be used for each specimen. From left to right, the designation indicates six items. The first indicates the girder type. "C" is Texas Type C girders while "A" is AASHTO-PCI Type II girders. The next indicator gives the number of strands. The C-16 specimens had 16 straight 1/2 in. diameter strands, the C-14 specimen had 10 straight and four draped 1/2 in. diameter strands, while the A-22 had 12 straight and 10 draped 7/16 in. diameter strands. The third figure indicates the presence or absence of passive (unstressed) reinforcing steel in the precompressed tension zone. "NP" represents no passive reinforcement. "UP" indicates unconI fined passive reinforcement. "CP" represents confined well-distributed passive reinforcement. The next indicator represents the maximum nominal, extreme fiber concrete tensile stress based on uncracked section calculations in multiples of $\sqrt{f'_{ct}}$, where f'_{ct} is the concrete cylinder strength at the time testing began. The next figure indicates the presence or absence of overloads. "OL" represents occasional overloads (greater than 1.04 times the maximum fatigue load) during static tests. "NO" indicates no overloads during static testing. The last indicator gives the number of cycles (in millions) at the time fatigue testing was discontinued.

For example,

C -16-CP-5.5-OL-9.43

C: Texas Type C

16: 16 straight strands

CP: Confined well-distributed Passive reinforcement

5.5: the maximum nominal concrete stress during fatigue loading was $5.5\sqrt{f'_{ct}}$ based on uncracked section calculations

OL: Overloads during the occasional static tests

9.43: fatigue testing was stopped at 9.43 million cycles

5.2 Typical AASHTO Girder Design

A hypothetical bridge design using the AASHTO Specifications [78] will be presented in this section to show that moments and stresses

similar to those applied to the test specimens can be expected on typical bridge girders.

5.2.1 Design Loads

5.2.1.1 Dead Load

Girder: Texas Type C $A = 495 \text{ in.}^2$

Deck: Assume 8.5 in. $A = 8.5 \text{ in.} * S * 12 \text{ in./ft}$

where S is the spacing in ft

$$M_{DL} = 1/8 \left[(495 \text{ in.}^2 + 102 \text{ S in.}^2) * 0.145 \text{ k/ft}^3/144 \text{ in.}^2/\text{ft}^2\right] (48 \text{ ft})^2$$

$$= (144 + 30 \text{ S}) \text{ ft-kips}$$

Additional D.L.: 2 in. asphaltic overlay

$$M_{ADL} = 1/8 \left[(2 \text{ in.} * S * 12 \text{ in./ft}) * 0.090 \text{ k/ft}^3/144 \text{ in.}^2/\text{ft}^2\right] (48 \text{ ft})^2$$

$$= 4.3 \text{ S ft-kips}$$

5.2.1.2 Live Loads

5.2.1.2.1 HS Lane Load

Concentrated Load = 18^k for moment

Uniform Load = 0.64^k/(10 ft lane width)

$M_{Lane} = (9^k * 24 \text{ ft}) + 1/8 (0.64 \text{ k/ft}) (48\text{ft})^2$

$= 400$ ft-kips

5.2.1.2.2 HS 20-44 Truck Load

Maximum centerline moment occurs when the center wheels are at the centerline of the bridge and the wheel spacing is 14 ft.

Reaction 1 = (8^k * 10 ft * 32^k * 24 ft + 32^k * 38 ft)/48 ft

= 43 kips

Reaction 2 = 8^k + 32^k * 32^k - 43^k

= 29 kips

M_{truck} = 43^k * 24 ft - 32^k * 14 ft

= 584 ft-kips

$$M_{Truck} = 584 \text{ ft-kips}$$

5.2.1.3 Impact Factor

$$I = 50 / (L + 125)$$

where: L is the length in ft of the portion of the span which is loaded to produce the maximum stress in the member

L = 48 ft

I = 50 / (48 + 125) = 0.29

5.2.2 Determine Girder Spacing

Assume: Texas Type C-16 girders

Sixteen 1/2 in. diameter 270 ksi strands

f_{pi} = 0.7 * 270 ksi = 189 ksi

Losses = 20%

S_{bgird} = 4833 $in.^3$

Y_{bgird} = 17.09 in.

c.g.ps = 6.25 in.

f'_{cdeck} = 3000 psi

Effective width = (8.5 in. * 12) + 7 in.

= 109 in.

Y_{bcomp} = 33.16 in.

I_{comp} = 302 900 $in.^4$

S_{bcomp} = 9136 $in.^3$

$$6\sqrt{f'_c} = -P/A - P_e/S_{bgird} + M_{DL}/S_{bgird} + M_{LL}/S_{bcomp}$$

$$6\sqrt{5000}/1000 = -370^k/495\ in.^2 - (370^k * 10.84\ in.)/4833\ in.^3$$

$$+ (1728 + 360\ S)\ in.\text{-}k/4833$$

$$+ ((520 + 1.29 * 7008) * (S/10) * (S/11))/9136$$

S = 9.80 ft

This is a realistic value based on current designs.

5.2.3 Ultimate Capacity

D.L. = (144 + 30S + 4.3S) ft-kips

= 5760 in.-kips

L.L. = 584 ft-kips * (9.8/10) * (9.8/11) * 12 in./ft

= 6120 in.-kips

= 1.3 [D.L. + 5/3 (L.L. + Impact)]

M_{ult} = 1.3 [5760 in.-kips + 5/3 (6120 * 1.29)]

= 24,600 in.-kips

$$M_u = A_s^* f_{su}^* d\ (1 - 0.6\ (p^* f_{su}^*/f'_c)\ \phi$$

where: A_s^* = area of prestressing steel = 2.45 in.^{2}

b = width of flange or flanged member = 109 in.

d = distance from extreme compressive fiber to centroid of the prestressing force = 42.25 in.

f'_c = compressive strength at 28 days = 5000 psi

f'_s = ultimate strength of prestressing steel = 270 ksi

ϕ = strength capacity reduction factor (factory produced precast prestressed concrete members) = 1.0

p^* = ratio of prestressing steel

$= A_s^*/(bd) = 2.45 \text{ in.}^2/(109 \text{ in.} * 42.24 \text{ in.}) = 5.32\text{x}10^{-4}$

f_{su}^* = average stress in prestressing steel at ultimate load

$= f'_s (1 - 0.5\, p^* f'_s/f'_c)$

$= 270 \text{ ksi } (1 - 0.5\, (5.32\text{x}10^{-4} * 270 \text{ ksi})/5 \text{ ksi}) = 266 \text{ ksi}$

$$M_u = 2.45 \text{ in.}^2 * 266 \text{ ksi} * 42.25 \text{ in.}$$
$$(1 - 0.6 * 5.32\text{x}10^{4} * 266 \text{ ksi}/5 \text{ ksi}) * 1.0$$
$$= 27{,}100 \text{ in.-kips}$$

The ultimate capacity is sufficient.

5.2.4 Test Loads

The design dead load (girder and deck) moment on the hypothetical girder before it was composite with the slab was 5260 in.-kips. The Texas Type C test specimens had a centerline dead load moment of 3800 in.-kips. Assuming a composite section to girder section modulus ratio of approximately 1.9 and a 16 ft shear span, a pair of applied loads of 14.4 kips each would be required to produce a state of stress in the test specimens equivalent to that in the hypothetical girder. Additional applied loads of 2.6 kips each would be needed to account for the asphaltic overlay for a total dead load of 17 kips.

The live load moment in the hypothetical girder design was 6120 in.-kips. For a 16 ft shear span, loads of approximately 32 kips above the 17 kip applied loads to compensate for additional dead load (due to

a thicker slab, the asphaltic overlay, and a wider deck on the actual design bridge) would be required to produce the desired moment. The live loads increase to 41 kips with the impact factor of 0.29. Thus, total applied loads of 58 kips each are required to simulate prototype dead, live and impact loading. These would be design level loads thought of as producing the design extreme fiber nominal concrete tensile stress of $6\sqrt{f'_c}$. In the test program, a pair of concentrated loads of 60 to 61 kips (with a shear span of 16 ft) were applied to four Texas Type C specimens. Thus, the loads are very much in the range of actual bridge loads. However, as a result of lower prestress losses in the test girders than the 20 percent assumed (some as low as 8 to 10 percent), higher concrete strengths than the 5000 psi assumed (the mean test strength was 6300 for the Texas C-16 specimens), and higher desired concrete stresses for research purposes (as high as $10.5\sqrt{f'_{ct}}$), maximum loads in the vicinity of 70 to 75 kips were applied to three C-16 specimens. A similar procedure was used to establish the test loads for the Texas C-14 specimen and the three AASHTO-PCI Type II specimens.

Loads higher than those required to produce stresses of $6\sqrt{f'_c}$ were applied to generate data in the short life region of the stress range versus number of cycles (S/N) curve and to simulate older girders, girders with excessive prestress losses, or girders with fabrication errors. From comparison of the computed and applied test load levels, it is felt that moments and stresses experienced by the test specimens can be expected in bridge girders where the load distribution between girders is realistically considered in design.

5.3 Analytical Program PBEAM

PBEAM, developed by Suttikan [85], is a computer program:

> developed for the analysis of initial and time-dependent responses and strength in simple bending of partially or fully prestressed concrete members.... It accounts for the effects of nonlinearity of stress-strain responses of materials, variations with time of strength, creep, and shrinkage of concrete, and relaxation of bonded prestressing steel in different parts of the cross section.

Various equations to model strength, creep, shrinkage, and relaxation were available in PBEAM. The following equations were recommended by Suttikan and were used for loss calculations presented in this chapter.

Concrete Compressive Strength Equation:
Recommended by ACI Committee 209 [18]

$$(f'_c)_t/(f'_c)_{28} = t/(A1 + A2*t)$$

where: t is the age in days

$(f'_c)_t$ is the compressive strength at t days

$(f'_c)_{28}$ is the 28-day compressive strength

A1 and A2 are constants determined from girder concrete strength at release and at 28 days and are shown in Appendix A, Table A.1. For slab concrete strength, the values of 4.00 and 0.85 were used for A1 and A2, respectively, as recommended by Committee 209.

Creep Equation:
Recommended by ACI Committee 209 [18]

$$(C)_{t,t'} / C9 = CC_{LA} (t-t')^{C1} / [C2 + (t-t')^{C1}]$$

$$CC_{LA} = C3 (t')^{C4}, \text{ for moist cured concrete}$$

where: $(C)_{t,t'}$ is the creep coefficient at day t due to sustained load applied at day t'

t is the age in days

t' is the age in days when load is applied

CC_{LA} is the creep correction factor for age of concrete at loading

C1, C2, C3, C4 are constants. The recommended values are 0.60, 1.0, 1.25, and -0.118, respectively

C9 is the ultimate creep coefficient. An average value of 2.35 was initially used for C9 as recommended. This initial value was then modified by correction factors for relative humidity, minimum member thickness, slump, percent fines and air content. Modified C9 was subsequently used as the ultimate creep coefficient. These values are shown in Appendix A, Table A.2.

Shrinkage Equation:
Recommended by ACI Committee 209 [18]

$$(\epsilon_s)_t / S1 = t / (t + S2)$$

where: $(\epsilon_s)_t$ is the shrinkage strain at day t

t is the age in days

S1 is the ultimate shrinkage strain. An average value of -0.00080 in./in. was initially used as recommended for moist cured concrete. This value was modified by correction factors for relative humidity, minimum member thickness, slump, percent fines, air content, and cement factor (number of 94 lb sacks of concrete per cubic yard of mix). Modified S1 was subsequently used as the ultimate shrinkage strain. These values are shown in Appendix A, Table A.3.

S2 is a constant. The recommended value for moist cured concrete is 35.

Concrete Compressive Stress Versus Strain Equation: Hognestad Curve

for $0 \leq \varepsilon \leq \varepsilon_o$

$$f_c = f''_c \left[2\varepsilon / \varepsilon_o - (\varepsilon / \varepsilon_o)^2\right]$$

for $\varepsilon_o < \varepsilon \leq \varepsilon_u$

$$f_c = f''_c \left(\varepsilon_u - 0.85\ \varepsilon_o - 0.15\ \varepsilon\right) / \left(\varepsilon_u - \varepsilon_o\right)$$

where: ε is the concrete compressive strain

ε is the maximum concrete compressive strain at f'_c

$= 2\ f''_c / E_{ci}$

ε_u is the ultimate concrete compressive strain

$= 0.0038$ in./in.

f_c is the concrete compressive stress at

f'_c is the concrete cylinder strength

f''_c is the maximum concrete compressive stress in the concrete stress-strain curve

$= 0.85\ f'_c$

E_{ci} is the initial concrete modulus of elasticity

$= 1{,}800{,}000 + 480 \left| f'_c \right|$ psi

Strand Relaxation Equation:
Recommended by PCI Committee on Prestress Losses [71]

$$(f_{sr})_t = (f_{sr})_{t1} [(\log 24t - \log 24t1)/R2] [(f_s)_t/R1 - R3]$$

$$(f_s)_t / f_{sy} \geq R4; \; f_{sy} = 0.90 f_{pu}$$

where: $(f_{sr})_t$ is the steel relaxation stress at t

$(f_{sr})_{t1}$ is the steel relaxation stress at t1

$(f_s)_{t1}$ is the steel stress at t1

t is the age in days

t1 is the age in days at the beginning of the time interval. For mathematical correctness a value of 1/24 day (Log 24 * 1/24 = 0) is suggested if the initial age is the time stressing is completed.

f_{pu} is the ultimate steel strength

f_{sy} is the steel yield strength

R1,R2,R3 are constants. Based on actual relaxation tests using the same stressing bed and stressing procedure used for the test specimens, the values were 270, 45, and 0.55, respectively

R4 is a constant. The PCI recommended value for low-relaxation steel is 0.60.

5.4 Evaluation of Test Specimens

5.4.1 Determination and Comparison of Sections Stiffeners Indices (EI)

To calculate displacements, rotations and losses, the relation between applied moments and curvature must be known. In the elastic range, displacements and rotations are inversely proportional to EI. For an uncracked section, elastic strains at release (and hence losses) and at loads below the cracking load are primarily a function of the modulus of elasticity (E). An error in the determination of the modulus of elasticity (E) or the moment of inertia (I) can directly affect computation of prestress losses, serviceability calculations for live load deflections, and stress calculations for redundant structures.

The AASHTO Specifications [7,8] recommend a concrete modulus of $57,000\sqrt{f'_c}$. When the slab and girder compressive strengths are known, a transformed moment of inertia can be determined using the AASHTO

relationship. Uncracked section theoretical stiffness indices are compared to experimentally determined stiffness indices in Table 5.1. The moment of inertia is based on gross section properties ignoring steel areas. The experimentally determined stiffness index (EI_e) was calculated from measured deflections at the zero tension loads. The equation at the bottom of Table 5.1, used for the experimentally determined stiffness index (EI_e), was derived using the moment-area method and a 16 ft shear span. The ratio of the experimentally determined stiffness index to the theoretical index had a mean of 1.02 with a standard deviation of 7 percent. The zero tension load was used because at this point there is a deviation from linear load-deflection and load-strain behavior. Figure 5.1 indicates this significant change in load-strain behavior at approximately 36 kips, the zero tension load. During cycle one the section was uncracked at this load. After cracking, there is a drastic decrease in the load-strain slope at the zero tension load because above this load the prestressing strand provides all the internal tension force to maintain equilibrium.

5.4.2 Determination and Effect of Prestress Losses

Computations of nominal concrete tensile stresses and strand stress ranges are a function of the applied loads and the prestress losses. Figure 5.2 shows computed load versus strand stress for two hypothetical Texas Type C-16 girders. Example NL (normal losses) would have losses totaling 19 percent of the initial stress. The strand stress range between zero live load and a load that would produce a nominal concrete tensile stress of $6\sqrt{f'_c}$ is 23 ksi, based on cracked section behavior and the PBEAM [85] program. Assuming the same loads, but assuming actual losses of 46 percent, Example HL (high losses) would have a significantly greater strand stress range of 67 ksi, based on cracked section behavior and the PBEAM program. Both hypothetical sections are assumed to have girder and slab 28 day compressive strengths of 5000 psi and 3000 psi, respectively. The girder release strength at one day is assumed at 4000 psi. The slabs are assumed cast 30 days after the girders, and loads applied at 60 days. For Example NL, low relaxation strands are assumed with initial prestress of 0.70 f_{pu} (f_{pu} = 270 ksi). Average values were assumed for determination of creep, shrinkage, and relaxation losses. Example HL was deliberately assumed to be incorrectly prestressed to a realistic lower bound of 0.60 f_{pu} (f_{pu} = 270 ksi) using stress relieved strands. Extreme values were assumed for creep and shrinkage losses. The modulus of elasticity was assumed 10 percent below that used for Example NL. All of these values could occur in practice.

This example demonstrates the affect prestress losses have on strand stress range. High losses can be caused by fabrication errors and variations in material properties as assumed here as well as by incorrect storage procedures or as a result of time effects during the service life or any combination of these and other factors. Without

TABLE 5.1 Comparison of Section Stiffness Index Values (EI_e)

Specimen	Zero Tension Load P_o (kips)	Measured Centerline Deflection at P_o Δ_o (in.)	Experimentally Determined EI_e ($\times 10^8$ k-in.^{2})	Theoretical EI_T ($\times 10^8$ k-in.^{2})	$\frac{EI_e}{EI_T}$
C-16-NP-10.5-NO-0.58	36	0.19	12.9	11.8	1.09
C-16-NP-7.2-OL-1.48	35	0.19	12.5	11.8	1.06
C-16-NP-10.1-NO-0.91	25	0.15	11.3	11.2	1.01
C-16-NP-6.0-NO-1.91	37.5	0.22	11.6	12.5	0.93
C-14-NP-5.5-OL-2.29	46	0.24	13.0	12.0	1.08
A-22-NP-6.2-OL-2.84	30	0.24	8.5	8.4	1.01
A-22-NP-6.2-NO-5.00	30 (estimated--see text)	0.23	8.8	8.4	1.04
A-22-NP-3.5-OL-5.95(NF)	30	0.22	9.2	8.5	1.08
C-16-UP-8.0-NO-1.73	48	0.31	10.5	10.8	0.97
C-16-CP-7.2-NO-2.54	42.5	0.26	11.1	12.8	0.88
C-16-CP-5.5-OL-9.43	42.5	0.24	12.0	11.0	1.09
					====
				x =	1.02
				=	0.07

$EI_e = P_o / \Delta_o \times (6.783 \times 10^6$ in.$^3)$

Shear span was 16 ft for all specimens during initial loading.

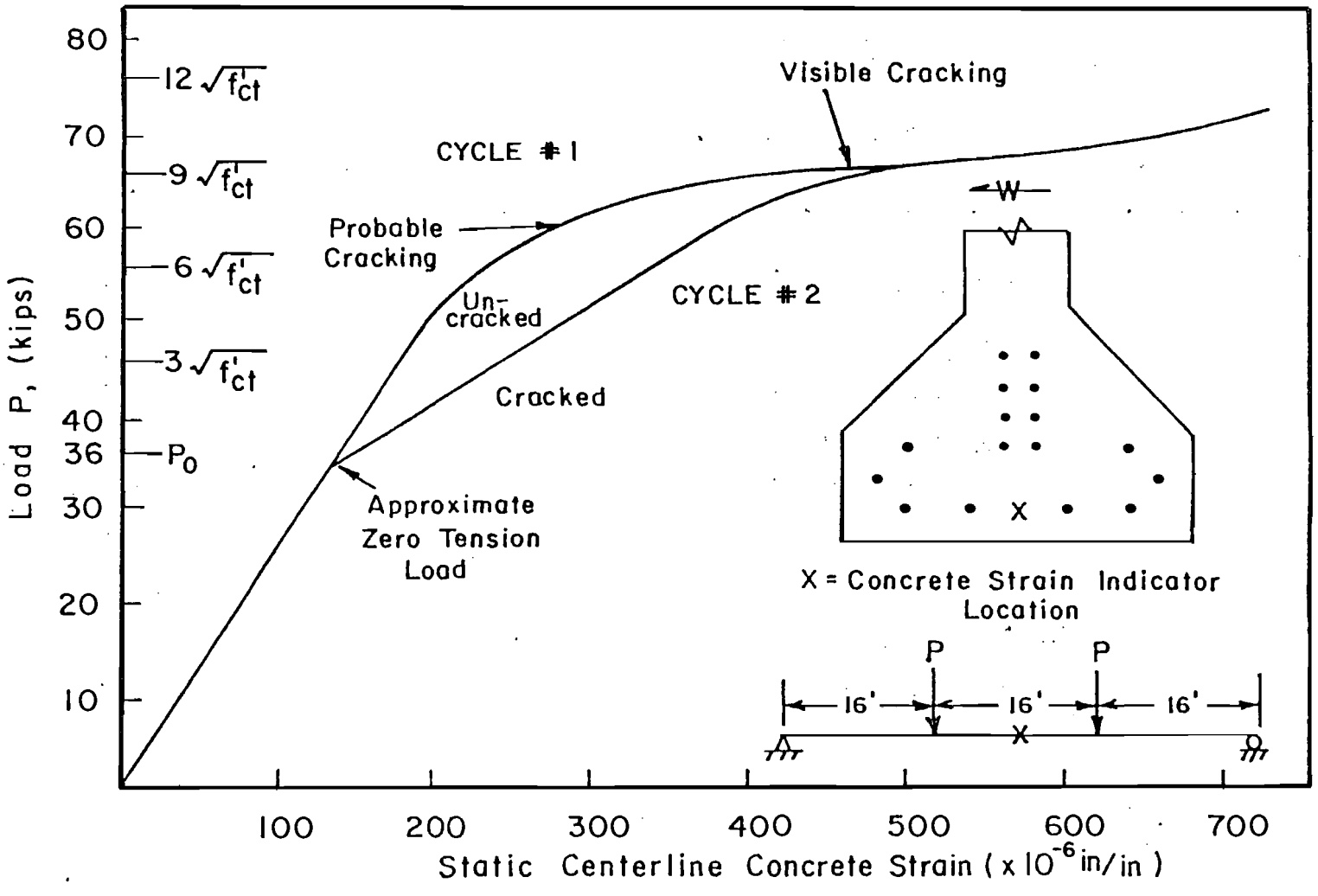

Fig. 5.1 Determination of zero tension load for Specimen C-16-NP-10.5-NO-0.58

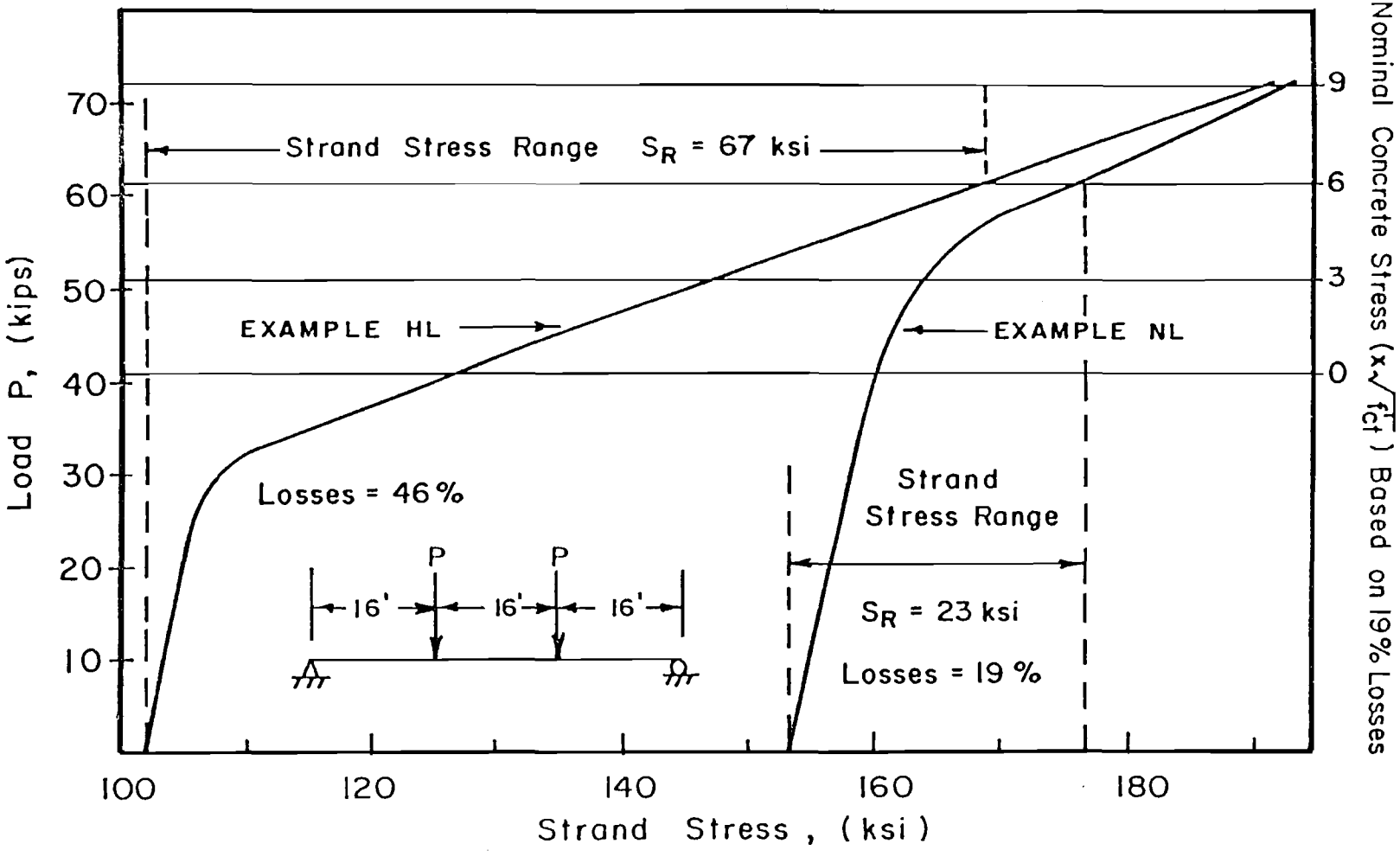

Fig. 5.2 Effect of prestress losses on strand stress ranges for two hypothetical Texas Type C-16 girders

strict quality control and knowledge of the actual material properties, actual prestress losses could be significantly different from the assumed design values.

Time dependent prestress losses determined from the loss equations using the program PBEAM [85] are compared in Table 5.2 to the actual losses determined from cracking loads for the test girders. Concrete strength and strand relaxation properties were known and realistic values were assumed for creep and shrinkage properties and the concrete stress strain relationship in the PBEAM input. The actual effective prestress force (P_{em}) and losses were calculated using the measured zero tension load given in Table 5.1. Figure 5.1 shows the characteristic change in load deflection behavior at zero tension. Using this load and the following equation, the effective prestress force, P_{em}, was determined. The equation was set equal to zero because by definition the zero tension load produces no stress in the extreme tension fibers.

$$0 = \frac{-P_e}{A_g} - \frac{P_e e}{S_g} + \frac{M_{DL}}{S_g} + \frac{P_o * SS}{S_{comp}}$$

where: P_e is the effective prestress force

A_g is the area of the girder

e is the strand eccentricity

S_g is the girder section modulus

M_{DL} is the moment applied to the girder before it is composite with the slab

P_o is the zero tension load

SS is the shear span

S_{comp} is the composite girder section modulus

The analytical program consistently underestimated the prestress losses for all but two of the Texas Type C specimens. The mean difference between predicted and measured loads for the five Type C specimens with no passive reinforcement (C-16-NP and C-14-NP) was approximately -2.6 percent of the initial prestress force. The standard deviation was 2.4 percent. For two of these specimens the measured and predicted losses were identical. The mean difference for the three Type C specimens with passive reinforcement (C-16-UP and C-16-CP) was -5.0 percent of the initial force, with a standard deviation of 1.3 percent. It is unlikely that losses can ever be predicted to within 3.0 percent. Such accuracy is sufficient for practical purposes.

TABLE 5.2 Comparison of Predicted and Measured Prestressed Losses

Specimen	Initial Force P_i (kips)	Predicted Effective Force P_{ea} (kips)	Predicted Losses L_p (percent)	Measured Effective Force P_{em} (kips)	Measured Losses L_{em} (percent)	$L_p - L_m$ (percent)
C-16-NP-10.5-NO-0.58	453	384	15.2	368	18.9	-3.7
C-16-NP-7.2-OL-1.48	448	368	17.9	368	17.9	0
C-16-NP-10.1-NO-0.91	390	336	13.8	319	18.1	-4.3
C-16-NP-6.0-NO-1.91	458	402	12.2	380	17.1	-4.9
C-14-NP-5.5-OL-2.29	424	356	16.0	356	16.0	0
A-22-NP-6.2-OL-2.84	377	259	31.3	329	12.7	18.6
A-22-NP-6.2-NO-5.00	377	259	31.3	329	12.7	18.6
A-22-NP-3.5-OL-5.95(NF)	377	256	32.1	329	12.7	19.4
C-16-UP-8.0-NO-1.73	502	458	8.8	440	12.4	-3.6
C-16-CP-7.2-NO-2.54	490	437	10.8	407	17.0	-6.2
C-16-CP-5.5-OL-9.43	470	432	8.1	408	13.3	-5.2

$L_p - L_m$: Type C-NP $\bar{x} = -2.6$, $\sigma = 2.4$ Type C-_P $\bar{x} = -5.0$, $\sigma = 1.3$ Type A-22 $\bar{x} = 18.7$, $\sigma = 0.5$

PBEAM [85] seriously overestimated the losses for the AASHTO-PCI Type II (A-22) specimens. The average difference between the measured losses and the predicted losses was approximately 19 percent of the total prestress force. The standard deviation was less than 0.5 percent. The actual losses for these specimens were approximately the same as for the Texas Type C girders. This overestimation again illustrates the extreme uncertainty of current provisions for determining prestress losses and consequently for estimating strand stress ranges. Without the measured load-deflection and load-strain curves and computed zero tension loads, the computed stress ranges would be significantly in error for these girders.

Passive reinforcement does help control losses. Such reinforcement acts as compression steel even in the tension flange of a pretensioned girder and reduces creep and shrinkage effects. The average measured loss for the four C-16 specimens with no passive reinforcement (C-16-NP) was 18 percent. The specimens with passive steel (C-16-_P) averaged losses of only 14.2 percent. This was with only 2 sq. in. of reinforcing steel in the lower flange. Figure 5.3 shows two C-16 specimens, one with passive steel, one without. Both were cycled at approximately $6\sqrt{f'_{ct}}$. The specimen without passive reinforcement (C-16-NP-6.0-NO-1.91) has losses of approximately 17 percent, a strand stress range of approximately 28 ksi, and experienced 1.91 million cycles before fatigue failure. Specimen C-19-CP-5.5-OL-9.43 had losses of approximately 13 percent, and withstood 9.43 million fatigue cycles before failure. Thus, a small amount of well distributed conventional reinforcement reduced losses, controlled and distributed cracking, and greatly extended the fatigue life.

5.4.3 Comparison of Cracking Stresses

The AASHTO Specifications [7,8] recommend that the tensile cracking stress be assumed equal to the modulus of rupture which is defined as $7.5\sqrt{f'_c}$ for normal weight concrete. Table 5.3 shows the stresses produced by loads at which cracking was first visible as well as the probable cracking stresses determined from concrete and steel strain readings and load deflection curves during static loading. The table also compares the probable cracking stress to the AASHTO recommendation.

Concrete strains decrease and steel strains increase drastically after cracking. Figures 5.1 and 5.4 show how the probable cracking loads were determined at a load where the load-strain curve deviated significantly from linear behavior. The measured concrete strain increased at cracking in Fig. 5.1 because the indicator was a gage mounted on an aluminum bar that strained with the concrete until cracking. At that time, the bar acted as reinforcing or prestressing steel and carried a large portion of the tension force.

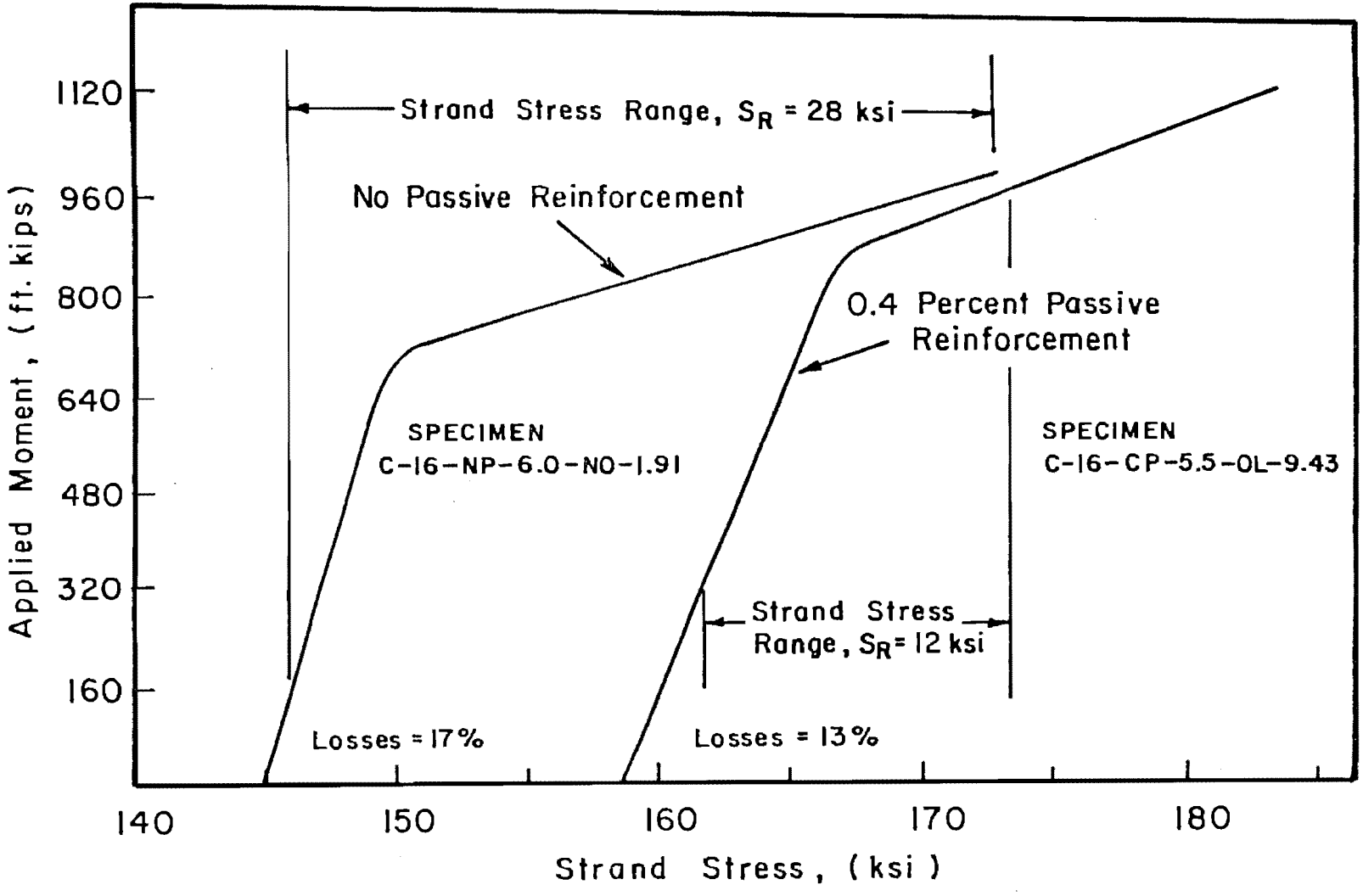

Fig. 5.3 Effect of passive steel on prestress losses and stress ranges

TABLE 5.3 Comparison of Cracking Stresses

Specimen	Visible Cracking		Probable Cracking		
	Load (kips)	Nominal Concrete Stress N_v ($\times \sqrt{f'_{ct}}$)	Load (kips)	Nominal Concrete Stress N_{cr} ($\times \sqrt{f'_{ct}}$)	$\frac{N_{cr}}{7.5\sqrt{f'_{ct}}}$
C-16-NP-10.5-NO-0.58	70	10.1	60	7.2	0.96
C-16-NP-7.2-OL-1.48	67.5	9.2	62.5	7.8	1.04
C-16-NP-10.1-NO-0.91	56	8.8	50	7.1	0.95
C-16-NP-6.0-NO-1.91	70	8.8	60	6.1	0.81
C-14-NP-5.5-OL-2.29	77.5	9.1	70	6.9	0.92
A-22-NP-6.2-OL-2.84	55	9.7	45	5.8	0.77
A-22-NP-6.2-NO-5.00	46[r]	6.2	46[r]	6.2	0.83
A-22-NP-3.5-OL-5.95(NF)	55	9.6	45	5.8	0.77
C-16-UP-8.0-NO-1.73	75	8.1	70	6.6	0.88
C-16-CP-7.2-NO-2.54	70	7.3	65	5.9	0.79
C-16-CP-5.5-OL-9.43	65	6.8	65	6.8	0.91

[r] Cracked during repetitive loading after 1180 cycles

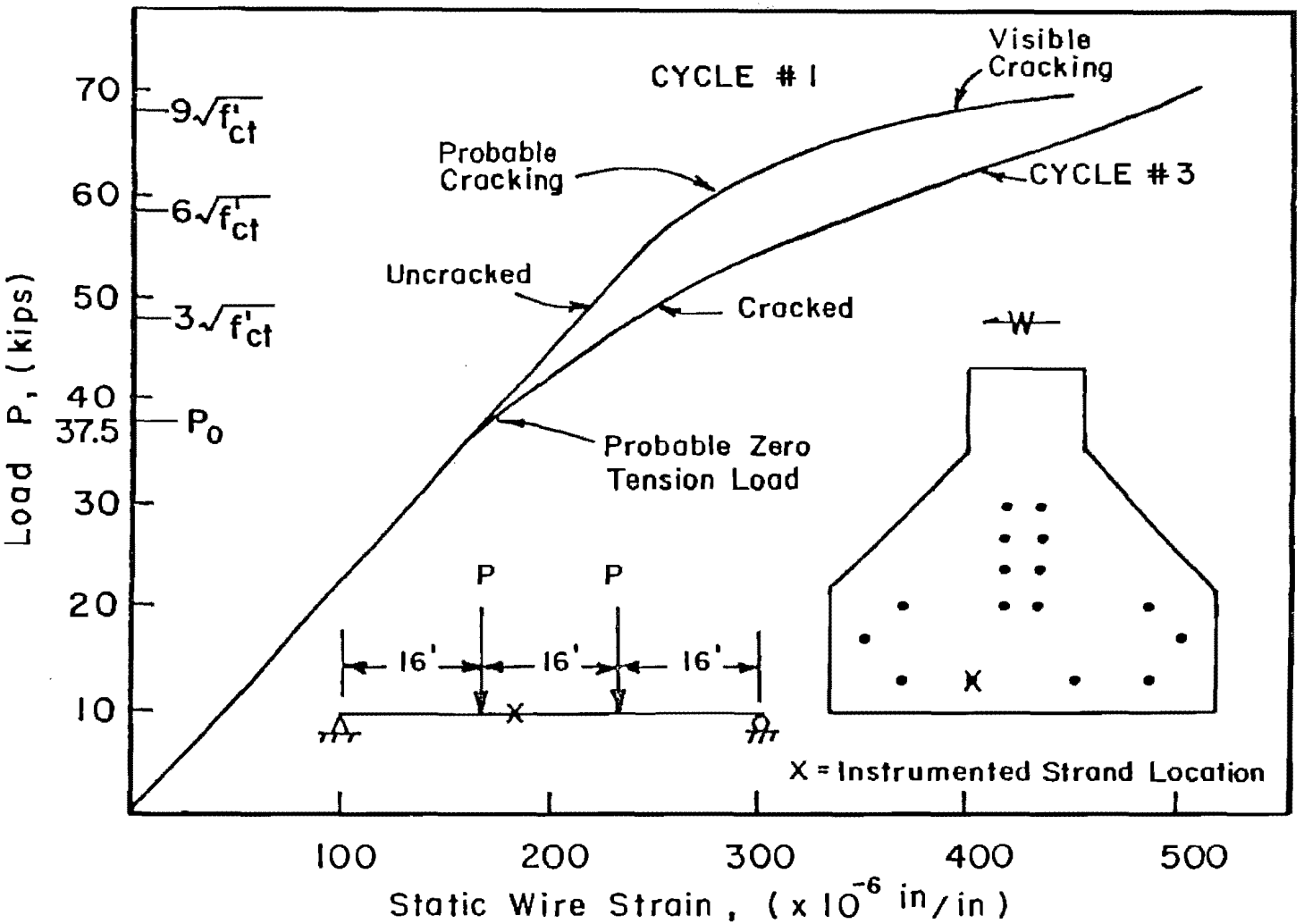

Fig. 5.4 Determination of zero tension load for Specimen C-16-NP-6.0-NO-1.91

The average probable cracking stress under initial loading was $6.6\sqrt{f'_{ct}}$ (where f'_{ct} was the concrete compressive strength on the day the specimens were cracked). The standard deviation was $0.7\sqrt{f'_c}$. The average stress is below the AASHTO recommendation by 12 percent but is similar to the suggested pure tension, split cylinder value of 6.7 to $7.0\sqrt{f'_c}$ [36,53,89]. This seems reasonable because in a deep specimen there is very little strain gradient effect as might occur in the more shallow modulus of rupture specimens [18]. Magura and Hognestad [54] (Section 2.3.10) also reported cracking stresses that were less than the modulus of rupture. All their specimens were full scale highway girders with composite slabs. Two specimens cracked at 86 percent of the modulus of rupture, one during static testing, one during fatigue testing after 5000 cycles. One specimen cracked at 92 percent of the modulus of rupture after 4.59 million cycles. A fourth specimen cracked at 94 percent after 4.7 million cycles. Assuming a modulus of rupture of $7.5\sqrt{f'_c}$, these stresses would be 6.4 to $7.1\sqrt{f'_c}$.

The implications of this difference between actual and assumed cracking stresses could potentially cause fatigue problems if highway bridges are designed by current specifications, and flexural members actually experience design level stresses. Flexural cracking will occur (along with a corresponding increase in strand stress range) with moderate overloads or due to fatigue of concrete in tension (Section 2.2.1.2) if prestressed concrete bridge elements carry loads that produce the AASHTO allowable tensile stress of $6.0\sqrt{f'_c}$. For the test specimens discussed in this report, all loads, prestress losses, and material properties were known accurately. These values can vary significantly for in-service girders, indicating that there is even a higher probability of cracking in service. A realistic factor of safety should be provided if crack free applications are desired.

5.4.4 Comparison of Applied Loads and Dynamically Amplified Loads

Fatigue tests that last millions of cycles must be performed at an accelerated rate in the interest of time. For a vehicle traveling 55 miles per hour (80.7 ft/sec) over the 48 ft span, loads would be applied and removed (1 cycle) in 0.60 sec, which is 1.68 cycles per second. The specimens in this test program were tested at between 2.5 and 3.0 cycles per second, roughly 1.5 to 1.8 times the actual value.

Table 5.4 shows the applied loads and the dynamically amplified loads and compares the maximum values. The applied loads were determined directly from load cells and a peak detector, which read the loads during fatigue testing. The dynamically amplified loads were also determined from the peak detector but from centerline deflection measurements. The actual maximum and minimum deflections were read dynamically. These deflections were converted to equivalent static loads using static load deflection curves. Specimen C-16-NP-10.5-NO-

TABLE 5.4 Comparison of Applied Loads and Dynamically Amplified Loads

Specimen	Applied Loads		Dynamically Amplified Loads		
	P_{min} (kips)	P_{max} (kips)	P'_{min} (kips)	P'_{max} (kips)	$\frac{P'_{max}}{P_{max}}$
C-16-NP-10.5-NO-0.58	47.5	71.5	46	74	1.03
C-16-NP-7.2-OL-1.48	10	60.8	10	60.8	1.00
C-16-NP-10.1-NO-0.91	27.1	60.8	34	64	1.05
C-16-NP-6.0-NO-1.91[a]	10	80	10	83	1.04
C-14-NP-5.5-OL-2.29	10	65	6	68	1.05
A-22-NP-6.2-OL-2.84	10	46	11	48	1.04
A-22-NP-6.2-NO-5.00	10	46	13	48	1.04
A-22-NP-3.5-OL-5.95(NF)	10	39	10	39	1.00
C-16-UP-8.0-NO-1.73	24	75	24	77	1.03
C-16-CP-7.2-NO-2.54	19	70	24	73	1.04
C-16-CP-5.5-OL-9.43	20	61	20	61	1.00
					====
					$\bar{x}$ = 1.03
					σ = 0.02

[a] Shear span was 12 ft during fatigue testing for this specimen, 16 ft for all others

0.58 is shown as an example. The dynamically measured maximum and minimum applied loads were 71.5 and 47.5 kips, respectively. The resulting dynamically measured centerline deflection was 0.34 in. to 0.94 in. at 312,000 cycles. During a static test at 315,000 cycles, these deflections corresponded to static loads of 46 and 74 kips. This interpretation procedure is valid because deflections are a function of loads. In this case, the dynamic loads are due to the applied loads and to the inertial mass effects of the specimen. The rate of loading causes the mass to accelerate slightly above the acceleration due to gravity, hence a slightly larger deflection results.

Table 5.4 indicates that the average dynamic amplification of the maximum load was approximately 3 percent, with a standard deviation of 2 percent. The lowest ratio of P'_{max} (dynamic maximum load) to P_{max} (applied load) was 1.00, which indicates no dynamic amplification. This was the case for three specimens. The maximum P'_{max} to P_{max} ratio indicated a dynamic load amplification of only 5 percent. Since even the largest amplification is quite small compared to the applied loads, it can be concluded that there was no significant dynamic load amplification.

5.4.5 Comparison of Strand Stress Range

A primary purpose of the experimental program was to determine if beam fatigue life could be determined from strand fatigue data generated from tests in air. The first portion of this section presents analytical and measured strand stress ranges and shows how overloads and passive reinforcement affect fatigue life. The last portion of this section compares beam fatigue results using nominal concrete and strand stress ranges. Available fatigue models are also used to evaluate the beam fatigue results.

5.4.5.1 Analytical and Measured Strand Stress Ranges

To use current strand and steel fatigue models, strand stress ranges must be known. For experimental specimens, strain gages can be installed on the prestressing wires of a strand and stress ranges can be determined directly. One problem with this technique is the randomness of flexural cracking. Unless a strain gage is directly at a crack, strains less than the maximum value will be read. In tests by Rabbat et al. [76], flexural cracks were forced to occur (with the help of sheet metal crack formers) at the location of strain gages, so stresses close to the maximum were determined. For the specimens in this test program, no crack formers were used. Therefore, the presence of a strain gage at a flexural crack was random.

Table 5.5 shows the maximum measured static and dynamic stress ranges for each specimen. In some cases, the static stress ranges are

TABLE 5.5 Comparison of Strand Stress Ranges

Specimen	Dynamic Loads Min/Max (kips)	Measured Strand Stress Range Before Deterioration Began		Analytical Stress Range[a] (ksi)
		Dynamic (ksi)	Static (ksi)	
C-16-NP-10.5-NO-0.58	46/74	30.5	5.3	43.7
C-16-NP-7.2-OL-1.48	10/60.8	7.9	38.1*	24.0
C-16-NP-10.1-NO-0.91	34/64	24.1	21.4	49.1
C-16-NP-6.0-NO-1.91	10/83	29.0*	18.3	27.8
C-14-NP-5.5-OL-2.29	6/68	18.3	16.8	24.7
A-22-NP-6.2-OL-2.84	11/48	NA	NA	20.9
A-22-NP-6.2-NO-5.00	13/48	NA	NA	20.5
A-22-NP-3.5-OL-5.95(NF)	10/39	2.0	5.8	7.5
C-16-UP-8.0-NO-1.73	24/77	20.1*	18.6	20.7
C-16-CP-7.2-NO-2.54	24/73	7.6	16.8	22.5
C-16-CP-5.5-OL-9.43	20/61	9.0	7.2	11.7

* Indicates that strain gage was probably in the vicinity of a flexural crack

[a] Using Program PBEAM

NA - Not Available

higher which indicates that gage which was read statically was closer to a flexural crack than the gage which was read dynamically. When the dynamic value is higher, it indicates that this strain gage was probably in the vicinity of a flexural crack. Analytical stress ranges are also shown in Table 5.5. Typically, a designer will not have access to measured stress ranges and must depend on analytical values. For this reason and because of the randomness of flexural cracking relative to strain gages, analytical stress ranges will be used for comparison purposes. Table 5.5 indicates that in three cases, strain gages were probably in the vicinity of a flexural crack. For these cases the measured stress ranges were equal to or greater than the analytical predictions and confirm the analytical values. The analytical stress ranges were determined using the program PBEAM [85] and the actual prestress losses determined from the measured decompression loads.

5.4.5.2 Manual Determination of Strand Stress Ranges

5.4.5.2.1 Graphical Determination of Strand Stress Range

Approximate stress ranges can be calculated manually by assuming no concrete tensile capacity, a linear stress strain relationship, and by placing the neutral axis at various levels of the cross section. The strand stresses and applied loads are determined for the assumed neutral axes. By connecting the different load-stress values with straight lines, as shown in Fig. 5.5, the approximate load-strand stress curve can be found. The maximum and minimum stresses can be found graphically. The stress range is the difference between these two values. These graphical values are compared to the PBEAM determined analytical values in Fig. 5.5. Considering the uncertainty in the prestress losses calculations, this graphical method is probably acceptable for an initial estimation of strand stress ranges.

5.4.5.2.2 Graphical Strand Stress Range for Specimen C-16-NP-10.5-NO-0.58

From the following given properties for Specimen C-16-NP-10.5-NO-0.58, the strand stress range between the applied loads of 46 and 74 kips will be determined.

Girder Properties:

A_g = 495 in.^{2}

I_g = 82,602 in.^{4}

c.g. bottom = 17.09 in.

Prestressing Steel

E_{ps} = 28.700 ksi

n = 6.88

A_{ps} = 16 strands @ 0.153

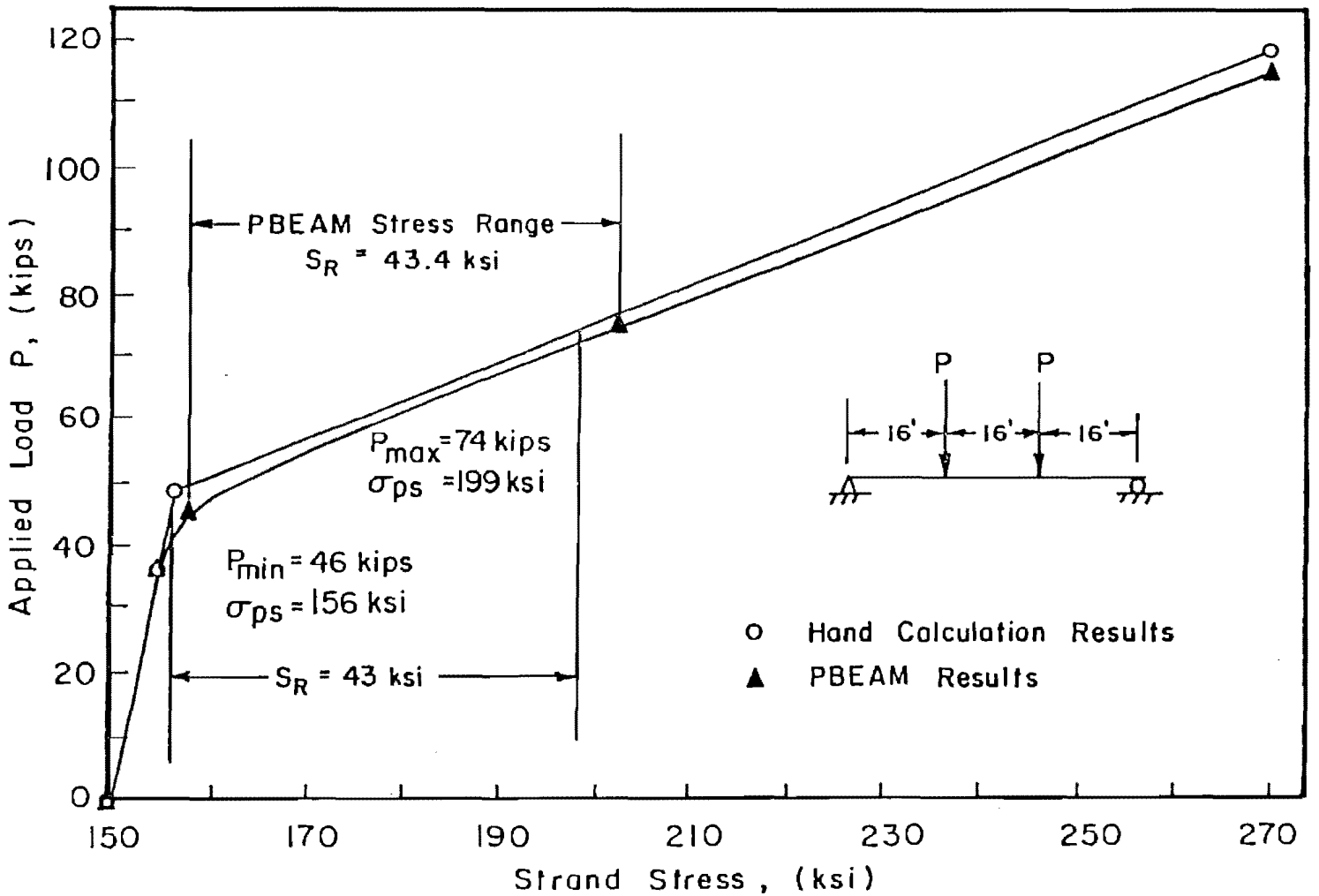

Fig. 5.5 Approximate and analytical strand stress ranges for Specimen C-16-NP-10.5-NO-0.58

c.g. top = 22.91 in. $= 2.45\ in.^2$

$S_b = 4833\ in.^3$ $c.g._{ps} = 6.25$ in.
$S_t = 3605\ in.^3$

$f'_{cgtest} = 5350$ psi $E_c = 57\ \ 5350 = 4200$ ksi

Slab Properties:

$f'_{cstest} = 5780$ psi $n = 1.04$

$A_{transformed} = 77$ in. * 1.04 * 7.75 in. $= 620\ in.^2$

Composite Properties:

$I_{comp} = 283{,}200\ in.^4$ $M_{DL} = 3800$ in.-kips

c.g.c.bot. = 31.99 in.

$S_{cb} = 8853\ in.^3$

Determine effective prestress force after losses:

In this example the measured force reported in Table 5.5 will be used.

Strand stress = $368^k/2.45\ in.^2 = 150.2$ ksi

$P_e = 368$ kips

Applied load = 0 kips

Determine the dead load state-of-stress:

Bottom fibers:

$$\sigma_b = \frac{-P_e}{A_g} - \frac{P_e e}{S_b} + \frac{M_{DL}}{S_b}$$

$$= \frac{-368k}{495\ in.^2} - \frac{368k\ (17.09 - 6.25\ in.)}{4833\ in.^3} + \frac{3800\ in.\text{-}k}{4833\ in.^3}$$

$$= -0.743\ ksi - 0.825\ ksi + 0.786\ ksi$$

$$= -0.782\ ksi$$

Top fibers:

$$\sigma_z = \frac{-P_e}{A_g} + \frac{P_e e}{S_t} - \frac{M_{DL}}{S_b}$$

$$= -743 + \frac{368k * 10.84 \text{ in.}}{3605 \text{ in.}^3} - \frac{3800 \text{ in.-k}}{3605 \text{ in.}^3}$$

$$= -0.743 \text{ ksi} + 1.107 \text{ ksi} - 1.054 \text{ ksi}$$

$$= -0.690 \text{ ksi}$$

Determine decompression moment:

$$0.782 \text{ ksi} = M_o/8853 \text{ in.}^3$$

$$M_o = 6923 \text{ in.-kips}$$

For a 192 in. shear span, the applied load would be 36.0 kips. This corresponds to the zero tension load of 36.0 kips reported in Table 5.1.

Determine the strand stress range from zero to M_o:

$$\Delta\sigma = 6923 \text{ in.-kips} * (31.99 - 6.25 \text{ in.})/283{,}200 \text{ in.}^4$$

$$= 0.629 \text{ ksi}$$

$$S_r = 0.629 \text{ ksi} * 6.88 = 4.3 \text{ ksi}$$

Strand stress = 150.2 + 4.3 ksi = 154.5 ksi

Applied load = 36.0 kips

Determine the internal moment and the strand stress with the neutral axis at the bottom of the web:

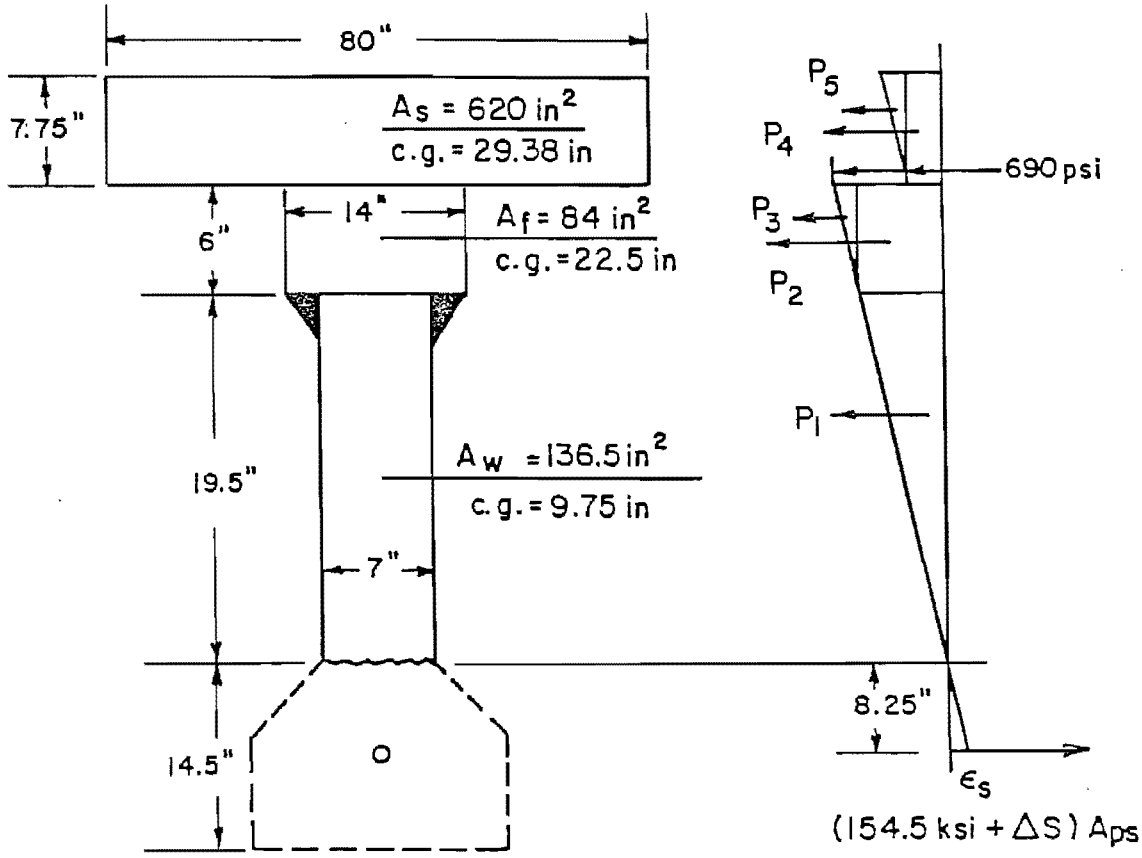

$m = \epsilon_s / 8.25\ in.$

$T = (154.5\ ksi + \Delta_s) A_{ps}$

$= (154.5\ ksi + 8.25\ in. * m * E_s)\ A_{ps}$

$C = P_1 + P_2 + P_3 + P_4 + P_5$

$C = m * 9.75\ in. * E_c * 136.5\ in.^2$

$+ m * 19.5\ in. * E_c * 84\ in.^2$

$+ m * 3\ in. * E_c * 84\ in.^2$

$+ (m * 25.5 * E_c * 620\ in.^2 - 0.691\ ksi * 620\ in.^2)$

$+ m * 3.875 * E_c * 620\ in.^2$

--

Determine ultimate capacity:

Setting T = C and solving for m:

$$378.2 \text{ kips} + 579{,}600\ m = 4{,}458{,}700\ m \quad P_1$$
$$+\ 6{,}829{,}100\ m \quad P_2$$
$$+\ 1{,}050{,}600\ m \quad P_3$$
$$+\ 65{,}914{,}900\ m \quad P_4$$
$$-\ 428.4 \text{ kips}$$
$$+\ 10{,}016{,}500\ m \quad P_5$$

$$m = 9.085 \times 10^{-6}$$

Determine concrete compressive forces and internal moment:

P_1 =	50.4 kips	*	(13 in. + 8.25 in.)	=	1071 in.-kips
P_2 =	62.0 kips	*	(22.5 + 8.25 in.)	=	1907
P_3 =	9.5 kips	*	(23.5 + 8.25 in.)	=	302
P_4 =	170.5 kips	*	(29.38 + 8.25 in.)	=	6415
P_5 =	91.0 kips	*	(30.67 + 8.25 in.)	=	3541
C =	383.4 kips				13,240 in.-kips

$T = (154.5 \text{ ksi} + 8.25 \text{ in.} * m * E_s)\ A_{ps}$

$= (156.7 \text{ ksi})\ A_{ps}$

$= 383.5 \text{ kips} \quad T = C$

$M_{DL} = 3800$ in.-kips

$P = 49.2$ kips

Strand Stress = 156.7 ksi

Applied Load = 49.2 kips

Determine ultimate capacity:

$$M_u = A_s^* f_{su}^* d (1 - 0.6 (p^* f_{su}^*)/f_c') \phi$$

where: A_s^* = area of prestressing steel = 2.45 in.^{2}

b = width of flange or flanged member = 80 in.

d = distance from extreme compressive fiber to centroid of the prestressing force = 41.5

f_c' = compressive strength at 28 days = 5350 psi

f_s' = ultimate strength of prestressing steel = 270 ksi

ϕ = strength capacity reduction factor (factory produced precast prestressed concrete members) = 1.0

p^* = ratio of prestressing steel

$= A^*s/(bd) = 2.45 \text{ in.}^2/(80 \text{ in.} * 41.5 \text{ in.}) = 7.38 \times 10^{-4}$

f_{su}^* = average stress in prestressing steel at ultimate load

$= f_s' (1 - 0.5 (p^* f_s')/f_c')$

$= 270 \text{ ksi } (1 - 0.5 (7.38 \times 10^{-4} * 270 \text{ ksi})/(5.35 \text{ ksi}))$

$= 265$ ksi

$M_u = 2.45 \text{ in.}^2 * 265 \text{ ksi} * 41.5 \text{ in.}$

$(1-0.6 * 7.38 \times 10^{-4} * 265 \text{ ksi}/5.35 \text{ ksi})$

$= 26{,}400$ kips

M_{DL} = 3800 in.-kips

M_{AL} = 22,600 in.-kips

For a 192 in. shear span, P_{ult} = 117 kips. This corresponds to the value shown in Table 5.11.

Strand stress = 270 ksi

Applied load = 117 kips

The results are plotted in Fig. 5.5 where a stress range of 43 ksi is predicted using the graphical method. The nonlinear program PBEAM [85] predicted a strand stress range of 43.4 ksi. This indicates that reasonable values can be calculated manually for designers who do not have access to programs such as PBEAM.

5.4.5.3 Effect of Passive Steel and Prestress Losses on Stress Range

Strand stress ranges are directly influenced by prestress losses and the presence of passive reinforcement. Figure 5.2 shows dramatically how variations in prestress losses can substantially affect strand stress ranges. As losses increase above the expected value, strand stress ranges can increase drastically. Figure 5.3 shows how passive reinforcement can reduce stress ranges both by controlling prestress losses and by providing a greater area of steel to carry the tension force (this reduces the strand stress since it increases the effective tension area).

5.4.5.4 Graphical Presentation of Beam Fatigue Results

Figure 5.6 shows the beam fatigue results plotted on a log-log scale, which is typical of fatigue plots. Failure was defined as the point that fatigue testing was stopped, which was characterized by a drastic increase in centerline deflection at the maximum static load. It was also often accompanied by massive concrete spalling and audible wire breaks. Analytical stress ranges are plotted with circles, triangles, and squares. Maximum measured static or dynamic stress ranges are connected to the analytical points with solid lines. In only one specimen did measured stress range values significantly exceed the analytical values. All beams in which the analytical stress range exceeded 10 ksi experienced fatigue failures.

5.4.5.5 Effects of Occasional Overloads on Fatigue Life

Table 5.5 shows that the main variable between Specimens A-22-MP-6.2-OL-2.84 and A-22-NP-6.2-NO-5.00 was the presence of a few modest static overloads. Figure 5.7 shows that Specimen A-22-NP-6.2-OL-2.84 was loaded approximately 20 percent above the maximum fatigue load during the initial and subsequent static tests. As a result of the initial overload, flexural cracking occurred. The specimen withstood 2.84 million cycles before fatigue failure. The maximum load during the static ultimate test was 49 kips. Specimen A-22-NP-6.2-NO-5.00 was not overloaded (loads above the maximum fatigue load) prior to the ultimate test after 5.00 million cycles, as shown in Fig. 5.7. Flexural cracking occurred after 1180 fatigue cycles at a maximum nominal concrete tensile stress of $6.2\sqrt{f'_{ct}}$. The ultimate load was 79 kips (60 percent greater

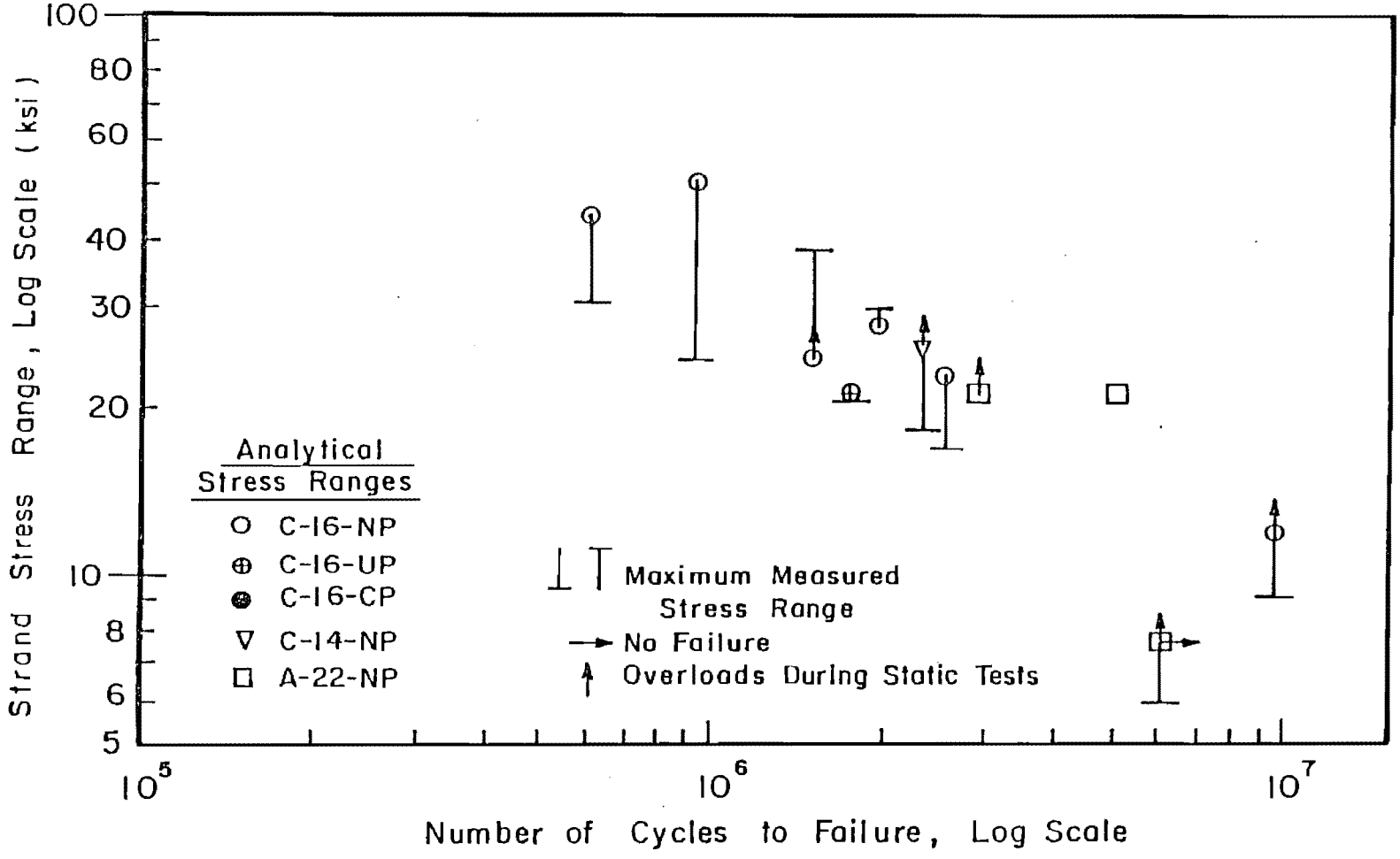

Fig. 5.6 Analytical and measured strand stress ranges versus number of cycles to failure

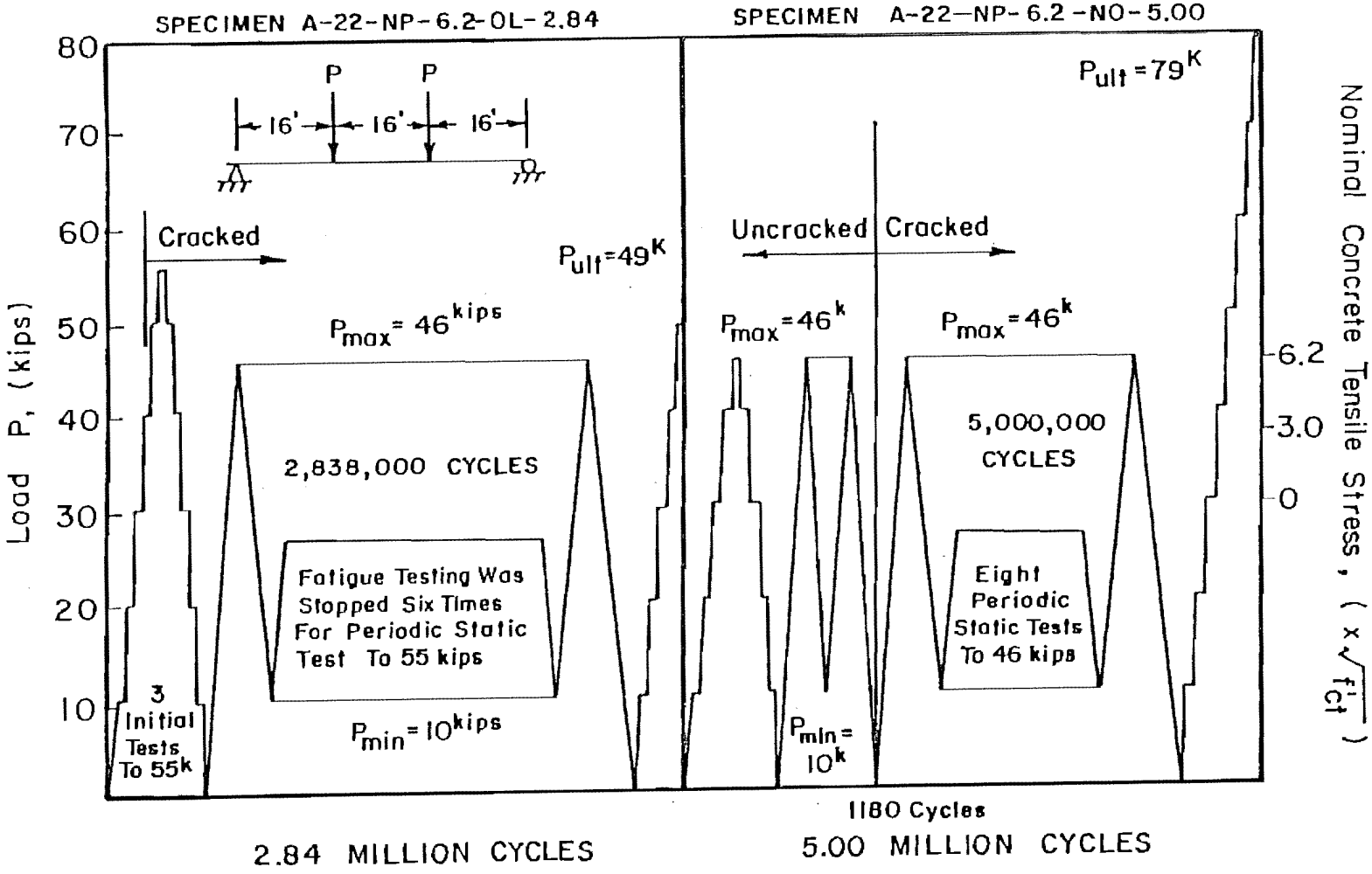

Fig. 5.7 Effects of modest overloads on fatigue life

than the value for the occasionally overloaded companion specimen). A comparison between these two specimens, which were cast at the same time using a commercial long line stressing bed, indicates that very occasional overloads (in this case 20 percent above the fatigue load) can drastically reduce fatigue life. The large length of prestressing strand tested in a beam specimen probably reduces the inherent randomness of fatigue data so the presence of overloads appears to be extremely detrimental.

Ozell, Ardaman, and Abeles explained how overloads and varying load ranges reduce fatigue life. Ozell and Ardaman [65] (Section 2.3.2) stated that:

> The fracture of the wires at points bordering the tension cracks in the beam substantiates the belief that these cracks form stress concentrations in the strands, especially as a result of overloads, rendering them vulnerable to fatigue and ultimately causing the breaking of wires.

Abeles [15] (Section 2.2.1.4, "Bond Between Concrete and Steel") attributed the problem to bond deterioration, reporting that "varying ranges of loads intensify bond deterioration." He [15] further states that:

> It may be expected that with excellent bond the conditions in prestressed concrete beams are better than with the steel tested in the air, whereas with very bad bond the conditions are considerably worse....
>
> ... The early occurrence of the bond break may reduce the fatigue life of a prestressed concrete beam to only 40% of that which it would have if bond break did not occur.

The fatigue life of Specimen A-22-NP-6.2-OL-2.84, which experienced overloads 20 percent above the cyclic load nine times during static tests, was approximately 60 percent of the fatigue life of the companion specimen with no overloads. These test results indicate that even a small number of overload cycles can be extremely detrimental to a single girder. To put this into perspective, the reader must remember that in an actual bridge, loads are not carried by a single girder. There is lateral distribution, so overloads may not be as detrimental. Also, the overload produced a maximum nominal concrete tensile stress of $10\sqrt{f'_{ct}}$.

5.4.5.6 Beam Fatigue Results and Failure Models

The background for a rational fatigue design approach for pretensioned concrete bridge girders is presented in this section. The data base includes the eleven full size flexural specimens reported on

in this study and the six full size specimens tested by Rabbat et al. [76]. Where strand stress ranges are used, the analytical results determined from program PBEAM will be utilized for the eleven specimens tested in this program. For the Rabbat et al. specimens, the reported measured experimental stress ranges, as shown in Table 5.6, will be used. The corresponding analytical values could not be determined because of the lack of information on material properties, loading times, and actual prestress losses.

5.4.5.6.1 Evaluation of Fatigue Results Using Nominal Concrete Tensile Stress

AASHTO Specifications [7,8] allow $6\sqrt{f'_c}$ tension stress in the extreme fibers of the precompressed tension zone of prestressed concrete flexural members. It has been implicitly assumed that fatigue failure would not occur at this design level for a significant number of cycles. The maximum nominal concrete stresses for the specimens tested in this program are shown in Table 5.7. Figure 5.8 shows a plot of nominal concrete tensile stress as a function of $\sqrt{f'_{ct}}$ versus fatigue life. It indicates that fatigue failures will occur at and below the AASHTO design limit of $6\sqrt{f'_c}$ and can occur at $6\sqrt{f'_c}$ at less than 2 million cycles. The figure also shows that at a maximum nominal tensile stress of approximately $5.5\sqrt{f'_{ct}}$ one specimen failed after 2.29 million cycles and another failed after 9.43 million cycles. This is approximately a fourfold difference and indicates that this design parameter is inappropriate. Figure 5.9 shows the same data plotted using maximum nominal concrete tensile stress (in psi units) versus the fatigue life as the variables. Again, the scatter is unacceptable.

The primary disadvantage of using nominal concrete stress as the main design parameter is that once a section cracks, the concrete no longer resists tensile forces. The parameter is then meaningless. It has been shown that cracking can occur due to random, unpredictable overloads, fabrication errors, time effects, and cyclic deterioration of concrete. An alternative criteria is needed to evaluate the fatigue strength of prestressed concrete bridge girders.

5.4.5.6.2 Evaluation of Fatigue Results Using Strand Fatigue Test Models and Structural Steel Fatigue Models

Flexural fatigue failure of prestressed concrete girders is primarily caused by fatigue failure of prestressing steel. Strand stress ranges that are adequate to cause fatigue failure can occur once a member is cracked and the prestressing steel is required to provide the entire internal flexural tension force. Such fatigue failures would not be a problem if the girders could absolutely be protected from cracking. Because failure is by brittle fatigue fracture of prestressing steel with no apparent fretting or corrosion fatigue, it

TABLE 5.6 Fatigue Results of Specimens Tested by Rabbat et al. [76]

Specimen	Nominal Concrete Tensile Stress (x f'_c)	Measured Strand Stress Range at 2.5 Million Cycles (ksi)	Fatigue Life (millions)	Ultimate Load as a Percentage of Calculated Load (percent)	Ultimate Deflection (in.)
G10	6	19.0	3.63	59	1.4
G10A	0	NI	5.0(NF)	104	21
G11	6	18.2	3.78	41	1.2
G12	0	15.5	5.0(NF)	102	31
G13	6	20.1	3.20	NUT	NUT
G14	0	12.8	5.0(NF)	104	28

NI = No strain gage instrumentation

NF = No fatigue failure

NUT = No ultimate test

TABLE 5.7 Maximum Nominal Concrete Tensile Stresses

Specimen	Maximum Nominal Concrete Tensile Stress During Fatigue Loading ($x\sqrt{f'_{ct}}$)	(psi)	Fatigue Life (millions)
C-16-NP-10.5-NO-0.58	10.5	770	0.58
C-16-NP-7.2-OL-1.48	7.2	570	1.48
C-16-NP-10.1-NO-0.91	10.1	820	0.91
C-16-NP-6.0-NO-1.91	6.0	500	1.91
C-14-NP-5.5-OL-2.29	5.5	420	2.29
A-22-NP-6.2-OL-2.84	6.2	520	2.84
A-22-NP-6.2-NO-5.00	6.2	520	5.00
A-22-NP-3.5-OL-5.95(NF)	3.5	290	5.95(NF)
C-16-UP-8.0-NO-1.73	8.0	610	1.73
C-16-CP-7.2-NO-2.54	7.2	610	2.54
C-16-CP-5.5-OL-9.43	5.5	410	9.43

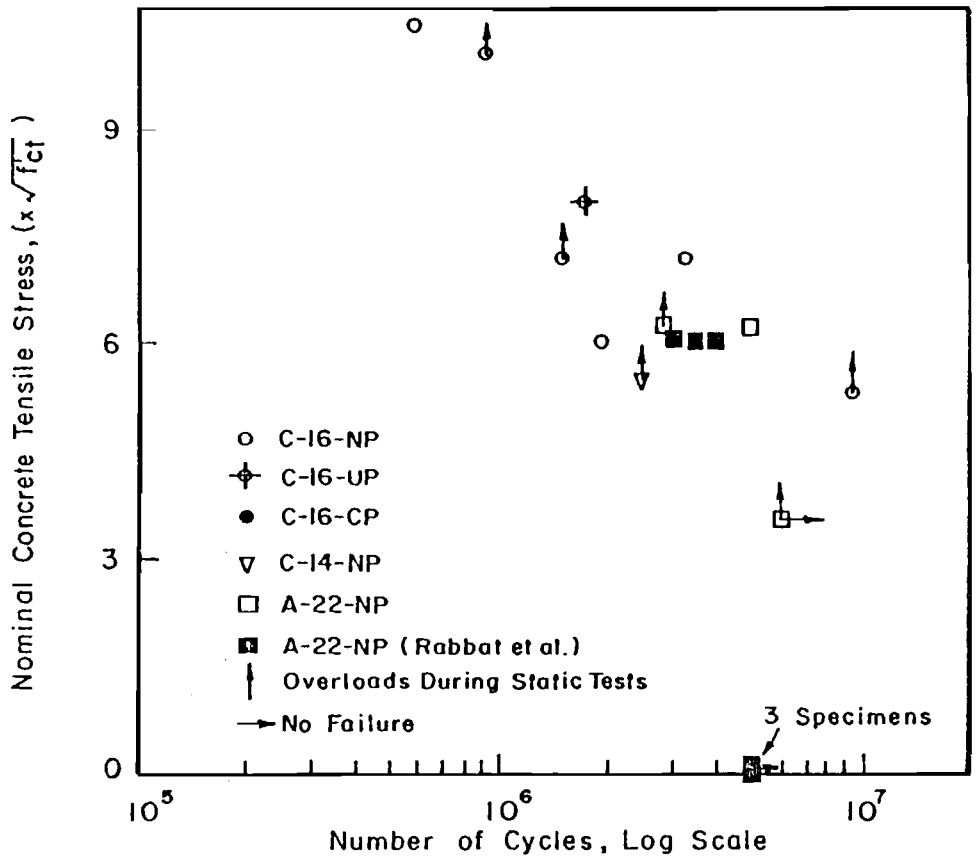

Fig. 5.8 Nominal concrete tensile stress as a function of $\sqrt{f'_{ct}}$ versus number of cycles to failure

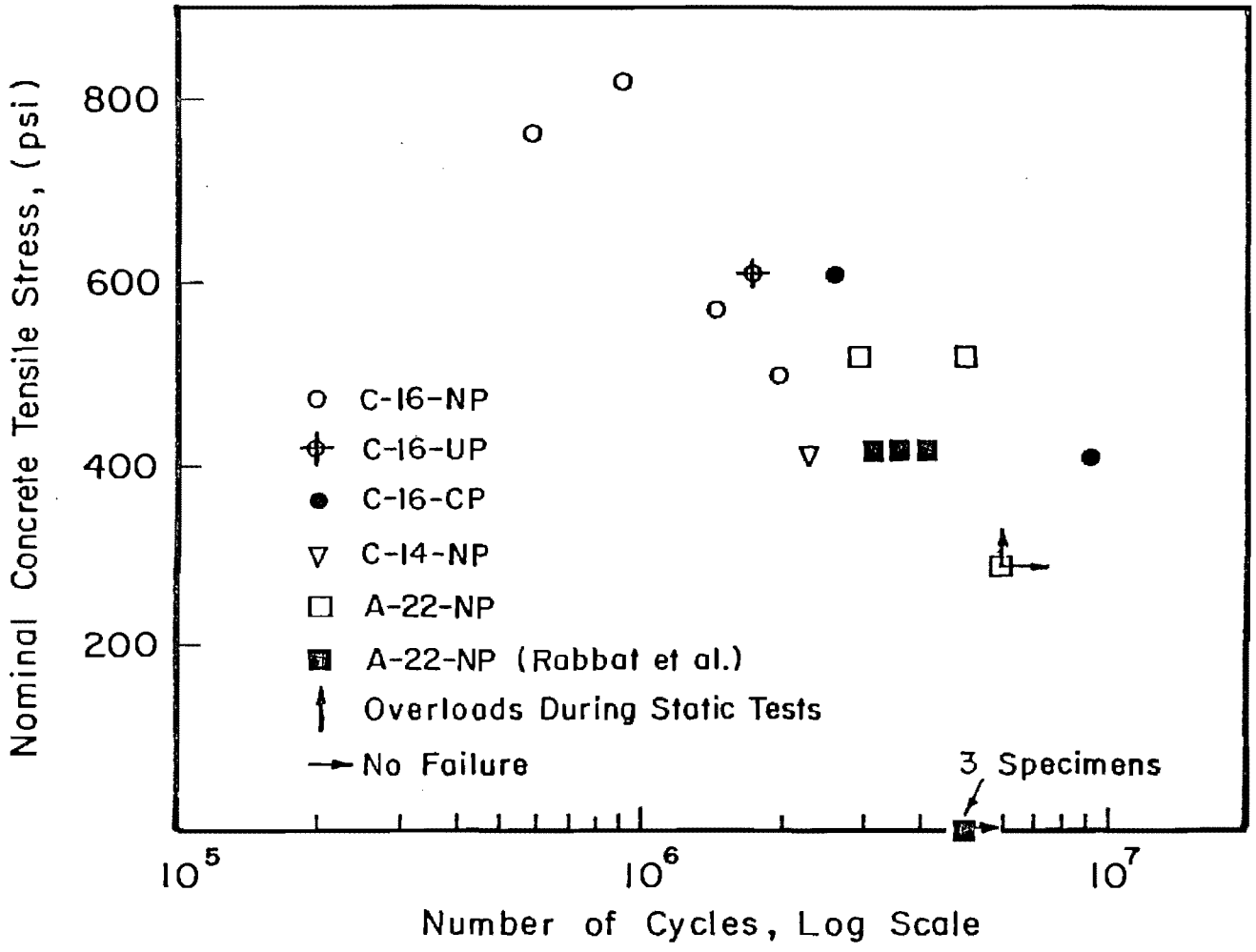

Fig. 5.9 Nominal concrete tensile stress in psi versus number of cycles to failure

seems logical that fatigue results for individual strands could be used to predict fatigue lives of pretensioned concrete members. Paulson [73] reviewed numerous strand fatigue test programs and generated additional data points to add to the data base. His recommended model and the data used to develop it are shown in Fig. 5.10. Only strand fatigue failures occurring outside the gripping regions are included. The strand fatigue model is a conservative, one-sided tolerance limit where there is a 95 percent probability that at least 97.5 percent of the distribution will be above the limit. An endurance limit of 20 ksi was suggested, but not verified by Paulson. This endurance limit has been dropped from the model shown here as it conflicts with beam data.

Beam fatigue results are plotted in Fig. 5.11 along with Paulson's strand fatigue model and the AASHTO Category B [7,8] fatigue design model for redundant load path structures. The previous scatter which was shown in Figs. 5.8 and 5.9, where nominal concrete tensile stress was the major variable, is greatly reduced. All but two fatigue failure specimens are clustered in a band, close to and on the conservative side of the strand fatigue model modified to have no endurance limit. The two specimens which are on the unconservative side fall reasonably close to the line (3 to 4 ksi off). The strand model appears to be more accurate for pretensioned concrete members that contain prestressing strand than the AASHTO Category B model for structural steel. However, presentation of the closely related AASHTO Category B values suggests a way to tie any pretensioned concrete girder fatigue criteria to the larger problem associated with predicting fatigue loading in terms of type highway and daily truck traffic counts.

5.4.5.6.2.1 Premature Failure of Two Specimens with Passive Reinforcement

The two specimens which experienced failures that plot on the unconservative side of the strand fatigue model both contained passive reinforcement. The passive reinforcing steel stress ranges were similar to the strand stress ranges shown in Table 5.5 (Specimen C-16-UP-8.0-NO-1.73, S_R = 20.7 ksi, Specimen C-16-CP-5.5-OL-9.43, S_R = 11.7 ksi) and are at or below the reinforcing steel fatigue endurance limit [19,42] of approximately 22 ksi. The two specimens failed prematurely for different reasons. Figure 5.12 indicates that in Specimen C-16-UP-8.0-NO-1.73 the passive reinforcement, which was concentrated near the bottom fiber of the girder, was effective in controlling crack widths (and strand stress ranges) only at the level of the passive steel. It was not effective in controling cracking in the web and upper portion of the lower flange. The post mortem investigation of this girder revealed that none of the passive reinforcing steel failed in fatigue and that only 15 percent of the wire fatigue fractures were at the level of the reinforcing steel although 25 percent of the strands were in this region. The reinforcing steel controlled strand stresses and crack

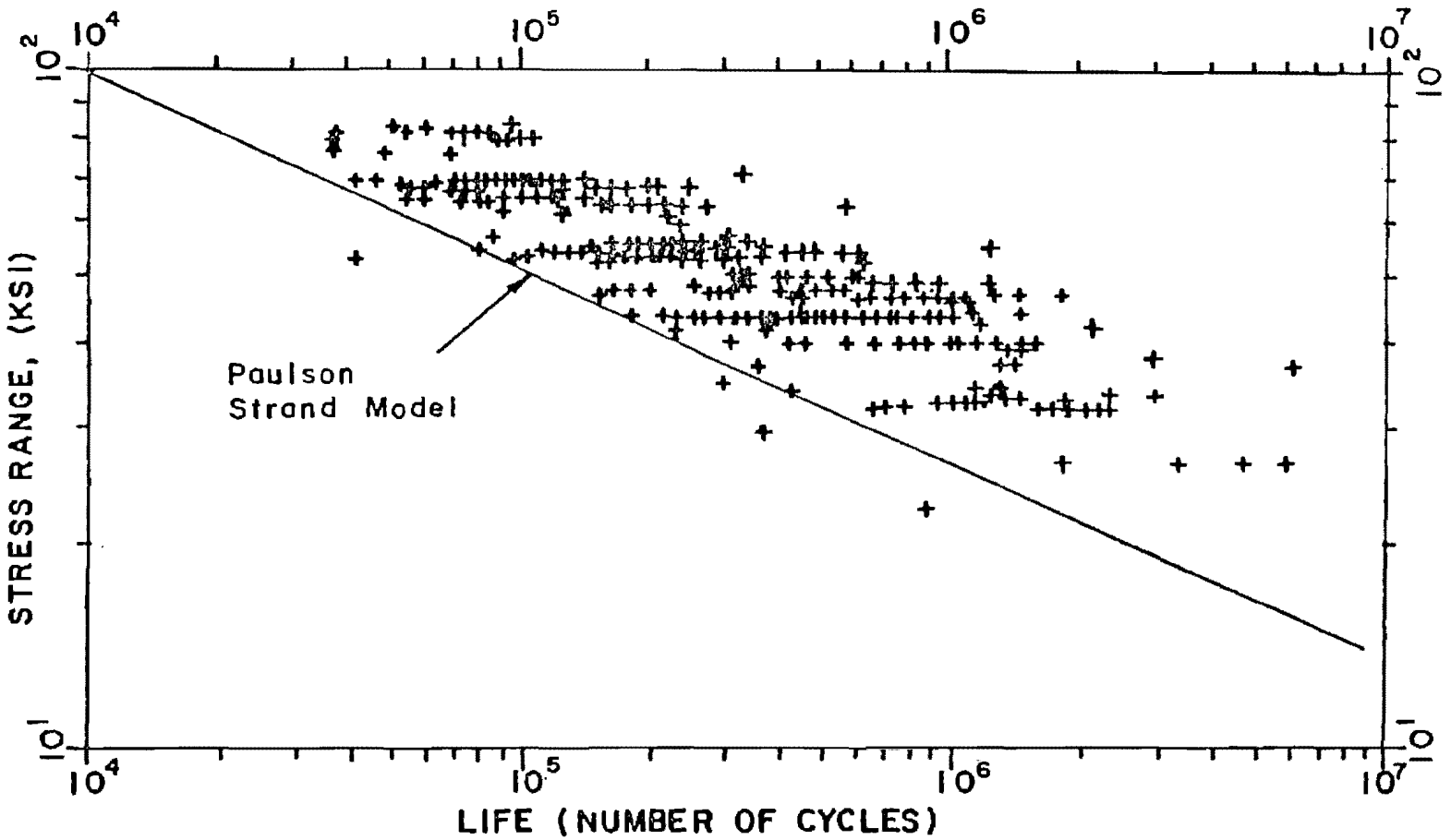

Fig. 5.10 Paulson's "in-air" strand fatigue model

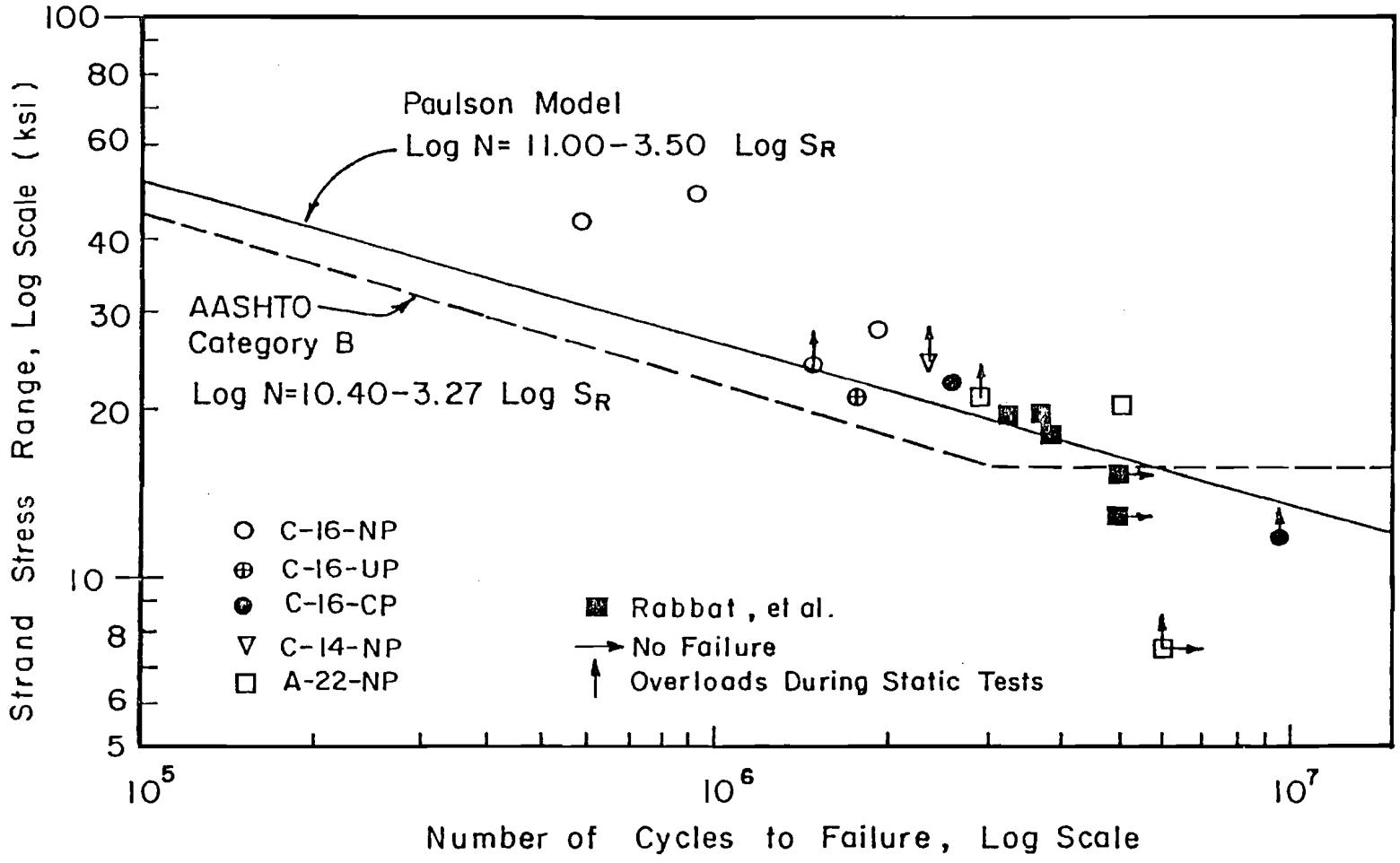

Fig. 5.11 Beam results with Paulson's fatigue model and AASHTO Category B (nonredundant load path structures) fatigue models

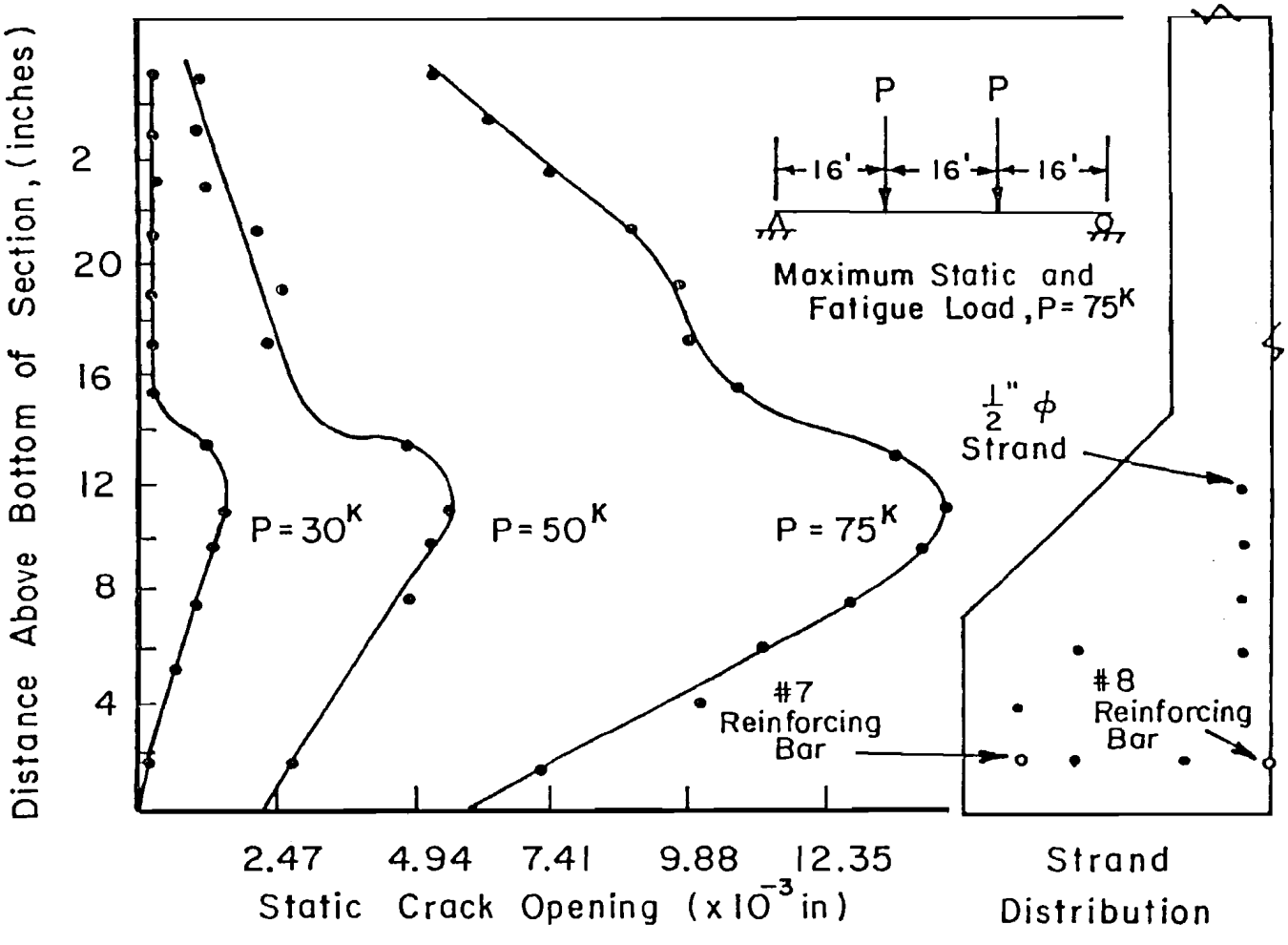

Fig. 5.12 Crack opening profile at various loads for Specimen C-16-UP-8.0-NO-1.73

widths in the bottom of the section where it was placed but not elsewhere.

Specimen C-16-CP-5.5-OL-9.43 failed somewhat prematurely due to the effect of the occasional modest overloads and the local high reinforcing steel stresses which occurred as a result of strand bond deterioration during the static load cycles. Occasional overloads accelerated the crack propagation. Gerwick and Venuti [39] (Section 2.2.1.4) state that:

> Bond progressively is lost along the steel, particularly along smooth bars, strand, and wire.... Due to slippage of the prestressing steel, the conventional unstressed steel usually is subjected to a slightly higher stress range.

Figure 5.13 indicates an unloading of the strand and a transfer of tension forces from prestressing steel to reinforcing steel after cracking for Specimen C-16-CP-5.5-OL-9.43 during the initial loading cycle. Figure 5.14 shows hysteretic loops indicating a gradual transfer of stress from strand to bars after cycling had begun. Notice how the strand stress decreases during progressive cycles. Reinforcing steel stresses must increase to maintain equilibrium of the section. The resulting reinforcing bar stress range could be safely above the analytically predicted value of 11.7 ksi because the endurance limit for reinforcement is approximately 20 ksi [19,42].

Occasional overloads, as described previously, force crack propagation and thus intensify bond deterioration. This is probably the reason Specimen C-16-CP-5.5-OL-9.43 (which had a few occasional overloads during static tests) failed prematurely while Specimen C-16-CP-7.2-NO-2.54 (which did not experience overloads during static testing) did not. Further evidence of bond deterioration of prestressing steel, and a accompanying increase in reinforcing steel stress can be seen in Fig. 5.15 which contrasts locations of reinforcing steel and wire fatigue fractures at the principal failure cracks for the two C-16-CP specimens. Notice the large number of reinforcing steel fatigue fractures for both specimens. Specimen C-16-CP-7.2-NO-2.54 had an analytically predicted reinforcing steel stress range of approximately 23 ksi, which is close to the endurance limit but should not cause this large number of fatigue failures at only 2.54 million cycles. Specimen C-16-CP-5.5-OL-9.43 had an analytically predicted reinforcing steel stress range of only 12 ksi, which is below the endurance limit and should not cause failures at any number of cycles.

Specimen C-16-CP-7.2-NO-2.54 had slightly increased reinforcing steel stress range as a result of strand slip. The result was possibly a slight decrease in fatigue life. Specimen C-16-CP-5.5-OL-9.43 had a significant increase in reinforcing steel stress range due to strand slip and more importantly modest overloads during occasional static load

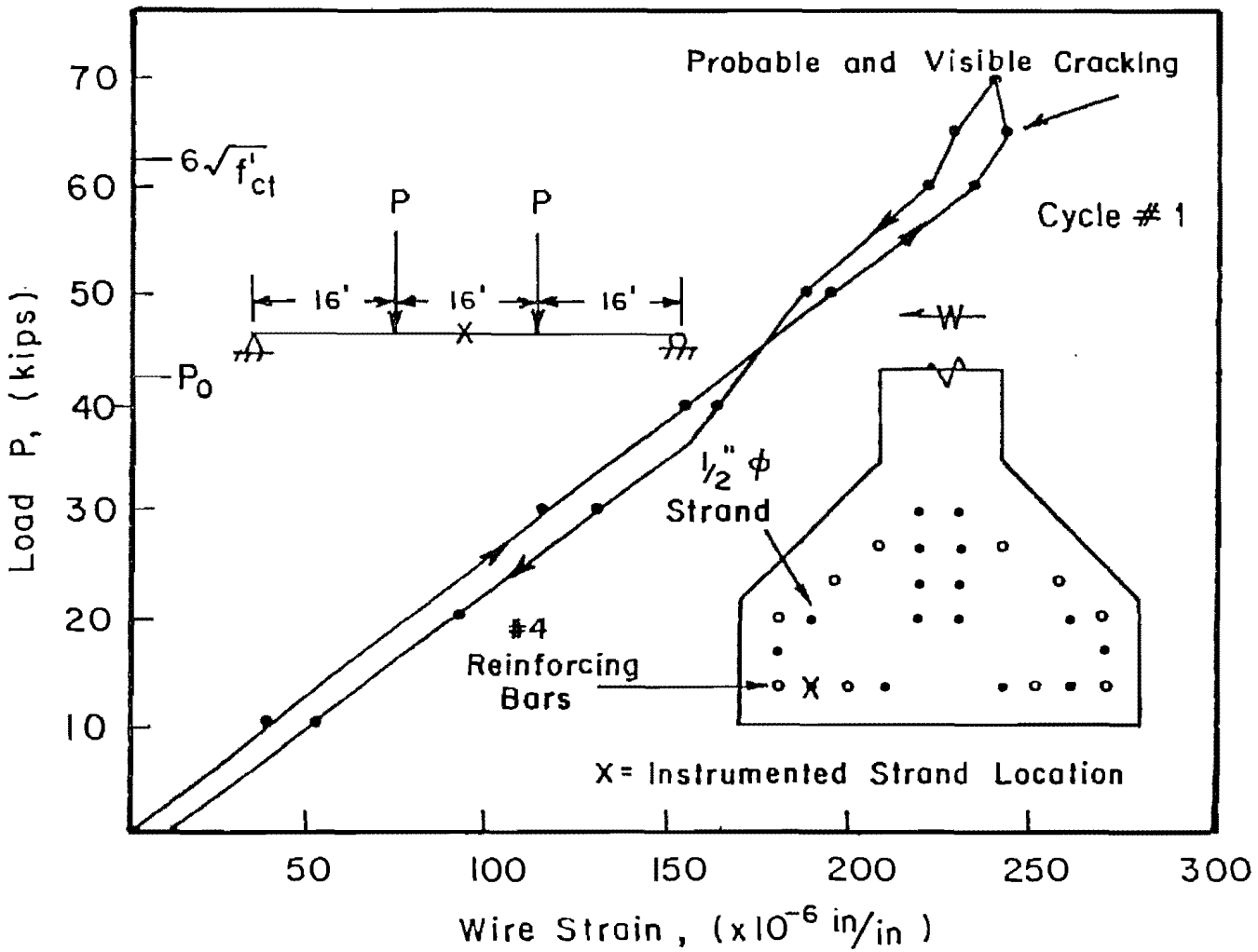

Fig. 5.13 Transfer of tension load from prestressing strands to reinforcing bars after flexural cracking for Specimen C-16-CP-5.5-OL-9.43

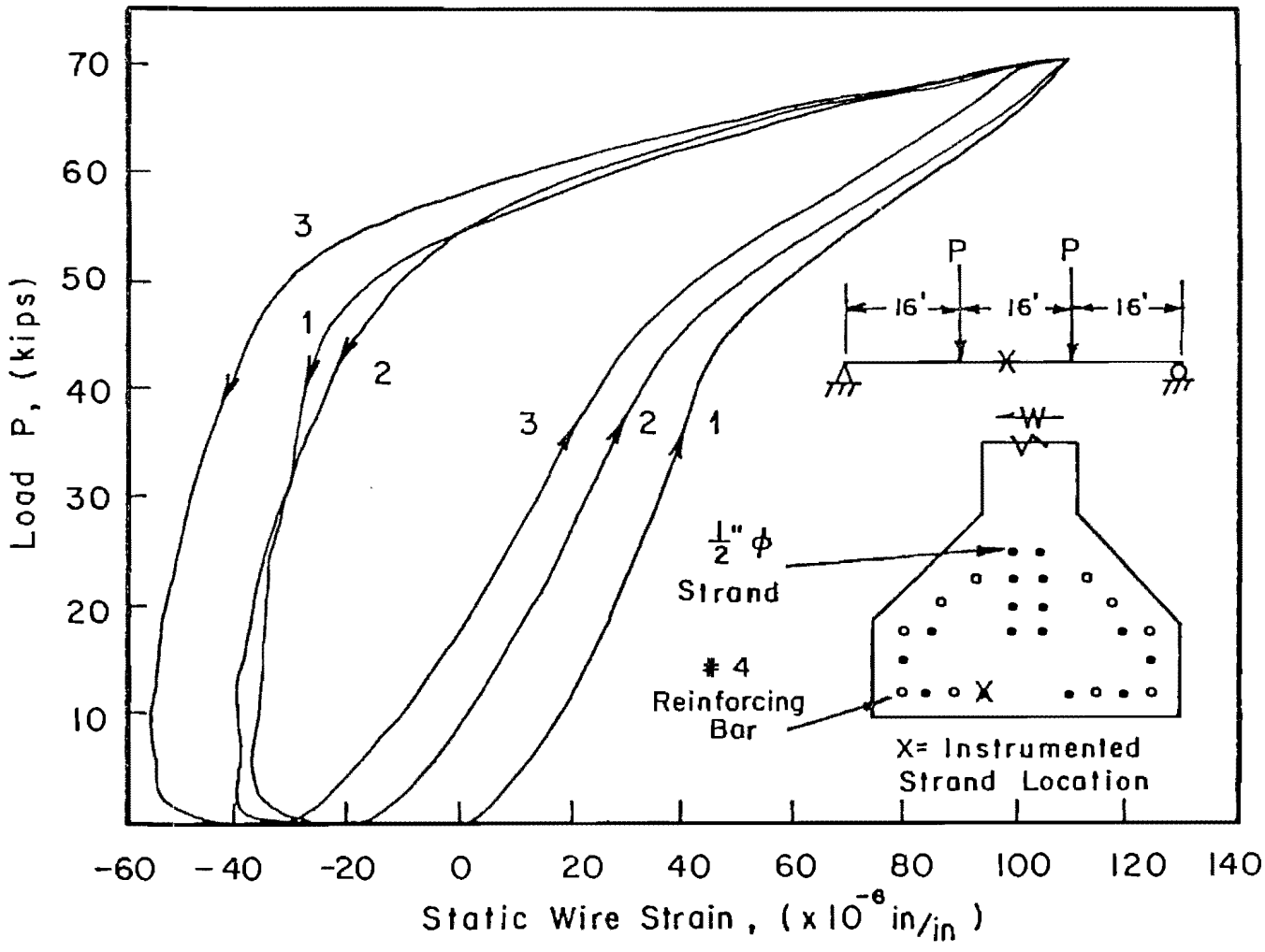

Fig. 5.14 Hysteretic loops during static cycles

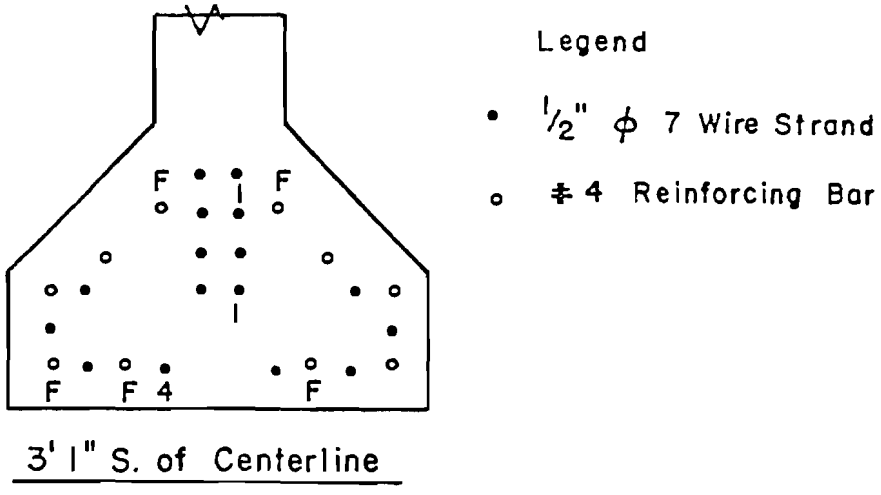

a) Failure Location For Specimen C-16-CP-7.2-NO-2.54

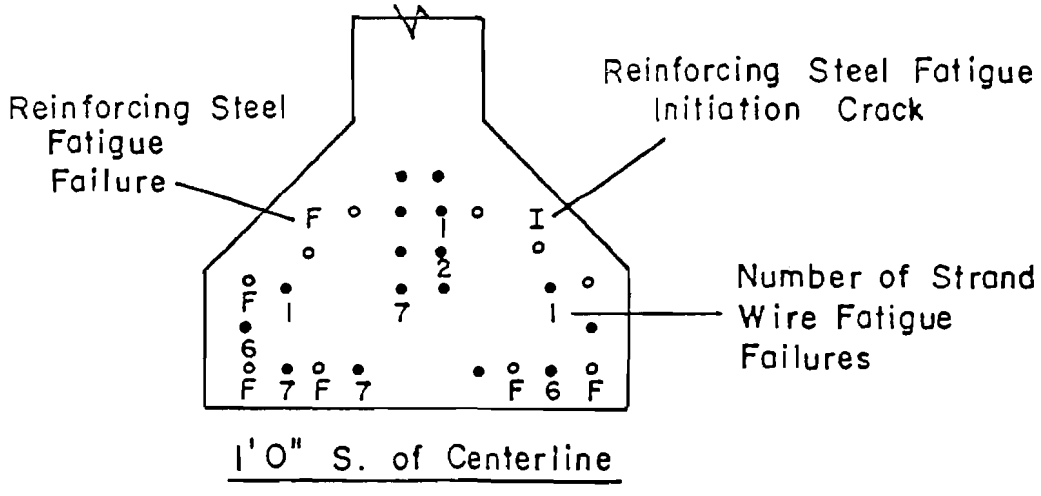

b) Failure Location For Specimen C-16-CP-5.5—OL-9.43

Fig. 5.15 Location of reinforcing steel and wire fatigue fractures

cycles. The result was marked reinforcing steel fatigue failures and a marked decrease in fatigue life.

5.4.5.6.2.2 Comments on Strand and Structural Steel Fatigue Models

In general, the strand fatigue model is a good predictor of beam fatigue lives. The statistical shift in Paulson's model to obtain the 95 percent confidence level appears to eliminate any length affects. His suggested 20 ksi endurance limit does not appear to be valid. Paulson's suggested limit lacked experimental basis, as shown in Fig. 5.10, and appears to be too high. The AASHTO endurance limit for redundant load path steel structures (Category B) of 16 ksi appears valid for application to pretensioned concrete girders if a fatigue life of 6 million cycles is considered adequate for all cases. A 16 ksi effective endurance limit for the strand fatigue model would also be adequate at 6 million cycles. The 6 million cycle fatigue life was selected arbitrarily and is probably sufficiently high for most bridge applications. It is very disturbing that Specimen C-16-CP-5.5-OL-9.43 failed below the AASHTO Category B endurance limit. This suggests that even 10 million cycles of fatigue testing may not be sufficient to define an endurance limit.

The strand fatigue model is applicable to beam fatigue results with several limitations. Prestress losses and actual girder loads must be known accurately. The loads actually applied to highway girders may include overloads above legal limits. Design procedures should consider such occasional overloads. Inclusion of passive reinforcement provides substantial toughness to resist such occasional overloading. Actual distribution factors are also required to determine realistic girder loads.

5.4.5.6.3 A Nominal Concrete Stress Limit for Design

Prestressed concrete designers in the United States are accustomed to using nominal concrete tensile stresses for design criteria. As stated previously, this design parameter is meaningless once a section cracks. A designer thus has two choices: he may perform a cracked section analysis to determine strand stress ranges and the accompanying fatigue life based on the Paulson strand model or he may limit nominal concrete tensile stresses to a very low value such that even under occasional overloads the resulting strand stress ranges will not be sufficient to cause fatigue problems.

A nominal concrete tensile stress of $3\sqrt{f'_c}$ produces cracked section strand stress ranges for loads above zero tension of less than 4 ksi. Assuming girder and slab 28 day compression strengths of 5000 psi and 3000 psi, respectively, the cracked C-16-NP specimens would have a

strand stress range from zero tension to a load that produced a nominal concrete stress of $3\sqrt{f'_c}$ of only 3 ksi. The C-16 specimens with passive steel would have even lower stress ranges as a result of the passive steel. The cracked C-14-NP specimen would have a strand stress range of less than 4 ksi for loads between zero tension and loads that produced a tensile stress of $3\sqrt{f'_c}$, and the cracked A-22-NP specimens would have a stress range of approximately 3 ksi for these same loads.

With an unusually high precompression stress in the bottom of a girder of 1000 psi and assuming the strands were at that level with a modular ratio of 7.2 ($29{,}000 \text{ ksi}/57\sqrt{5000}$), the strand stress range from zero live load to zero tension would be 7.2 ksi (7.2 * 1.0 ksi). When added to the maximum cracked section stress range (for loads above zero tension) of 4 ksi, this produces strand stress ranges of less than 12 ksi, which is below the suggested 6 million cycle effective endurance limit of 16 ksi.

The suggested maximum nominal concrete tensile stress of $3\sqrt{f'_c}$ was the AASHTO limit prior to 1971 [1] and is suggested by ACI Committee 443 [24], Concrete Bridge Structures, as the limit for prestressed flexural members without bonded passive reinforcement. The $3\sqrt{f'_c}$ limit would work fine for the four cross sections tested. For new and different shapes and steel distributions, a cracked section analysis would have to be performed once for each section and steel distribution to determine if strand stress ranges were sufficiently low. Prestress losses and actual dead and live loads would have to be known accurately as with the more rational strand fatigue method. If a nominal tensile stress limit is used to implicitly guard against fatigue failure, the limit should be $3\sqrt{f'_c}$ in the absence of adequate, well distributed and well confined passive reinforcement.

5.4.6 Cracked Section Stiffness Indices (EI_{cr})

To calculate deflections of a girder in a cracked state, a nonlinear calculation can be performed or cracked section stiffness indices (EI) can be used. Considering the randomness of flexural fatigue crack spacing, as well as the variability of crack widths and heights, the empirically derived cracked section stiffness index is probably sufficient.

For loads less than the zero tension load, the entire section is in compression and linear elastic section properties can be assumed for calculating deflections. Section 5.4.1 indicates that theoretical stiffness indices (EI_e) can be used to predict actual deflections quite closely for loads less than the decompression load (zero tension load). Once the zero tension load is reached, flexural cracks begin to open and a reduced section resists applied loads. The cracked section stiffness indices in Table 5.8 were computed for loads above zero tension ($P_s - P_o$). They assume a cracked section between load points, an uncracked

TABLE 5.8 Cracked Section Stiffness Indices (EI_{cr})

Specimen	Maximum Static Load Above P_o $P_s - P_o$ P_{so} (kips)	Difference in Centerline Deflection Between P_s & P_o Δ_{so} (in.)	Computed Cracked Section EI from Measured Deflections, EI_{cr} ($x10^8$k-in.^{2})	Computed Uncracked Section EI from Measured Deflections, EI_e ($x10^8$k-in.^{2})	$\frac{EI_{cr}}{EI_e}$
C-16-NP-10.5-NO-0.58	36.8	0.68	2.7	12.9	0.21
C-16-NP-7.2-OL-1.48	37.0	0.24	9.6	12.5	0.77
C-16-NP-10.1-NO-0.91	36.5	0.64	2.9	11.3	0.25
C-16-NP-6.0-NO-1.91	30.0	0.25	6.0	11.6	0.52
C-14-NP-5.5-OL-2.29	24.0	0.23	5.7	13.0	0.44
A-22-NP-6.2-OL-2.84	25.0	0.32	4.4	8.5	0.52
A-22-NP-6.2-NO-5.00	16.0	0.18	5.2	8.8	0.59
A-22-NP-3.5-OL-5.95(NF)	25.0	0.31	4.5	9.2	0.49
C-16-UP-8.0-NO-1.73	27.0	0.36	4.0	10.5	0.38
C-16-CP-7.2-NO-2.54	27.5	0.35	4.2	11.1	0.38
C-16-CP-5.5-OL-9.43	22.5	0.21	6.0	12.0	0.50
					====
			NP Specimens		$\bar{x}$ = 0.47
					σ = 0.18
			P Specimens		$\bar{x}$ = 0.42
					σ = 0.07

$$EI_{cr} = \frac{(41472 \text{ in.}^2 - x^2/2)\, P_{so}\, x}{\Delta_{so} - P_{so}\, x^3/(3 * EI_e)}$$

x is the shear span length in inches

section outside the load points, and linear load-deflection behavior after the flexural cracks open at the zero tension load. The equation at the bottom of Table 5.8 was derived using the moment-area method.

The average cracked section stiffness index (EI_{cr}) for the specimens with no passive reinforcement was 47 percent of the measured uncracked stiffness index (EI_e) with a standard deviation of 18 percent. The relatively large standard deviation reflects the scatter of the data. For the specimens with passive reinforcement, the mean was 42 percent, and the standard deviation was a much smaller 8 percent.

Figure 5.16 shows the stiffness index ratio (EI_{cr}/EI_e) plotted versus fatigue life. The ratio generally increases as fatigue life increases until approximately 3 million cycles. After 3 million cycles the ratio is approximately 0.50. This trend appears to be opposite of the logical trend of increased cracking and deflections (reduced EI_s) as cycling progresses. It must be remembered that fatigue life is a function of strand stress range. For long life specimens, the strand stress is low and hence less flexural cracking results. A cracked section stiffness index of approximately 50 percent of the uncracked value is probably a reasonable estimation in this case. For high stress ranges, extensive cracking occurs, deflections increase and fatigue occurs at a low number of cycles. Assuming a 93 percent confidence level, a cracked section stiffness index of 20 percent of the uncracked index is a conservative limit for estimating deflections for specimens without passive reinforcement. A cracked section stiffness of 30 percent should be used for girders with passive reinforcement. These reduced stiffnesses can thus be used to estimate deflections at loads above the zero tension load. These deflections are then added to elastic deflections at loads less than the zero tension load to obtain total deflections.

5.4.7 Number of Cycles to First Indication of Deterioration

For inspection purposes, it is useful to know the interval of time between first indication of fatigue distress and failure. With all members, visible flexural cracking preceded fatigue distress. The number of cycles to first indications of deterioration and the indicators are shown in Table 5.9. These slight changes ordinarily occur at approximately 70 percent of the fatigue life and are shown in Figs. 5.17 and 5.18.

Small changes are only apparent when strain gages and potentiometers are used, so they cannot be measured with in-service girders. Visible and audible indicators of deterioration, which are useful for inspection purposes, are shown in Table 5.10. The total number of cycles referenced in both tables is the fatigue life and indicates the end of fatigue testing. A significant loss of strength and extensive cracking had occurred by this time.

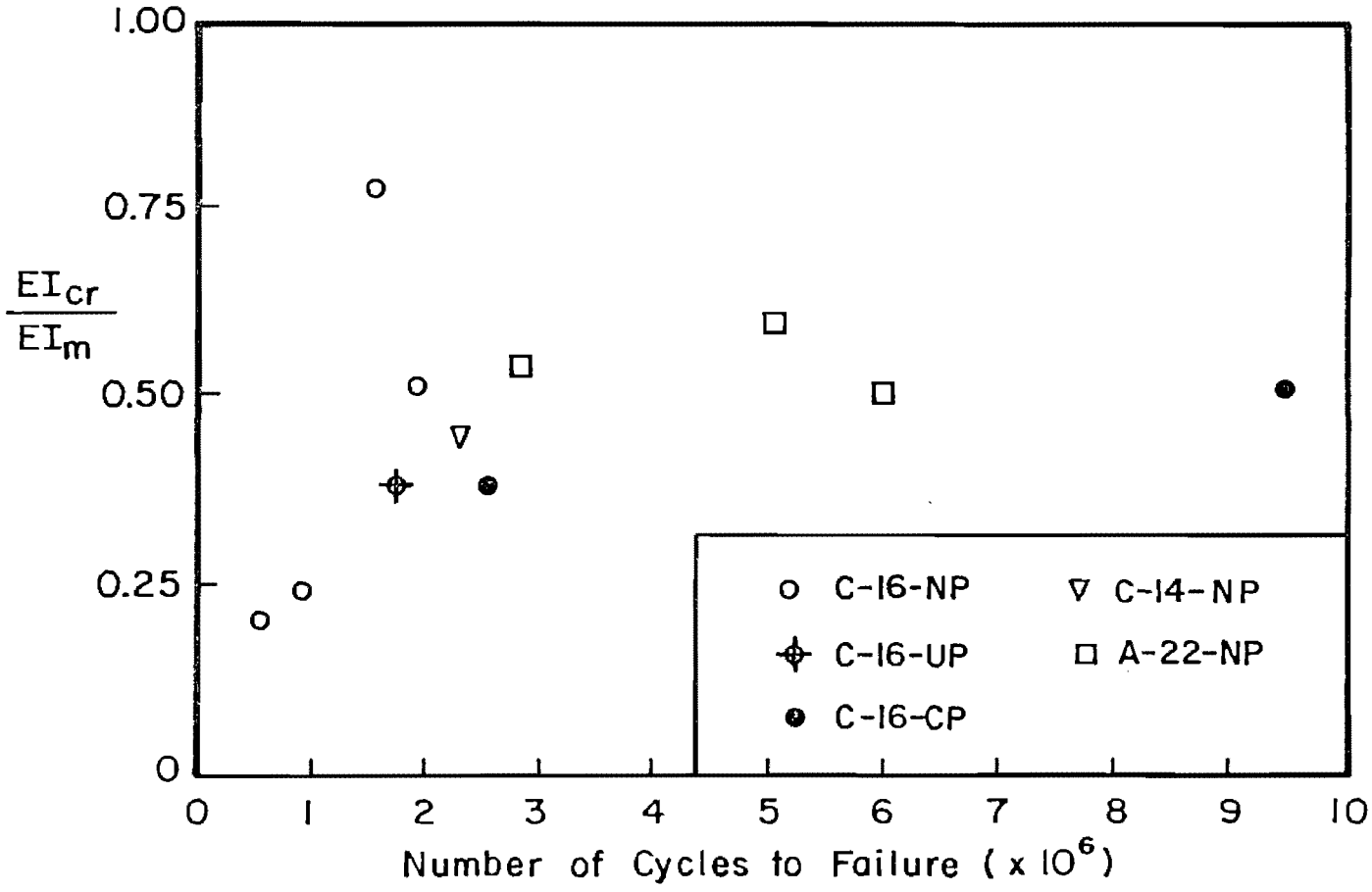

Fig. 5.16 Stiffness indices for cracked sections versus number of cycles

TABLE 5.9 Number of Cycles to First Indication of Deterioration

Specimen	First Indication of Deterioration		
	Indicator	Number of Cycles (millions)	Percentage of Total Number of Cycles
C-16-NP-10.5-NO-0.58	Increased centerline deflection	0.480	83
C-16-NP-7.2-OL-1.48	Increased centerline deflection	0.990	67
C-16-NP-10.1-NO-0.91	Increased centerline deflection	0.638	70
C-16-NP-6.0-NO-1.91	Increased centerline deflection	1.08	57
C-14-NP-5.5-OL-2.29	Increased static wire strain	1.03	45[b]
		2.02	62[c]
A-22-NP-6.2-OL-2.84	Increased crack width	1.38	49
A-22-NP-6.2-NO-5.00	Increased centerline deflection	4.50	90
A-22-NP-3.5-OL-5.95(NF)	Specimen did not experience fatigue failure		
C-16-UP-8.0-NO-1.73	Increased centerline deflection; increased wire strain	1.15	66
C-16-CP-7.2-NO-2.54	Increased centerline deflection; increased wire strain; increased crack width	2.30	91
C-16-CP-5.5-OL-9.43	Increased wire strain	5.00	53

[a] The last number in the alphanumeric specimen label indicates the number of cycles, in millions, to failure

[b] 2.29 million cycles at $5.5\sqrt{f'_{ct}}$

[c] 3.28 million total cycles

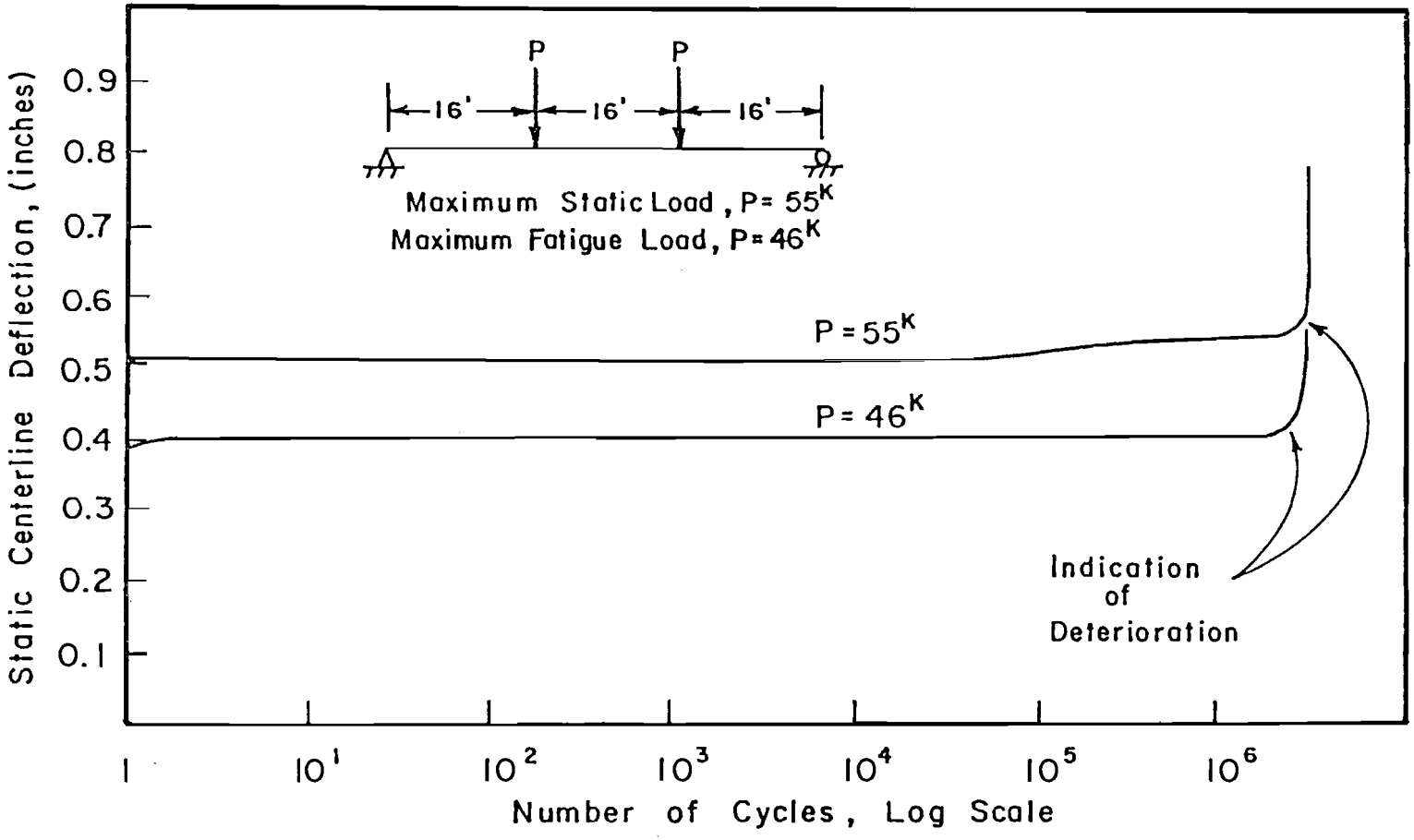

Fig. 5.17 Indication of deterioration for Specimen A-22-NP-6.2-OL-2.84

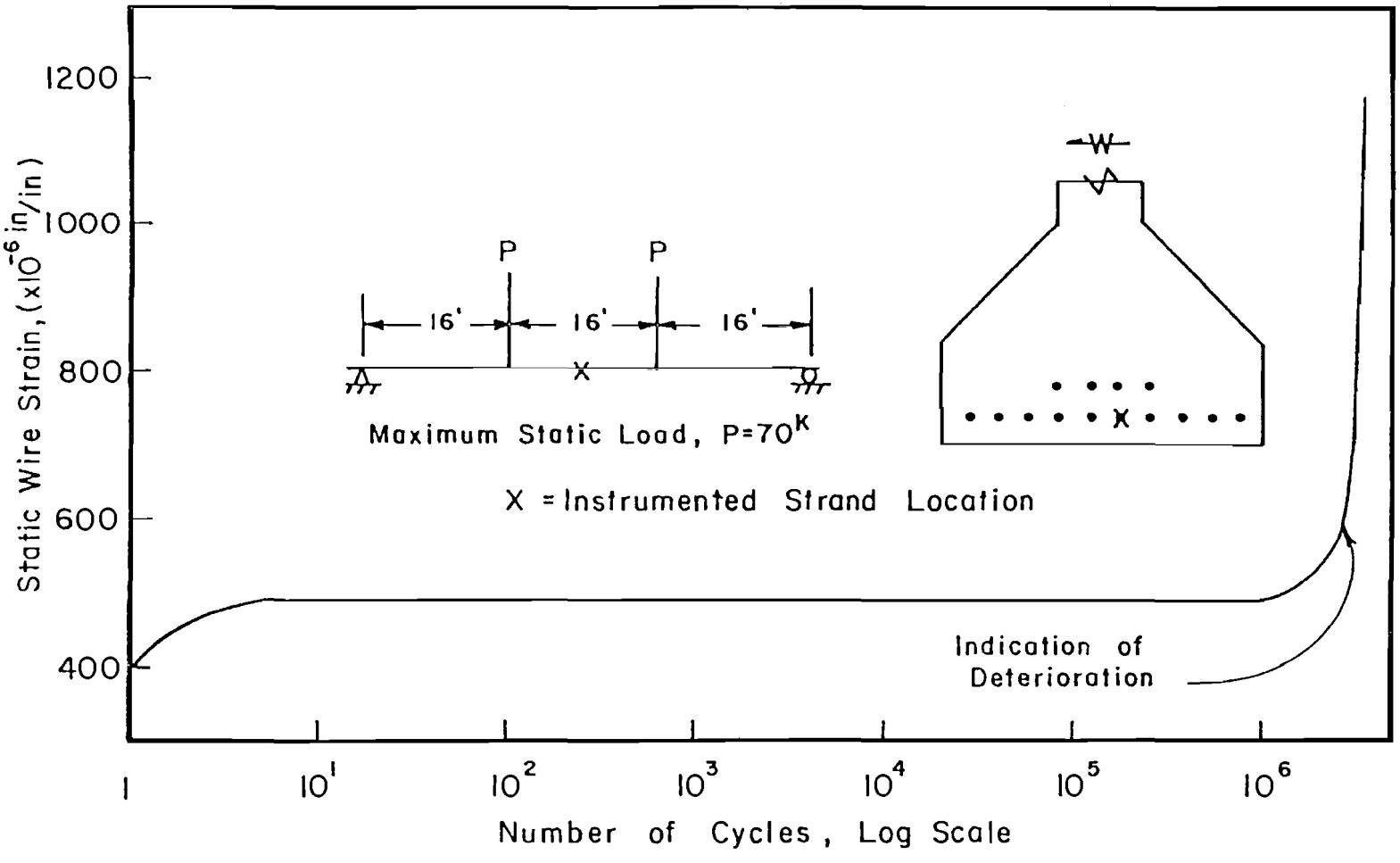

Fig. 5.18 Indication of deterioration for Specimen C-14-NP-5.5-OL-2.29

TABLE 5.10 Number of Cycles to Audible or Visible Indication of Deterioration

Specimen[a]	Audible or Visible Indicator of Deterioration Indicator	Number of Cycles (millions)	Percentage of Total Number of Cycles
C-16-NP-10.5-NO-0.58	Audible breaks	0.540	93
	Hor. cracks in lower flange	0.570	98
	Spalling	0.578	100
C-16-NP-7.2-OL-1.48	Spalling, visible breaks	1.460	99
	Audible breaks	1.478	100
C-16-NP-10.1-NO-0.91	Audible breaks	0.837	92
	Flexural cracks did not close	0.837	92
	Hor. cracking-spalling	0.894	98
C-16-NP-6.0-NO-1.91	Strand slip	1.08	57
	Spalling, visible breaks	1.50	79
C-14-NP-5.5-OL-2.29 (b/c)	Audible breaks	2.06/3.05	90/93
	Flexural cracks did not close	2.06/3.05	90/93
	Spalling, visible breaks	2.20/3.19	96/97
A-22-NP-6.2-OL-2.84	Audible wire breaks	2.64	93
	Squeeking noise at flex. crack	2.81	99
	No spalling		

TABLE 5.10 Number of Cycles to Audible or Visible Indication of Deterioration (continued)

Specimen[a]	Audible or Visible Indicator of Deterioration Indicator	Number of Cycles (millions)	Percentage of Total Number of Cycles
A-22-NP-6.2-NO-5.00	Audible wire breaks	4.50	90
	Powder from flexural crack	4.90	98
	No spalling	4.90	98
A-22-NP-3.5-OL-5.95(NF)	Specimen did not experience fatigue failure		
C-16-UP-8.0-NO-1.73	Spalling, visible breaks	1.20	69
	Audible wire breaks	1.61	93
C-16-CP-7.2-NO-2.54	Audible wire breaks	2.37	94
	Spalling, vislble breaks	2.50	99
C-16-CP-5.5-OL-9.43	Audible wire breaks	6.01	64
	No spalling		

[a] The last number in the alphanumeric specimen label indicates the number of cycles to failure in millions.
[b] 2.29 million cycles at $5.5\sqrt{f'_{ct}}$
[c] 3.28 million total cycles

A member has to deteriorate considerably after the first indication of distress before recognizable indicators are apparent at approximately 85 percent of the total fatigue life. With four specimens (three A-22 specimens and one C-16-CP specimen), no spalling or clearly visible signs of distress were apparent before major failure occurred. The A-22 specimens had 7/16 in. diameter strands (the Type C specimens had 1/2 in. diameter strands), 2.5 in. of concrete cover (the Type C specimens had 2.0 in. of cover), and stirrups that passed below all the bottom strands. The strands in the Type C-NP specimens were not as well confined. The C-16-CP specimens had confining reinforcing steel around the strands and reinforcing steel which probably helped control spalling for Specimen C-16-CP-5.5-0L-9.43.

Figure 5.19 shows all specimens tested in this test program and the number of cycles to indication of distress. For several specimens, particularly the draped strand ones (A-22-NP and C-14-NP), there was only a short period of time between apparent signs of distress and fatigue failure.

5.4.8 Comparison of Actual and Calculated Ultimate Capacities

After a significant number of wire fatigue breaks have occurred, it is important to know the actual capacity of a girder. For all fatigued specimens a static test to ultimate was performed. The actual and calculated ultimate capacities are presented in Table 5.11. The actual capacity to calculated capacity ratio is shown to indicate the remaining strength after fatigue failure. The average capacity was approximately 70 percent of the calculated capacity, with a standard deviation of approximately 13 percent. The lowest value was 49 percent of the calculated ultimate.

Specimen A-22-NP-3.5-0L-5.95 (NF) did not experience fatigue failure. The actual capacity was 11 percent above the calculated capacity. The static ultimate test was stopped at a deflection of approximately 23 in. for safety reasons. There was not a loss of strength at this point, but the load versus deflection curve indicated yielding of the strands.

Figure 5.20 shows the drastic difference in ductility and load capacity of two A-22 girders that experienced fatigue distress and Specimen A-22-NP-3.5-0L-5.95 (NF) which did not. The ultimate centerline deflections, also shown in Table 5.11, after a significant number of wire fatigue failures were well below the 22.7 in. centerline deflection for Specimen A-22-NP-3.5-0L-5.95 (NF), which did not experience fatigue distress. This large deflection is typical of full scale prestressed concrete girders. The results of fatigue tests by Rabbat et al. [76] shown in Table 5.6 indicate that deflections of 21 in. to 31 in. were achieved for three specimens with no fatigue damage.

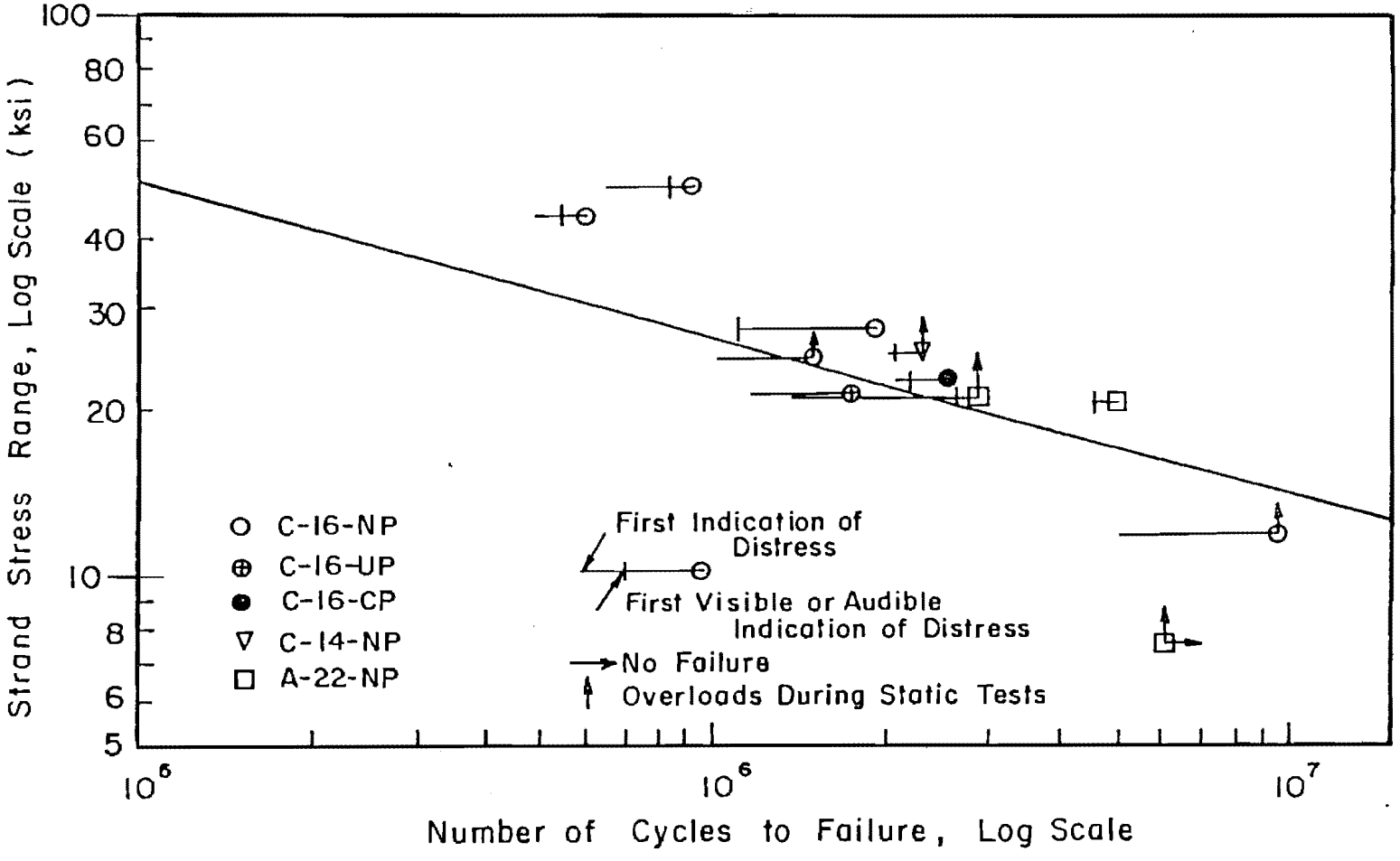

Fig. 5.19 Indication of first indication of deterioration for test specimens

TABLE 5.11 Ultimate Loads and Deflections

Specimen	Ultimate Load P_{ult} (kips)	Ultimate Capacity P_{uc} (kips)	$\frac{P_{ult}}{P_{uc}}$	Centerline Deflection at P_{ult} (in.)	Maximum Deflection/ Load (in./kips)
C-16-NP-10.5-NO-0.58	100	117	0.85	4.8	4.8
C-16-NP-7.2-OL-1.48	65.3	117	0.56	1.3	1.3
C-16-NP-10.1-NO-0.91	69.8	117	0.60	1.9	2.2/68.5
C-16-NP-6.0-NO-1.91	115	156	0.74	5.3	6.0/106
C-14-NP-5.5-OL-2.29	84	114	0.74	2.6	2.6
A-22-NP-6.2-OL-2.84	49	100	0.49	1.4	1.5/48
A-22-NP-6.2-NO-5.00	79	100	0.79	2.9	4.8/66
A-22-NP-3.5-OL-5.95(NF)	111	100	1.11	22.7	22.7
C-16-UP-8.0-NO-1.73	112	146	0.77	3.4	5.4/100
C-16-CP-7.2-NO-2.54	118	144	0.82	4.9	6.8/90
C-16-CP-5.5-OL-9.43	84	144	0.58	2.75	3.6/63

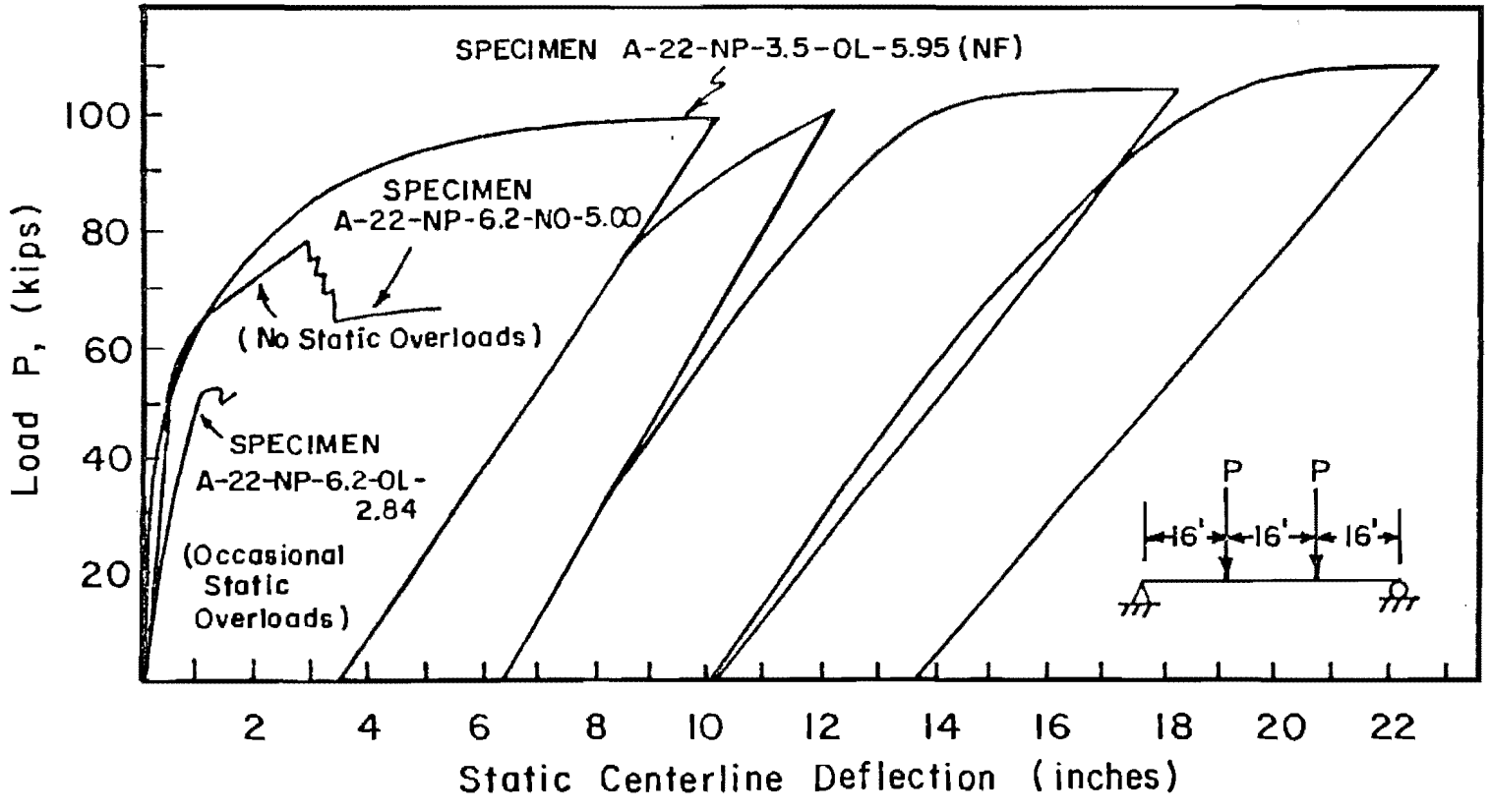

Fig. 5.20 Effects of fatigue distress and overloads on ultimate capacity and ductility

Mangura and Hognestad [54] (Section 2.3.10) reported centerline deflections of approximately 22 in. and 30 in. at ultimate load for two fatigue specimens that did not experience wire fatigue fractures.

Passive reinforcement increases ductility during ultimate testing. Table 5.11 indicates that all three C-16-_P specimens continued to support a reduced load and provide additional ductility after the ultimate load was obtained. Additional ductility after ultimate was often not available for specimens with no passive reinforcement. Figure 5.21 shows the increased ductility for a specimen with passive reinforcing steel in the lower flange (C-16-CP-7.2-NO-2.54) when compared to the specimen (C-16-NP-7.2-OL-1.48) with no passive reinforcement. Notice also the increased ultimate load as a percent of the ultimate capacity for Specimen C-16-CP-7.2-NO-2.54. Both specimens were cycled at a maximum nominal concrete tensile stress of $7.2\sqrt{f'_{ct}}$.

5.4.9 Number of Wire Fatigue Break Locations

Table 5.12 indicates that wire fatigue fractures can be distributed at several flexural cracks in the same girder. The number of break locations varied from zero for a specimen that did not fail due to fatigue loading to eight different locations in two girders. Numerous break locations in the same girder indicate that prestressing strands are stressed approximately equally in the constant moment region. A small number of break locations indicate high strand stresses concentrated at a small number of flexural cracks. A few cases of multiple fatigue breaks at relatively close flexural cracks indicate that prestressing wires in a seven wire strand can actually rebond and develop high stresses after a fatigue fracture.

Table 5.12 shows that occasional static overloads significantly reduced the number of break locations for the C-16 specimens with and without passive reinforcement. Even the small occasional overloads applied in this program apparently caused crack propagation, debonding, an increase in curvature, and an accompanying significant increase in crack widths at a few flexural cracks. The result is higher strand stress ranges at these cracks. Warner and Hulsbos [90] (Section 2.3.5) state that:

> ... an examination of the deformations measured in the test beams indicates that steel stress varies greatly along the length of the beam, even in regions of constant moment and in fact will attain a maximum value only at the widest crack.

Occasional overloads increase strand stresses and significantly reduce beam fatigue life.

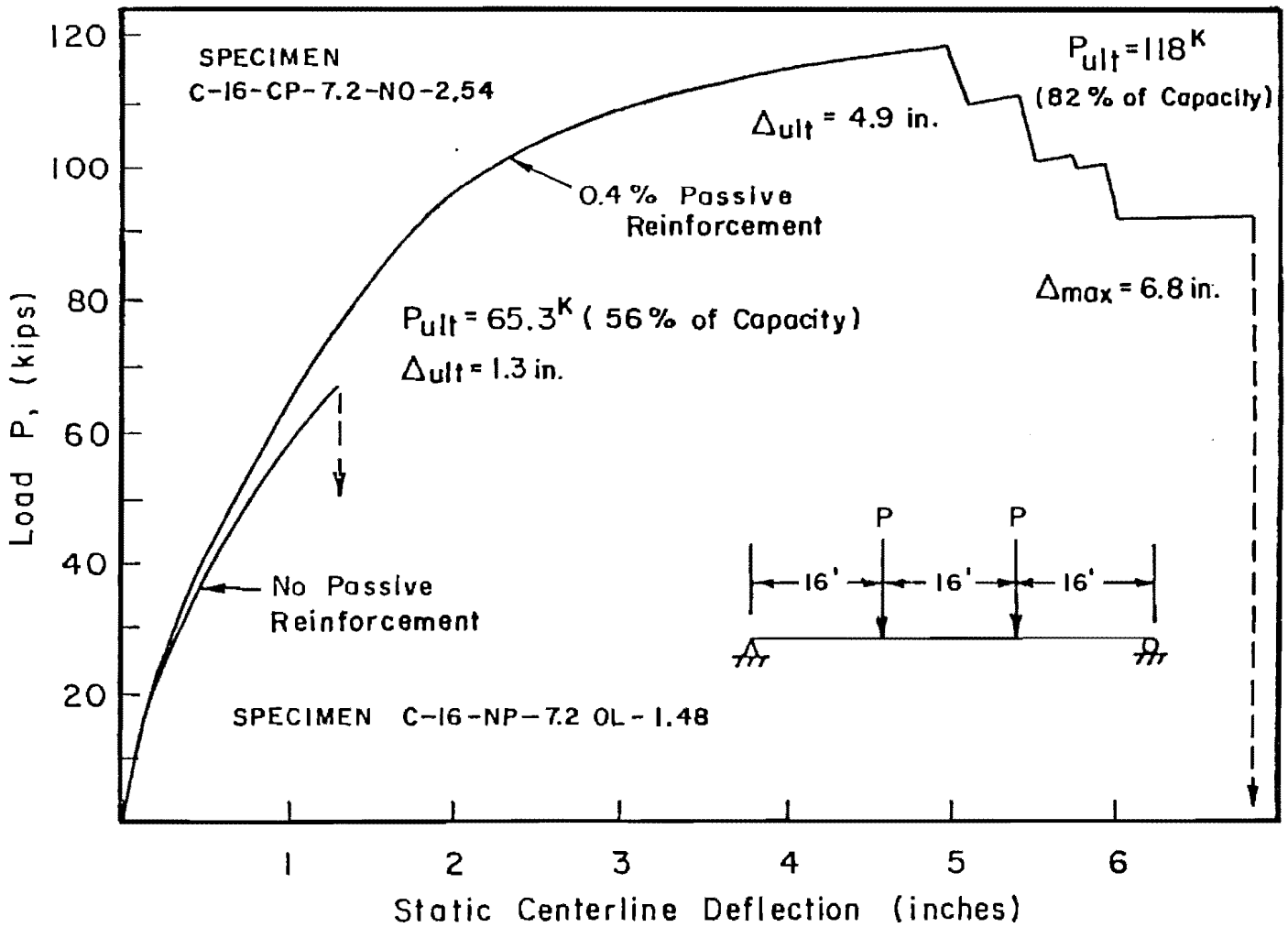

Fig. 5.21 Effects of passive steel on ultimate capacity and ductility

TABLE 5.12 Number of Wire Fatigue Break Locations

Specimen	Number of Wire Breaks	Number of Reinforcing Bar Breaks	Number of Reinforcing Bar Fatigue Initiation Cracks	Number of Break Locations
C-16-NP-10.5-NO-0.58	33	NA	NA	6
C-16-NP-7.2-OL-1.48	56	NA	NA	1
C-16-NP-10.1-NO-0.91	88	NA	NA	8
C-16-NP-6.0-NO-1.91	34	NA	NA	5
C-14-NP-5.5-OL-2.29	35	NA	NA	3
A-22-NP-6.2-OL-2.84	66	NA	NA	1 (drape pt)
A-22-NP-6.2-NO-5.00	33	NA	NA	1
A-22-NP-3.5-OL-5.95(NF)	0	NA	NA	0
C-16-UP-8.0-NO-1.73	46	0	0	8
C-16-CP-7.2-NO-2.54	39	10	4	6
C-16-CP-5.5-OL-9.43	48	8	3	3

NA - Not Applicable

5.5 Fatigue Design Procedure for Pretensioned Concrete Highway Girders

The results of this limited number of tests must be put into perspective. The applied loads (static and dynamic), losses, and material properties could be determined accurately for all specimens. This is not true in service conditions, in-service conditions could be better or worse. With the single girder test specimen used there was no possibility of or uncertainty regarding lateral distribution of load to adjacent girders. Such lateral distribution occurs in actual bridges. Conservatism in lateral load distribution factors, if present in actual bridges, could introduce an additional safety margin not present in laboratory girder tests. On the other hand, the applied loads in the tests were well-controlled. Actual service applications could expose bridge girders to heavy illegal overloads. The damaging effect of only a few intermittent overloads found in this study is very disturbing in this regard. Putting the results in overall perspective, it should be noted that all test specimens experienced a relatively large number of full live load cycles prior to failure. Any highway girder would probably be in-service a substantial number of years before it accumulates design level load cycles of this magnitude. The results must be viewed in terms of the proposed application of the girders in bridges with various potential traffic counts and lives. The attempt to incorporate a design procedure related to the AASHTO procedure for structural steel members permits this.

The examination of the results of this project suggest the step-by-step procedure for fatigue design of pretensioned concrete highway girders which is presented in this section. The AASHTO [7,8] Category B allowable stress ranges for structural steel (redundant load path structures) will be used as the general fatigue model. This model was chosen because it is currently in the AASHTO Specifications and provides an accepted basis for relating highway types and traffic counts to allowable stress ranges. As shown in Fig. 5.11, the AASHTO Category B model is a reasonably correct and conservative model up to a 6 million cycle fatigue life.

The recommended procedure is outlined in Fig. 5.22 and explained in the following statements:

1. Conservatively determine girder loads, including the probability overloads.

2. Because the load-strand stress range relationship is nonlinear, use an iterative approach. Assume a maximum nominal concrete tensile stress of $3\sqrt{f'_c}$. Proceed with a trial bridge design determining girder type, spacing, number of strands, and strand layout.

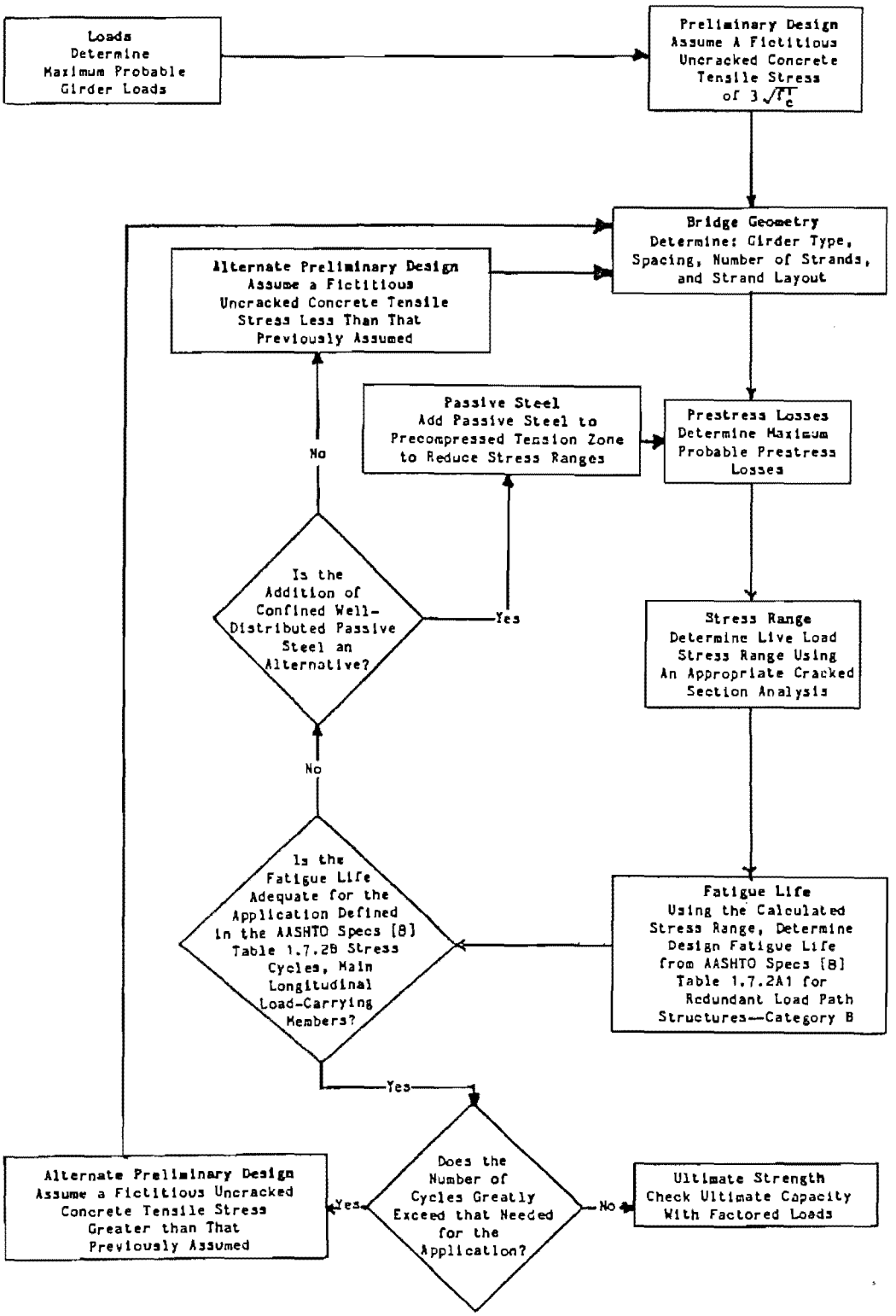

Fig. 5.22 Fatigue design for pretensioned concrete girders

3. Conservatively determine prestress losses for the trial section.

4. With the given loads, trial section, and prestress losses perform a cracked section analysis to determine the strand stress range between zero and full live load. A nonlinear program similar to PBEAM [85] or approximate manual calculations as shown in Section 5.4.5.2 can be used.

5. Enter Table 1.7.2A1 for redundant load path structures from the AASHTO Specifications [8] and determine the allowable number of cycles for this stress range (Fig. 5.23). The 16 ksi stress range should only be assumed valid to 6 million cycles.

6. If the allowable number of cycles is not adequate for the proposed traffic application given in AASHTO Specifications [8] Table 1.7.2B, also shown in Fig. 5.24, a new trial section can be determined assuming a lower nominal concrete tensile stress. Alternatively, passive reinforcement can be added to reduce stress ranges and provide fatigue toughness.

   a. If a lower concrete tensile stress is used, revise the $3\sqrt{f'_c}$ limit in step 2 and iterate to an acceptable stress range/number of cycles value.

   b. If passive reinforcement is added, recompute prestress losses in step 3 and iterate to an acceptable stress range/number of cycles value.

7. If the allowable number of cycles greatly exceeds the required value for the proposed traffic applications, the $3\sqrt{f'_c}$ limit in step 2 can be increased, and then design should iterate to an acceptable stress range/number of cycles value.

TABLE 1.7.2A1
REDUNDANT LOAD PATH STRUCTURES (1)

Category See Table 1.7.2A2	Allowable Range of Stress, F_{sr} (ksi) (MPa)			
	For 100,000 Cycles	For 500,000 Cycles	For 2,000,000 Cycles	For over 2,000,000 Cycles
A	60 (413.69)	36 (248.21)	24 (165.47)	24 (165.47)
B	45 (310.26)	27.5 (189.60)	18 (124.10)	16 (110.31)
C	32 (220.63)	19 (131.00)	13 (89.63)	10, 12* (68.95), (82.74)*
D	27 (186.16)	16 (110.31)	10 (68.95)	7 (48.26)
E	21 (144.79)	12.5 (86.18)	8 (55.15)	5 (34.47)
F	15 (103.42)	12 (82.74)	9 (62.05)	8 (55.15)

*For transverse stiffener welds on girder webs or flanges.

NON REDUNDANT LOAD PATH STRUCTURES (2)

Category See Table 1.7.2A2	Allowable Range of Stress F_{sr} (ksi) (MPa)			
	For 100,000 Cycles	For 500,000 Cycles	For 2,000,000 Cycles	For over 2,000,000 Cycles
A	36 (248.21)	24 (165.47)	24 (165.47)	24 (165.47)
B	27.5 (189.60)	18 (124.10)	16 (110.31)	16 (110.31)
C	19 (131.00)	13 (89.63)	10, (68.95) 12*(82.74)	9, (62.05) 11*(75.84)
D	16 (110.31)	10 (68.95)	7 (48.26)	5 (34.47)
E	12.5 (86.18)	8 (55.15)	5 (34.47)	2.5 (17.24)
F	12 (82.74)	9 (62.05)	8 (55.15)	7 (48.26)

*For transverse stiffener welds on girder webs or flanges.

(1) Structure types with multi-load paths where a single fracture in a member cannot lead to the collapse. For example, a simply supported single span multi-beam bridge or a multi-element eye bar truss member has redundant load paths.

(2) Structure types with a single load path where a single fracture can lead to a catastrophic collapse. For example, flange and web plates in one or two girder bridges, main one-element truss members, hanger plates, caps at single or two column bents have non-redundant load paths.

Fig. 5.23 AASHTO Specifications [8] Table 1.7.2A1

TABLE 1.7.2B—Stress Cycles

Main (Longitudinal) Load Carrying Members

Type of Road	Case	ADTT*	Truck Loading	Lane Loading†
Freeways, Expressways, Major Highways and Streets	I	2500 or more	2,000,000**	500,000
	II	less than 2500	500,000	100,000
Other Highways and Streets not included in Case I or II	III		100,000	100,000

Transverse Members and Details Subjected to Wheel Loads

Type of Road	Case	ADTT*	Truck Loading
Freeways, Expressways, Major Highways and Streets	I	2500 or more	over 2,000,000
	II	less than 2500	2,000,000
Other Highways and Streets	III	. . .	500,000

*Average Daily Truck Traffic (one direction).
†Longitudinal members should also be checked for truck loading.
**Members shall also be investigated for "over 2 million" stress cycles produced by placing a single truck on the bridge distributed to the girders as designated in Article 1.3.1(B) for one traffic lane loading.

Fig. 5.24 AASHTO Specifications [8] Table 1.7.2B

CHAPTER 6

SUMMARY, CONCLUSIONS AND RECOMMENDATIONS

6.1 Summary

As a result of potentially unfavorable results found in previous tests by Rabbat et al. [76], this test program was initiated to determine the fatigue strength of full scale pretensioned concrete bridge girders. The initial portion of the test program was reported by Paulson et al. and involved the development of a strand in air fatigue model based on both previously reported tests and new data. Eleven full scale pretensioned girder specimens were tested in the current flexural fatigue portion of the research project.

This report summarizes the flexural fatigue tests of full scale precast pretensioned girders with unshored cast-in-place slabs. It includes an extensive literature review of fatigue of the constituent materials (concrete, reinforcing steel, and prestressing steel), of fatigue of prestressed members, of the evolution of prestressed concrete design provisions in the AASHTO Specifications, and of the development of specifications and code provisions relating to fatigue of prestressed concrete. The report also includes a detailed description of the fabrication procedures, material properties, initial static loading procedure, and the techniques used to determine the actual prestress force. Detailed summaries are given of the fatigue and ultimate behavior of the eleven specimens including static and dynamic loads, deflections, stresses and crack measurements. A post mortem investigation was performed on all specimens to determine the locations and types of wire and reinforcing steel fractures. The main experimental variables included maximum load level as indicated by the nominal concrete tensile stresses based on uncracked gross section calculations; girder strand stress ranges; cross sections (which included AASHTO-PCI Type II girders and Texas Type C girders); strand patterns including both draped and straight strands; provision of passive reinforcing steel in the precompressed tension zone; distribution and confinement of passive reinforcement; degree of precracking of sections; and the presence or absence of occasional modest overloads during static tests. A nonlinear program was used in the analysis of experimental results to determine the level of prestressing, extent of prestress losses and the effective strand stress ranges. Comparisons were made not only between these eleven specimens, but to other reported test results, and to recommended and existing fatigue design procedures. The report synthesizes this information and presents design recommendations suitable for inclusion within the general AASHTO fatigue design framework.

6.2 Conclusions

In any experimental program involving a very limited number of fatigue tests, it is difficult to draw sweeping conclusions. However, for the type girder widely used in pretensioned girder and slab bridges, the following conclusions seem justified.

6.2.1 Primary Conclusions

1. Pretensioned concrete bridge girders without well-distributed, confined passive reinforcement which are actually subjected to loads producing nominal tensile tresses of $6\sqrt{f'_c}$ can fail as a result of fatigue of prestressing strands at less than 3.0 million cycles.

2. The fatigue life of pretensioned concrete girders can be predicted using the following modification of the strand fatigue model developed by Paulson [73]:

$$\text{Log } N = 11.0 - 3.50 \text{ Log } S_r$$

where: N is the fatigue life in number of cycles

S_r is the strand stress range; maximum stress - minimum stress (ksi)

No endurance limit can be set, but it appears that stress ranges below 5 ksi would be insignificant. The probable stress range must be determined accurately or conservatively considering the effects of prestress losses, of section cracking, and the probability of overloads.

3. In order to relate the design of pretensioned concrete girders to the general AASHTO fatigue provisions, it appears adequate to design these girders for stress ranges similar to AASHTO structural steel Category B values for redundant load path structures.

4. A small number (less than 10) of occasional modest overload cycles (20 percent above the normal applied load level) can produce extremely detrimental effects in the form of increased strand stress ranges and sharply reduced fatigue lives.

5. Prestress losses directly influence strand stress ranges and hence fatigue life. Realistic, conservative estimates of minimum prestress forces must be used in assessing girder fatigue life.

6. Confined, well-distributed passive reinforcing steel can substantially increase fatigue life by reducing prestress losses, controlling crack propagation, and thus limiting strand stress ranges.

7. The use of the current AASHTO Specification allowable nominal concrete tensile stress of $6\sqrt{f'_c}$ without specific inclusion of well-distributed, confined supplementary reinforcement will not ensure adequate fatigue life.

6.2.2 Secondary Conclusions

1. Prestressing strand in cracked pretensioned concrete girders appears to have an endurance limit below 10 ksi if an endurance limit exists.

2. Effective prestress level can be determined from strain and deflection measurements when the section is cracked.

3. In this test series with frequency of loading in the 2.5 to 3.0 Hz range, dynamic load amplification was insignificant.

4. Approximate strand stress ranges for the cracked concrete sections can be calculated readily using either a nonlinear computer program (PBEAM) or approximate manual calculations based on prestressed concrete fundamentals and equilibrium.

5. Static and dynamic measurements of strand strain near or at flexural cracks tend to confirm analytical stress ranges.

6. Passive reinforcement was not totally effective in reducing strand stress ranges because of the different bond characteristics between reinforcing steel and strand.

7. Fatigue damage to girders significantly reduced ultimate capacity and ductility.

8. Confined, well-distributed passive reinforcement increased both the fatigue life and the developable percentage of ultimate capacity after fatigue testing, as well as greatly improved ductility.

9. Results from the eleven specimens tested indicate there was no significant difference in fatigue life between the two girder shapes tested (Texas Type C and AASHTO-PCI Type II).

10. No correlation was found between draping of prestressing strands and premature failure at pretensioned concrete beams.

6.3 Recommendations

6.3.1 Design Recommendations

1. In order to determine the fatigue life of pretensioned concrete girders, a rational design procedure should be used which must include an accurate determination of girder loads and a conservative assessment of prestress loads. These values should be used with a cracked section analysis (no concrete tensile capacity) to determine probable strand stress ranges in a trial section. The fatigue life may then be determined from the strand stress range by using either the strand fatigue model:

$$\text{Log } N = 11.0 - 3.5 \text{ Log } S_r$$

where: N is the fatigue life in number of cycles

S_r is the strand stress range; maximum stress - minimum stress (ksi)

or the more conservative AASHTO Category B fatigue model for redundant structural steel members. If the fatigue life governed stress range is not acceptable, the girder design will have to be modified to decrease the strand stress range by reducing girder spacing, by increasing prestressing steel area, or by adding confined, well-distributed passive reinforcement.

2. An effective endurance limit of 16 ksi can be used with either fatigue model. This corresponds to the stress range sustained for a fatigue life of 6 million cycles. No actual fatigue endurance limit greater than 10 ksi was found in these pretensioned girder tests (which included loading to 10 million cycles).

3. An indirect design procedure using a fictitious maximum nominal concrete tensile stress of $3\sqrt{f'_c}$ is probably sufficiently conservative to prevent fatigue damage in pretensioned girders without passive reinforcement at lives up to 6 million cycles. As with a cracked section analysis, loads and losses must be known accurately or calculated conservatively.

4. For full size girders the split cylinder strength of approximately $6.5\sqrt{f'_c}$ is a more realistic predictor in determining cracking stresses than the currently indicated modulus of rupture of $7.5\sqrt{f'_c}$.

5. A cracked section stiffness index (EI) of approximately 20 percent of the uncracked value can conservatively be used to estimate deflections due to loads above the zero tension load.

6. Confined, well-distributed passive reinforcing steel is recommended to reduce prestress losses and hence creep deflections, reduce strand stress ranges, and increase strength and ductility under fatigue and ultimate load conditions.

7. In many existing girders and in new girders designed for relatively few cyclic load applications, high strand stress ranges may exist. Inspection programs should be alerted to watch for potential fatigue problems. Flexural concrete cracking always preceded fatigue deterioration. Substantial increases in crack widths or girder deflections under applied loads provide warning of incipient fatigue failures.

6.3.2 Research Recommendations

1. Since limited foreign test results indicate that the fatigue strength of posttensioned girders may be even lower than pretensioned girders, the effect of posttensioning should be immediately examined.

2. Further research should be performed to determine actual loads on pretensioned bridge girders under service conditions.

3. Research should assess the effect of variable load histories and the cumulative damage due to varying load ranges on prestressed concrete girders.

4. Extremely high cycle-low stress range strand and beam fatigue tests need to be performed to determine pretensioned concrete beam fatigue endurance limits.

5. Future research on fatigue of prestressed concrete must include a careful determination of the effective prestress in each specimen at the time of testing.

6. Minimal girder fatigue test instrumentation should include strain gage instrumented strands and reinforcing steel, deflection and crack width potentiometers, and load cells. All instrumentation should be read dynamically during fatigue testing to determine dynamic effects.

7. Future fatigue test programs should include thorough post mortem investigations to determine the location and number of fatigue breaks.

8. More information is needed on the cyclic compressive creep of concrete to determine its effect on fatigue life.

9. Adequate information is lacking on bond fatigue and flexural crack propagation, particularly as they relate to overloads.

10. All future prestressed concrete girder research should include provisions to measure material creep, shrinkage, and stress-strain properties and to assess effective prestress. The data should be used with analytical programs to determine how closely prestress losses can be predicted. This is particularly important with passive reinforcement to control losses.

11. Long and short term prestress losses of full scale prestressed members need further investigation.

APPENDIX A

CONCRETE PROPERTIES USED IN INPUT FOR PROGRAM PBEAM [85]

TABLE A.1 Concrete Compressive Strength Equation Factors

Specimen	Release Strength (psi,days)	28-Day Strength (psi)	Concrete Compressive Strength Equation Factors (A1)	(A2)
C-16-NP-10.5-NO-0.58	4300 (14)	5300	6.51	0.767
C-16-NP-7.2-OL-1.48	4800 (7)	5970	2.28	0.919
C-16-NP-10.1-NO-0.91	4700 (14)	5780	6.43	0.770
C-16-NP-6.0-NO-1.91	4950 (6)	6690	2.68	0.904
C-14-NP-5.5-OL-2.29	4500 (6)	5600	1.87	0.933
A-22-NP-6.2-OL-2.84	4032 (1)	7050*	0.733	0.974
A-22-NP-6.2-NO-5.00	4032 (1)	7050*	0.733	0.974
A-22-NP-3.5-OL-5.95(NF)	4032 (1)	7050*	0.733	0.974
C-16-UP-8.0-NO-1.73	5730 (13)	5800	0.296	0.989
C-16-CP-7.2-NO-2.54	6330 (7)	7100	1.14	0.959
C-16-CP-5.5-OL-9.43	5210 (11)	5840	2.19	0.922

* Strength at 450 days

A.1 Determination of the Ultimate Creep Coefficient

Initial Creep Coefficient = 2.35

Humidity Correction: CCH = 1.27 - 0.0067 (humidity,%)

Assume 70%	CCH = 1.27 - 0.0067 (70%)	= 0.801

Minimum thickness correction: CCT = 1.14 - 0.023 (thickness, in.)

Type C Girder, t = 7 in.	CCT = 1.14 - 0.023 (7 in.)	= 0.979
Type II Girder, t = 6 in.	CCT = 1.14 - 0.023 (6 in.)	= 1.00
Slab, t = 7.75 in.	CCT = 1.14 - 0.023 (7.75 in.)	= 0.962

Air content correction: CCA = 1.0 $A \leq 6\%$

Assume 5%	CCA	= 1.0

Slump correction: CCS = 0.82 + 0.067 (slump, in.)

Values shown in Table A.2

Percent Fines Correction: CCF = 0.88 + 0.0024 (fines,%)

Values shown in Table A.2

Ultimate creep coefficient = 2.35 * CCH * CCT * CCA * CCS * CCF

TABLE A.2 Determination of the Ultimate Creep Coefficient

Specimen	Slump (in.) Girder / Slab	Slump Correction Girder / Slab	Fines (percent) Girder / Slab	Fines Correction Girder / Slab	Ult. Creep Coefficient Girder / Slab
C-16-NP-10.5-NO-0.58	8.0	1.36	29.7	0.951	2.38
	4.0	1.09	26.9	0.945	1.86
C-16-NP-7.2-OL-1.48	6.0	1.22	30.8	0.954	2.15
	3.0	1.02	27.5	0.946	1.75
C-16-NP-10.1-NO-0.91	6.0	1.22	29.2	0.950	2.14
	6.0	1.22	30.3	0.953	2.11
C-16-NP-6.0-NO-1.91	3.5	1.05	29.3	0.950	1.85
	4.0	1.09	32.3	0.958	1.89
C-14-NP-5.5-OL-2.29	6.0	1.22	29.1	0.950	2.14
	8.0	1.36	20.8	0.930	2.28
A-22-NP-6.2-OL-2.84	4.5	1.12	27.7	0.946	2.00
	5.5	1.19	24.2	0.938	2.02
A-22-NP-6.2-NO-5.00	4.5	1.12	27.7	0.946	2.00
	6.0	1.22	24.3	0.938	2.08
A-22-NP-3.5-OL-5.95(NF)	4.5	1.12	27.7	0.946	2.00
	8.0	1.36	32.5	0.958	2.35
C-16-UP-8.0-NO-1.73	7.0	1.29	29.3	0.950	2.26
	8.0	1.36	26.5	0.944	2.32
C-16-CP-7.2-NO-2.54	6.5	1.26	29.3	0.950	2.20
	8.0	1.36	28.9	0.950	2.33
C-16-CP-5.5-OL-9.43	5.0	1.16	29.1	0.950	2.02
	6.5	1.26	32.5	0.958	2.18

A.2 Determination of Ultimate Shrinkage Strains

Initial Shrinkage Strain:	Moist cured concrete ISS = -0.0008	
	Steam cured concrete ISS = -0.00073	
Humidity Correction:	CSH = 1.40 - 0.010 (humidity,%)	
Assume 70%	CSH = 1.40 - 0.010 (70%)	= 0.70
Minimum Thickness Correction:	CST = 1.23 - 0.038 (thickness,in.)	
Type C Girder, t = 7 in.	CST = 1.23 - 0.038 (7 in.)	= 0.964
Type II Girder, t = 6 in.	CST = 1.23 - 0.038 (6 in.)	= 1.00
Slab, t = 7.75 in.	CST = 1.23 - 0.038 (7.75 in.)	= 0.936
Air Content Correction:	CSA = 0.95 + 0.0080 (air,%)	
Assume 5%	CSA = 0.95 + 0.0080 (5%)	= 0.990
Slump Correction:	CSS = 0.89 + 0.041 (slump,in.)	
Slump values shown in Table A.3		
Cement Content Correction:	CSC = 0.75 + 0.034 (sacks)	
Cement content values shown in Table A.3		
Percent Fines Correction:	CSF = 0.30 + 0.0140 (fines,%)	
Percent fines by weight shown in Table A.3		

Ultimate Shrinkage Strain = ISS * CSH * CST * CSA * CSS * CSC * CSF

TABLE A.3 Determination of Ultimate Shrinkage Strains

	Slump (in.)		Cement Content (sacks)		Fines (percent)		Ultimate Shrinkage Strains ($x10^{-3}$)	
	Girder	Slab	Girder	Slab	Girder	Slab	Girder	Slab
C-16-NP-10.5-NO-0.58	8.0		7.2		29.7		-4.64	
	4.0		6.0		26.9		-3.53	
C-16-NP-7.2-OL-1.48	6.0		6.2		30.8		-4.27	
	3.0		6.0		27.5		-3.43	
C-16-NP-10.1-NO-0.91	6.0		6.8		29.2		-4.22	
	6.0		6.0		30.3		-4.07	
C-16-NP-6.0-NO-1.91	3.5		7.2		29.3		-3.90	
	4.0		6.0		32.3		-3.92	
C-14-NP-5.5-OL-2.29	6.0		7.1		29.1		-3.89	
	8.0		6.4		20.8		-3.61	
A-22-NP-6.2-OL-2.84	*4.5		7.5		27.7		-3.76	
	5.5		6.9		24.2		-3.64	
A-22-NP-6.2-NO-5.00	*4.5		7.5		27.7		-3.76	
	6.0		7.0		24.3		-3.73	
A-22-NP-3.5-OL-5.95(NF)	*4.5		7.5		27.7		-3.76	
	8.0		6.1		32.5		-4.57	
C-16-UP-8.0-NO-1.73	7.0		7.3		29.3		-4.46	
	8.0		6.9		26.5		-4.17	
C-16-CP-7.2-NO-2.54	6.5		7.3		29.3		-4.38	
	8.0		7.0		28.9		-4.40	
C-16-CP-5.5-OL-9.43	5.0		7.2		29.1		-4.11	
	6.5		6.1		32.5		-4.33	

* Steam cured concrete

REFERENCES

1. AASHO, Interim Specifications, American Association of State Highway Officials, Washington, 1971.

2. AASHO, Standard Specifications for Highway Bridges, 7th Ed., American Association of State Highway Officials, Washington, 1957.

3. AASHO, Standard Specifications for Highway Bridges, 8th Ed., American Association of State Highway Officials, Washington, 1961.

4. AASHO, Standard Specifications for Highway Bridges, 9th Ed., American Association of State Highway Officials, 1965.

5. AASHO, Standard Specifications for Highway Bridges, 10th Ed., American Association of State Highway Officials, Washington, 1969.

6. AASHO, Standard Specifications for Highway Bridges, 11th Ed., American Association of State Highway Officials, Washington, 1973.

7. AASHTO, Interim Specifications: Bridges, American Association of State Highway and Transportation Officials, Washington, 1980.

8. AASHTO, Standard Specifications for Highway Bridges, 12th Ed., American Association of State Highway and Transportation Officials, Washington, 1977.

9. Abeles, P.W., "Design of Partially Prestressed Concrete Beams," American Concrete Institute Journal, October 1967, pp. 669-677.

10. Abeles, P.W., "Partial Prestressing in England," Prestressed Concrete Institute Journal, February 1963, pp. 51-72.

11. Abeles, P.W., "Partial Prestressing and Possibilities for Its Practical Application," Prestressed Concrete Institute Journal, June 1959, pp. 35-51.

12. Abeles, P.W., "Static and Fatigue Tests on Partially Prestressed Concrete Construction," Journal of the American Concrete Institute, December 1954, pp. 361-376.

13. Abeles, P.W., Barton, F.W., and Brown, E.I.,II, "Fatigue Behavior of Prestressed Concrete Bridge Beams," First International Symposium on Concrete Bridge Design, SP-23, American Concrete Institute, Detroit, 1969, pp. 579-599.

14. Abeles, P.W., Brown, E.I., II, and Hu, C.H., "Behavior of Under-Reinforced Prestressed Concrete Beams Subjected to Different Stress Ranges," Abeles Symnposium on Fatigue of Concrete, SP-41, American Concrete Institute, Detroit, 1974, pp. 279-299.

15. Abeles, P.W., Brown, E.I.,II, and Hu, C.H., "Fatigue Resistance of Under-Reinforced Prestressed Beams Subjected to Different Stress Ranges: Miner's Hypothesis," Abeles Symposium on Fatigue of Concrete, SP-41, American Concrete Institute, Detroit, 1974, pp. 237-277.

16. Abeles, P.W., Brown, E.I.,II, and Morrow, J.W., "Development and Distribution of Cracks in Rectangular Prestressed Beams During Static and Fatigue Loading," Prestressed Concrete Institute Journal, October 1964, pp. 36-51.

17. ACI-ASCE Joint Committee 323, "Tentative Recommendations for Prestressed Concrete," Journal of the American Concrete Institute, January 1958, pp. 545-578.

18. ACI Committee 209, "Prediction of Creep, Shrinkage, and Temperature Effects in Concrete Structures," ACI Manual of Concrete Practice, Part 1, 1984, pp. 209R-1 - 209R-92.

19. ACI Committee 215, "Considerations for Design of Concrete Structures Subjected to Fatigue Loading," ACI Manual of Concrete Practice, Part 1, 1984, pp. 215R-1 - 215R-25.

20. ACI Committee 215, "Considerations for Design of Concrete Structures Subjected to Fatigue Loading," American Concrete Institute Journal, March 1974, pp. 97-121.

21. ACI Committee 318, "Building Code Requirements for Reinforced Concrete (ACI 318-77)," American Concrete Institute, Detroit, 1977, 103pp.

22. ACI Committee 318, "Building Code Requirements for Reinforced Concrete (ACI 318-83)," American Concrete Institute, Detroit, 1983, 111pp.

23. ACI Committee 443, "Analysis and Design of Reinforced Concrete Bridge Structures," ACI Journal, April 1974, pp. 171-200.

24. ACI Committee 443, "Analysis and Design of Reinforced Concrete Bridge Structures," American Concrete Institute, Detroit, 1977, 116pp.

25. Anderson, A.R., "An Adventure in Prestressed Concrete," Reflections on the Beginnings of Prestressed Concrete in America, 1981, pp. 214-237.

26. Bachman, P.M., "Static and Shear Fatigue of Pretensioned Concrete I-Girders," unpublished M.S. Thesis, The University of Texas at Austin, May 1985.

27. Bachmann, H., "From Full to Partial Prestressing," Institut fur Baustatik und Konstruktion, ETH Zurich, Report No. 132, August 1982. Also, Concrete International, October 1983, pp. 36-39.

28. Bate, S.C.C., "An Experimental Study of Strand in Prestressed Concrete Beams Under Static and Repeated Loading," Proceedings, Institute of Civil Engineers, London, V. 23, December 1962, pp. 625-638.

29. Bieschke, L.A., and Klingner, R.E., "The Effect of Transverse Strand Extensions on the Behavior of Precast Prestressed Panel Bridges," Research Report 303-1F, Center for Highway Research, The University of Texas at Austin, June 1982.

30. Broek, D., Elementary Engineering Fracture Mechanics, 3rd Revised Ed., Martinus Nijhoff Publishers, Boston, 1982, 469pp.

31. Canteli, A.F., Esslinger, V., and Thürlimann, B., "Ermudungsfestigkeit von Buvuehrungs und Spannstahlen," Institut fur Baustatik-und Konstruktion, ETH Zurich, Report No. 8002-1, February 1984.

32. Edwards, A.D., and Picard, A., "Fatigue Characteristics of Prestressing Strand," Proceedings, Institute of Civil Engineers, London, Part 2, Vol. 53, September 1972, pp. 323-336.

33. Edwards, A.D., and Yannopoulos, "Local Bond-Stress-Slip Relationships Under Repeated Loading," Magazine of Concrete Research, Vol. 30, No. 103, June 1978, pp. 62-72.

34. Ekberg, C.E., Jr., "The Characteristics of Prestressed Concrete Under Repetitive Loading," PCI Journal, December 1956, pp. 7-16.

35. Ekberg, C.E., Jr., Walther, R.E., and Slutter, R.G., "Fatigue Resistance of Prestressed Concrete Beams in Bending," Journal of the Structural Division, ASCE, 83 (ST4), Proc. 1304.

36. Ferguson, P.M., Reinforced Concrete Fundamentals, 3rd Ed., John Wiley and Sons, New York, 1973, 750pp.

37. Fisher, J.W., and Viest, I.M., "Behavior of AASHO Road Test Bridge Structures Under Repeated Overstress," Highway Research Board, Special Report 73, 1962, pp. 19-51.

38. Frantz, G.C., and Breen, J.E., "Control of Cracking on the Side Faces of Large Reinforced Concrete Beams," Research Report 198-1F, Center for Highway Research, The University of Texas at Austin, September 1978.

39. Gerwick, B.C., and Venuti, W.J., "High- and Low-Cycle Behavior of Prestressed Concrete in Offshore Structures," Society of Petroleum Engineers Journal, August 1980, pp. 304-310.

40. Hanson, J.M., and Hulsbos, C.L., "Fatigue Tests of Two Prestressed Concrete I-Beams with Inclined Cracks," Highway Research Record, Highway Research Board, No. 103, 1965, pp. 14-30.

41. Hanson, J.M., Hulsbos, C.L., and Van Horn, D.A., "Fatigue Tests of Prestressed Concrete I-Beams," Proceedings, ASCE, Vol. 96, ST11, November 1970, pp. 2443-2464.

42. Hanson, J.M., Somes, M.F., and Helagson, T., "Investigation of Design Factors Affecting Fatigue Strength of Reinforcing Bars-Test Program," Abeles Symposium on Fatigue of Concrete, SP-41, American Concrete Institute, Detroit, 1974, pp. 71-105.

43. Hanson, N.W., "Influence of Surface Roughness of Prestressing Strand on Bond Performance," Prestressed Concrete Institute Journal, February 1969, pp. 32-45.

44. Hawkins, N.M., and Shah, S.P., "American Concrete Institute Considerations for Fatigue," Proceedings, IABSE, Vol. 37, 1982, pp. 41-50.

45. Helagson, T., and Hanson, J.M., "Investigation of Design Factors Affecting Fatigue Strength of Reinforcing Bars-Statistical Analysis," Abeles Symposium on Fatigue of Concrete, SP-41, American Concrete Institute, Detroit, 1974, pp. 107-137.

46. Howells, H., and Raithby, K.D., "Static and Repeated Loading Tests on Lightweight Prestressed Concrete Bridge Beams," Transport and Road Research Laboratory Report 804, Crowthorne, Berks, England, 1977.

47. Irwin, C.A.K., "Static and Repetitive Loading Tests on Full-Scale Prestressed Concrete Bridge Beams," Transport and Road Research Laboratory Report 802, Crowthorne, Berkshire, England, 1977.

48. Johnston, D.W., and Zia, P., "Bond Characteristics of Epoxy Coated Reinforcing Bars," Research Report ERSD-110-79-4, Center for Transportation Engineering Studies, North Carolina State University, August 1982.

49. Karr, P.H., and Hanson, N.W., "Bond Failure Tests of Beams Simulating Pretensioned Concrete Crossties," Prestressed Concrete Institute Journal, September-October 1975, pp. 65-80.

50. Karr, P.H., and Magura, D.D., "Effect of Strand Blanketing on Performance of Pretensioned Girders," Prestressed Concrete Institute Journal, December 1965, pp. 20-43.

51. Knudsen, K.E., and Eney, W.J., "Endurance of a Full-Scale Pretensioned Concrete Beam," Proceedings, Highway Research Board, Vol. 36, 1957, pp. 103-128.

52. Lin, T.Y., "Partial Prestressing Design--Philosophy and Approach," Concrete Design: U.S. and European Practices, SP-59, American Concrete Institute, Detroit, 1979, pp. 257-267.

53. Lin, T.Y., and Burns, N.H., Design of Prestressed Concrete Structures, 3rd Ed., John Wiley and Sons, New York, 1981, 646pp.

54. Magura, D.D., and Hognestad, E., "Tests of Partially Prestressed Concrete Girders," Proceedings, ASCE, Vol. 92, ST1, February 1966, pp. 327-350.

55. Menn, C., "Partial Prestressing From the Designer's Point of View," Concrete International, March 1983, pp. 52-59.

56. Miller, I., and Freund, J.E., Probability and Statistics for Engineers, 2nd Ed., Prentice-Hall, Englewood Cliffs, New Jersey, 1977, 529pp.

57. Moustafa, S.E., "Design of Partially Prestressed Concrete Flexural Members," Prestressed Concrete Institute Journal, May-June 1977, pp. 12-29.

58. Murdock, J.W., and Kesler, C.E., "Effect of Range of Stress on Fatigue of Plain Concrete Beams," Journal of the American Concrete Institute, August 1958, pp. 221-231.

59. Naaman, A.E., "Fatigue in Partially Prestressed Concrete Beams," Fatigue of Concrete Structures, SP-75, American Concrete Institute, Detroit, 1982, pp. 25-46.

60. Naaman, A.E., "Partially Prestressed Concrete Design, American Viewpoint," International Symposium: Nonlinearity and Continuity in Prestressed Concrete, Vol. 1, University of Waterloo, Waterloo, Ontario, Canada, July 1983, pp. 147-169.

61. Nordby, G.M., "Fatigue of Concrete--A Review of Research," Journal of the American Concrete Institute, August 1958, pp. 191-219.

62. Nordby, G.M., and Venuti, W.J., "Fatigue and Static Tests of Steel Strand Prestressed Beams of Expanded Shale Concrete and Conventional Concrete," Journal of the American Concrete Institute, August 1957, pp. 141-160.

63. Ople, F.S., Jr., and Hulsbos, C.L., "Probable Fatigue Life of Plain Concrete with Stress Gradient," Journal of the American Concrete Institute, January 1966, pp. 59-81.

64. Ozell, A.M., "Fatigue Tests of Prestressed Concrete I-Beams with Depressed Strands," Fourth Congress, Federation Internationale de la Precontrainte, 1962, pp. 128-135.

65. Ozell, A.M., and Ardaman, E., "Fatigue Tests of Pre-Tensioned Prestressed Beams," Journal of the American Concrete Institute, October 1956, pp. 413-424.

66. Ozell, A.M., and Diniz, J.F., "Composite Prestressed Concrete Beams Under Repetitive Loading," Prestressed Concrete Institute Journal, March 1958, pp. 19-27.

67. Ozell, A.M., and Diniz, J.F., "Fatigue Tests of Prestressed Concrete Beams Pretensioned with 1/2 Inch Strands," Prestressed Concrete Institute Journal, June 1958, pp. 79-88.

68. Ople, F.S., and Hulsbos, C.L., "Probable Fatigue Life of Plain Concrete with Stress Gradient," Journal of the American Concrete Institute, January 1966, pp. 59-81.

69. PCI Building Code Committee, "PCI Standard Building Code for Prestressed Concrete (Tentative)," STD-110-59T, Prestressed Concrete Institute, Chicago, November 1959, 22pp.

70. PCI Building Code Committee, "Prestressed Concrete Building Code Requirements," STD-110-61, Prestressed Concrete Institute, Chicago, 1961, 15pp.

71. PCI Committee on Prestress Losses, "Recommendations for Estimating Prestress Losses," PCI Journal, Vol. 20, No. 4, July-August 1975, pp. 43-75.

72. Paulson, C., "A Fatigue Study of Prestressing Strand," unpublished M.S. Thesis, The University of Texas at Austin, August 1982.

73. Paulson, C., Frank, K.H., and Breen, J.E., "A Fatigue Study of Prestressing Strand," Research Report 300-1, Center for Highway Research, The University of Texas at Austin, April 1983.

74. "Prestressed Girder Shines," ENR, October 27, 1983, p. 16.

75. Price, K.M., and Edwards, A.D., "Fatigue Strength in Shear of Prestressed Concrete I-Beams," American Concrete Institute Journal, April 1971, pp. 282-292.

76. Rabbat, B.G., Karr, P.H., Russell, H.G., and Bruce, N.G., Jr., "Fatigue Tests of Full Size Prestressed Girders," Research Report 113, Portland Cement Association, June 1978.

77. Reese, G.A., "Fatigue Strength of Prestressed Concrete Girders," unpublished M.S. Thesis, The University of Texas at Austin, August 1983.

78. "Retired Girders Undergo Lab Tests," ENR, August 11, 1983, pp. 26-27.

79. Rileem Committee 36-RDL, "Long Term Random Dynamic Loading of Concrete Structures (Tentative Edition)," 1982.

80. Rowe, R.E., "An Appreciation of the Work Carried Out on Fatigue in Prestressed Concrete Structures," Magazine of Concrete Research, Vol. 9, No. 25, March 1957, pp. 3-8.

81. Saito, M., and Imai, S., "Direct Tension Fatigue of Concrete by the Use of Friction Grips," American Concrete Institute Journal, September-October 1983, pp. 431-438.

82. Sawko, F., and Saha, G.P., "Fatigue of Concrete and Its Effect Upon Prestressed Concrete Beams," Magazine of Concrete Research, Vol. 20, No. 62, March 1968, pp. 21-30.

83. Shah, S.P., and McGarry, F.J., "Griffith Fracture Criterion and Concrete," Journal of the Engineering Mechanics Division, ASCE, Vol. 97, EM6, December 1971, pp. 1663-1676.

84. Slutter, R.G., and Ekberg, C.E., "Static and Fatigue Tests of Prestressed Concrete Railway Slabs," Proceedings, American Railway Engineering Association, 1959, pp. 1-50.

85. Suttikan, C., "A Generalized Solution for Time Dependent Response and Strength of Non Composite and Composite Prestressed Concrete Beams," Ph.D. Dissertation, The University of Texas at Austin, August 1978.

86. Thürlimann, B., "A Case for Partial Prestressing," PCA-University of Toronto Structural Concrete Symposium, Toronto, May 1971, pp. 252-301.

87. Thürlimann, B., "Prestressed Concrete--Facts and Trends," Institut fur Baustatik und Konstruktion, ETH Zurich, Report No. 114, July 1981.

88. Venuti, W.J., "A Statistical Approach to the Analysis of Fatigue Failure of Prestressed Concrete Beams," Journal of the American Concrete Institute, November 1965, pp. 1375-1393.

89. Wang, C., and Salmon, C.G., Reinforced Concrete Design, 3rd Ed., Harper and Row, New York, 1979, 918pp.

90. Warner, R.F., and Hulsbos, C.L., "Probable Fatigue Life of Prestressed Concrete Beams," Prestressed Concrete Institute Journal, April 1966, pp. 16-39.

91. Warner, R.F., and Hulsbos, C.F., "Probable Fatigue Life of Under-Reinforced Prestressed Concrete Beams," Publications, Vol. 22, IABSE, Zurich, 1962, pp. 337-352.

92. Waschеidt, H., "On the Fatigue Strength of Embedded Concrete Reinforcing Steel," Doctoral Thesis, Technical University of Aachen, Germany, 1965.

93. Zollman, C.L., "Dynamic American Engineers Sustain Magnel's Momentum," Reflections on the Beginnings of Prestressed Concrete in America, 1981, pp. 33-75.

94. Zollman, C.L., "Magnel's Impact on the Advent of Prestressed Concrete," Reflections on the Beginnings of Prestressed Concrete in America, 1981, pp. 5-32.

95. Overman, T.R., "Flexural Fatigue Behavior of Pretensioned Concrete Girders," unpublished M.S. thesis, The University of Texas at Austin, December 1984.

(Continued from inside front cover)

183-8 "The Resilient and Fatigue Characteristics of Asphalt Mixtures Processed by the Dryer-Drum Mixer," by Manuel Rodriguez and Thomas W. Kennedy, December 1976.

183-9 "Fatigue and Repeated-Load Elastic Characteristics of Inservice Portland Cement Concrete," by John A. Crumley and Thomas W. Kennedy, June 1977.

183-10 "Development of a Mixture Design Procedure for Recycled Asphalt Mixtures," by Ignacio Perez, Thomas W. Kennedy, and Adedare S. Adedimila, November 1978.

183-11 "An Evaluation of the Texas Blackbase Mix Design Procedure Using the Indirect Tensile Test," by David B. Peters and Thomas W. Kennedy, March 1979.

183-12 "The Effects of Soil Binder and Moisture on Blackbase Mixtures," by Wei-Chou V. Ping and Thomas W. Kennedy, May 1979.

184-1 "The TEXAS Model for Intersection Traffic—Development," by Clyde E. Lee, Thomas W. Rioux, and Charlie R. Copeland, December 1977.

184-2 "The TEXAS Model for Intersection Traffic — Programmer's Guide," by Clyde E. Lee, Thomas W. Rioux, Vivek S. Savur, and Charlie R. Copeland, December 1977.

184-3 "The TEXAS Model for Intersection Traffic—User's Guide," by Clyde E. Lee, Glenn E. Grayson, Charlie R. Copeland, Jeff W. Miller, Thomas W. Rioux, and Vivek S. Savur, July 1977.

184-4F "Application of the TEXAS Model for Analysis of Intersection Capacity and Evaluation of Traffic Control Warrants," by Clyde E. Lee, Vivek S. Savur, and Glenn E. Grayson, July 1978.

188-1 "Behavior of Stage-Cast Inverted T-Beams with the Precast Flange in Tension," by S. A. A. Wahidi and R. W. Furlong, August 1976.

188-2F "Strength and Behavior of Stage-Cast Inverted T-Beams," by Richard W. Furlong, August 1978.

196-1F "Design of Reinforcement for Notched Ends of Prestressed Concrete Girders," by Gangadharan Menon and Richard W. Furlong, August 1977.

198-1F "Control of Cracking on the Side Faces of Large Reinforced Concrete Beams," by G. C. Frantz and J. E. Breen, September 1978.

209-1F "Fatigue Loading of Cantilever Sign Structures from Truck Wind Gusts," by Bruce M. Creamer, Karl H. Frank, and Richard E. Klingner, April 1979.

212-1F "Design Criteria for Median Turn Lanes," by C. Michael Walton, Thomas W. Horne, and William K. Fung, March 1978.

244-1 "Analysis of Single Piles Under Lateral Loading," by Barry J. Meyer and Lymon C. Reese, December 1979.

245-1F "Texas Traffic Data Acquisition Program," by Han-Jei Lin, Clyde E. Lee, and Randy Machemehl, February 1980.

514-1F "Effects of Temperature Change on Plastic Crash Cushions," by Victor N. Toth and Clyde E. Lee, January 1976.

1053-1F "Social Service Agency Transportation Services: Current Operations and the Potential for the Increased Involvement of the Taxi Industry," by Walter L. Cox and Sandra Rosenbloom, August 1977.

RR 16 "The Prediction of Passenger Riding Comfort from Acceleration Data," by Craig C. Smith, David Y. McGehee, and Anthony J. Healey, March 1976.

RR 35 "Perceived Environmental Utility Under Alternative Transportation Systems: A Framework for Analysis," by Pat Burnett, March 1976.

RR 36 "Monitoring the Effects of the Dallas/Fort Worth Regional Airport — Volume I: Ground Transportation Impacts," by William J. Dunlay, Jr., Lyndon Henry, Thomas G. Caffery, Douglas W. Wiersig, and Waldo A. Zambrano, December 1976.

RR 37 "Monitoring the Effects of the Dallas/Fort Worth Regional Airport — Volume II: Land Use and Travel Behavior," by Pat Burnett, David Chang, Carl Gregory, Arthur Friedman, Jose Montemayor, and Donna Prestwood, July 1976.

RR 38 "The Influence on Rural Communities of Interurban Transportation Systems, Volume II: Transportation and Community Development: A Manual for Small Communities," by C. Michael Walton, John Huddleston, Richard Dodge, Charles Heimsath, Ron Linehan, and John Betak, August 1977.

RR 39 "An Evaluation of Promotional Tactics and Utility Measurement Methods for Public Transportation Systems," by Mark Alpert, Linda Golden, John Betak, James Story, and C. Shane Davies, March 1977.

RR 40 "A Survey of Longitudinal Acceleration Comfort Studies in Ground Transportation Vehicles," by L. L. Hoberock, July 1976.

RR 43 "A Pavement Design and Management System for Forest Service Roads — A Working Model," by Freddy L. Roberts, B. Frank McCullough, Hugh J. Williamson, and William R. Wallin, February 1977.

RR 45 "Characteristics of Local Passenger Transportation Providers in Texas," by Ronald Briggs, January 1977.

RR 46 "The Influence on Rural Communities of Interurban Transportation Systems, Volume I: The Influence on Rural Communities of Interurban Transportation Systems," by C. Michael Walton, Richard Dodge, John Huddleston, John Betak, Ron Linehan, and Charles Heimsath, August 1977.

RR 47 "Effects of Visual Distraction on Reaction Time in a Simulated Traffic Environment," by C. Josh Holahan, March 1977.

RR 48 "Personality Factors in Accident Causation," by Deborah Valentine, Martha Williams, and Robert K. Young, March 1977.

RR 49 "Alcohol and Accidents," by Robert K. Young, Deborah Valentine, and Martha S. Williams, March 1977.

RR 50 "Alcohol Countermeasures," by Gary D. Hales, Martha S. Williams, and Robert K. Young, July 1977.

RR 51 "Drugs and Their Effect on Driving Performance," by Deborah Valentine, Martha S. Williams, and Robert K. Young, May 1977.

RR 52 "Seat Belts: Safety Ignored," by Gary D. Hales, Robert K. Young, and Martha S. Williams, June 1978.

RR 53 "Age-Related Factors in Driving Safety," by Deborah Valentine, Martha Williams, and Robert K. Young, February 1978.

RR 54 "Relationships Between Roadside Signs and Traffic Accidents: A Field Investigation," by Charles J. Holahan, November 1977.

RR 55 "Demographic Variables and Accidents," by Deborah Valentine, Martha Williams, and Robert K. Young, January 1978.

RR 56 "Feasibility of Multidisciplinary Accident Investigation in Texas," by Hal L. Fitzpatrick, Craig C. Smith, and Walter S. Reed, September 1977.

RR 60 "A Pavement Design and Management System for Forest Service Roads — Implementation," by B. Frank McCullough and David R. Luhr, January 1979.

RR 61 "Multidisciplinary Accident Investigation," by Deborah Valentine, Gary D. Hales, Martha S. Williams, and Robert K. Young, October 1978.

RR 62 "Psychological Analysis of Degree of Safety in Traffic Environment Design," by Charles J. Holahan, February 1979.

RR 63 "Automobile Collision Reconstruction: A Literature Survey," by Barry D. Olson and Craig C. Smith, December 1979.

RR 64 "An Evaluation of the Utilization of Psychological Knowledge Concerning Potential Roadside Distractors," by Charles J. Holahan, December 1979.